Preprocedural planning, procedural guidance and follow-up assessment in percutaneous coronary intervention using multimodality coronary imaging

Suwannasom, P.

Publication date
2017

Document Version
Final published version

License
Other

Multimodality Coronary Imaging in Percutaneous Coronary Intervention
Pannipa Suwannasom

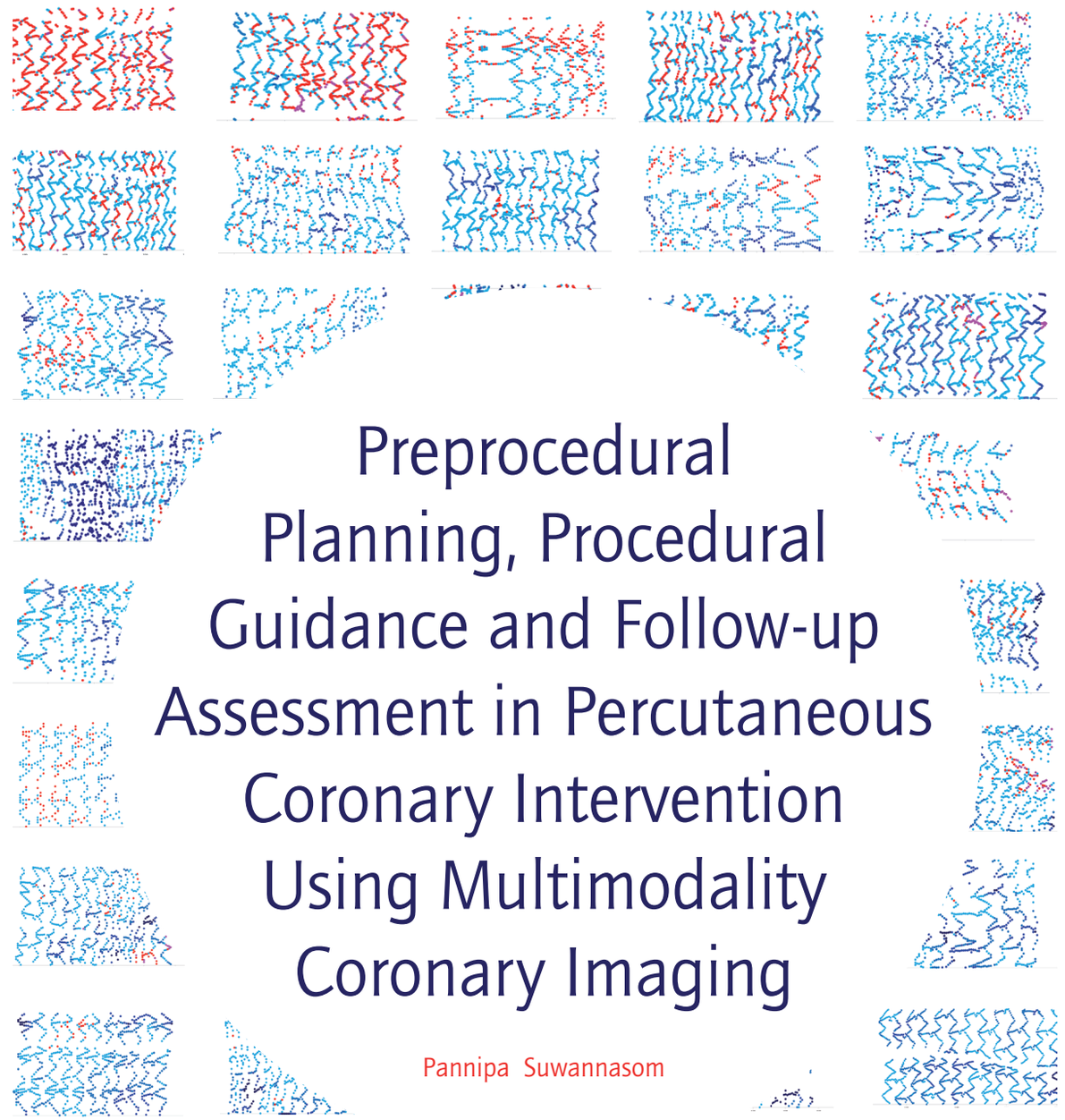

Preprocedural Planning, Procedural Guidance and Follow-up Assessment in Percutaneous Coronary Intervention Using Multimodality Coronary Imaging

Pannipa Suwannasom

Preprocedural Planning, Procedural Guidance and Follow-up Assessment in Percutaneous Coronary Intervention Using Multimodality Coronary Imaging

Pannipa Suwannasom

Layout: Optima Grafische Communicatie, Rotterdam, the Netherlands (www.ogc.nl)
Printed by: Optima Grafische Communicatie, Rotterdam, the Netherlands (www.ogc.nl)
ISBN: 978-94-92683-15-1

Financial support by the Academic Medical Center – University of Amsterdam and Northern Region Heart Center, Chiang Mai University are gratefully acknowledged.

Additional financial support for publication of this thesis was provided by:
Cardialysis B.V., Medis Medical Imaging Systems B.V., and Qvanteg AG

Preprocedural Planning, Procedural Guidance and Follow-up Assessment in Percutaneous Coronary Intervention Using Multimodality Coronary Imaging

ACADEMISCH PROEFSCHRIFT

ter verkrijging van de graad van doctor
aan de Universiteit van Amsterdam
op gezag van de Rector Magnificus
prof. dr. ir. K.I.J. Maex
ten overstaan van een door het College voor Promoties ingestelde commissie,
in het openbaar te verdedigen in de Agnietenkapel
op donderdag 14 september 2017, te 14:00 uur

door Pannipa Suwannasom
geboren te Uttaradit, Thailand

Promotores:	prof. dr. R.J. de Winter	AMC-UvA
	prof. dr. P.W.J.C. Serruys	Imperial College London
Copromotores:	dr. Y. Onuma	Erasmus Universiteit Rotterdam
	dr. J.J. Wykrzykowska	AMC-UvA
Overige leden:	prof. dr. C. von Birgelen	Universiteit Twente
	prof. dr. A.C. van der Wal	AMC-UvA
	prof. dr. R.J.G. Peters	AMC-UvA
	prof. dr. B.J.M. Mulder	AMC-UvA
	prof. dr. Y.B.W.E.M. Roos	AMC-UvA
	prof. dr. J.H.C. Reiber	Universiteit Leiden

Faculteit der Geneeskunde

TABLE OF CONTENTS

Chapter 1

General introduction and outline of the thesis

Pannipa Suwannasom

GENERAL INTRODUCTION

Coronary artery disease and the current treatment

Since its introduction 60 years ago, the selective coronary diagnostic angiogram, became a strong foundation of coronary artery disease (CAD) assessment. Coronary artery bypass graft surgery has been introduced in 1964[1] and first balloon angioplasty in an awake patient has been performed in 1977[2]. The development of these two techniques led to major advances in the treatment of coronary artery disease. There has been considerable progress in the development of the catheterization techniques and related device for percutaneous coronary intervention especially coronary stent technology. The coronary stent has provided a solution to subacute occlusion after balloon angioplasty[3-5], however, the bare metal stent still had a high restenosis rate and large proportion of patients needed repeat revascularization[4]. This problem has been effectively addressed by the development of drug eluting stents (DES), which reduced in-stent restenosis by delivering antiproliferative agents to the lesion[6-8]. However, the late and very late stent thrombosis in DES has raised concern about the global safety profile of first generation DES back in 2006[9]. Registries of all comers treated with the first-generation DES showed late stent thrombosis rate of 0.53% per year, with a continued increase to 3% over 4 years [10,11]. Post-mortem histopathological study in stent thrombosis patients showed a strong correlation of late stent thrombosis with the number of uncovered struts with evidence of a persistent inflammatory reaction around the stent struts[12,13]. This stimulated an intensive research on DES safety and introduced of the second-generation DES with thinner struts and permanent more biocompatible and less pro-inflammatory polymer. The frequency of stent thrombosis in second-generation DES was decreased to 0.7% at a mean follow-up of 21.7 months[14]. The complications related with the permanent polymer have motivated researchers to develop newer stent platform. The newer generation of DES have been designed, which coat drug on biodegradable polymer[15-19] or coat drug on stent with special techniques without polymer[20-22]. In parallel with the development of DES, the new BMS platform, with new designs, metal composition, thinner strut and surface modification also has been developed to actively inhibit neointimal hyperplasia[23,24].

Aside from the metallic stent platform, the novel technology of fully bioresorbable scaffolds (BRS) has been developed to offer the transient scaffolding of the vessel and elute antiproliferative drug to inhibit excessive growth of neointima[25]. To date, there are two types of coronary drug-eluting BRS technologies with an acquired CE mark, the PLLA-based BRS platform and the magnesium-based BRS[26.] The most widespread BRS platform is the fully bioresorbable everolimus-eluting polylactide scaffold, ABSORB BVS (Abbott Vascular, Santa Clara, CA). Due to the inherent difference of the mechanical properties of PLLA-based BRS from the metallic stent, this novel technology has required new imaging modalities and methodology for the assessment of its safety and efficacy in comparison with the metallic stents[27,28].

Intracoronary imaging

As outlined above, the new stent platforms required the appropriate imaging techniques to evaluate their safety and efficacy in short- and long-term follow-up[29]. It has been known that coronary angiography has limited reliability in evaluating lesion severity due to the dependency of image projection and high observer variability[30]. To overcome the intrinsic limitation of coronary angiography, the adjunctive invasive intracoronary imaging has been used to support the operator for procedural planning[31], assessing the stent performance[32] and monitoring the stent safety and efficacy at long-term follow-up[33,34]. The catheter-based imaging modalities available to date examine the coronary artery using either acoustic-based or light-based signals. Intravascular ultrasound (IVUS) is an acoustic-based imaging modality with axial resolution of 100 to 200 μm and lateral resolution of 250 μm[35]. IVUS algorithm offers the accurate measurement of luminal and vessel area, therefore, it is an attractive method for plaque quantification[36]. Optical coherence tomography (OCT) is a light-based imaging technique, which uses the scattering and absorption of near infrared light to generate the coronary images[37[. OCT provides an excellent axial resolution that can demonstrate plaque morphology, unrecognized plaque rupture, thrombus, strut apposition, edge dissection and neointimal thickness in more detail than IVUS[37].

OUTLINE OF THE THESIS: PREPROCEDURAL PLANNING, PROCEDURAL GUIDANCE AND FOLLOW-UP ASSESSMENT IN PERCUTANEOUS CORONARY INTERVENTION USING MULTIMODALITY CORONARY IMAGING

Remaining challenges in the treatment of coronary artery disease: procedural planning

Invasive coronary angiography is the gold-standard diagnostic method for treatment planning, the major drawback of this imaging technique is its invasive nature. It has been two decades that multislices coronary computed tomography angiography (CCTA) was introduced as an alternative method to evaluate coronary anatomy[38]. The improvement of image resolution of CCTA provide unlimited projections and reconstruction of 3-dimensional view compared with 2-dimensional view of conventional angiography. Beyond detection coronary stenosis sites, CCTA also provides fast and comprehensive atherosclerotic disease burden[39,40]. In addition, physiologic information can be derived from CCTA (FFR-CT)[41], which has promising prognostic implications.

To date clinical guidelines have recommended the use of anatomical SYNTAX score and heart team approach to decide on the revascularization strategy in patients with multivessel CAD. Due to noninvasive nature of CCTA, many studies have tried to compare the use of CCTA and conventional coronary angiography to evaluate lesions

complexity and planning for treatment. The feasibility and reproducibility of CCTA SYNTAX score have been studied and found that SYNTAX score assessed by CCTA is feasible and comparable to invasive coronary angiography with high reproducibility[42,43]. The challenge in this field has been to improve the ability of CCTA to provide assessment of coronary anatomy equivalent to the conventional coronary angiography[44].

The application of CCTA in diagnosis of CAD and procedural planning has recently also been extended to evaluation of in-stent restenosis. In the metallic stents, the evaluation of stent patency has been hampered due to partial volume and beam-hardening artifacts from the metallic material. These limitations are no longer present in polymeric BRS. Owing to the radiolucent properties of the polymeric material, the vessels treated with polymeric BRS would be the good candidates to be followed-up by CCTA[45]. The polymeric BRS is not only allowed CCTA to adequately delineate the lumen within the scaffold but also provided the volumetric analysis of plaque within scaffolded segments and non-intervene vessels[46]. Recently, CCTA has also shown its feasibility in providing noninvasive functional assessment (FFR-CT) in polymeric BRS treated segment[45]. However, the questions remain to be explored is the reliability of CCTA in evaluating treated segment compared with other coronary imaging techniques (QCA, IVUS, OCT). Another concerning issue of the CT technology is the reliability of CCTA derived FFR in intervened vessels when compared with standard invasive FFR.

Remaining challenges in percutaneous coronary intervention: multimodality imaging to evaluate stent safety and efficacy

Recent meta-analysis reported that IVUS-guided DES implantation superior to angiography-guided percutaneous coronary intervention in reducing the risk of major adverse cardiac events and stent thrombosis[47]. However, the results from meta-analyses may not be applied for BRS platform due to the lack of supporting evidence. In the absence of specific intracoronary imaging guidance, BVS exhibited higher device asymmetry and eccentricity than metallic EES post-implantation as assessed by IVUS[32]. Understanding of the clinical prognostic value of the imaging-based device performance measures such as acute gain, expansion, eccentricity and asymmetry indices either in metallic or polymeric devices is still limited.

There has been a considerable effort to develop new coronary stent platforms that could offer safety and efficacy in the CAD treatment. The accumulating evidences from histo-pathological and intracoronary imaging findings of the previous generation DES are the foundation for the development of new stent platform. The previous animal study on histology has shown the association between stretch and deep injury of the coronary artery and neointimal proliferation[48]. Post-mortem data showed that uncovered stent strut was associated with stent thrombosis[49] and it may link to the permanent polymer drug-coating that constitute to delayed vascular healing[50]. With the excellent

resolution of OCT, it allows the evaluation of the degree of injury, so called " embedment" between strut and three layers of coronary arteries. The mechanistic insights into the vascular healing after new stent implantation can also be assessed by OCT. The remaining challenges in this field and areas of uncertainty are: 1) the quantification of vessel wall-stent/scaffold interaction after the implantation of the scaffold/stent struts and the impact of embedment to the clinical outcomes and; 2) the standardization of methodology that permits a relative assessment of the speed and degree of vascular "healing" in patients treated with different types of stent and at different points in time.

The aims of this thesis are 1) to demonstrate application of the multimodality imaging for planning and follow-up assessment in PCI from non-invasive coronary imaging to invasive intracoronary imaging; 2) to explore advanced OCT application for evaluating new stent technologies.

Part A: An overview of bioresorbable vascular scaffold in the treatment of coronary artery disease

In **chapter 2,** we will provide an overview of drug-eluting BRS for the treatment of coronary artery disease. The mechanisms of active agent release from such scaffolds; currently available drug-eluting BRS and also discussed their future applications.

Part B: Multimodality imaging for preprocedural planning

In **chapter 3** we will present a comparison study between a purely noninvasive CCTA assessment with an invasive angiographic evaluation for the selection of the revascularization strategy in patients with multivessel CAD. In view of the limited accuracy in visual estimation of vessel sizing, in **chapter 4** we will present the application of quantitative coronary angiography maximal lumen diameter (QCA-Dmax) in the ABSORB clinical trial program for vessel sizing. We will explore the relation between the QCA-Dmax and clinical outcomes in 1,232 patients from 3 study cohorts of bioresorbable scaffold. In **chapter 5,** we will demonstrate the impact of implantation of oversized BVS and metallic everolimus-eluting stent (EES) confirmed by pre-procedural IVUS on the actual device expansion.

Part C: Multimodality imaging for assessment of acute device performance

In **chapter 6**, we will describe the algorithm of the embedment analysis and its reproducibility to use as surrogate parameter of acute injury caused by implantation of devices. In **chapter 7,** we will demonstrate the difference in lumen dimension measurements between optical coherence tomography (OCT) and quantitative coronary angiography (QCA) in the polymeric BRS and metallic stent. In **chapter 8,** we will investigate by IVUS, acute gain at the site of the pre-procedural minimal lumen area (MLA) achieved by either the polymeric BRS or the metallic EES and identify the factors contributing to the acute

performance of these devices. In **chapter 9,** we will subsequently explore the impact of post-procedural asymmetry, expansion, and eccentricity indices as assessed by IVUS in metallic EES and BRS and their respective impact on clinical events at 1-year follow-up.

Part D: Multimodality imaging for evaluating safety and efficacy of stent from short- to medium-term follow-up

In **chapter 10**, we will first evaluate the clinical safety and feasibility of a bare metal cobalt-chromium stent with an active surface oxide layer modification by using QCA and OCT post-implantation and at 6-month follow-up. In this chapter, we will present the postprocedural, 6-month and 1 year clinical outcomes after stent implantation. In **chapter 11**, we will present a study evaluating vascular healing afterpolymer-free sirolimus-eluting stents implantationat 3 and 6 months with optical coherence tomography imaging.

Part E: Multimodality imaging for evaluating safety and efficacy of stent in long-term follow-up

In **chapter 12,** we will demonstrate the feasibility of non-invasive coronary imaging for investigating the vessel treated with polymeric BRS at 18 months after implantation. This chapter will provide simple method to identify the metallic radio-opaque markers (MRMs) and discriminate them from the calcified nodules which could mimic the appearance of MRMs. We will use this method to identify the region of interest and perform in-scaffold quantitative luminal analysis then compared with QCA, IVUS and OCT. It has been known that OCT is the reliable imaging technique that could provide lumen assessment close to actual vessel size. In **chapter 13**, we will specifically compare the accuracy of CCTA for in-scaffold quantitative evaluation at 18 months post-implantation with OCT by matching the same cross-section.

In **chapter 14**, we will evaluate the vascular response and healing at 2 years of overlapping BVS segment compared to non-overlapping BVS segment as assessed by OCT. In **chapter 15**, we will demonstrate the application of multimodality imaging to follow-up the change of coronary artery aneurysm after implantation of BVS up to 5 years. From chapter 16 to chapter 18, we will explore the serial changes of the vessels treated with BVS from post-implantation until 5-year follow-up in various aspects. In **chapter 16**, we will investigate using OCT the changes of the lumen eccentricity and asymmetry at 5 years after implantation of BVS and their impacts to the long-term clinical outcomes. In **chapter 17**, the edge vascular response with the geometric changes will be carefully evaluated by using serial OCT analysis. Thereafter, in **chapter 18**, we will focus on the changes of plaque composition in the scaffolded segment compared to the non-scaffolded segment by using multimodality imaging (IVUS, IVUS-VH, OCT).

REFERENCE

1. Head SJ, Kieser TM, Falk V, Huysmans HA, Kappetein AP. Coronary artery bypass grafting: Part 1--the evolution over the first 50 years. European heart journal. 2013;34(37):2862-2872.
2. Gruntzig A. Transluminal dilatation of coronary-artery stenosis. Lancet (London, England). 1978;1(8058):263.
3. Fischman DL, Leon MB, Baim DS, et al. A randomized comparison of coronary-stent placement and balloon angioplasty in the treatment of coronary artery disease. Stent Restenosis Study Investigators. The New England journal of medicine. 1994;331(8):496-501.
4. Serruys PW, de Jaegere P, Kiemeneij F, et al. A comparison of balloon-expandable-stent implantation with balloon angioplasty in patients with coronary artery disease. Benestent Study Group. The New England journal of medicine. 1994;331(8):489-495.
5. Sigwart U, Puel J, Mirkovitch V, Joffre F, Kappenberger L. Intravascular stents to prevent occlusion and restenosis after transluminal angioplasty. The New England journal of medicine. 1987;316(12):701-706.
6. Morice MC, Serruys PW, Sousa JE, et al. A randomized comparison of a sirolimus-eluting stent with a standard stent for coronary revascularization. The New England journal of medicine. 2002;346(23):1773-1780.
7. Sousa JE, Costa MA, Abizaid A, et al. Lack of neointimal proliferation after implantation of sirolimus-coated stents in human coronary arteries: a quantitative coronary angiography and three-dimensional intravascular ultrasound study. Circulation. 2001;103(2):192-195.
8. Silber S, Colombo A, Banning AP, et al. Final 5-year results of the TAXUS II trial: a randomized study to assess the effectiveness of slow- and moderate-release polymer-based paclitaxel-eluting stents for de novo coronary artery lesions. Circulation. 2009;120(15):1498-1504.
9. Camenzind E, Steg PG, Wijns W. Stent thrombosis late after implantation of first-generation drug-eluting stents: a cause for concern. Circulation. 2007;115(11):1440-1455; discussion 1455.
10. Daemen J, Wenaweser P, Tsuchida K, et al. Early and late coronary stent thrombosis of sirolimus-eluting and paclitaxel-eluting stents in routine clinical practice: data from a large two-institutional cohort study. Lancet (London, England). 2007;369(9562):667-678.
11. Wenaweser P, Daemen J, Zwahlen M, et al. Incidence and correlates of drug-eluting stent thrombosis in routine clinical practice. 4-year results from a large 2-institutional cohort study. Journal of the American College of Cardiology. 2008;52(14):1134-1140.
12. Joner M, Finn AV, Farb A, et al. Pathology of drug-eluting stents in humans: delayed healing and late thrombotic risk. Journal of the American College of Cardiology. 2006;48(1):193-202.
13. Nebeker JR, Virmani R, Bennett CL, et al. Hypersensitivity cases associated with drug-eluting coronary stents: a review of available cases from the Research on Adverse Drug Events and Reports (RADAR) project. Journal of the American College of Cardiology. 2006;47(1):175-181.
14. Baber U, Mehran R, Sharma SK, et al. Impact of the everolimus-eluting stent on stent thrombosis: a meta-analysis of 13 randomized trials. Journal of the American College of Cardiology. 2011;58(15):1569-1577.
15. Nakazawa G, Torii S, Ijichi T, et al. Comparison of Vascular Responses Following New-Generation Biodegradable and Durable Polymer-Based Drug-Eluting Stent Implantation in an Atherosclerotic Rabbit Iliac Artery Model. Journal of the American Heart Association. 2016;5(10).
16. Wilson GJ, Marks A, Berg KJ, et al. The SYNERGY biodegradable polymer everolimus eluting coronary stent: Porcine vascular compatibility and polymer safety study. Catheterization and

cardiovascular interventions : official journal of the Society for Cardiac Angiography & Interventions. 2015;86(6):E247-257.
17. Byrne RA, Kastrati A, Massberg S, et al. Biodegradable polymer versus permanent polymer drug-eluting stents and everolimus-versus sirolimus-eluting stents in patients with coronary artery disease: 3-year outcomes from a randomized clinical trial. Journal of the American College of Cardiology. 2011;58(13):1325-1331.
18. Kang SH, Park KW, Kang DY, et al. Biodegradable-polymer drug-eluting stents vs. bare metal stents vs. durable-polymer drug-eluting stents: a systematic review and Bayesian approach network meta-analysis. European heart journal. 2014;35(17):1147-1158.
19. Zhang Y-J, Pan D-R, Pang S, Wu W, Xu B. Biodegradable or biocompatible polymer drug-eluting stent: a Gordian knot. EuroIntervention. 2015;11(3):250-252.
20. Desch S, Schloma D, Mobius-Winkler S, et al. Randomized comparison of a polymer-free sirolimus-eluting stent versus a polymer-based paclitaxel-eluting stent in patients with diabetes mellitus: the LIPSIA Yukon trial. JACC Cardiovascular interventions. 2011;4(4):452-459.
21. Shiratori Y, Cola C, Brugaletta S, et al. Randomized Comparison Between Polymer-Free Versus Polymer-Based Paclitaxel-Eluting Stent. Circulation: Cardiovascular Interventions. 2014;7(3):312.
22. Urban P, Meredith IT, Abizaid A, et al. Polymer-free Drug-Coated Coronary Stents in Patients at High Bleeding Risk. New England Journal of Medicine. 2015;373(21):2038-2047.
23. Zhang K, Liu T, Li JA, Chen JY, Wang J, Huang N. Surface modification of implanted cardiovascular metal stents: from antithrombosis and antirestenosis to endothelialization. Journal of biomedical materials research Part A. 2014;102(2):588-609.
24. Zhang Q, Shen Y, Tang C, Wu X, Yu Q, Wang G. Surface modification of coronary stents with SiCOH plasma nanocoatings for improving endothelialization and anticoagulation. Journal of biomedical materials research Part B, Applied biomaterials. 2015;103(2):464-472.
25. Onuma Y, Serruys PW. Bioresorbable scaffold: the advent of a new era in percutaneous coronary and peripheral revascularization? Circulation. 2011;123(7):779-797.
26. Suwannasom P, Sotomi Y, Tateishi H, et al. Bioresorbable drug-eluting scaffolds for treatment of vascular disease. Expert opinion on drug delivery. 2016;13(5):725-739.
27. Chamie D, Garcia-Garcia H, Costa RA, Onuma Y, Abizaid A, Serruys PW. Role of invasive imaging in acute and long-term assessment of bioresorbable scaffold technology. Catheterization and cardiovascular interventions : official journal of the Society for Cardiac Angiography & Interventions. 2016;88(S1):38-53.
28. Garcia-Garcia HM, Serruys PW, Campos CM, et al. Assessing bioresorbable coronary devices: methods and parameters. JACC Cardiovascular imaging. 2014;7(11):1130-1148.
29. Byrne RA, Serruys PW, Baumbach A, et al. Report of a European Society of Cardiology-European Association of Percutaneous Cardiovascular Interventions task force on the evaluation of coronary stents in Europe: executive summary. European heart journal. 2015;36(38):2608-2620.
30. Garrone P, Biondi-Zoccai G, Salvetti I, et al. Quantitative coronary angiography in the current era: principles and applications. Journal of interventional cardiology. 2009;22(6):527-536.
31. Gomez-Lara J, Diletti R, Brugaletta S, et al. Angiographic maximal luminal diameter and appropriate deployment of the everolimus-eluting bioresorbable vascular scaffold as assessed by optical coherence tomography: an ABSORB cohort B trial sub-study. EuroIntervention. 2012;8(2):214-224.
32. Brugaletta S, Gomez-Lara J, Diletti R, et al. Comparison of in vivo eccentricity and symmetry indices between metallic stents and bioresorbable vascular scaffolds: insights from the ABSORB

and SPIRIT trials. Catheterization and cardiovascular interventions : official journal of the Society for Cardiac Angiography & Interventions. 2012;79(2):219-228.
33. Choi SY, Maehara A, Cristea E, et al. Usefulness of minimum stent cross sectional area as a predictor of angiographic restenosis after primary percutaneous coronary intervention in acute myocardial infarction (from the HORIZONS-AMI Trial IVUS substudy). The American journal of cardiology. 2012;109(4):455-460.
34. Witzenbichler B, Maehara A, Weisz G, et al. Relationship between intravascular ultrasound guidance and clinical outcomes after drug-eluting stents: the assessment of dual antiplatelet therapy with drug-eluting stents (ADAPT-DES) study. Circulation. 2014;129(4):463-470.
35. Mintz GS, Nissen SE, Anderson WD, et al. American College of Cardiology Clinical Expert Consensus Document on Standards for Acquisition, Measurement and Reporting of Intravascular Ultrasound Studies (IVUS). A report of the American College of Cardiology Task Force on Clinical Expert Consensus Documents. Journal of the American College of Cardiology. 2001;37(5):1478-1492.
36. Mintz GS, Garcia-Garcia HM, Nicholls SJ, et al. Clinical expert consensus document on standards for acquisition, measurement and reporting of intravascular ultrasound regression/progression studies. EuroIntervention. 2011;6(9):1123-1130, 1129.
37. Tearney GJ, Regar E, Akasaka T, et al. Consensus standards for acquisition, measurement, and reporting of intravascular optical coherence tomography studies: a report from the International Working Group for Intravascular Optical Coherence Tomography Standardization and Validation. Journal of the American College of Cardiology. 2012;59(12):1058-1072.
38. Achenbach S, Moshage W, Ropers D, Nossen J, Daniel WG. Value of electron-beam computed tomography for the noninvasive detection of high-grade coronary-artery stenoses and occlusions. The New England journal of medicine. 1998;339(27):1964-1971.
39. Maurovich-Horvat P, Ferencik M, Voros S, Merkely B, Hoffmann U. Comprehensive plaque assessment by coronary CT angiography. Nat Rev Cardiol. 2014;11(7):390-402.
40. Min JK, Shaw LJ. Noninvasive diagnostic and prognostic assessment of individuals with suspected coronary artery disease: coronary computed tomographic angiography perspective. Circulation Cardiovascular imaging. 2008;1(3):270-281; discussion 281.
41. Gaur S, Ovrehus KA, Dey D, et al. Coronary plaque quantification and fractional flow reserve by coronary computed tomography angiography identify ischaemia-causing lesions. European heart journal. 2016;37(15):1220-1227.
42. Papadopoulou SL, Girasis C, Dharampal A, et al. CT-SYNTAX score: a feasibility and reproducibility Study. JACC Cardiovascular imaging. 2013;6(3):413-415.
43. Pozo E, Alvarez-Acosta L, Alonso D, et al. Diagnostic accuracy of coronary ct for the quantification of the syntax score in patients with left main and/or 3-vessel coronary disease. Comparison with invasive angiography. International journal of cardiology. 2015;182:549-556.
44. Cavalcante R, Onuma Y, Sotomi Y, et al. Non-invasive Heart Team Assessment of Multivessel Coronary Disease with Coronary Computed Tomography Angiography Based on SYNTAX Score II Treatment Recommendations: Design and Rationale of the Randomized SYNTAX III Revolution trial. EuroIntervention. 2016.
45. Onuma Y, Dudek D, Thuesen L, et al. Five-year clinical and functional multislice computed tomography angiographic results after coronary implantation of the fully resorbable polymeric everolimus-eluting scaffold in patients with de novo coronary artery disease: the ABSORB cohort A trial. JACC Cardiovascular interventions. 2013;6(10):999-1009.

46. Campos CM, Garcia-Garcia HM, Muramatsu T, et al. Impact of the Everolimus-eluting Bioresorbable Scaffold in Coronary Atherosclerosis. Revista espanola de cardiologia (English ed). 2016;69(2):109-116.
47. Elgendy IY, Mahmoud AN, Elgendy AY, Bavry AA. Outcomes With Intravascular Ultrasound-Guided Stent Implantation: A Meta-Analysis of Randomized Trials in the Era of Drug-Eluting Stents. Circulation Cardiovascular interventions. 2016;9(4):e003700.
48. Schwartz RS, Huber KC, Murphy JG, et al. Restenosis and the proportional neointimal response to coronary artery injury: results in a porcine model. Journal of the American College of Cardiology. 1992;19(2):267-274.
49. Finn AV, Joner M, Nakazawa G, et al. Pathological correlates of late drug-eluting stent thrombosis: strut coverage as a marker of endothelialization. Circulation. 2007;115(18):2435-2441.
50. John MC, Wessely R, Kastrati A, et al. Differential Healing Responses in Polymer- and Nonpolymer-Based Sirolimus-Eluting Stents. JACC: Cardiovascular Interventions. 2008;1(5):535-544.

Chapter 2

Bioresorbable drug-eluting scaffolds for treatment of vascular disease: reviewed

Pannipa Suwannasom, Yohei Sotomi, Hiroki Tateishi, Erhan Tenekecioglu, Yaping Zeng, Robin P. Kraak, Joanna J. Wykrzykowska, Robbert J. de Winter, Patrick W. Serruys, Yoshinobu Onuma

Expert Opin Drug Deliv. 2016;13(5):725-39.

ABSTRACT

Introduction

Theoretical advantages of fully bioresorbable scaffold (BRS) stem from transient vessel support without rigid caging. Therefore, it could reduce long-term adverse events associated with the presence of foreign materials.

Areas covered

This article will provide an overview of: drug-eluting BRS for various applications in the treatment of vascular disease; The mechanisms of active agent release from such scaffolds; currently available drug-eluting BRS and their future applications are also discussed.

Expert opinion

The current BRS have been developed in order to achieve optimal vascular patency while providing long-term safety. The clinical efficacy and safety of BRS in coronary treatment have been reported as equal to that of the current metallic drug eluting stents in simple lesions. The application of BRS can potentially be expanded to other vascular beds. The research in bioengineering for the appropriate materials should not only focus on biocompatibility but also should be tailored according to the sites of implantation, which may require different strength and supporting period. The ultimate goal in this field is to develop a biocompatible device that provides equivalent and complementary therapy to other devices, and is able to disappear when the mechanical support and drug delivery are no longer require

Article highlights

- BRS provides temporary drug elution and scaffolding until the vessel has healed.
- Sirolimus-derivative agents developed through modifications on the carbon C40 of the macrocyclic ring except novolimus and myolimus.
- The polymer composition, coating thickness, and stent design greatly influence the drug release behavior.
- The most dominant release mechanism of drug incorporated in DES is diffusion-based drug delivery.
- The current BRSs are composed of either a polymer or bioresorbable metal alloy.
- Different materials have different chemical compositions, mechanical properties, and therefore bioabsorption times.

- The BRS application in vasculature has expanded beyond treatment of coronary disease, such as congenital heart disease and peripheral vascular disease.

1. INTRODUCTION

The first reference to stent used in cardiovascular literature comes from Dotter in 1983. [1] At that time, Dotter reported the results of transluminal expandable Nitinol Stent Grafting in peripheral vascular disease. Four years later, the first report of the clinical use of coronary stents was published,[2] followed by the landmarks BENESTENT and STRESS trials.[3,4] This technology has provided a solution to acute vessel occlusion by sealing the dissection flaps and preventing elastic recoil. The rate of subacute occlusion was reduced to 1.5%, making emergency bypass surgery a rare occurrence. Despite the use of stent, the restenosis rates of bare metal stent were still high (22% at 7 months), and the neointimal hyperplasia inside the stent was even more prominent than with angioplasty, necessitating repeat treatment in large proportion of patients.[3] In-stent restenosis is caused by the migration and proliferation of vascular smooth muscle cells (SMCs) in response to the trauma to the vessel wall.[5]

To circumvent the problem of in-stent restenosis, drug eluting stents (DES) have been introduced in clinical practice to prevent neointimal hyperplasia by delivering antiproliferative agents to the lesion.[6,7] Both large-scale randomized trials and all-comer registries showed excellent results in terms of reducing the need for repeat revascularization. However, the early enthusiasm has been tempered in recent years following widespread concerns regarding the increased risk of late and very late stent thrombosis. [8–12] This problem has been now largely solved with the development of metallic stents with thin struts covered by a thin biodegradable polymer or metallic DES without polymer to minimize stent thrombosis. Considering the serious and often debilitating consequences of stent thrombosis, bioresorbable technology has been developed to eliminate the presence of the permanent foreign material. Such bioresorbale device further eliminates deleterious caging effects of the permanent metallic endoluminal prosthesis, namely their permanent effects on vessel geometry, wall shear stress, and cell signaling.[13]

The novel technology of fully bioresorbable scaffold (BRS) offers the possibility of transient scaffolding of the vessel to prevent acute vessel closure and recoil whilst also transiently eluting an antiproliferative drug to counteract the constrictive remodeling and excessive neointimal hyperplasia.[14] The BRS application in vasculature has expanded beyond treatment of coronary disease. The scaffold has been applied as vasculature support in congenital heart disease. It is also being tested as a reservoir for local drug delivery in cancer treatment and gene therapy.

This article will provide (1) an overview of landscape of drug-eluting BRS for various applications in vasculature, (2) mechanisms of active agent release from a scaffold for treatment, and (3) currently available drug-eluting BRS in vasculature that acquired Con-

formité Européenne (CE) mark, those under clinical investigation and those in preclinical phase trials.

2. THEORETICAL CONCEPT OF BIORESORBABLE DEVICES IN VASCULATURE

Theoretical advantages of BRS stem from transient vessel support without rigid caging. The potential benefits of BRS over current metallic DES technology proposed by authors are summarized as follows:

2.1. A reduction in long-term adverse events from permanent materials

As drug elution and scaffolding are temporary until the vessel has healed, no foreign material potentially triggering very late stent thrombosis (such as non-endothelialized struts and drug polymers)[15] could persist in the long term.

2.2. The removal, through bioresorption, of the stented vessel's rigid caging

This can facilitate the return of vasomotion, physiological cyclic shear stress, late luminal enlargement, and late expansive remodeling. Furthermore, this might also reduce the problems of jailing the ostium of side branches as seen with permanent metallic stent struts (non-apposed in front of the side-branch struts).

2.3. Suitability for future treatment options

The treatment of complex multivessel disease frequently results in the use of multiple long DESs, so-called full metal jacket stenting. In such cases, repeat revascularization – either percutaneous or surgical – is potentially challenging because of the metallic caging of distal runoffs with previously implanted stents. The use of a BRS implies no restriction to future percutaneous or surgical revascularization.

2.4. Allowing the use of noninvasive imaging techniques such as multislice computed tomographic angiography or magnetic resonance imaging for follow-up

Presently, metallic stents can cause a blooming effect with these imaging modalities making interpretation more difficult.[16] The polymeric scaffold should not restrict the use of multislice computed tomographic (MSCT) or magnetic resonance imaging (MRI) as it is nonmetallic. Even with metallic BRS, such as magnesium or iron, MSCT and MRI can be efficiently used once bioresorption is completed. MSCT has provided reliable assessment of the angiographic results up to 3–5 years after translucent scaffold implantation. [17,18]

2.5. Reservoir for the local delivery of drugs

Since the duration of bioresorption is modifiable, according to the type of polymers/copolymers, a fine-tuned elution of multiple drugs can potentially be achieved (e.g. early elution of anti-proliferative agent from a coated polymer and chronic elution of anti-inflammatory or other agent from the backbone polymer).

2.6. Relief of anxiety of implanted foreign materials

The use of BRS eliminates patient's concern about having an implant in their bodies for the rest of their lives.[19]

2.7. Pediatric application

Congenital heart disease (e.g. pulmonary stenosis, aortic coarctation, aorto-pulmonary collaterals, atrial septal defect) can be potentially treated with BRS.[20–23] After bioresorption, scaffolded arteries can adapt a natural growth pattern. However, this indication for the treatment is still off-label, and the long-term results need to be monitored.

2.8. Peripheral vascular disease

BRS may prevent the late complications related to stent placement such as strut fracture from high stresses due to complex vascular motion.[24] BRS may provide a superior flexibility and a vessel support only for the time that is needed.

3. DRUG RELEASE CONTROL FROM BIORESOBABLE DRUG- ELUTING SCAFFOLD

BRS can keep the vessel lumen patent and simultaneously serve as a drug/protein delivery platform. However, most drugs and all proteins are destroyed when exposed to high melting temperature. Certain drugs, such as steroids, can be incorporated in small drug quantities into poly-L-lactic acid (PLLA) fiber during the melting process without compromising the mechanical properties of the scaffold.[25] In order to make a BRS carry adequate amount of antiproliferative agent, coating layer controlling drug release is added to the scaffold backbone. There are three main release mechanisms for drugs incorporated into DES: (1) diffusion-based drug delivery: the most common release mechanism for drugs incorporated into DES [26]; (2) erosion-based drug delivery: drug is released due to the polymer degradation and erosion from coating.[27]; (3) dissolution-based delivery: the drug particles may either be incorporated into a polymer or coated directly onto the device surface.[28] Dissolution is mostly used in polymer-free metallic DES. The current drug-eluting BRS are coated with biodegradable polymers; therefore, drug release kinetics depend on the kinetics of polymer degradation time.

The polymer composition, coating thickness, and stent design greatly influence the drug release behavior. The total achievable drug load and the prolongation of release depend on the coating thickness and the integrity of polymer during device expansion. Hydrophilic characteristics of the polymer promote biocompatibility while the hydrophobic characteristics control drug elution.[29] Prolongation of drug release and increase of drug load remain to be a challenge for BRS technologies. BRS platform might allow the incorporation of the drugs into the entire stent or scaffold made up of polymers or metal alloy. The drug release mechanism might either be the diffusion control or the stent degradation or the combination of both processes.[26]

4. DRUGS USED IN CORONARY BRS

The primary aim of loading a drug on BRS is to prevent neointimal hyperplasia; therefore, the antiproliferative agents which retard hyper-proliferation and migration of SMCs, have anti-inflammatory and antithrombogenic characteristics are the major candidates for DES application. Several immunosuppressive, antiproliferative drugs, or even statins [30,31] have been tested. However, only two classes of antiproliferative agents have proven their efficacies in preventing neointimal hyperplasia and in-stent restenosis: paclitaxel and the rapamycin analogs (limus family). The current family of drug-eluting BRS can be classified into (i) limus family elution from biodegradable coating; (ii) non-limus drug elution from biodegradable coating.

4.1. Mechanism of action of antiproliferative drug available in current BRS

4.1.1. Limus family elution from biodegradable coating

There are eight limus family compounds being used in coronary metallic DES. These compounds target either the mammalian target of rapamycin (mTOR) (sirolimus, everolimus, zotarolimus, biolimus A9, myolimus, and novolimus) or calcineurin (tacrolimus and pimecrolimus).[32] Nevertheless, only mTOR inhibitors have been tested in BRS. Amongst six of mTOR inhibitors, there are only three substances: sirolimus, everolimus, and novolimus, which are being used in the current BRS platforms.

(1) Sirolimus is a natural macrocyclic lactone with potent immunosuppressive and antiproliferative properties; it is also known as Rapamycin. It is synthesized by the bacterium Streptomyces hygroscopicus.[33] Initially, it was developed as an antifungal agent, but was soon discovered of immuno-suppressive activity and antitumor activity. It has also allowed for a positive turn in coronary artery stenosis treatment. The chemical structure of sirolimus and its analogs are shown in Figure 1, All mTOR inhibitors share an almost identical lipophilic chemical structure and bind to their major cytosolic FK-506

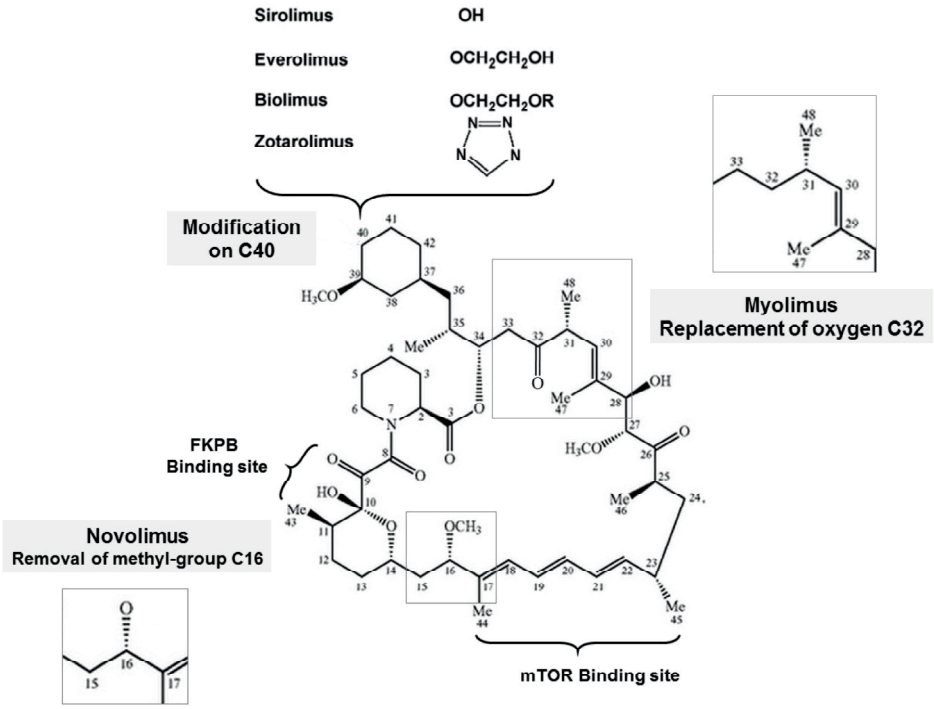

a. Limus family

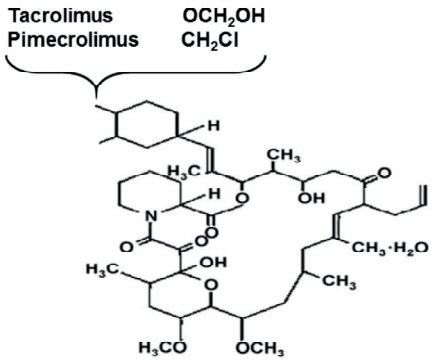

b. Calcineurin inhibitor

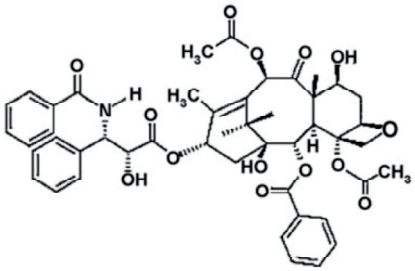

c. Paclitaxel

figure caption 1. Chemical structure of sirolimus analogues, calcinuerin inhibitors and paclitaxel. Adapted from [38]

Abbreviation: FKBP = FK-506 binding protein-12; mTOR = mammalian target of rapamycin

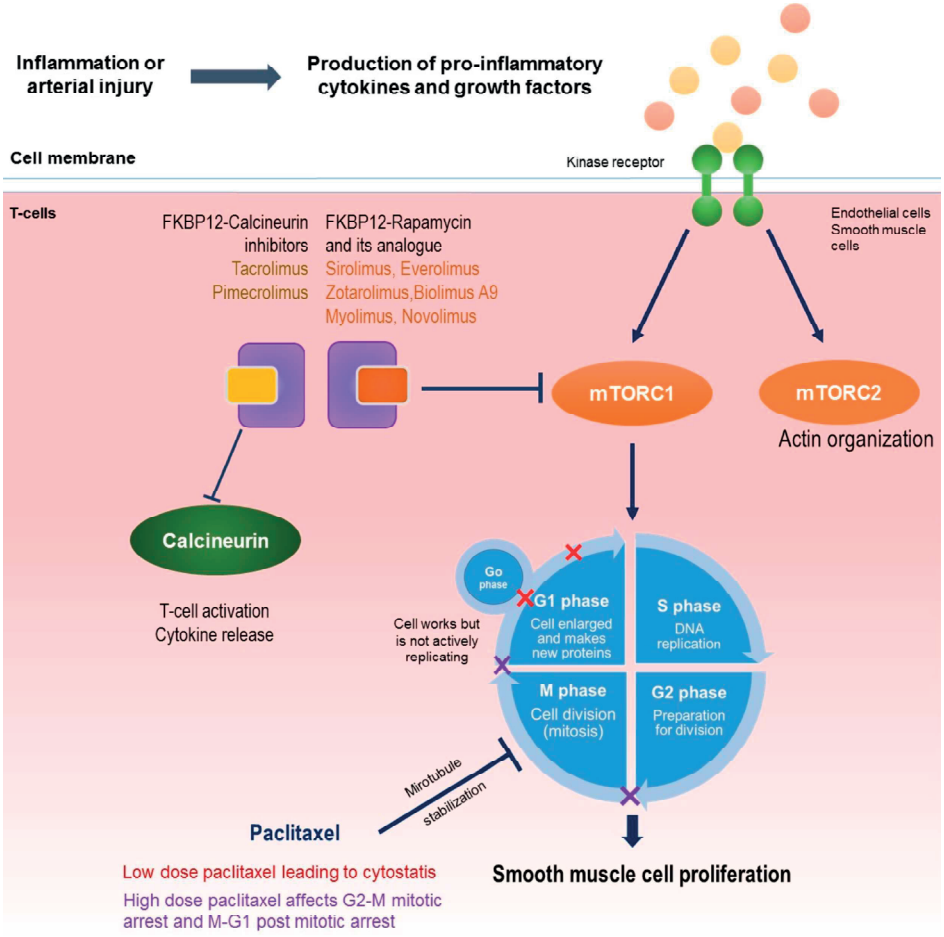

figure caption 2. Mechanism of action of sirolimus and its analogues, calcineurin inhibitors and paclitaxel. Sirolimus form a complex with the cytosolic immunophilin FKBP-12 and inhibits the mammalian target of rapamycin (mTOR). Inhibition of mTORC1 results in blockage of late G1 phase (in red cross). Paclitaxel inhibits its disassembly of microtubules, mitotic progression and cell proliferation. Paclitaxel inhibits cell proliferation and migration in a dose-dependent. It is cytostatic at low dose (inhibit G2-M phase in purple cross), at high dose, it can cause mitotic arrest and local vascular cytotoxic. Adapted from [39] and [40].

binding protein-12 (FKBP12) forming a complex which subsequently inhibits the mTOR. mTOR is a serine/threonine kinase which is a member of the phosphatidylinositol-3-kinase-related protein kinase family. mTORC1 ivs involved with critical steps of the cell cycle, including the checkpoints that govern DNA damage and repair.[34] Inhibition of mTORC1 induces cell-cycle arrest at the juncture of the G1 and S phase,[35] resulting in inhibition of SMCs proliferation [36] and migration.[37] Therefore, the mechanism of sirolimus analogues is cytostatic rather than cytotoxic (see Figure 2).

Sirolimus includes two separated moieties, the TOR-binding and the FKBP12-binding regions (see Figure 1a). The formation of a rapamycin–FKBP12 complex binds directly to mTOR and inhibits the mTOR function and the mTOR- mediated signaling network.[41] Other antirestenotic properties of Sirolimus include the inhibition of total protein and collagen synthesis involved in extracellular matrix formation and promoting a contractile rather than a proliferative phenotype.[42]

(2) Everolimus is a hydroxyethyl ether derivative of sirolimus, with a 2-hydroxyethyl group in carbon C40 (see Figure 1a). Everolimus has immuno-suppressive potential, which relies on preventing lymphocyte and SMC proliferation mediated by inflammatory cytokines and growth factors.[43] A stent-based delivery of everolimus was found to selectively clear macrophages in rabbit atherosclerotic plaques by autophagy.[44] Due to its molecular and chemical structure, the lipophilic properties of everolimus are greater compared to sirolimus, leading to a more rapid absorption into the arterial wall [43] and lower half-life than sirolimus.[32]

(3) Myolimus is a macrocyclic lactone which is produced by replacement of the oxygen on C32 of the macrocyclic ring (see Figure 1a), and has a comparable potency, in terms of inhibition of SMCs, to sirolimus.[40]

(4) Novolimus is a macrocyclic lactone, which has been developed by removal of a methyl-group from carbon C16. Notably, this differs from the other macrocyclic lactone agents that are used in DES, which have been developed through modifications on the carbon C40 of the macrocyclic ring (see Figure 1a). Nevertheless, in a similar fashion to these other agents in limus family, Novolimus has been shown in in vitro studies to have a high potency to inhibit human SMCs, comparable to that of sirolimus.[45,46]

4.1.2. Non-limus drug elution from biodegradable coating

Paclitaxel is a lipophilic molecule with potent antiproliferative and antimigratory activity. The drug binds specifically to the ß-tubulin subunit of microtubules and appears to antagonize the disassembly of microtubules, and thus, aberrant structures derived from microtubules accumulate in the mitotic phase of the cell cycle. Paclitaxel impacts primarily the M phase of the cell cycle, inhibiting growth factor-induced DNA synthesis and cell proliferation and leads to apoptosis or cell death. Compared with the limus family, the mode of action of paclitaxel is primarily cytotoxic. It has narrow toxic-therapeutic window and has hydrophobic properties.[33] Paclitaxel has been used in the first generation of magnesium BRS before changing to sirolimus in the new generation.

Table 1 Mechanical properties and degradation time for different polymers.

Polymer composition	Tensile modulus of elasticity (Gpa)	Tensile strength (Mpa)	Elongation at break (%)	Degradation time (months)
Poly(L-lactide)	3.1-3.7	60-70	2-6	>24
Poly (DL-lactide)	3.1-3.7	45-55	2-6	12-6
Poly (glycolide)	6.5-7.0	90-110	1-2	6-12
50/50 DL-lactide/glycolide	3.4-3.8	40-50	1-4	1-2
82/18 L-lactide/glycolide	3.3-3.5	60-70	2-6	12-18
70/30 L-Lactide/ε- caprolactone	0.02-0.04	18-22	>100	12-24
78/22 L-lactide/ poly(4-hydroxybutyrate	1.0	36	126	>12
Magnesium alloy	40-45	220-330	2-20	1-3
Iron	200	300	25	>48
Cobalt chromium	210-235	1449	~40	Biostable
Stainless steel 316L	193	668	40+	Biostable
Nitinol	45	700-1100	10-20	Biostable

Adapted from Onuma Y et al.[47]
Tensile modulus is the tendency of an object to deform along an axis when opposing forces are applied along that axis. Tensile strength is defined as the maximum stress that a material can withstand without significant contraction in cross-section while being stretched.
Abbreviation: Gpa = Giga pascal, Mpa = Mega pascal

5. LANDSCAPE OF MATERIALS AND TECHNOLOGIES TO CREATE BRS

The key mechanical traits for candidate materials for coronary indications include: high-elastic moduli to impart radial stiffness, large break strains to impart the ability to withstand deformations from the crimped to expanded states, and low-yield strains to reduce the amount of recoil and over-inflation necessary to achieve the target deployment. Stent developers look to increase stent strut dimensions to compensate for mechanical shortcomings of bioresorbable materials. As the thickness of these struts increases, strain levels imposed on the material increases proportionally.

The current BRSs are composed of either a polymer or bioresorbable metal alloy. Numerous different polymers are available, each with different chemical compositions, mechanical properties, and subsequently bioresorption times. The mechanical properties of material being tested as a BRS platform are summarized in Table 1.

6. CURRENTLY AVAILABLE DRUG-ELUTING BRS IN VASCULAR DISEASE

6.1. Drug-eluting BRS in coronary artery disease

This section is focused on currently available drug-eluting BRS that were (1) clinically successful and acquired CE mark, (2) under clinical investigation, or (3) in preclinical

phase. A shortsummary of first in man trial results of each platform is tabulated in Table 2.

6.1.1. Coronary drug-eluting BRS with an acquired CE mark

6.1.1.1. Absorb BVS 1.1. Absorb Bioresorbable Vascular Scaffold (BVS) backbone (Abbott Vascular, Santa Clara, California, USA) is made of semicrystalline polymer called PLLA. [50] The thickness of the strut is 156 µm. The struts are either directly joined or linked by straight bridges. Because the devices are radiolucent under fluoroscopy, two adjacent cylindrical radio-opaque platinum markers have been incorporated in the proximal and distal edges of the polymeric device. The coating consists of poly-D,L-lactide (PDLLA), which is a random copolymer of D- and L-lactic acid with lower crystallinity than the BVS backbone and fully bioresorbable. The coating contains and controls the release of everolimus, with a coating-to-drug ratio of 1:1.[50,64] The second-generation Absorb BVS 1.1 claims to elute 75% of loaded everolimus within 30 days and with the same dose density (100 mg/cm2) as the cobalt–chromium everolimus-coated Xience V coronary stent. The release kinetics of everolimus in Absorb™ are purely diffusion-controlled.[32] The diffusion follows an inherently Fickian first-order release behavior proportional to square-root of time, according to the well-known relationship from Higuchi.[47]

The bioresorption process of PLLA is as follows: First, hydration of the polymer occurs. The semicrystalline property of polylactide allows water to penetrate deeply inside the implant. Second, depolymerization by hydrolysis is observed and reduction in molecular weight takes place. The latter starts from the time of implantation, gradually progresses and is completed at 36 months. Third, polymer fragmentation into segments of low-weight polymer due to the scission of amorphous tie chains linking the crystalline regions, resulting in subsequent gradual loss of the radial strength, starts from the 6th month after implantation and is completed at the 12th month after implantation. Final process is assimilation or dissolution of monomers. Phagocytes can assimilate small particles less than 2 µm and convert them to soluble monomeric anions. Lastly, the soluble monomer (e.g. L-lactate) is changed into pyruvate, which eventually enters the Krebs cycle and is further converted into carbon dioxide and water, eliminated by the lungs and kidneys.[65]

To date, Absorb BVS is the most extensively studied BRS. In the ABSORB-III randomized trial, Absorb BVS was non-inferior to Xience for target-lesion failure at 1 year.[66] This observation is also supported by a patient level meta-analysis involving 3738 patients enrolled into the ABSORB II, ABSORB III, ABSORB JAPAN and ABSORB CHINA, EVERBIO-II, and TROFI-II randomized trials.[67] These trials included patients with relatively simple lesions. Performance of this device in all-comers patient population is being studied in the AIDA trial, which is nearing enrollment completion. Its primary endpoint of TVF will be reported in 2 years.[68]

Table 2 Summary of first-in-man drug-eluting BRS implanted in coronary artery disease

Scaffold	Clinical study	Number of patients	Status	Major endpoints	Angiographic endpoint (LLL)	TLR	MACE	Ref
METALLIC								
DREAMS 1.0	BIOSOLVE-I	46	complete	Target lesion failure at 6 and 12 months	6M: 0.64 mm	6M: 4.3%	--	[48]
					12M: 0.52 mm	6M: 6.5%		
DREAM 2.0	BIOSOLVE-II	123	Complete	In segment Late Lumen Loss at 6 months	6M: 0.27 mm	6M: 2.0%	--	[49]
POLYMERIC								
BVS 1.0	ABSORB cohort-A	30	complete	Clinical endpoints at 1 year, Angiographic endpoints	6M: 0.44 mm	6M: 0%	5Y: 3.4%	[50]
BVS 1.1	ABSORB cohort-B	101	complete	LLL, TLR and MACE at 6 months, 1, 2 and 3 years	6M: 0.19 mm	12M: 3.6%	2Y: 9.0%	[51]
					12M: 0.27 mm		3Y: 10%	
DESolve (myolimus)	DESolve I	16	ongoing	LLL at 6 months	8M: 0.19 mm	12 M: 6.7 %	--	[52]
DESolve (novolimus)	DESolve NX	126	ongoing	Procedural success, LLL at 6 months, MACE at 1, 6, and 12 months, 2, 3, 4, and 5 years	6M: 0.21 mm	6M: 1.6%	6M: 3.25%	[53]
ReZolve	RESTORE	50	ongoing	TLR at 6 months, LLL at 12 months	12M: 0.20 at for n=8	6 M: 2 out of 12	6M: 2 out of 12	[54]
XINSORB	XINSORB FIM	30	Complete	MACE at 30 days FU and LLL at 180 days FU	6M: 0.18 mm	18M: 3.3%	1 definite ST, 18 at 18 M.	[55]
ReZolve2	RESTORE II	125	ongoing	MACE at 6 and 12 months, LLL at 9 months	--	--	--	[56]
Fantom	FANTOM I	7	ongoing	ID-TLR at 4 months	--	--	--	[57]
Fantom	FANTOM II	220	ongoing	MACE at 6 months, LLL at 6 months	--	--	--	[58]
AmM FORTITUDE	MEND II	50	ongoing	Incidence of TVF, in-scaffold LLL at 9 months	--	--	--	[59]
AmM FORTITUDE	RENASCENT	120	ongoing	Incidence of TVF, in-scaffold LLL at 9 months	--	--	--	[60]
NeoVas	NeoVas BCS FIM	30	ongoing	TLF at 30 days	--	--	--	[61]
MeRES 100	MeRES-1 FHU	108	ongoing	Ischemic driven MACE at 180 days.	--	--	--	[62]
FAST	FAST FIM	30	ongoing	Clinical procedural success, in-scaffold LLL at 6 months	--	--	--	[63]

Abbreviation: 6M=6 Months, 12M=12 Months, 5Y=5 Years, LLL=Late Lumen Loss, TLR=Target Lesion Revascularization, MACE=Major Cardiovascular Events, 2Y=2 Years, 3 Years, 8M=8 Months, FU=Follow-Up, 18M=18 Months, ST=Scaffold thrombosis, ID-TLR=Ischemic Driven-Target Lesion Revascularization, TVF=Target Vessel Failure, TLF=Target Lesion Failure.

6.1.1.2. DESolve. DESolve® (Elixir Medical, Sunnyvale, CA) also has a PLLA backbone with antiproliferative drug, novolimus, which is an active metabolite of sirolimus. There are two platinum markers at each end of the scaffold. The coating polymer is a biodegradable polylactide-based polymer. The drug–polymer matrix is applied to the surface of the stent, without a primer polymer coating underneath, using a proprietary spray resulting in a coating thickness of <3μm. The dose of novolimus used on the DESolve is 5 μg/mm of stent length and 85% release over 4 weeks (data on file at Elixir Medical). DESolve has already received CE mark for DESolve 100, where the strut thickness is reduced from 150 μm to 100 μm. A new generation DESolve Cx with strut thickness of 120 μm is now being tested in clinical trial. The important features of the DESolve distinguishing it from BVS are (1) intrinsic self-correcting properties of the device in case of minor strut malapposition, (2) relative elasticity/ductility that provides a wide range of expansion without risk of strut fracture.

6.1.2. Coronary drug-eluting BRS under clinical investigation

6.1.2.1. Magnesium stent. Mg and Mg-based alloys are light-weight metallic materials, which are extremely biocompatible and have similar mechanical properties to natural bone. Magnesium is the fourth commonest cation within the human body. In contrast to polymeric material, magnesium has a 10- fold higher tensile strength and is capable of significant elongation at break. The bioresorption rate of the magnesium alloy varies from 2 to ≥12 months by manipulation of the alloy with alloying elements, such as rare earths (4% yttrium and a 3% rare earth mixture composed of neodymium, cerium, and dysprosium).[69]

Degradation of the alloy includes two steps: first, the magnesium alloy is converted to hydrated magnesium oxide. Second, magnesium oxide is converted to magnesium phosphate, which is in turn replaced by amorphous calcium phosphate.[49] The degradation of Mg produces an electronegative charge that results in the stent being thrombogenic.[70] During this process, metallic magnesium is removed by diffusion from the amorphous matrix and is absorbed by the body. The amorphous calcium phosphate remains in the tissue together with the other elements of the alloy and the markers. About 95% of the magnesium is converted at 12 months.

In the porcine model, the magnesium stent has been shown to be rapidly endothelialized, and within 60 days is largely degraded into inorganic salts, with little associated inflammatory response.[71] Of note, magnesium is not detectable under computed tomography or MRI.[72] This feature enables the device to be evaluated by noninvasive coronary imaging already at baseline at implantation.

Recently, the first-in-man second-generation drug-eluting absorbable metal scaffold (DREAMS 2G; Biotronik AG, Buelach, Switzerland) has been investigated in BIOSOLVE-II trial. DREAM 2G strut thickness is 150 μm with two permanent X-ray markers made from

tantalum at the distal and proximal scaffold ends. The surface of the scaffold backbone is completely coated with PLLA (7 μm), which incorporates sirolimus. The sirolimus load is 1.4 μg/mm^2 scaffold surface. The results showed a sustained favorable clinical and safety profile up to 6 months. In addition, vasomotion was restored at 6 months. No definite or probable scaffold thrombosis was noted for DREAMS 2G and the rates of target lesion failure and revascularization were low (see Table 2).[49]

6.1.2.2. FANTOM™ stent. FANTOM™ stent (Reva Medical Inc., San Diego, CA, USA) is a tyrosine polycarbonate stent. Tyrosine poly (desaminotyrosyltyrosine ethyl ester) carbonate is resorbable and radio-opaque following the chemical modification of tyrosine to incorporate iodine molecules. The polymer degrades into water, carbon dioxide, and ethanol; in addition, tyrosine is also metabolized by the Kreb's cycle. The preclinical data showed that the late lumen gain in the arterial segments treated by tyro- sine polycarbonate stent may be coupled with positive (outward) remodeling.[73]

Fantom scaffold was made using a modified polymer based on phenyl ring structure; the strut thickness is reduced from 230 μm to 125 μm. The Fantom scaffold is radio-opaque at implantation due to iodine binding, has a crossing profile of 1.3 mm and can be implanted with a single-step inflation. The CE-mark clinical trial has completed enrollment and awaiting for 6 months angiographic follow-up.

6.1.2.3. XINSORB. The stent was designed and fabricated by HuaAn Biotech., Co. Ltd. The stent is composed of bioabsorbable PLLA as its backbone with a thickness of 150 μm. The molecular weight of PLLA used for XINSORB stent is 300 kDa. The radial strength of XINSORB is more than 1 N. The coating is PDLLA mixed with PLLA. The dose of sirolimus on the XINSORB stent is 8 μg/mm. About 80% of sirolimus is eluted from the polymer in 28 days ex vivo. Preclinical studies showed that the acute absolute/percent recoil of XINSORB stent was similar to that of commercialized DES.[74,75] The results of the first-in-man trial showed that 6-month late loss is 0.18 ± 0.21 mm with a diameter stenosis of 10.6%. The follow-up residual area obstruction on optical coherence tomography and intravascular ultrasound were 11.3% and 3.1%, respectively.[55]

6.1.2.4. Mirage bioresorbable micro-fiber scaffold. Mirage Bioresorbable Micro-fiber Scaffold (Mirage BRMS, Manli Cardiology, Singapore) is a monofilament scaffold made of PLLA with a helix coil design mounted on three backbones. It is coated with biodegradable PLA at its abluminal side, which releases sirolimus.[76] The helical coil design gives high flexibility to the scaffold. The strut thickness is 125 μm in scaffolds with diameters ≤3 mm and 150 μm in scaffolds with diameters ≥3.5 mm. The bioresorption time is nearly 14 months. The additional features of the MIRAGE BRMS include: no time limitation for staying in the artery before deployment, re-entering artery is allowed, and there is no need for the gradual balloon inflation during deployment.

Other drug-eluting BRS platforms that have been tested in clinical trials include Fortitude® (Amaranth, Singapore), Neovasc (Lepu medical, China), MeRES 100 (Meril

Life science, India), and FAST (Boston Scientific, US). All of them are sirolimus-eluting BRS with a PLLA backbone. The Fortitude BRS is made from an ultrahigh molecular weight PLLA, which is subsequently processed by casting in the solution to produce highly amorphous tubing before the scaffold cutting process.[60] This scaffold could be dilated more than two times its initial diameter without losing its mechanical strength. MeRES BRS is a hybrid geometry scaffold between an open cell design in mid-portion and a closed cell design at both ends. This provides high radial strength and avoids over expansion at the edges.[62]

6.1.3. Coronary drug-eluting BRS in the developmental stage

The On-AVS stent (OrbusNeich, Fort Lauderdale, Florida, USA) has a PLLA/PDLA/L-lactic-co-e-caprolactone platform and has CD34+ antibodies for endothelial progenitor cell (EPC) capture at the luminal side of its struts and sirolimus coating at abluminal surface. The CD34+ antibodies attract circulating EPCs promoting quick maturation of functional endothelium. This accelerated healing strategy aims to lower the risk of restenosis and potentially reduce stent thrombosis.[77]

The DCBS stent (ART/Terumo, France/Japan) is made from a PLLA/PDLA. It has been developed from previous ART Pure BRS platform but has a thinner strut and is loaded with sirolimus. The animal data showed satisfactory drug effect.[78] The BRS platforms and their research status are summarized in Table 3.

6.2. BRS in peripheral vascular disease

The metallic stents have been used for the treatment of lower limb stenosis for many years. Although they reduce vessel recoil and restenosis in short-term, the in-stent restenosis rate at longer term follow-up still remains a major limitation of this treatment. Dynamic deformations from repetitive movement exert significant biomechanical forces on the wall that enhance intimal hyperplasia. Therefore, the BRS has been introduced in peripheral vascular treatment, as it is an ideal mechanical implant that could mimic or conform to the vessel wall. BRS made of magnesium and PLLA has been implanted in peripheral arteries in clinical trials.[92,93]

So far, two dedicated BRS without drug elution for treatment of peripheral artery disease have acquired a CE mark. The first one is the Igaki-Tamai stent (Kyoto medical, Kyoto, Japan). The scaffold is made of PLLA and was approved for CE mark after completion of PERSEUS study.[92] The second scaffold is REMEDY™ (ENDOCOR GmBH, Hamburg, Germany) that is also made from PLLA. Galyfos et al. reported the pooled analysis results comparing the metallic stent versus the polymeric BRS. The metallic stent was associated with a higher 30- day amputation/death rate and less 6-month primary patency rate, compared to polymeric BRS.[94] The ongoing clinical trials evaluating BRS in peripheral vascular disease are summarized in Table 4.

Table 3 Drug release characteristics of current bioresorbable drug-eluting scaffold

Drug	Stent name (manufacturer)	Stent platform	Strut thickness, μm	Coating material	Coating thickness	Radial support	Resorption time	Reported release profile	Drug dose	Status	Site of implantation	ref
Paclitaxel	DREAMS 1.0 (Biotronik)	WE43 alloy, 93% Mg and 7% rare earth elements	120	PLGA	1 μm	3–6 months	9 months	Controlled release in 3 months, both paclitaxel release and magnesium degradation completed	0.07 μg/mm2	Discontinued	Coronary	[79]
Sirolimus	DREAM 2G (Biotronik)	WE43 alloy, 93% Mg and 7% rare earth elements	150	PLLA	1 μm	3–6 months	9 months	Over 3 to 6 months	1.4 μg/mm2	Clinical trials	Coronary	[80]
	ReZolve (Reva Medical)	PTD-PC	115-230	--	--	4–6 months	4–6 months	--	80 μg	Discontinued	Coronary	[56]
	Fantom (Reva Medical)	PTD-PC	125	Bioresorbable polymer	--	--	within 3 years	--	115 μg	Clinical trials	Coronary	[58]
	IDEAL BTI 1st generation (Xenogenics)	Poly-lactic anhydride containing 2 salicylic acid molecules linked to 1 sebacic acid molecule	200 2nd gen 175	SA/AA	--	3 months	9-12 months	complete after 30 days	8.3 μg/mm	Discontinued	Coronary	[81]
	XINSORB (HuaAn Biotech)	PLLA	160	PDLLA + PLLA	--	--	2 to 3 years	About 80% of sirolimus eluted from the polymer in 28 days ex vivo	8 μg/mm	Clinical trials	Coronary	[74,82]
	MIRAGE BRMS (Manli)	PLLA	125 for diameter 3.0 mm and 150 for 3.5 mm	PLLA	--	--	14 months	--	--	Clinical trials	Coronary	[83]
	FORTITUDE (Amaranth)	PLLA	120	Bioresorbable polymer	--	3–6 months	3–6 months	--	--	Clinical trials	Coronary	[84]

Table 3 Drug release characteristics of current bioresorbable drug-eluting scaffold (continued)

Drug	Stent name (manufacturer)	Stent platform	Strut thickness, μm	Coating material	Coating thickness	Radial support	Resorption time	Reported release profile	Drug dose	Status	Site of implantation	ref
	NeoVas (Lepu Medical)	PLLA	180	PDLA	--	--	24 months	--	15.3 μg/mm	Clinical trials	Coronary	[61]
	Microport BRS (Microport)	PLLA	100-125	PDLLA	< 5	180 days	--	--	4 μg/mm	Pre-clinical study	Coronary	[85]
	MERES 100 (Meril Life Science, India)	PLLA	100	PDLLA	3-4	--	2 years	--	1.25 μg/mm2	Clinical trials	Coronary	[62]
	DCBS (ART/Terumo)	PLLA+ PDLLA	--	--	--	--	--	--	--	Pre-clinical study	Coronary	[78]
	--	PLLA/P4HB	250	PLLA/P4HB	--	--	--	--	2.3 μg/mm^2	Research stage (in-vitro)	Peripheral	[86]
	-- (University of Rostock ,Germany)	PLLA	270	PLLA	--	--	--	--	1.5 μg/mm2.	Pre-clinical study	Peripheral (Carotid)	[87]
Dual elution Sirolimus+ CD 34 antibody	On-AVS (OrbusNeich)	PLLA, PLCL, PDLA	150	PLLA+ PDLA	--	--	18 months	--	100 μg/cm2	Preclinical underway	Coronary	[88]
Everolimus	BVS 1.0 (Abbott)	PLLA	156	PLLA	2-4 μm	weeks	18-24 months	75% of loaded everolimus within 30 days	100 μg/cm^2	Discontinued	Coronary	[50]
	BVS 1.1 (Abbott)	PLLA	156	PLLA	2-4 μm	6 months	24-48 months	75% of loaded everolimus within 30 days	100 μg/cm2	CE mark	Coronary	[47,50]

Table 3 Drug release characteristics of current bioresorbable drug-eluting scaffold (continued)

Drug	Stent name (manufacturer)	Stent platform	Strut thickness, μm	Coating material	Coating thickness	Radial support	Resorption time	Reported release profile	Drug dose	Status	Site of implantation	ref
	FAST (Boston scientific)	PLLA	100	PLGA	--	--	1 to 2 years	complete around 90 days	--	Clinical trials	Coronary	[63]
Myolimus	DESolve (Elixir)	PLLA	150	matrix of polylactide-based polymer	--	3–4 months	12 months	more than 85% of the drug is released over 4 weeks.	3 μg/mm	Discontinued	Coronary	[52]
Novolimus	DESolve (Elixir)	PLLA	100	Bioresorbable polymer	< 3 μm	3–4 months	12 months	more than 85% of the drug is released over 4 weeks.	5 μg/mm	CE mark	Coronary	[83]
Mitomycin C	--	PLCL	--	--	--	--	--	33% of loaded MMC released over 12 weeks	--	Preclinical study	Tracheal	[89]
Cisplatin	--	PCL	--	PLGA	--	--	--	Cisplatin released in 4 weeks through linear diffusion-control	--	Preclinical study	Tracheal	[90]

Abbreviation:Mg = Magnesium, PLLA = Poly L-lactic acid, PDLA = Poly-D-lactic acid, PDLLA = Poly-DL-lactic acid, BVS = Bioresorbable Vascular Scaffold, SA/AA = Salicylic acid / Adipic Acid, PTD-PC = Poly-Tyrosine-derived polycarbonate, PLCL = poly(L-lactide-co-ε-caprolactone), MMC = mitomycin C, PCL =poly (l-caprolactone. PLGA = Poly (d,l)-lactide-co-glycolide. Adapted from Iqbal et al. [121] and Huang et al.[35]

Table 4 Summary clinical trials used bioresorbable scaffolds for peripheral vascular treatment

Scaffold (manufacturer)	Material	Drug eluting	Clinical study	Type of vessel	Number of patients	Status	Endpoints	Result	Ref
AMS (Biotronik)	Magnesium	No	AMS-INSIGHT	Infrapopliteal	117	complete	30-day Major amputation/ death, 6-month patency rate	No difference regarding complications, lower patency rate in AMS	[93]
AMS (Biotronik)	Magnesium	No	BEST-BTK	Infrapopliteal	20	complete	3 months patency, limb salvage	3-month limb salvage: 94.7% Survival 94%	[95]
Igaki-Tamai (Kyoto medical)	PLLA	No	PERSEUS	SFA	103	complete	Primary technical success, major adverse events 12 and 24-month Patency Number of interventions	100% technical success No major adverse events	[92]
Igaki-Tamai (Kyoto medical)	PLLA	No	GAIA	SFA	30	complete	Technical success, restenosis rate, TLR rate, changes in ABI, and quality of life by evaluating the WIQ.	Comparable results to bare metal stents 6 months patency 61.7%, 6 months TLR 25%	[96]
REMEDY™ (Endocore GMBH)	PLLA	No	Linni et al†	CFA	80	complete	30-day primary patency, 1-year patency rates, limb salvage and survival	Primary patency rates 92.5% at 30-day and 80% at 1-year.	[97]
REMEDY™ (Endocore GMBH)	PLLA	No	ALSTER	SFA and iliac lesions	600	ongoing			
REMEDY™ (Endocore GMBH)	PLLA	No	Silingardi R et al.	SFA	35	complete	Clinical examination and patency rate at 24 and 36 months	Primary and secondary patency rates: 77.1% and 97.1% at 24 and 36 months.	[98]
REMEDY™ (Endocore GMBH)	PLLA	No	Belgian REMEDY study	SFA	100	complete	Technical success, freedom from TLR, primary patency	High technical success 100%, 6 months primary patency 70.2%	[99]
Absorb (Abbott Vascular)	PLLA	Everolimus	Varcoe RL et al.	below the knee	14	complete	Safety, midterm restenosis rate, and clinical improvement	Immediate technical success was 100% no amputation, bypass surgery, or evidence of binary restenosis on 12 month follow-up	[100]

Table 4 Summary clinical trials used bioresorbable scaffolds for peripheral vascular treatment (continued)

Scaffold (manufacturer)	Material	Drug eluting	Clinical study	Type of vessel	Number of patients	Status	Endpoints	Result	Ref
ESPRIT BVS (Abbott Vascular)	PLLA	Everolimus	ESPRIT I	SFA, CIA, EIA	35	ongoing	Amputation, death (1-6-12 months) thrombosis, clinical improvement, ABI improvement	6 months primary patency100%, 6 months clinical improvement 93.1%, ABI improvement, no major complications, 98% technical success	[101]
STANZA (480 biomedical)	NA	No	STANCE	SFA	60	ongoing	Major adverse events at 6 months		[102]
STANZA (480 biomedical)	NA	Paclitaxel	SPRINT	SFA	70	ongoing	Patency at 6 month, Major Adverse Events at 30 days		[103]

Abbreviation : PLLA = Poly L-lactic acid, SFA = superficial femoral artery, CIA = common iliac artery, EIA = External iliac artery, TLR= target lesion revascularization, ABI = ankle-brachial index, WIQ= walking impairment questionnaire, NA=not available

The novel material in peripheral BRS is a polymer blend of high olecular weight PLLA and poly (4-hydroxybutyrate) (P4HB), with a mass ratio of 78/22. P4HB is a strong, pliable thermoplastic biopolymer produced in a recombinant fermentation process using Escherichia coli K12. It has been considered in several biomedical devices such as suture material, heart valves and vascular grafts. P4HB appears to degrade faster than PLLA. Its degradation product (4-hydroxybutyrate) is a natural human metabolite present in several organs.[86] P4HB serves an important role in this technology by acting as a toughening agent that makes it possible to balloon expand the slotted P4HB–PLLA tube without fracture of the stent struts.[104] It provides adequate mechanical characteristics for a broad range of peripheral vascular and nonvascular applications.

The sirolimus-eluting PLLA/P4HB stent has been studied in porcine carotid arteries. The results showed sufficient mechanical stability, reduction of neointimal response without thrombotic complication.[87] Grabow et al. developed sirolimus-eluting PLLA/P4HB stent for the treatment of peripheral artery disease. The balloon-expandable slotted-tube PLLA/P4HB stent showed low recoil and high collapse pressure. In particular, recoil (4.2%) and collapse pressure (1.1 bar) were comparable to those of commercially available peripheral metallic stents, for which recoil values of 2.5–4.8%, and collapse pressures of 0.8–1.2 bars are acceptable. These characteristics were achieved with a strut thickness of 300 μm.[86] The challenge in this field is manufacturing a stent platform since the availability of bioresorbable and biocompatible polymer or metal are limited. Moreover, the radial strength of device needs to be reinforced by means of polymer-processing (extrusion, annealing, spinning, microfiber, and microbraiding) in order to be comparable to the metallic stent. The ideal degradation time and rate also need to be explored in the long-term follow-up since the vascular support to prevent acute recoil and healing might be variable depending on the site of implantation.[94]

6.3. BRS in congenital heart disease

Metallic stents have been the only tools available to pediatric interventional cardiologists,[105] until recently. Pediatricians have to apply the metallic stents, that have been designed and tested for adult disease, to pediatric patients in an off-label indication.[106–109] Implantation of nonresorbable stent in pediatric patients seems to be an imperfect solution as permanent implants do not allow vessel growth. The ideal stent for pediatric treatment would provide a short-term scaffolding and to disappear at mid-term, which would enable the vessel to enlarge according to the natural growth of the patient.

There are few reports on the usage of BRS in congenital heart disease. These reports are so far limited to metallic BRS. Zartner et al., reported successful treatment of the ligated left pulmonary artery with a 3 mm non-drug-eluting magnesium stent (AMS, Biotronik, Switzerland).[110] In a case report of Schranz et al., critical re-coarctation in an infant was successfully treated by magnesium stent (3.0–4.0 mm).[111]

There is a great need for a dedicated BRS with a large diameter and a small delivery system to treat pediatric patients with congenital heart diseases. The development of such a device is, however, particularly challenging due to their relatively low radial strength.[112,113] Veeram et al. recently reported that a novel double opposed helical design with PLLA fibers. This design could be used to manufacture larger diameter stents for use in congenital heart disease.[114] Polymeric BRS made of polyhydroxybutyrate (PHB) and polycaprolactone showed a weaker vessel support and faster degradation of polymers, resulting in stent collapse at 1 month. Moreover, it has a higher inflammatory response compared to PLLA and metal stents.[115,116] The PHB stents led to destruction of the internal elastic membrane and resulted in undesirable effects such as: growth of mural capillary vessels, invasion of multinucleated foreign body giant cells and in one animal, obstruction of the lumen at 10 weeks.[116]

7. FUTURE PERSPECTIVE

BRS with dual-drug elution

Theoretically, the ideal device would carry an antiproliferative drug to suppress SMC proliferation and an anti-inflammatory drug to reduce inflammation, promote vascular healing, and also have an anti-thrombotic effect.[26,32,117] The concept of dual-drug BRS is no longer limited to antiproliferative agents but also expanded to gene-eluting stents. It is possible that small interfering (siRNA) local delivery via stent can be an effective treatment option for control of both malignant tumors around a nonvascular stent as well as SMC proliferation around a vascular stent.[118] Despite successes in the animal model, however, clinical application of siRNA-delivering stent has yet to be tried.[119]

Theranostics BRS with nano-particles

The term theranostic indicates technology with concurrent and complementary therapeutic and diagnostic capabilities. [120] BRS may provide vascular support for de-novo coronary artery stenosis or in-stent restenosis, delivery of therapeutic particles to specific sites with minimum toxicity, and controlling rate of therapy release.[121] Simultaneously, BRS may facilitate novel post-stent imaging and diagnostic methods for atherosclerosis, restenosis and thrombosis, and ease of tracking drug release kinetic in vivo by embedding imaging agents.[122] All of these functions could be integrated in a single platform in the future.

8. CONCLUSION

The BRS technology offers the possibility of transient scaffolding of the vessel. Since the BRS does not definitively cage definitely any vascular structures, the technology is not only applicable to the field of coronary artery disease but also applicable to peripheral vascular disease and congenital heart abnormalities. The currently available drug eluting BRS have demonstrated their ability to prevent restenosis and have shown good results in terms of long-term safety end-points in coronary treatment. The body of evidence supporting the application of the BRS in other vascular beds such as peripheral artery and pediatric aorta/arteries is growing and long-term clinical follow-up is required. Further improvement of the devices in mechanical properties and the development of dedicated BRS for different clinical indications are ongoing.

9. EXPERT OPINION

An extensive research has been conducted to prove the efficacy and safety of the BRS especially in coronary artery treatment. Available data shows that BRS can be used safely and effectively to treat de novo coronary artery lesions. Long-term follow-up of FIM trials suggests that there would be additional benefits over permanent caging such as restoration of vasomotion and late lumen enlargement.

The main deficiencies of currently approved drug-eluting BRS are (i) weaker mechanical properties (e.g. tensile strength, elongation at break) compared to permanent metallic stents made of stainless steel or cobalt–chromium; (ii) thicker and wider scaffold struts which might result in more flow disturbance potentially increasing acute thrombotic events. To overcome these shortcomings, the second-generation BRS should be mechanically stronger and have thinner struts. Various post-processing methods of polymers are being explored and investigated (extrusion, annealing, electro spinning, microfiber and microbraiding) to achieve such superior design. When next-generation (Mirage [Manli], FAST [Boston scientific] and 3rd generation Absorb BVS [Abbott]) devices become available in the clinical setting, at least some of the current limitations of BRS will be addressed. Only when those limitations are fully addressed, do the BRS devices have a chance to become work-horse 'stents' to be applied in treatment of so-called 'all-comers' 'real world' patient populations.

One of the potential advantages of magnesium BRS over polymeric BRS is its higher tensile strength and higher elongation at break, which could translate into a more fracture resistant and mechanically robust device. On the other hand, the complete absorption of magnesium occurs much faster (approximately 1–3 months) than PLLA (>24 months). The fast resorption of magnesium was considered as one of the reasons

of failure in the PROGRESS trial where the late recoil of the device was a prominent etiology of restenosis. The second and the third-generation of magnesium BRS therefore use polymeric coating to slow down the biodegradation by limiting access of water to magnesium and to enable longer drug release. Despite the inherent mechanical advantage, the current magnesium scaffold still has a thick strut (150 μm) just as polymeric BRS. If next generation magnesium BRS should succeed to make the struts thinner and stronger, it might offer some advantage of the polymeric BRS.

According to the European task force recommendation [123], the following additional analyses are required for non-clinical evaluation of BRS: (i) bench testing that should be performed through time of significant mass loss, (ii) biochemical analysis of degradation products in BRS is mandatory, and (iii) critical time points of follow-up should cover complete resorption as determined by histopathology. In clinical assessment, BRS should be directly compared with a CE-approved metallic DES or with other CE-approved bioresorbable coronary stents.

The indication for BRS is not only limited to the field of coronary artery disease, it could also expanded to peripheral vascular disease and congenital heart abnormalities. Therefore, the design, material and degradation time of the 'ideal' BRS drug-eluting vascular stent would also depend on the implantation site since the need for support is different. The research on BRS in noncoronary applications is still in its infancy; however, the dedicated devices for the particular indications with improved and optimized mechanical properties are being developed.

REFERENCES

1. Dotter CT, Buschmann RW, McKinney MK, et al. Transluminal expandable nitinol coil stent grafting: preliminary report. Radiology. 1983;147(1):259–260.
2. Sigwart U, Puel J, Mirkovitch V, et al. Intravascular stents to prevent occlusion and restenosis after transluminal angioplasty. N Engl J Med. 1987;316(12):701–706. doi:10.1056/NEJM198703193161201.
3. Serruys PW, De Jaegere P, Kiemeneij F, et al. A comparison of balloon-expandable-stent implantation with balloon angioplasty in patients with coronary artery disease. Benestent Study Group. N Engl J Med. 1994;331(8):489–495.doi:10.1056/ NEJM199408253310801.
4. Fischman DL, Leon MB, Baim DS, et al. A randomized comparison of coronary-stent placement and balloon angioplasty in the treatment of coronary artery disease. Stent Restenosis Study Investigators. N Engl J Med. 1994;331(8):496–501. doi:10.1056/ NEJM199408253310802.
5. Marx SO, Totary-Jain H, Marks AR. Vascular smooth muscle cell proliferation in restenosis. Circ Cardiovasc Inte. 2011;4(1):104–111. doi:10.1161/CIRCINTERVENTIONS.110.957332.
6. Sousa JE, Costa MA, Abizaid AC, et al. Sustained suppression of neointimal proliferation by sirolimus-eluting stents: one-year angiographic and intravascular ultrasound follow-up. Circulation. 2001;104(17):2007–2011.
7. Morice MC, Serruys PW, Sousa JE, et al. A randomized comparison of a sirolimus-eluting stent with a standard stent for coronary revascularization. N Engl J Med. 2002;346(23):1773–1780. doi:10.1056/NEJMoa012843.
8. Ong AT, McFadden EP, Regar E, et al. Late angiographic stent thrombosis (LAST) events with drug-eluting stents. J Am Coll Cardiol. 2005;45(12):2088–2092. doi:10.1016/j.jacc.2005.02.086.
9. McFadden EP, Stabile E, Regar E, et al. Late thrombosis in drugeluting coronary stents after discontinuation of antiplatelet therapy. Lancet. 2004;364(9444):1519–1521. doi:10.1016/S0140-6736 (04)17275-9.
10. Camenzind E, Steg PG, Wijns W. Stent thrombosis late after implantation of first-generation drug-eluting stents: a cause for concern. Circulation. 2007;115(11):1440–1455. discussion 1455. doi:10.1161/ CIRCULATIONAHA.106.666800.
11. Lagerqvist B, James SK, Stenestrand U, et al. Long-term outcomes with drug-eluting stents versus bare-metal stents in Sweden. N Engl J Med. 2007;356(10):1009–1019. doi:10.1056/NEJMoa067722.
12. Pfisterer M, Brunner-La Rocca HP, Pt B, et al. Late clinical events after clopidogrel discontinuation may limit the benefit of drugeluting stents: an observational study of drug-eluting versus baremetal stents. J Am Coll Cardiol. 2006;48(12):2584–2591. doi:10.1016/j.jacc.2006.10.026.
13. Serruys PW, Garcia-Garcia HM, Onuma Y. From metallic cages to transient bioresorbable scaffolds: change in paradigm of coronary revascularization in the upcoming decade? Eur Heart J. 2012;33 (1):16–25. doi:10.1093/eurheartj/ehr384.
14. Waksman R. Biodegradable stents: they do their job and disappear. J Invasive Cardiol. 2006;18(2):70–74.
15. Joner M, Finn AV, Farb A, et al. Pathology of drug-eluting stents in humans: delayed healing and late thrombotic risk. J Am Coll Cardiol. 2006;48(1):193–202. doi:10.1016/j.jacc.2006.03.042.
16. Spuentrup E, Ruebben A, Mahnken A, et al. Artifact-free coronary magnetic resonance angiography and coronary vessel wall imaging in the presence of a new, metallic, coronary magnetic resonance imaging stent. Circulation. 2005;111(8):1019–1026. doi:10.1161/01. CIR.0000156462.97532.8F.

17. Onuma Y, Dudek D, Thuesen L, et al. Five-year clinical and functional multislice computed tomography angiographic results after coronary implantation of the fully resorbable polymeric everolimus-eluting scaffold in patients with de novo coronary artery disease: the ABSORB cohort A trial. JACC Cardiovasc Interv. 2013;6(10):999–1009. doi:10.1016/j.jcin.2013.05.017.
18. Serruys PW, Onuma Y, Garcia-Garcia HM, et al. Dynamics of vessel wall changes following the implantation of the absorb everolimus-eluting bioresorbable vascular scaffold: a multi-imaging modality study at 6, 12, 24 and 36 months. EuroIntervention. 2014;9(11):1271–1284. doi:10.4244/EIJV9I11A217.
19. Ormiston JA, Serruys PW. Bioabsorbable coronary stents. Circ Cardiovasc Interv. 2009;2(3):255–260. doi:10.1161/ CIRCINTERVENTIONS.109.859173.
20. Jux C, Bertram H, Wohlsein P, et al. Interventional atrial septal defect closure using a totally bioresorbable occluder matrix: development and preclinical evaluation of the BioSTAR device. J Am Coll Cardiol. 2006;48(1):161–169. doi:10.1016/j.jacc.2006.02.057.
21. Luu B, Esmaeili A, Schranz D, et al. Bioresorbable vascular scaffold implantation for successful treatment of a symptomatic coronary lesion in a 17-year-old boy after Kawasaki disease. Pediatr Cardiol. 2015;36(7):1539–1541. doi:10.1007/s00246-015-1215-4.
22. Nappi F, Spadaccio C, Fraldi M, et al. Use of bioresorbable scaffold for neopulmonary artery in simple transposition of great arteries: tissue engineering moves steps in pediatric cardiac surgery. Int J Cardiol. 2015;201:639–643. doi:10.1016/j.ijcard.2015.08.124.
23. Castro Rodriguez J, Dessy H, Demanet H. Implantation of an absorb bioresorbable vascular scaffold in the stenotic aortopulmonary collateral artery of a young child with Alagille syndrome. Catheter Cardiovasc Inter Official J Soc Cardiac Angiography Interventions. 2015;86(2):E76–80. doi:10.1002/ccd.26019.
24. Berglund J, Guo Y, Wilcox J. Challenges related to development of bioabsorbable vascular stents. EuroIntervention. 2009;5(F):F72–F79. doi:10.4244/EIJV5IFA12.
25. Zilberman M, Eberhart RC. Drug-eluting bioresorbable stents for various applications. Annu Rev Biomed Eng. 2006;8:153–180. doi:10.1146/annurev.bioeng.8.013106.151418.
26. Seidlitz A, Wentzlaff M, Weitschies W. Controlling drug delivery from coronary stents: are we aiming for the right targets? Ther Deliv. 2015;6(6):705–720. doi:10.4155/tde.15.25.
27. Siepmann J, Gopferich A. Mathematical modeling of bioerodible, polymeric drug delivery systems. Adv Drug Deliv Rev. 2001;48(2–3):229–247. • Mechanism of erosion-based delivery.
28. Siepmann J, Siepmann F. Mathematical modeling of drug dissolution. Int J Pharm. 2013;453(1):12–24. doi:10.1016/j. ijpharm.2013.04.044.
29. Hezi-Yamit A, Sullivan C, Wong J, et al. Impact of polymer hydro-philicity on biocompatibility: implication for DES polymer design. J Biomed Mater Res A. 2009;90(1):133–141. doi:10.1002/jbm.a.32057.
30. Walter DH, Schachinger V, Elsner M, et al. Effect of statin therapy on restenosis after coronary stent implantation. Am J Cardiol. 2000;85 (8):962–968.
31. Lee CH, Chang SH, Lin YH, et al. Acceleration of re-endothelialization and inhibition of neointimal formation using hybrid biodegradable nanofibrous rosuvastatin-loaded stents. Biomaterials.2014;35(15):4417–4427. doi:10.1016/j.biomaterials.2014.02.017.
32. Huang Y, Ng HC, Ng XW, et al. Drug-eluting biostable and erodible stents. J Control Release. 2014;193:188–201. doi:10.1016/j. jconrel.2014.05.011.
33. Costa MA, Simon DI. Molecular basis of restenosis and drug-eluting stents. Circulation. 2005 review of restenosis mechanism;111 (17):2257–2273. doi:10.1161/01.CIR.0000163587.36485.A7.
34. Schmelzle T, Hall MN. TOR, a central controller of cell growth. Cell. 2000;103(2):253–262.

35. Braun-Dullaeus RC, Ziegler A, Bohle RM, et al. Quantification of the cell-cycle inhibitors p27(Kip1) and p21(Cip1) in human atherectomy specimens: primary stenosis versus restenosis. J Lab Clin Med.2003;141(3):179–189. doi:10.1067/mlc.2003.23.
36. Marx SO, Jayaraman T, Go LO, et al. Rapamycin-FKBP inhibits cell cycle regulators of proliferation in vascular smooth muscle cells. Circ Res. 1995;76(3):412–417.
37. Sun J, Marx SO, Chen H-J, et al. Role for p27Kip1 in vascular smooth muscle cell migration. Circulation. 2001;103(24):2967–2972.
38. Kukreja N, Onuma Y, Daemen J, et al. The future of drug-eluting stents. Pharmacological Res. 2008;57(3):171–180.doi:10.1016/j. phrs.2008.01.012.
39. Papafaklis MI, Chatzizisis YS, Naka KK, et al. Drug-eluting stent restenosis: effect of drug type, release kinetics, hemodynamics and coating strategy. Pharmacol Ther. 2012;134(1):43–53. doi:10.1016/j.pharmthera.2011.12.006.
40. Garg S, Serruys PW. Coronary stents: current status. J Am Coll Cardiol. 2010;56(10, Supplement):S1–S42. doi:10.1016/j.jacc.2010.06.007.
41. Tsang CK, Qi H, Liu LF, et al. Targeting mammalian target of rapamycin (mTOR) for health and diseases. Drug Discov Today. 2007;12(3–4):112–124. doi:10.1016/j.drudis.2006.12.008.
42. Martin KA, Rzucidlo EM, Bl M, et al. The mTOR/p70 S6K1 pathway regulates vascular smooth muscle cell differentiation. Am J Physiol Physiol. 2004;286(3):C507–C517. doi:10.1152/ajpcell.00201.2003.
43. Kahan BD, Wong RL, Carter C, et al. A phase I study of a 4-week course of SDZ-RAD (RAD) quiescent cyclosporine-prednisone-treated renal transplant recipients. Transplantation. 1999;68(8):1100–1106.
44. Verheye S, Martinet W, Kockx MM, et al. Selective clearance of macrophages in atherosclerotic plaques by autophagy. J Am Coll Cardiol. 2007;49(6):706–715. doi:10.1016/j.jacc.2006.09.047.
45. Serruys PW, Garg S, Abizaid A, et al. A randomised comparison of novolimus-eluting and zotarolimus eluting coronary stents: 9- month follow-up results of the EXCELLA II study. EuroIntervention. 2010;6(2):195–205. doi:10.4244/.
46. Costa JR Jr., Abizaid A, Feres F, et al. EXCELLA First-in-Man (FIM) study: safety and efficacy of novolimus-eluting stent in de novo coronary lesions. EuroIntervention. 2008;4(1):53–58.
47. Onuma Y, Serruys PW. Bioresorbable scaffold: the advent of a new era in percutaneous coronary and peripheral revascularization? Circulation. 2011;123(7):779–797. doi:10.1161/CIRCULATIONAHA.110.971606.
48. Haude M, Erbel R, Erne P, et al. Safety and performance of the drug- eluting absorbable metal scaffold (DREAMS) in patients with de- novo coronary lesions: 12 month results of the prospective, multi-centre, first-in-man BIOSOLVE-I trial. Lancet. 2013;381(9869):836–844. doi:10.1016/S0140-6736(12)61765-6. • First-in-man trial of drug-eluting metallic BRS.
49. Haude M, Ince H, Abizaid A, et al. Safety and performance of the second-generation drug-eluting absorbable metal scaffold in patients with de-novo coronary artery lesions (BIOSOLVE-II): 6 month results of a prospective, multicentre, non-randomised, first-in-man trial. Lancet. 2016;387(10013):31–39. doi:10.1016/ S0140-6736(15)00447-X.
50. Ormiston JA, Serruys PW, Regar E, et al. A bioabsorbable everolimus-eluting coronary stent system for patients with single de-novo coronary artery lesions (ABSORB): a prospective open-label trial. Lancet. 2008;371(9616):899–907. doi:10.1016/S0140-6736(08)60415-8. • First-in-man trial of drug-eluting bioresorbable scaffold.
51. Serruys PW, Onuma Y, Ormiston JA, et al. Evaluation of the second generation of a bioresorbable everolimus drug-eluting vascular scaffold for treatment of de novo coronary artery stenosis:

six- month clinical and imaging outcomes. Circulation. 2010;122 (22):2301–2312. doi:10.1161/ CIRCULATIONAHA.110.970772.

52. Verheye S, Ormiston JA, Stewart J, et al. A next-generation biore- sorbable coronary scaffold system: from bench to first clinical evaluation: 6- and 12-month clinical and multimodality imaging results. JACC Cardio Inte. 2014;7(1):89–99.doi:10.1016/j. jcin.2013.07.007.
53. Abizaid A, Maeng M, Witzenbichler B, et al., et al. Prospective, Multi-Center Evaluation of the DESolve Nx Novolimus- ElutingBioresorbable Coronary Scaffold: First Report of One Year Clinical and Imaging Outcomes. TCT 2013. Poster presentation. Available at https://auth.cardiosource. org/EasyConnect/ Integration/Post.aspx, (2013).
54. Anderson A, Brachmann J, Dudek D, et al. REVA RESTORE TRIAL.Interim 12-Month Clinical Results of the ReZolve?Bioresorbable Scaffold and ReZolve2 Clinical Program Update. [cited 9 Oct 2015]. Available from: http://files.shareholder.com/downloads/ ABEA-5 J M ECA/0x0 x665612/92C095C8-7B42-41BD-95C4- 86720C133228/12-monthRESTORE trial data and ReZolve2 update. PDF
55. Ge J. Bioresorbable rapamycin-eluting scaffold (FIM of Xinsorb in China) Euro PCR2015. [cited 9 Oct 2015]. Available from: http:// www.pcronline.com/Lectures/2015/Bioresorbable-polymer-target- release-rapamycin-eluting-scaffold-Huaan-Biotech-China
56. Gogas BD, Farooq V, Onuma Y, et al. The ABSORB bioresorbable vascular scaffold: an evolution or revolution in interventional car- diology? Hellenic J Cardiol. 2012;53(4):301–309.
57. FANTOM I. REVA Medical, inc. CVPIPELINE BY MARKETMONITORS INC., [cited 9 Oct 2015]. Available from: https://www.cvpipeline. com/sectors/DES/trials/12728
58. Fantom, REVA Medical, inc. CVPIPELINE BY MARKETMONITORS INC., [cited 8 October 2015]. Available from: https://www.cvpipeline. com/sectors/DES/products
59. MEND-II. Amaranth Medical, Inc. CVPIPELINE BY MARKETMONITORS INC., [cited 9 Oct 2015]. Available from: https://www.cvpipeline. com/sectors/DES/meetings/300/abstracts/446289
60. RENASCENT (Restoring Endolumical Narrowing using Bioresorbable Scaffolds – European Trial). [cited 9 Oct 2015]. Available from: https://www.cvpipeline.com/sectors/DES/trials/13747
61. NeoVas, Beijing Lepu Medical Device, Inc. CVPIPELINE BY MARKETMONITORS INC., [Last accessed 8 October 2015]. Available from: https://www.cvpipeline.com/sectors/DES/products
62. Granada J. Fully bioresorbable PLLA-based sirolimus-eluting MeRes 100 scaffold (Meril Life Science, India) Euro PCR2015. [cited 9 Oct 2015]. Available from: http://www.pcronline.com/ Lectures/2015/ Fully-bioresorbable-PLLA-based-sirolimus-eluting-MeRes-100-scaf fold-Meril-Life-Science-India
63. FAST, Boston Scientific. Assess safety and performance of the FAST fully resorbable scaffold in subjects with single de novo native coronary artery target lesions. [Last accessed 21 December 2015]. Available from: https://www.cvpipeline.com/sectors/DES/trials/15274
64. Doostzadeh J, Clark LN, Bezenek S, et al. Recent progress in percutaneous coronary intervention: evolution of the drug-eluting stents, focus on the XIENCE V drug-eluting stent. Coron Artery Dis. 2010;21(1):46–56. doi:10.1097/MCA.0b013e328333f550.
65. Hollinger JO, Battistone GC. Biodegradable bone repair materials.Synthetic polymers and ceramics. Clin Orthop Relat Res.1986;207:290–305.
66. Ellis SG, Kereiakes DJ, Metzger DC, et al. Everolimus-eluting bioresorbable scaffolds for coronary artery disease. N Engl J Med 2015;373(20):1905–1915. doi:10.1056/ NEJMoa1509038.
67. Cassese S, Byrne RA, Ndrepepa G, et al. Everolimus-eluting bioresorbable vascular scaffolds versus everolimus-eluting metallic stents: a meta-analysis of randomised controlled trials. The Lancet. 2016;387(10018):537–544. doi:10.1016/S0140-6736(15)00979-4.

68. Woudstra P, Grundeken MJ, Kraak RP, et al. Amsterdam Investigator-initiateD Absorb strategy all-comers trial (AIDA trial): a clinical evaluation comparing the efficacy and performance of ABSORB everolimus-eluting bioresorbable vascular scaffold strategy vs the XIENCE family (XIENCE PRIME or XIENCE Xpedition) everolimus-eluting coronary stent strategy in the treatment of coronary lesions in consecutive all-comers: rationale and study design. Am Heart J.2014;167(2):133–140. doi:10.1016/j. ahj.2013.09.017.
69. Erbel R, Di Mario C, Bartunek J, et al. Temporary scaffolding of coronary arteries with bioabsorbable magnesium stents: a prospective, non-randomised multicentre trial. The Lancet. 2007;369(9576):1869–1875. doi:10.1016/S0140-6736(07)60853-8.
70. Heublein B, Rohde R, Kaese V, et al. Biocorrosion of magnesium alloys: a new principle in cardiovascular implant technology? Heart.2003;89(6):651–656.
71. Waksman R, Pakala R, Kuchulakanti PK, et al. Safety and efficacy of bioabsorbable magnesium alloy stents in porcine coronary arteries. Catheter Cardiovasc Interv. 2006;68(4):607–617. discussion 618-609. doi:10.1002/ccd.20727.
72. Brown DA, Lee EW, Loh CT, et al. A new wave in treatment of vascular occlusive disease: biodegradable stents–clinical experience and scientific principles. Journal of Vascular and Interventional Radiology: JVIR. 2009;20(3):315–324. quiz 325. doi:10.1016/j.jvir.2008.11.007.
73. Strandberg E, Zeltinger J, Schulz DG, et al. Late positive remodeling and late lumen gain contribute to vascular restoration by a non-drug eluting bioresorbable scaffold: a four-year intravascular ultrasound study in normal porcine coronary arteries. Circ Cardiovasc Interv. 2012;5(1):39–46. doi:10.1161/CIRCINTERVENTIONS.111.964270.
74. Wu Y, Shen L, Wang Q, et al. Comparison of acute recoil between bioabsorbable Poly-L-lactic acid XINSORB stent and metallic stent in porcine model. J Biomed Biotechnol. 2012;2012:413956. doi:10.1155/2012/413956.
75. Shen L, Wang Q, Wu Y, et al. Short-term effects of fully bioabsorbable PLLA coronary stents in a porcine model. Polym Bull. 2012;68 (4):1171–1181. doi:10.1007/s00289-011-0682-x.
76. Costa RA, Liew H, Abizaid A, et al. TCT-546 6-month angiographic results of the novel mirage microfiber sirolimus-eluting bioresorbable vascular scaffold - a quantitative coronary angiography analysis from the prospective, randomized mirage clinical trial. J Am Coll Cardiol. 2015;66(15_S). doi:10.1016/j.jacc.2015.08.563.
77. Sethi R, Lee C-H. Endothelial progenitor cell capture stent: safety and effectiveness. J Interv Cardiol. 2012;25(5):493–500. doi:10.1111/ j.1540-8183.2012.00740.x.
78. Lafont A. Sirolimus-eluting fully bioresorbable scaffold with mixed PLLA/PDLA (ART/Terumo, France/Japan) Euro PCR 2015. Available from: http://www.pcronline.com/Lectures/2015/Sirolimus-eluting- fully-bioresorbable-scaffold-with-mixed-PLLA-PDLA-ART-Terumo- France-Japan, (2015).
79. Haude M, Erbel R, Erne P, et al. TCT-38 Three-year clinical data of the BIOSOLVE-I Study with the paclitaxel-eluting bioabsorbable magnesium scaffold (DREAMS) and multi-modality imaging analysis. J Am Coll Cardiol. 2013;62(18_S1):B13–B13. doi:10.1016/j. jacc.2013.08.768.
80. Campos CM, Muramatsu T, Iqbal J, et al. Bioresorbable drug-eluting magnesium-alloy scaffold for treatment of coronary artery disease. Int J Mol Sci. 2013;14(12):24492–24500. doi:10.3390/ijms141224492.
81. Jabara R, Pendyala L, Geva S, et al. Novel fully bioabsorbable salicylate-based sirolimuseluting stent. EuroIntervention. 2009;5(F): F58–F64. doi:10.4244/EIJV5IFA10.
82. Chen JH, Wu YZ, Shen L, et al. First-in-man implantation of the XINSORB bioresorbable sirolimus-eluting scaffold in China. Chin Med J. 2015;128(9):1275–1276. doi:10.4103/0366-6999.156155.

83. DeSolve, Elixir Medical Corporation. VPIPELINE BY MARKETMONITORS INC., [cited 8 October 2015)]. Available from: https://www.cvpipeline.com/sectors/DES/products
84. FORTITUDE, Amaranth Medical, Inc. CVPIPELINE BY MARKETMONITORS INC., [Last accessed 8 October 2015]. Available from: https://www.cvpipeline.com/sectors/DES/products
85. Virmani R. A novel biodegradable PLLA-based sirolimus-eluting scaffold (Microport, China) Euro PCR 2015. Available from: http:// www.pcronline.com/Lectures/2015/A-novel-biodegradable-PLLA- based-sirolimus-eluting-scaffold-Microport-China, (2015).
86. Grabow N, Bunger CM, Kischkel S, et al. Development of a sirolimus-eluting poly (L-lactide)/ poly(4-hydroxybutyrate) absorbable stent for peripheral vascular intervention. Biomedizinische Technik. Biomed Eng. 2013;58(5):429–437. doi:10.1515/bmt-2012-0050.
87. Bunger CM, Grabow N, Sternberg K, et al. Sirolimus-eluting biode-gradable poly-L-lactide stent for peripheral vascular application: a preliminary study in porcine carotid arteries. J Surg Res. 2007;139 (1):77–82. doi:10.1016/j.jss.2006.07.035.
88. On AVS, OrbusNeich. CVPIPELINE BY MARKETMONITORS INC., [Last accessed 8 October 2015]. Available from: https://www.cvpipeline. com/sectors/DES/products
89. Zhu GH, Ng AHC, Venkatraman SS, et al. A novel bioabsorbable drug-eluting tracheal stent. Laryngoscope. 2011;121(10):2234–2239. doi:10.1002/lary.22175.
90. Chao Y-K, Liu K-S, Wang Y-C, et al. Biodegradable cisplatin-eluting tracheal stent for malignant airway obstruction: In vivo and in vitro studies. Chest. 2013;144(1):193–199. doi:10.1378/ chest.12-2282.
91. Iqbal J, Onuma Y, Ormiston J, et al. Bioresorbable scaffolds: rationale, current status, challenges, and future. Eur Heart J. 2014;35 (12):765–776. doi:10.1093/eurheartj/eht542.
92. Biamino G, Schmidt A, Scheinert D. Treatment of SFA lesions with PLLA biodegradable stents: results of the PERSEUS study. J Endovasc Ther. 2005;12(supplement):5.
93. Bosiers M, Peeters P, D'Archambeau O, et al. AMS INSIGHT–absorbable metal stent implantation for treatment of below-the-knee critical limb ischemia: 6-month analysis. Cardiovasc Intervent Radiol. 2009;32(3):424–435. doi:10.1007/s00270-008-9472-8.
94. Galyfos G, Geropapas G, Stefanidis I, et al. Bioabsorbable stenting in peripheral artery disease. Cardiovasc Revascularization Med. 2015;16 (8):480–483. doi:10.1016/j.carrev.2015.08.005.
95. Peeters P, Bosiers M, Verbist J, et al. Preliminary results after application of absorbable metal stents in patients with critical limb ischemia. J Endovascular Ther. 2005;12(1):1–5. doi:10.1583/04-1349R.1.
96. Werner M, Micari A, Cioppa A, et al. Evaluation of the biodegradable peripheral Igaki-Tamai stent in the treatment of de novo lesions in the superficial femoral artery: the GAIA study. JACC Cardiovasc Interv. 2014;7(3):305–312. doi:10.1016/j.jcin.2013.09.009.
97. Linni K, Ugurluoglu A, Hitzl W, et al. Bioabsorbable stent implantation vs. common femoral artery endarterectomy: early results of a randomized trial. J Endovascular Ther. 2014;21(4):493–502. doi:10.1583/14-4699R.1.
98. Silingardi R, Lauricella A, Coppi G, et al. Midterm results of endo- vascular treatment of superficial femoral artery disease with biode- gradable stents: single-center experience. J Vasc Interv Radiol JVIR. 2015;26(3):374–381.e371. doi:10.1016/j.jvir.2014.10.050.
99. Vermassen F, Bouckenooghe I, Moreels N, et al. Role of bioresorb- able stents in the superficial femoral artery. J Card Surgery. 2013;54 (2):225–234.
100. Varcoe RL, Schouten O, Thomas SD, et al. Initial experience with the absorb bioresorbable vascular scaffold below the knee: six-month clinical and imaging outcomes. J Endovasc Therapy. 2015;22 (2):226–232. doi:10.1177/1526602815575256.

101. Lammer J the 26th annual International Symposium on Endovascular Therapy, Florida (USA) (2014).
102. 480 Biomedical I. 480 Biomedical Bioresorbable Scaffold System in the Treatment of de Novo Superficial Femoral Artery (SFA) Lesions (STANCE). [cited 8 October 2015]. Available from: https://clinical trials.gov/ct2/show/NCT01403077.
103. 480 Biomedical I. Treatment of SFA Lesions With 480 Biomedical STANZA? Drug-Eluting Resorbable Scaffold (DRS) System (SPRINT). [cited 8 October 2015]. Available from: https://clinicaltrials.gov/ct2/ show/NCT02097082
104. Williams SF, Rizk S, Martin DP. Poly-4-hydroxybutyrate (P4HB): a new generation of resorbable medical devices for tissue repair and regeneration. Biomedizinische Technik. Biomedical Engineering. 2013;58(5):439–452. doi:10.1515/bmt-2013-0009.
105. Crystal MA, Ing FF. Pediatric interventional cardiology: 2009. Curr Opin Pediatr. 2010;22(5):567–572. doi:10.1097/MOP.0b013e32833e1328.
106. Dohlen G, Chaturvedi RR, Benson LN, et al. Stenting of the right ventricular outflow tract in the symptomatic infant with tetralogy of Fallot. Heart. 2009;95(2):142–147. doi:10.1136/hrt.2007.135723.
107. Desai T, Stumper O, Miller P, et al. Acute interventions for stenosed right ventricle-pulmonary artery conduit following the right-sided modification of norwood-sano procedure. Congenit Heart Dis. 2009;4(6):433–439. doi:10.1111/j.1747-0803.2009.00347.x.
108. Frazer JR, Ing FF. Stenting of stenotic or occluded iliofemoral veins, superior and inferior vena cavae in children with congenital heart disease: Acute results and intermediate follow up. Catheterization and Cardiovascular Interventions. 2009;73(2):181–188. doi:10.1002/ ccd.21790.
109. Stapleton GE, Hamzeh R, Mullins CE, et al. Simultaneous stent implantation to treat bifurcation stenoses in the pulmonary arteries: initial results and long-term follow up. Catheterization and Cardiovascular Interventions. 2009;73(4):557–563. doi:10.1002/ccd.21838.
110. Zartner P, Cesnjevar R, Singer H, et al. First successful implantation of a biodegradable metal stent into the left pulmonary artery of a preterm baby. Catheterization and Cardiovascular Interventions.2005;66(4):590–594. doi:10.1002/ccd.20520.
111. Schranz D, Zartner P, Michel-Behnke I, et al. Bioabsorbable metal stents for percutaneous treatment of critical recoarctation of the aorta in a newborn. Catheterization and Cardiovascular Interventions. 2006;67 (5):671–673. doi:10.1002/ccd.20756.
112. Garg S, Serruys PW. Coronary stents: looking forward. J Am Coll Cardiol. 2010;56(10, Supplement):S43–S78. doi:10.1016/j.jacc.2010.06.008.
113. Waksman R. Promise and challenges of bioabsorbable stents. Catheterization and Cardiovascular Interventions. 2007;70(3):407–414. doi:10.1002/ccd.21176.
114. Veeram Reddy SR, Welch TR, Wang J, et al. A novel biodegradable stent applicable for use in congenital heart disease: Bench testing and feasibility results in a rabbit model. Catheterization and Cardiovascular Interventions. 2014;83(3):448–456. doi:10.1002/ ccd.24936.
115. Rosa DS, Guedes CGF, Bardi MAG. Evaluation of thermal, mechanical and morphological properties of PCL/CA and PCL/CA/PE-g- GMA blends. Polym Test. 2007;26(2):209–215. doi:10.1016/j.polymertesting.2006.10.003.
116. Unverdorben M, Spielberger A, Schywalsky M, et al. Apolyhydroxybutyrate biodegradable stent: preliminary experience in the rabbit. Cvir. 2002;25(2):127–132. doi:10.1007/s00270-001-0118-3.
117. Tsukie N, Nakano K, Matoba T, et al. Pitavastatin-incorporated nanoparticle-eluting stents attenuate in-stent stenosis without delayed endothelial healing effects in a porcine coronary artery model. J Atheroscler Thromb. 2013;20(1):32–45.

118. Yin RX, Yang DZ, Wu JZ. Nanoparticle drug- and gene-eluting stents for the prevention and treatment of coronary restenosis. Theranostics. 2014;4(2):175–200. doi:10.7150/thno.7210.
119. Kwon H, Park S. Local delivery of antiproliferative agents via stents.Polymers. 2014;6(3):755. doi:10.3390/polym6030755.
120. Jokerst JV, Gambhir SS. Molecular imaging with theranostic nano- particles. Acc Chem Res. 2011;44(10):1050–1060. doi:10.1021/ ar200106e.
121. Gundogan B, Tan A, Farhatnia Y, et al. Bioabsorbable stent quo vadis: a case for nano-theranostics. Theranostics. 2014;4(5):514–533. doi:10.7150/thno.8137.
122. Nakano K, Egashira K, Masuda S, et al. Formulation of nanopar- ticle-eluting stents by a cationic electrodeposition coating technology: efficient nano-drug delivery via bioabsorbable polymeric nanoparticle-eluting stents in porcine coronary arteries. JACC Cardiovasc Interv. 2009;2(4):277–283. doi:10.1016/j. jcin.2008.08.023.
123. Byrne RA, Serruys PW, Baumbach A, et al. Report of a European Society of Cardiology–European Association of Percutaneous Cardiovascular Interventions Task Force on the evaluation of coronary stents in Europe: executive summary. Eur Heart J. 2015;36 (38):2608–2620. doi:10.1093/ eurheartj/ehv203.

Chapter 3

Noninvasive Coronary Computed Tomography Angiography Based Heart Team Assessment Using The SYNTAX Score II For The Selection Of The Revascularization Strategy In Patients With Multivessel Coronary Artery Disease: An Analysis Of The SYNTAX II Trial

Rafael Cavalcante, Pannipa Suwannasom, Yoshinobu Onuma, Yohei Sotomi, Nicola Ryan, Gianluigi de Maria, Carlos Collet, Marie-Angele Morel, Gerrit-Anne van Es, Vasim Farooq, Adrian Banning, Javier Escaned, Patrick W. Serruys

(submitted)

ABSTRACT

Aims

To compare a purely noninvasive coronary computed tomography angiography (CTA) assessment with an invasive angiographic evaluation for the selection of the revascularization strategy in patients with multivessel coronary disease enrolled in the SYNTAX II trial.

Methods and results

Sixty-eight consecutive patients with 3-vessel coronary disease enrolled in the SYNTAX II trial who underwent coronary CTA were included in the present study. Two independent corelab Heart Teams analyzed coronaryCTA scans and conventional angiograms in a blinded fashion. The primary endpoint was the level of agreement between treatment recommendations of both heart teams using the SYNTAX scoreII and measured by the weighted kappa statistic. SYNTAX score II showed excellent agreement between coronaryCTA and invasive angiography (ICC=0.96, $p<0.001$). Invasive angiography assessment lead to a recommendation for "PCI only" in 1 case, suggested "equipoise" in 62 and recommended "CABG only" in 5 cases, while CTA assessment lead to a recommendation for "PCI only" in 2 cases, suggested "equipoise" in 59 and recommended "CABG only" in 7 cases. There were no cases with disagreement between "CABG only" and "PCI only". The weighted kappa for treatment recommendation between the two imaging modalities was 0.50 (95%CI 0.17 to 0.82).

Conclusion

Recommendations for CABG or PCI based on the SYNTAX score II derived from coronaryCTA and conventional angiography show moderate agreement. Coronary CTA appears promising to help guide the Heart Team decision regarding the choice of revascularization strategy in patients with multivessel coronary disease. Key words: Coronary CT angiography, multivessel coronary disease, PCI, CABG

INTRODUCTION

In patients with severe coronary artery disease (CAD), a multidisciplinary "Heart Team" (HT) approach has become the standard-of-care for the decision making process of selecting the most appropriate revascularization strategy, whether percutaneous coronary intervention (PCI) or coronary artery bypass graft (CABG).[1] This approach is supported by the most recent multi-society guidelines.[1, 2] The HT decision tree is based on coronary anatomy and several other factors that may interfere with prognosis for both PCI and CABG, as well as on patients personal preferences.

Specifically in the subgroup of multivessel disease, the quantification of coronary anatomic complexity with the use of the angiographic anatomic SYNTAX score has proven to predict prognosis.(3) This score is, therefore, also recommended as tool to help HT decision.[1, 2] Nevertheless, since factors other than anatomic complexity also play a significant role in outcomes after revascularization, the SYNTAX score II (SSII) was created by adding, to the purely anatomic angiographic score, clinical comorbidities with proven prognostic impact.[4] This score, validated in a large external population, predicts 4 years all-cause mortality for both PCI and CABG and generates a recommended revascularization strategy based on possible differences in predicted mortality.[5]

For the assessment of coronary anatomy, invasive coronary angiography (ICA) has been the gold standard since its introduction. More recently coronary computed tomography angiography (CTA) was introduced as a non-invasive alternative.[6] Furthermore, the application of an adapted anatomic SYNTAX score on coronary CTA images has been shown to be feasible and reproducible.[7-9]

The objective of the present study was to evaluate 1 a purely noninvasive coronary CTA based Heart Team assessment using the SYNTAX score II for the selection of the revascularization strategy in patients with multivessel CAD. This non invasive approach was compared with the standard-of-care invasive angiographic evaluation in patients enrolled in the ongoing multicenter SYNTAX II trial.

METHODS

The SYNTAX II trial

The design of the SYNTAX II trial was previously described elsewhere.[10,11] In brief, patients with multivessel CAD were enrolled in an open label, single arm,10 multicenter registry design. (ClinicalTrials.gov number, NCT02015832) After undergoing coronary angiography and having an indication for revascularization, the patients had their SYNTAX score II calculated in an online calculator (available at www.syntaxscore.com). This score uses the anatomic SYNTAX score, gender, age, creatinine clearance, left ventricular

ejection fraction, presence of left main disease, chronic obstructive pulmonary disease and peripheral vascular disease to provide individual 4 years predicted all-cause mortality rates associated with both PCI and CABG. When no statistical difference (based on the 95% predictive interval of the difference) existed between both predicted mortality rates ("Equipoise"), or when the existing difference was in favor of PCI ("PCI only"), the patient was included in the trial to undergo state-of-the-art PCI with second generation drug eluting stents guided by fractional flow reserve (FFR) and intravascular ultrasound (IVUS). When the difference favored CABG ("CABG only"), the patient was sent to surgery and followed in a separate registry.(10,11)

Study Population

The SYNTAX II trial enrolled 454 patients. The use of coronary CTA in the trial was optional but encouraged to be analyzed in the context of this exploratory substudy. All prospectively enrolled patients who underwent both coronary CTA and ICA were included in the present analysis. The only exclusion criteria were poor quality or unavailable coronary CTA imaging. (Fig. 1)

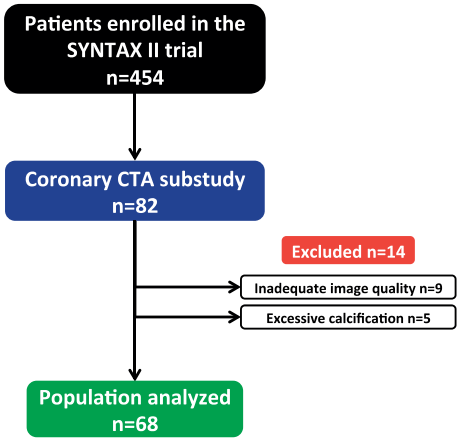

figure caption 1. Study flowchart.

Coronary CTA imaging acquisition protocol

All coronary CTA were performed using multidetector scanners according to current acquisition guidelines.[6] Patients without contraindications received beta blockers to lower the heart rate and sublingual nitrates. All scans were performed with ECG gating. Analyses were performed off-line by an independent Core Laboratory (Cardialysis BV, Rotterdam, The Netherlands). The CT data were analyzed on a dedicated workstation (Multi-Modality Workstation, Siemens AG) using a validated cardiovascular analysis package (Circulation, Siemens AG).

Core laboratory Heart Teams and Imaging analyses

At the Core laboratory (Cardialysis BV, Rotterdam, The Netherlands), two heart teams independently and blindly assessed either coronary CTA or invasive conventional angiograms and calculated the anatomic SYNTAX score and SYNTAX score II for each case. For the calculation of the anatomic SYNTAX score on CTA images, the criteria previously described and validated by our group were used and imputed in the online calculator.[7]

Study endpoints

The primary endpoint of the present study was the level of agreement between the non-invasive and invasive SYNTAX score II derived treatment recommendations regarding the mode of revascularization ("PCI only", "equipoise" or "CABG only"). As secondary endpoints we assessed the levels of agreement between anatomic SYNTAX scores and SYNTAX II scores for PCI for both CTA and ICA based assessments. Since the SYNTAX score II CABG (and its derived 4 years predicted mortality) does not take into account the anatomic SYNTAX score, no comparison between CTA and ICA was performed for this parameter.

STATISTICAL ANALYSIS

Continuous variables are presented as mean ± standard deviation (SD) and categorical variables are presented as counts and proportions. For the assessment of the primary endpoint we used the Kappa statistic with linear weighting to evaluate the agreement of both assessments in recommending "PCI only", "equipoise" or "CABG only". For the comparison between anatomic SYNTAX scores, SYNTAX score II and PCI predicted mortality rates we used absolute agreement intraclass correlation coefficients (ICC) with two-way mixed models and Bland-Altman analysis. Inter-observer variability for the coronary CTA anatomic SYNTAX score calculation was assessed with ICC. A two-sided alpha error of <0.05 was considered statistically significant. All analyses were performed using SPSS 21.0 (IBM corp).

RESULTS

Study population

Of the 454 patients enrolled in the SYNTAX II trial, a total of 82 subjects underwent coronary CTA assessment prior to enrollment. Of these 82 cases, 14 were excluded due to insufficient image quality (n=9) or heavy calcification precluding appropriate analysis (n=5). The population of the present study thus comprises 68 patients from centers in

Spain, United Kingdom, Netherlands and Poland (Figure 1). Overall, mean age was 65.6 ± 8.9 years, 95.6% were male, 76.5% had hypertension and 29.4% had Diabetes Mellitus. The clinical presentation was chronic stable angina or silent ischemia in 86.8% of the cases (Table 1).

Table 1. Baseline characteristics.

	n=68
Age (years)	65.6 ± 8.9
Male gender	95.6% (65)
Ejection Fraction (%)	58.7 ± 7.5
Creatine Clearance (ml/min)	82.2 ± 29.3
Left Main Disease	0
Chronic obstructive pulmonary disease	10.3% (7)
Peripheral Vascular Disease	4.4% (3)
Body mass index (Kg/m^2)	28.5 ± 4.0
Hypertension	76.5% (52)
Diabetes Mellitus	29.4% (20)
Hyperlipidemia	70.6% (48)
Current smoking	10.3% (7)
Previous Stroke	4.4% (3)
Previous Myocardial Infarction	5.9% (4)
Clinical presentation	
Silent ischemia	5.9% (4)
Stable angina	80.9% (55)
Unstable angina	11.8%(8)

Anatomic SYNTAX score and SYNTAX score II

Table 2 summarizes the SYNTAX scores data on both invasive and non invasive assessments and Figure 2 depicts a case example of calculation of anatomic SYNTAX score and SYNTAX score II on invasive and non-invasive images.

Coronary CTA and invasive angiography had a weak albeit statistically significant correlation for the anatomic SYNTAX score (r=0.43; p<0.001) and a strong correlation for the SYNTAX score II PCI (r=0.96; p<0.001) (Figure 3). Average anatomic SYNTAX score was higher in the CTA non-invasive assessment as compared to conventional invasive angiography (23.2 ± 7.2 vs. 21.6 ± 6.6, respectively) and showed only fair agreement between the two imaging modalities with an ICC of 0.42 (95%CI 0.21 – 0.60), p<0.001. SYNTAX score II and 4 years predicted PCI mortality rates for CTA and ICA showed excellent agreement with ICCs of 0.96 (95%CI 0.94 – 0.98), p<0.001 and 0.96 (95%CI 0.93 – 0.97), p<0.001; respectively (Table 2). On Bland-Altman analysis, mean difference between CTA

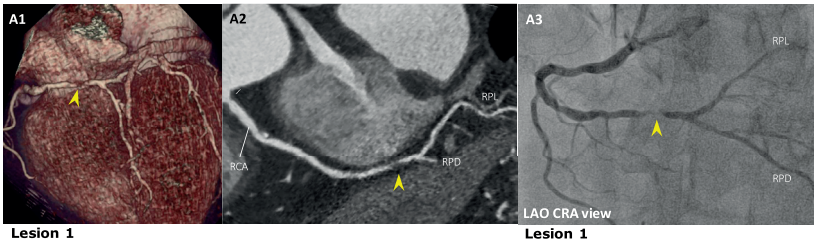

Lesion 1	
(segment 3): 1x2=	2
Sub total lesion 1	2

Lesion 1	
(segment 3): 1x2=	2
Sub total lesion 1	2

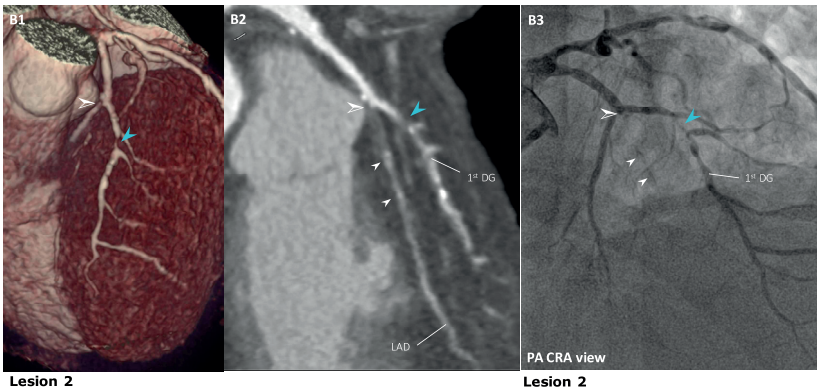

Lesion 2	
(segment 9): 1x2=	2
Sub total lesion 2	2
Lesion 3	
(segment 7): 2.5x5=	12.5
Age T.O. is unknown	1
+ Blunt stump	1
the first segment beyond the T.O. visualized by contrast: 7	0
+ sidebranch: Yes, all sidebranches ≥ 1.5mm	1
Bifurcation Type: Medina 0,1,0:	1
Angulation <70 degree	1
Sub total lesion 3	17.5

Lesion 2	
(segment 9): 1x2=	2
Sub total lesion 2	2
Lesion 3	
(segment 7): 2.5x5=	12.5
Age T.O. is unknown	1
+ Blunt stump	1
the first segment beyond the T.O. visualized by contrast: 7	0
+ sidebranch: Yes, all sidebranches ≥ 1.5mm	1
Bifurcation Type: Medina 0,1,0:	1
Sub total lesion 3	16.5

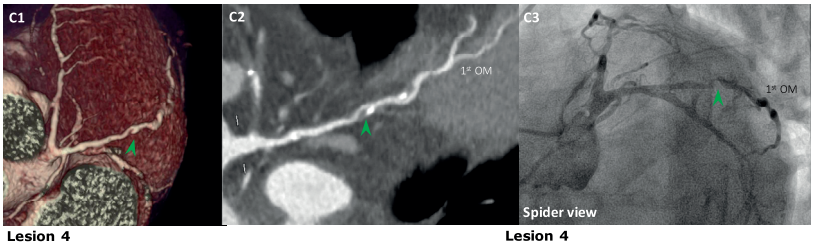

Lesion 4 **Lesion 4**

Figure 2. Coronary CT angiography in a 78-year-old man with a past medical history of hypertension presenting with stable angina Canadian Cardiology Society class III. The patient had a creatinine clearance of 65 mL/min and a left ventricular ejection fraction of 70%. There was no left main disease, no history of chronic obstructive pulmonary disease or of peripheral vascular disease. On the left and mid panels, volume rendering technique (VRT) and curved multiplanar reconstruction (MPR) images of distal right coronary artery (RCA), left anterior descending artery (LAD) and 1st diagonal branch and left circumflex artery (1st OM) are shown. The corresponding invasive coronary angiography of each major epicardial vessel is seen in the right side panels. Anatomic SYNTAX scores and SYNTAX II scores were calculated from both images and are shown in the bottom.

Table 2. Anatomic SYNTAX score and SYNTAX score II in coronary CTA and invasive angiography.

	Coronary CTA	Invasive Angiography	ICC (95% CI)	p value
Anatomic SYNTAX score	23.2 ± 7.2	21.6 ± 6.6	0.42 (0.21 – 0.60)	<0.001
SYNTAX score II PCI	30.1 ± 7.4	29.7 ± 7.6	0.96 (0.94 – 0.98)	<0.001
4y predicted mortality PCI (%)	8.3 ± 6.1	8.1 ± 6.3	0.96 (0.93 – 0.97)	<0.001

CI – Confidence interval; CTA – Computed tomography angiography; ICC – Intraclass correlation coefficient; PCI – Percutaneous coronary intervention.

and ICA for the anatomic SYNTAX score was 1.6 ± 7.4 (limits of agreement: -13.2 to 16.4) while for the SYNTAX score II was 0.5 ± 2.1 (limits of agreement: -3.8 to 4.7) (Figure 4). Coronary CTA anatomic SYNTAX score was assessed by two independent observers in 16 patients (23.5%) and showed good inter-observer variability with an ICC of 0.83 for the final score.

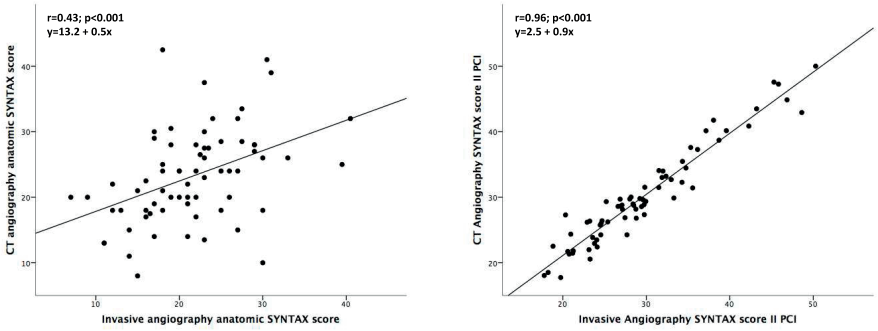

Figure 3. Scatter plots of anatomical SYNTAX score (A) and SYNTAX score II PCI (B) calculated from coronary CTA and invasive angiography.

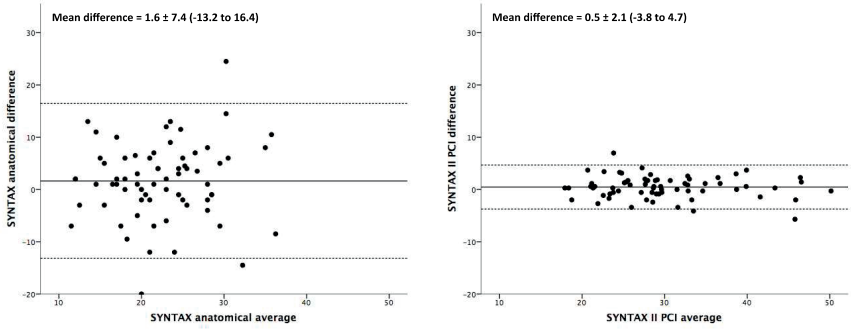

Figure 4. Bland-Altman plots of anatomical SYNTAX score (A) and SYNTAX score II PCI (B) calculated from coronary CTA and invasive angiography.

Heart Team Treatment Recommendations (Primary Endpoint)

Based on the SYNTAX score predicted mortality differences for PCI and CABG, the treatment recommendation after non-invasive CTA assessment alone was "PCI only" in 2 cases, "CABG only" in 7 cases and either 1 strategy ("Equipoise") in 59 patients. When invasive angiography alone was assessed, treatment recommendation was "PCI only" in 1 case, "CABG only" in 5 cases and either strategy ("Equipoise") in 62 cases. The two imaging modalities recommended the same revascularization strategy in 61 (89.7%) cases. The agreement according to the weighted Kappa statistic was moderate ($\kappa = 0.50$, SE 0.28, 95%CI 0.17 to 0.82) (Table 3).

Table 3. Treatment recommendation based on SYNTAX score II calculated from Coronary CTA and invasive angiography. The two imaging techniques showed moderate agreement for treatment recommendation with a weighted Kappa of $\kappa = 0.50$ (SE 0.28, 95%CI 0.17 to 0.82).

		Invasive Angiography			
		PCI only	Equipoise	CABG only	Total
Coronary CTA	PCI only	1	1	0	2
	Equipoise	0	57	2	59
	CABG only	0	4	3	7
	Total	1	62	5	68

DISCUSSION

The findings of the present study can be summarized as follows: 1) Coronary CTA SYNTAX score II shows excellent agreement with invasive angiography SYNTAX score II; 2) SYNTAX score II derived Heart Team treatment recommendations based on coronary CTA and ICA show moderate agreement.

Since the introduction of coronary CTA with multidetector scanners, the cardiology community has speculated about the possibility of sending a patient to CABG based on a purely non-invasive assessment. However, given the limitations associated with even the most up-to-date technology; mainly spatial resolution; CT angiography is yet to become an alternative to conventional invasive cineangiography, especially in complex multivessel disease.[12]

The assessment of coronary anatomy with the use of the anatomic SYNTAX score is currently recommended in multinational guidelines to guide the selection of the most appropriate revascularization strategy for patients with multivessel coronary disease.[1, 2] Recent data demonstrated an acceptable concordance (ICC=0.64) and good correlation between CTA and ICA derived anatomic SYNTAX scores.[8] Using purely anatomic criteria to recommend CABG, Suh et al, showed that coronary CTA and CTA SYNTAX

score had high specificity and positive predictive value for selecting CABG candidates as compared to the standard of invasive coronary angiography.[9]

One limitation of such analyses is that it presumes that coronary anatomy is the sole factor to be taken into account when selecting the best revascularization strategy. This is complicated by the not small variability associated with the calculation of the anatomic SYNTAX score, even when using only the conventional invasive angiogram. In a previous analysis of the SYNTAX trial, the weighted kappa values for inter and intra-observer variability were 0.45 and 0.59, respectively.[13] When corelab anatomic SYNTAX scores were compared to those calculated by the site investigators at each hospital, an overall underestimation by the sites was observed with a mean difference (corelab minus site) of 3.83 and wide limits of agreement from -18.57 to +26.23.[14] In the present analysis, when comparing to imaging techniques we found somewhat similar variability for the anatomic SYNTAX score (Table 2, Figures 3 and 4).

The SYNTAX score II was developed, among other factors, to overcome this limitation by putting coronary anatomy as one of the factors (instead of the only factor) that should drive revascularization strategy selection.(4) By doing this, it reduces the variability of the assessment either of multiple observers, as seen in the SYNTAX I trial[14] or by different imaging modalities such as CTA and ICA, as we demonstrated in the present analysis (Table 2, Figures 3 and 4).

A Heart team decision-making process should preferably account for all factors driving prognosis and interaction for treatment effect with the mode of revascularization in order to accurately select the best treatment for a given patient. The SYNTAX score II provides an individual, customized mortality prediction that helps this process. In the present analysis we demonstrated that following this principle, a purely non-invasive coronary anatomy assessment with coronary CT angiography showed moderate agreement with the standard-of-care of the conventional invasive angiography assessment. These data supports the idea that, as technology advances, we are not far from being able to send a patient to coronary bypass surgery after a solely non-invasive CT assessment together with a careful multidisciplinary heart team evaluation of all clinical factors driving prognosis.

In fact, the present study worked as a pilot for the development of the SYNTAX III Revolution randomized trial, that will test this hypothesis by randomizing two Heart teams to assess either the coronary CTA using the Revolution 512-slice scanner (General Electric Healthcare) or the invasive angiogram and give a treatment recommendation regarding the revascularization strategy. This trial will provide further insight into this relevant scientific issue.

Strengths and limitations

The present analysis is limited by the small and selected sample size of patients included. Since the inclusion of the SYNTAX II trial mandated by protocol that patients should not have a "CABG only" recommendation by the SYNTAX II score, this population is largely underrepresented in this series. Furthermore, a non negligible 17% (14 of 82) of screened patients were excluded due to lack of adequate image quality. This was more frequently due to problems with imaging acquisition and related with the lack of a standardized acquisition protocol for all the centers involved, although in 5% (4 of 82) the limitation was excessive coronary calcification precluding adequate analysis.

Nevertheless, the fact that this is the first study to assess this concept with the new SYNTAX score II is the main strength of our study. Furthermore, by design it showed the performance of coronary CT in a very complex all-comers 3-vessel disease population with indication for PCI. Thus, our findings can be interpreted as a rather robust analysis of this common clinical scenario.

Conclusions

A purely non-invasive coronary CTA guided selection of the revascularization strategy using the SYNTAX score II showed moderate agreement with the standard of-care conventional invasive angiography assessment. Coronary CTA shows promise as a non-invasive method to guide the heart team decision-making process for the treatment of patients with multivessel coronary disease.

REFERENCES

1. Windecker S, Kolh P, Alfonso F, Collet JP, Cremer J, Falk V, et al. 2014 ESC/EACTS Guidelines on myocardial revascularization: The Task Force on Myocardial Revascularization of the European Society of Cardiology (ESC) and the European Association for Cardio-Thoracic Surgery (EACTS) Developed with the special contribution of the European Association of Percutaneous Cardiovascular Interventions (EAPCI). Eur Heart J. 2014;35(37):2541-619.
2. Levine GN, Bates ER, Blankenship JC, Bailey SR, Bittl JA, Cercek B, et al. 2011 ACCF/AHA/SCAI Guideline for Percutaneous Coronary Intervention: a report of the American College of Cardiology Foundation/American Heart Association Task Force on Practice Guidelines and the Society for Cardiovascular Angiography and Interventions. Circulation. 2011;124(23):e574-651.
3. Serruys PW, Morice MC, Kappetein AP, Colombo A, Holmes DR, Mack MJ, et al. Percutaneous coronary intervention versus coronary-artery bypass grafting for severe coronary artery disease. N Engl J Med. 2009;360(10):961-72.
4. Farooq V, van Klaveren D, Steyerberg EW, Meliga E, Vergouwe Y, Chieffo A, et al. Anatomical and clinical characteristics to guide decision making between coronary artery bypass surgery and percutaneous coronary intervention for individual patients: development and validation of SYNTAX score II. Lancet. 2013;381(9867):639-50.
5. Campos CM, van Klaveren D, Farooq V, Simonton CA, Kappetein AP, Sabik JF, et al. Long-term forecasting and comparison of mortality in the Evaluation of the Xience Everolimus Eluting Stent vs. Coronary Artery Bypass Surgery for Effectiveness of Left Main Revascularization (EXCEL) trial: prospective validation of the SYNTAX Score II. Eur Heart J. 2015;36(20):1231-41.
6. Raff GL, Abidov A, Achenbach S, Berman DS, Boxt LM, Budoff MJ, et al. SCCT guidelines for the interpretation and reporting of coronary computed tomographic angiography. J Cardiovasc Comput Tomogr. 2009;3(2):122-36.
7. Papadopoulou SL, Girasis C, Dharampal A, Farooq V, Onuma Y, Rossi A, et al. CT-SYNTAX score: a feasibility and reproducibility Study. JACC Cardiovasc Imaging.30 2013;6(3):413-5.
8. Pozo E, Álvarez-Acosta L, Alonso D, Pazos-Lopez P, de Siqueira ME, Jacobi A, et al. Diagnostic accuracy of coronary ct for the quantification of the syntax score in patients with left main and/or 3-vessel coronary disease. Comparison with invasive angiography. Int J Cardiol. 2015;182:549-56.
9. Suh YJ, Hong YJ, Lee HJ, Hur J, Kim YJ, Hong SR, et al. Accuracy of CT for Selecting Candidates for Coronary Artery Bypass Graft Surgery: Combination with the SYNTAX Score. Radiology. 2015;276(2):390-9.
10. Campos CM, Stanetic BM, Farooq V, Walsh S, Ishibashi Y, Onuma Y, et al. Risk stratification in 3-vessel coronary artery disease: Applying the SYNTAX Score II in the Heart Team Discussion of the SYNTAX II trial. Catheter Cardiovasc Interv. 2015.
11. Escaned J, Banning A, Farooq V, Echavarria-Pinto M, Onuma Y, Ryan N, et al. Rationale and design of the SYNTAX II trial evaluating the short to long-term outcomes of state-of-the-art percutaneous coronary revascularisation in patients with de novo three-vessel disease. EuroIntervention. 2016;12(2):e224-34.
12. Gonçalves PeA, Rodríguez-Granillo GA, Spitzer E, Suwannasom P, Loewe C, Nieman K, et al. Functional Evaluation of Coronary Disease by CT Angiography. JACC Cardiovasc Imaging. 2015;8(11):1322-35.
13. Serruys PW, Onuma Y, Garg S, Sarno G, van den Brand M, Kappetein AP, et al. Assessment of the SYNTAX score in the Syntax study. EuroIntervention. 2009;5(1):50-6.

14. Zhang YJ, Iqbal J, Campos CM, Klaveren DV, Bourantas CV, Dawkins KD, et al. Prognostic value of site SYNTAX score and rationale for combining anatomic and clinical factors in decision making: insights from the SYNTAX trial. J Am Coll Cardiol.6 2014;64(5):423-32.

Chapter 4

Relation Between Bioresorbable Scaffold Sizing Using QCA-Dmax and Clinical Outcomes at 1 Year in 1,232 Patients From 3 Study Cohorts (ABSORB Cohort B, ABSORB EXTEND, and ABSORB II)

Yuki Ishibashi, Shimpei Nakatani, Yohei Sotomi, Pannipa Suwannasom, Maik J. Grundeken, Hector M. Garcia-Garcia, Antonio L. Bartorelli, Robert Whitbourn, Bernard Chevalier, Alexandre Abizaid, John A. Ormiston, Richard J. Rapoza, Susan Veldhof, Yoshinobu Onuma, Patrick W.Serruys

JACC Cardiovasc Interv. 2015 Nov;8(13):1715-26.

ABSTRACT

Objectives

This study sought to investigate the clinical outcomes based on the assessment of quantitative coronary angiography–maximal lumen diameter (Dmax).

Background

Assessment of pre-procedural Dmax of proximal and distal sites has been used for Absorb scaffold size selection in the ABSORB studies.

Methods

A total of 1,248 patients received Absorb scaffolds in the ABSORB Cohort B (ABSORB Clinical Investigation,Cohort B) study (N = 101), ABSORB EXTEND (ABSORB EXTEND Clinical Investigation) study (N = 812), and ABSORB II (ABSORB II Randomized Controlled Trial) trial (N = 335). The incidence of major adverse cardiac events (MACE) (a composite of cardiac death, any myocardial infarction [MI], and ischemia-driven target lesion revascularization) was analyzed according to the Dmax subclassification of scaffold oversize group versus scaffold nonoversize group.

Results

Of 1,248 patients, pre-procedural Dmax was assessed in 1,232 patients (98.7%). In 649 (52.7%) patients, both proximal and distal Dmax values were smaller than the nominal size of the implanted scaffold (scaffold oversize group), whereas in 583 (47.3%) of patients, the proximal and/or distal Dmax were larger than the implanted scaffold (scaffold nonoversize group). The rates of MACE and MI at 1 year were significantly higher in the scaffold oversize group than in the scaffold nonoversize group (MACE 6.6% vs. 3.3%; log-rank $p < 0.01$, all MI: 4.6% vs. 2.4%; log-rank $p = 0.04$), mainly driven by a higher MI rate within 1 month post-procedure (3.5% vs. 1.9%; $p = 0.08$). The independent ACE determinants were both Dmax smaller than the scaffold nominal size (odds ratio [OR]: 2.13, 95% confidence interval [CI]: 1.22 to 3.70; $p < 0.01$) and the implantation of overlapping scaffolds (OR: 2.10, 95% CI: 1.17 to 3.80; $p = 0.01$).

Conclusions

Implantation of an oversized Absorb scaffold in a relatively small vessel appears to be associated with a higher 1-year MACE rate driven by more frequent early MI.

The performance of the secondgeneration Absorb bioresorbable everolimus-eluting scaffold was investigated in the ABSORB II (ABSORB II Randomized Controlled Trial) as well as in the Cohort B1, Cohort B2, and ABSORB EXTEND (ABSORB EXTEND Clinical Investigation) studies, and demonstrated excellent clinical results (1–7). As the Absorb scaffold has a strict upper limit of expansion, quantitative coronary angiography (QCA)-guided implantation was a mandatory requirement in ABSORB EXTEND (7) and ABSORB II (1). The aim was to allow the selection of a scaffold size matching that of the reference vessel diameter. For reasons related to the potential labeling by the regulator, the sponsoring corporation did not want to require the use of intravascular imaging for sizing the vessel and for selection of the device size. The concerns about appropriate deployment of the Absorb scaffold with angiography guidance arose mainly from optical coherence tomography (OCT) substudies demonstrating an increased frequency of malapposition when the Absorb scaffold was implanted in a too large vessel (8). Another matter of concern is the risk of scaffold disruption (9), particularly when the device has already reached its maximal limit of expansion and is overexpanded in an attempt to correct persistent malapposition. Conversely, an OCT substudy showed an excess of proximal and/or distal edge dissections when the Absorb scaffold was implanted in vessels smaller than the device nominal size (8). However, the impact of quantitative angiographic guidance on clinical outcomes is so far unknown. Therefore, the aim of this study was to investigate the relationship between clinical outcomes and maximal diameter (Dmax) by QCA, which was used as a guide for appropriate selection and deployment of the Absorb scaffold in 2 cohorts of patients from the ABSORB Cohort B study, ABSORB EXTEND study, and ABSORB II trial.

METHODS

Study design and population.

We analyzed the results of Absorb scaffold implantation in 1,248 patients enrolled between 2009 and 2013 in the ABSORB Cohort B study (2,4), ABSORB EXTEND study (7), and ABSORB II (1) randomized controlled trial. The design of each study is described elsewhere (4,6,7,10). In the ABSORB Cohort B, a 3.0 x18-mm Absorb scaffold only was available. In the ABSORB EXTEND and ABSORB II studies, patients were treated as follows (1,7): 1) a 3.5-mm Absorb scaffold was used when both the proximal and distal Dmax were within an upper limit of 3.8 mm and a lower limit of 3.0 mm: 2) a 3.0-mm Absorb scaffold was used when both the proximal and distal maximal lumen diameters were within an upper limit of 3.3 mm and a lower limit of 2.5 mm: 3) a 2.5-mm Absorb scaffold was used when both the proximal and the distal Dmax were within an upper limit of 3.0 mm and a lower limit of 2.25 mm: and 4) scaffold overlap was allowed. Patients

demographic data and baseline characteristics were similar among 3 studies as well as pre-procedure minimal lumen diameter (MLD) and % diameter stenosis. All of these trials were sponsored and funded by Abbott Vascular. The research ethics committee of each participating institution approved the protocol, and all enrolled patients provided written informed consent before inclusion.

Study device.

The details of the study device (Absorb, Abbott Vascular, Santa Clara, California) have been described in detail previously (5,6). In brief, the balloon-expandable Absorb scaffold comprises a poly-L-lactide backbone (6) coated with an amorphous drug-eluting coating matrix composed of poly-D,L-lactide polymer containing everolimus.

QCA ANALYSIS

QCA guidance of Absorb implantation relies on the angiographic diameter function curve of the pre-treatment vessel segment that contains 3 nonambiguous data points; namely, the MLD and the Dmax with respect to the MLD of the proximal (proximal Dmax) and distal (distal Dmax) vessel segments of interest (8,11) (Figure 1). QCA analyses were undertaken by the sites before Absorb implantation, and post-procedurally by an independent core laboratory (Cardialysis BV, Rotterdam, the Netherlands) using a Coronary Angiography Analysis System (Pie Medical Imaging, Maastricht, the Netherlands).

Definitions and endpoints.

The patient population in the present study was stratified by the difference between the angiographic maximal diameter and the nominal diameter of the implanted scaffold. The selection of device size was considered "oversized" (scaffold oversize group) when the patient received 1 or more devices in vessels in which both the proximal and the distal Dmax were smaller than the nominal size of the device. Patients who received Absorb scaffolds in vessels with either a proximal or a distal Dmax or both Dmax larger than the nominal size of the device constituted the "scaffold nonoversize group". When a patient received 2 or 3 overlapping Absorb scaffolds in a long lesion, the nominal size of the proximally implanted device was compared with the proximal Dmax, whereas the nominal size of the distally implanted device was compared with the distal Dmax. In the cases of device failure (n = 10), the difference between Dmax and the implanted metallic stent was calculated. An additional analysis was performed using a different criterion (nominal scaffold diameter within 0.4 or 0.5 mm of Dmax) and is presented in Online Tables 1 and 2.

In the present analysis, the primary clinical outcome assessed was ischemia-driven major adverse cardiac events (ID-MACE), defined as a composite of cardiac death, any myocardial infarction (MI classified as Q-wave or non–Q-wave MI), and ischemia-driven

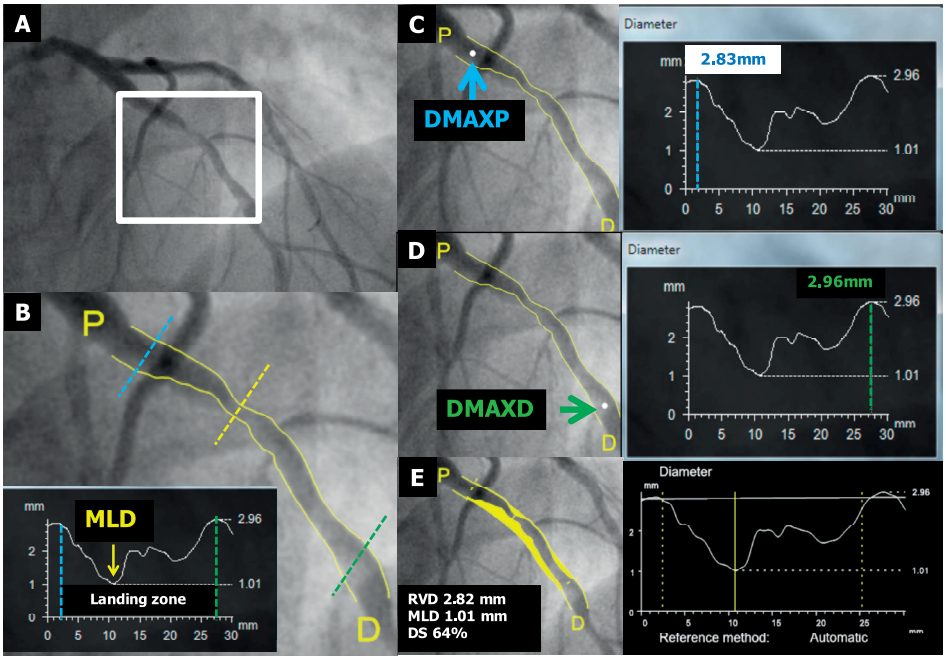

Figure 1. The Method to Measure QCA Proximal and Distal Dmax.
The method used to measure proximal and distal Dmax with QCA is shown. In the pre-procedural angiography (A), the operator has to define the landing zone where the scaffold will be implanted (B). Within the landing zone, the peak of the diameter function curve proximal to the minimal lumen diameter is defined as proximal (P) Dmax (C), whereas the peak diameter function curve distal (D) to the minimal lumen diameter is defined as distal Dmax (D). In this case, the proximal and distal Dmax of 2.83 and 2.96 mm led to the correct sizing of the Absorb (3.0 mm) with regard to the vessel diameter (E). DMAXD =maximal lumen diameter distal; DMAXP =maximal lumen diameter proximal; MLD =minimal lumen diameter; QCA = quantitative coronary angiography; RVD =reference vessel diameter.

target lesion revascularization (ID-TLR) by coronary artery bypass graft or percutaneous coronary intervention. Cardiac death was defined as any death due to a proximate cardiac cause (e.g., MI, low-output failure, fatal arrhythmia). Unwitnessed death and death of unknown cause were classified as cardiac death. MI classification and criteria for diagnosis were defined according to the per-protocol definition. Q-wave MI was the development of a new, pathological Q-wave. Non–Q-wave MI was adjudicated if there was an elevation of CK levels to ≥2 times the upper limit of normal with elevated creatine kinase-myocardial band levels in the absence of new pathological Q waves (12). Notably, this definition of per-protocol MI was consistently applied in all trials included in the present analysis. Target vessel myocardial infarction (TVMI) was defined as MI that occurred in the entire major coronary vessel proximal and distal to the target lesion, which includes upstream and downstream branches and the target lesion itself. ID-TLR was defined as any repeat percutaneous intervention of the target lesion or bypass

surgery of the target vessel with either a positive functional ischemia study, ischemic symptoms, or an angiographic MLD stenosis ≥50% by core laboratory QCA, or revascularization of a target lesion with diameter stenosis ≥70% by core laboratory QCA without either ischemic symptoms or a positive functional study. Definite and probable scaffold thrombosis (ST) was adjudicated according to the Academic Research Consortium definitions (13–15). All clinical outcomes were adjudicated by an independent clinical events committee.

Source document verification and clinical follow-up.

In the ABSORB Cohort B and ABSORB II studies, we verified source documents in 100% of patients through 1-year follow-up. In the ABSORB EXTEND trial, source document verification was routinely performed in 100% of patients through 30-day follow-up, subsequently in a random 20% of patients, and in 100% of all reported events for the remaining follow-up period.

Statistical analysis.

All analyses were conducted using the intention-to-treat population. For the present analyses, individual data were based on a patient-level basis. Categorical variables were compared by Fisher exact test. Continuous variables are presented as mean ±SD and were compared by nonparametric test. Time-to-event variables are presented as Kaplan-Meier curves. To determine the independent predictors of MACE, firstly univariate logistic regression models were constructed using the following variables: age, male sex, current smoking, hypertension requiring treatment, dyslipidemia requiring treatment, any diabetes, unstable angina, pre-procedural diameter stenosis, pre-procedural MLD, lesion length, angulation >45°, bifurcation lesions, calcified lesions, pre-procedural visible thrombus, Type B2/C lesions, target vessel treatment with 2.5-mm device, treatment with overlapping scaffolds, and scaffold implantation in a vessel with both proximal and distal Dmax smaller than the nominal device size. Secondly, significant variables ($p < 0.10$) in the univariate analysis were forcedly entered into a multivariable logistic regression model to predict for MACE. A 2-sided p value <0.05 was considered significant for all tests. All statistical tests were performed with SPSS, version 22.0 for windows (IBM, Chicago, Illinois).

RESULTS

Of a total population of 1,248 patients, pre-procedural Dmax was assessed by the core laboratory in 1,232 (98.7 %) patients. Figure 2 displays individual values of proximal and distal Dmax in patients who received Absorb scaffolds of either 2.5-mm, 3.0-mm, or 3.5-

mm nominal size. The nominal size of the implanted Absorb scaffold was larger than both proximal and distal Dmax in 649 patients (scaffold oversize group 52.7%).

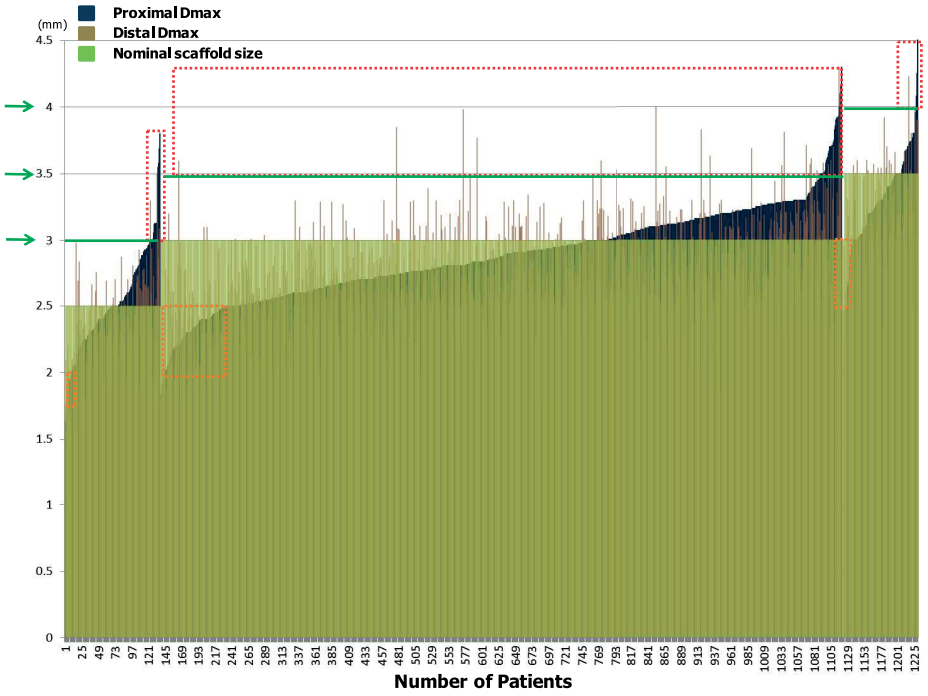

Figure 2. Proximal and Distal Dmax Compared With Nominal Size of the Scaffold. The graph represents the proximal Dmax value, the distal Dmax value and the nominal size of the implanted Absorb scaffold(s) in 1,232 patients. The Dmax measurement is based on core lab assessment. According to the manufacturer, the 2.5-mm, 3.0-mm, and 3.5-mm scaffolds cannot be dilated beyond their nominal size of 3.0 mm, 3.5 mm, and 4.0 mm, respectively. The limit of expansion of the scaffold is depicted by a green continuous line. Theoretically, dotted red areas indicate implantation of a too "small" Absorb scaffold in a relatively large vessel, and dotted orange areas indicate implantation of a too "large" Absorb scaffold in a relatively small vessel. Device size selection with regard to Dmax was considered appropriate in 867 (70.4%) patients and inappropriate in 365 (29.6%) patients. Dmax = maximal lumen diameter

Clinical and angiographic characteristics between the scaffold oversize group and the scaffold nonoversize group are detailed in Table 1. The 2 groups did not significantly differ with regard to main baseline clinical characteristics, whereas pre-procedural MLD, reference vessel diameter, and both proximal and distal Dmax were significantly smaller in the scaffold oversize group than in the scaffold nonoversize group.

The scaffold oversize group was associated with a higher risk of ID-MACE than the scaffold nonoversize group. As illustrated in Figure 3, the graphical presentation clearly shows that a higher number of these patients can be seen in the lower left quadrant (scaffold oversize group) than in the other quadrants of the graph (6.6% vs. 3.3%, p

Table 1. Clinical and pre- and post-procedural angiographic characteristics

	Scaffold oversize group (N=649)	Scaffold non-oversize group (N=583)	*p* value
Age , yrs	61.6 ± 10.7	60.8 ± 10.1	0.20
Male	73.8 (479)	75.1 (438)	0.60
Current smoker	1.7 (141)	24 (140)	0.34
Hypertension requiring treatment	67.6 (439)	67.9 (396)	0.95
Dyslipidemia requiring treatment	69.8 (453)	69 (402)	0.76
Any diabetes mellitus	24 (156)	26.2 (153)	0.39
Unstable Angina	24.8 (161)	22.9 (133)	0.46
Prior history of myocardial infarction	28.1 (182)	27.8 (162)	0.95
Lesion location			
Right coronary artery	21.9 (142)	33.6 (196)	<0.01
Left anterior descending artery	49.8 (323)	41.9 (244)	0.01
Left circumflex artery or ramus	9.9 (64)	9.6 (56)	0.92
Left main coronary artery	0 (0)	0.2 (1)	0.47
ACC/AHA lesion complexity			
A	1.9 (12)	2.1 (12)	0.84
B1	53.9 (349)	52.8 (307)	0.73
B2	41.2 (267)	43.5 (25)	0.45
C	3.1 (20)	1.7 (10)	0.14
TIMI Flow 0 or 1	0.6 (4)	0.2 (1)	0.38
Calcification (moderate or severe)	13.4 (87)	14.4 (84)	0.62
Angulation ≥ 45°	2.6 (17)	2.2 (13)	0.71
Bifurcation	4.0 (26)	4.8 (28)	0.58
Thrombus	1.5 (10)	1.9 (11)	0.67
Pre-procedural			
Reference vessel diameter , mm	2.50 ± 0.33	2.79 ± 0.39	<0.01
Proximal Dmax ,mm	2.66 ± 0.30	3.11 ± 0.34	<0.01
Distal Dmax ,mm	2.58 ± 0.31	2.94 ± 0.38	<0.01
Minimum lumen diameter, mm	1.05 ± 0.30	1.15 ± 0.33	<0.01
Diameter stenosis , %	57.9 ± 10.9	58.6 ± 10.2	0.22
Obstruction lesion length ,mm	12.2 ± 5.9	13.0 ± 5.7	0.03
Device related			
2.5-mm scaffold	8.6 (56)	13.9 (81)	<0.01
3.0-mm scaffold	82.4 (535)	77.4 (451)	0.03
3.5-mm scaffold	8.9 (58)	8.8 (51)	0.92
Average nominal diameter	2.97 ± 0.24	3.00 ± 0.21	0.03
Post-procedural			
Reference vessel diameter, mm	2.58 ± 0.30	2.82 ± 0.34	<0.01
Minimum lumen diameter, mm	2.19 ± 0.28	2.37 ± 0.31	<0.01

Table 1. Clinical and pre- and post-procedural angiographic characteristics (continued)

	Scaffold oversize group (N=649)	Scaffold non-oversize group (N=583)	*p* value
Diameter stenosis in percentage, %	15.3 ± 6.5	15.9 ± 10.2	0.09
Acute decrease, % diameter stenosis	42.5 ± 12.5	42.5 ± 12.4	0.98
Acute gain ,mm	1.13 ± 0.34	1.21± 0.38	<0.01
Acute gain / pre-procedural RVD, mm	0.46 ± 0.14	0.44 ± 0.14	0.02
Bailout treatment with metallic stent	1.9 (12)	0.7 (4)	0.08

Values are mean±SD, or % (n). Clinical and pre- and post-procedural angiographic characteristics are according to the distribution of Dmax measurements minus the nominal scaffold size in the scaffold oversize group versus the scaffold nonoversize group.

ACC/AHA . American College of Cardiology/American Heart Association lesion characteristics; Dmax = maximal lumen diameter; RVD = reference vessel diameter; TIMI = Thrombolysis In Myocardial Infarction.

< 0.01). MACE occurred in 46 of 760 patients when a relatively large device size was selected, whereas it occurred in 16 of 472 patients when a relatively small device size was selected (6.1% vs. 3.4%, p = 0.04).

The MACE and MI rates at 1 year and 2 years were significantly higher in the scaffold oversize group than in scaffold nonoversize group (1-year MACE: 6.6% vs. 3.3%; log-rank p < 0.01, 2-year MACE: 8.7% vs. 5.9%; log-rank p = 0.03, 1-year TVMI: 4.5% vs. 2.1%, 2-year MI: 5.5% vs. 3.0%; log-rank p = 0.04), mainly driven by a higher rate of TVMI within 1 month after the procedure (3.5% vs. 1.9%; p = 0.08) (Figure 4, Tables 2 and 3). Among the events of MI (44 of 1,232), periprocedural MI (PMI) occurred in 28 cases (63.6%). MI occurred after 48 h in 36% of all MI events. In the scaffold oversize group, PMI occurred in 64% (18 cases), whereas in the scaffold nonoversize group, the PMI rate was 35.7% (10 cases). There were no statistically significant differences in the incidence of overall angiographic complications that could be documented at the end of the procedure for patients who had TVMI within 1 month (3.1% vs. 1.7%; p = 0.14) (Table 3). The incidence of ST tended to be higher in the scaffold oversize group than in the scaffold nonoversize group (Table 2) (1.54% vs. 0.51%, OR: 3.03 [0.83 to 11.05]; p =0.10). The acute definite ST rate was 0.15% and 0% in the scaffold oversize group and the scaffold nonoversize group, respectively (p = 1.0). Subacute and late definite ST were not significantly different among the 2 groups (Online Table 3). A case of a definite early ST is shown in Figure 5.

When the appropriateness of scaffold size was defined by nominal scaffold diameter within 0.5 mm of Dmax, there was no statistically significant difference in MACE between the 2 groups, (appropriate 4.5% vs. inappropriate 6.3%; p = 0.20). When the cutoff of 0.4 mm is used, there was a significant difference in MACE between appropriate and inappropriate scaffold deployment (3.4% vs. 6.8%; p = 0.006) (Online Figures 1 and 2, Online Table 3).

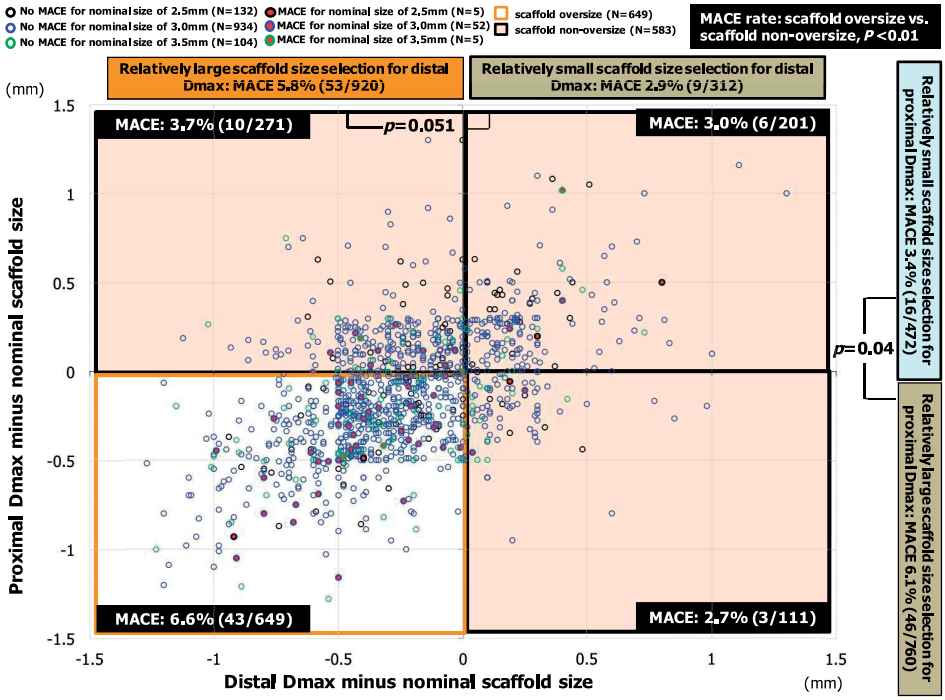

Figure 3. Distribution of the Difference Between Dmax and Nominal Scaffold.
Distribution of proximal and distal Dmax measurements minus nominal scaffold size in patients with or without major adverse cardiac events is shown. When the appropriateness of scaffold size was defined by nominal scaffold diameter within 0.5 mm of Dmax, the differences between the distal Dmax and nominal scaffold size are plotted on the y-axis and x-axis, respectively. The red filled circles represent the patients who experienced ID-MACE at 1 year. The graphical presentation demonstrates that major adverse cardiac events (MACE) were more frequently observed in patients in whom both proximal and distal Dmax were smaller than the device nominal size (6.6% vs. 3.3%, p < 0.01) (lower left quadrant). Dmax = maximal lumen diameter; ID-MACE = ischemia-driven major adverse cardiac event(s).

Independent predictor of mace after implantation of absorb scaffold(s)

With multivariable logistic regression analysis, the independent determinants of 1-year MACE were: implantation of the Absorb scaffold(s) in a vessel with both proximal and distal Dmax smaller than the device nominal size (OR: 2.13, 95% CI: 1.22 to 3.70; p < 0.01) and overlapping scaffolds (OR: 2.10, 95% CI: 1.17 to 3.80; p = 0.01) (Table 4).

DISCUSSION

The main findings of this study are: 1) 52.7% (n = 649) of patients had an "oversize" scaffold implantation; 2) The MACE and MI rates at 1 year were significantly higher in the scaffold

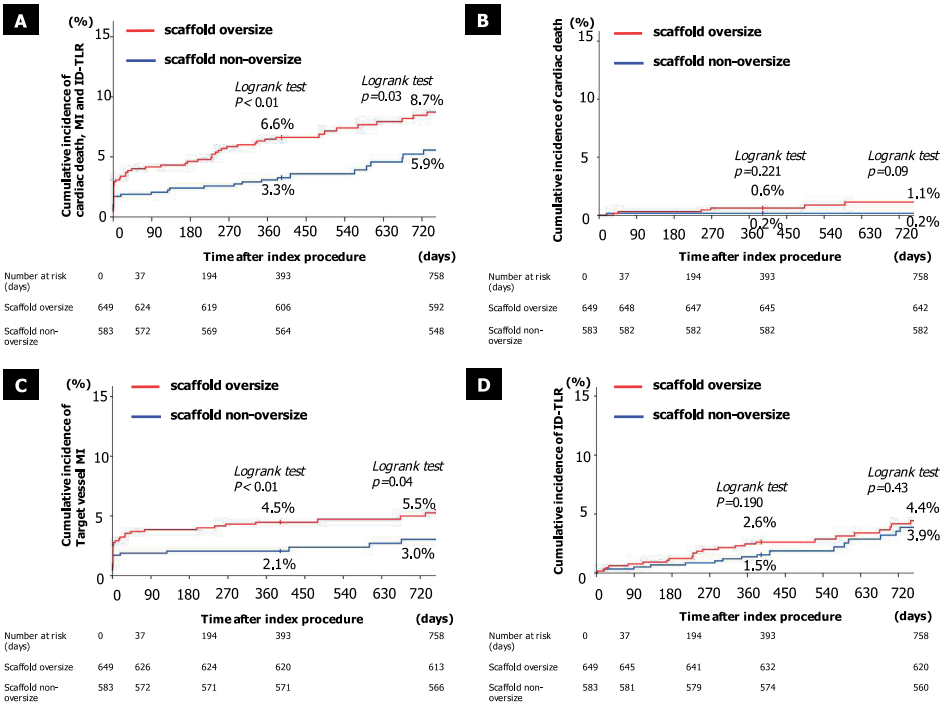

Figure 4. Time-to-Event Curves of MACE and Its Components

Time-to-event curves of MACE (A) and its components (B: death, C: target vessel MI; D: ID-TLR) at 2 years, according to study group. ID-TLR = ischemia-driven target lesion revascularization; MACE = major adverse cardiac event(s); MI = myocardial infarction.

oversize group than in the scaffold nonoversize group (MACE: 6.6% vs. 3.3%, log-rank p < 0.01, all MI: 4.6% vs. 2.4%; log-rank p = 0.04), mainly driven by a higher rate of MI within 1 month after the procedure (3.5% vs. 1.9%; p = 0.08); the incidence of definite ST tended to be higher in the scaffold oversize group than in the scaffold nonoversize group (1.54% vs. 0.51%,OR: 3.03 [0.83 to 11.05]; p = 0.10); 3) The independent determinants of MACE were both Dmax smaller than the device nominal size (OR: 2.13, 95% CI: 1.22 to 3.70; p < 0.01) and overlapping scaffolds (OR: 2.10, 95% CI:1.17 to 3.80; p = 0.01).

As illustrated in the scaffold oversize group in Figure 3, proximal and distal Dmax were significantly smaller than in the scaffold nonoversize group (proximal Dmax: 2.66 ± 0.30 mm vs. 3.11 ± 0.34 mm; p < 0.01, distal Dmax: 2.58 ± 0.31 mm vs. 2.94 ± 0.38 mm; p < 0.01, respectively) (Table 1). In the population described in the scaffold oversize group, 2.5-mm device size scaffolds were less frequently selected (8.6% vs. 13.9%; p < 0.01) as compared with 3.0-mm scaffolds (82.4% vs. 77.4%; p = 0.03). In the scaffold oversize group, acute gain normalized for preprocedural reference vessel diameter was higher (0.46 ± 0.14 vs. 0.44 ± 0.14; p = 0.02) and bailout treatment with metallic stents was more

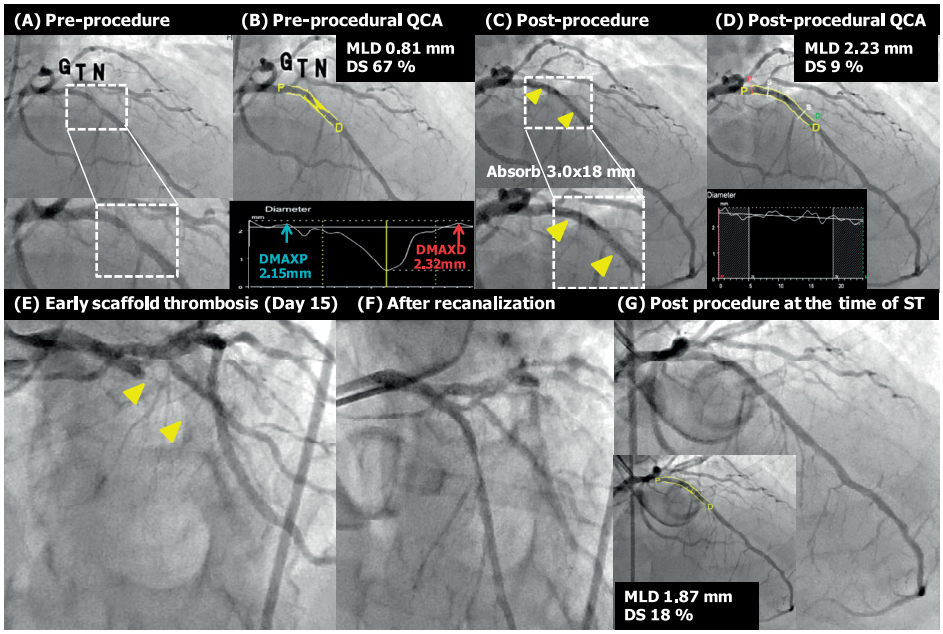

Figure 5. A Case Example of a Definite Early Thrombosis of Absorb Scaffold Implanted in the Mid-LAD
The patient received a 3.0-mm device in a too-small vessel (proximal and distal Dmax 2.15 mm and 2.32 mm, respectively [A and B]). After Absorb scaffold implantation (C and D, arrowheads), QCA showed an excellent result with a residual DS of 9%. Fifteen days after the procedure, the patient presented with a STEMI due to early scaffold thrombosis (E) that was treated with a manual aspiration only (F and G). DS =diameter stenosis; LAD =left anterior descending coronary artery; ST =scaffold thrombosis; STEMI =ST-segment elevation myocardial infarction; other abbreviations as in Figure 1.

frequently performed (1.9% vs. 0.7%; p = 0.08) compared with the nonoversize group (Table 1). Implanting Absorb scaffold(s) in a vessel with both proximal and distal Dmax smaller than the device nominal size may cause edge dissections due to the higher balloon/device–artery ratio during scaffold deployment.

Retrospective subanalysis [8] of the ABSORB Cohort B study demonstrated that after implantation of a 3.0 × 18-mm device, patients with a Dmax ranging between 2.5 and 3.3 mm had better acute OCT outcomes as compared with patients with a Dmax out of range. The implantation of a "small" Absorb scaffold in a relatively large vessel can cause incomplete strut apposition at the edge and may be associated with scaffold disruption [9] when aggressive postdilation with a larger balloon is attempted to correct such malapposition (Figure 6A). Conversely, implantation of a "large" Absorb scaffold in a relatively small vessel can cause vessel injury or underexpansion of the scaffold (Figure 6B).

Table 2. Incidence of clinical events at 1 year

Clinical outcomes	Scaffold oversize group (N=649)		Scaffold non-oversize group (N=583)		OR [95%CI]	p value
	% (n)	95% CI	% (n)	95% CI		
Cardiac Death	0.62 (4)	0.17-1.57	0.17 (1)	0.00-0.95	3.61 [0.40-32.39]	0.38
Myocardial infarction	4.62 (30)	3.14-5.53	2.40 (14)	1.32-4.00	1.97 [1.03-3.75]	0.049
QMI	1.23 (8)	0.53-2.41	0.34 (2)	0.04-1.23	3.63 [0.77-17.14]	0.11
NQMI	3.39 (22)	2.14-5.09	2.06 (12)	1.07-3.57	1.67 [0.82-3.40]	0.17
TVMI	4.47 (29)	3.01-6.35	2.06 (12)	1.07-3.57	2.23 [1.13-4.40]	0.025
Ischemia Driven TLR	2.62 (17)	1.53-4.16	1.54 (9)	0.71-2.91	1.72 [0.76-3.88]	0.23
Composite of cardiac death, all MI and clinically indicated target lesion revascularization (MACE)	6.63 (43)	4.84-8.82	3.26 (19)	1.97-5.04	2.11 [1.21-3.66]	< 0.01
Composite of cardiac death, target vessel MI and clinically indicated target lesion revascularization (DoCE)	6.32 (41)	4.57-8.47	2.92 (17)	1.71-4.63	2.25 [1.26-3.99]	< 0.01
Composite of all death, all MI and all revascularization (PoCE)	8.01 (52)	6.04-10.37	4.46 (26)	2.93-6.47	1.87 [1.15-3.03]	0.01
Scaffold thrombosis, n (%)	1.54 (10)	0.74-2.82	0.51 (3)	0.11-1.50	3.03 [0.83-11.05]	0.10
Definite ST	0.92 (6)	0.34-2.00	0.51 (3)	0.11-1.50	1.80 [0.45-7.25]	0.51
Probable ST	0.31 (2)	0.04-1.11	0 (0)	0.00-1.01	NA	1.0
Possible ST	0.31 (2)	0.04-1.11	0 (0)	0.00-1.01	NA	1.0

Incidence of clinical events at 1 year are according to the distribution of Dmax measurements minus the nominal scaffold size in the scaffold oversize group versus the scaffold nonoversize group. CI = confidence interval; Dmax = maximal lumen diameter; DoCE = device-oriented composite endpoint; MACE = major adverse cardiac event(s); MI = myocardial infarction; NQMI = non–Q-wave myocardial infarction; OR = odds ratio; PoCE = patient-oriented composite endpoint; QMI = Q-wave myocardial infarction; ST = scaffold thrombosis; TLR = target lesion revascularization; TVMI = target vessel myocardial infarction

Clinical outcomes with respect to dmax.

The present study clearly demonstrates that implanting Absorb scaffold(s) in a vessel with both proximal and distal Dmax smaller than the device nominal size (OR: 2.13, 95% CI: 1.22 to 3.70; nominal size is associated with a higher risk of IDMACE (6.6% vs. 3.3%; $p < 0.01$). The difference in 1-year MACE was observed in the scaffold oversize group and was mainly driven by a higher MI rate (4.5% vs. 2.1%; $p < 0.01$). Scaffold expansion below nominal diameters can lead to a denser polymer surface pattern and a higher polymer-toartery ratio (Online Figure 3). Furthermore, the expanding radial force may be suboptimal in these underdeployed configurations; presumably, these unfavorable final expansion diameters might cause micro thrombus formation at the strut level and

Table 3. Incidence of TVMI

	Scaffold oversize group (N=649)	Scaffold non-oversize group (N=583)	P value
TVMI at 12 months after index procedure	4.5 (29)	2.1(12)	0.025
TVMI within 1 month after index procedure	3.5 (23)	1.9 (11)	0.08
TVMI between 1 month and 12 months after index procedure	0.9 (6)	0.2(1)	0.13
Overall angiographic complications at the end of procedure for TVMI within 1 month	3.1 (20)	1.7 (10)	0.14
Side branch occlusion	2.3 (15)	1.4 (8)	0.29
Coronary dissection	1.1 (7)	0.3 (2)	0.18
Side branch occlusion + coronary dissection	0.3(2)	0 (0)	0.50
Device non-related angiographic complications for TVMI within 1 month Coronary dissection due to balloon dilatation	0.3 (2)	0.3 (2)	1.0

Values are % (n). Abbreviations as in Table 2.

side-branch occlusion. However, no statistically significant difference in the incidence of overall angiographic complications could be documented at the end of the procedure for the patients who sustained MI within 1 month (scaffold oversize group: 3.1% vs. scaffold nonoversize group: 1.7%; p = 0.14) (Table 3).

With multivariable logistic regression analysis, the independent determinants of 1-year MACE were: implantation of an Absorb scaffold(s) in a vessel with both proximal and distal Dmax smaller than device nominal size (OR: 2.13, 95% CI: 1.22 to 3.70; p < 0.01) and overlapping scaffolds (OR: 2.10, 95% CI: 1.17 to 3.80; p = 0.01) (Table 4). Of note, in a juvenile porcine model, overlapping Absorb scaffolds showed delayed healing on histology and with OCT assessment and slower tissue coverage than nonoverlapping scaffolds. Indeed, the neoendothelial coverage of the overlapping segments was 80.1% and 99.5% at 28 and 90 days after implantation, respectively; accordingly, coverage in humans may need up to 18 months to be completed[16]. Among the 62 patients with MACE, MI occurred in 14 (22.6%) patients who were treated with overlapping scaffolds and were mainly PMI (12 [19.4%]). Thus, overlapping of scaffolds might be a contributing factor of MACE.

Practical implications of the selection of appropriately sized absorb scaffolds.

Previously, we have focused mainly on the upper limit of 0.5 mm Dmax due to the well-known issues of device malapposition and disruption in case of over dilation. However, scaffold underexpansion due to the deployment of a scaffold in a vessel with a smaller size, may be associated with a higher post-procedural MI rate due to several different mechanisms. The oversized scaffold could create vessel dissection or microperforation in a small target vessel. Alternatively, the underexpansion of the scaffold may lead to a

Table 4. Predictors of MACE after implantation of the Absorb scaffold(s)

	Univariate logistic regression		Multivariate logistic regression	
	OR (95% CI)	p-value	OR (95% CI)	p-value
Patient-related factors				
Age (yrs)	1.01(0.98-1.03)	0.64		
Male	0.83(0.47-1.46)	0.52	-	-
Current smoker	0.80(0.42-1.53)	0.51	-	-
Hypertension requiring treatment	1.00(0.90-1.10)	0.96	-	-
Dyslipidemia requiring treatment	1.54(0.84-2.83)	0.16	-	-
Any diabetes mellitus	0.78(0.42-1.46)	0.44	-	-
Unstable Angina	0.69(0.35-1.34)	0.27	-	-
Prior myocardial infarction	1.01(0.99-1.04)	0.20	-	-
Lesion-related factor assessed by angiography				
Pre-procedural Diameter Stenosis (%)	0.99(0.97-1.02)	0.55	-	-
Pre-procedural Minimum Lumen Diameter (mm)	0.76(0.33-1.72)	0.51	-	-
Obstruction length (mm)	0.99(0.94-1.04)	0.64	-	-
Smallest Dmax (out of proximal and distal)	0.51(0.22-1.14)	0.10	-	-
Angulation ≥ 45 degree	0.64(0.09-4.81)	0.67	-	-
Moderate / severe calcification	0.65(0.28-1.54)	0.33	-	-
Pre-procedural visible thrombus	0.94(0.12-7.13)	0.95	-	-
Bifurcation lesion	CS	CS	-	-
Type B2/C lesion	1.02(0.61-1.71)	0.93	-	-
Left anterior descending artery	0.73(0.43-1.23)	0.24	-	-
Nominal scaffold size/post-procedural MLD	3.11(0.73-13.16)	0.12	-	-
Treatment-related factors				
Treatment with overlapping devices	2.08(1.15-3.75)	0.02	2.10(1.17-3.80)	0.01
2.5 mm device implanted	0.69(0.27-1.75)	0.44	-	-
Implanting Absorb scaffold(s) in a vessel with both proximal and distal Dmax smaller than nominal size of the device	2.11(1.21-3.66)	0.01	2.13(1.22-3.70)	<0.01

CS = complete separation; ITT = intention to treat; MLD = minimal lumen diameter; other abbreviations as in Table 2.

denser polymer surface pattern and a larger strut footprint to vessel surface area causing side branch occlusion or microthrombus formation.

In the present study, the size selection of Absorb scaffolds with the cutoff value of 0.5-mm Dmax has been shown to be clinically relevant. As presented in the Results and Online Appendix, more events were observed when the mismatch between the device and the vessel size was beyond 0.4 mm. It could therefore be recommended that the device–vessel mismatch regarding Dmax should be within 0.4 mm.

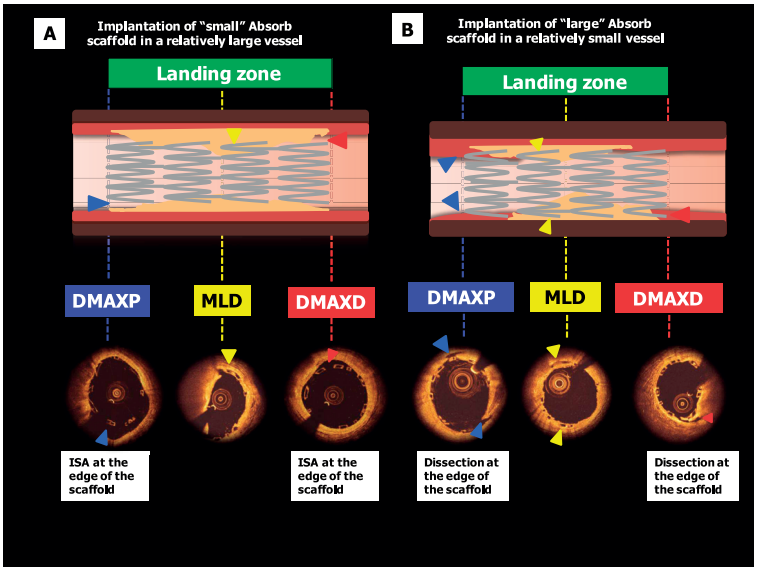

Figure 6. The Potential Consequences of a Device–Vessel Mismatch Implantation
Implantation of a too "small" Absorb scaffold in a relatively large vessel can cause incomplete apposition of the device edges (A, top panel, blue and red arrowheads). Incomplete scaffold apposition (blue and red arrow heads) and scaffold under-expansion (yellow arrowhead) are visible in the OCT images (A, bottom panel). Implantation of a too "large" Absorb scaffold in a relatively small vessel can cause vessel injury (B, top panel, blue and red arrowheads). Edge dissections (blue and red arrowheads) are visible in the OCT images (B, bottom panel). ISA =incomplete scaffold apposition; OCT =optical coherence tomography; other abbreviations as in Figure 1.

The current analysis showed that the device–vessel mismatch regarding the pre-procedural angiography has a clinical impact. There were no differences in MACE in the population with a post-procedure diameter stenosis ≥10% and <10% (MACE: 5.3% vs. 4.1%; p = 0.46) or in patients with a diameter stenosis ≥20% and <20% (MACE: 5.14% vs. 4.69%; p = 0.77). Therefore, the observed relationship between device–vessel mismatch and clinical outcomes seems to specifically relate to pre-procedural angiographic measurement. It is still unclear how far the pre-procedural device–vessel mismatch could be corrected by postdilation with high-pressure or low-pressure balloons. Currently, operators with a large experience of BRS implantation are intuitively promoting a strategy of a high-pressure post-dilation with a noncompliant balloon size 0.25 or 0.5 mm larger than the nominal size of the device. A randomized trial on post-dilation strategy (systematic vs. nonsystematic) will be able to clarify what the optimal implantation technique or this polymeric coronary device is.

It has been shown that QCA underestimates coronary lumen diameter, whereas OCT provides correct assessment of lumen dimension [17]. Mattesini et al. [18,19] reported that when OCT is used to guide and optimize Absorb scaffold implantation, postimplan-

tation area stenosis, minimal lumen area, and eccentricity index were similar to those observed after deployment of second-generation metallic drug eluting stents. The different approach for lesion preparation and routine use of OCT guidance during Absorb scaffold implantation might have contributed to these results. In addition, recent studies demonstrated with multivariable analysis that persistent dissections shown by OCT were independent predictors of PMI (OR: 5.3, 95% CI: 1.2 to 24.3), raising concerns about the relationship between these minor vessel injuries and a potential higher risk of early TVMI [20]. Taking into account the weakness of QCA for accurately measuring vessel lumen dimension and its inability to assess incomplete scaffold apposition and/or acute scaffold disruption, coregistration [21] of OCT imaging and x-ray angiography may be useful for optimizing the percutaneous treatment of coronary artery disease with bioresorbable vascular scaffolds. In future studies, a clinical scientific question would be whether the pre-procedural usage of intravascular imaging could further improve clinical outcomes.

Study limitations.

The current study does not provide mechanistic data to support the occurrence of clinical adverse events caused by sizing mismatch due to a lack of routine intravascular imaging (e.g., intravascular ultrasound, OCT, etc.). Further investigation using intravascular imaging is needed to establish the relationship between acute mechanistic complications (such as underexpansion, dissection, and malapposition, and so on) and late adverse events.

CONCLUSIONS

Selection of an appropriate scaffold size according to the vessel Dmax showed a trend toward less frequent ID-TLR, whereas implantation of an oversized Absorb scaffold in a relatively small vessel may be associated with a higher risk of MACE at 1 year. The current results need to be confirmed in the large-scale randomized trials that are on-going, and the mechanistic etiologies should be further elucidated in imaging studies.

PERSPECTIVES

WHAT IS KNOWN? QCA-Dmax–guided scaffold size selection has been proposed to optimize the scaffold implantation procedure. However, the relationship between clinical outcomes and QCA-Dmax is unknown.

WHAT IS NEW? The device-vessel size mismatch has an impact on clinical event after implantation of Absorb scaffold.

WHAT IS NEXT? The current results should be confirmed in large-scale randomized trials, and the mechanistic etiologies should be further elucidated in studies using intravascular imaging.

REFERENCES

1. Serruys PW, Chevalier B, Dudek D, et al. A bioresorbable everolimus-eluting scaffold versus a metallic everolimus-eluting stent for ischaemic heart disease caused by de-novo native coronary artery lesions (ABSORB II): an interim 1-year analysis of clinical and procedural secondary outcomes from a randomised controlled trial.Lancet 2015;385:43–54.
2. Serruys PW, Onuma Y, Garcia-Garcia HM, et al. Dynamics of vessel wall changes following the implantation of the Absorb everolimus-eluting bioresorbable vascular scaffold: a multi-imaging modality study at 6, 12, 24 and 36 months.EuroIntervention 2014;9:1271–84.
3. Onuma Y, Dudek D, Thuesen L, et al. Five-year clinical and functional multislice computed tomography angiographic results after coronary implantation of the fully resorbable polymeric everolimus-eluting scaffold in patients with de novo coronary artery disease: the ABSORB cohort A trial. J Am Coll Cardiol Intv 2013;6:999–1009.
4. Serruys PW, Onuma Y, Dudek D, et al. Evaluation of the second generation of a bioresorbable everolimus-eluting vascular scaffold for the treatment of de novo coronary artery stenosis: 12-month clinical and imaging outcomes. J Am Coll Cardiol 2011;58:1578–88.
5. Serruys PW, Ormiston JA, Onuma Y, et al. A bioabsorbable everolimus-eluting coronary stent system (ABSORB): 2-year outcomes and results from multiple imaging methods. Lancet 2009;373:897–910.
6. Ormiston JA, Serruys PW, Regar E, et al.A bioabsorbable everolimus-eluting coronary stent system for patients with single de-novo coronary artery lesions (ABSORB): a prospective open-label trial. Lancet 2008;371:899–907.
7. Abizaid A, Costa JR Jr., Bartorelli AL, et al. The ABSORB EXTEND study: preliminary report of the twelve-month clinical outcomes in the first 512 patients enrolled. EuroIntervention 2015;10:1396–401.
8. Gomez-Lara J, Diletti R, Brugaletta S, et al. Angiographic maximal luminal diameter and appropriate deployment of the everolimus-eluting bioresorbable vascular scaffold as assessed by optical coherence tomography: an ABSORB cohort B trial sub-study. EuroIntervention 2012;8:214–24.
9. Onuma Y, Serruys PW, Muramatsu T, et al. Incidence and imaging outcomes of acute scaffold disruption and late structural discontinuity after implantation of the absorb everolimus-eluting fully bioresorbable vascular scaffold: optical coherence tomography assessment in the ABSORB Cohort B trial (A Clinical Evaluation of the Bioabsorbable Everolimus Eluting Coronary Stent System in the Treatment of Patients With De Novo Native Coronary Artery Lesions). J Am Coll Cardiol Intv 2014;7:1400–11.
10. Diletti R, Serruys PW, Farooq V, et al. ABSORB II randomized controlled trial: a clinical evaluation to compare the safety, efficacy, and performance of the Absorb everolimus-eluting bioresorbable vascular scaffold system against the XIENCE everolimus-eluting coronary stent system in the treatment of subjects with ischemic heart disease caused by de novo native coronary artery lesions: rationale and study design. Am Heart J 2012;164:654–63.
11. Farooq V, Gomez-Lara J, Brugaletta S, et al. Proximal and distal maximal luminal diameters as a guide to appropriate deployment of the ABSORB everolimus-eluting bioresorbable vascular scaffold:a sub-study of the ABSORB Cohort B and the on-going ABSORB EXTEND Single Arm Study. Catheter Cardiovasc Interv 2012;79:880–8.
12. Vranckx P, Farooq V, Garg S, et al. Different cardiac biomarkers to detect peri-procedural myocardial infarction in contemporary coronary stent trials: impact on outcome reporting. Heart 2012;98:1424–30.

13. Vranckx P, Kint PP, Morel MA, Van Es GA, Serruys PW, Cutlip DE. Identifying stent thrombosis, a critical appraisal of the academic research consortium (ARC) consensus definitions: a lighthouse and as a toe in the water. EuroIntervention 2008;4 Suppl C:C39–44.
14. Applegate RJ, Sacrinty MT, Little WC, Santos RM, Gandhi SK, Kutcher MA. Incidence of coronary stent thrombosis based on academic research consortium definitions. Am J Cardiol2008;102:683–8.
15. Mauri L, Hsieh WH, Massaro JM, Ho KK, D'Agostino R, Cutlip DE. Stent thrombosis in randomized clinical trials of drug-eluting stents. N Engl J Med 2007;356:1020–9.
16. FarooqV, SerruysPW,HeoJH, et al. Intracoronary optical coherence tomography and histology of overlapping everolimus-eluting bioresorbable vascular scaffolds in a porcine coronary artery-model: the potential implications for clinical practice. J Am Coll Cardiol Intv 2013;6:523–32.
17. Tsuchida K, van der Giessen WJ, Patterson M, et al. In vivo validation of a novel threedimensional quantitative coronary angiography system (CardiOp-B): comparison with a conventional two-dimensional system (CAAS II) and with special reference to optical coherence tomography. EuroIntervention 2007;3:100–8.
18. Mattesini A, Pighi M, Konstantinidis N, et al. Optical coherence tomography in bioabsorbable stents: mechanism of vascular response and guidance of stent implantation. Minerva Cardioangiol 2014;62:71–82.
19. Mattesini A, Secco GG, Dall'Ara G, et al. ABSORB biodegradable stents versus secondgeneration metal stents: a comparison study of 100 complex lesions treated under OCT guidance. J Am Coll Cardiol Intv 2014;7:741–50.
20. Porto I, Di Vito L, Burzotta F, et al. Predictors of periprocedural (type IVa) myocardial infarction, as assessed by frequency-domain optical coherence tomography. Circ Cardiovasc Interv 2012;5: 89–96, S1–6.
21. Hebsgaard L, Nielsen TM, Tu S, et al. Coregistration of optical coherence tomography and X-ray angiography in percutaneous coronary intervention. The Does Optical Coherence Tomography Optimize Revascularization (DOCTOR) fusion study. Int J Cardiol 2014;182C:272–8.

Online Appendix. Table 1. Incidence of clinical events at 1 year based on the appropriateness of the scaffold size selection within 0.5 mm

	appropriately-sized (cutoff 0.5mm) (n=867 pts)		inappropriately-sized (cutoff 0.5 mm) (n=365 pts)			
Clinical outcomes	% (n)	95% CI	% (n)	95% CI	OR [95%CI]	p value
Cardiac Death	0.35 (3)	0.07-1.01	0.55 (2)	0.07-1.96	1.58 [0.26-9.54]	0.64
Myocardial infarction	3.23 (28)	2.16-4.63	4.38 (16)	2.53-7.02	1.37 [0.73-2.57]	0.32
QMI	0.69 (6)	0.25-1.50	1.10 (4)	0.30-2.78	1.59 [0.45-5.67]	0.49
NQMI	2.54 (22)	1.60-3.82	3.29 (12)	1.71-5.67	1.31 [0.64-2.68]	0.45
TVMI	3.00 (26)	1.97-4.36	4.11 (15)	2.32-6.69	1.39 [0.72-2.65]	0.38
Ischemia Driven TLR	1.61 (14)	0.89-2.69	3.29 (12)	1.71-5.67	2.07 [0.95-4.52]	0.08
Composite of cardiac death, all MI and clinically indicated target lesion revascularization (MACE)	4.50 (39)	3.22-6.10	6.30 (23)	4.04-9.31	1.26 [0.73-2.20]	0.20
Composite of cardiac death, target vessel MI and clinically indicated target lesion revascularization (DoCE)	4.38 (38)	3.12-5.97	5.48 (20)	3.38-8.34	1.43 [0.84-2.43]	0.46
Composite of all death, all MI and all revascularization (PoCE)	5.77 (50)	4.31-7.53	7.67 (28)	5.16-10.90	1.36 [0.84-2.19]	0.25
Scaffold thrombosis	1.04 (9)	0.48-1.96	1.10 (4)	0.30-2.78	1.06[0.32-3.45]	1.0
-Definite ST	0.58 (5)	0.19-1.34	1.10 (4)	0.30-2.78	1.91[0.51-7.15]	0.46
-Probable ST	0.23 (2)	0.03-0.83	0 (0)	0.00-1.01	NA	1.0
-Possible ST	0.23 (2)	0.03-0.83	0 (0)	0.00-1.01	NA	1.0

QMI: Q-wave myocardial infarction; NQMI: non-Q-wave myocardial infarction; TVMI: target vessel myocardial infarction; TIR: target lesion revascularization; MACE: major adverse cardiac events; MI: myocardial infarction;; DoCE: device oriented composite end point; PoCE: patient oriented composite end point; ST: scaffold thrombosis.

Online Appendix. Table 2. Incidence of clinical events at 1 year based on the appropriateness of the scaffold size selection within 0.4 mm

	appropriately-sized (cutoff 0.4 mm) (n=645 pts)		inappropriately-sized (cutoff 0.4 mm) (n=587pts)			
Clinical outcomes	% (n)	95% CI	% (n)	95% CI	OR [95%CI]	p value
Cardiac Death	0.31 (2)	0.04-1.12	0.51 (3)	0.11-1.49	1.65 [0.28-9.92]	0.67
Myocardial infarction	2.79 (18)	1.66-4.37	4.43 (26)	2.91-6.42	1.61 [0.88-2.98]	0.13
QMI	0.78 (5)	0.25-1.80	0.85 (5)	0.28-1.98	1.10 [0.32-3.82]	1.00
NQMI	2.02 (13)	1.08-3.42	3.58 (21)	2.23-5.42	1.80 [0.90-3.64]	0.12
TVMI	2.64 (17)	1.54-4.19	4.09 (24)	2.64-6.02	1.58 [0.84-2.96]	0.20
Ischemia Driven TLR	1.09 (7)	0.44-2.22	3.24 (19)	1.96-5.01	3.05 [1.27-7.31]	0.01
Composite of cardiac death, all MI and clinically indicated target lesion revascularization (MACE)	3.57 (23)	2.27-5.30	6.64 (39)	4.77-8.97	1.93 [1.14-3.26]	0.02
Composite of cardiac death, target vessel MI and clinically indicated target lesion revascularization (DoCE)	3.26 (21)	2.03-4.93	6.30 (37)	4.48-8.58	2.00 [1.16-3.46]	0.02
Composite of all death, all MI and all revascularization (PoCE)	4.65 (30)	3.16-6.57	8.18 (48)	6.09-10.70	1.83 [1.14-2.92]	0.01
Scaffold thrombosis	1.09 (7)	0.44-2.22	1.02 (6)	0.38-2.21	0.94 [0.32-2.82]	1.00
-Definite ST	0.78 (5)	0.25-1.80	0.58 (4)	0.19-1.74	0.88 [0.24-3.29]	1.00
-Probable ST	0.16 (1)	0.00-0.86	0.17 (1)	0.00-0.95	1.10 [0.07-17.6]	1.00
-Possible ST	0.16 (1)	0.00-0.86	0.17 (1)	0.00-0.95	1.10 [0.07-17.6]	1.00

QMI: Q-wave myocardial infarction; NQMI: non-Q-wave myocardial infarction; TVMI: target vessel myocardial infarction; TIR: target lesion revascularization; MACE: major adverse cardiac events; MI: myocardial infarction;; DoCE: device oriented composite end point; PoCE: patient oriented composite end point; ST: scaffold thrombosis.

Online Appendix. Table 3. The incidence rate of stent thrombosis according to the distribution of Dmax measurements minus nominal scaffold size of patients who received a scaffold in a vessel with both proximal and distal Dmax smaller than device nominal size (scaffold oversize group) vs. the others (scaffold non-oversize group)

	scaffold oversize group		scaffold non-oversize group		
	(n=649 pts)		(N=583 pts)		
Variable	% (n)	95% CI	% (n)	95% CI	p value
Definite ST	0.92 (6)	0.34-2.00	0.51 (3)	0.11-1.50	0.51
Probable ST	0.31 (2)	0.04-1.11	0 (0)	0.00-0.63	0.50
Possible ST	0.31 (2)	0.04-1.11	0 (0)	0.00-0.63	0.50
Acute	0.15 (1)	0.00-0.86	0 (0)	0.00-0.63	1.00
-Definite	0.15 (1)	0.00-0.86	0 (0)	0.00-0.63	1.00
-Probable	0 (0)	0.00-0.57	0 (0)	0.00-0.63	NA
-Possible	0 (0)	0.00-0.57	0 (0)	0.00-0.63	NA
Subacute	0.62 (4)	0.17-1.57	0.34 (2)	0.04-1.23	0.69
-Definite	0.46 (3)	0.10-1.35	0.34 (2)	0.04-1.23	1.00
-Probable	0.15 (1)	0.00-0.86	0 (0)	0.00-0.63	1.00
-Possible	0 (0)	0.00-0.57	0 (0)	0.00-0.63	NA
Late	0.77 (5)	0.25-1.79	0.17 (1)	0.00-0.95	0.22
-Definite	0.31 (2)	0.04-1.11	0.17 (1)	0.00-0.95	1.00
-Probable	0.15 (1)	0.00-0.86	0 (0)	0.00-0.63	1.00
-Possible	0.31 (2)	0.04-1.11	0 (0)	0.00-0.63	0.50

Scaffold thrombosis was categorized as acute (< 1 day), subacute (1-30 days) and late (31 to 365 days) and was defined according to the ARC guidelines as follows: definite: acute coronary syndrome and angiographic or pathologic confirmation of scaffold thrombosis; probable: unexplained death ≤ 30 days or TV-MI without angiographic information

Comparisons were performed by fisher exact test.

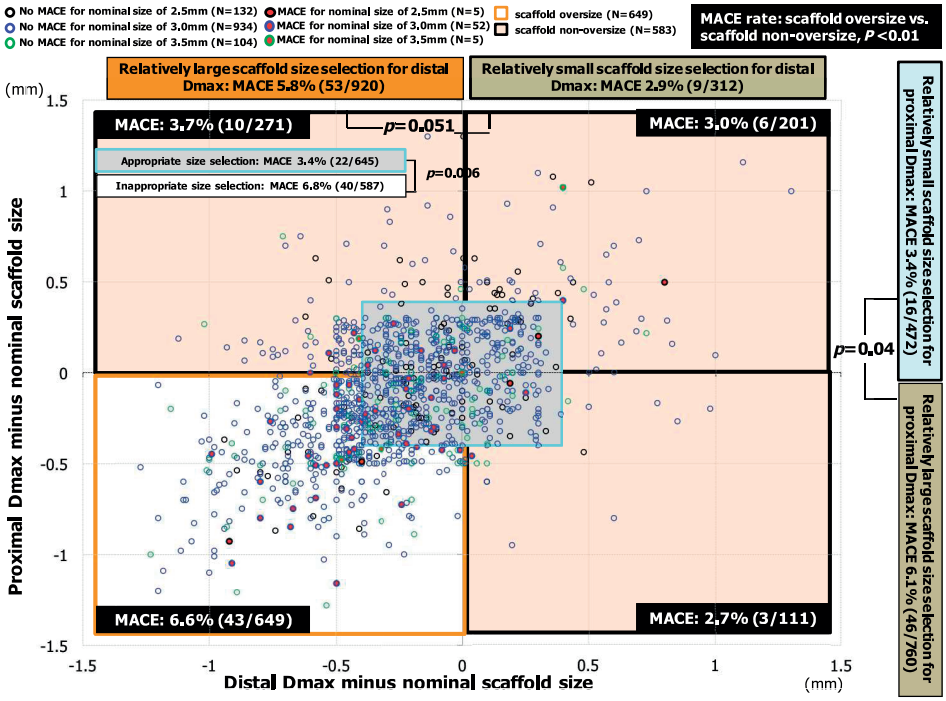

online appendix figure 1. Distribution of proximal and distal Dmax measurements minus nominal scaffold size in patients with or without major adverse cardiac events is shown. When the appropriateness of scaffold size was defined by nominal scaffold diameter within 0.4 mm of Dmax, blue box. The differences between the distal Dmax and nominal scaffold size are plotted on the Y-axis and X-axis, respectively. The red filled circles represent the patients who experienced ID-MACE at 1 year. The graphical presentation demonstrates that major adverse cardiac events were more frequently observed in patients who were categorized in inappropriate scaffold implantation group (outside blue box), the events were higher than appropriate group (inside blue box) MACE: major adverse cardiac events; Dmax: maximum lumen diameter.

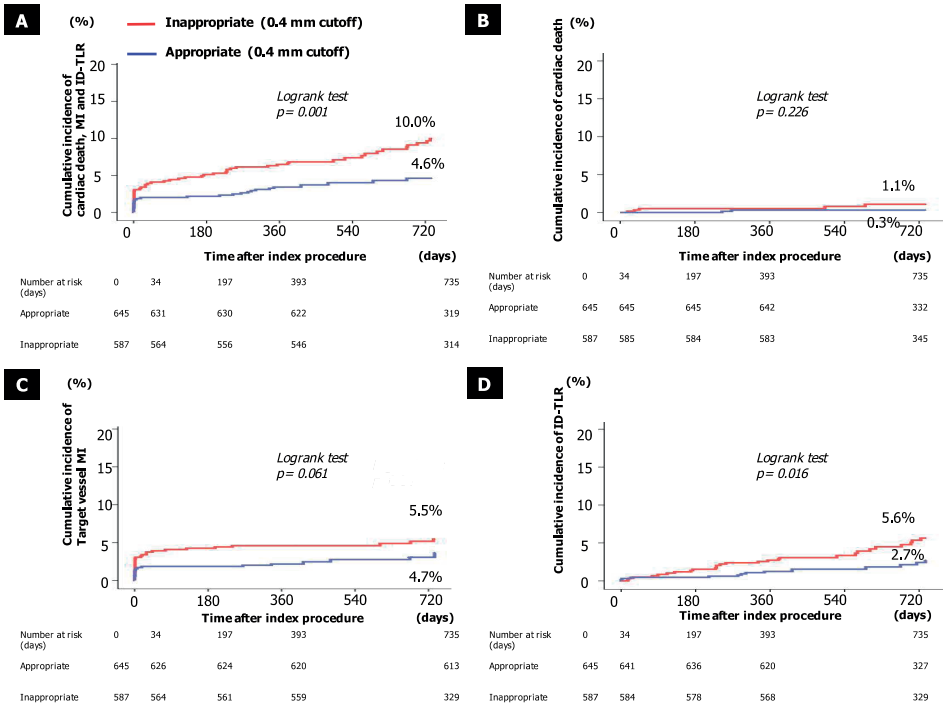

online appendix figure 2. Time-to-event curves for MACE (A) and their components (B: death, C: target vessel MI; D: ID-TLR) in patients with inappropriate or appropriate scaffold size when use 0.4 mm as a cutoff value.

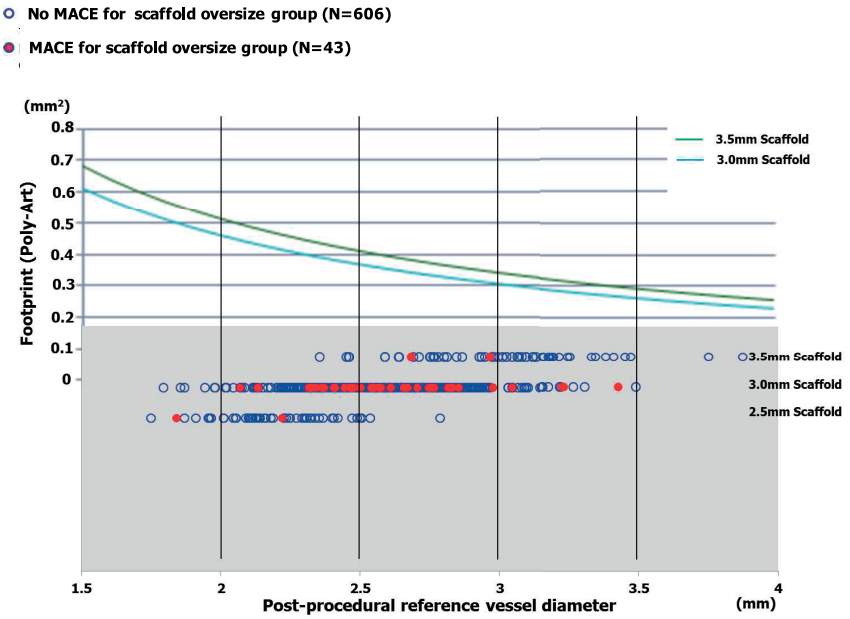

online appendix figure 3. Correlation between scaffold footprint and post-procedural reference vessel diameter in patients with "scaffold oversize group" group. Scaffold expansion below nominal diameters can lead to a denser polymer surface pattern and a higher polymer-to-artery ratio.
MACE: major adverse cardiac events

Chapter 5

Impact of devices oversizing on final device expansion between everolimus-eluting bioresorbable vascular scaffold and everolimus-eluting metallic stent in the ABSORB II trial

Pannipa Suwannasom, Yohei Sotomi, Erhan Tenekecioglu, Joanna J. Wykrzykowska, Steven Haine, Rod Stables, Adrian Banning, Alexander Ghanem, Gianluca Campo, Robbert J. de Winter, Bernard Chevalier, Yoshinobu Onuma, Patrick W. Serruys

(submitted)

ABSTRACT

Background

Implantation of the oversized bioresorbable vascular scaffolds(BVS) is associated with adverse cardiac events from angiographic-derived data. We sought to investigate the actual device expansion after implantation of oversized device as confirmed by intravascular ultrasound.

Methods and Results

Paired pre- and post-procedural intravascular ultrasound (IVUS) was performed in 451 patients (297 BVS and 154 metallic EES) in the ABSORB II trial. Device was considered oversized when both pre-procedural proximal and distal maximal lumen area were smaller than the nominal area of the device. Deployment index (DI) was calculated as minimal stent area/nominal area of the device. The incidence of major adverse cardiac events (MACE) at 1 year was analyzed in the oversized group versus the non-oversized group. The proportion of oversized device was not different between BVS(36.0%) and metallic EES(31.2%), p=0.30. The oversized group had a lower DI than in the non-oversized group (BVS[0.60±0.12 vs. 0.72±0.15, p<0.001] and EES[0.69±0.10 vs. 0.81±0.16, p<0.001]). The DI could not be corrected with post-dilation of the scaffold if the device had been oversized. Oversized scaffold group had a higher MACE rate, predominantly driven by periprocedural MI rates , than in the non-oversized scaffold group (9.3% vs. 3.7%, p=0.043). There was no significant difference in MACE observed in the metallic EES between oversized and non-oversized devices (4.2% vs. 2.8%, p=0.67).

Conclusion

Oversized scaffold/stent implantation is associated with under-deployment of devices. The correlation of device oversizing to the peri-procedural myocardial infarction rate is greater in patients treated with BVS than those treated with metallic EES.

INTRODUCTION

The bioresorbable vascular scaffold (BVS) is a novel coronary device with unique properties different from a metallic stent platform[1]. Given the limited accuracy of visual estimation of vessel sizing[2], the quantitative coronary angiography maximal lumen diameter (QCA-Dmax) was introduced in the ABSORB clinical trial program to prevent device-vessel mismatch[3, 4]. A pooled analysis in 1,232 patients from 3 cohorts (ABSORB Cohort B, ABSORB Extend and ABSORB II) demonstrated that implantation of an oversized BVS in a relatively small vessel appears to be associated with an increased in major adverse cardiac events (MACE) at 1 year, mainly driven by more frequent early MI[5]. It has been hypothesized that BVS oversizing is associated with a relative underdeployment of device[5] and contributes to high percentage of abluminal strut surface area (ASSA) in small vessels[6] . The latter may have resulted in an increase in thrombogenicity and disturbance in microcirculation[7], and potentially may have induced microthrombi and micromyocardial necrosis[8]

However, the above theoretical consideration has never been validated against the actual findings from intracoronary imaging. Furthermore, the impact of device oversizing on the final expansion between the BVS and metallic everolimus-eluting stent (EES) has never been investigated. The main objective of the present study was to investigate: 1) the actual deployment status after implantation of oversized device confirmed by intravascular ultrasound (IVUS) and; 2) the impact of device oversizing between the two stent platforms, and clinical outcomes at 1 year.

METHODS

Study design and population

The design of the ABSORB II trial has been previously described[9]. In summary, the ABSORB II trial is a prospective, single-blinded, randomized controlled trial that compared the safety and efficacy of the Absorb BVS versus the metallic EES in 501 patients having one or two de-novo native coronary lesions in different epicardial vessels with a minimum and maximum lumen diameter between 2.25 mm and 3.8 mm, respectively, as assessed by online QCA and a maximum lesion length of 48 mm. For the purpose of the study, only patients who had paired IVUS pre- and post-implantation were included in the analysis.

Study Device

The study device characteristics (Absorb BVS and Xience, Abbott Vascular, Santa Clara, CA) have been described in details previously[9]. In brief, the balloon expandable Absorb

scaffold is comprised of a Poly-L-lactide (PLLA) backbone coated with an amorphous drug-eluting coating matrix composed of Poly-D, L-lactide (PDLLA) polymer containing everolimus at 100 μg/cm^2. The control device was the second-generation everolimus-eluting stent Xience (Abbott Vascular, Santa Clara, CA), which is a balloon-expandable metallic stent, manufactured from a flexible cobalt chromium alloy, and coated with a thin non-adhesive, durable, biocompatible acrylic, and fluorinated everolimus-releasing copolymer. The Xience stent and Absorb scaffold share the similar MULTI-LINK design, and both devices are similar in terms of drug, drug dose density, and elution profile.

Imaging acquisition and analysis

IVUS image acquisition

Pre-procedural IVUS was mandatory before dilation of the target lesion. If not technically feasible (for example, the IVUS catheter could not cross the lesion), pre-dilatation with a small balloon was allowed to facilitate the IVUS catheter passage. IVUS pullbacks were performed after intracoronary injection of 200 μg nitroglycerin and acquired with a 3.2-French, 45-MHz rotational IVUS catheter (Revolution® 45 MHz; Volcano Corporation, Rancho Cordova, CA), using automated pullbacks at 0.5 mm per second and 30 frames per second. Post-procedural IVUS image was obtained after the final procedure (device implantation with or without post-dilatation). All pullbacks were analyzed off-line at 1 mm longitudinal intervals and analyzed by an independent core laboratory (Cardialysis BV, Rotterdam, The Netherlands) using a commercial software (QIvus 2.2, Medis, Leiden, The Netherlands).

Pre- and post-procedural IVUS analysis

The region of interest (ROI) of pre-procedural IVUS was co-located to the post-procedural IVUS scaffold segment by dedicated software (IvusOctRegistration, Division of Image Processing [LKEB], Leiden, The Netherlands) (see details in Figure 1). The scaffold segments were identified by the first and the last cross-sectional IVUS frame in which the scaffold/stent struts could be identified. The post-procedural region of interest was the segment beginning 5 mm distal from the scaffold segment and extending 5 mm proximal from the scaffold segment.

By using pre-procedural minimal lumen area (MLA) as a reference, the largest lumen area distal to MLA in the distal landing zone of the device was defined as distal maximal lumen area (distal Amax). The largest lumen area proximal to MLA in the proximal landing zone of the device was defined as proximal maximal lumen area (proximal Amax) (figure 1). The nominal device area at the nominal pressure was derived from the formula of $\pi(D/2)^2$. Reference lumen area (RLA) was the average of the mean lumen area between the 5 mm proximal and distal segments to the edges of the scaffold/stent according to the MUSIC study criteria[10].

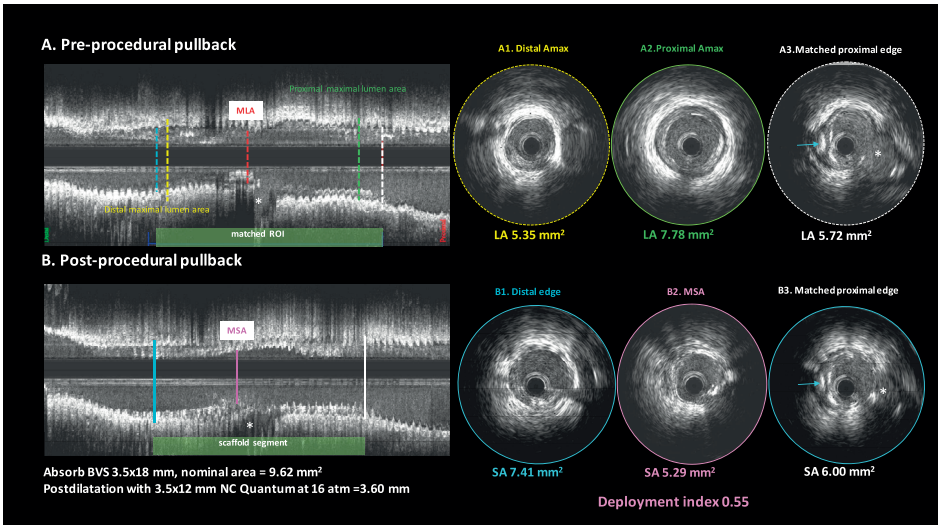

Figure 1. The calculation of Amax
The pre-procedural region of interest (ROI) (panel A) was defined by co-location of the post-procedural scaffold/stent segment (panel B). The co-location procedure was performed by matching identical landmarks, such as side-branch (white star), cardiac vein and calcium spots (blue arrow) between pre- and post-procedural IVUS. Subsequently, both IVUS pullback were synchronized by dedicated software. By using pre-procedural MLA as a reference (red line), the largest lumen area distal to MLA in the distal landing zone of the device (between red dotted line and blue dotted line in the left-hand side) was defined as distal maximal lumen area (distal Amax, yellow frame). The largest lumen area proximal to MLA in the proximal landing zone of the device (between red dotted line and white dotted line in the right-hand side) was defined as proximal maximal lumen area (proximal Amax, white frame). The nominal scaffold area was larger than the distal and proximal Amax. After implantation, the scaffold was post-dilated with non-compliance balloon 3.5x12 mm at 16 atm. Deployment index was 0.55.
Abbreviation: Amax: Maximal lumen area; MLA:minimal stent/scaffold area

The expansion of device was assessed by deployment index. Deployment index was calculated by the ratio of minimal stent or scaffold area (MSA) to the expected nominal device area at nominal pressure. Incomplete scaffold apposition (ISA) is defined as the absence of contact between the stent struts and the lumen wall[11].

Oversizing definitions

The oversizing definition in the present study was derived from QCA maximal lumen diameter as described by Ishibashi et al.(5). We used area instead of diameter in order to circumvent the limitation of QCA Dmax that use only one view to evaluate vessel size. Device was considered "oversized" when the patient received 1 or more devices in vessels in which both the pre-procedural proximal and distal Amax were smaller than the nominal area of the device. The remaining patients who did not meet above criteria were considered "non-oversizing". This group consisted of patients who had either proximal or distal areas smaller than or equal to the nominal area. When a patient received 2

or 3 overlapping Absorb scaffolds or metallic EESs in a long lesion, the nominal size of the proximally implanted device was compared with the proximal Amax, whereas the nominal size of the distally implanted device was compared with the distal Amax.

Clinical endpoints

In the present analysis, the primary clinical outcome was a composite of major adverse cardiac events (MACE) at 1 year, defined as a composite of cardiac death, any myocardial infarction (MI) and ischemia-driven target lesion revascularization (ID-TLR) by coronary bypass graft surgery or percutaneous coronary intervention. MI classification and criteria for diagnosis were defined according to the per protocol definition[9]. Definite and probable scaffold/stent thrombosis (ST) was adjudicated according to the Academic Research Consortium definitions[12]. An independent clinical events committee adjudicated all clinical outcomes.

Statistical analysis

All statistical analyses were performed using IBM SPSS Statistics, version 23.0 (IBM Corp, Armonk, NY). IVUS was analyzed per lesion. All continuous variables were presented as mean ± standard deviation (SD) or median and interquartile range (IQR; 1st to 3rd) as appropriate. Unpaired t-test or nonparametric Mann-Whitney U test were used for comparisons of continuous variables and Chi-square test was used for categorical variables. Pearson's correlation coefficient were used to evaluate the relationship between the appropriateness of device oversizing and the deployment index. Differences were considered to be statistically significant if p-value was < 0.05.

The endpoint analyses were performed according to the intention-to-treat principle and presented as a patient-level analysis. Whenever a patient received more than one lesion treatment, the lesion with the oversized implantation was selected as a representative of that patient. One-year clinical outcomes were compared between oversized and non-oversized group by the log-rank test.

RESULTS

Patient population, clinical and procedural characteristics

Out of 501 patients who were enrolled in the ABSORB-II trial, 451 had paired IVUS pre- and post-implantation. Absorb scaffolds were implanted in 297 patients whereas metallic EES were implanted in 154 patients. The proportion of patients who received oversized devices was not significantly different between the two platforms (BVS 36.0% vs. metallic EES 31.2%, p=0.30). Clinical and angiographic characteristics between the oversized device group and the non-oversized device group are detailed in Table 1.

Device-vessel mismatch and the expansion of the devices

As shown in table 2, both BVS and metallic EES oversized groups had a lower deployment index than in the non-oversized groups (BVS oversized 0.60±0.12 vs. BVS non-oversized 0.72±0.15, p<0.001; metallic EES oversized 0.69±0.10 vs. metallic EES non-oversized 0.81 ±0.16, p<0.001), which indicated an under-deployment of the devices. The relationship between the appropriateness of pre-procedural device sizing (distal Amax minus nominal scaffold or stent area) and the device deployment index was demonstrated in figure 2. There was a moderate correlation between appropriateness of pre-procedural device sizing and deployment index (BVS r=0.61, p<0.001 and metallic EES r=0.41, p<0.001). The same figures also showed that the rate of post-dilation was not different between adequately deployed and underdeployed device, suggesting that the post-dilation may have little effect to correct underdeployed device if the initial sizing was inappropriate.

Device oversizing and incidence of major adverse cardiac events

Table 3 details the incidence of clinical events at 393 days . Oversized scaffold implantation was associated with a higher risk of MACE than in the non-oversized scaffold implantation (9.3% vs. 3.7%, p=0.043) whereas there was no significant difference in MACE rate between oversized and non-oversized group in the metallic EES arm (4.2% vs. 2.8%, p=0.67). Figure 2A demonstrated that the BVS oversize with under-deployment contributed to higher event rates than other conditions (10.3% vs. 2.8%, p= 0.006) whereas the metallic EES under-deployment did not (Figure 2B). High incidence of MACE in the BVS oversized group was driven by high event rates of MI (8.4% vs. 3.2%, p=0.047), especially within 37 days after the index procedure (8.4% vs. 2.6%, p=0.024). The incidence of definite and probable ST was not significantly different between the oversized and non-oversized group for both devices, albeit event rate was too low to assess this.

The level of cardiac enzymes post-implantation between oversized and non-oversized group was compared and showed in table 4. The BVS oversized group had a higher peak CK-MB and cTn ratio than in the BVS non-oversized group whereas there were no such differences observed in metallic EES arm. When the three enzymes were subcategorised according to the per protocol (CK > 2xULN), third universal definition(cTn > 5xULN) and SCAI definition(CK-MB ≥ 10xULN, or cTn > 70x ULN)[13], there were no differences between the oversized and non-oversized and between the two platforms .

An exploratory analysis was performed in the very small vessels subgroup (either proximal or distal Amax less than 4.0 mm^2, n= 47 in BVS arm and n=19 in metallic EES arm), there were no significant differences in MACE rates between BVS and metallic EES implanted in vessel size less than 4.0 mm^2 (BVS 8.5% vs. metallic EES 5.3%, p=0.65).

Table 1 Clinical, Pre- and Post-Procedural Angiographic Characteristics and procedural details

	BVS oversize	BVS non-oversize	p-value	EES oversize	EES non-oversize	p-value	p-value oversize	p-value non-oversize
	n=107	n=190		n=48	n=106		BVS vs. EES	BVS vs. EES
Age, yrs	61.9±10.1	60.6±10.2	0.26	61.7±9.5	60.7±10.1	0.56	0.93	0.88
Male	82(76.6)	140(73.3)	0.57	35(72.9)	88(83.0)	0.15	0.62	0.07
Current smoker	25(23.4)	52(27.4)	0.45	10(20.8)	23(21.7)	0.90	0.73	0.28
Hypertension requiring treatment	72(67.3)	119(62.6)	0.42	28(58.3)	76(71.7)	0.10	0.28	0.12
Dyslipidemia requiring treatment	77(72.0)	129((67.9)	0.47	36(75.0)	80(75.5)	0.95	0.69	0.17
Any diabetes mellitus	27(25.2)	38(20.0)	0.29	11(22.9)	27(25.5)	0.73	0.76	0.28
Unstable angina	26(24.3)	34(17.9)	0.19	14(29.2)	19(17.9)	0.12	0.52	0.99
Prior history of myocardial infarction	27(25.2)	54(28.6)	0.54	17(35.4)	28(26.4)	0.26	0.19	0.69
Treated coronary								
Right coronary artery	29(27.1)	46(24.2)	0.58	11(22.9)	32(30.2)	0.35	0.58	0.26
Left anterior descending artery	42(39.3)	97(51.1)	0.05	20(41.7)	59(55.7)	0.12	0.78	0.45
Left circumflex artery	36(33.6)	47(24.7)	0.10	17(35.4)	15(14.2)	0.003	0.83	0.03
Lesion classification								
A/B1	59(55.1)	115(70.5)	0.37	31(64.6)	49(46.2)	0.04	0.27	0.02
B2/C	48(44.9)	75(39.4)	0.37	16(33.3)	56(52.8)	0.03	0.18	0.03
Calcification (moderate or severe)	15(14.0)	21(11.1)	0.45	2(4.3)	22(20.8)	0.01	0.08	0.02
Angulation ≥45°	3(2.8)	6(3.2)	0.86	1(2.1)	5(4.8)	0.44	0.81	0.49
Jailed side branches, %	0	8(4.2)	0.03	2(4.3)	3(2.9)	0.66	0.03	0.56
Procedural details								
Balloon dilation prior to device implantation	107(100.0)	190(100.0)	na	48(100.0)	104(98.1)	0.34	na	0.06
Pre-dilation nominal balloon diameter, mm	2.57±0.39	2.62±0.33	0.26	2.67±0.37	2.65±0.34	0.68	0.14	0.53
Pre-dilation balloon pressure, atm	14.4±3.1	14.2±2.9	0.14	14.5±4.3	14.3±3.4	0.15	0.85	0.76

Table 1 Clinical, Pre- and Post-Procedural Angiographic Characteristics and procedural details (continued)

	BVS oversize	BVS non-oversize	p-value	EES oversize	EES non-oversize	p-value	p-value oversize	p-value non-oversize
	n=107	n=190		n=48	n=106		BVS vs. EES	BVS vs. EES
Pre-dilation balloon length, mm	11.8±2.8	12.3±3.0	0.61	11.9±3.2	12.7±3.1	0.77	0.94	0.39
Device size 2.5 mm	16(15.0)	29(15.3)	0.94	5(10.4)	11(10.4)	0.99	0.45	0.24
Device size 3.0 mm	54(50.5)	129(67.9)	0.003	26(54.2)	73(68.9)	0.08	0.67	0.86
Device size 3.5 mm	37(34.6)	32(16.8)	0.001	17(35.4)	21(19.8)	0.04	0.92	0.52
Nominal diameter of implanted device, mm	3.10±0.34	3.01±0.28	0.02	3.13±0.32	3.04±0.27	0.11	0.64	0.28
Maximal device inflation pressure, atm	13.1±2.8	13.5±2.5	0.19	13.7±2.6	14.1±2.5	0.41	0.19	0.06
Stent length, mm	25.0±12.0	23.2±9.9	0.15	22.0±9.1	23.9±8.2	0.20	0.13	0.51
Overlapped implantation	22(20.6)	30(15.8)	0.29	5(10.4)	17(16.0)	0.36	0.12	0.96
Balloon dilation after device implantation	63(58.9)	120(63.2)	0.47	24(50.0)	70(66.0)	0.06	0.30	0.62
Post-dilation nominal balloon diameter, mm	3.20±0.38	3.17±0.30	0.62	3.34±0.42	3.28±0.38	0.46	0.13	0.04
Post-dilation balloon pressure, atm	15.4±3.1	15.3±3.2	0.71	17.2±3.2	16.7±3.3	0.47	0.02	0.004
Post-dilation balloon length, mm	13.4±4.3	13.3±2.9	0.93	13.5±4.1	14.4±3.7	0.31	0.91	0.03

Data are shown in mean±SD or medial (IQR 1st-3rd) or n(%). Abbreviation: BVS: bioresorbable vascular scaffold, Dmax: maximal lumen diameter

Table 2 IVUS findings pre- and post-implantation

	BVS oversize	BVS non-oversize	p-value	EES oversize	EES non-oversize	p-value	p-value oversize	p-value non-oversize
	n=107	n=190		n=48	n=106		BVS vs. EES	BVS vs. EES
Pre-implantation								
Proximal Amax, mm^2	6.02±1.77	8.98±2.28	<0.001	6.22±1.72	9.03±2.56	<0.001	0.51	0.87
Distal Amax, mm^2	5.21±1.61	7.11±2.47	<0.001	5.68±2.02	7.37±2.19	<0.001	0.13	0.36
Amax smaller than 4 mm^2	33(30.8)	14(7.4)	<0.001	14(29.2)	5(4.7)	<0.001	0.83	0.37
Mean lumen area, mm^2	3.92±0.99	5.40±1.32	<0.001	4.15±1.19	5.42±1.47	<0.001	0.20	0.92
Minimal lumen area, mm^2	1.80±0.51	2.19±0.80	<0.001	1.94±0.61	2.23±0.93	0.05	0.12	0.69
Mean vessel area, mm^2	10.35±3.25	12.26±3.34	<0.001	11.14±3.54	12.81±3.36	0.005	0.18	0.17
Minimal vessel area, mm^2	7.73±2.99	9.20±3.07	<0.001	8.39±3.29	9.85±3.27	0.011	0.22	0.09
Post-implantation								
Reference lumen area, mm^2	4.72±1.65	5.82±1.76	<0.001	5.16±1.74	5.83±1.77	0.002	0.16	0.96
Mean vessel area, mm^2	12.25±3.48	13.79±3.51	<0.001	13.17±3.65	14.73±3.59	0.014	0.14	0.03
Minimal vessel area, mm^2	9.92±3.32	11.12±3.41	0.004	10.76±3.49	12.04±3.49	0.038	0.16	0.03
Mean stent area, mm^2	5.64±1.39	6.28±1.40	<0.001	6.31±1.52	7.05±1.61	0.008	0.007	<0.001
Minimal stent area, mm^2	4.52±1.27	5.12±1.39	<0.001	5.36±1.52	5.95±1.56	0.03	0.001	<0.001
Percentage of frame with malapposition,%	2.03±7.99	2.15±6.19	0.88	1.08±3.49	3.80±9.94	0.07	0.43	0.08
Mean ISA distance, mm	0.33±0.24	0.42±0.42	0.43	0.24±0.26	0.53±0.33	0.04	0.42	0.30
ISA area, mm^2	0.02±0.08	0.04±0.25	0.25	0.01±0.02	0.06±0.18	0.05	0.39	0.62
Deployment index	0.60±0.12	0.72±0.15	<0.001	0.69±0.10	0.81±0.16	<0.001	<0.001	<0.001
Device/artery ratio**	1.40±0.35	1.05±0.24	<0.001	1.31±0.29	1.08±0.28	<0.001	0.14	0.58

Data are shown in mean±SD or median (IQR 1st-3rd) or n(%).†available in 377 patients. *Optimal scaffold/stent expansion (OSE) was defined as MSA ≥ 90% of the average RLA or ≥ 100% of lumen area of the reference segment with the lowest lumen area. If MSA ≥ 9 mm2, OSE was defined as MSA ≥ 80% of the average RLA. ** calculated from nominal device area at nominal pressure divide by the largest Amax pre-procedure. Abbreviation: Amax: maximal lumen area at the landing zone; ISA:incomplete stent/scaffold apposition; MSA: minimal scaffold/stent area.

Table 3 Incidence of Clinical Events at 393 days

Clinical outcomes	BVS oversize	BVS non-oversize	p-value	EES oversize	EES non-oversize	p-value	p-value non-oversize	p-value oversize
	n=107	n=190		n=48	n=106		BVS vs. EES	BVS vs. EES
Cardiac death	0	0	na	0	0	na	na	na
Myocardial infarction at 393 days	9(8.4)	6(3.2)	0.047	1(2.1)	1(0.9)	0.56	0.22	0.14
QMI	1(0.9)	1(0.5)	0.65	0	0	na	0.45	0.50
NQMI	8(7.5)	5(2.6)	0.05	1(2.1)	1(0.9)	0.56	0.32	0.18
TVMI	8(7.5)	6(3.2)	0.09	1(2.1)	1(0.9)	0.56	0.23	0.18
Periprocedural MI	8(7.5)	5(2.6)	0.05	1(2.1)	1(0.9)	0.14	0.32	0.14
MI within 37 days after index procedure	9(8.4)	5(2.6)	0.024	1(2.1)	1(0.9)	0.56	0.18	0.32
MI between 37 days and 393 days after index procedure	0	1(0.5)	0.45	0	0	na	na	0.45
Ischemia-driven TLR at 393 days	3(2.8)	1(0.5)	0.09	1(2.1)	2(1.9)	0.93	0.26	0.29
Composite of cardiac death, all MI, and clinically indicated target lesion revascularization (MACE) at 393 days	10(9.3)	7(3.7)	0.043	2(4.2)	3(2.8)	0.67	0.69	0.27
Scaffold/stent thrombosis at 393 days	2(1.9)	1(0.5)	0.25	0	0	na	0.45	0.34
Definite ST	2(1.9)	0	0.06	0	0	na	na	0.34
Probable ST	0	1(0.5)	0.47	0	0	na	0.45	na
Acute to subacute definite and probable ST	2(1.9)	1(0.5)	0.25	0	0	na	0.45	0.34

Data are shown in n (%)Abbreviation: QMI: Q-wave myocardial infarction; NQMI: non-Q-wave myocardial infarction; TLR: target lesion revascularization; MI: myocardial infarction; MACE: major adverse cardiac events; ST: scaffold/stent thrombosi

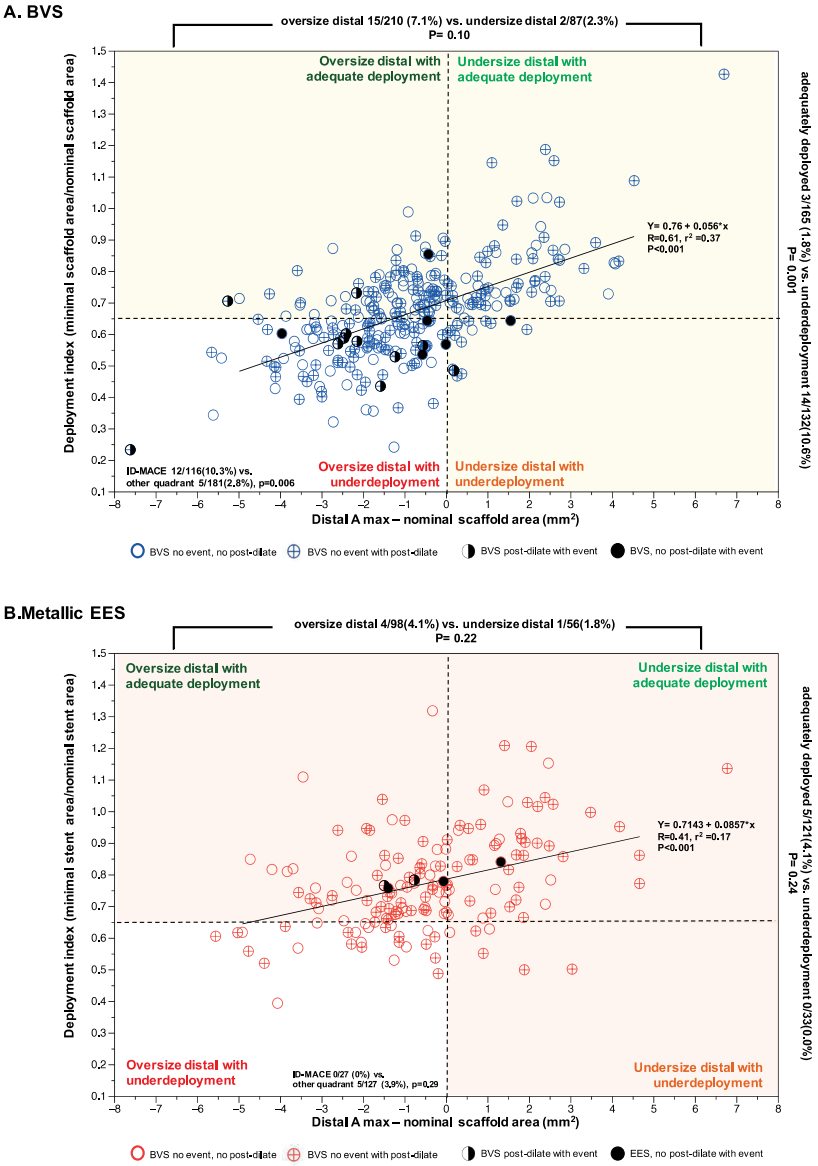

Figure 2. Distribution of the pre-procedural sizing (distal Amax- nominal device area) and status of device expansion as assessed by deployment index (minimal stent area/nominal device area) in each device (BVS; Fig 2A and metallic EES; Fig 2B).

It is clearly shown that MACE rate in BVS oversize and under-deployment after scaffold implantation is higher than the other quadrants (shaded in yellow). Post-dilation rate was not different between adequate deployment and under-deployment (cut-off 0.65) which indicated that under-deployment was unable to be corrected by post-dilation alone. However, this observation was observed only in the BVS arm while in the metallic EES arm was not.

Table 4 Comparison of the Peak Value of Cardiac Enzyme Rise Post-Procedure in the oversized and non-oversized groups

	BVS oversize	BVS non-oversize	p-value	EES oversize	EES non-oversize	p-value	p-value oversize	p-value non-oversize
	n=107	n=190		n=48	n=106		BVS vs. EES	BVS vs. EES
Post CK ratio	0.83±0.81	0.65±0.53	0.43	0.65±0.72	0.66±0.63	0.66	0.19	0.87
Post CK-MB ratio	1.89±3.13	1.05±1.31	0.02	1.13±0.98	1.11±1.96	0.18	0.03	0.75
Post cTn ratio	3.6 (1.27-15.43)	2.57 (0.98-7.88)	0.02	4.14 (1.32-11.86)	2.47 (1.10-8.26)	0.16	0.81	0.73
CK > 2xULN	9(8.7)	7(4.0)	0.10	1(2.1)	2(2.0)	0.96	0.13	0.35
cTn > 5xULN	50(49.5)	73(41.0)	0.17	0	4(3.9)	0.17	0.67	0.87
CK-MB ≥ 5x ULN	10(9.3)	6(3.4)	0.03	21(45.7)	40(40.0)	0.52	0.03	0.82
CK-MB ≥ 10x ULN	2(1.9)	0	0.07	0	1(1.0)	0.49	0.34	0.19
cTn > 35xULN	12(11.9)	10(5.6)	0.06	2(4.3)	5(5.0)	0.86	0.15	0.83
cTn > 70xULN	8(7.9)	7(3.9)	0.16	1(2.2)	2(2.0)	0.94	0.18	0.38

Data are shown in mean±SD or median (IQR 1st-3rd).
Abbreviation: CK: creatinine kinase; CK-MB:creatinine kinase-MB type; cTn: cardiac troponin

DISCUSSION

The main findings of the current analysis are the following: 1)device underdeployment was more frequently observed in the oversized device group than in the non-oversized device group; 2) despite post-dilation, it might not be possible to correct the device underexpansion if the initial sizing was inappropriate ; 3)Implantation of an oversized metallic stent did not contribute to increased MACE rates whereas implantation of the oversized BVS was associated with early peri-procedural MI (according to the pre protocol definition).

Clinical application of the present study and device sizing

Previously, Ishibashi et al reported that "oversized" scaffold implantation was observed in 52.7% as assessed by QCA-Dmax[5] whereas the current analysis found the frequency of oversized scaffold and oversized metallic EES implantation was 36.0% and 31.2%, respectively. The low incidence of "oversized" device implantation in the present study may relate to the existing systematic difference between QCA and IVUS[14]. Lumen dimensions as measured with QCA is systematically smaller than IVUS-assessed dimensions[14, 15]. Nevertheless, the present study showed a consistent association between oversized implantation of scaffold and a increased periprocedural MI rates. Therefore, either QCA Dmax or IVUS Amax lead to a similar conclusion and could be used as a guidance for scaffold sizing.

Recently, Puricel et al[7] reported that the risk of ScT appeared to increase when oversized scaffolds were implanted in relatively small vessels. Post hoc subgroup analysis in the ABSORB-III trial showed that the 1-year target lesion failure, individual components and ST for both BVS and metallic EES were higher in small vessels than in larger vessels without statistical significance[2]. The present study demonstrated that there was no statistical difference between the two platforms implanted in very small vessel subgroup (Amax < 4 mm^2). This could imply that oversized scaffold implantation had impact not only in small vessels but consistently affected the clinical outcomes when the oversized scaffolds were implanted in vessel of all sizes.

In current practice, the operators would intuitively respond to suboptimal device expansion by performing post-dilation and anticipating that it may improve the final stent/scaffold area. The current analysis showed that performing post-dilation was not associated with an increase of deployment index. As illustrated in figure 2, post-dilation dots were widely scattered and not confined in the upper quadrants (high deployment index), suggesting that post-dilation may have little effect to improve scaffold expansion if the initial sizing was inappropriate . Sotomi et al[16] recently demonstrated that the balloon-artery ratio positively correlated with the expansion of devices and suggested that pre- and postdilatation balloon sizing based on OCT-derived RVD might be recommended. Therefore, intracoronary imaging either OCT or IVUS should be considered to select the most proper BVS size.

The clinical application of the present study is that the operator should select BVS size such that its nominal area does not exceed both proximal and distal maximal lumen area in order to avoid an oversizing and thus relative underdeployment. A systematic assessment of vessel size pre-procedure and final device expansion by intracoronary imaging will be a useful tool to achieve the optimal results. Whether this optimal sizing technique using intravascular imaging will lead also to improved clinical outcomes needs to be further studied in prospective trials.

Potential mechanism of peri-procedural MI in oversized BVS

The present study showed that BVS oversizing was associated with post-procedural CK-MB and cTn rising. No such association was observed in the metallic EES arm. Iakovou et al reported that aggressive stent expansion resulted in rise of the cardiac enzymes. However, there was no significant rise of cardiac enzymes in the metallic EES arm compared to BVS arm despite higher post-dilatation diameter, pressure and deployment index (table 4).This suggests that the mechanism of cardiac enzyme rise in the BVS arm may be different from the metallic EES.

Previously, the randomized data of the ABSORB-II trial[17] showed that PMI rates were not different between Absorb and metallic EES. There was also no difference in the rate of side branch occlusion[17]. In the current analysis, the angiographic assessment (data

not shown) showed that the BVS oversized group has a lower incidence of side branch occlusion than the EES oversized group (0% vs.4.2%, p=0.03). The prolapsed area between BVS oversized and BVS non-oversized group was not different. Consequently, the focus has been moved to the increase of scaffold footprint [7, 18] due to the underdeployment. Normally, there was a marked difference in percentage of ASSA (1.5-3 times) and strut volume (5-7 times) between BVS and metallic EES[6]. When the implanted scaffold was oversized and underdeployed, it would substantially increase the scaffold footprint that may interfere the local flow hemodynamics and initiate platelet aggregation pathway[6]. This findings would explain one of different mechanism of PMI between BVS and metallic EES.

The MI in the present study was driven by PMI defined by per protocol definition. When the analysis was performed by using SCAI definition, there was no difference in MI rates between groups. The present study showed that the MI rate between 37 days and 393 days after index procedure was very low in both platforms together with non-statistically significant differences in the revascularization rates in both devices. One may concern that PMI has limited clinical relevance and may not affect long term clinical outcome[19]. Nevertheless, the elevation of cardiac enzymes followed oversized BVS implantation reflected that continued refinement of the device such as thinner strut may be advantageous in newly developed bioresorbable platforms .

Limitation

The following limitations need to be addressed; 1) the trial protocol was not designed to explore the IVUS guided device selection and expansion, in other words, the findings of periprocedural IVUS did not impact the device selection by the operator; 2) The method to evaluate proximal and distal maximal lumen area are somewhat difficult to perform in current clinical practice since it needs special software to co-localize angiography and IVUS images with respect to the landing zone. The advancement of co-registration software in the IVUS online workstation may enable this application in the future clinical practice.

Conclusion

Oversized scaffold/stent implantation is associated with device under-deployment. This cannot be corrected with subsequent aggressive post-dilation. The major mechanism, by which device oversizing contributed to the peri-procedural MIs was the relatively increase in strut footprint from the underdeployment of the scaffold. Precise vessel sizing before implantation may prevent potential complications related to the underdeployment of the device.

REFERENCE

1. Onuma Y, Serruys PW. Bioresorbable scaffold: the advent of a new era in percutaneous coronary and peripheral revascularization? Circulation. 2011;123(7):779-97.
2. Steinvil A, Rogers T, Torguson R, Waksman R. Overview of the 2016 U.S. Food and Drug Administration Circulatory System Devices Advisory Panel Meeting on the Absorb Bioresorbable Vascular Scaffold System. JACC Cardiovascular interventions. 2016;9(17):1757-64.
3. Gomez-Lara J, Diletti R, Brugaletta S, Onuma Y, Farooq V, Thuesen L, et al. Angiographic maximal luminal diameter and appropriate deployment of the everolimus-eluting bioresorbable vascular scaffold as assessed by optical coherence tomography: an ABSORB cohort B trial sub-study. EuroIntervention. 2012;8(2):214-24.
4. Farooq V, Gomez-Lara J, Brugaletta S, Gogas BD, Garcia-Garcia HM, Onuma Y, et al. Proximal and distal maximal luminal diameters as a guide to appropriate deployment of the ABSORB everolimus-eluting bioresorbable vascular scaffold: a sub-study of the ABSORB Cohort B and the on-going ABSORB EXTEND Single Arm Study. Catheterization and cardiovascular interventions 2012;79(6):880-8.
5. Ishibashi Y, Nakatani S, Sotomi Y, Suwannasom P, Grundeken MJ, Garcia-Garcia HM, et al. Relation Between Bioresorbable Scaffold Sizing Using QCA-Dmax and Clinical Outcomes at 1 Year in 1,232 Patients From 3 Study Cohorts (ABSORB Cohort B, ABSORB EXTEND, and ABSORB II). JACC Cardiovascular interventions. 2015;8(13):1715-26.
6. Kawamoto H, Jabbour RJ, Tanaka A, Latib A, Colombo A. The Bioresorbable Scaffold: Will Oversizing Affect Outcomes? JACC Cardiovascular interventions. 2016;9(3):299-300.
7. Puricel S, Cuculi F, Weissner M, Schmermund A, Jamshidi P, Nyffenegger T, et al. Bioresorbable Coronary Scaffold Thrombosis: Multicenter Comprehensive Analysis of Clinical Presentation, Mechanisms, and Predictors. Journal of the American College of Cardiology. 2016;67(8):921-31.
8. Serruys PW, Suwannasom P, Nakatani S, Onuma Y. Snowshoe Versus Ice Skate for Scaffolding of Disrupted Vessel Wall. JACC Cardiovascular interventions. 2015;8(7):910-3.
9. Diletti R, Serruys PW, Farooq V, Sudhir K, Dorange C, Miquel-Hebert K, et al. ABSORB II randomized controlled trial: a clinical evaluation to compare the safety, efficacy, and performance of the Absorb everolimus-eluting bioresorbable vascular scaffold system against the XIENCE everolimus-eluting coronary stent system in the treatment of subjects with ischemic heart disease caused by de novo native coronary artery lesions: rationale and study design. American heart journal. 2012;164(5):654-63.
10. de Jaegere P, Mudra H, Figulla H, Almagor Y, Doucet S, Penn I, et al. Intravascular ultrasound-guided optimized stent deployment. Immediate and 6 months clinical and angiographic results from the Multicenter Ultrasound Stenting in Coronaries Study (MUSIC Study). Eur Heart J. 1998;19(8):1214-23.
11. Mintz GS, Nissen SE, Anderson WD, Bailey SR, Erbel R, Fitzgerald PJ, et al. American College of Cardiology Clinical Expert Consensus Document on Standards for Acquisition, Measurement and Reporting of Intravascular Ultrasound Studies (IVUS). A report of the American College of Cardiology Task Force on Clinical Expert Consensus Documents. Journal of the American College of Cardiology. 2001;37(5):1478-92.
12. Vranckx P, Kint PP, Morel MA, Van Es GA, Serruys PW, Cutlip DE. Identifying stent thrombosis, a critical appraisal of the academic research consortium (ARC) consensus definitions: a lighthouse and as a toe in the water. EuroIntervention. 2008;4 Suppl C:C39-44.

13. Moussa ID, Klein LW, Shah B, Mehran R, Mack MJ, Brilakis ES, et al. Consideration of a new definition of clinically relevant myocardial infarction after coronary revascularization: an expert consensus document from the Society for Cardiovascular Angiography and Interventions (SCAI). Journal of the American College of Cardiology. 2013;62(17):1563-70.
14. Okamura T, Onuma Y, García-García HM, van Geuns R-JM, Wykrzykowska JJ, Schultz CJ, et al. First-in-man evaluation of intravascular optical frequency domain imaging (OFDI) of Terumo: a comparison with intravascular ultrasound and quantitative coronary angiography. EuroIntervention. 2011;6(9):1037-45.
15. Kubo T, Akasaka T, Shite J, Suzuki T, Uemura S, Yu B, et al. OCT Compared With IVUS in a Coronary Lesion Assessment: The OPUS-CLASS Study. JACC: Cardiovascular Imaging. 2013;6(10):1095-104.
16. Sotomi Y, Onuma Y, Dijkstra J, Eggermont J, Liu S, Tenekecioglu E, et al. Impact of Implantation Technique and Plaque Morphology on Strut Embedment and Scaffold Expansion of Polylactide Bioresorbable Scaffold- Insights From ABSORB Japan Trial. Circulation journal 2016 [Epub ahead of print].
17. Ishibashi Y, Muramatsu T, Nakatani S, Sotomi Y, Suwannasom P, Grundeken MJ, et al. Incidence and Potential Mechanism(s) of Post-Procedural Rise of Cardiac Biomarker in Patients With Coronary Artery Narrowing After Implantation of an Everolimus-Eluting Bioresorbable Vascular Scaffold or Everolimus-Eluting Metallic Stent. JACC Cardiovascular interventions. 2015;8(8):1053-63.
18. Kawamoto H, Panoulas VF, Sato K, Miyazaki T, Naganuma T, Sticchi A, et al. Impact of Strut Width in Periprocedural Myocardial Infarction: A Propensity-Matched Comparison Between Bioresorbable Scaffolds and the First-Generation Sirolimus-Eluting Stent. JACC Cardiovascular interventions. 2015;8(7):900-9.
19. Lansky AJ, Stone GW. Periprocedural myocardial infarction: prevalence, prognosis, and prevention. Circulation Cardiovascular interventions. 2010;3(6):602-10.

Chapter 6

Quantitative assessment of the stent/scaffold strut embedment analysis by optical coherence tomography

Yohei Sotomi, Hiroki Tateishi, Pannipa Suwannasom, Jouke Dijkstra, Jeroen Eggermont, Shengnan Liu, Erhan Tenekecioglu, Yaping Zheng, Mohammad Abdelghani, Rafael Cavalcante, Robbert J. de Winter, Joanna J. Wykrzykowska, Yoshinobu Onuma, Patrick W. Serruys, Takeshi Kimura

Int J Cardiovasc Imaging. 2016 Jun;32(6):871-83.

ABSTRACT

The degree of stent/scaffold embedment could be a surrogate parameter of the vessel wall-stent/scaffold interaction and could have biological implications in the vascular response. We have developed a new specific software for the quantitative evaluation of embedment of struts by optical coherence tomography (OCT). In the present study, we described the algorithm of the embedment analysis and its reproducibility. The degree of embedment was evaluated as the ratio of the embedded part versus the whole strut height and subdivided into quartiles. The agreement and the inter- and intra-observer reproducibility were evaluated using the kappa and the interclass correlation coefficient (ICC). A total of 4 pullbacks of OCT images in 4 randomly selected coronary lesions with 3.0 x18 mm devices [2 lesions with Absorb BVS and 2 lesions with XIENCE (both from Abbott Vascular, Santa Clara, CA, USA)] from Absorb Japan trial were evaluated by two investigators with QCU-CMS software version 4.69 (Leiden University Medical Center, Leiden, The Netherlands). Finally, 1481 polymeric struts in 174 cross-sections and 1415 metallic struts in 161 cross-sections were analyzed. Inter- and intra-observer reproducibility of quantitative measurements of embedment ratio and categorical assessment of embedment in Absorb BVS and XIENCE had excellent agreement with ICC ranging from 0.958 to 0.999 and kappa ranging from 0.850 to 0.980. The newly developed embedment software showed excellent reproducibility. Computer-assisted embedment analysis could be a feasible tool to assess the strut penetration into the vessel wall that could be a surrogate of acute injury caused by implantation of devices.

INTRODUCTION

The advent of OCT technology with a high resolution enabled us to assess quite precisely the appearance of metallic or polymeric struts embedded in the vessel wall. The degree of embedment could be one of surrogate parameters of the vessel wall-stent/ scaffold interaction after the implantation of the scaffold/stent struts [1–4]. Historically, in the era of metallic stents, the association between stretch and deep injury of the coronary artery and neointima formation was demonstrated in a porcine model [5–7]. The vessel injury is also one aspect of vessel wallstent/ scaffold interaction. Several concerns on clinical outcomes following Absorb everolimus-eluting bioresorbable scaffold [Absorb BVS] (Abbott Vascular, Santa Clara, CA, USA) implantation stem from its inherent material property (poly L-lactic acid), scaffold design, mechanical properties of the device, etc. Recent publications reported the potential association between the larger abluminal scaffold surface area ("footprint") of the Absorb BVS with a higher incidence of peri-procedural myocardial infarction when compared to metallic stents [8, 9]. The vessel wall and stent/scaffold interaction might play a role in this result as reported by Kawamoto et al. [10]. The surface area of the Absorb BVS is 27 %, whereas that of XIENCE Cobalt chromium everolimus-eluting stent [CoCr-EES] (Abbott Vascular, Santa Clara, CA, USA) is 13 % [9]. When the same force is applied, Absorb BVS struts create less parietal pressure compared to metallic struts, which could result in less embedment of Absorb BVS struts [1]. The degree of embedment (less protrusion of the device in the lumen) also strongly influences the endothelial shear stress in the microenvironment surrounding the struts, which is associated with neointimal formation and platelet aggregation, etc. [1, 4, 11–13].

When OCT started to be applied to metallic stents and/or polymeric scaffolds, specific and appropriate methods of analysis related to each device were used and enables fair comparison between the two devices due to the light transparency of one device versus the higher opacity of the other device [14]. Reporting of the degree of embedment seems important to describe the difference in device-vessel interaction [14].

Before the era of bioresorbable scaffolds, clinical relevance of metallic stent strut embedment with neointimal coverage was evaluated [15]. However, there was no quantitative assessment of degree of strut embedment. Now we have accurate imaging technology and comparative methodology for the assessment of metallic stents and polymeric scaffolds. We have developed a new specific method for the quantitative and accurate evaluation of embedment of struts by optical coherence tomography (OCT). In the present study, we described the algorithm of the embedment analysis and its reproducibility.

METHODS

Study subjects

A total of 4 pullbacks of OCT images in 4 randomly selected coronary lesions with 3.0 × 18 mm devices (2 lesions with 3.0 × 18 mm Absorb BVS and 2 lesions with 3.0 × 18 mm XIENCE CoCr-EES were evaluated in this analysis. These OCT pullbacks came from ABSORB Japan, a prospective, multicentre, randomized, single-blind, active-controlled clinical trial in which 400 patients were recruited in Japan. Patients were randomized in a 2:1 ratio to treatment with the Absorb BVS or the XIENCE Prime/Xpedition CoCr-EES. The details of the trial were described elsewhere [16].

Optical coherence tomography data acquisition

OCT pullbacks were obtained at baseline after the stent or scaffold implantation by a Frequency-domain ILUMIEN OPTIS system using a Dragonfly™ Duo catheter (St. Jude Medical Inc., Saint Paul, MN, USA) with 10–15 μm axial and 20–40 μm lateral resolution [17] at a rotation speed of 180 frames/s with non-occlusive technique [18]. After infusion of intracoronary nitroglycerine, the imaging wire was withdrawn by a motorized pull-back at a constant speed of 18 mm/s, while contrast was infused through the guiding catheter at a continuous rate of 2–4 mL/min. Accordingly, OCT images were obtained per 100 μm in longitudinal length.

Development of embedment analysis by optical coherence tomography

The embedment parameters measured by the software are strut thickness, embedment strut width and embedment depth.

In the polymeric scaffold (Absorb BVS), its black core was framed by a light reflecting structure of 30 μm (layer of the amorphous polylactide containing and releasing everolimus) (Fig. 1). Therefore, actual strut thickness of Absorb BVS was calculated as follows: Corrected Strut Thickness = strut thickness (black core thickness) + 0.06 mm [2 × 30 μm (the thickness of bright border)]. Actual embedment depth of Absorb BVS was also corrected as: Corrected embedment depth = embedment depth + 0.03 mm (the thickness of abluminal bright border). Actual embedment strut width was calculated as follows: Corrected embedment strut width = width of strut (black core) + 0.06 mm [2 × 30 lm (the thickness of bright border for both sides). In the metallic stent (XIENCE), no additional correction was performed. In the following sentences, "strut thickness", "embedment depth" and "embedment strut width" are corrected in case of Absorb BVS and non-corrected in case of XIENCE, respectively.

The parameters evaluated in the embedment analysis are demonstrated in Fig. 2. The "embedment ratio" (degree of embedment in percentage) was calculated using the following formula: embedment depth (the distance between the mid-point of the

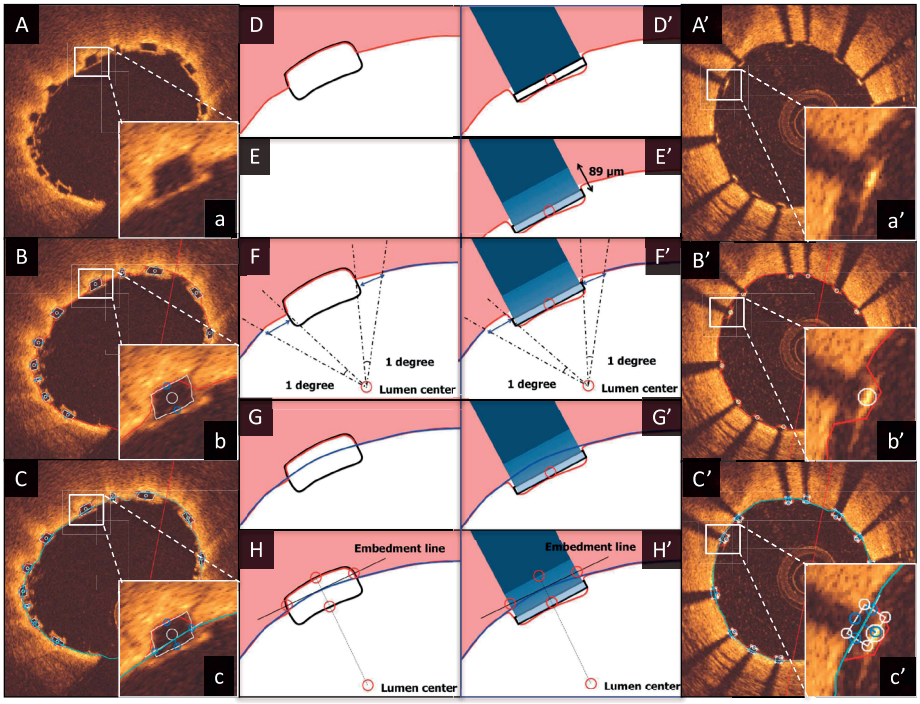

Figure 1. Algorithm for embedment analysis.
The algorithm for embedment analysis in Absorb BVS (A–H) and XIENCE (A'–H') is demonstrated in this figure. A–C and A'–C' indicate the actual analysis display, a–c and a'–c' show the magnified views of a single strut, and D–H and D'–H' illustrate the step-by-step algorithm for embedment analysis. As a first step, automatic lumen contour detection and automatic strut detection were performed (D, D'). After detection of the abluminal side of the metallic struts, the entire body of the strut was automatically drawn by simulating the virtual contour of the struts using the thickness of the strut indicated by the manufacturer (XIENCE: 89 µm) (E'). The following steps were the same between Absorb BVS and XIENCE. After erasing a part of the lumen contour surrounding a strut (strut part and bilateral 1 degree measured from the lumen center) (F, F'), interpolated lumen lines were connected through the strut automatically (G, G'). "Embedment Line" was automatically delineated as described in the main text (H, H'). This additional line was used for embedment analysis to compute the following embedment measurements. "Embedment depth" was the distance between the back position of struts and the Embedment Line measured along the line from the back position through the lumen center. "Embedment strut width" was the distance between the intersection point(s) of the Embedment Line and the strut contour

abluminal strut border to the interpolated lumen contour)/the thickness of the strut ×100 (%).

The embedment of struts was classified into 6 classes (Embedment Class [EC] 0–5) based on the degree of embedment (percentage) as indicated in Fig. 3. If struts were malapposed (indicated as negative value of percentage in the software), this was classified as EC0. When the strut was partially embedded in the vessel wall, the degree of

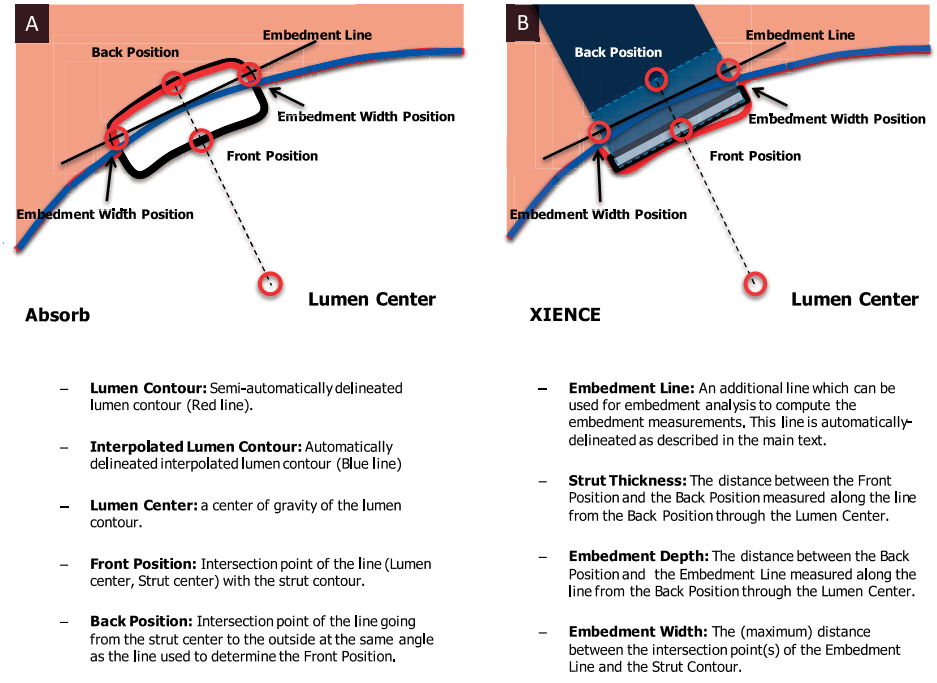

Figure 2. Parameters for embedment analysis. Parameters of embedment analysis for Absorb BVS (A) and XIENCE (B)

embedment was categorized by each quartile (0 % ≤ EC1 < 25 %, 25 % ≤ EC2 < 50 %, 50 % ≤ EC3 < 75 %,75 % ≤ EC4 < 100 %). When the tissue was covering the endoluminal surface of struts, the struts were considered as "buried", EC5 (≥100 %).

Embedment analysis algorithm

All the OCT analysis was performed with a special version of QCU-CMS version 4.69 (Leiden University Medical Center, Leiden, The Netherlands). The OCT analysis was performed every 200 µm cross-section in the stent/scaffold segments. All struts from both investigators were completely matched before the assessment of embedment. Struts located at a side branch ostium were excluded from the embedment analysis. The algorithm for embedment analysis is illustrated in the Fig. 1. At the first step automatic lumen contour detection and automatic strut detection were performed. The details of the strut detection algorithm are described elsewhere [19, 20]. For the polymeric scaffold (Absorb BVS), the black core of struts were delineated using automatic detection, and if necessary manually corrected. For the metallic stents, the center of the reflective border of the metallic strut was detected automatically by the software. If the automatically detected strut point was not located at the correct point, manual correction was

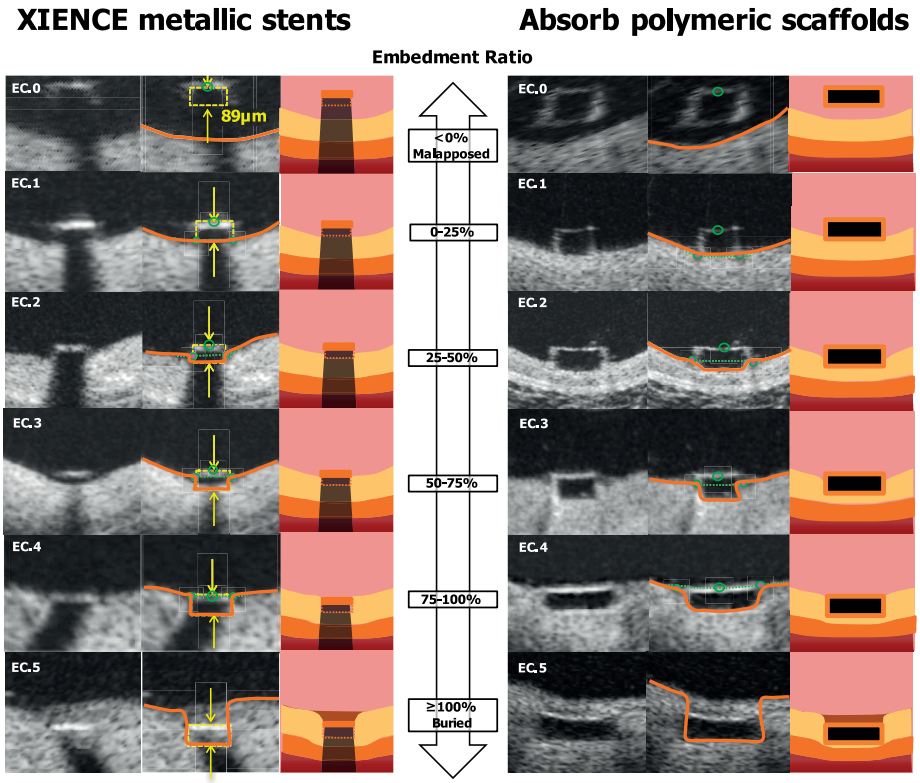

Figure 3. Embedment categorization.
The embedment of struts was classified into 6 classes (Embedment Class [EC] 0–5) based on the degree of embedment (percentage). If struts were malapposed (indicated as negative value of percentage in the software), this was classified as EC0. When the strut was partially embedded in the vessel wall, the degree of embedment was categorized by each quartile (0 % ≤ EC1<25 %,25 % ≤ EC2<50 %, 50 % ≤ EC3<75 %, 75 % ≤ EC4<100 %). When the tissue was covering the endoluminal surface of struts, the struts were considered as "buried", EC5 (≥100 %)

performed additionally. The abluminal side of the metallic struts could not be directly delineated; however, this could be automatically drawn by simulating the virtual contour of the struts using the thickness of the strut indicated by the manufacturer (XIENCE: 89 µm). The following steps were the same for Absorb BVS and XIENCE. First, the parts of the lumen contour surrounding a strut (the strut part plus 1 degree to both sides of a strut from the lumen center) were removed and, using spline interpolation, a new interpolated lumen was automatically computed. The lumen center was detected automatically as a center of gravity of the lumen contour. Next, for each strut an "Embedment Line" was computed automatically as follows: based on the intersection of the interpolated lumen contour with lines from the lumen center through the start/end angle of each strut plus 2.5° to each side, an intersection line was computed. This intersection line

was then moved to touch the interpolated lumen along a line from the lumen center through the center of the intersection line. This additional line was used for embedment analysis to compute the following embedment measurements. "Embedment depth" was the distance between the back position and the embedment line measured along the line from the back position through the lumen center. "Embedment strut width" was the largest distance between the intersection point(s) of the embedment line with the strut contour. The embedment strut width was evaluated only when the embedment line intersected the strut contour. If there was no intersection between the embedment line and the strut contour, embedment strut width was not analyzed.

Assessment of reproducibility

For the assessment of intra- and inter-observer reproducibility, two analysts (Observer A, HT and Observer B, YS) performed OCT embedment analysis. For the intraobserver reproducibility, one of the analysts (YS) repeated all the measurements on the same pullbacks after an interval of 4 weeks. For the evaluation of inter-observer reproducibility, the parameters of strut embedment were compared between the two analysts. The agreement between the two analysts for the embedment categorization was also determined.

Statistical analysis

Quantitative measurements to assess the inter- and intraobserver reproducibility are presented at strut level analysis. Data are expressed as mean ± standard deviation or median and inter-quartile range, if appropriate. Intra- and inter-observer reproducibility was evaluated by the following methods. The reproducibility of embedment parameter measurements (embedment ratio and embedment strut width) at strut level was evaluated with the interclass correlation coefficient (ICC) for concordance (ICCc) and absolute agreement (ICCa) with its 95 % confidence intervals (CI). An ICC < 0.4 indicates bad agreement, an ICC between 0.4 and 0.75 indicates moderate agreement, and ICC values > 0.75 indicates excellent agreement [21]. The correlation between different observations was analyzed by simple linear regression. Measurement agreement was determined by comparing measurements of each analysis using the Bland–Altman method [22]. Data are given as plots showing the absolute difference between corresponding measurements of both observers (y-axis) against the average of both observers (x-axis). The relative difference between measurements (absolute difference divided by the average) gives the bias; its standard deviation gives the random variation. The limits of agreement were calculated as mean bias ± 1.96SD. The Cohen's k (kappa) test was used to assess intra- and inter-observer agreement for embedment categorization. The kappa coefficient was categorized as <0.20 = poor, 0.21–0.40 = fair, 0.41–0.60 = moderate, 0.61–0.80 = substantial, and 0.81–1.00 = almost perfect [23]. Statistical significance was assumed at

a probability (P) value of < 0.05. All statistical analyses were performed with SPSS (version 23.0.0, IBM, New York) and MedCalc Statistical Software version 14.12.0 (MedCalc Software bvba, Ostend, Belgium).

RESULTS

Population characteristics

A total of 177 and 188 cross-sections were recognized in the scaffolded and stented segments, respectively. In 3 of 177 and 27 of 188 cross-sections, automatic lumen detection did not work appropriately due to poor image quality. In the remaining 174 and 161 cross-sections, 1481 polymeric struts and 1415 metallic struts were matched and analyzed for embedment assessment. The embedment analysis for one case took on average 25 ± 6 min for 18 mm device with 200 μm intervals (theoretically 90 cross-sections). We performed manual correction in 3.9 ± 0.7 % of all the struts.

Reproducibility of quantitative measurements

Inter- and intra-observer reproducibility of quantitative measures are shown in Table 1. The assessments of embedment ratio in Absorb BVS and XIENCE had excellent agreement in both inter- and intra-observer reproducibility (Absorb BVS: inter-observer ICCc of multiple raters, 0.958 [95 % confidence interval 0.954–0.962]; intra-observer ICCc of multiple raters, 0.965 [0.962–0.969]; XIENCE: inter-observer ICCc of multiple raters, 0.999 [0.999–0.999]; intra-observer ICCc of multiple raters, 0.999 [0.999–0.999]). The assessments of embedment strut width in Absorb BVS and XIENCE also had excellent agreement in both inter- and intra-observer reproducibility (Absorb BVS: inter-observer ICCc of multiple raters, 0.974 [0.971–0.977]; intra-observer ICCc of multiple raters, 0.971 [0.968–0.974]; XIENCE: interobserver ICCc of multiple raters, 0.992 [0.991–0.993]; intra-observer ICCc of multiple raters, 0.991 [0.989–0.992]). Simple linear regression and Bland–Altman plots for embedment ratio and embedment strut width are shown in Figs. 4, 5, 6, 7. Cumulative frequency distribution curves of embedment ratio and embedment strut width are indicated in Fig. 8.

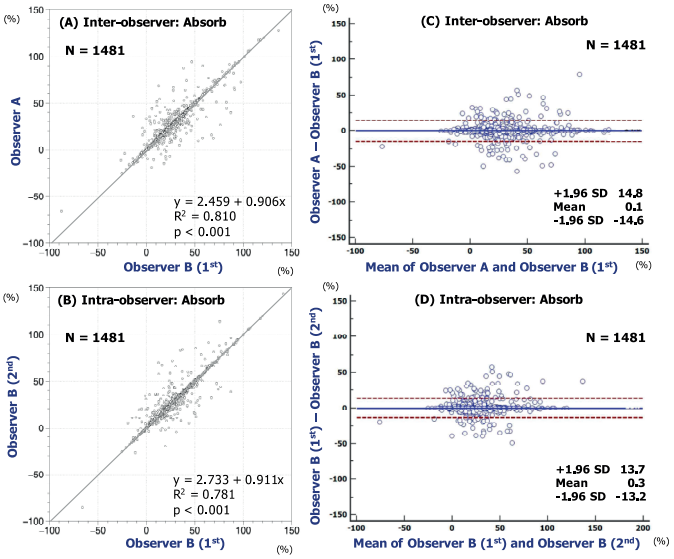

Figure 4. Reproducibility for embedment ratio of Absorb BVS.
Simple linear regression analyses are indicated in A (inter-) and B (intra-observer). Bland–Altman plots indicate inter- (C) and intra-observer (D) reproducibility to assess the embedment ratio of Absorb BVS

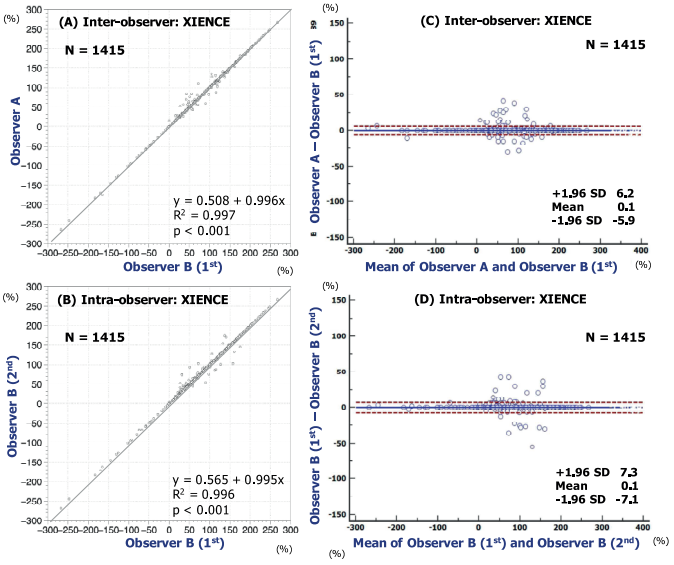

Figure 5. Reproducibility for embedment ratio of XIENCE.
Simple linear regression analyses are indicated in A (inter-) and B (intra-observer). Bland–Altman plots indicate inter- (C) and intra-observer (D) reproducibility to assess the embedment ratio of XIENCE

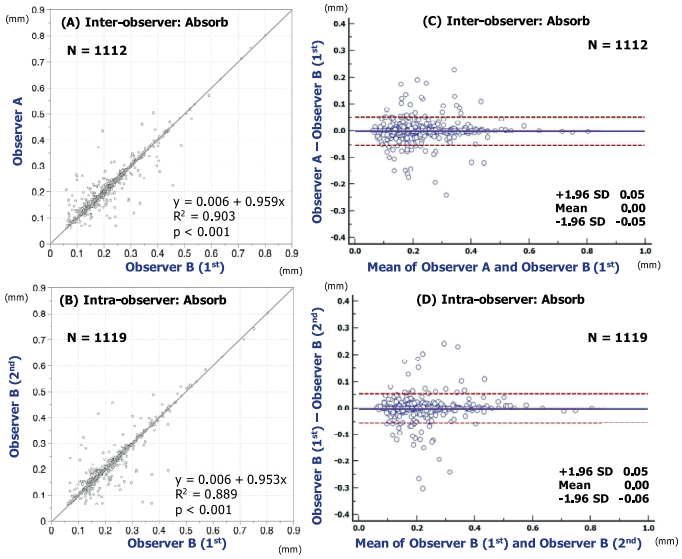

Figure 6. Reproducibility for embedment strut width of Absorb BVS.
Simple linear regression analyses are indicated in A (inter-) and B (intraobserver). Bland–Altman plots indicate inter- (C) and intra-observer (D) reproducibility to assess the embedment strut width of Absorb BVS

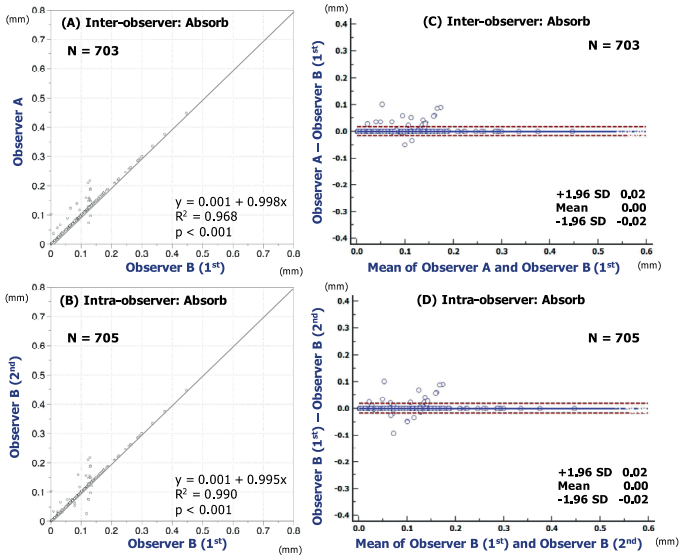

Figure 7. Reproducibility for embedment strut width of XIENCE.
Simple linear regression analyses are indicated in A (inter-) and B (intraobserver). Bland-Altman plots indicate inter- (C) and intra-observer (D) reproducibility to assess the embedment strut width of XIENCE

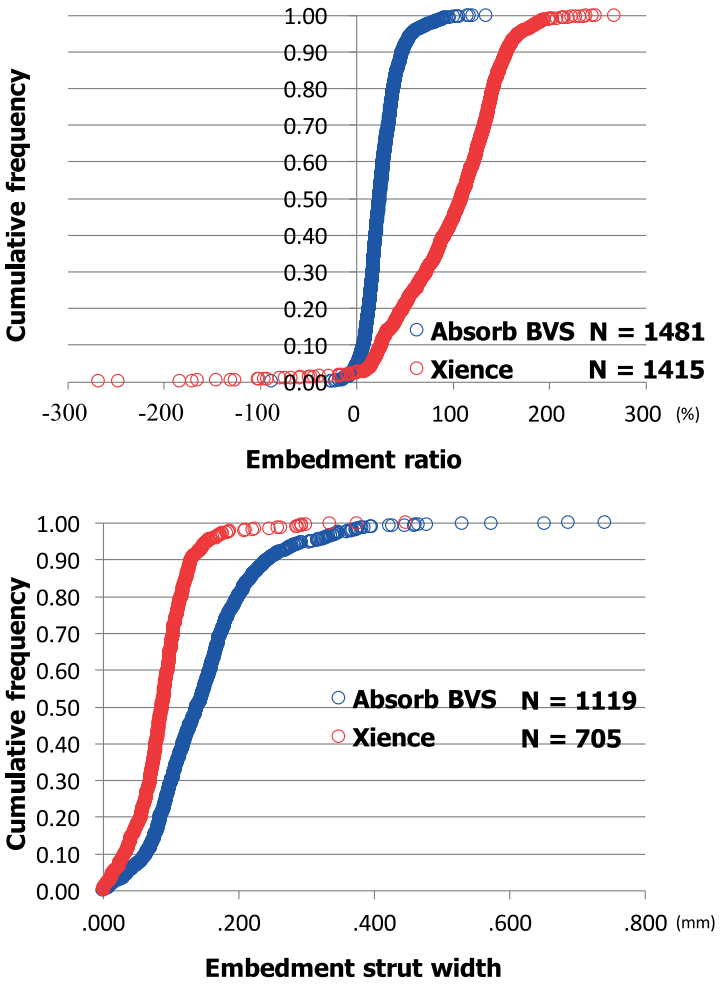

Figure 8. Cumulative frequency distribution curves.
Cumulative frequency distribution curves of embedment ratio (A) and embedment strut width (B) assessed by observer B (1st)

Reproducibility of qualitative measurements

The inter- and intra-observer reproducibility of embedment category at strut level analysis is shown in Table 2. Inter-and intra-observer reproducibility to assess embedment category was very good both in Absorb BVS (inter-observer kappa, 0.850; intra-observer kappa, 0.867) and XIENCE (inter-observer kappa, 0.976; intra-observer kappa, 0.980), but better in the XIENCE than in the Absorb BVS.

Table 1 Inter- and intra-observer reproducibility of quantitative measures

	No. of matched struts	Inter-observer variability	Observer A versus observer B (1st)	ICCc	ICCa
		Analyzable matched struts	Absolute difference [95 % CI]		
Embedment ratio (%)					
Absorb BVS	1481	1481	−0.08 [−0.51–0.36]		
Single measures				0.919 [0.911–0.927]	0.919 [0.911–0.927]
Average measures				0.958 [0.954–0.962]	0.958 [0.954–0.962]
XIENCE	1415	1415	0.14 [−0.02–0.30]		
Single measures				0.998 [0.998–0.999]	0.998 [0.998–0.999]
Average measures				0.999 [0.999–0.999]	0.999 [0.999–0.999]
Strut embedment width (mm)					
Absorb BVS	1481	1112	−0.000 [−0.002–0.002]		
Single measures				0.95 [0.943–0.955]	0.95 [0.943–0.955]
Average measures			0.974 [0.971–0.977]	0.974 [0.971–0.977]	
XIENCE	1426	703	0.001 [0.000–0.002]		
Single measures				0.984 [0.981–0.986]	0.984 [0.981–0.986]
Average measures				0.992 [0.991–0.993]	0.992 [0.990–0.993]

Table 1 Inter- and intra-observer reproducibility of quantitative measures (continued)

	No. of matched struts	Intra-observer variability	Observer B (1st) versus observer B (2nd)	ICCc	ICCa
		Analyzable matched struts	Absolute difference [95 % CI]		
Embedment ratio (%)					
Absorb BVS	1481	1481	−0.33 [−0.80–0.15]		
Single measures				0.933 [0.926–0.939]	0.933 [0.926–0.939]
Average measures				0.965 [0.962–0.969]	0.965 [0.962–0.969]
XIENCE	1415	1415	0.08 [−1.09–0.27]	0.998 [0.998–0.999]	0.998 [0.998–0.998]
Single measures				0.999 [0.999–0.999]	0.999 [0.999–0.999]
Average measures					
Strut embedment width (mm)					
Absorb BVS	1481	1119	0.001 [−0.001–0.002]		
Single measures				0.944 [0.937–0.95]	0.944 [0.937–0.95]
Average Measures				0.971 [0.968–0.974]	0.971 [0.968–0.974]
XIENCE	1426	705	0.001 [−0.000–0.001]		
Single measures				0.982 [0.979–0.984]	0.982 [0.979–0.984]
Average measures				0.991 [0.989–0.992]	0.991 [0.989–0.992]

Table 2 The inter- and intra-observer reproducibility of embedment category

	Observer A						Total	Inter-observer agreement (Kappa)
	Embedment category							
	0	1	2	3	4	5		
Observer B (1st)								
Absorb BVS								
Embedment category								
0	54	11	0	0	0	0	65	0.850
1	8	652	33	4	0	0	697	
2	2	40	534	7	3	0	586	
3	0	3	12	80	6	1	102	
4	0	0	2	3	19	1	25	
5	0	0	0	0	0	6	6	
Total	64	706	581	94	28	8	1481	
XIENCE								
Embedment category								
0	33	0	0	0	0	0	33	0.976
1	0	96	2	0	0	0	98	
2	0	1	149	8	1	0	159	
3	0	0	2	145	3	1	151	
4	0	0	0	2	184	0	186	
5	0	0	0	0	2	786	788	
Total	33	97	153	155	190	787	1415	
Observer B (1st)								
Absorb BVS								
Embedment category								
0	53	10	2	0	0	0	65	0.867
1	6	656	30	5	0	0	697	
2	1	31	543	9	2	0	586	
3	0	3	14	80	5	0	102	
4	0	0	2	0	22	1	25	
5	0	0	0	0	0	6	6	
Total	60	700	591	94	29	7	1481	
XIENCE								
Embedment category								
0	33	0	0	0	0	0	33	0.98
1	0	97	1	0	0	0	98	
2	0	0	154	5	0	0	159	
3	0	0	3	144	3	1	151	
4	0	0	0	1	185	0	186	
5	0	0	0	0	4	784	788	
Total	33	97	158	150	192	785	1415	

DISCUSSION

The present study demonstrated a high reproducibility for in vivo quantitative assessment of scaffold/stent embedment by OCT. The assessments of embedment ratio in Absorb BVS and XIENCE had excellent agreement in both inter- and intra-observer reproducibility. Inter- and intraobserver reproducibility to assess embedment category was also very good both in Absorb BVS and XIENCE. The algorithm and semi-automatic program for embedment analysis was reproducible and appeared to be feasible to use in future studies.

Clinical application of embedment analysis

Before the era of OCT, namely in the era of metallic stents, angiography and intravascular ultra sound, there was no accurate assessment of embedment. The scientific interest for embedment came from the need for accurate and quantitative evaluation of the vessel wall and stent/scaffold interaction. The previous animal studies on histology indicated a clear relationship between injury and neointimal proliferation [5–7]. The assessment of embedment on OCT could have been a surrogate parameter of vessel wall injury in these early days [1].

Our results indicated that the boundary of agreement in the continuous value of embedment ratio was as narrow as 15 %; and the kappa value in the embedment category was as high as 0.850, which may allow us to use continuous values or categories of embedment for scientific purpose.

From a practical point of view, we can also use OCT embedment assessment to evaluate the quality of stent/ scaffold implantation. We would be able to express the results in percentage of embedment and, as usual, we would have strut level assessment, cross sectional level assessment, and scaffold/lesion level assessment.

Embedment strut width and vessel-stent/scaffold interaction

The width of the strut could also influence the embedment of the strut. When the same force is applied, a device with a smaller contact area would generate a higher pressure to the vessel wall according to the simple principle: Pressure = Force/Area, resulting in more embedded struts. Embedded struts denote penetration of the cutting edge of the struts through fibrous, calcific, and necrotic plaques, implying larger injury of the vessel. On the other hand, Kawamoto et al. reported the potential association between the larger footprint of the Absorb BVS and higher incidence of peri-procedural myocardial infarction when compared with metallic stent [8, 9]. Even if the embedment of struts is small, a larger footprint (larger width of struts) itself could contribute to larger amount of vessel wall-stent/scaffold interaction.

The relationship amongst embedment depth, embedment strut width, and vessel injury will be a topic of research in the upcoming year [1]. Our algorithm demonstrated excellent reproducibility for the assessment of embedment strut width as well.

Advantages and disadvantages of embedment

Whatever is embedded in the vessel wall does not impact the flow in the lumen. Flow area increases as embedment increases; and in terms of shear stress, the deeper the struts are embedded, the less disturbed the shear stress will be [13]. However, there seems to be a down side in the sense that the embedment might also be the expression of a kind of injury that can trigger the neointimal hyperplasia as a response to injury [5–7]. Eluted cytotoxic and cytostatic drugs have been introduced to inhibit the excessive neointimal formation. On that theoretical basis, we should not expect an excess of neointima despite the embedment and injury to the vessel wall. The relationship between the injury (degree of embedment) and neointimal hyperplasia will be the topic of future studies.

LIMITATION

Selection bias of the patients and cross-sections was the major limitation of this analysis. The sample size of the enrolled patients was quite limited, although the strut number was sufficient to evaluate the reproducibility of the method. A total of 30 cross-sections from 365 cross-sections were excluded from the analysis due to incapability of automatic lumen detection (masked by residual blood). This automatic detection, a key factor for the excellent reproducibility of this embedment algorithm, was highly influenced by the OCT image quality. Some sample showed as much as 50 % of difference in embedment ratio. These differences stemmed from the struts and lumen contours manually corrected by analysts. In some struts and lumen contours, we needed to manually correct the strut point and contours because of the error of the automatic detection [19, 20]. Although we have created a protocol for manual correction to improve the reproducibility as much as possible, this kind of manual work affected the accuracy of the analysis. Finally, in the current study, we focused only on the embedment analysis and its reproducibility, which is just one aspect of vessel injury assessment. Further investigation would be necessary to assess the vessel injury comprehensively.

CONCLUSIONS

The newly developed embedment analysis by OCT showed excellent reproducibility in stented/scaffolded coronary segments. Computer-assisted embedment analysis could be a feasible tool for future clinical application and clinical studies.

REFERENCES

1. Serruys PW, Suwannasom P, Nakatani S, Onuma Y (2015) Snowshoe versus ice skate for scaffolding of disrupted vessel wall. JACC Cardiovasc Interv 8(7):910–913. doi:10.1016/j.jcin.2015.04.005
2. Methe H, Balcells M, Alegret Mdel C, Santacana M, Molins B, Hamik A, Jain MK, Edelman ER (2007) Vascular bed origin dictates flow pattern regulation of endothelial adhesion molecule expression. Am J Physiol Heart Circ Physiol 292(5):H2167– H2175. doi:10.1152/ajpheart.00403.2006
3. Jimenez JM, Davies PF (2009) Hemodynamically driven stent strut design. Ann Biomed Eng 37(8):1483–1494. doi:10.1007/ s10439-009-9719-9
4. Bourantas CV, Papafaklis MI, Kotsia A, Farooq V, Muramatsu T,Gomez-Lara J, Zhang YJ, Iqbal J, Kalatzis FG, Naka KK, Fotiadis DI, Dorange C, Wang J, Rapoza R, Garcia-Garcia HM, Onuma Y, Michalis LK, Serruys PW (2014) Effect of the endothelial shear stress patterns on neointimal proliferation following drug-eluting bioresorbable vascular scaffold implantation: an optical coherence tomography study. JACC Cardiovasc Interv 7(3):315–324. doi:10.1016/j.jcin.2013.05.034
5. Schwartz RS, Huber KC, Murphy JG, Edwards WD, Camrud AR, Vlietstra RE, Holmes DR (1992) Restenosis and the proportional neointimal response to coronary artery injury: results in a porcine model. J Am Coll Cardiol 19(2):267–274
6. Gunn J, Arnold N, Chan KH, Shepherd L, Cumberland DC, Crossman DC (2002) Coronary artery stretch versus deep injury in the development of in-stent neointima. Heart 88(4):401–405
7. Schwartz RS, Chronos NA, Virmani R (2004) Preclinical restenosis models and drug-eluting stents: still important, still much to learn. J Am Coll Cardiol 44(7):1373–1385. doi:10.1016/j.jacc.2004.04.060
8. Kawamoto H, Panoulas VF, Sato K, Miyazaki T, Naganuma T, Sticchi A, Figini F, Latib A, Chieffo A, Carlino M, Montorfano M, Colombo A (2015) Impact of strut width in periprocedural myocardial infarction: a propensity-matched comparison between bioresorbable scaffolds and the first-generation sirolimus-eluting stent. JACC Cardiovasc Interv 8(7):900–909. doi:10.1016/j.jcin.2015.02.011
9. Ormiston JA, Webber B, Ubod B, Darremont O, Webster MW (2015) An independent bench comparison of two bioresorbable drug-eluting coronary scaffolds (Absorb and DESolve) with a durable metallic drug-eluting stent (ML8/Xpedition). EuroIntervention11(1):60–67. doi:10.4244/EIJY15M02_03
10. Kawamoto T, Okura H, Koyama Y, Toda I, Taguchi H, Tamita K, Yamamuro A, Yoshimura Y, Neishi Y, Toyota E, Yoshida K (2007) The relationship between coronary plaque characteristics and small embolic particles during coronary stent implantation. J Am Coll Cardiol 50(17):1635–1640. doi:10.1016/j.jacc.2007.05.050
11. Koskinas KC, Chatzizisis YS, Antoniadis AP, Giannoglou GD (2012) Role of endothelial shear stress in stent restenosis and thrombosis: pathophysiologic mechanisms and implications for clinical translation. J Am Coll Cardiol 59(15):1337–1349. doi:10. 1016/j.jacc.2011.10.903
12. Papafaklis MI, Bourantas CV, Farooq V, Diletti R, Muramatsu T, Zhang Y, Fotiadis DI, Onuma Y, Garcia Garcia HM, Michalis LK, Serruys PW (2013) In vivo assessment of the three-dimensional haemodynamic micro-environment following drug-eluting bioresorbable vascular scaffold implantation in a human coronary artery: fusion of frequency domain optical coherence tomography and angiography.EuroIntervention 9(7):890. doi:10.4244/EIJV9I7A147
13. Mejia J, Ruzzeh B, Mongrain R, Leask R, Bertrand OF (2009) Evaluation of the effect of stent strut profile on shear stress distribution using statistical moments. Biomed Eng Online 8:8. doi:10.1186/1475-925x-8-8

14. Nakatani S, Sotomi Y, Ishibashi Y, Grundeken MJ, Tateishi H, Tenekecioglu E, Zeng Y, Suwannasom P, Regar E, Radu MD, Raber L, Bezerra H, Costa MA, Fitzgerald P, Prati F, Costa RA, Dijkstra J, Kimura T, Kozuma K, Tanabe K, Akasaka T, Di Mario C, Serruys PW, Onuma Y (2015) Comparative analysis method of permanent metallic stents (XIENCE) and bioresorbable poly-L-lactic (PLLA) scaffolds (Absorb) on optical coherence tomography at baseline and follow-up. EuroIntervention. doi:10.4244/eijy15m10_03
15. Kim JS, Ha J, Kim BK, Shin DH, Ko YG, Choi D, Jang Y, Hong MK (2014) The relationship between post-stent strut apposition and follow-up strut coverage assessed by a contour plot optical coherence tomography analysis. JACC Cardiovasc Interv 7(6):641–651. doi:10.1016/j.jcin.2013.12.205
16. Kimura T, Kozuma K, Tanabe K, Nakamura S, Yamane M, Muramatsu T, Saito S, Yajima J, Hagiwara N, Mitsudo K, Popma JJ, Serruys PW, Onuma Y, Ying S, Cao S, Staehr P, Cheong WF, Kusano H, Stone GW (2015) A randomized trial evaluating everolimus- eluting Absorb bioresorbable scaffolds vs. everolimuseluting metallic stents in patients with coronary artery disease: ABSORB Japan. Eur Heart J. doi:10.1093/eurheartj/ehv435
17. Bezerra HG, Costa MA, Guagliumi G, Rollins AM, Simon DI (2009) Intracoronary optical coherence tomography: a comprehensive review clinical and research applications. JACC Cardiovasc Interv 2(11):1035–1046. doi:10.1016/j.jcin.2009.06.019
18. Prati F, Cera M, Ramazzotti V, Imola F, Giudice R, Giudice M, Propris SD, Albertucci M (2008) From bench to bedside: a noveltechnique of acquiring OCT images. Circ J 72(5):839–843
19. Wang A, Nakatani S, Eggermont J, Onuma Y, Garcia-Garcia HM, Serruys PW, Reiber JH, Dijkstra J (2014) Automatic detection of bioresorbable vascular scaffold struts in intravascular optical coherence tomography pullback runs. Biomed Opt Express 5(10):3589–3602. doi:10.1364/boe.5.003589
20. Wang A, Eggermont J, Dekker N, Garcia-Garcia HM, Pawar R, Reiber JH, Dijkstra J (2013) Automatic stent strut detection in intravascular optical coherence tomographic pullback runs. Int J Cardiovasc Imaging 29(1):29–38. doi:10.1007/s10554-012-0064-y 21. Fleiss JL (1986) The design and analysis of clinical experiments. Wiley, New York
22. BlandJM A (1986) Statistical methods for assessing agreement between two methods of clinical measurement. Lancet 1(8476):307–310
23. Landis JR, Koch GG (1977) The measurement of observer agreement for categorical data. Biometrics 33(1):159–174

Chapter 7

Is quantitative coronary angiography reliable in assessing the lumen gain after treatment with the everolimus eluting bioresorbable polylactide scaffold: a quantitative coronary angiography and optical coherence tomography comparison in the Absorb Japan randomized trial?

Yohei Sotomi, Yoshinobu Onuma, Pannipa Suwannasom, Hiroki Tateishi, Erhan Tenekecioglu, Yaping Zheng, Rafael Cavalcante, Hans Jonker, Jouke Dijkstra, Nicolas Foin, Jaryl Ng Chen Koon, Carlos Collet, Robbert J. de Winter, Joanna J. Wykrzykowska, Gregg W. Stone, Jeffrey J. Popma, Ken Kozuma, Kengo Tanabe, Patrick W. Serruys, Takeshi Kimura

EuroIntervention. 2016 Oct 10;12(8):e998-e1008

ABSTRACT

Aims

The current study aimed to assess the difference in lumen dimension measurements between optical coherence tomography (OCT) and quantitative coronary angiography (QCA) in the polymeric bioresorbable scaffold and metallic stent.

Methods and results

In the randomised ABSORB Japan trial, 87 lesions in the Absorb arm and 44 lesions in the XIENCE arm were analysed. Post-procedural OCT-QCA lumen dimensions were assessed in matched proximal/distal non-stented/non-scaffolded reference (n=199), scaffolded (n=145) and stented (n=75) cross-sections at the two device edges using the Bland-Altman method. In the non-stented/non-scaffolded reference segments, QCA systematically underestimated lumen diameter (LD) compared with OCT (accuracy, –0.26 mm; precision, 0.47 mm; 95% limits of agreement as a mean bias±1.96 standard deviation, –1.18-0.66 mm). When compared to OCT, QCA of the Absorb led to a more severe underestimation of the LD (–0.30 mm; 0.39 mm; –1.06-0.46 mm) than with the XIENCE (–0.14 mm; 0.31 mm; –0.75- 0.46 mm). QCA underestimated LD by 9.1%, 4.9%, and 9.8% in the reference, stented, and scaffolded segments, respectively. The protrusion distance of struts was larger in the Absorb arm than in the XIENCE arm (135±27 μm vs. 18±26 μm, $p<0.001$), and may have contributed to the observed differences.

Conclusions

In-device QCA measurement was differently affected by the presence of a metallic or polymeric scaffold, a fact that had a significant impact on the QCA assessment of acute gain and post-procedural minimum LD. (ClinicalTrials.gov, Identifier: NCT01844284)

INTRODUCTION

In contrast to metallic stents, the Absorb™ bioresorbable poly-L-lactide (PLLA) scaffolds (Abbott Vascular, Santa Clara, CA, USA) are partially translucent and radiolucent to gamma radiation, with the exception of the radiopaque platinum markers at the edges. Therefore, imaging interpretation of Absorb scaffolds with optical coherence tomography (OCT) or quantitative coronary angiography (QCA) has to be critically appraised.

OCT is widely recognised as a gold standard for the measurement of luminal dimensions for both metallic stents and polymeric scaffolds due to its resolution (<20 μm) and accuracy[1]. The comparative methodologies of lumen measurement by OCT in polymeric scaffolds and metallic stents have been introduced and applied for the current clinical trials[2-4].

QCA is known to underestimate the lumen dimension systematically compared to OCT[5]. However, in the assessment of metallic stents, this difference between QCA and OCT might also be influenced by the radiopacity of the material, since the radiopacity of metallic stents could theoretically impact on the densitometric and edge software analysis of QCA[6]. In the assessment of polymeric scaffolds, their radiolucency theoretically does not impact on the QCA analysis, whereas their increased strut protrusion into the lumen could hinder the intracoronary laminar flow, which might result in underestimation of the lumen dimension due to altered contact of the contrast medium with the vessel wall[7,8]. Therefore, polymeric scaffolds and metallic stents – because of their inherent material properties – could introduce an incremental element of discrepancy between measurements by OCT and QCA. However, this hypothesis has not been investigated so far.

The purpose of the current study was to assess the difference between OCT and QCA measurements in polymeric scaffolds and metallic stents, and to investigate the mechanisms of discrepancy, if it occurs.

METHODS

Study design

ABSORB Japan was a prospective, multicentre, randomised, single-blind, active-controlled clinical trial in which 400 patients undergoing coronary stent implantation in Japan were randomised in a 2:1 ratio to treatment with the Absorb everolimus-eluting BVS or the XIENCE Prime®/Xpedition® cobalt-chromium everolimus-eluting stent (both Abbott Vascular)[3]. The details of the trial have been described elsewhere[3]. A total of 38 investigational sites in Japan participated in the study. The study was conducted according to the Declaration of Helsinki. Prior to initiating the study, the institutional

review board at each investigational site approved the clinical trial protocol. All patients provided written informed consent before enrolment.

Patients were randomised in a 2:1 ratio to Absorb vs. XIENCE using a central randomisation service. Randomisation was stratified by the presence of diabetes mellitus and the number of lesions to be treated. Patients were allocated randomly to one of the three intravascular imaging subgroups: intravascular ultrasound (IVUS) group (150 patients), OCT group 1 (125 patients), or OCT group 2 (125 patients), based on the schedules of intravascular imaging. In the present investigation, we analysed OCT data and QCA data from OCT group 1[3]. The study flow chart is shown in Figure 1.

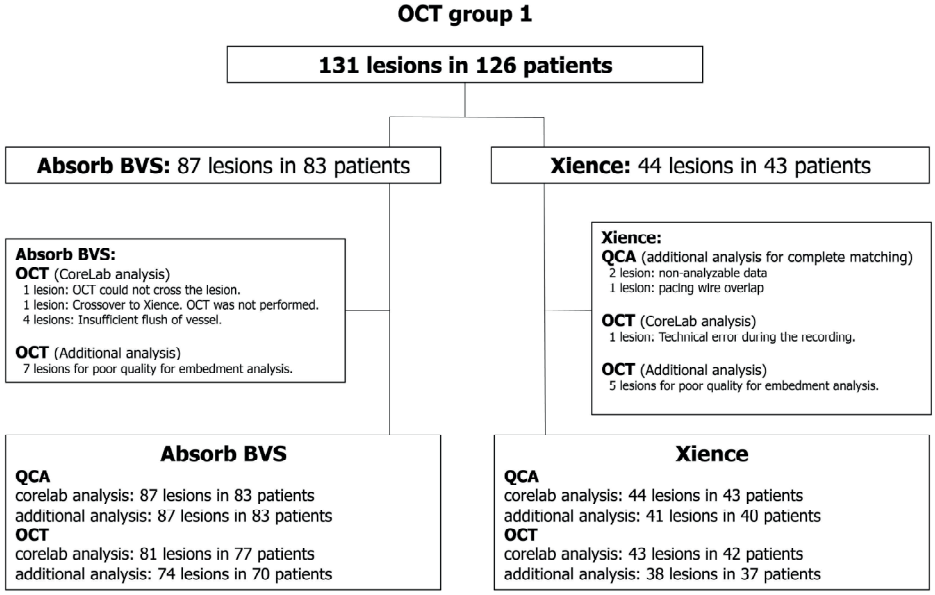

Figure 1. Study flow chart

Quantitative coronary angiography

An angiographic core laboratory performed QCA analysis (QAngio® XA 7.3; Medis medical imaging systems bv, Leiden, The Netherlands). The following parameters were analysed by the core lab: mean lumen diameter (LD), minimum lumen diameter (MLD), interpolated reference vessel diameter (RVD), percentage diameter stenosis (%DS), minimum lumen area (MLA) based on the edge detection method9. MLA assessed by QCA was calculated from the MLD, which was provided by the software, using the formula: $MLA=3.14x(MLD/2)^2$[2,6] (Appendix Figure 1). In addition to the core lab analysis of QCA, we performed QCA by the edge detection method at the co-localised position with the OCT cross-sections. This QCA analysis was performed according to standard procedures,

using single-plane orthogonal projections of the target lesion with the CAAS system version 5.11 (Pie Medical Imaging BV, Maastricht, The Netherlands). For each lesion, the LDs at both device edges and a single LD at the extremities of the 5 mm proximal and distal to the device edges were analysed. The small radiopaque markers at the ends of the polymeric scaffolds and the radiopaque struts of metallic stents helped us to localise the in-device segment. Lumen area (LA) at each cross-section was calculated by the above-mentioned formula.

Optical coherence tomography

OCT pullbacks were obtained at baseline after the stent or scaffold implantation by a frequency-domain C7 system using a Dragonfly™ catheter (St. Jude Medical, St. Paul, MN, USA) at a rotation speed of 100 frames/s and constant pullback speed of 20 mm/s, a frequency-domain ILUMIEN™ OPTIS™ system using a Dragonfly™ Duo catheter (both St. Jude Medical) at a rotation speed of 180 frames/s and constant pullback speed of 18 mm/s, or an optical frequency domain imaging (OFDI) Lunawave® console using a FastView® catheter (both Terumo Europe N.V., Leuven, Belgium) at a rotation speed of 160 frames/s and constant pullback speed of 20 or 40 mm/s with a non-occlusive technique, while contrast was infused through the guiding catheter at a continuous rate of 2-4 mL/s.

The OCT measurements were performed with the QIvus® software (Medis) by the core laboratory (Cardialysis, Rotterdam, The Netherlands). With adjustment for the pullback speed, the analysis of continuous cross-sections was performed at each 1 mm longitudinal interval within the treated segment. The following parameters were evaluated: mean and (projected) MLD and area, mean and minimum (abluminal) scaffold/stent diameter and area[2]. The LD of the matched cross-section analysis was calculated using a circular model[10]. The details are shown in the Appendix.

The additional OCT analysis (strut protrusion analysis) was performed with a newly developed specific software, QCU-CMS software version 4.69 (Leiden University Medical Center, Leiden, The Netherlands)[11]. The protrusion distance was measured by the software (Appendix Figure 1). The details of the analysis are described elsewhere[11]. The protrusion analysis by OCT was performed every 200 μm cross-section in case of OCT and every 250 μm in case of OFDI in the stent/scaffold segments. The cases with complete pullback and good image quality as defined by >70% of analysable frames were included in this specific analysis[12]. Mean strut protrusion distance was calculated as the average of protrusion distance in a lesion level and a cross-section level.

Comparison of QCA and OCT

The discrepancies between QCA and OCT were compared among scaffolded segment, stented segment, and proximal/distal reference segment. As described above, in each

lesion, the treated segment and the peri-treated regions (defined by a length of 5 mm proximal and distal to the device edge) were analysed.

For matching of an OCT cross-section with a corresponding QCA cross-section, the following criteria were used in this study. Case examples for matched cross-sections in XIENCE and Absorb cases are shown in Figure 2. For the scaffolded segment, OCT cross-sections with proximal and distal metallic markers were matched with corresponding QCA cross-sections which were recognised using the radiopaque metallic markers of the polymeric device. For the stented segment, OCT cross-sections at both stent edges were matched with the corresponding QCA cross-sections which were recognised by radiopaque strut edges. The identification of the stent edges on OCT was defined as the point where the visualisation of the stent arc was circumferential, implying that the stent edge to some extent may include metallic struts. For proximal/distal reference segments, 5 mm proximal and 5 mm distal cross-sections in OCT and QCA analyses were analysed as matched cross-sections. Bifurcation segments in which the side branch occupied more than 45° of the cross-section were excluded in order to avoid tracing interpolation when quantifying the lumen[12]. In case the metallic marker of the Absorb could not be identified due to the wire shadow artefact or insufficient flush of blood, the cross-section and the associated proximal or distal edge cross-sections were not included in the analysis.

Statistical analysis

Data are expressed as mean ± standard deviation or median and interquartile range with differences (95% confidence interval). Group means for continuous variables with normal and non-normal distributions were compared using Student's t-tests and Mann-Whitney U tests, respectively. Categorical variables were compared using the Pearson's chi-square test or Fisher's exact test, as appropriate. Generalised estimating equations modelling was performed to take into account the clustered nature of >1 stent/ scaffold analysed from the same patients, which might result in unknown correlations among measurements within these scaffold clusters. Measurement agreements in LD at cross-section level and mean LD, MLD, MLA at lesion level by QCA and those by OCT were determined by comparing measurements of each analysis using the Bland-Altman method. Data are given as plots showing the absolute difference between corresponding measurements of both methods (y-axis) against the average of both methods (x-axis). Assuming OCT as a gold standard, the accuracy between OCT and QCA measurements and its precision were calculated. The 95% limits of agreement were calculated as mean bias ± 1.96 standard deviation. Simple linear regression analysis was used to evaluate the relationship between the strut protrusion distance and the OCT-QCA discrepancy. The Pearson correlation coefficient was used to evaluate the strength and direction of the linear relationship between the OCT-QCA discrepancy and strut protrusion. Statistical

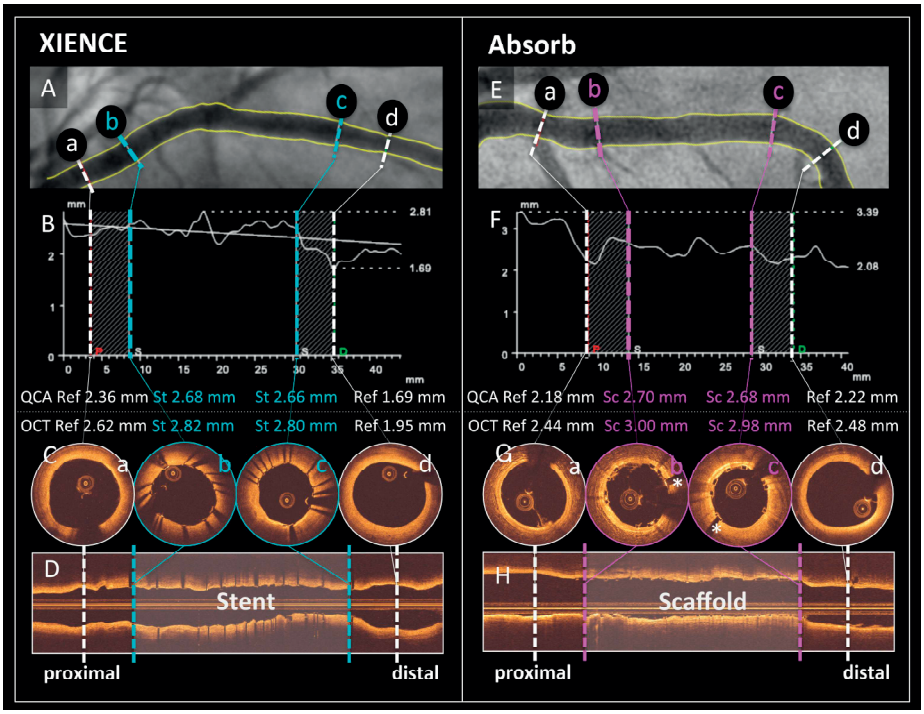

Figure 2. Case examples for matched cross-sections. Case examples of XIENCE (A-D) and Absorb (E-H) are shown. Cross-sections at reference (white) vessel (a, d) and stented (light blue)/scaffolded (pink) vessel (b, c) on QCA (A, B, E, & F) were matched with those on OCT (C, D, G, & H). *Metallic marker of Absorb. OCT: optical coherence tomography; QCA: quantitative coronary angiography; Ref: reference cross-section; Sc: scaffolded cross-section; St: stented cross-section

significance was assumed at a probability (p) value of <0.05. All statistical analyses were performed with SPSS, Version 23.0.0 (IBM Corp., Armonk, NY, USA) or MedCalc statistical software, version 14.12.0 (MedCalc Software bvba, Ostend, Belgium).

RESULTS

Patient characteristics

From a total of 126 patients in the OCT group 1, 87 lesions from 83 patients in the Absorb arm and 44 lesions from 43 patients in the XIENCE arm were analysed. Baseline clinical characteristics are shown in Table 1. Lesion and procedural characteristics are summarised in Table 2. All baseline characteristics and the procedural variables were well balanced between both arms.

Table 1. Baseline characteristics

	Absorb (N=83)	XIENCE (N=43)	Difference [95% CI]
Age (year)	65.9±9.8(83)	67.6±11.2(43)	-1.7[-5.7,2.3]
Gender	79.5%(66/83)	72.1%(31/43)	7.43%[-7.49%,23.91%]
Risk Factors			
Current Tobacco Use	20.5%(17/83)	18.6%(8/43)	1.88%[-13.91%,15.16%]
Hypertension	79.5%(66/83)	86.0%(37/43)	-6.53%[-18.88%,8.64%]
Dyslipidemia	83.1%(69/83)	81.4%(35/43)	1.74%[-11.24%,17.20%]
Family History of Premature CAD	9.2%(7/76)	7.5%(3/40)	1.71%[-11.51%,11.62%]
Prior MI	16.0%(13/81)	18.6%(8/43)	-2.56%[-17.97%,10.44%]
All Diabetes Mellitus	38.6%(32/83)	41.9%(18/43)	-3.31%[-21.03%,13.94%]
Type I Diabetes	0.0%(0/83)	0.0%(0/43)	0%[-8.20%,4.42%]
Type II Diabetes	38.6%(32/83)	41.9%(18/43)	-3.31%[-21.03%,13.94%]
HbA1c (%)	6.12±0.81(83)	6.17±0.65(43)	-0.05[-0.32,0.21]
Serum Creatinine (mg/dl)	0.86±0.18(83)	0.83±0.23(43)	0.03[-0.05,0.11]
eGFR (ml/min/1.73m^2)	68.5±16.6(83)	70.6±18.3(43)	-2.10[-8.75,4.54]

Data are expressed as mean ± standard deviation, percentage and number with 95% confidence interval.

Results of pre- and post-procedural QCA and post-procedural OCT are shown in Table 3. Post-procedural in-device MLD by QCA was significantly smaller in the Absorb arm than in the XIENCE arm (2.42 ± 0.38 mm vs. 2.58 ± 0.43 mm, p = 0.031). In-device acute gain by QCA was smaller in the Absorb arm than in the XIENCE arm (1.47 ± 0.43 mm vs. 1.60 ± 0.42 mm, p = 0.086). In post-procedural OCT analysis, projected MLD was similar in both arms (Absorb 2.75±0.42 mm vs. XIENCE 2.72 ± 0.54 mm, p = 0.71). Both arms had similar mean lumen area and minimum lumen area.

Comparison of QCA with OCT parameters in absorb and XIENCE

Measurement agreements between QCA and OCT for mean LD, MLD, and MLA in a lesion level analysis are shown in Figure 3. When OCT was used as a gold standard, the Absorb arm had an accuracy of –0.36 mm between QCA and OCT, which was 0.20 mm less than the XIENCE arm. MLD and MLA were also more severely underestimated by QCA in the Absorb arm than in the XIENCE arm.

Agreement between QCA and OCT parameters in the matched cross-section analysis

A total of 199 cross-sections at proximal/distal reference segments, 75 cross-sections at stented segments, and 145 cross-sections at scaffolded segments were evaluated in the matched cross-section analysis. Agreement between QCA and OCT parameters is shown in Figure 4. In proximal/distal reference segments without stents/scaffolds, QCA

Table 2. Lesion and procedural characteristics (per lesion analysis)

	Absorb (N=83) (L=87)	XIENCE (N=43) (L=44)	Difference [95% CI]
Target Vessel			
Left anterior descending artery	51.7%(45/87)	45.5%(20/44)	6.27%[-11.53%,23.39%]
Left circumflex artery or Ramus	19.5%(17/87)	31.8%(14/44)	-12.28%[-28.58%,2.91%]
Right coronary artery	28.7%(25/87)	22.7%(10/44)	6.01%[-10.57%,20.25%]
Left main coronary artery	0.0%(0/87)	0.0%(0/44)	0%[-8.03%,4.23%]
Aneurysm	1.2%(1/86)	2.3%(1/44)	-1.11%[-10.69%,4.35%]
Calcification (Moderate or Severe)	22.1%(19/86)	34.1%(15/44)	-12%[-28.55%,3.70%]
Tortuosity (Moderate or Severe)	7.0%(6/86)	9.1%(4/44)	-2.11%[-14.75%,7.12%]
Eccentric	89.5%(77/86)	79.5%(35/44)	9.99%[-2.44%,24.85%]
Thrombus	0.0%(0/86)	0.0%(0/44)	0%[-8.03%,4.28%]
Bifurcation	34.5%(30/87)	43.2%(19/44)	-8.7%[-25.92%,8.37%]
ACC/AHA Lesion Class			
A	4.6%(4/87)	2.3%(1/44)	2.32%[-7.61%,9.22%]
B1	16.1%(14/87)	15.9%(7/44)	0.18%[-14.66%,12.31%]
B2	58.6%(51/87)	52.3%(23/44)	6.35%[-11.13%,23.70%]
C	20.7%(18/87)	29.5%(13/44)	-8.86%[-25.19%,6.08%]
Pre Dilatation	100.0%(87/87)	100.0%(44/44)	0%[-4.23%,8.03%]
Number of Total Study Devices	1.0±0.2(87)	1.0±0.0(44)	0.0[-0.0,0.1]
Diameter of Study Devices (mm)	3.03±0.38(87)	3.06±0.41(44)	-0.03[-0.17,0.12]
Length of Total Study Devices (mm)	20.6±5.6(87)	19.9±5.2(44)	0.7[-1.2,2.7]
Post Dilatation	77.0%(67/87)	77.3%(34/44)	-0.26%[-14.23%,15.90%]
Procedure Duration (min)	53.3±26.6(83)	51.9±24.1(43)	1.4[-8.0,10.7]
Procedure Complication	4.8%(4/83)	4.7%(2/43)	0.17%[-11.03%,7.87%]
Clinical Device Success	98.8%(85/86)	100.0%(44/44)	-1.16%[-6.30%,6.92%]
Clinical Procedure Success	97.6%(80/82)	97.7%(42/43)	-0.11%[-6.43%,9.78%]

Data are expressed as mean ± standard deviation, percentage and number with 95% confidence interval.

underestimated LD by 0.26 mm on average compared with OCT. When compared to OCT, QCA of the Absorb polymeric scaffolds led to a more severe underestimation of the LD (accuracy –0.30 mm; precision 0.39 mm) than with the XIENCE metallic stents (accuracy –0.14 mm; precision 0.31 mm). The same trend was observed in LA. Delta accuracy compared to the accuracy of reference segments (–0.26 mm in average compared with OCT. When compared to OCT, QCA of the Absorb polymeric scaffolds led to a more severe underestimation of the LD (accuracy –0.30 mm; precision 0.39 mm) than with the XIENCE metallic stents (accuracy –0.14 mm; precision 0.31 mm). The same trend was observed in LA. Delta accuracy compared to the accuracy of reference segments (–0.26 mm on LD, –1.13 mm^2 in LA) was significantly different between the XIENCE and

Table 3. Results of quantitative coronary angiography and optical coherence tomography

	Absorb	XIENCE	Difference [95%CI]	P-Value
QCA analysis	L=87	L=44		
Lesion Length (mm)	13.8±5.5	13.4±5.0	0.4[-1.6,2.3]	0.71
Pre-Procedure Reference Vessel Diameter (mm)	2.68±0.45	2.76±0.50	-0.08[-0.26,0.10]	0.39
Pre-Procedure Minimum Lumen Diameter (mm)	0.95±0.36	0.98±0.34	-0.04[-0.16,0.09]	0.58
Pre-Procedure Percent Diameter Stenosis (%DS)	65±12	64±10	0.1[-3.9,4.1]	0.95
Post-Procedure In-Device Minimum Lumen Diameter (mm)	2.42±0.38	2.58±0.43	-0.17[-0.32,-0.02]	0.031
Post-Procedure In-Device Percent Diameter Stenosis (%DS)	11±7	8±7	3.0[0.4,5.6]	0.023
In-Device Acute Gain (mm)	1.47±0.43	1.60±0.42	-0.14[-0.29,0.02]	0.086
OCT analysis (Post-Procedural)	L=81	L=43		
Mean Lumen Diameter (mm)	3.03±0.42	3.02±0.52	-0.01[-0.18,0.16]	0.94
(Projected) Minimum Lumen Diameter (mm)	2.75±0.42	2.72±0.54	-0.03[-0.21,0.14]	0.71
Mean Lumen Area (mm^2)	7.37±2.01	7.40±2.42	0.04[-0.77,0.84]	0.93
Minimum Lumen Area (mm^2)	6.09±1.81	6.03±2.24	-0.06[-0.79,0.68]	0.88
Mean Stent/Scaffold Diameter (mm)*	3.11±0.43	3.16±0.51	0.05[-0.12,0.22]	0.54
(Projected) Minimum Stent/Scaffold Diameter (mm)*	2.57±0.43	2.73±0.54	0.16[-0.02,0.34]	0.073
Mean Stent/Scaffold Area (mm^2)*	7.74±2.10	8.05±2.49	0.31[-0.53,1.15]	0.46
Minimum Stent/Scaffold Area (mm^2)*	6.55±1.99	6.90±2.44	0.35[-0.46,1.15]	0.40
Mean Strut Area (mm^2)	0.27±0.04	0.08±0.01	-0.19[-0.20,-0.18]	<0.001
Protrusion Distance (mm)	135±27(L=74)	18±26(L=38)	-117[-128,-107]	<0.001

* "Abluminal" Stent/Scaffold data are indicated. Data are expressed as mean ± standard deviation, percentage and number with 95% confidence interval.

the Absorb arms (LD: XIENCE +0.12±0.31 mm vs. Absorb –0.04±0.39 mm, p=0.002; LA: +0.37±1.55 mm^2 vs. –0.26±1.90 mm^2, p=0.014).

Correlation between the OCT-QCA discrepancy and stent/scaffold parameters

In a lesion level analysis (Table 3), the protrusion distance of struts into the lumen was larger in the Absorb arm than in the XIENCE arm (135±27 μm vs. 18±26 μm, p<0.001). In a cross-section level analysis, mean protrusion distance had a moderate correlation with the OCT-QCA discrepancy of LD both in XIENCE and Absorb (correlation coefficient –0.418 for XIENCE, –0.440 for Absorb, both p<0.001) (Figure 5). Lumen eccentricity had very weak correlation with the discrepancy in both arms (correlation coefficient 0.221 for XIENCE, p=0.057; –0.184 for Absorb, p=0.027).

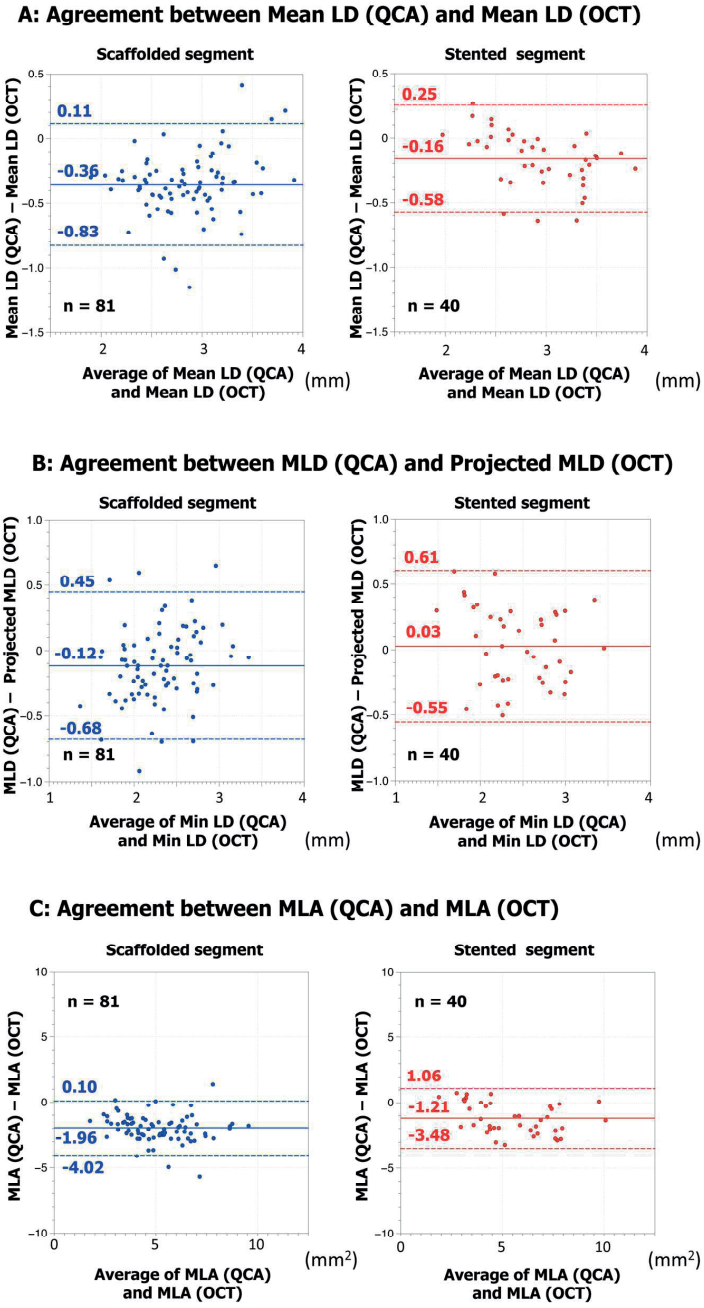

Figure 3. Measurement agreement between QCA and OCT. In the Absorb arm, QCA underestimated mean LD 0.20 mm more than in the XIENCE arm (A). MLD (B) and MLA (C) were also more severely underestimated by QCA in the Absorb arm than in the XIENCE arm. LD: lumen diameter; MLA: minimum lumen area; MLD: minimum lumen diameter; OCT: optical coherence tomography; QCA: quantitative coronary angiography

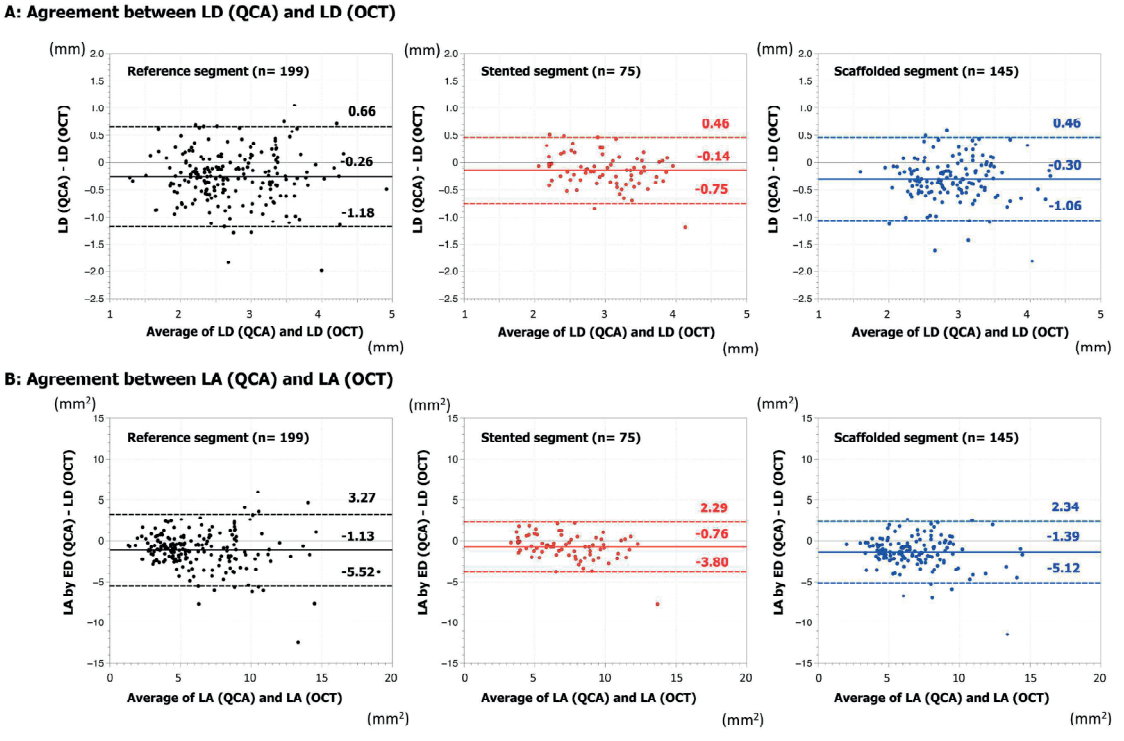

Figure 4. Agreement between OCT and QCA in matched cross-section analysis.
In a matched cross-section analysis, lumen diameter (A) and lumen area (B) in 199, 75, and 145 cross-sections were evaluated at proximal/distal reference (black), stented (red), and scaffolded (blue) segments, respectively. Mean bias (solid line) and 95% limits of agreement (mean bias±1.96 standard deviation) (dotted line) are indicated. LA: lumen area; LD: lumen diameter; OCT: optical coherence tomography; QCA: quantitative coronary angiography

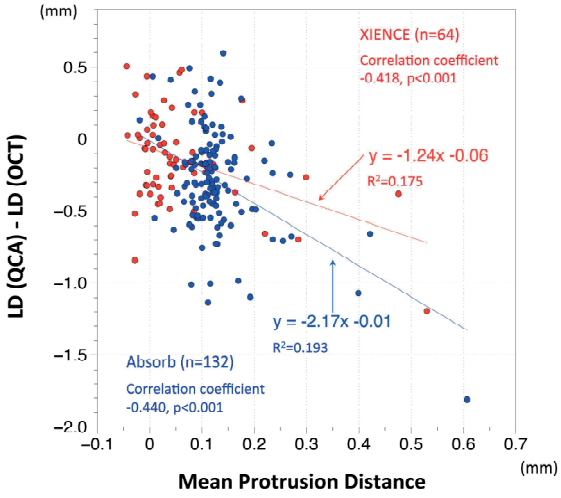

Figure 5. Correlation between the OCT-QCA LD discrepancy and stent/scaffold protrusion. Correlation between the OCT-QCA LD discrepancy and mean protrusion distance in XIENCE (red circle) and Absorb (blue circle) is shown in scatter plots. Mean protrusion distance had a moderate correlation with the OCT-QCA discrepancy of LD in both XIENCE and Absorb. LD: lumen diameter; OCT: optical coherence tomography; QCA: quantitative coronary angiography

DISCUSSION

The main findings of the present study are summarised as follows. 1) In proximal/distal reference segments without stents/scaffolds, QCA underestimated LD by 0.26 mm on average compared with OCT. When compared to OCT, QCA of the Absorb polymeric scaffolds led to a more severe underestimation of the luminal dimension (accuracy –0.30 mm) than with the XIENCE metallic stents (accuracy –0.14 mm). 2) Strut protrusion into the lumen had a moderate correlation with the underestimation of QCA compared to OCT in both XIENCE and Absorb.

OCT is widely recognised as a gold standard for the measurement of luminal dimensions for both metallic stents and polymeric scaffolds due to its resolution and accuracy[1]. Detection of the vessel wall by OCT is the result of the backscattering reflection of the light from the most superficial (20 μm) endoluminal layer of the vessel wall, while the detection of luminal dimension by angiography is the result of a more or less laminar contact of contrast medium with the vessel wall which is influenced by the velocity of the most outer layer of laminar flow along the vessel wall. Therefore, the QCA measurement, by nature, underestimates the true dimension which is almost perfectly defined by OCT [1,5,13]

The results of the present study are in line with previous reports[1,5,13]. Figure 6 summarises the relative difference of QCA-LD versus OCT-LD. In the reference segments,

QCA underestimated LD by 9.1% compared to OCT. In the stented segments, QCA underestimated LD less (4.9%), whereas in the scaffolded segments QCA more severely underestimated LD (9.8%) compared to OCT. Figure 7 illustrates computational flow dynamics demonstrating the possible causes of discrepancy between luminal dimensions as determined by OCT or QCA in the native (reference), stented, and scaffolded vessels. In the stented vessel, laminar flow of contrast is disturbed by the protruded struts and cannot get into close contact with the vessel wall compared to the native unstented/unscaffolded vessels. However, high radiopacity of metallic struts could cause an artefactual outward enlargement of the lumen contours (blooming artefact of metal), resulting in less underestimation in the stented vessels than in the scaffolded vessels. A radiolucent polymeric strut does not cause any inherent X-ray artefact in the brightness function and analysis by QCA. In the scaffolded vessels, the laminar flow disturbance is larger than in the stented vessels due to more strut protrusions, resulting in less close contact of the contrast medium with the vessel wall. Thereby, scaffolded vessels generate possibly a more severe underestimation of the lumen dimension on QCA than the one observed in the native vessels.

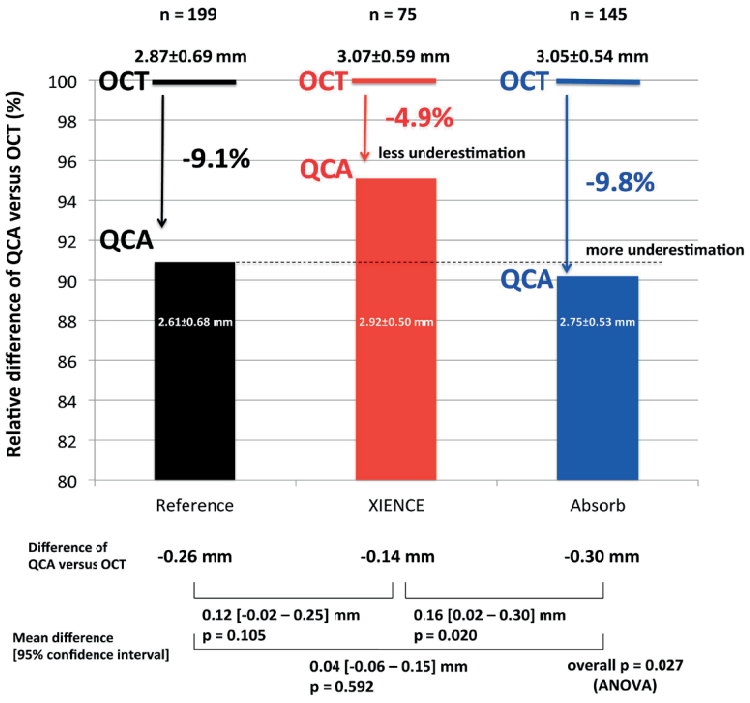

Figure 6. Relative difference of QCA-LD versus OCT-LD. In the reference segments (black), QCA underestimated LD by 9.1% compared to OCT; in the stented segments (red), QCA underestimated LD less (4.9%), whereas, in the scaffolded segments (blue), QCA underestimated LD more severely (9.8%) compared to OCT. OCT: optical coherence tomography; QCA: quantitative coronary angiography

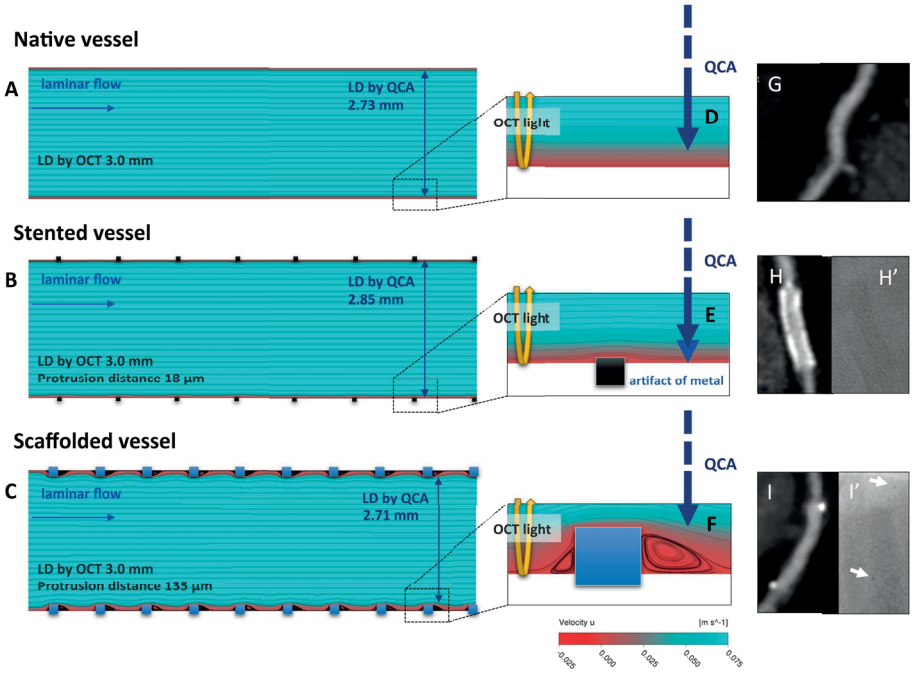

Figure 7. Possible causes of discrepancy between luminal dimensions as determined by OCT or QCA in the native, stented, and scaffolded vessels. Computational flow dynamics in native (A & D), stented (B & E), and scaffolded (C & F) vessels demonstrated the difference of contact of contrast with the vessel wall. The differences of radiopacity are demonstrated in MSCT (G, H, & I) and angiographic images (H' & I'). White arrows in panel I': metallic markers of Absorb. LD: lumen diameter; OCT: optical coherence tomography; QCA: quantitative coronary angiography

Material property

The more radiopaque the metal is, the larger the luminal dimensions become on QCA. The basic algorithm of edge detection relies on the average weight of the first and second derivative of the brightness function, and presence of metal in the vessel wall will interfere with the edge detection[6], a fact that has been repeatedly demonstrated for highly radiopaque metals such as tantalum, nitinol, and platinum[6,14]. Fortunately, cobalt-chromium is a metal with low radiopacity and thus there is less interference with edge detection, although a small but detectable effect can be demonstrated compared with the reference segment[14]. In other words, radiopacity has a tendency to enlarge artefactually the contour of the lumen, whereas the lumen contour might artefactually be reduced by the degree of strut protrusion. In contrast to metallic stents, the Absorb PLLA scaffolds are totally radiolucent. The material (PLLA) itself therefore does not interfere with the densitometric assessment by QCA but causes underestimation of the lumen dimension due to the physical hindrance for the contrast medium to contact the vessel wall as described above. Overall, the overestimation of the lumen with metallic stents

and underestimation with polymeric scaffolds could generate lower acute gain and post-procedural MLD for the polymeric scaffold when compared to the metallic stent by QCA.

Laminar flow disturbance

When the struts protrude into the lumen of coronary arteries, the lumen physically loses some space for contrast medium, which could result in underestimation of size by QCA analysis. The Absorb scaffold has 157 μm of strut thickness and 27% of vessel wall area coverage while the XIENCE has 89 μm and 13%, respectively. Contrast medium cannot be in direct contact with the vessel, at least not in this stent/scaffold occupied surface area. In addition, the flow dynamics of a coronary artery are pulsatile, laminar, and non-Newtonian. When a stent is deployed, the individual struts promote blood flow separation, creating upstream and downstream recirculation zones[15]. In the recirculation zones, contrast medium cannot be physically in contact with the vessel wall[16]. When the strut shape is the same (e.g., both Absorb and XIENCE have rectangular shapes), the larger strut thickness creates reversal of flow upstream and downstream to the strut more frequently[7,15]. In the present study, a moderate correlation between OCT-QCA discrepancy of LD and protrusion distance would suggest that the laminar flow disturbance could be at least one of the mechanisms of OCT-QCA discrepancy.

Assessment of acute gain

In current clinical trials, "acute gain", defined as the difference between pre- and post-procedural MLD, is assessed by QCA as a parameter of device performance[3,4]. The present study would imply the unfairness of this assessment for Absorb compared to XIENCE. For the assessment of MLD, the lower degree of underestimation in metallic stents and the more severe underestimation in polymeric scaffolds would logically generate a large discrepancy and unfairness for the comparison of the device performance. In the present study, in-device acute gain by QCA was smaller in the Absorb arm than in the XIENCE arm (Absorb 1.47±0.43 mm vs. XIENCE 1.60±0.42 mm, p=0.086), while post-procedural MLD by OCT as a substitute parameter of acute gain by OCT in both arms was similar (Absorb 2.75±0.42 mm vs. XIENCE 2.72±0.54 mm, p=0.71). Since pre-procedural OCT was not performed in this study population, the acute gain by OCT is not available. However, we could assume the similarity of pre-procedural MLD in both arms due to the randomised approach. Currently, we do not have an appropriate quantitative angiographic method to assess the impact of a slight change in radiopacity on the lumen dimension measurement.

The difference in QCA analysis and the absence of difference in OCT analysis could raise the question whether the commonly used acute gain analysis by QCA for the comparison of Absorb with XIENCE is appropriate and accurate. The QCA acute gain data from previous trials comparing polymeric scaffolds and metallic stents might be critically reconsidered[3,4,17].

LIMITATIONS

First, the coronary sites matched by OCT and QCA may not have been exactly identical, especially at proximal/distal reference segments. Although the matching was performed with the radiopaque struts of XIENCE and the metallic markers of the Absorb at stented/scaffolded segments, the proximal/distal reference segments were determined as 5 mm proximal and distal from these matched cross-sections. The length on QCA and on OCT could not be identical due to the well-known unavoidable foreshortening effect of conventional angiography. Second, in the correlation analysis, cross-sections with malapposed struts were also included in the protrusion distance analysis. The impact of malapposed struts on laminar flow varies according to the malapposed distance[18]. The precise haemodynamics in the vessel with malapposed struts still remain to be elucidated. Therefore, the correlation between the OCT-QCA discrepancy and the protrusion distance could be just a hypothesis-generating finding, and further investigations are still warranted.

CONCLUSIONS

Using OCT and an untreated segment as a method and vessel of reference, it has been demonstrated that QCA is differently affected by the presence of a metallic stent or a polymeric scaffold, a fact that has a significant impact on the QCA assessment of acute gain and post-procedural MLD.

Impact on daily practice

The difference in radiopacity of polymer and metal theoretically influences the edge detection method of QCA for the assessment of Absorb polymeric scaffolds and XIENCE metallic stents. In the ABSORB Japan randomised trial, when compared to OCT, QCA underestimated LD by 9.1%, 4.9%, and 9.8% in the reference, stented, and scaffolded segments, respectively, a fact that had a significant impact on the QCA assessment of acute gain and post-procedural minimum LD. The present study would imply the unfairness of the assessment for Absorb compared to XIENCE, which could raise the question of whether the commonly used acute gain analysis by QCA for the comparison of Absorb with XIENCE is appropriate and accurate. The QCA acute gain data from previous trials comparing Absorb and XIENCE might be critically reconsidered.

REFERENCES

1. Gutierrez-Chico JL, Serruys PW, Girasis C, Garg S, Onuma Y, Brugaletta S, Garcia-Garcia H, van Es GA, Regar E. Quantitative multi-modality imaging analysis of a fully bioresorbable stent: a head-to-head comparison between QCA, IVUS and OCT. Int J Cardiovasc Imaging. 2012;28:467-78.
2. Nakatani S, Sotomi Y, Ishibashi Y, Grundeken MJ, Tateishi H, Tenekecioglu E, Zeng Y, Suwannasom P, Regar E, Radu MD, Raber L, Bezerra H, Costa MA, Fitzgerald P, Prati F, Costa RA, Dijkstra J, Kimura T, Kozuma K, Tanabe K, Akasaka T, DiMario C, Serruys PW, Onuma Y. Comparative analysis method of permanent metallic stents (XIENCE) and bioresorbable poly-L- lactic (PLLA) scaffolds (Absorb) on optical coherence tomogra- phy at baseline and follow-up. EuroIntervention. 2015 Oct 9;11(6). [Epub ahead of print].
3. Kimura T, Kozuma K, Tanabe K, Nakamura S, Yamane M, Muramatsu T, Saito S, Yajima J, Hagiwara N, Mitsudo K, Popma JJ, Serruys PW, Onuma Y, Ying S, Cao S, Staehr P, Cheong WF, Kusano H, Stone GW. A randomized trial evaluating everolimus- eluting Absorb bioresorbable scaffolds vs. everolimus-eluting metallic stents in patients with coronary artery disease: ABSORB Japan. Eur Heart J. 2015;36:3332-42.
4. Sabate M, Windecker S, Iniguez A, Okkels-Jensen L, Cequier A, Brugaletta S, Hofma SH, Raber L, Christiansen EH, Suttorp M, Pilgrim T, Anne van Es G, Sotomi Y, Garcia-Garcia HM, Onuma Y, Serruys PW. Everolimus-eluting bioresorbable stent vs. durable polymer everolimus-eluting metallic stent in patients with ST-segment elevation myocardial infarction: results of the randomized ABSORB ST-segment elevation myocardial infarction- TROFI II trial. Eur Heart J. 2016;37:229-40.
5. Okamura T, Onuma Y, Garcia-Garcia HM, van Geuns RJ, Wykrzykowska JJ, Schultz C, van der Giessen WJ, Ligthart J, Regar E, Serruys PW. First-in-man evaluation of intravascular opti- cal frequency domain imaging (OFDI) of Terumo: a comparison with intravascular ultrasound and quantitative coronary angiography. EuroIntervention. 2011;6:1037-45.
6. Strauss BH, Rensing BJ, den Boer A, van der Giessen WJ, Reiber JH, Serruys PW. Do stents interfere with the densitometric assessment of a coronary artery lesion? Cathet Cardiovasc Diagn.1991;24:259-64.
7. Koskinas KC, Chatzizisis YS, Antoniadis AP, Giannoglou GD. Role of endothelial shear stress in stent restenosis and thrombosis: pathophysiologic mechanisms and implications for clinical transla- tion. J Am Coll Cardiol. 2012;59:1337-49.
8. Serruys PW, Suwannasom P, Nakatani S, Onuma Y. Snowshoe Versus Ice Skate for Scaffolding of Disrupted Vessel Wall. JACC Cardiovasc Interv. 2015;8:910-3.
9. Tsuchida K, Garcia-Garcia HM, Ong AT, Valgimigli M, Aoki J, Rademaker TA, Morel MA, van Es GA, Bruining N, Serruys PW. Revisiting late loss and neointimal volumetric measurements in a drug-eluting stent trial: analysis from the SPIRIT FIRST trial. Catheter Cardiovasc Interv. 2006;67:188-97.
10. Bruining N, Tanimoto S, Otsuka M, Weustink A, Ligthart J, de Winter S, van Mieghem C, Nieman K, de Feyter PJ, van Domburg RT, Serruys PW. Quantitative multi-modality imaging analysis of a bioabsorbable poly-L-lactic acid stent design in the acute phase: a comparison between 2- and 3D-QCA, QCU and QMSCT-CA. EuroIntervention. 2008;4:285-91.
11. Sotomi Y, Tateishi H, Suwannasom P, Dijkstra J, Eggermont J, Liu S, Tenekecioglu E, Zheng Y, Abdelghani M, Cavalcante R, de Winter RJ, Wykrzykowska JJ, Onuma Y, Serruys PW, Kimura T. Quantitative assessment of the stent/scaffold strut embedment analysis by optical coherence tomography. Int J CardiovascImaging. 2016;32:871-83.
12. Bezerra HG, Attizzani GF, Sirbu V, Musumeci G, Lortkipanidze N, Fujino Y, Wang W, Nakamura S, Erglis A, Guagliumi G, Costa MA. Optical coherence tomography versus intravascular ultrasound

to evaluate coronary artery disease and percutaneous coronary intervention. JACC Cardiovasc Interv.2013;6:228-36.

13. Kubo T, Akasaka T, Shite J, Suzuki T, Uemura S, Yu B, Kozuma K, Kitabata H, Shinke T, Habara M, Saito Y, Hou J, Suzuki N, Zhang S. OCT compared with IVUS in a coronary lesion assessment: the OPUS-CLASS study. JACC Cardiovasc Imaging.2013;6:1095-104.
14. O'Brien BJ, Stinson JS, Larsen SR, Eppihimer MJ, Carroll WM. A platinum-chromium steel for cardiovascular stents. Biomaterials. 2010;31:3755-61.
15. Jimenez JM, Davies PF. Hemodynamically driven stent strut design. Ann Biomed Eng. 2009;37:1483-94.
16. Teresa Parra, Ruben Perez, Miguel A. Rodriguez, Francisco Castro, Robert Z. Szasz, Artur Gutkowski. Numerical Simulation of Swirling Flows - Heat Transfer Enhancement. Journal of Fluid Flow, Heat and Mass Transfer. 2015;2:1-6.
17. Serruys PW, Chevalier B, Dudek D, Cequier A, Carrie D, Iniguez A, Dominici M, van der Schaaf RJ, Haude M, Wasungu L,Veldhof S, Peng L, Staehr P, Grundeken MJ, Ishibashi Y, Garcia- Garcia HM, Onuma Y. A bioresorbable everolimus-eluting scaffold versus a metallic everolimus-eluting stent for ischaemic heart disease caused by de-novo native coronary artery lesions (ABSORB II): an interim 1-year analysis of clinical and procedural secondary out- comes from a randomised controlled trial. Lancet. 2015;385:43-54.
18. Foin N, Gutierrez-Chico JL, Nakatani S, Torii R, Bourantas CV, Sen S, Nijjer S, Petraco R, Kousera C, Ghione M, Onuma Y, Garcia-Garcia HM, Francis DP, Wong P, Di Mario C, Davies JE, Serruys PW. Incomplete stent apposition causes high shear flow disturbances and delay in neointimal cover- age as a function of strut to wall detachment distance: implications for the man- agement of incomplete stent apposition. Circ Cardiovasc Interv.2014;7:180-9.
19. Serruys PW, Onuma Y, Ormiston JA, de Bruyne B, Regar E, Dudek D, Thuesen L, Smits PC, Chevalier B, McClean D, Koolen J, Windecker S, Whitbourn R, Meredith I, Dorange C, Veldhof S, Miquel-Hebert K, Rapoza R, Garcia-Garcia HM. Evaluation of the second generation of a bioresorbable everolimus drug-eluting vas- cular scaffold for treatment of de novo coronary artery stenosis: six-month clinical and imaging outcomes. Circulation. 2010;122:2301-12.

APPENDIX - OPTICAL COHERENCE TOMOGRAPHY METHODOLOGY

We analysed lumen area, flow area, abluminal and endoluminal stent/scaffold area according to the previous publication[2]. Lumen area was measured using the continuous interface between a blood and non-blood structure. The flow area concept was introduced in 2010 to describe the vessel lumen filled by circulating blood, which reflects the blood supply conductance to the myocardium[19]. Abluminal and endoluminal stent/scaffold contours were delineated by a curvilinear interpolation connecting the midpoints of the abluminal and endoluminal leading edges of the reflective borders, respectively. In the present study, we reported lumen area, and abluminal stent/scaffold area as a stent/scaffold area. Lumen diameter of matched cross-section analysis was calculated using a circular model[10].

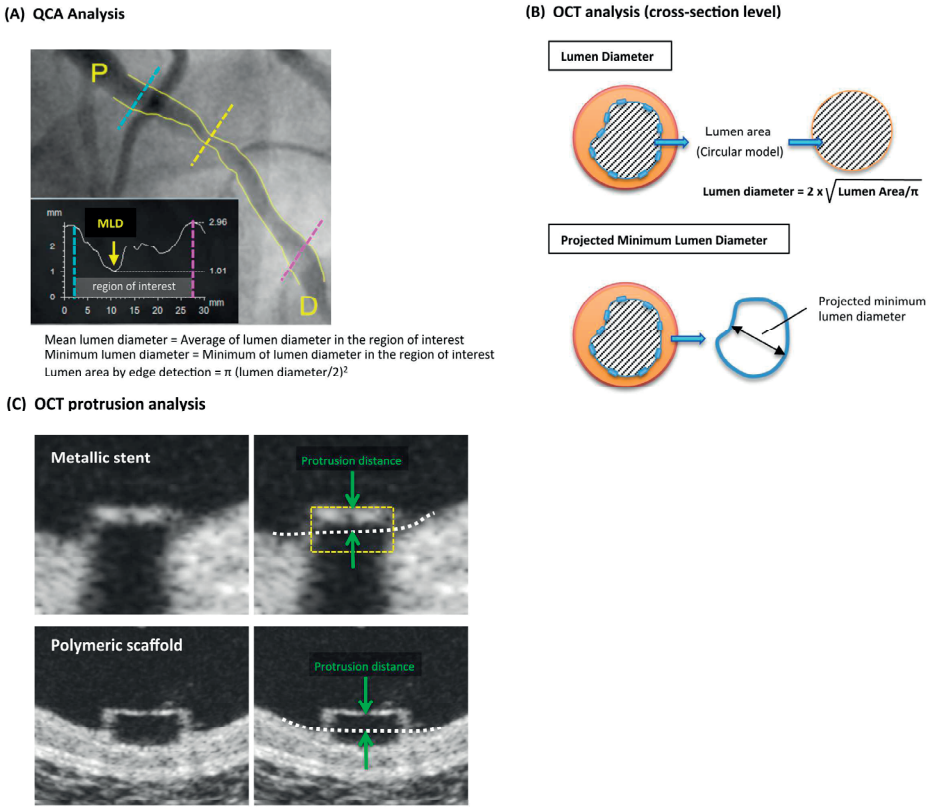

online appendix figure 1. Methodology for QCA and OCT analysis. Methods used to measure parameters with QCA (A), OCT (B), and OCT protrusion analysis (C) are shown. Standard methodology for the assessment of QCA and OCT was applied in this study (A & B)[9]. In OCT protrusion analysis, protrusion distance (green) was automatically computed by the software using the interpolated lumen contour (white dotted line) and virtual metallic struts (yellow dashed box)[11]. OCT: optical coherence tomography; QCA: quantitative coronary angiography

Chapter 8

Acute Gain in Minimal Lumen Area Following Implantation of Everolimus-Eluting ABSORB Biodegradable Vascular Scaffolds or Xience Metallic Stents: Intravascular Ultrasound Assessment from the ABSORB II Trial

Yohei Sotomi, Yuki Ishibashi, Pannipa Suwannasom, Shimpei Nakatani, Yun-Kyeong Cho, Maik J. Grundeken, Yaping Zheng, Hiroki Tateishi, Pieter C. Smits, Paul Barragan, Ron Kornowski, Anthony H. Gershlick, Stephan Windecker, Robert-Janvan Geuns, Antonio L. Bartorelli, Robbert J. de Winter, Jan G.P Tijssen, Patrick W. Serruys, Yoshinobu Onuma

JACC Cardiovasc Interv. 2016 Jun 27;9(12):1216-27

ABSTRACT

Objectives

The study compared, by intravascular ultrasound (IVUS), acute gain (AG) at the site of the pre-procedural minimal lumen area (MLA) achieved by either the Absorb (Abbott Vascular, Santa Clara, California) scaffold or the Xience stent and identified the factors contributing to the acute performance of these devices.

Background

It is warranted that the acute performance of Absorb matches that of metallic stents; however, concern exists about acute expansion and lumen gain with the use of Absorb.

Methods

Of a total of 501 patients (546 lesions) in the ABSORB II (ABSORB II Randomized Controlled Trial) randomized trial, 445 patients with 480 lesions were investigated by IVUS pre- and post-procedure. Comparison of MLA pre- and post-procedure was performed at the MLA site by matching pre- and post-procedural IVUS pullbacks.

Results

Lower AG on IVUS (lowest tertile) occurred more frequently in the Absorb arm than in the Xience arm (3.46 mm^2 vs. 4.27 mm^2, respectively; $p < 0.001$; risk ratio: 3.04; 95% confidence interval: 1.94 to 4.76). The plaque morphology at the MLA cross-section was not independently associated with IVUS acute gain. The main difference in AG in MLD by angiography was observed at the time of device implantation (Xience vs. Absorb, Δ + 1.50 mm vs. Δ+ 1.23 mm, respectively), whereas the gain from post-dilation was similar between the 2 arms (Δ+ 0.16 mm vs. Δ+ 0.16 mm) when patients underwent post-dilation, although expected balloon diameter was smaller in the Absorb arm than in the Xience arm ($p = 0.003$) during post-dilation.

Conclusion

At the site of the pre-procedural MLA, the increase of the lumen post-procedure was smaller in the Absorb-arm than in the Xience arm. To achieve equivalent AG to Xience, the implantation of Absorb may require more aggressive strategies at implantation, pre- and post-dilation than the technique used in the ABSORB II trial. (ABSORB II Randomized Controlled Trial [ABSORB II]; NCT01425281)

The fully bioresorbable scaffold is a novel device to treat coronary artery stenosis, potentially minimizing the long-term complications seen with metallic drug-eluting stents. The everolimus-eluting Absorb bioresorbable vascular scaffold (Absorb, Abbott Vascular, Santa Clara, California) made of poly-L-lactide (PLLA) provides a temporary coronary scaffolding for at least 6 months and becomes fully resorbed by approximately 3 years [1]. The first-in-humans trial using the Absorb showed excellent safety results with potential late benefits such as late lumen enlargement and restoration of vasomotion[2]. The ABSORB II (ABSORB II Randomized Controlled Trial; NCT01425281) study is the first randomized trial between the Absorb scaffold and Xience metallic stents in patients with up to 2 de novo native coronary lesions[3,4].

It is warranted that the acute performance of Absorb matches that of metallic stents; however, concern exists about acute expansion and lumen gain with the use of a polymeric device. In the ABSORB first-in-humans trial, post-procedural intravascular ultrasound (IVUS) imaging demonstrated that implantation of an Absorb scaffold resulted in a more eccentric lumen with nonhomogeneous scaffold expansion compared with metallic stents [5]. Furthermore, nonrandomized matched population from the ABSORB and SPIRIT trials demonstrated that angiographic acute gain in lumen diameter tends to be smaller in the Absorb than in the Xience[6]. This trend was also observed in the randomized Japanese ABSORB trial [7–9]. In the ABSORB II randomized trial, pre-procedural and post-procedural documentary IVUS imaging were mandatory and provided a unique opportunity to evaluate the scaffold/stent expansion at the precise site of preprocedural minimal lumen area (MLA) and to relate the degree of expansion to the mechanical performance of both devices, procedural parameters of implantation and tissue composition derived from IVUS analyses[4].

Therefore, the purpose of this study was to investigate the IVUS acute gain at the site of minimal lumen area between the Absorb scaffold and the Xience stent and to identify the factors contributing to the acute performance of these devices.

METHODS

Study design and population

The ABSORB II study was a randomized controlled trial comparing the safety and efficacy of the Absorb everolimus-eluting bioresorbable vascular scaffold and the Xience everolimus-eluting metallic stent in patients with up to 2 de novo native coronary lesions. Details of the study are available elsewhere [3]. After successful pre-dilation of the target lesion, 2:1 randomization was performed. Of a total of 501 patients (546 lesions), 335 patients (364 lesions) were randomly assigned to receive Absorb device, and 166 patients (182 lesions) were assigned to receive the Xience device. Grayscale IVUS and

IVUS-virtual histology (VH) imaging pre-procedure and postimplantation was mandatory but documentary. No treatment recommendation on the basis of IVUS imaging was made in the protocol.

Study device

The Absorb device has an amorphous poly-DL-lactide (PDLLA) coating that contains and controls the release of the antiproliferative drug everolimus. The scaffold is made of semicrystalline PLLA. PLLA is completely biodegraded by hydrolysis into water and CO_2 via the Krebs cycle. Physically, the scaffold has struts with an approximate thickness of 150 µm. The Xience device is an everolimus-eluting, cobalt chromium alloy device with a platform consisting of serpentine rings connected by links fabricated from a single piece. The overall strut thickness including the drug coating is approximately 90 µm.

Procedure and IVUS acquisition.

Pre-procedural IVUS was mandatory before dilation of the target lesion. If it was not technically feasible (e.g., the IVUS catheter could not cross the lesion), pre-dilation with a small balloon was allowed to facilitate the IVUS catheter insertion.

IVUS images were obtained with a rotational 45-MHz IVUS catheter (Revolution, Volcano Corp., Rancho Cordova, California). After intracoronary injection of 200 µg of nitroglycerin, IVUS pullbacks were performed with the use of an automated motorized device at a pullback speed of 0.5 mm/s. Lesions were treated with routine interventional techniques that included mandatory pre-dilation with a balloon shorter and 0.5 mm smaller in diameter than the study device. The size of stent/scaffold was determined by the target vessel diameter, which was measured by pre-procedural on-line quantitative coronary angiography (QCA) [3,10]. All patients enrolled in the ABSORB II trial were treated as follows: 1) a 3.5-mm device was used when both the proximal and distal maximal lumen diameters were within an upper limit of 3.8 mm and a lower limit of 3.0 mm; 2) a 3.0-mm device was used when both the proximal and the distal maximal lumen diameters were within an upper limit of 3.3 mm and a lower limit of 2.5 mm; 3) a 2.5-mm device was used when both the proximal and the distal maximal lumen diameters were within an upper limit of 3.0 mm and a lower limit of 2.25 mm; and 4) scaffold/stent overlap was allowed. Post-dilation with a balloon shorter than the implanted scaffold/stent was performed at the discretion of the operators. Post-procedural IVUS images were obtained at the end of the procedure (post-device implantation or post-dilation). All pullbacks were analyzed offline by an independent core laboratory (Cardialysis BV, Rotterdam, the Netherlands) using commercially available software (QIvus version 2.2, Medis, Leiden, the Netherlands).

Measurement of acute gain on IVUS.

To assess the acute performance of the Absorb and Xience stent at the site of the worst stenosis pre-procedure, the difference of lumen area between pre- and postprocedural IVUS images at the site of the preprocedural minimal lumen area (MLA) was measured as acute gain in MLA. Pre-procedural MLA was defined as the smallest lumen area within the target lesion. After identifying the frame of the pre-procedural MLA site, matching of pre- and post-procedural IVUS images was performed by identifying common landmarks, such as side branches, bifurcations, large calcifications, or echogenic metallic marker on the device. Matching was performed using a dedicated software (QCU-CMS software, Medis). The preprocedural image of the MLA was matched and compared with the post-procedural lumen area at the same site. The lower acute gain was defined as the lowest tertile from the whole population.

Analysis of IVUS and procedural parameters.

Contour detection was performed by experienced IVUS core laboratory analysts who were unblinded to the device type. IVUS metrics including vessel, stent/ scaffold, and lumen area were measured at 0.5-mm intervals. To identify the lesion factors in the evaluation of acute gain, analysis was also performed using the following parameters: plaque burden, lumen eccentricity, presence of calcium, remodeling index [11] from grayscale IVUS and tissue composition parameters (absolute value and percentage) from IVUS-VH. Plaque burden was obtained by the plaque plus medium cross-sectional area divided by the vessel crosssectional area [1]). Eccentricity index was calculated as the ratio of the projected minimal and maximal lumen or scaffold/stent diameter at the MLA crosssection[5,13]. Pre-treatment reference segments were selected as sites with the least amount of plaque proximal and distal to the MLA sites before the takeoff of any major side branch[11]. The remodeling index (RI) was calculated as the vessel area at the MLA site divided by the average of the proximal and distal reference vessel areas. Negative remodeling was defined as an RI <0.88, intermediate remodeling as an RI of 0.88 to 1.00, and positive remodeling as an RI >1.00 [11].

Location and circumferential distribution of calcium was quantified in grayscale IVUS. Calcium was defined as bright echoes with acoustic shadowing. The location of the calcium was defined as superficial, deep, or both [14]. If the leading edge of the acoustic shadowing appeared within the shallowest 50% of the plaque thickness, it was defined as superficial calcium. If the leading edge of the acoustic shadowing appeared within the deepest 50% of the plaque thickness, it was defined as deep calcium. The largest continuous arc of calcium and summed arc of calcium at the site of pre-interventional lumen area were measured in degrees with a protractor centered on the lumen. In addition, the arc of calcium was classified as 1 quadrant (≤ 90º), 2 quadrants (91 º to 180 º), 3 quadrants (181 º to 270 º), or 4 quadrants (271º to 360 º). By IVUS-VH analysis, tissue

at the site of preprocedural MLA was divided into 4 basic plaque tissue components: fibrous tissue, fibrofatty tissue, necrotic core, and dense calcium [15]. In the compliance charts (pressure-diameter relationships) for Absorb and Xience (Prime, Xpedition, and so forth) provided by the manufacturer, the inner diameters of the devices were described. Expected device diameter was obtained from the device compliance chart, using the nominal device diameter and the maximal pressure during implantation. During post-dilation, the expected balloon diameter was obtained from the balloon compliance chart data provided by the various manufacturers of balloons, using the nominal diameter of the balloon and the maximal pressure during the procedure. In case the pressure during the procedure exceeded the highest pressure on the chart, the highest diameter on the chart was used for the calculation.

Angiographic assessment

Online QCA analyses were undertaken by the sites before Absorb implantation to define Dmax [10], and pre- and postprocedural offline QCA were performed by an independent core laboratory (Cardialysis BV) using the coronary angiography analysis system (Pie Medical Imaging, Maastricht, the Netherlands). The minimal lumen diameter (MLD) changes at different phases of the procedure were measured before procedure, after device implantation, and immediately after postdilation. Additionally, minimal diameter of balloon was measured during scaffold/stent implantation at maximal inflation pressure and during post-dilation at maximal inflation pressure. Acute recoil was defined as follows: When a stent/ scaffold delivery balloon was used for stent/scaffold expansion, acute absolute stent/scaffold recoil was defined as the difference between the mean diameter of the stent/scaffold delivery balloon at the highest pressure at implantation of the stent/scaffold (X) and the mean luminal diameter of the stented/scaffolded segment after implantation (Y). Acute absolute stent/ scaffold recoil was calculated as: [X – Y]. When a postdilation balloon was used in the procedure, acute absolute recoil was defined as the difference between the mean diameter of the post-dilation balloon at the highest pressure in the post-dilated segment (X') and themean luminal diameter after post-dilation (Y'). The angiogram of X and Y was performed in the same angiographic view so that the 2 images were perfectly matched.

Statistical analysis

Categorical variables are presented as counts and percentages. Continuous variables are presented as mean ± SD. A p value of <0.05 was considered statistically significant. Generalized estimating equations modeling was performed to take into an account the clustered nature of >1 stents/scaffolds per patient, which might result in unknown correlations among measurements within these scaffold clusters. Paired analysis was performed in the patients with analyzable pre- and postprocedural IVUS images. Logis-

tic regression analysis was performed to find the relationship of the following factors with IVUS lower acute gain in lumen area: sex, age, obesity (body mass index ≥ 30 kg/m^2), treated vessel, pre-procedural MLA, pre-procedural lumen eccentricity, plaque area, and vessel area (all measurements at the site of MLA). In addition, presence or absence of calcium as well as arc of calcium at the site ofMLA, tissue composition at the site of MLA, remodeling index [11], type of stent/scaffold, and maximal expected inner device or balloon diameter throughout procedure (in cases with or without post-dilation) were also included in the logistic regression analysis. In the multivariate model, MLA was not included due to strong interaction with plaque area and vessel area. Statistical analyses were performed with SPSS version 23.0.0 software (IBM, Armonk, New York).

RESULTS

Baseline characteristics

Of 501 patients with 546 lesions who were enrolled in the ABSORB II trial, 445 patients with 480 lesions (291 patients with 313 lesions in the Absorb arm and 154 patients with 167 lesions in the Xience arm) had both preprocedural and post-procedural IVUS analyses for acute lumen area gain assessment (Figure 1). There were no significant differences in baseline patient demographics and pre-procedural angiography data (Table 1).

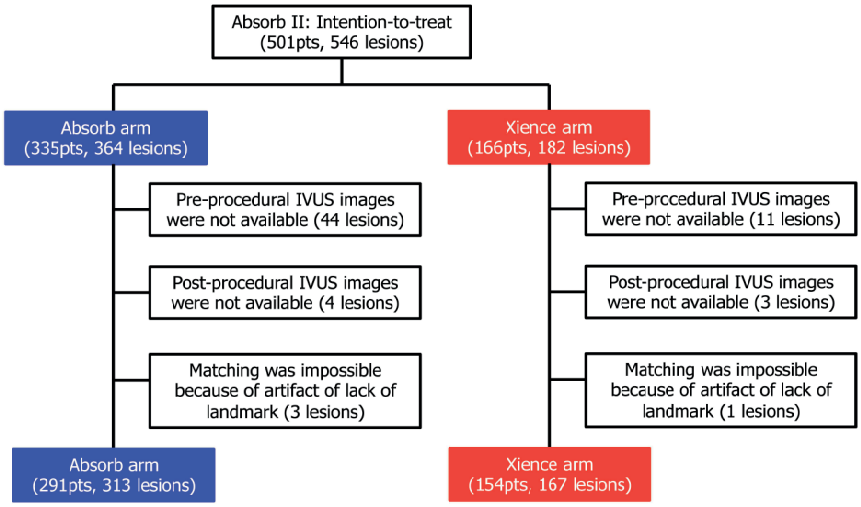

Figure 1. Study Flow Chart

Of 501 patients with 546 lesions, enrolled in the ABSORB II trial, 445 patients with 480 lesions (291 patients with 313 lesions in Absorb and 154 patients with 167 lesions in Xience) had both pre-procedural and post-procedural IVUS analyses for acute lumen area gain at the original minimal lumen area site. pts = patients.

Table 1. Clinical Characteristics and Procedural Variables (N = 445)

	ABSORB	XIENCE	*P* value
	(N=291)	(N=154)	
Demographics			
Male gender	217 (74.6)	123 (79.9)	0.241
Age (years)	61 ± 10	61 ± 10	0.786
Current smoking	77 (26.5)	33 (21.4)	0.251
Lipid disorder requiring medication	201 (69.1)	116 (75.3)	0.258
Hypertension requiring medication	188 (64.6)	104 (67.5)	0.802
Diabetes mellitus	64 (22.0)	38 (24.7)	0.554
Stable angina	187 (64.3)	100 (64.9)	0.917
Body mass index (BMI, kg/m^2)	27.8 ± 4.1	28.1 ± 3.7	0.542
Obesity (BMI ≥30 kg/m^2)	67 (23.1)	44 (28.6)	0.208
Lesion (N=480)	313 lesions	167 lesions	
Pre-procedural angiography			
Lesion location			0.184
Left anterior descending artery	146 (46.7)	81 (48.5)	
Left circumflex artery	88 (28.1)	35 (21.0)	
Right coronary artery	79 (25.2)	51 (30.5)	
Lesion classification†			0.456
A	4 (1.3)	1 (0.6)	
B1	181 (58.0)	85 (51.5)	
B2	125 (40.1)	78 (47.3)	
C	2 (0.6)	1 (0.6)	
Quantitative coronary angiography			
Interpolated percent diameter stenosis (%)	58.3 ± 11.1	59.1 ± 11.4	0.448
Minimal lumen diameter (mm)	1.08 ± 0.32	1.07 ± 0.31	0.627
Reference vessel diameter (mm)	2.60 ± 0.37	2.64 ± 0.40	0.327
Maximal diameter at proximal reference segment (mm)	2.84 ± 0.45	2.87 ± 0.46	0.476
Maximal diameter at distal reference segment (mm)	2.69 ± 0.45	2.74 ± 0.43	0.258
Procedural variables			
Pre-dilatation			
Pre-dilatation before IVUS	115 (36.7)	59 (35.3)	0.842
Pre-dilatation performed	313 (100.0)	165 (98.8)	0.121
Nominal diameter of pre-dilatation balloon (mm)	2.60 ± 0.36	2.64 ± 0.35	0.236
Maximal pressure during pre-dilatation (atm)	12.2 ± 3.0	12.5 ± 3.1	0.300

Table 1. Clinical Characteristics and Procedural Variables (N = 445) (continued)

	ABSORB (N=291)	XIENCE (N=154)	*P* value
Device implantation			
Nominal diameter of device			0.139
2.5 mm	52 (16.6)	17 (10.2)	
2.75 mm	0 (0)	1 (0.6)	
3.0 mm	190 (60.7)	107 (64.1)	
3.5 mm	71 (22.7)	42 (25.1)	
Maximal pressure during device implantation (atm)	13.1 ± 2.7	13.8 ± 2.5	0.008 *
Expected inner device diameter (mm)	3.34 ± 0.33	3.28 ± 0.33	0.109
Post-dilatation			
Post-dilatation performed	194 (62.0)	102 (61.1)	0.844
Nominal diameter of post-dilatation balloon (mm)‡	3.16 ± 0.34	3.28 ± 0.37	0.01 *
Maximal pressure during post-dilatation (atm)¶	15.3 ± 3.2	16.7 ± 3.4	0.001 *
Expected diameter of post-dilatation balloon (mm)¶	3.27 ± 0.35	3.40 ± 0.39	0.003 *
Maximal expected diameter of balloon (with or without post-dilatation, mm)	3.37 ± 0.33	3.38 ± 0.36	0.896

Data are expressed as mean ± SD, as n (%)
* $p < 0.05$
† Data was available in 477 lesions.
‡ Data was available in 292 lesions.
¶ Data was available in 290 lesions.

Differences in procedural implantation strategy between absorb and xience

Table 1 indicates the differences in procedural strategy between Absorb and Xience. Pre-dilation strategy was comparable between both arms. At the time of the device implantation, no differences in device size selection and expected inner device diameter were observed, whereas maximal pressure during device implantation was higher in Xience than in Absorb. At the time of post-dilation, nominal diameter of the balloon, maximal pressure, and expected balloon diameter were smaller in the Absorb arm than in the Xience arm.

IVUS analysis

A representative case of acute gain in MLA is presented in Figure 2. Overall, the pre-procedural MLA was comparable between the 2 arms. However, pre-procedural vessel area (Xience 11.61 mm^2 vs. Absorb 10.71 mm^2, respectively; $p = 0.014$) and plaque area

(Xience 9.47 mm^2 vs. Absorb 8.63 mm^2, respectively; p= 0.016) at the site of MLA were significantly larger in the Xience arm than in the Absorb arm. The post-procedural lumen area at the site of pre-procedural MLA was significantly smaller in the Absorb arm (5.55 mm^2 vs. 6.40 mm^2, respectively; $p < 0.001$). The amount of change in plaque area and plaque burden was significantly smaller in the Absorb arm than in the Xience arm (-1.12 mm^2 vs. -1.60 mm^2, respectively; $p = 0.005$; and -22.6% vs. -25.9%, respectively; $p < 0.001$). The increase of vessel area tended to be smaller in the Absorb arm (2.34 mm^2 vs. 2.66 mm^2, respectively; $p = 0.066$). As a result, there were significant differences in acute gain for the minimal lumen areas (3.46 mm^2 vs. 4.27 mm^2, respectively; $p < 0.001$) (Table 2, Figure 3).

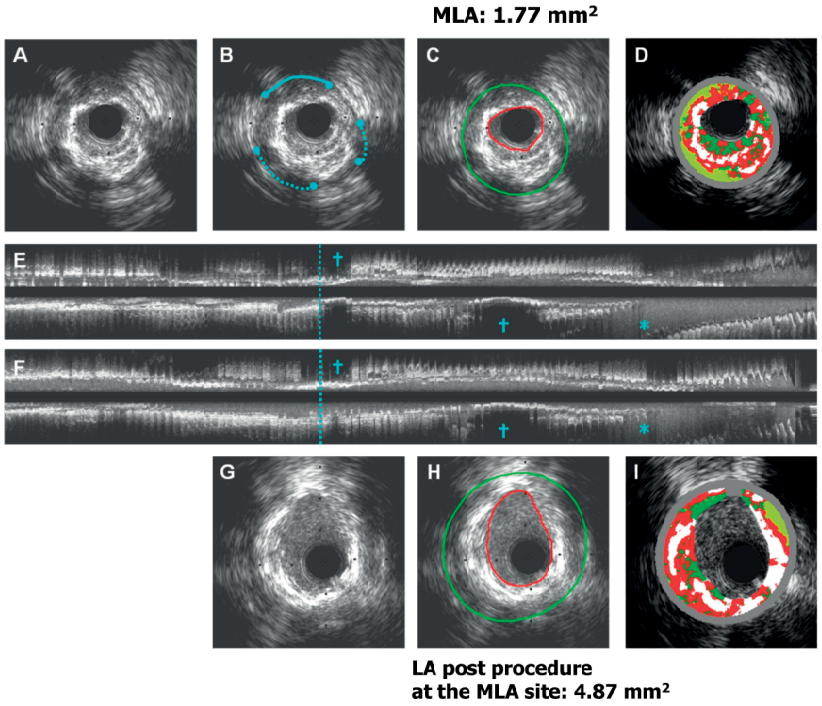

Figure 2. Representative Case of IVUS Acute Gain

Examples of IVUS pullbacks before (A–E) and after procedure (F–I). Vessel and lumen contours were drawn (C) at the site of pre-procedural minimal lumen area (dotted line in longitudinal view [E, F]). Calcium, defined as bright echoes with acoustic shadowing, was measured in its circumferential extension (largest continuous arc of calcium [solid arc]: 101.3°, summed arc of calcium [solid and dotted arcs]: 214.1° [B]), and location (superficial calcium). Tissue component (D) was assessed by IVUS-VH. After matching pre- (E) and post-procedural IVUS pullbacks (F), vessel and lumen areas were obtained at the corresponding site (H). Lumen area in C was 1.77 mm^2 and 4.87 mm^2 in H. Therefore, acute lumen gain was 3.10 mm^2 (green line = vessel contour; red line = lumen contour; blue asterisk = side branch; blue dagger = calcification). LA = lumen area; MLA = minimal lumen area; IVUS-VH = intravascular ultrasound-virtual histology.

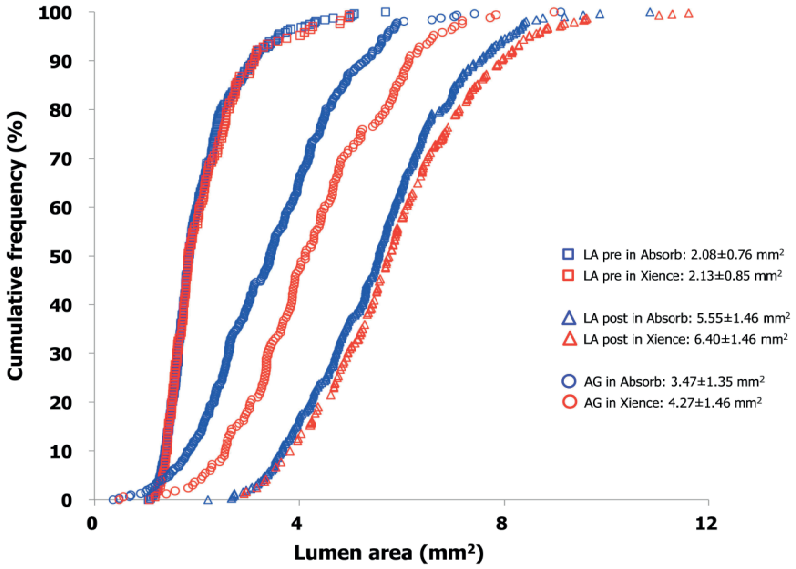

Figure 3. Cumulative Frequency Distribution Curve of Pre- and Post-MLA and Acute Gain Cumulative frequency distribution curve of AG at the MLA site pre-procedure [AG = (MLA_{post} – MLA_{pre})] for Absorb and Xience. Pre-procedural MLA was similar between the 2 arms. The post-procedural lumen area at the site of the pre-procedural MLA was significantly smaller in the Absorb arm than in the Xience arm (5.55 mm^2 vs. 6.40 mm^2, respectively; $p < 0.001$). The amount of change in lumen area was significantly smaller in the Absorb arm than in the Xience arm (3.46 mm^2 vs. 4.27 mm^2, respectively; $p < 0.001$). AG = acute gain; MLA = minimal lumen area.

Device expansion in minimal lumen area

When device expansion [16,17] was defined as the ratio of post-procedural lumen area at the site of pre-procedural MLA to the expected inner device area calculated from the largest balloon used during procedure, the Absorb scaffold achieved on average 62±12% of the predicted lumen area, whereas the Xience stent achieved 71±15% ($p < 0.001$) (Figure 4). Location of calcium as well as the arc of calcium and the amount of NC did not affect device expansion (Figure 5).

QCA MLD changes at different phases during procedure.

Figure 6 shows the MLD by QCA and MLA by IVUS changes at different phases during the procedure in the patients who had both pre- and post-procedural IVUS analyses.

The Main difference in acute gain in MLD by QCA was observed at the time of device implantation (Xience vs. Absorb, Δ +1.50 mm vs. Δ + 1.23 mm, respectively), whereas the gain from post-dilation was similar between the 2 arms (Δ + 0.16 mm vs. Δ + 0.16 mm) when patients underwent post-dilation. Acute recoil during device implantation was similar in both devices (Xience vs. Absorb, 0.20 ± 0.18 mm vs. 0.19 ± 0.19 mm, respectively; $p = 0.716$), whereas acute recoil during post-dilation was larger in the Xience than in the Absorb (0.21± 0.21 mm vs. 0.13±0.20 mm, respectively; $p = 0.006$).

Table 2. IVUS data at the site of pre-procedural minimal lumen area

	Pre-procedure			Post-procedure			Change from pre and post		
	ABSORB	XIENCE	P value	ABSORB	XIENCE	P value	ABSORB	XIENCE	P value
	n=313	n=167		n=313	n=167		n=313	n=167	
Grayscale IVUS									
Lumen area (mm^2)	2.08 ± 0.76	2.13 ± 0.85	0.502	5.55 ± 1.46	6.40 ± 1.68	<0.001	3.46 ±1.35	4.27 ±1.46	<0.001
Vessel area (mm^2)	10.71 ± 3.67	11.61 ± 3.89	0.014	13.05 ± 3.83	14.28 ± 4.01	0.001	2.34 ±1.80	2.66 ±1.82	0.066
Plaque area (mm^2)	8.63 ± 3.47	9.47 ± 3.71	0.016	7.51 ± 2.82	7.88 ± 2.94	0.181	-1.12 ±1.75	-1.60 ±1.76	0.005
Plaque burden (%)	79.0 ± 8.3	80.2 ± 8.5	0.143	56.4 ± 8.1	54.3 ± 7.8	0.007	-22.6 ± 8.2	-25.9 ±7.3	<0.001
Minimal lumen diameter (mm)	1.47 ± 0.23	1.48 ± 0.25	0.660	2.41 ± 0.37	2.66 ± 0.45	<0.001			
Maximal lumen diameter (mm)	1.75 ± 0.37	1.77 ± 0.38	0.591	2.86 ± 0.40	3.00 ± 0.41	<0.001			
Lumen eccentricity	0.86 ± 0.10	0.85 ± 0.10	0.711	0.84 ± 0.08	0.89 ± 0.11	<0.001			
Presence or absence of calcium (%)			0.987						
No	114 (36.4)	61 (36.5)							
1 quadrant (1~90 degrees)	130 (41.5)	67 (40.1)							
2 quadrants (91~180 degrees)	41 (13.1)	24 (14.4)							
3 quadrants (181~270 degrees)	15 (4.8)	9 (5.4)							
4 quadrants (270~360 degrees)	13 (4.2)	6 (3.6)							
Largest continuous arc of calcium (degrees)	45.5 ± 58.8	51.8 ± 67.0	0.306						
Summed arc of calcium (degrees)	54.3 ± 69.3	60.7 ± 75.0	0.362						
Remodeling pattern (%)[§]			0.802						
Positive remodeling	94 (30)	46 (28)							
Intermediate remodeling	83 (27)	43 (26)							
Negative remodeling	132 (42)	75 (45)							

Table 2. IVUS data at the site of pre-procedural minimal lumen area (continued)

	Pre-procedure			Post-procedure			Change between pre and post		
	ABSORB	XIENCE	P value	ABSORB	XIENCE	P value	ABSORB	XIENCE	P value
IVUS-VH									
Fibrous tissue (% of total plaque area)	27.70 ± 16.07	26.70 ± 14.69	0.504	27.30 ± 10.99	21.71 ± 8.86	<0.001	-0.41 ± 15.11	-4.99 ± 15.22	0.002
Fibro-fatty tissue (% of total plaque area)	52.70 ± 22.81	54.00 ± 21.61	0.551	31.49 ± 19.77	30.08 ± 17.65	0.440	-21.25 ± 20.07	-23.92 ± 17.17	0.139
Necrotic core (% of total plaque area)	15.64 ± 10.23	15.48 ± 9.94	0.867	28.58 ± 10.70	30.65 ± 10.12	0.043	13.03 ± 10.96	15.17 ± 10.65	0.044
Dense calcium (% of total plaque area*)	3.95 ± 6.02	3.82 ± 5.81	0.822	12.56 ± 11.21*	17.56 ± 12.90*	<0.001	8.56 ± 10.13	13.74 ± 12.47	<0.001

Data are expressed as mean ± SD, as n (%). § 7 missing data.

* The polymeric or metallic struts are detected as (pseudo)calcium on IVUS-VH IVUS-VH = intravascular ultrasound-virtual histology.

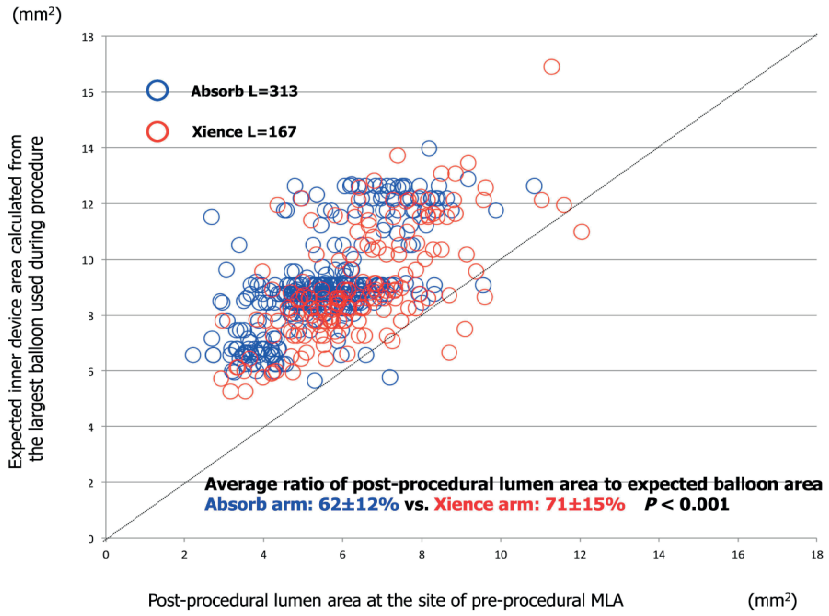

Figure 4. Device Expansion of Absorb and Xience
When device expansion was defined as the ratio of post-procedural lumen area at the site of the pre-procedural MLA to the expected inner device area calculated from the largest balloon used during procedure, the Absorb scaffold achieved, on average, 62±12% only of the predicted lumen area, whereas the Xience stent achieved 71±15% (p < 0.001). MLA =minimal lumen area.

Predictors of lower acute gain.

Lower acute gain (lowest tertile) occurred more frequently in the Absorb arm than in the Xience arm (risk ratio: 3.04; 95% confidence interval [CI]: 1.94 to 4.76) (Table 3). Results of logistic regression analysis are summarized in Online Table 1. Sex, age, obesity, treated vessel, pre-procedural lumen eccentricity at the site of MLA, presence or absence of calcium as well as arc of calcium at the site of MLA, tissue composition at the site of MLA were not independent predictors for lower acute gain. The following variables were significantly associated with lower acute gain in the multivariate model: Absorb use, maximal inner device or balloon diameter throughout procedure, vessel and plaque areas at the MLA site, and negative remodeling. Differences in IVUS acute gain between Absorb and Xience were consistent across these variables (Table 3).

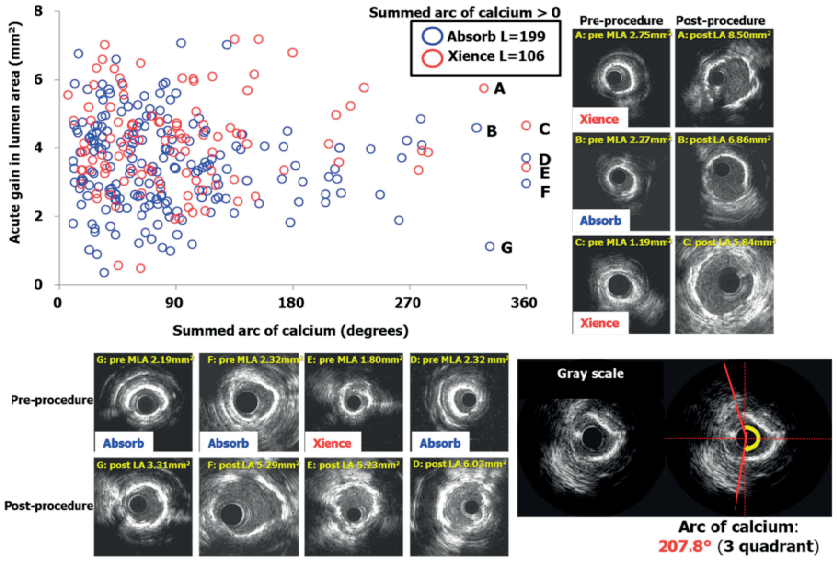

Figure 5. Relationship Between Circumferential Distribution of Calcium and Acute Gain
The relationship between circumferential distribution of calcium and acute gain (blue circles =Absorb; red circles =Xience). Presence or absence of calcium as well as the arc of calcium by IVUS grayscale did not affect acute gain and device expansion at the site of minimal lumen area. IVUS =intravascular ultrasound; MLA =minimal lumen area.

DISCUSSION

Main findings

The main findings of this study are: lower acute gain occurred more frequently in the Absorb arm than in the Xience arm (3.46 mm^2 vs. 4.27 mm^2, respectively; $p < 0.001$; risk ratio: 3.04; 95% CI: 1.94 to 4.76); plaque morphology at the MLA cross-section was not independently associated with acute gain; and on angiography, acute device recoil was comparable, but expansion of the device was different. The influence of post-dilation on MLD was somewhat limited.

Impact of lesion morphology on lumen enlargement.

There are conflicting data about the impact of lesion morphology on lumen enlargement. In previous reports, the expansion of drug-eluting stents was drastically influenced by IVUS (grayscale/virtual histology) plaque morphology (including the arc and length of lesion calcium) or quantitative lesion site geometry (lesion vessel area, plaque area, and plaque burden) [16–18]. In the present study, the impact of plaque component on acute gain in lumen area was not retained in the multivariate analysis, although in univariate analysis, higher amounts of fibrotic plaque, necrotic core, and dense calcium showed

Table 3. Incidence of lower acute gain

Incidence of lower acute gain

	Absorb		Xience		Risk ratio	p value for interaction
All patients	41%	(128/313)	19%	(31/167)	3.04 (1.94-4.76)	
Maximal expected diameter of balloon with or without post-dilatation						
Lower tertile (≤3.28)	70%	(78/112)	35%	(25/72)	4.31 (2.30-8.10)	
Mid-tertile (>3.28, ≤3.40)	32%	(37/117)	9%	(3/34)	4.78 (1.37-16.64)	0.872
Higher tertile (>3.40)	16%	(13/84)	5%	(3/61)	3.54 (0.96-13.02)	
Vessel Area at MLA site						
Lower tertile (≤9.10)	67%	(75/112)	45%	(21/47)	2.51 (1.25-5.04)	
Mid-tertile (>9.10, <12.30)	33%	(35/105)	13%	(7/53)	3.29 (1.35-8.02)	0.305
Higher tertile (≥12.30)	19%	(18/96)	5%	(3/67)	4.92 (1.39-17.46)	
Plaque Area at MLA site						
Lower tertile (≤7.10)	69%	(79/114)	46%	(20/44)	2.71 (1.33-5.53)	
Mid-tertile (>7.10, <9.95)	35%	(35/101)	16%	(9/58)	2.89 (1.27-6.56)	0.475
Higher tertile (≥9.95)	14%	(14/98)	3%	(2/65)	5.25 (1.15-23.94)	
Remodeling†						
Negative (RI<0.88)	41%	(54/132)	17%	(13/75)	3.30 (1.65-6.59)	
Intermediate (0.88≤ RI≤1.00)	39%	(32/83)	26%	(11/43)	1.83 (0.81-4.13)	0.835
Positive (RI>1.0)	43%	(40/94)	15%	(7/46)	4.13 (1.67-10.18)	

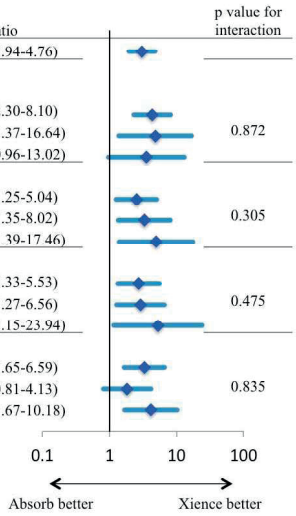

†Remodeling index: 7 missing dataMLA= minimal lumen area; RI = remodeling index.

lower acute gain in lumen area in both arms. In the present study, presence or absence of calcium as well as the arc of calcium by IVUS grayscale did not affect the acute gain and device expansion at MLA (Figure 5).

Differences in procedural strategy between absorb and xience.

Differences in acute performance can be driven not only by differences in the mechanical properties of the Absorb scaffold and the Xience metallic stent but also by different initial implantation strategies [6,19,20]. Within precise boundaries of expansion (e.g., 3.0 to 3.5 mm for a device of 3.0 mm), the stress-strain relationship of the metallic and polymeric struts are comparable, and the mechanical strength of the Absorb scaffold is not different from that of the metallic stent [21]. However, when the scaffold is over-expanded (>3.5 mm for a 3.0-mm device), the strut crowns begin approaching their geometrical limit. The radial support is maximized, while their tensile strength limit is also reached [22]. Therefore, pre-dilation, optimal expansion, and avoidance of over-expansion are encouraged during the procedure with the Absorb device.

Maximal expected balloon diameters in cases with or without post-dilation were similar between Absorb and Xience. However, the ratio of post-procedural lumen area at the site of pre-procedural MLA to the expected inner device area calculated from the largest balloon used during procedure was smaller in the Absorb than in the Xience (Figure 4). This result might imply the necessity of more aggressive strategy during implantation

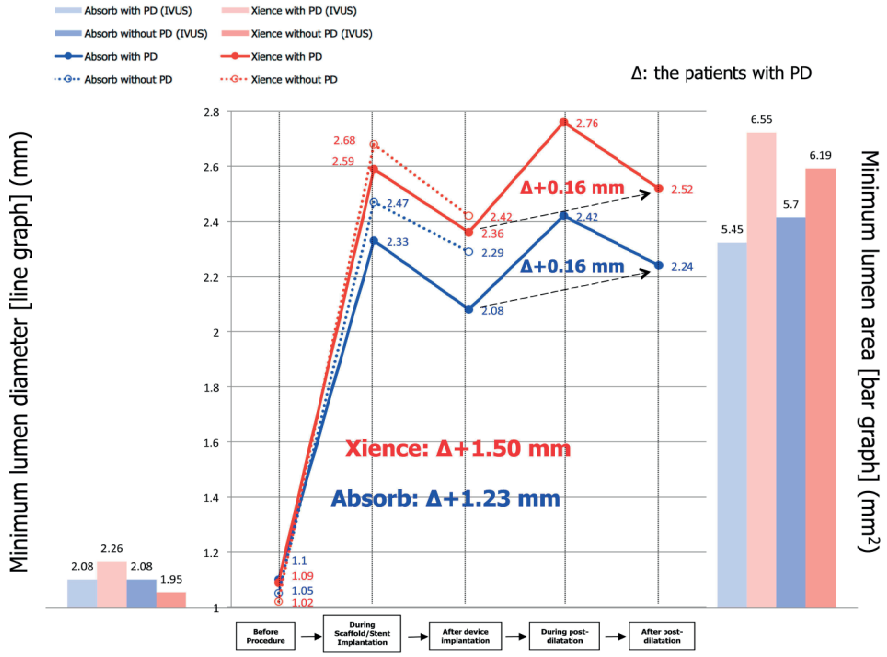

Figure 6. Minimal Lumen Diameter Changes by QCA and MLA Changes by IVUS at Different Phases of the Procedure

The minimal lumen diameter changes by QCA (line graph) and MLA changes by IVUS (bar graph) at different phases of the procedure in patients who had both pre- and post-procedural IVUS analyses. Change of MLD by QCA and MLA by IVUS of the Absorb and the Xience are depicted by blue and red, respectively. Dotted lines show minimal lumen diameter changes for those lesions that were not post-dilated, whereas solid lines show minimal lumen diameter change of the lesions that underwent post-dilation. Differences in acute gains were mainly observed at the time of device implantation (Δ+1.50 mm vs. Δ+1.23 mm), whereas the gain from post-dilation was similar between the 2 arms (Δ+0.16 mm vs. Δ+0.16 mm), when patients underwent post-dilation. IVUS =intravascular ultrasound; MLA =minimal lumen area; QCA =quantitative coronary angiography.

and post-dilation of Absorb compared to Xience due to the device mechanical properties (i.e., tensile strength and radial force).

When QCA was performed to assess MLD changes at different phases during the procedure, differences between the 2 arms were already significant at the time of device balloon expansion (Δ+ 1.50 mm for Xience vs. Δ+ 1.23 mm for Absorb; $p < 0.01$) (Figure 6), despite the fact that the expected inner devices' diameters at implantation were similar in both arms. Acute device recoil amounts were comparable between the 2 arms [4]. Despite less aggressive post-dilation in the Absorb arm than in the Xience arm, the angiographic gains from post-dilation between the 2 arms were similar (ΔD+ 0.16 mm vs. Δ+ 0.16 mm, respectively; $p = 0.97$) (Figure 6). These angiographic analyses implied

differences of the mechanical properties of both devices and the necessity of different procedural strategies for implantation.

The issue of recoil in QCA and IVUS seemingly somewhat contradicted each other. Another possibility is that the limited accuracy of the measurements by QCA and IVUS due to their resolutions could cause this contradiction. Their accuracy could be affected differently in implanted polymeric scaffolds and metallic stents. Moreover, the recoils were assessed by QCA and IVUS in a different fashion and settings. With IVUS, post-procedural MLA was compared to the virtual expected balloon dimensions at the time of maximal balloon inflation. In QCA, recoil was assessed from the difference in diameter between inflation balloon device and stented/ scaffolded diameter of the vessel post-implantation.

Clinical implication

On the basis of previous reports[23] of disrupted polymeric scaffolds due to over-expansion, the protocol did not recommend post-dilation of the bioresorbable scaffold device. However, on angiography, a significant difference in the initial expansion was noted (Absorb < Xience). To achieve with the Absorb an acute lumen gain equivalent to that of the Xience, device balloon expansion with higher pressures and/or more aggressive post-dilation should be considered within the limits of the recommended diameters due to the difference in inherent device mechanical properties (i.e., tensile strength and radial force). Because the device balloon of the Absorb is semi-compliant, implantation with a high pressure might result in over-expansion of the device or edge dissection. One of the possible contributing factors to lower acute gain in the Absorb is the lack of systematic post-dilation with a noncompliant balloon with a diameter of 0.25 or 0.5 mm larger than the nominal diameter of the polymeric device.

The following 3 clinical questions remain: How does an aggressive lesion preparation (pre-dilation, rotational atherectomy or cutting/scoring balloon) impact acute gain? Can a high implantation pressure with the Absorb device improve acute gain? How does an aggressive post-dilation impact acute gain? These questions should be answered in future trials.

Study limitations

If the IVUS catheter could not cross the lesion, pre-dilation with a small balloon was performed. The incidence of pre-dilation before IVUS was similar between the Absorb and Xience arms, but initial lesion geometry and morphology could not be evaluated in 12% of lesions. The analysts in core laboratory were not blinded to the device type, which could result in potential bias in data acquisition. Aorto-ostial lesions, bifurcations, chronic total occlusions, and lesions with heavy calcification on angiography were excluded from the present study. Thus, our conclusions should not be extrapolated to

more complex lesion subsets. Lastly, in the present study, we did not evaluate—due to the small number of the events—the relationship between IVUS findings and clinical events such as scaffold thrombosis that is our current concern after implantation of Absorb.

CONCLUSIONS

At the site of pre-procedural MLA, the Absorb scaffold showed lower acute gain than Xience stents. To achieve acute gain equivalent to that of Xience, Absorb deployment may require preparation of the lesion and more aggressive strategies at implantation and post-dilation than the technique used in the ABSORB II trial due to the difference in inherent device mechanical properties.

PERSPECTIVES

WHAT IS KNOWN? It is warranted that the acute performance of Absorb matches that of metallic stents; however, concern exists about acute expansion and lumen gain with the use of Absorb.

WHAT IS NEW? Lower IVUS acute gain occurred more frequently in the Absorb arm than in the Xience arm. The plaque morphology at the MLA cross-section was not independently associated with acute gain. On angiography, device acute recoil was comparable but expansion of the device was different.

WHAT IS NEXT? Further studies are needed to evaluate the impact of more aggressive strategies at implantation, pre- and post-dilation than the technique used in the ABSORB II trial on acute performance of Absorb.

REFERENCES

1. Serruys PW, Onuma Y, Garcia-Garcia HM, et al. Dynamics of vessel wall changes following the implantation of the Absorb everolimus-eluting bioresorbable vascular scaffold: a multi-imaging modality study at 6, 12, 24 and 36 months. EuroIntervention 2014;9:1271–84.
2. Onuma Y, Serruys PW. Bioresorbable scaffold: the advent of a new era in percutaneous coronary and peripheral revascularization? Circulation 2011;123:779–97.
3. Diletti R, Serruys PW, Farooq V, et al. ABSORB II randomized controlled trial: a clinical evaluation to compare the safety, efficacy, and performance of the Absorb everolimus-eluting bioresorbable vascular scaffold system against the Xience everolimuseluting coronary stent system in the treatment of subjects with ischemic heart disease caused by de novo native coronary artery lesions: rationale and study design. Am Heart J 2012;164:654–63.
4. Serruys PW, Chevalier B, Dudek D, et al. A bioresorbable everolimus-eluting scaffold versus a metallic everolimus-eluting stent for ischaemic heart disease caused by de-novo native coronary artery lesions (ABSORB II): an interim 1-year analysis of clinical and procedural secondary outcomes from a randomised controlled trial. Lancet 2015;385:43–54.
5. Brugaletta S, Gomez-Lara J, Diletti R, et al. Comparison of in vivo eccentricity and symmetry indices between metallic stents and bioresorbable vascular scaffolds: insights from the ABSORB and SPIRIT trials. Catheter Cardiovasc Interv 2012;79:219–28.
6. Zhang YJ, Bourantas CV, Muramatsu T, et al.Comparison of acute gain and late lumen loss after PCI with bioresorbable vascular scaffolds versus everolimus-eluting stents: an exploratory observational study prior to a randomised trial. Euro-Intervention 2014;10:672–80.
7. Kimura T, Kozuma K, Tanabe K, et al. A randomized trial evaluating everolimus-eluting Absorb bioresorbable scaffolds vs. everolimuseluting metallic stents in patients with coronary artery disease: ABSORB Japan. Eur Heart J 2015; 36:3332–42.
8. Gao R, Yang Y, Han Y, et al. Bioresorbable vascular scaffolds versus metallic stents in patients with coronary artery disease: ABSORB China trial. J Am Coll Cardiol 2015;66:2298–309.
9. Ellis SG, Kereiakes DJ, Metzger DC, et al. Everolimus-eluting bioresorbable scaffolds for coronary artery Disease. N Engl J Med 2015;373:1905–15.
10. Ishibashi Y, Nakatani S, Sotomi Y, et al. Relation between bioresorbable scaffold sizing using QCA-Dmax and clinical outcomes at 1 Year in 1,232 patients from 3 study cohorts (ABSORB Cohort B, ABSORB EXTEND, and ABSORB II). J Am Coll Cardiol Intv 2015;8:1715–26.
11. Inaba S, Mintz GS, Farhat NZ, et al. Impact of positive and negative lesion site remodeling on clinical outcomes: insights from PROSPECT. J Am Coll Cardiol Img 2014;7:70–8.
12. Mintz GS, Nissen SE, Anderson WD, et al. American College of Cardiology clinical expert consensus document on standards for acquisition, measurement and reporting of intravascular ultrasound studies (IVUS). A report of the American College of Cardiology Task Force on Clinical Expert Consensus Documents. J Am Coll Cardiol 2001;37:1478–92.
13. de Jaegere P, Mudra H, Figulla H, et al. Intravascular ultrasound-guided optimized stent deployment. Immediate and 6 months clinical and angiographic results from the Multicenter Ultrasound Stenting in Coronaries Study (MUSIC Study). Eur Heart J 1998;19:1214–23.
14. Mintz GS, Popma JJ, Pichard AD, et al. Patterns of calcification in coronary artery disease. A statistical analysis of intravascular ultrasound and coronary angiography in 1155 lesions. Circulation 1995;91:1959–65.
15. Garcia-Garcia HM, Costa MA, Serruys PW. Imaging of coronary atherosclerosis: intravascular ultrasound. Eur Heart J 2010;31:2456–69.

16. de Ribamar Costa J Jr.,Mintz GS, Carlier SG, et al. Intravascular ultrasound assessment of drug-eluting stent expansion. Am Heart J 2007;153:297–303.
17. He Y, Maehara A, Mintz GS, et al. Intravascular ultrasound assessment of cobalt chromium versus stainless steel drug-eluting stent expansion. Am J Cardiol 2010;105:1272–5.
18. Lee WS, Kim SW, Lee KJ, Kim TH, Kim CJ, Ryu WS. Under-expansions of drug eluting stents in patients with acute coronary syndrome are associated with plaque components as well as vessel size or plaque burden. Circulation 2009;120:S913.
19. Onuma Y, Serruys PW, Gomez J, et al., ABSORB Cohort A and B investigators. Comparison of in vivo acute stent recoil between the bioresorbable everolimus-eluting coronary scaffolds (revision 1.0 and 1.1) and the metallic everolimuseluting stent. Catheter Cardiovasc Interv 2011;78:3–12.
20. Tanimoto S, Bruining N, van Domburg RT, et al. Late stent recoil of the bioabsorbable everolimus-eluting coronary stent and its relationship with plaque morphology. J Am Coll Cardiol 2008;52:1616–20.
21. Ormiston JA, Serruys PW, Regar E, et al. A bioabsorbable everolimus-eluting coronary stent system for patients with single de-novo coronary artery lesions (ABSORB): a prospective open-label trial. Lancet 2008;371:899–907.
22. Onuma Y, Serruys PW, Perkins LE, et al. Intracoronary optical coherence tomography and histology at 1 month and 2, 3, and 4 years after implantation of everolimus-eluting bioresorbable vascular scaffolds in a porcine coronary artery model: an attempt to decipher the human optical coherence tomography images in the ABSORB trial. Circulation 2010;122:2288–300.
23. Onuma Y, Serruys PW, Muramatsu T, et al. Incidence and imaging outcomes of acute scaffold disruption and late structural discontinuity after implantation of the Absorb everolimus-eluting fully bioresorbable vascular scaffold: optical coherence tomography assessment in the ABSORB cohort B trial (A Clinical Evaluation of the Bioabsorbable Everolimus Eluting Coronary Stent System in the Treatment of Patients With De Novo Native Coronary Artery Lesions). J Am Coll Cardiol Img 2014;7:1400–11.

Online supplement table 1. Independent predictors for lower acute gain

	Univariate analysis		Multivariate analysis		Variables not in model
			Variables in model		
	OR [95%CI]	P value	OR [95%CI]	P value	P value
Male gender	0.543 [0.352-0.837]	0.006 *			0.483
Age (year)	0.998 [0.98-1.018]	0.874			0.906
Obesity (BMI>30 kg/mm^2)	0.582 [0.368-0.923]	0.021 *			0.375
Absorb usage	3.035 [1.935-4.763]	<0.001 *	5.028 [2.659-9.507]	<0.001 *	
Target vessel (Reference: LCX)					
LAD	1.031 [0.705-1.508]	0.876			0.987
RCA	0.433 [0.269-0.697]	0.001 *			0.504
Maximal expected diameter of balloon with or without post-dilatation (mm)	0.016 [0.006-0.040]	<0.001 *	0.010 [0.003-0.035]	<0.001 *	
At the site of minimal lumen area					
Pre-procedural minimal lumen area**	1.155 [0.914-1.461]	0.228			
Pre-procedural lumen eccentricity	1.779 [0.236-13.395]	0.576			0.205
Pre-procedural plaque area	0.674 [0.618-0.736]	<0.001 *	0.213 [0.134-0.340]	<0.001 *	
Pre-procedural vessel area	0.726 [0.674-0.783]	<0.001 *	3.078 [2.041-4.640]	<0.001 *	
Presence of calcium at the site of MLA	0.785 [0.53-1.161]	0.225			0.334
Total arc of calcium at the site of MLA	0.998 [0.996-1.001]	0.258			0.493
Remodeling index (Reference: 0.88 - 1.00)					
< 0.88 (Negative remodeling)	0.942 [0.641-1.383]	0.759	0.461 [0.250-0.850]	0.013 *	
>1.00 (Positive remodeling)	1.029 [0.678-1.562]	0.894			0.53
Tissue composition					
Fibrotic	1.021 [1.009-1.034]	0.001 *			0.67
Fibrofatty	0.979 [0.97-0.988]	<0.001 *			0.55

Online supplement table 1. Independent predictors for lower acute gain (continued)

	Univariate analysis		Multivariate analysis		Variables not in model
			Variables in model		
	OR [95%CI]	P value	OR [95%CI]	P value	P value
Necrotic core	1.034 [1.014-1.054]	0.001 *			0.324
Dense calcium	1.039 [1.006-1.072]	0.02 *			0.152

* $p < 0.05$

** Minimal lumen area was not included in the multivariate model due to strong interaction with plaque area and vessel area

Abbreviations: MLA, minimal lumen area; LAD, left anterior descending artery; LCX, left circumflex artery; RCA, right coronary artery.

Chapter 9

The impact of post-procedural asymmetry, expansion and eccentricity of bioresorbable everolimus-eluting scaffold and metallic everolimus-eluting stent on clinical outcomes in the ABSORB II trial

Pannipa Suwannasom, Yohei Sotomi, Yuki Ishibashi, Rafael Cavalcante, Felipe N. Albuquerque, Carlos Macaya, John A. Ormiston, Jonathan Hill, Irene M. Lang, Mohaned Egred, Jean Fajadet, Maciej Lesiak, Jan G.P Tijssen, Joanna J. Wykrzykowska, Robbert J. de Winter, Bernard Chevalier, Patrick W. Serruys, Yoshinobu Onuma

JACC Cardiovasc Interv. 2016 Jun 27;9(12):1231-42

ABSTRACT

Objectives

The study sought to investigate the relationship between post-procedural asymmetry, expansion, and eccentricity indices of metallic everolimus-eluting stent (EES) and bioresorbable vascular scaffold (BVS) and their respective impact on clinical events at 1-year follow-up.

Background

Mechanical properties of a fully BVS are inherently different from those of permanent metallic stent.

METHODS

The ABSORB II (A bioresorbable everolimus-eluting scaffold versus a metallic everolimus-eluting stent for ischaemic heart disease caused by de-novo native coronary artery lesions) trial compared the BVS and metallic EES in the treatment of a de novo coronary artery stenosis. Protocol-mandated intravascular ultrasound imaging was performed pre- and post-procedure in 470 patients (162 metallic EES and 308 BVS). Asymmetry index (AI) was calculated per lesion as: (1 - minimum scaffold/stent diameter/maximum scaffold/stent diameter). Expansion index and optimal scaffold/ stent expansion followed the definition of the MUSIC (Multicenter Ultrasound Stenting in Coronaries) study. Eccentricity index (EI) was calculated as the ratio of minimum and maximum scaffold/stent diameter per cross section. The incidence of device-oriented composite endpoint (DoCE) was collected.

Results

Post-procedure, the metallic EES group was more symmetric and concentric than the BVS group. Only 8.0% of the BVS arm and 20.0% of the metallic EES arm achieved optimal scaffold/stent expansion ($p < 0.001$). At 1 year, there was no difference in the DoCE between both devices (BVS 5.2% vs. EES 3.1%; $p = 0.29$). Post-procedural devices asymmetry and eccentricity were related to higher event rates while there was no relevance to the expansion status. Subsequent multivariate analysis identified that post-procedural AI >0.30 is an independent predictor of DoCE (hazard ratio: 3.43; 95% confidence interval: 1.08 to 10.92; $p = 0.037$).

Conclusions

BVS implantation is more frequently associated with post-procedural asymmetric and eccentric morphology compared to metallic EES. Post-procedural devices asymmetry were independently associated with DoCE following percutaneous coronary intervention. However, this approach should be viewed as hypothesis generating due to low event rates. (ABSORB II Randomized Controlled Trial [ABSORB II]; NCT01425281)

Bioresorbable vascular scaffolds (BVS) (Absorb BVS; Abbott Vascular, Santa Clara, California) have emerged as a novel technology with several potential advantages compared to permanent metallic stents in the treatment of coronary artery disease [1]. Data from randomized control trials showed that the scaffold efficacy is noninferior to the available metallic drug eluting stent (DES) [2,3]. However, the use of BVS remains limited to noncomplex coronary lesions because their limitations stemming from the inherent differences in the mechanical properties of polymeric material of BVS compared to metallic DES (e.g., a lesser radial strength) [4].

Previously, difference in acute stent performance between the Absorb BVS and metallic everolimus-eluting stent (EES) has been investigated [5]. In the absence of specific intracoronary imaging guidance, BVS exhibited higher device asymmetry and eccentricity than metallic EES post-implantation as assessed by intravascular ultrasound (IVUS), without detectable impact on major adverse cardiac event rate at 6 months [5]. However, the understanding of the prognostic value of the device performance such as expansion, eccentricity and asymmetry indices in clinical practice remains limited mainly due to the observational nature of the studies, use of old stent platforms [6], small sample sizes [7], and short follow-up duration [6,7]. It is of interest to investigate the acute performance of a new scaffold/stent platform and their relationships to device-oriented composite endpoint (DoCE) in a larger sample size and in the context of a randomized trial [3]). The aim of this study was to assess the impact of post-procedural scaffold/stent asymmetry, expansion, and eccentricity indices on early and late clinical events treated either with a metallic or polymeric devices.

METHODS

Study population.

The ABSORB II (A bioresorbable everolimus-eluting scaffold versus a metallic everolimus-eluting stent for ischaemic heart disease caused by de-novo native coronary artery lesions) trial is a prospective, single-blinded, randomized, active controlled trial. The study included 501 patients with de novo coronary lesions, randomized in 2:1 ratio to receive either treatment with an everolimus-eluting bioresorbable scaffold (Absorb BVS) or with an everolimus-eluting metallic stent (Xience, Abbott Vascular, Santa Clara, California). The details of inclusion and exclusion criteria have been described previously (8). For the purpose of the study, only patients with post-procedural IVUS were included. Of 501 patients, 31 patients were excluded due to the reasons listed in Figure 1. Consequently, the total 470 patients with post-procedural IVUS were included in the analyses.

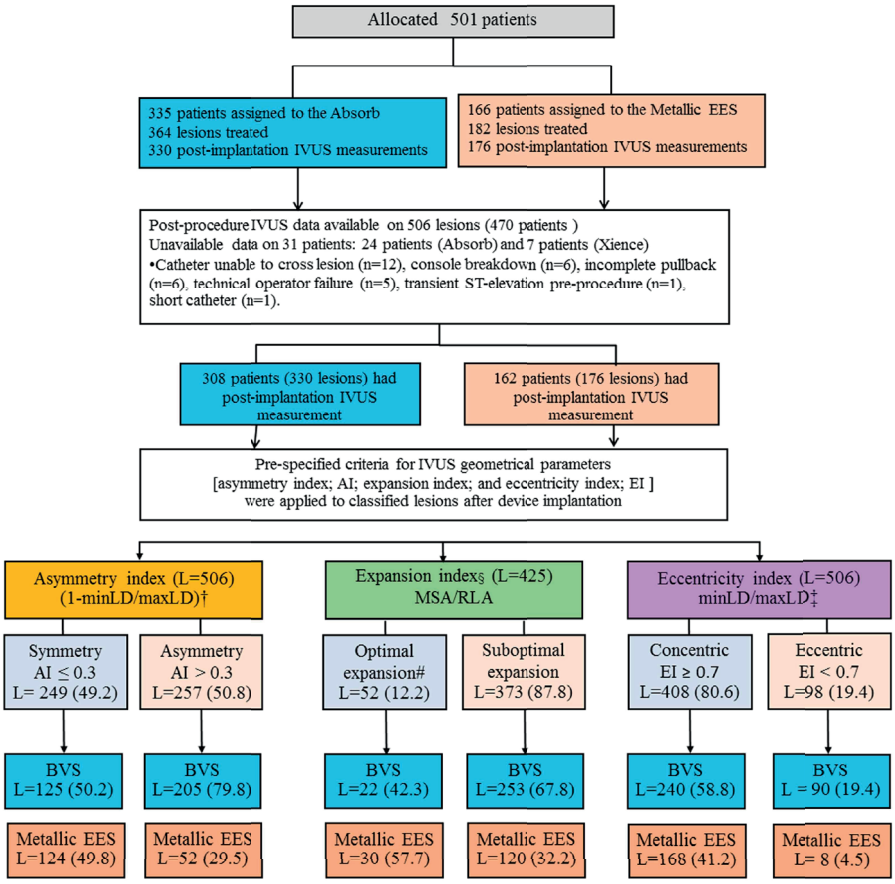

Figure 1. Study flow chart

†Being calculated per pullback; §available in 425 lesions due to the presence of side branches both proximal and distal edge of the scaffold/stent; ‡being calculated per cross-section. AI =asymmetry index; BVS =bioresorbable vascular scaffold; EES =everolimus-elutingstent(s); EI =eccentricity index; IVUS =intravascular ultrasound; L =lesion; LD =lumen diameter; MSA =minimal scaffold/stent area; RLA =reference lumen area.

Study device

The details of the study device (Absorb BVS) have been described previously [8,9]. In brief, the balloon-expandable Absorb scaffold comprises a poly-L-lactide backbone coated with an amorphous drug-eluting coating matrix composed of poly-D,L-lactide polymer containing everolimus 100 mg/cm^2. The control device was the second generation EES Xience, which is a balloon expandable metallic stent, manufactured from a flexible cobalt chromium alloy, and coated with a thin non adhesive, durable, biocompatible acrylic, and fluorinated everolimus-releasing copolymer [8]. The Xience stent and Absorb scaffold share the same basic MULTI-LINK design, and both devices are similar in terms of drug, drug dose density, and elution profile.

Imaging acquisition and analysis

Quantitative angiographic assessment

In each patient, the scaffold/stent segments and the periscaffold/stent segments (defined by a 5 mm length proximal and distal to the scaffold edge) were analyzed by quantitative coronary angiography (QCA) pre- and post-procedure. QCA was performed at an independent core lab (Cardialysis BV, Rotterdam, the Netherlands) with the CAAS system (CAAS 5.10, Pie Medical BV, Maastricht, the Netherlands). The QCA measurements details are described elsewhere [8,10–12].

IVUS acquisition

Grayscale IVUS was acquired with a 3.2-F, 45 MHz rotational IVUS catheter (Revolution 45 MHz, Volcano Corporation, Rancho Cordova, California), using automated pullbacks at 0.5 mm/s and 30 frames/s. All pullbacks were analyzed off-line at 1 mm longitudinal intervals and analyzed by an independent core laboratory (Cardialysis BV) using a commercial software (QIvus 2.2, Medis, Leiden, the Netherlands).

Pre- and post-procedural IVUS analysis

The methods of quantitative IVUS have been previously reported [3,8]. The pre-procedure segments were defined by coregistration with post-procedural IVUS using identical landmarks such as side-branches and calcium locations. Matching was done using dedicated software (Ivus OCTRegistration, Division of Image Processing, Leiden, the Netherlands). Pretreatment reference segments were selected as sites with the least amount of plaque proximal and distal to the minimal lumen area (MLA) sites prior to the takeoff of any major side branches. The scaffold/stent segments were identified by the first and the last cross-sectional IVUS frame in which the scaffold/ stent struts could be identified and/or where the proximal or distal metallic markers could be identified. The post-procedural region of interest was the segment beginning at 5 mm distal of the scaffold/ stent segment extending to the proximal 5 mm of the scaffold/stent segment [13].

IVUS parameter definitions

Calcification on pre-procedural IVUS appears as bright echoes with acoustic shadowing of the deeper arterial structures. Location and circumferential distribution of calcium were quantified on grayscale IVUS. The largest continuous arc of calcium and summed arc of calcium at the site of the pre-interventional lumen area were measured in degrees with a protractor centered on the lumen. Remodeling was assessed by the remodeling index, expressed as the vessel area at the MLA site divided by the average vessel area of the proximal and distal reference segment. Three remodeling categories were defined as follows: positive remodeling, remodeling index >1.00; intermediate remodeling, remodeling index 0.88 to 1.00; and negative remodeling, remodeling index <0.88 [14].

Incomplete apposition was defined as 1 or more scaffold/stent struts separated from the vessel wall. The acute device performance was evaluated by 3 parameters. First, asymmetry index (AI) was calculated per lesion (1- minimum scaffold/stent diameter/ maximum scaffold/stent diameter throughout an entire pullback) [5,15]. Scaffold/stent diameter in each cross-section were measured through each gravitational center for each sectorial degree [16]; minimal scaffold/stent diameter was the minimal value of minimal scaffold/stent diameter throughout scaffold segment, and maximal scaffold/ stent diameter was the maximal value of maximal scaffold/stent diameter throughout scaffold/stent segment. Therefore, the minimum scaffold/stent diameter and maximum scaffold/stent diameter could derive from different cross sections in the scaffold segment. A lesion was characterized as asymmetric when the value of AI was over 0.3 [6]. Conversely, a lesion with AI ≤0.3 was defined as a symmetric lesion. The AI cutoff of 0.3 was derived from the MUSIC study in which the symmetric stent expansion was defined as a ratio of minimum lumen diameter and maximum lumen diameter throughout an entire pullback ≥0.70 (which corresponds to AI of 0.30) had favorable angiographic results at 6 months' follow-up. Second, scaffold/stent expansion index was calculated by the ratio of minimum scaffold/stent area (MSA) to the average reference lumen area (RLA) [6]. The optimal scaffold/stent expansion (OSE) was defined according to criteria of the MUSIC study [6] as MSA ≥90% of the average RLA or ≥100% of lumen area of the reference segment with the lowest lumen area. If MSA ≥9 mm^2, OSE was defined as MSA ≥80% of the average RLA. Third, eccentricity index (EI) was calculated as a parameter for the circularity of the cross section using the formula of minimal scaffold/stent diameter divided by maximal scaffold/stent diameter. Therefore, the calculation of minimal and-maximal scaffold/ stent diameter was derived from the same crosssection [5,6,15]. The IVUS cross sections with the lowest EI value per pullback were used for the analysis.A lesion with EI ≥0.7 was defined as concentric while EI <0.7 was defined as eccentric lesion [17,18].

Clinical endpoints and definition

In the present analysis, the primary clinical outcome was a device-oriented composite endpoint (DoCE) at 1 year, defined as a composite of cardiac death, myocardial infarction (MI) (defined by Q-wave and non–Q-wave MI from nonattributed to nontarget vessels), and ischemia-driven target lesion revascularization by coronary bypass graft or percutaneous coronary intervention. All clinical endpoint definitions are described in the Online Appendix. Definite and probable scaffold/stent thrombosis was adjudicated according to the Academic Research Consortium definitions[19]. An independent clinical events committee adjudicated all clinical outcomes.

Statistical analysis

All statistical analyses were performed using SAS release 9.1 (SAS Institute Inc., Cary, North Carolina) or IBM SPSS Statistics, version 23.0 (IBM Corp., Armonk, New York). QCA and IVUS were analyzed per lesion. All continuous variables were presented as mean ± SD or median (interquartile range) as appropriate. Unpaired *t* test or nonparametric Mann-Whitney *U* test was used for comparisons of continuous variables and chi-square test was used for categorical variables. For lesion-level data, a model with a generalized estimating equation approach was used to compensate for any potential cluster effect of more than 1 vessel scaffold/stent implantation in the same patient and presented as least-squares mean with 95% confidence interval (CI). Differences were considered to be statistically significant if the p value was <0.05.

The endpoints analyses were performed according to the intention-to-treat principle and presented at a patient-level. Whenever a patient received more than 1 lesion treatment, the lesion with the lowest scaffold/stent EI was selected as representative of that patient. One-year clinical outcomes according to post-procedural asymmetry, optimal stent expansion, and eccentricity status were separately compared by the log-rank test. A multivariate Cox proportional hazards model was performed to determine the independent determinants of DoCE. A multivariate Cox proportional hazards analyses was performed to determine the independent determinants of DoCE. The first model was constructed using significant variables in the univariate analysis. The second model was constructed with forward stepwise Cox multivariable regression analysis, entry, and removal criteria of 0.05 and 0.10, respectively. Adjusted hazard ratio (HR) with 95% CI was calculated. The proportional hazards assumption of the Cox regression model was checked by using time-dependent Cox models. If any of the pre-defined IVUS parameters showed statistical significance from logistic regression analysis, receiver-operating characteristic curve and c-index were used to justify the cutoff value. The sensitivity analysis are detailed in the Online Appendix.

RESULTS

Clinical, angiographic results and procedural characteristics

Of the 470 patients, 308 patients (330 lesions) were randomly assigned to BVS arm whereas 162 patients (176 lesions) were assigned to metallic EES arm. Baseline clinical, angiographic results and procedural characteristics are detailed in Table 1. There were no significant differences in the patient's baseline characteristics comparing both devices. Patients treated with the BVS had a higher post-procedural diameter stenosis and lower acute gain compared to the metallic EES. The post-dilation balloon size and pressure in the BVS group were lower than the metallic EES.

Table 1 Baseline clinical and angiographic findings and procedural details based on device type

	BVS	Metallic EES	p-value
	(N= 308, L=330)	(N= 162, L=176)	
Age, year	63.7±10.0	63.3±9.8	0.73
Male sex	231(75.0)	128(79.0)	0.33
Current smokers	78(25.3)	35(21.6)	0.37
Diabetes	69(22.4)	39(24.1)	0.68
Hypertension	210(68.2)	115(71.0)	0.53
Hyperlipidemia requiring medication	217(70.5)	120(74.1)	0.41
Previous PCI	108(35.1)	57(35.2)	0.98
Previous myocardial infarction	85(27.6)	48(29.6)	0.54
Unstable angina	61(19.8)	36(22.2)	0.78
Lesion location			0.52
Left anterior descending	151(45.8)	83(47.2)	
Left circumflex	93(28.2)	40(22.7)	
Right coronary artery	86(26.1)	53(30.1)	
Type B2/C lesion	142(43.0)	86(48.8)	0.21
Calcification, moderate or severe	39(11.9)	28(16.0)	0.19
Pre-procedural angiographic findings			
Reference vessel diameter, mm	2.60±0.37	2.63±0.40	0.44
Proximal Dmax, mm	2.84±0.44	2.87±0.46	0.47
Distal Dmax, mm	2.69±0.45	2.73±0.43	0.32
Minimal lumen diameter, mm	1.08±0.32	1.06±0.31	0.52
Diameter stenosis,%	58.6±11.1	59.4±11.3	0.43
Obstructive lesion length, mm	13.76±6.29	13.66±6.51	0.87
Post-procedural angiographic findings			
Reference vessel diameter, mm	2.65±0.35	2.79±0.33	<0.001
Minimal lumen diameter, mm	2.24±0.33	2.51±0.33	<0.001
Diameter stenosis,%	15.6±6.4	10.3±5.1	<0.001
Acute gain, mm	1.17±0.38	1.45±0.37	<0.001
Percentage acute gain, %	42.8±12.1	49.0±11.7	<0.001
Procedural details			
Balloon dilation prior to device implantation	330(100)	174(98.9)	0.05
Diameter implanted device, mm	3.03±0.31	3.06±0.28	0.18
Maximal device inflation pressure, atm	13.2±2.7	13.8±2.5	0.008
Stent length, mm	24.0±10.9	23.4±8.9	0.53
Overlapped implantation	58(17.6)	152(13.6)	0.25
Balloon dilation after device implantation	206(62.4)	107(60.8)	0.72
Maximal diameter balloon post-dilation, mm	3.09±0.33	3.16±0.36	0.04
Maximal post-dilation balloon inflation, atm	14.3±3.4	15.1±3.4	0.01
Maximal post-dilation balloon length, mm	16.9±4.6	17.8±5.4	0.05

Values are mean±SD or n(%).

BVS = bioresorbable vascular scaffold; Dmax = maximal lumen diameter; EES = everolimus-eluting stent(s); L = number of lesions; PCI = percutaneous coronary intervention.

IVUS findings pre- and post-procedure between BVS and metallic EES

IVUS findings between the 2 devices are tabulated in Table 2.Pre-procedure, the presence of calcium and the sum arc of calcium were similar for both devices. Pre-procedural lumen EI of metallic EES arm was lower than the BVS arm (0.59 [IQR: 0.57 to 0.61] vs. 0.61 [IQR: 0.60 to 0.62]; p = 0.041), whereas the pre-procedural AI was not significantly different. Post-procedure, MSA measured 4.87 (IQR: 4.72 to 5.02) mm^2 in the BVS group and 5.72 (IQR: 5.49 to 5.94) mm^2 in the metallic EES group (p < 0.001). Lesions treated with BVS were more eccentric (27.3% vs. 4.5%; p < 0.001) and asymmetric (62.1% vs. 29.5%; p < 0.001) than lesions treated with metallic EES. Among 506 lesions, the scaffold/stent expansion index was calculated in 425 lesions, while in the remaining 71 lesions the scaffold/stent expansion indices could not be calculated due to the presence of side branches both at the proximal and distal edges of the scaffold/stent. Notably, only 8.0% in BVS arm and 20.0% in metallic EES could achieve optimal scaffold stent expansion (p < 0.001).

Device-oriented composite endpoint at 1 year as stratified by IVUS parameters.

At 1 year, the DoCE rates were 5.2% in BVS and 3.1% in EES, respectively (p = 0.29). DoCE and the components as stratified by the pre-defined IVUS parameters are shown in Table 3. The DoCE rates were similar between the OSE group and suboptimal stent expansion group (4.2% vs. 4.4%; p = 0.93). When stratified by the AI, the asymmetric group was associated with a higher risk of DoCE than the symmetric group. As showed in Figure 2, DoCE occurred in 4 of 224 patients in the symmetric group, whereas it occurred in 17 of 246 patients in the asymmetric group (1.8% vs. 6.9 %; p = 0.007). A higher event rate in the asymmetric group was primarily driven by a higher incidence of MI (majority was periprocedural MI), while the incidence of cardiac death, definite/probable scaffold/stent thrombosis were not significantly different between both groups. However, upon stratification by the EI, eccentric lesions had higher rates of DoCE, target lesion revascularization, and definite/probable scaffold/stent thrombosis than concentric lesions (Table 3). Of note, as showed in Figure 2, all eccentric lesions belonged to the asymmetric lesions group.

IVUS predictors for DoCE after scaffold/ stent implantation.

Table 4 shows the univariate predictors of DoCE after scaffold/stent implantation for the entire population and each device. Subsequent multivariate analysis (Table 5) from both 2 models identified that AI >0.30 after implantation was an independent predictor for the occurrence of DoCE (adjusted HR: 3.43; 95% CI: 1.08 to 10.92; p = 0.037), whereas there was no consistency of the statistical significances of pre-procedural diameter stenosis, pre-procedural negative remodeling lesion, total stent length and overlapping

Table 2 Intravascular Ultrasound findings pre- and post-implantation according to implanted devices

	BVS	Metallic EES	p-value
	(N= 308, L=330)	(N= 162, L=176)	
Pre-implantation			
Mean lumen area, mm^2	4.84(4.68-4.99)	5.03(4.81-5.25)	0.156
Minimal lumen area, mm^2	2.04(1.96-2.12)	2.13(2.01-2.26)	0.203
Lumen eccentricity index	0.61(0.60-0.62)	0.59(0.57-0.61)	0.041
Asymmetry index	0.60(0.59-0.61)	0.61(0.60-0.62)	0.323
Mean vessel area, mm^2	11.51(11.13-11.89)	12.34(11.81-12.87)	0.013
Minimal vessel area, mm^2	8.62(8.28-8.96)	9.43(8.93-9.93)	0.009
Total plaque area, mm^2	6.67(6.39-6.95)	7.30(6.88-7.71)	0.015
Presence of calcium	200(114)	106(63.1)	0.897
Sum arc of calcium	54.26(46.68-61.83)	60.31(48.98-71.64)	0.384
Remodeling index	0.91(0.89-0.94)	0.92(0.89-0.95)	0.775
Negative arterial remodeling	132(41.6)	77(46.4)	0.897
Post-implantation			
Reference lumen area	6.53(6.28-6.78)	6.92(6.61-7.23)	0.057
Mean vessel area, mm^2	13.11(12.72-13.50)	14.22(13.70-14.75)	0.001
Minimal vessel area, mm^2	10.57(10.21-10.94)	11.59(11.09-12.10)	0.001
Mean stent area, mm^2	6.01(5.85-6.16)	6.78(6.55-7.02)	<0.001
Minimal stent area, mm^2	4.87(4.72-5.02)	5.72(5.49-5.94)	<0.001
Total plaque area, mm^2	7.07(6.80-7.34)	7.41(7.05-7.77)	0.139
Percentage of frame with malapposition,%	2.00(1.27-2.73)	2.74(1.54-3.94)	0.299
Mean ISA distance, mm	0.37(0.27-0.47)	0.45(0.35-0.55)	0.251
ISA area, mm^2	0.98(0.45-1.51)	1.15(0.78-1.52)	0.622
Prolapse area, mm^2	0.00	0.00(0.00-0.01)	0.001
Scaffold/stent asymmetry index	0.33(0.32-0.34)	0.27(0.26-0.27)	<0.001
Device asymmetry after implantation†	205(62.1)	52(29.5)	<0.001
Expansion index†	0.70(0.68-0.72)	0.76(0.74-0.78)	<0.001
Optimal scaffold/stent expansion*	22(8.0)	30(20.0)	<0.001
Ratio of MSA to expected nominal scaffold/stent area	0.67(0.66-0.69)	0.77(0.75-0.79)	<0.001
Minimum scaffold/stent eccentricity index	0.74(0.73-0.75)	0.81(0.80-0.81)	<0.001
Device eccentricity after implantation‡	90(27.3)	8(4.5)	<0.001
Δ pre- vs. post-procedural AI	0.27(0.26-0.28)	0.34(0.33-0.36)	<0.001
Δ pre- vs. post-procedural EI	-0.13(-0.14--0.12)	-0.22(-0.23--0.20)	<0.001
Eccentric & asymmetric lesions post-implantation	90(27.3)	8(4.5)	<0.001

Values are median (interquartile range) or n (%). Generalized estimated equation analysis was used. *Optimal scaffold/stent expansion (OSE) was defined as MSA ≥ 90% of the average RLA or ≥ 100% of lumen area of the reference segment with the lowest lumen area. If MSA ≥ 9 mm2, OSE was defined as MSA ≥ 80% of the average RLA. † A lesion was characterized as asymmetric when the value of AI was over 0.3.‡ A lesion was characterized as eccentric when the value of EI was less than 0.7.

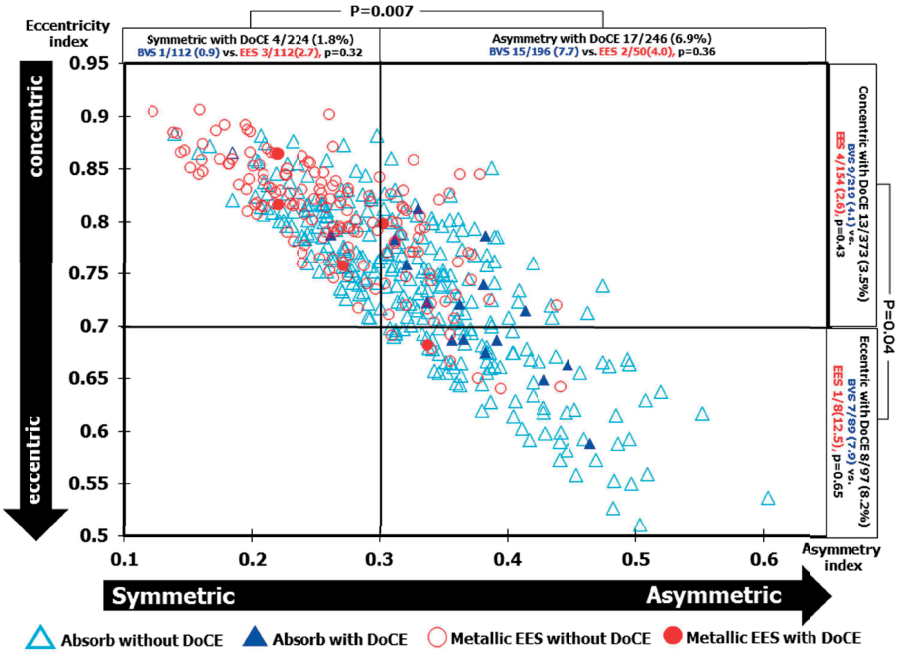

Figure 2. Distribution of Geometrical Morphology According to Type of Device in the ABSORB II Trial and the Incidence of DoCE Over 1-Year Follow-Up
DoCE = device oriented cardiovascular endpoint; other abbreviations as in Figure 1.

implantation across the 2 models. The cutoff of 0.30 was justified by receiver-operating characteristic curve analysis and demonstrated in Online Figure 1.

Upon comparison of patients with asymmetric versus symmetric lesions: there was a lower prevalence of diabetes (22% vs. 27.2%; p = 0.04); lesions were more complex (type B2/C) and more moderate to severe calcification; the reference vessel diameter was smaller and the lesion length was longer in the asymmetric subgroup, respectively. Furthermore, the baseline MLA, post-procedural MSA, and expansion index were lower in the asymmetric group, along with a higher prevalence of eccentric device after implantation (38.1% vs. 0%; p < 0.001; respectively) (Online Table 1).

The interaction between the subgroup and asymmetry status was performed to confirm if the influence of asymmetry on adverse events was consistent among the subset of patients. As shown in Figure 3, post-implantation device asymmetry compared with symmetry was consistent in all subgroups. As the sample size was small for most subgroups, caution should be used in the interpretation of these results and in drawing conclusions.

Table 3 Incidence of device oriented clinical endpoints at 1-year follow-up according to the criteria of optimal expansion, asymmetry and eccentricity of device post-implantation.

Clinical outcomes	OSE	SSE	p-value†	Symmetry	Asymmetry	p-value¶	Concentric	Eccentric	p-value§
	N=48	N=343		N=224	N=246		N=373	N=97	
Cardiac Death	0(0)	0(0)	NA	0(0)	0(0)	NA	0(0)	0(0)	NA
Myocardial infarction	0(0)	13(3.8)	0.17	3(1.3)	14(5.7)	0.01	12(3.2)	5(5.2)	0.36
QMI	0(0)	2(0.6)		0(0)	2(0.8)		1(0.3)	1(1.0)	
NQMI	0(0)	11(3.2)		3(1.3)	12(4.9)		11(2.9)	4(4.1)	
MI from nonattributed to nontarget vessels	0(0)	12(3.5)	0.19	2(0.9)	14(5.7)	0.004	11(2.9)	5(5.2)	0.29
Peri-procedural MI	0(0)	11(3.2)	0.68	4(1.8)	11(4.5)	0.046	10(2.7)	4(4.1)	0.46
Ischemia Driven TLR	2(4.2)	5(1.5)	0.19	2(0.9)	5(2.0)	0.29	2(0.5)	5(5.2)	0.001
Composite of cardiac death, MI from nonattributed to nontarget vessels I and clinically indicated target lesion revascularization (DoCE)	2(4.2)	15(4.4)	0.93	4(1.8)	17(6.9)	0.007	13(3.5)	8(8.2)	0.04
Composite of cardiac death, all MI and clinically indicated target lesion revascularization (MACE)	2(4.2)	16(4.7)	0.87	5(2.2)	17(6.9)	0.02	14(3.8)	8(8.2)	0.06
Definite/probable ST	0(0)	3(0.9)	0.51	0(0)	3(1.2)	0.09	1(0.3)	2(2.1)	0.04
-Definite ST‡	0(0)	2(0.6)		0(0)	2(0.8)		0(0.0)	2(2.1)	
-Probable ST#	0(0)	1(0.3)		0(0)	1(0.4)		1(0.3)	0(0)	

Data are shown in n (%) ‡ event occur at 0 and 2 days post-procedure; # event occur 335 days post-procedure. †compare between OSE and SSE; ¶compared between symmetry group and asymmetry group. § compared between concentric group and eccentric group. There were no significant differences of events between BVS and Metallic EES in each group.

Abbreviation: OSE:optimal scaffold/stent expansion; SSE: suboptimal scaffold/stent expansion; QMI: Q-wave myocardial infarction; NQMI: non-Q-wave myocardial infarction; TLR: target lesion revascularization; MI: myocardial infarction; MACE: major adverse cardiac events; DoCE: device oriented composite end point; ST: scaffold/stent thrombosis

Table 4 Univariate Analysis for Predictors of DoCE After Scaffold/Stent Implantation

	Overall		Absorb BVS		metallic EES	
	HR (95% CI)	p Value	HR (95% CI)	p Value	HR (95%CI)	p Value
I. Patient-related factors						
Age (yrs)	1.02(0.97-1.06)	0.46	1.01(0.96-1.06)	0.75	1.04(0.95-1.15)	0.37
Male	0.53 (0.15-1.82)	0.31	0.68 (0.19-2.45)	0.56	29.31 (0.003-2.72e5)	0.47
Current smoker	1.09(0.79-1.50)	0.62	1.22(0.86-1.74)	0.26	0.32(0.02-6.60)	0.32
Hypertension requiring treatment	0.94(0.59-1.49)	0.8	1.01(0.59-1.75)	0.96	0.78(0.31-1.93)	0.59
Dyslipidemia requiring treatment	0.79(0.50-1.25)	0.31	0.83(0.49-1.39)	0.48	0.72(0.29-1.78)	0.47
Any diabetes mellitus	0.99(0.76-1.28)	0.93	2.08(0.46-9.40)	0.34	0.20(0.03-1.23)	0.08
Unstable Angina	0.90(0.29-2.74)	0.85	0.69(0.25-1.91)	0.48	0.83(0.14-5.13)	0.84
II. Lesion-related factors assessed by QCA and IVUS pre-procedure						
QCA:type B2/C lesions	0.72(0.30-1.74)	0.47	1.36(0.50-3.71)	0.56	1.64(0.27-10.09)	0.59
QCA:obstruction length per mm	0.95(0.87-1.04)	0.26	0.95(0.86-1.05)	0.29	0.95(0.80-1.13)	0.55
QCA:percentage diameter stenosis	0.96(0.93-1.00)	0.07	0.97(0.92-1.01)	0.12	0.96(0.89-1.05)	0.38
QCA:reference diameter per mm	0.50(0.19-1.36)	0.18	0.20(0.04-0.96)	0.045	0.62(0.07-5.91)	0.68
QCA:curvature per cm^{-1}	0.71(0.25-2.01)	0.52	0.26(0.03-2.31)	0.22	0.30(0.01-17.55)	0.56
IVUS:lesion length to MLA ratio	1.06(0.99-1.13)	0.06	1.06(0.99-1.14)	0.08	1.05(0.91-1.23)	0.50
IVUS:sum arc of calcium at MLA frame	1.00(0.99-1.00)	0.34	1.00(1.00-1.01)	0.32	1.00(0.99-1.01)	0.76
IVUS:minimal vessel area per mm^2	1.01(0.87-1.17)	0.89	0.96(0.81-1.14)	0.62	1.08(0.84-1.40)	0.54
IVUS:minimal lumen area per mm^2	0.65(0.26-1.65)	0.36	0.60(0.24-1.50)	0.27	0.87(0.27-2.77)	0.81
IVUS:lumen eccentricity index	0.09(0.00-3.57)	0.19	0.84(0.55-1.28)	0.41	0.62(0.31-1.25)	0.18
IVUS:lumen asymmetry index¶	1.13(0.63-2.03)	0.69	1.07(0.56-2.07)	0.83	1.39(0.40-4.87)	0.60
IVUS:total plaque area per mm^2	1.04(0.88-1.24)	0.62	0.97(0.79-1.19)	0.78	1.21(0.91-1.60)	0.19
IVUS:lesion with negative remodeling†	0.31(0.10-0.93)	0.04	0.32(0.09-1.15)	0.08	0.29(0.03-2.66)	0.27
III. Procedure-related factors						
Treatment with Absorb	1.72(0.62-4.79)	0.29	NA	NA	NA	NA

Table 4 Univariate analysis for predictors of device-oriented composite endpoint (DoCE) after scaffold/stent implantation. (continued)

	Overall		Absorb BVS		metallic EES	
	HR (95% CI)	p Value	HR (95% CI)	p Value	HR (95%CI)	p Value
Pre-dilation balloon diameter per mm	1.30(0.38-4.45)	0.67	0.78(0.19-3.24)	0.73	7.24(0.68-77.56)	0.10
Pre-dilation balloon pressure per atm	1.07(0.93-1.22)	0.38	1.13(0.96-1.33)	0.15	0.90(0.66-1.24)	0.53
Device diameter per mm	0.83(0.19-3.54)	0.80	0.77(0.15-3.85)	0.75	1.50(0.06-36.63)	0.80
Total stent length per mm†	1.05(1.02-1.08)	0.002	1.05(1.02-1.09)	0.002	1.01(0.92-1.11)	0.83
Maximal device inflation pressure	1.12(0.93-1.34)	0.24	1.08(0.88-1.33)	0.45	1.30(0.87-1.96)	0.20
Overlapping implantation†	3.33(1.33-8.34)	0.01	3.95(1.40-11.13)	0.009	1.53(0.16-14.37)	0.71
Post-dilation performed	1.01(0.41-2.49)	0.98	1.31(0.44-3.87)	0.63	0.42(0.07-2.61)	0.86
Post-dilation balloon diameter per mm	1.33(0.37-4.79)	0.66	1.73(0.37-8.18)	0.49	0.89(0.08-10.72)	0.93
Post-dilation balloon length per mm	0.99(0.89-1.08)	0.76	0.95(0.85-1.08)	0.44	1.06(0.91-1.24)	0.44
Post-dilation balloon pressure per atm	1.04(0.92-1.19)	0.51	1.03(0.88-1.19)	0.74	1.14(0.88-1.46)	0.32
IV. Post-procedural results						
QCA:percentage diameter stenosis	0.99(0.93-1.06)	0.80	0.99(0.91-1.07)	0.78	0.90(0.75-1.09)	0.29
QCA:percentage of acute gain	0.98(0.94-1.01)	0.19	0.98(0.94-1.02)	0.30	0.99(0.91-1.07)	0.71
QCA:minimal lumen diameter per mm	0.49(0.13-1.81)	0.28	0.34(0.07-1.74)	0.20	2.72(0.20-37.71)	0.46
IVUS:minimum stent area per mm^2	0.85(0.61-1.16)	0.30	0.78(0.52-1.16)	0.22	1.14(0.65-1.99)	0.64
IVUS:mean stent area per mm^2	0.91(0.67-1.22)	0.52	0.85(0.59-1.23)	0.38	1.18(0.69-2.00)	0.55
IVUS:scaffold/stent eccentricity index	0.01(0.00-3.02)	0.12	0.73(0.38-1.37)	0.33	0.55(0.13-2.42)	0.43
IVUS:scaffold/stent asymmetry index¶	1.74(1.03-2.93)	0.04	1.81(0.98-3.36)	0.06	1.12(0.28-4.53)	0.88
IVUS:scaffold/stent expansion index	0.31(0.01-8.91)	0.49	0.85(0.57-1.27)	0.42	1.13(0.59-2.17)	0.72
IVUS:total plaque area per mm^2	1.02(0.85-1.26)	0.86	0.95(0.77-1.18)	0.66	1.23(0.89-1.71)	0.21
Being classified in EA group	2.49(1.00-6.19)	0.05	1.99(0.72-5.53)	0.19	5.36(0.53-54.44)	0.16
Asymmetry index > 0.3 after implantation†	4.08(1.35-12.33)	0.01	9.20(1.20-70.60)	0.03	1.51(0.25-9.35)	0.66

¶ per 0.1 increase; †variables that were selected into multivariable model.

CI = confidence interval; EA = eccentric and asymmetric; HR = hazard ratio; IVUS = intravascular ultrasound; MLA = minimal lumen area; QCA = quantitative coronary angiography; other abbreviations as in Tables 2 and 3.

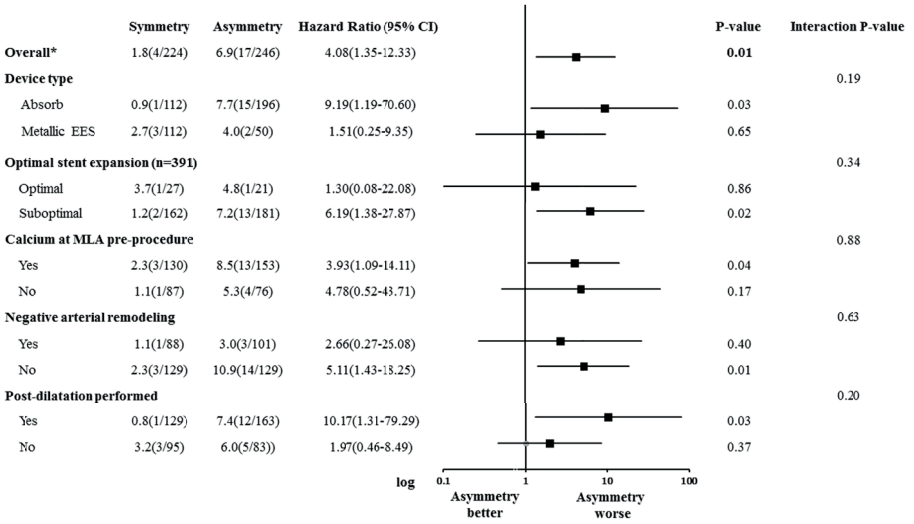

Figure 3. Subgroup Analyses of the 1-Year Rates of Device Oriented Cardiac Events Between Asymmetric Versus Symmetric of Device Post-Implantation

Probability for interaction represents the likelihood for interaction between the variable and the post-implantation asymmetry status. CI = confidence interval; EES = everolimus-eluting stent(s); MLA = minimal lumen area.

Table 5 Multivariate Analysis for Predictors of DoCE After Scaffold/Stent Implantation

Multivariate analyses using variables in univariate analysis, p-value< 0.05		
	HR (95%)	p Value
IVUS:lesion with negative remodeling	0.32(0.11-0.99)	0.049
Total stent length per mm	1.02(0.97-1.07)	0.41
Overlapping implantation	1.35(0.28-6.49)	0.71
Asymmetry index > 0.3 after implantation	3.43(1.08-10.92)	0.037
Forward stepwise Cox multivariable regression analysis		
	HR (95%)	p Value
%diameter stenosis pre-procedure	0.944 (0.91-0.98)	0.006
Overlapping implantation	3.18 (1.19-8.50)	0.021
Asymmetry index > 0.3 after implantation	4.06 (1.15-14.36)	0.030

DISCUSSION

The present study investigated the impact of acute scaffold/stent performance of BVS and the second generation DES on clinical outcomes. The current analyses suggested that post-procedural AI >0.30 was associated with adverse clinical outcomes.

Importance of AI over expansion index: are these 2 parameters similar in evaluating optimal deployment?

MSA and expansion index have been widely used as indicators of optimal scaffold/stent expansion whereas there was less attention dedicated to post-implantation device asymmetry and eccentricity. Indeed, these parameters aim to evaluate the optimal device performance, so called "expansion." The present study showed that post-implantation device asymmetry (AI >0.30) is one of the predictors of DOCE while MSA, expansion index, and EI were not. Furthermore, the asymmetric lumen has worse outcomes especially in patients with suboptimal expansion. However, a non significant p value for interaction (p = 0.34) suggested that this influence was not different in patients with or without optimal expansion. Thus, the current study suggested that a single variable of the expansion index is not enough to predict future events without taking into consideration the homogeneity of the stent/scaffold expansion and it seemed that AI was a more discriminant parameter compared to the EI.

The discrepancy of the present study with previous publications could be explained by the following reasons. First, the criteria of optimal stent expansion used in previous reports varied considerably. For example, the optimal stent expansion criteria in some studies depended on the discretion of the treating operator [20,21]. Some used absolute value of MSA≥5.0 mm^2[22] or the ratio of MSA to crosssection area of the fully inflated post-dilation balloon [23]. Additionally, the outcomes measured in each study were also different. Second, the criteria applied to evaluate the optimal device expansion in the present study was based on IVUS guidance stent implantation trial while IVUS in the ABSORB II trial was only documentary. Third, the current analysis was a comparison between metallic EES and BVS in a randomized design, while previous trials were conducted in the first-generation DES platform, mostly in nonrandomized studies, only with post-procedural IVUS and shorter clinical follow-up (6 months).

How does device asymmetry contribute to DoCE?

The present analysis showed that AI >0.30 is associated with a high rate of MI and primarily represented by periprocedural MI, which could potentially be explained by disruption of the laminar flow and induced flow disturbances in asymmetric lesions. Low shear stress could induce platelet aggregation, microthrombi formation with potential embolization, leading to micromyocardial necrosis [24].

Additionally, the present study also showed a higher target lesion revascularization in the eccentric device subgroup. Potential explanations could be the following. First, the pharmacokinetic models have shown that substantial inhomogeneities in drug concentration exist for different strut placements and geometry [25]. An inhomogeneous strut istribution in eccentric and asymmetric lesions may cause lower local drug concentration, subsequent neointimal hyperplasia and restenosis that could explain the increased target lesion revascularization incidence: Second, the heterogeneous EES due to the asymmetric and eccentric lumen may further accentuate the plaque eccentricity and further amplify the low EES effect. The low EES area is at high risk for rapid worsening plaque distribution [26] that may result in more restenosis at follow-up.

When the univariate analysis was performed separately in the metallic EES arm and Absorb arm (Table 4), AI >0.30 did no longer demonstrated statistical significance in the metallic EES arm. As shown in Figure 3, the influence of asymmetric lumen on clinical outcomes tended to be more emphasized in the Absorb arm (HR: 9.19; 95% CI: 1.19 to 70.60) than in the metallic EES arm (HR: 1.51; 95% CI: 0.25 to 9.35) although the p value for interaction failed to reach statistical significance ($p = 0.06$). Therefore, to avoid post-implantation device asymmetry, intravascular imaging may have an important role in the detection and correction of these morphologic abnormalities. Recently, Hong et al.[27] reported that IVUS-guided EES implantation, compared with angiographyguided stent implantation, resulted in significantly lower rates of major adverse cardiac events. It remains to demonstrate whether post-procedural eccentricity and asymmetry could be corrected by aggressive post-dilation or whether this strategy should be avoided and prevented by an aggressive lesion preparation. Mattesini et al. [15] showed that both BVS and second-generation DES could achieve similar asymmetry, eccentricity indices, minimal and mean scaffold/stent areas with optical coherence tomography guidance to achieve optimal expansion at the discretion of the treating operator by further postdilation. Also, the diameter and pre-dilation balloon pressure were higher in the ABSORB compared to the DES group. In addition, post-dilation balloon pressure was higher in the ABSORB group while the postdilation balloon diameter was similar. Aggressive lesion preparation in combination with a high pressure post-dilation may have corrected the preprocedural eccentricity and asymmetry. Further research with a large clinical trial assessing the role of intravascular imaging guidance for lesion preparation and device post-dilation to achieve optimal scaffold/stent expansion is of interest to clarify its impact on clinical outcomes.

Study limitations.

First, multivariate analyses could not be performed extensively due to limited number of events. In the present analysis, 2 multivariate models contributed different independent predictors of DoCE, nevertheless, AI >0.30 is the only variable that remains significant

in the analyses. Hence findings should be interpreted with caution and are hypothesis generating in nature. Second, the relatively simple lesions characteristics might have limited our ability to generalize our findings, especially to patients with complex lesions that we commonly see in the daily clinical practice. Third, the expansion index was evaluated in 391 patients due to missing data in 79 patients (16.8%). Fourth, because the 1-year follow-up of the ABSORB II trial is purely clinical, we could not evaluate the restenosis process on angiography or IVUS and relate the asymmetry and eccentricity assessment to neointimal hyperplasia.

CONCLUSIONS

In this ABSORB II IVUS substudy, asymmetry, expansion, and eccentricity was used to investigate its relationship to the incidence of DoCE. Postprocedural device asymmetry and eccentricity were related to a higher event rates while the expansion status was not. Post-intervention AI >0.30 should be avoided to reduce asymmetry or eccentricity-related complication, although the results are hypothesis generating.

PERSPECTIVES

WHAT IS KNOWN? Minimal stent area and expansion index have been widely used as indicators of optimal scaffold/stent expansion whereas the impact of postimplantation device asymmetry and eccentricity on clinical events is unclear.

WHAT IS NEW? The current analyses suggested that post-procedural AI >0.30 was associated with adverse clinical outcomes.

WHAT IS NEXT? It remains to demonstrate whether post-procedural eccentricity and asymmetry could be corrected by aggressive post-dilation or whether this strategy should be avoided and prevented by an aggressive lesion preparation.

REFERENCES

1. Onuma Y, Serruys PW. Bioresorbable scaffold: the advent of a new era in percutaneous coronary and peripheral revascularization? Circulation 2011;123:779–97.
2. Ellis SG, Kereiakes DJ, Metzger DC, et al. Everolimus-eluting bioresorbable scaffolds for coronary artery disease. N Engl J Med 2015;373:1905–15.
3. Serruys PW, Chevalier B, Dudek D, et al. A bioresorbable everolimus-eluting scaffold versus a metallic everolimus-eluting stent for ischaemic heart disease caused by de-novo native coronary artery lesions (ABSORB II): an interim 1-year analysis of clinical and procedural secondary outcomes from a randomised controlled trial. Lancet 2015;385:43–54.
4. Ormiston JA, Webber B, Ubod B, Darremont O, Webster MW. An independent bench comparison of two bioresorbable drug-eluting coronary scaffolds (Absorb and DESolve) with a durable metallic drug-eluting stent (ML8/Xpedition). EuroIntervention 2015;11:60–7.
5. Brugaletta S, Gomez-Lara J, Diletti R, et al. Comparison of in vivo eccentricity and symmetry indices between metallic stents and bioresorbable vascular scaffolds: insights from the ABSORB and SPIRIT trials. Catheter Cardiovasc Interv 2012;79:219–28.
6. de Jaegere P, Mudra H, Figulla H, et al. Intravascular ultrasound-guided optimized stent deployment. Immediate and 6 months clinical and angiographic results from the Multicenter Ultrasound Stenting in Coronaries Study (MUSIC Study). Eur Heart J 1998;19:1214–23.
7. Otake H, Shite J, Ako J, et al. Local determinants of thrombus formation following sirolimus-eluting stent implantation assessed by optical coherence tomography. J Am Coll CardiolIntv 2009;2:459–66.
8. Diletti R, Serruys PW, Farooq V, et al. ABSORB II randomized controlled trial: a clinical evaluation to compare the safety, efficacy, and performance of the Absorb everolimus-eluting bioresorbable vascular scaffold system against the XIENCE everolimus-eluting coronary stent system in the treatment of subjects with ischemic heart disease caused by de novo native coronary artery lesions: rationale and study design. Am Heart J 2012;164:654–63.
9. Serruys PW, Onuma Y, Ormiston JA, et al. Evaluation of the second generation of a bioresorbable everolimus drug-eluting vascular scaffold for treatment of de novo coronary artery stenosis: six-month clinical and imaging outcomes.Circulation 2010;122:2301–12.
10. Gomez-Lara J, Diletti R, Brugaletta S, et al. Angiographic maximal luminal diameter and appropriate deployment of the everolimus-eluting bioresorbable vascular scaffold as assessed by optical coherence tomography: an ABSORB cohort B trial sub-study. EuroIntervention 2012;8:214–24.
11. Farooq V, Gomez-Lara J, Brugaletta S, et al. Proximal and distal maximal luminal diameters as a guide to appropriate deployment of the ABSORB everolimus-eluting bioresorbable vascular scaffold: a sub-study of the ABSORB Cohort B and the on-going ABSORB EXTEND Single Arm Study. Catheter Cardiovasc Interv 2012;79:880–8.
12. Ishibashi Y, Nakatani S, Sotomi Y, et al. Relation between bioresorbable scaffold sizing Using QCA-Dmax and clinical outcomes at 1 year in 1,232 patients from 3 study cohorts (ABSORB Cohort B, ABSORB EXTEND, and ABSORB II). J Am Coll Cardiol Intv 2015;8:1715–26.
13. Mintz GS, Nissen SE, Anderson WD, et al. American College of Cardiology Clinical Expert Consensus Document on Standards for Acquisition, Measurement and Reporting of Intravascular Ultrasound Studies (IVUS). A report of the American College of Cardiology Task Force on Clinical Expert Consensus Documents. J Am Coll Cardiol 2001;37:1478–92.
14. Inaba S, Mintz GS, Farhat NZ, et al. Impact of positive and negative lesion site remodeling on clinical outcomes: insights from PROSPECT. J Am Coll Cardiol Img 2014;7:70–8.

15. Mattesini A, Secco GG, Dall'Ara G, et al. ABSORB biodegradable stents versus secondgeneration metal stents: a comparison study of 100 complex lesions treated under OCT guidance. J Am Coll Cardiol Intv 2014;7:741–50.
16. Tsuchida K, Garcia-Garcia HM, Ong AT, et al. Revisiting late loss and neointimal volumetric measurements in a drug-eluting stent trial: analysis from the SPIRIT FIRST trial. Catheter Cardiovasc Interv 2006;67:188–97.
17. von Birgelen C, Gil R, Ruygrok P, et al. Optimized expansion of the Wallstent compared with the Palmaz-Schatz stent: on-line observations with two- and three-dimensional intracoronary ultrasound after angiographic guidance. Am Heart J 1996;131:1067–75.
18. Nakano M, Wagatsuma K, Iga A, et al. Impact of highly asymmetric stent expansion after sirolimus-eluting stent implantation on twelvemonth clinical outcomes. J Cardiol 2007;49:313–21.
19. Vranckx P, Kint PP, Morel MA, Van Es GA, Serruys PW, Cutlip DE. Identifying stent thrombosis, a critical appraisal of the academic research consortium (ARC) consensus definitions: a lighthouse and as a toe in the water. EuroIntervention 2008;4:C39–44.
20. Claessen BE, Mehran R, Mintz GS, et al. Impact of intravascular ultrasound imaging on early and late clinical outcomes following percutaneous coronary intervention with drugeluting stents. J Am Coll Cardiol Intv 2011;4:974–81.
21. Witzenbichler B, Maehara A, Weisz G, et al. Relationship between intravascular ultrasound guidance and clinical outcomes after drug-eluting stents: the assessment of dual antiplatelet therapy with drug-eluting stents (ADAPT-DES) study. Circulation 2014;129:463–70.
22. Sonoda S, Morino Y, Ako J, et al. Impact of final stent dimensions on long-term results following sirolimus-eluting stent implantation: serial intravascular ultrasound analysis from the sirius trial. J Am Coll Cardiol 2004;43: 1959–63.
23. Chieffo A, Latib A, Caussin C, et al. A prospective, randomized trial of intravascularultrasound guided compared to angiography guided stent implantation in complex coronarylesions: the AVIO trial. Am Heart J 2013;165:65–72.
24. Koskinas KC, Chatzizisis YS, Antoniadis AP, Giannoglou GD. Role of endothelial shear stress in stent restenosis and thrombosis: pathophysiologic mechanisms and mplications forclinical translation. J Am Coll Cardiol 2012;59: 1337–49.
25. Hwang CW, Wu D, Edelman ER. Physiological transport forces govern drug distribution for tent-based delivery. Circulation 2001;104:600–5.
26. Papafaklis MI, Takahashi S, Antoniadis AP, et al. Effect of the local hemodynamic environment on the de novo development and progression of eccentric coronary atherosclerosis in humans: insights from PREDICTION. Atherosclerosis 2015; 240:205–11.
27. Hong S, Kim B, Shin D, et al. Effect of intravascular ultrasound–guided vs angiography-guided everolimus-eluting stent implantation: The ivus-xpl randomized clinical trial. JAMA 2015;314:2155–63.

APPENDIX- CLINICAL ENDPOINTS DEFINITIONS

Cardiac death was defined as any death due to a proximate cardiac cause (e.g., MI, low-output failure, fatal arrhythmia). Unwitnessed death and death of unknown cause were classified as cardiac death. MI classification and criteria for diagnosis were defined according to the per protocol definition. Q-wave MI was the development of a new, pathological Q-wave. Non-Q-wave MI was adjudicated if there was an elevation of CK levels to ≥ two times the upper limit of normal with elevated CK-MB in the absence of new pathological Q waves. Notably, this definition of per-protocol MI was consistently applied in all trials included in the present analysis. ID-TLR was defined as any repeat percutaneous intervention of the target lesion or bypass surgery of the target vessel with either a positive functional ischemia study, ischemic symptoms and angiographic minimal lumen diameter stenosis ≥50% by core laboratory QCA, or revascularization of a target lesion with diameter stenosis ≥70% by core laboratory QCA without either ischemic symptoms or a positive functional study.

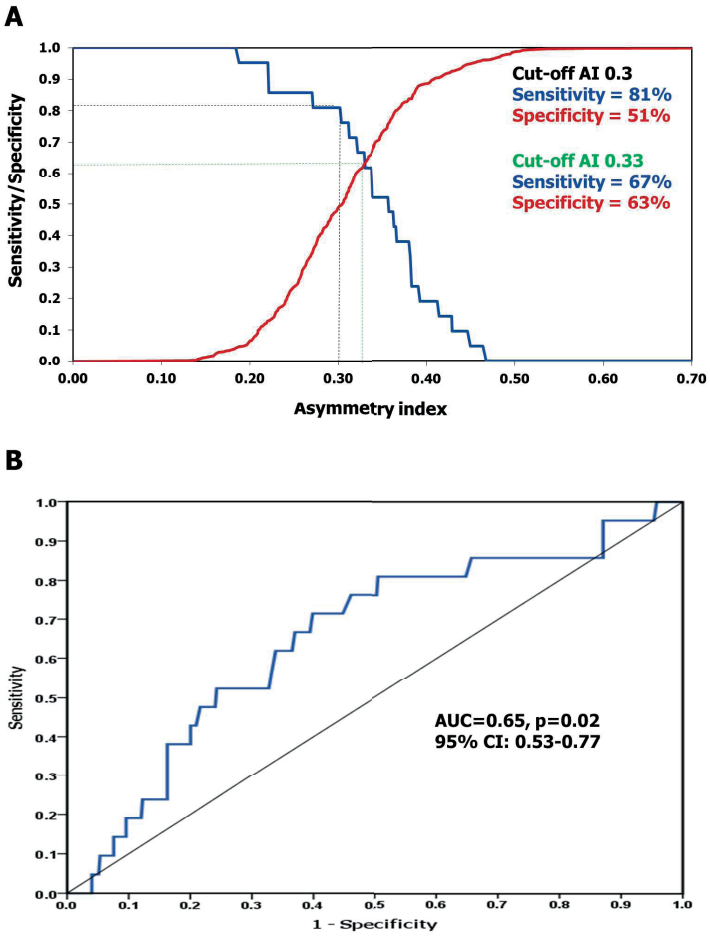

online appendix figure 1 Cumulative curves of sensitivity and specificity of scaffold/stent asymmetry index and receiver operating characteristic curves of scaffold/stent asymmetry index to predict device oriented cardiovascular endpoint. Panel A showed cumulative curves of sensitivity (Blue line) and specificity (Red line) of scaffold/stent asymmetry index. Panel B demonstrated ROC curves of scaffold/stent asymmetry index. Abbreviations: AI=asymmetry index; AUC=area under curve; CI=confident interval; EI=eccentricity index

Supplementary Table 1 Intravascular Ultrasound findings pre- and post-implantation according to symmetry of device post-implantation

	Symmetry	Asymmetry	p-value
	N=224, L=249	N=246, L=257	
Pre-procedure Intravascular Ultrasound			
Mean lumen area, mm^2	5.10±1.46	4.70±1.36	0.002
Minimal lumen area, mm^2	2.20±0.85	1.94±0.63	<0.001
Lumen eccentricity index	0.62±0.11	0.59±0.11	0.002
Asymmetry index	0.59±0.08	0.62±0.07	<0.001
Mean vessel area, mm^2	12.34±3.45	11.25±3.32	<0.001
Minimal vessel area, mm^2	9.68±3.27	8.13±2.87	<0.001
Presence of calcium, n(%)	159(66.3)	147(60.7)	0.21
Median sum arc of calcium	68.3(32.6-107.4)	71.6(43.6-113.9)	0.14
Total plaque area, mm^2	7.23±2.74	6.55±2.39	0.004
Remodeling index	0.93±0.18	0.91±0.21	0.35
Negative remodeling, n(%)	108(44.8)	101(41.7)	0.49
Post-procedure Intravascular Ultrasound			
Reference lumen area	7.05±2.10	6.29±1.90	<0.001
Minimal vessel area, mm^2	11.86±3.41	10.03±3.18	<0.001
Mean vessel area, mm^2	14.22±3.58	12.79±3.44	<0.001
Minimal scaffold/stent area, mm^2	5.73±1.44	4.61±1.29	<0.001
Mean scaffold/stent area, mm^2	6.63±1.53	5.94±1.43	<0.001
Mean ISA distance, mm	0.42±0.30	0.39±0.38	0.76
ISA area, mm^2	0.03±0.13	0.03±0.21	0.86
Expansion index (n=391)	0.75±0.13	0.69±0.16	<0.001
Optimal scaffold/stent expansion*, n(%)	31(14.6)	21(9.9)	0.13
Ratio of MSA to expected nominal scaffold/ stent area	0.78±0.16	0.64±0.14	<0.001
Scaffold/stent asymmetry index	0.24±0.04	0.37±0.05	<0.001
Scaffold/stent minimal eccentricity index	0.81±0.04	0.72±0.07	<0.001
Device eccentricity after implantation† n(%)	0(0)	98(38.1)	<0.001
Δ pre- vs. post-procedure AI	0.35±0.09	0.25±0.08	<0.001
Δ pre- vs. post-procedure EI	-0.19±0.12	-0.13±0.12	<0.001

Data are shown in n(%) or mean±SD or median (IQR 1st – 3rd). †available in 391 patients *Optimal stent/ scaffold expansion (OSE) was defined as MSA ≥ 90% of the average RLA or ≥ 100% of lumen area of the reference segment with the lowest lumen area. If MSA ≥ 9 mm2, OSE was defined as MSA ≥ 80% of the average RLA. † A lesion was characterized as asymmetric when the value of AI was over 0.3.† A lesion was characterized as eccentric when the value of EI was less than 0.7.

Abbreviation: EES:everolimus eluting stent; ISA: incomplete stent apposition; MSA:minimal stent/scaffold area; AI:asymmetry index; EI: eccentric index

Chapter 10

First-in-Man six-month results of a surface-modified Coronary Stent System in native coronary stenosis

Pannipa Suwannasom, Yohei Sotomi, Roberto Corti, David J. Kurz, Marco Roffi, Clemens von Birgelen, Stefano Buzzi, Arik Zucker, Jouke Dijkstra, Joanna J. Wykrzykowska, Robbert J. de Winter, Stephan Windecker, Yoshinobu Onuma, Patrick W. Serruys, Joost Daemen, Lorenz Räber

EuroIntervention 2017; 12(17):2118-2127

ABSTRACT

Aims

In pre-clinical studies, a bare metal cobalt-chromium stent with an active surface oxide layer modification (BMS_{mod}) has shown to effectively inhibited neointimal hyperplasia. We sought to assess both clinical safety and feasibility of the BMS_{mod}.

Methods and results

In this prospective, nonrandomized, first-in-man multicenter study, a total of 31 patients with de novo coronary lesions, reference lumen diameters of 2.5 - 3.5 mm and lesion length ≤16 mm were enrolled. Quantitative coronary angiography and optical coherence tomography(OCT) were performed at baseline and 6-month follow-up. Primary angiographic and OCT endpoints included in-stent late lumen loss (LLL) and mean neointimal thickness at 6 months, respectively. Device-oriented Composite Endpoint (DoCE) defined as cardiac death, myocardial infarction not clearly attributable to a non-intervention vessel, and clinically-indicated Target Lesion Revascularization[CI-TLR]) was analyzed according to the intention-to-treat principle.

In 31 patients (33 lesions), procedural success rate was 93.5%. At 6 months, angiographic LLL was 0.91±0.45 mm and binary angiographic restenosis occurred in 23.3% of lesions. Out of 33 lesions, OCT was performed in 27 lesions at both time points. Mean neointimal thickness amounted to 348±116 mm. At 6 months, the DoCE was 19.4% due to the occurrence of CI-TLR in 5 patients (including one late definite stent thrombosis of non-study stent).

Conclusion

In contrast to previous pre-clinical pathophysiological work, the BMS_{mod} did not prevent neointimal hyperplasia in a first-in-man clinical setting.

INTRODUCTION

Despite significant therapeutic successes achieved by the first-generation drug-eluting stent (DES) in reduction of restenosis and target vessel revascularization compared with bare metal stent (BMS), it has been shown that the first-generation DES was associated with an increase of very late stent thrombosis[1] and led to a mandatory of long-term dual antiplatelet therapy (DAPT)[2]. With regard to this concern, the second-generation DES has been developed and showed clinical advantage over first-generation DES, resulting in a 6-month duration of DAPT[3]. Nevertheless, the new BMS platform, with new designs, metal composition, thinner strut and surface modification also has been developed in parallel with the second-generation DES to actively inhibit neointimal hyperplasia and reduce clinical adverse event rates with short-term DAPT.

Qvanteq surface-modified coronary stent system is a Cobalt-Chromium(CoCr) BMS which underwent oxide surface layer modification (BMS_{mod}, Qvanteq AG, Zurich, Switzerland). The modification reduces nickel and cobalt concentrations in the surface oxide and simultaneously removes organic contamination, resulting in an ultra-hydrophilic surface that facilitates a fast endothelial growth[4]. It has been hypothesized that surface treatment may offer a safe and effective alternatives to DES with rapid healing and short duration of DAPT. In a porcine model with healthy coronary arteries, the BMS_{mod} demonstrated effective inhibition of neointimal formation[5].

The present first-in-man(FIM) study was designed to test the safety and feasibility of the BMS_{mod} for treating de novo coronary lesions.

METHODS

Patient population

The study enrolled 31 patients at six participating sites in Switzerland and Netherlands. A total of 31 patients over 18 years of age with stable or unstable angina (with stable haemodynamic condition) or silent ischemia with a single de novo target lesion of >50% diameter stenosis and <16 mm with a diameter 2.5-3.5 mm in one or two major epicardial arteries were included. Key exclusion criteria were: 1)evidence of ongoing acute myocardial infarction(MI) prior to the procedure; 2)stroke/transient ischemic attack in the past 6 months; 3)left ventricular ejection fraction <30%; 4)known hypersensitivity or contraindication to aspirin, heparin, clopidogrel or cobalt-chromium; 5)requirement for oral anticoagulation or prolonged need for DAPT; 6)other medical illness that may cause non-compliance with the protocol; 7)female of child bearing potential; 8)recipient of heart transplant. Angiographic exclusion criteria included: severe tortuous, calcified or angulated coronary anatomy of the study vessel; target lesion in left main stem;

involving a side branch >2.0 mm in diameter; aorto-ostial lesion; total occlusion; visible thrombus; restenotic lesion; arterial or saphenous vein graft lesions.

The study protocol was approved by all local institutional ethical committees and informed consent was obtained for every patient before any intervention was performed.

Device description

The BMS_{mod} is a CoCr stent that underwent surface treatment by modifying native oxide layer composition, as described elsewhere[4]. In vitro studies showed that treated surface reduce platelet adhesion while increase an adhesion of polymorphonuclear neutrophils[4]. The increase of neutrophils leads to the neutrophil-released protein "cathelicidin" which reduced neointimal formation[6]. Therefore, the BMS_{mod} is expected to have less thrombogenicity and in-stent restenosis[4,7]. The BMS_{mod} is a balloon expandable stent compatible to 6F guide catheter. The stent is arranged inside a container in an inert environment to protect its hydrophilic surface properties. It was mandatory to fill the guiding catheter with blood by back bleeding so that the stent's surface would be first in direct contact with blood.The balloon delivery system has two radiopaque markers to aid in the placement of the stent during fluoroscopy. The strut thickness is 80 μm for diameter 2.75 mm and 90 μm for diameter 3.00 mm.

Study procedure

Lesions were treated using standard interventional techniques with mandatory pre-dilatation prior to stent implantation. The following sizes of BMS_{mod} were used in the study: 15 mm and 20 mm length and either 2.75 and 3.00 mm diameter. The treating physicians performed the procedure using only angiographic guidance. OCT was performed after angiographic optimal stent placement and the physicians performing the procedure were blinded with respect to OCT images and results. Preprocedural antiplatelet therapy followed current guideline[8]. Post-procedure, patients were required to take clopidogrel 75 mg once daily for 1 month and aspirin 75-100 mg once daily indefinitely.

Angiographic and OCT evaluations were performed post-procedure and at 6 months. An independent Data Safety Monitoring Board monitored the individual and collective safety of the patients in the study on an ongoing basis.

Quantitative coronary analysis

Two-dimensional quantitative coronary analysis(QCA) was performed by an independent core lab (Cardialysis BV, Rotterdam, The Netherlands) with the CAAS system(CAAS 5.11; Pie Medical Imaging BV, Maastricht, The Netherlands).

OCT acquisition and analysis

OCT was performed using the three different frequency-domain OCT systems according to the availability at the participating sites (OPTIS™ integrated system; ILUMIEN™ OPTIS™ PCI Optimization™ System and Dragonfly™ Duo imaging catheter; C7-XR™ OCT Intravascular Imaging System and Dragonfly™ catheter; St. Jude Medical, St. Paul, MN, USA). All OCT images were analysed by an independent core laboratory (Cardialysis BV, Rotterdam, The Netherlands) with QIvus 2.2 software(Medis, Leiden, The Netherlands). Cross-sectional OCT images were analysed at 1 mm intervals.

OCT definition

A covered strut was defined as having neointimal thickness more than 0 μm[9]. Incomplete strut apposition(ISA) was defined as a clear separation between strut and vessel wall with a distance greater than the thickness of the strut. Healing Score(HS)[10] was calculated at every time-point as previously described in detail elsewhere. Stent expansion index was calculated by the ratio of minimum stent area(MSA) to the average reference lumen area(RLA). The optimal stent expansion(OSE) was defined according to criteria of the MUSIC study[11].

Evaluation degree of strut embedment and neointimal response

An exploratory analysis of strut embedment was performed using dedicated software(LKEB, Leiden University, the Netherlands) for quantification of the degree of strut embedment. The algorithm and reproducibility of the embedment software have been described elsewhere[12]. Briefly, the center of the reflective border of the metallic strut is detected automatically by the software. The abluminal side of the metallic struts is automatically drawn by simulating the virtual contour of the struts using the thickness of the strut indicated by the manufacturer. The degree of strut embedment is reported as "embedment depth". Embedment depth is the distance between the abluminal side and the embedment line measured along the line from the abluminal side through the lumen center. An example of the measurement of stent struts embedment are illustrated in figure 1.

Study endpoints

The primary angiographic endpoint was 6-month in-stent late lumen loss(LLL.) The primary OCT endpoint was 6-month mean neointimal thickness. The secondary clinical endpoints included Device-oriented Composite Endpoints(DoCE) (defined as Cardiac Death, MI not clearly attributable to a non-intervention vessel, and clinically-indicated target lesion revascularization[CI-TLR][13]) and its individual components of the composite end point, any revascularization at 6 and 12 months and stent thrombosis according to the academic research consortium(ARC) definitions[13] up to 12 months follow-up.

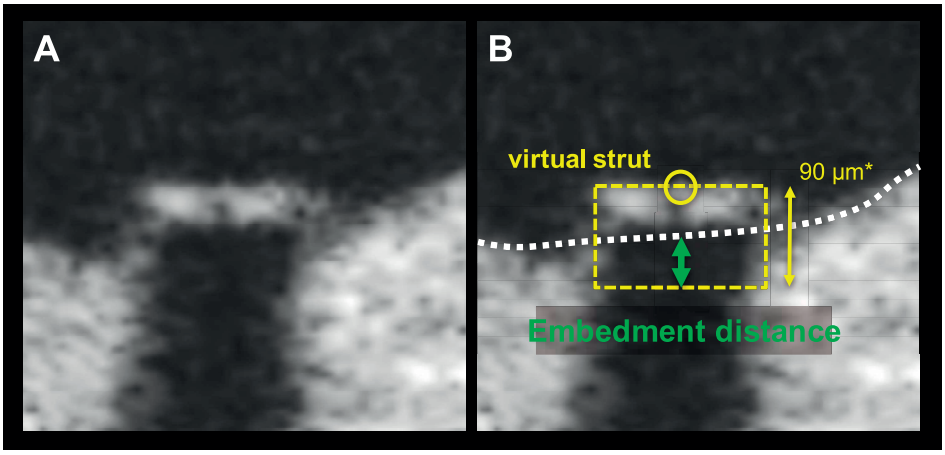

Figure 1. Method of the OCT embedment analysis
A strut example is illustrated without contour(A) and with contour(B). The dedicated software automatically creates the virtual struts (yellow dotted square) based on the strut thickness (BMS_{mod} 2.75 mm device = 80 µm; and *3.0 mm device = 90 µm) provided by the manufacturer. Embedment depth (green arrow) was computed using the interpolated lumen contour (white dotted line).

Periprocedural MI and spontaneous MI was defined by Third universal definition and WHO definition. Device success defined as DS <30% of the target site using the BMS_{mod}. The procedure success required DS <30%; no occurrence of DoCE during the hospital stay. All patients visited the outpatient clinic at 6 months. Telephone contacts were scheduled at 12 months.

Statistical analysis

Categorical variables were summarized with frequencies and percentages. The continuous variables were reported as mean ± standard deviation(SD) or median and interquartile ranges as appropriate. Wilcoxon Signed Ranks test was used to compare continuous variables between serial OCT and QCA data. The categorical variables were compared by Fisher's exact test. A two sided p-value <0.05 was considered statistically significant. The current study is a FIM and single-arm study, the sample size was not defined on the basis of an endpoint hypothesis but rather to provide some information about the device safety. The primary endpoint and all imaging-based findings were analysed based on the as-treated population. Clinical outcomes analyses were based on the intention-to-treat population.

The comparison between neointimal response(area, thickness, volume) and embedment depth was performed by dividing the analyzed cross-sections into 3 subsegments as: proximal, mid, and distal. The correlation between embedment depth and neointimal component was compared by using subsegment level. The statistical analysis was performed by SPSS version 23.0(IBM corp, Armonk, New York).

RESULTS

Baseline clinical characteristics

Thirty-one patients were included between October 2014 and August 2015. The baseline clinical characteristics are presented in Table 1. Procedure success was 93.5%(29/31) and device success was 93.9%(31/33) of the lesions because two study stents could not cross the lesions. There were 3 study stent dislodgements due to the larger profile of the study device (6F guide catheter compatibility) as compared to currently used lower profile devices (5F guide catheter compatibility) in today's clinical practice: the first stent got dislodged from the balloon during the use of a "mother-and-child" configuration (5Fr). A non-study stent(Promus Premier™; Boston Scientific, Marlborough, MA, USA) was subsequently implanted. In the second case, the stent dislodgement occurred in the Y-connector outside the patient when the investigator attempted to implant a study stent in the mid RCA. A non-study stent(Xience Prime™; Abbott Vascular, Santa Clara, CA, USA) was implanted. The last stent dislodgement occurred because the mandatory pre-dilatation of the lesion was omitted and the study stent device profile(1.6 mm) was too large for crossing the lesion(MLD 0.84 mm). The stent got dislodged while the operator retrieved it back into the guide catheter. Subsequently, pre-dilatation was performed and another study stent was successfully implanted in the index lesion.

Table 1 Baseline Characteristics

	N=31
Age (years)	63.1±9.5
Men,n(%)	21(67.7)
Current smokers,n(%)	8(25.8)
Diabetes,n(%)	3(9.7)
Hypertension,n(%)	13(41.9)
Hyperlipidemia,n(%)	20(64.5)
Family history of CAD,n(%)	11(35.5)
Previous PCI,n(%)	3(9.7)
Previous myocardial infarction,n(%)	4(12.9)
Stable angina,n(%)	22(71.0)
Silent ischemia,n(%)	4(12.9)

Abbreviation: CAD coronary artery disease; CABG: coronary artery bypass graft; PCI: percutaneous coronary intervention.

Angiographic and procedural characteristics

Baseline angiographic characteristics are depicted in table 2. Angiographic follow-up at 6 months was achieved in 28 patients(30 lesions)(Figure 2). Serial angiographic analyses

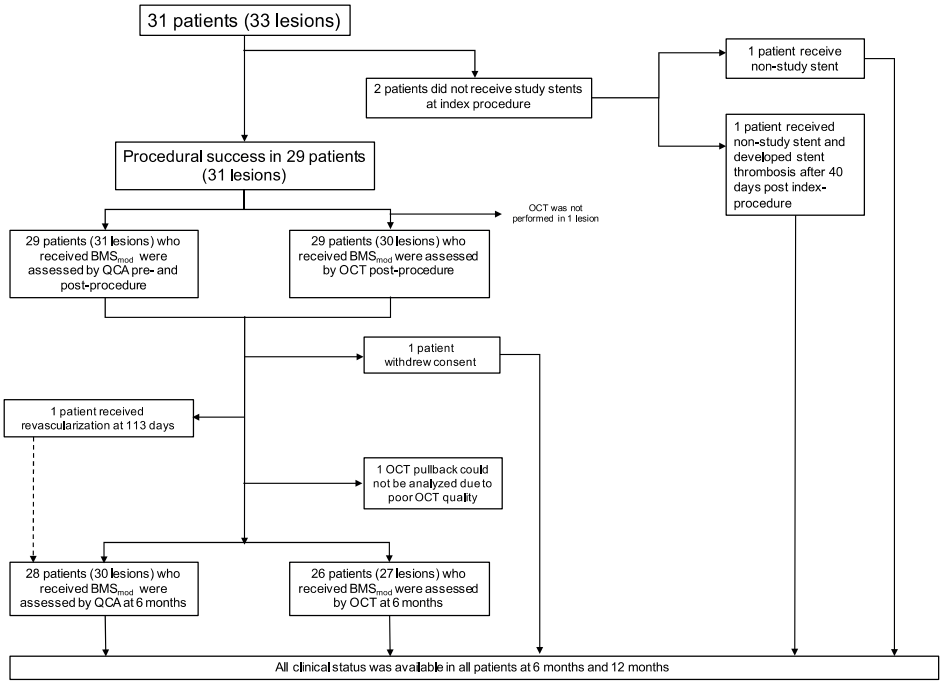

Figure 2. Study flow chart

at baseline, post-procedure, and 6-month follow-up (n = 30 lesions) are presented in Table 3. At 6 months, the mean in-stent late loss, in-stent percentage diameter stenosis, and the frequency of binary angiographic restenosis were 0.91±0.45 mm, 36.0±18.1%, and 23.3%, respectively. Figure 3 demonstrates the cumulative frequency of MLDs immediately after the index procedure, at 6-month follow-up and in-stent LLL.

OCT findings at baseline and at 6 months

At 6 months, OCT evaluation was performed in 26 patients(27 lesions). The results of paired OCT at baseline and 6-month follow-up are tabulated in Table 4. The 6-month mean neointimal thickness was 348±116μm with %NVO of 39.4±14.4%. The percentage of covered struts was 99.5±1.5% with a healing score of 4.3±13.9. ISA at baseline was reported in 13.9±11.8% of the analyzed struts, and that percentage was reduced to 0.3±1.0% at 6 months. There was no late acquired incomplete apposition.

Correlation of neointimal response to the embedment depth

The mean strut embedment depth was 70.4±28.4μm after stent implantation. The embedment depth was deepest in the middle segment, followed by proximal and distal

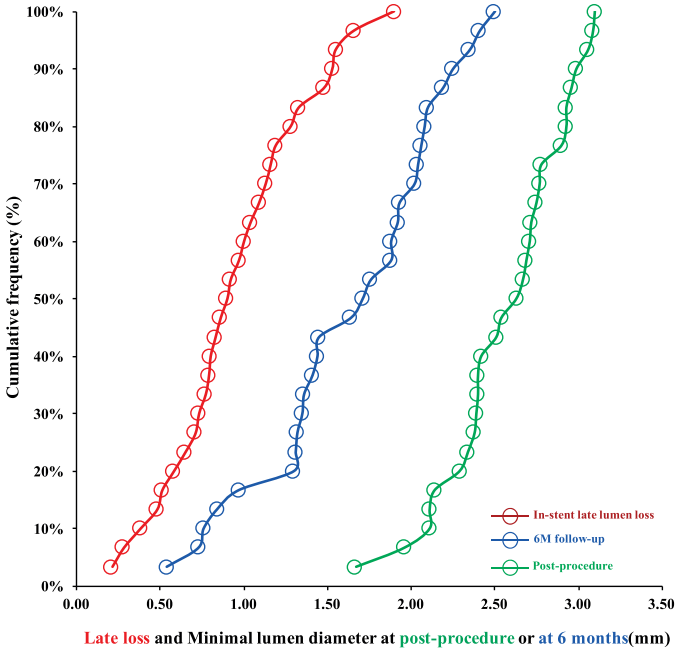

Figure 3. Cumulative frequency distribution curves of minimal luminal diameter at post-procedure (green line), at 6 months follow-up (blue line) and in-stent late lumen loss at 6 months (red line).

segment, respectively (Table 5). The neointimal thickness, neointimal area and neointimal volume were also numerically highest in the middle segment, however, there were no statistically significant differences between the proximal and distal segment. There was a moderate positive correlation between neointimal area, thickness and neointimal volume and embedment depth: r=0.320, p=0.005, r=0.424, p<0.001 and r=0.374, p=0.001, respectively (Figure 4 and Figure 5).

Device-oriented Composite Endpoints (DoCE)

Clinical data was available up to 12 months in all patients. Individual clinical endpoints are listed in Table 6. One periprocedural MI occurred (cTn 29.57xULN, CK-MB 6.43xULN with symptom). One patient experienced a definite late stent thrombosis of non-study stent at 40 days after index procedure. There were 5 cases of CI-TLR (including 1 case with definite stent thrombosis in a non-study stent). In total, DoCE rate at 6 months is 19.4% (6/31). Including only patients in which the device was implanted successfully, the DoCE rate at 6 months was 17.2% (5/29). No additional DoCE occurred between 7 months and 12 months.

Table 2 Baseline Angiographic Characteristics

	N=33
Target vessel	
Left anterior descending,n(%)	18(54.5)
Left circumflex artery,n(%)	9(27.3)
Right coronary artery,n(%)	6(18.2)
AHA/ACC lesion classification	
A/B1,n(%)	16(48.5)
B2,n(%)	17(51.5)
Moderate to heavy calcification,n(%)	7(21.2)
Obstruction length(mm)	12.19±3.75
Reference lumen diameter(mm)	2.83±0.47
Minimal lumen diameter(mm)	1.01±0.34
Mean lumen diameter(mm)	2.46±0.39
Diameter stenosis(%)	63.5±12.7
Pre-dilatation, n(%)	29(87.9)
pre-dilation balloon length(mm)	13.4±2.1
Total length of implanted stents(mm)	20.2±7.1
Mean nominal device diameter(mm)	2.9±0.1
Overlapping stents,n(%)	4(12.1)
Bailed-out stent,n(%)	3(9.1)
Post-dilation,n(%)	25(75.8)
Nominal post-dilation balloon diameter(mm)	3.4±0.5
Post-dilation balloon length(mm)	12.5±2.8
Balloon-artery ratio*	1.15±0.09
Acute success	
Device success,n(%)	31(93.9)
Procedure success,n(%)	29(93.5)

Abbreviation: AHA/ACC: American heart association/ American college of cardiology. *Balloon-artery ratio was calculated by nominal device or post-dilation balloon diameter at nominal pressure divided by interpolated reference lumen diameter post-procedure.

DISCUSSION

The main findings of this first-in-man study are the following; 1) while the surface technology itself appeared to be safe in the context of the present study, the BMS_{mod} was associated with in-stent angiographic late loss of 0.91 mm and 6-month binary restenosis rate of 23.3%; 2) the endothelialization of BMS_{mod} was almost complete at 6

Table 3 Quantitative Coronary Angiography at pre-procedure, post-procedure and 6-month in 30 paired lesions

	Pre-procedure	Post-procedure	6-month follow-up	p-value
	N=30	N=30	N=30	
Reference lumen diameter(mm)	2.85±0.48	2.90±0.42	2.58±0.49	<0.001
Minimal lumen diameter(mm)	1.03±0.34	2.58±0.36	1.65±0.53	<0.001
Diameter stenosis(%)	63.1±13.0	11.2±5.3	36.0±18.1	<0.001
Acute gain(mm)		1.56±0.47		
Late loss(mm)			0.91±0.45	
Binary restenosis(%)			7(23.3)	

months(percent covered strut 99.5%); 3) the 6-month mean neointimal thickness was 348±116 μm with %NVO of 39.4±14.4%.

The present study showed that the neointimal hyperplasia in the BMS_{mod} was not substantially reduced as compared to the expected LLL in currently used BMS[14](BMS_{mod} 0.91±0.45 mm, MULTI-LINK VISIONâ 0.87±0.37 mm). The same observation was also made in the OCT analysis; %NVO of the BMS_{mod} was comparable to the MULTI-LINK VISION® [Abbott Vascular](BMS_{mod} 39.4±14.4% vs. MULTI-LINK VISION 28.1±14.0%)[14].

The impact of surface modification to the neointimal response.

Recently, BMS_{mod} showed promising results in inhibiting neointimal proliferation in rabbit and swine models compared to untreated surface BMS and DES[5] , whereas BMS_{mod} efficacy in the current FIM study showed comparable results with current generation BMS.

Although the balloon-to-artery ratio was comparable between the previous animal models and the present FIM trial (1.14±0.05 vs. 1.15±0.09), the balloon-artery ratio at the MLA site would be greater than any other area in the vessel. Consequently, a huge stretch at the MLA site by the balloon could contribute to severe injury to the vessel wall. On the contrary, the balloon-to-artery ratio in the animal model was homogeneous throughout the stent length since there was no pathological stenosis. Therefore, the anti-restenotic property of the BMS_{mod} could not be adequately tested at 30 days in porcine model.

Vessel injury after implantation and neointimal response

Previously, Schwartz et al, reported that the mean histologic injury score significantly correlated with histologic neointimal thickness, percent area stenosis post-procedure and neointimal area; r= 0.80, p<0.001; r=0.74, p<0.001 and r=0.46, p=0.02, respectively[15]. However, the correlation of the neointimal response and the embedment depth in the present study was not as strong as in the histological assessment. Part of the

Table 4 OCT measurements in matched pairs at post-procedural and 6 months follow-up (n= 27 paired lesions)

	Baseline	6-months	p-value
	N=27	N=27	
Strut level analysis			
Total analyzed struts,n	6047	5883	
Number of struts per cross-section,n	11.6	11.5	
Percentage of covered struts		99.5±1.5	
Mean neointimal thickness,μm		348±116	
Maximal neointimal thickness,μm		800±212	
Number of malapposed struts,n	211	6	
Percentage of malapposed struts	13.9±11.8	0.3±1.0	<0.001
Cross-section level analysis			
Number of cross-sections per lesions,n	19.7±5.3	19.3±5.2	
Mean reference lumen area,mm^2	7.49±2.28	5.73±2.18	<0.001
Minimum lumen area,mm^2	6.36±1.51	3.22±1.64	<0.001
Mean lumen area,mm^2	7.73±1.83	4.64±2.03	<0.001
Minimum stent area,mm^2	6.49±1.59	6.29±1.82	0.23
Mean stent area,mm^2	7.59±1.72	7.35±2.07	0.07
Prolapse area or Neointimal area,mm^2	0.19±0.14	2.73±0.91	<0.001
Mean incomplete strut apposition area,mm^2	0.28±0.31	0.02±0.07	<0.001
Lesion-level analysis			
Neointimal or prolapse volume,mm^3	2.4±2.0	49.6±20.8	<0.001
Stent volume,mm^3	140.4±57.1	134.0±57.8	0.06
Lumen volume,mm^3	142.8±61.5	84.8±49.9	<0.001
Percentage of neointimal volume obstruction, %	1.6±0.9	39.4±14.4	<0.001
Asymmetry index	0.27±0.06	0.22±0.07	<0.001
Mean lumen eccentricity index	0.86±0.03	0.84±0.04	0.03
Stent expansion index*	0.88±0.15		
Optimal stent expansion,n(%)	13(52.0)		

*available in 25 lesions.

discrepancy might be explained by the different properties of diseased human coronary artery tissue as compared to healthy porcine models[16] and limitation of OCT resolution to detect media disruption.

Translation pre-clinical study to the first-in-man trial

Theoretically, the objectives of a FIM stent trial are to ascertain safety and feasibility but not mandatorily to address the question of efficacy of the device. There is a heavy ethical responsibility involved in FIM trials. In converting the pre-clinical result into therapeutic

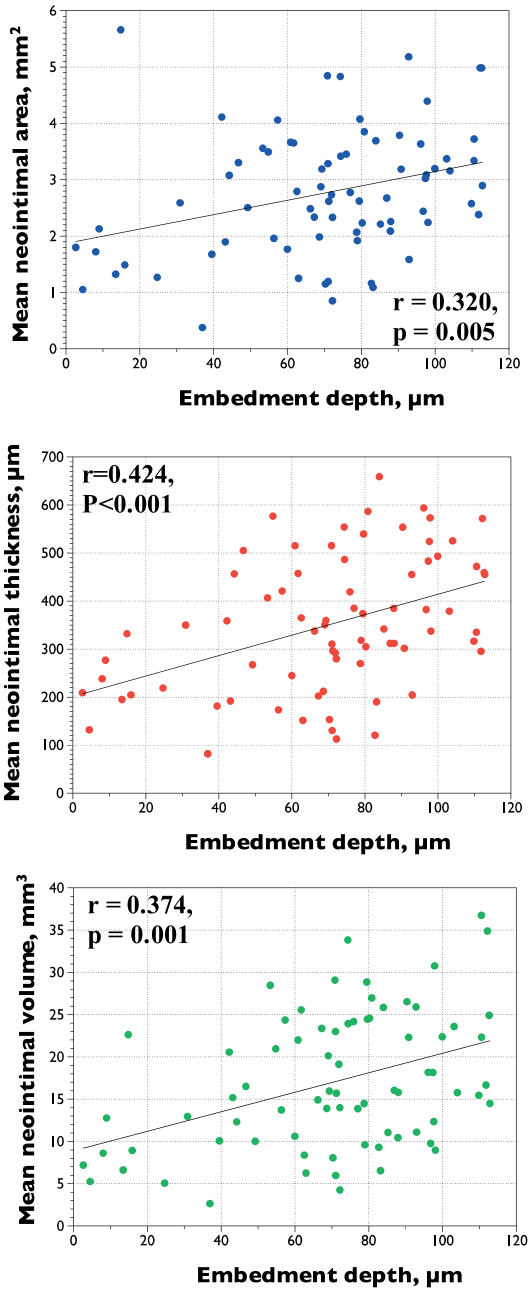

Figure 4. Correlation between the degree of strut embedment and neointimal response. Correlation between degree of strut embedment to mean neointimal area (panelA), neointimal thickness (panel B), and neointimal volume (panel C).

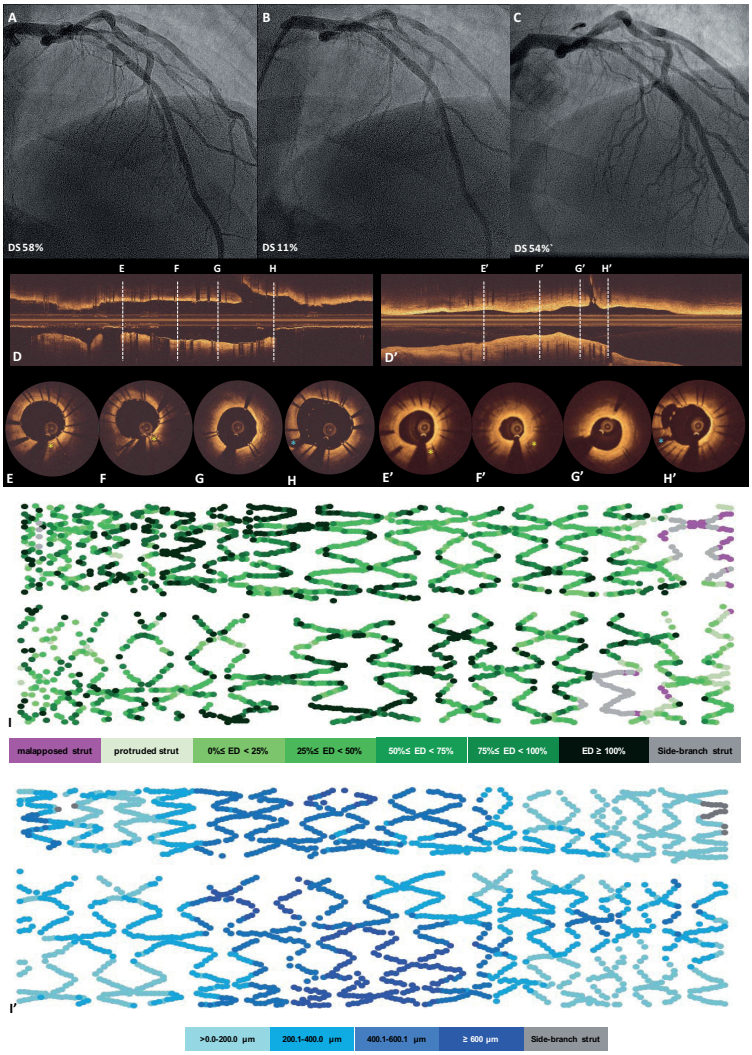

Figure 5. Case examples of embedment analysis at baseline and neointimal thickness at 6 months follow-up.

A patient received BMS_{mod} 3.0x20 mm in proximal left anterior ascending artery. Panel A, B and C demonstrated angiography pre-, post-procedure and at 6 months, respectively. The 6-month angiographic late loss was 1.28 mm. Optical coherence tomographic (OCT) imaging (longitudinal view: D, cross-sections: E–H) showed embedded (E-G), buried struts (F) and malapposed struts (H) at baseline. The yellow stars indicate calcific plaque, blue star indicates side-branch, both of them were used as anatomical landmarks for matching OCT images between baseline and 6-month follow-up. The corresponding longitudinal view and cross-section at 6-month follow-up show in panel D′ and E′- H′, respectively. Panel F′ showed minimal lumen area at 6-month follow-up was 2.48 mm^2. The OCT foldout view in panel I depicted the distribution of malapposed struts and embedment depth of each strut colour coded in pink and green, respectively. The healing score of the case at baseline was 234.9 and decreased to 11.54 at 6 months. The OCT foldout view in panel I′ depicted the distribution of the neointimal thickness of each strut, colour coded in blue shades.

Table 5 OCT measurement in subsegmental analysis (n=81 segments)

	In-stent segment	Proximal	Mid	Distal	p-value*
Mean embedment depth,μm	70.4±28.4	60.3±29.3	85.4±24.4	65.4±25.9	0.001 †,††
Mean neointimal area,mm^2	2.77±1.10	2.80±1.27	3.04±1.14	2.45±0.80	0.08
Mean neointimal thickness,μm	348±116	332±137	399±146	313±119	0.11
Mean neointimal volume,mm^3	17.3±7.9	16.70±8.2	19.7±8.7	15.4±6.3	0.15

*Comparison among subsegment (proximal, mid and distal) was performed by Kruskal-Wallis test. † Significant difference was found between mid and proximal segment, p =0.001; ††mid and distal segment, p=0.003, however, there was no significant difference between proximal and distal segment, p=0.547.

Table 6 Adverse cardiac events at 6 months and between 7-12 months

Event	At 6 months N=31	Between 7-12 months N=31
Cardiac death	0	0
Myocardial infarction		
Target vessel	1(3.2)	0
Non-target vessel	1(3.2)	0
Periprocedural MI	1(3.2)	0
Repeat PCI–ID-TLR	5*(16.1)	0
Device-oriented Composite Endpoints:DoCE (Cardiac Death, MI not clearly attributable to a non-intervention vessel, and ID-TLR)	6(19.4)	0
Repeat PCI–non-ID-TLR	1(3.2)	0
Repeat PCI–TVR	1(3.2)	0
Repeat PCI– non TVR	2(6.5)	2(6.5)
Patient-oriented Composite Endpoints :PoCE (All death, all MI and all revascularization)	10(32.2)	2(6.5)
CABG	0	0
Definite stent thrombosis (non-study stent)	1(3.2)	0

Data presented as n(%) and intention to treat analysis. *included case definite stent thrombosis of a non-study stent.

applications, it has been our experiences that stent treatment in healthy coronary arteries of juvenile growing animals (mainly pig) is frequently misleading and testing only the compatibility of the device with the biological environment without testing per se the anti-restenotic property of the device[17, 18]. In order to test the anti-restenotic properties, a certain level of injury should be induced and quantified by imaging to establish the relationship observed between vessel injury and neointimal hyperplasia[15]. Additionally, this type of pre-clinical work should be performed in mature animals that are not going to grow excessively at follow-up (e.g mini Yucatan swine) and the investigation should induce a quantified level of device injury [18].

Study limitations

The following limitations should be acknowledged 1) based on the characteristics of this FIM study, the study population was not large enough to fully address the question of efficacy; 2) based on an interim analysis and consideration of the 3 stent dislodgments, recruitment was stopped after 31 patients, instead after the planned 35 patients. The procedural success rate of the device in its current version was suboptimal warranting further refinement. Device dislodgements may be explained by the 6F compatibility profile of the study device that was larger than most stent platforms currently used in clinical practice together with a wrong device handling as described above. Thus, development of novel platforms should not target only inhibition of neointimal hyperplasia but the profile of the device on the delivery system should also be taken into account for deliverability, pushability and retention; 3) The OSE criteria are derived from IVUS criteria in MUSIC study, although OCT was used in the current study. A reported discrepancy between OCT and IVUS measurements could influence the assessment of OSE criteria[19]. However, the influence seems to be minimal since the stent expansion was assessed as a ratio of MSA to RLA, not as absolute values.

CONCLUSIONS

Despite the conceptual advantages of surface modification and effective inhibition of neointimal growth in animal models, this FIM study showed that the biocompatibility-focused surface modification is not sufficient to reduce the neointimal growth resulting from the overstretching dilatation of human coronary atherosclerotic narrowing. However, the observed efficacy was comparable with current generation BMS. Pre-clinical study with new stent platforms should induce a certain level of injury that would mimic the barotrauma in human atherosclerotic stenosis.

Impact on daily practice

Surface modification technology has demonstrated an effective inhibition of neointimal growth and rapid healing in preclinical studies. It has been speculated that such technology may offer alternatives to DES when short dual antiplatelet therapy is mandatory. This FIM study showed that the surface modification is not sufficient to reduce the neointimal growth in diseased human coronary arteries. Considering the recently well proven efficacy and safety of the drug-coated stents versus BMS in high bleeding risk patients, DES will remain in our armamentarium in the future unless new BMS platforms demonstrate a comparable antirestenotic capability to DES. In converting the future preclinical results of any new BMS plat-

forms into therapeutic applications, such devices should be tested for biocompatibility and antirestenotic properties by induction of a quantified level of device injury.

REFERENCE

1. Tada T,Byrne RA,Simunovic I,King LA,Cassese S, Joner M,Fusaro M,Schneider S, Schulz S,Ibrahim T,Ott I,Massberg S, Laugwitz K-L and Kastrati A. Risk of Stent Thrombosis Among Bare-Metal Stents, First-Generation Drug-Eluting Stents, and Second-Generation Drug-Eluting Stents: Results From a Registry of 18,334 Patients. JACC: Cardiovascular Interventions. 2013;6:1267-1274.
2. O'Gara PT,Kushner FG,Ascheim DD,Casey DE, Jr.,Chung MK,de Lemos JA,Ettinger SM,Fang JC,Fesmire FM, Franklin BA,Granger CB, Krumholz HM, Linderbaum JA, Morrow DA,Newby LK, Ornato JP, Ou N,Radford MJ,Tamis-Holland JE, Tommaso CL, Tracy CM, Woo YJ,Zhao DX,Anderson JL,Jacobs AK, Halperin JL,Albert NM, Brindis RG, Creager MA, DeMets D,Guyton RA,Hochman JS, Kovacs RJ,Kushner FG, Ohman EM, Stevenson WG and Yancy CW. 2013 ACCF/AHA guideline for the management of ST-elevation myocardial infarction Journal of the American College of Cardiology. 2013;61:485-510.
3. Levine GN,Bates ER, Bittl JA,Brindis RG, Fihn SD,Fleisher LA,Granger CB,Lange RA, Mack MJ,Mauri L,Mehran R, Mukherjee D,Newby LK,O'Gara PT,Sabatine MS, Smith PK and Smith SC, Jr. 2016 ACC/AHA Guideline Focused Update on Duration of Dual Antiplatelet Therapy in Patients With Coronary Artery Disease Journal of the American College of Cardiology. 2016;68:1082-115.
4. Milleret V,Ziogas A,Buzzi S,Heuberger R,Zucker A and Ehrbar M. Effect of oxide layer modification of CoCr stent alloys on blood activation and endothelial behavior. Journal of biomedical materials research Part B, Applied biomaterials. 2015;103:629-40.
5. Kolandaivelu K,Bailey L,Buzzi S,Zucker A,Milleret V,Ziogas A,Ehrbar M,Khattab AA, Stanley JR,Wong GK,Zani B, Markham PM,Tzafriri AR,Bhatt DL,Edelman ER. Ultra-Hydrophilic Stent Platforms Promote Early Vascular Healing and Minimize Late Tissue Response - A Potential Alternative to Second-Generation Drug Eluting Stents. Eurointervention. 2016 [Epub ahead of print]
6. Soehnlein O,Wantha S,Simsekyilmaz S,Doring Y,Megens RT,Mause SF,Drechsler M, Smeets R,Weinandy S,Schreiber F,Gries T,Jockenhoevel S,Moller M,Vijayan S,van Zandvoort MA,Agerberth B,Pham CT,Gallo RL,Hackeng TM,Liehn EA,Zernecke A,Klee D and Weber C. Neutrophil-derived cathelicidin protects from neointimal hyperplasia. Science translational medicine. 2011;3:103ra98.
7. Nazneen F,Herzog G,Arrigan DW,Caplice N,Benvenuto P,Galvin P and Thompson M. Surface chemical and physical modification in stent technology for the treatment of coronary artery disease. Journal of biomedical materials research Part B, Applied biomaterials. 2012;100:1989-2014.
8. Windecker S,Kolh P,Alfonso F,Collet JP,Cremer J,Falk V,Filippatos G,Hamm C,Head SJ, Juni P,Kappetein AP,Kastrati A,Knuuti J,Landmesser U,Laufer G,Neumann FJ,Richter DJ, Schauerte P,Sousa Uva M,Stefanini GG,Taggart DP,Torracca L,Valgimigli M,Wijns W and Witkowski A. 2014 ESC/EACTS Guidelines on myocardial revascularization European heart journal. 2014;35:2541-619.
9. Takano M,Inami S,Jang IK,Yamamoto M,Murakami D,Seimiya K,Ohba T and Mizuno K. Evaluation by optical coherence tomography of neointimal coverage of sirolimus-eluting stent three months after implantation. The American journal of cardiology. 2007;99:1033-8.
10. Raber L,Onuma Y,Brugaletta S,Garcia-Garcia HM,Backx B,Iniguez A,Jensen LO, Cequier-Fillat A,Pilgrim T,Christiansen EH,Hofma SH,Suttorp M,Serruys PW,Sabate M and Windecker S. Arterial healing following primary PCI using the Absorb everolimus-eluting bioresorbable vascular scaffold (Absorb BVS) versus the durable polymer everolimus-eluting metallic stent (XIENCE) in patients with acute ST-elevation myocardial infarction: rationale and design of the randomised TROFI II study. EuroIntervention 2015; [Epub ahead of print]

11. de Jaegere P,Mudra H,Figulla H,Almagor Y,Doucet S,Penn I,Colombo A,Hamm C, Bartorelli A,Rothman M,Nobuyoshi M,Yamaguchi T,Voudris V,DiMario C,Makovski S, Hausmann D,Rowe S,Rabinovich S, Sunamura M and van Es GA. Intravascular ultrasound-guided optimized stent deployment. Immediate and 6 months clinical and angiographic results from the Multicenter Ultrasound Stenting in Coronaries Study (MUSIC Study). European heart journal. 1998;19:1214-23.
12. Sotomi Y,Tateishi H,Suwannasom P,Dijkstra J,Eggermont J,Liu S,Tenekecioglu E, Zheng Y,Abdelghani M,Cavalcante R,de Winter RJ,Wykrzykowska JJ,Onuma Y,Serruys PW and Kimura T. Quantitative assessment of the stent/scaffold strut embedment analysis by optical coherence tomography. Int J Cardiovasc Imaging. 2016.
13. Cutlip DE,Windecker S,Mehran R,Boam A,Cohen DJ, van Es G-A,Gabriel Steg P, Morel M-a, Mauri L,Vranckx P,McFadden E,Lansky A,Hamon M, Krucoff MW, Serruys PW and Consortium obotAR. Clinical End Points in Coronary Stent Trials: A Case for Standardized Definitions. Circulation. 2007;115:2344-2351.
14. Serruys PW,Ong AT,Piek JJ,Neumann FJ,van der Giessen WJ,Wiemer M,Zeiher A, Grube E,Haase J,Thuesen L,Hamm C and Otto-Terlouw PC. A randomized comparison of a durable polymer Everolimus-eluting stent with a bare metal coronary stent: The SPIRIT first trial. EuroIntervention. 2005;1:58-65.
15. Schwartz RS,Huber KC,Murphy JG,Edwards WD,Camrud AR,Vlietstra RE and Holmes DR. Restenosis and the proportional neointimal response to coronary artery injury: results in a porcine model. Journal of the American College of Cardiology. 1992;19:267-74.
16. Hoffmann R,Mintz GS,Mehran R,Kent KM,Pichard AD,Satler LF and Leon MB. Tissue proliferation within and surrounding Palmaz-Schatz stents is dependent on the aggressiveness of stent implantation technique. The American journal of cardiology. 1999;83:1170-4.
17. van Beusekom H,Sorop O,Weymaere M,Duncker D and van der Giessen W. The neointimal response to stents eluting tacrolimus from a degradable coating depends on the balance between polymer degradation and drug release. EuroIntervention 2008;4:139-47.
18. Onuma Y,Serruys P,den Heijer P,Joesoef KS,Duckers H,Regar E,Kukreja N,Tanimoto S, Garcia-Garcia HM,van Beusekom H,van der Giessen W and Nishide T. MAHOROBA, first-in-man study: 6-month results of a biodegradable polymer sustained release tacrolimus-eluting stent in de novo coronary stenoses. European heart journal. 2009;30:1477-85.
19. Okamura T,Onuma Y,García-García HM,van Geuns R-JM,Wykrzykowska JJ,Schultz CJ, van der Giessen W,Ligthart JMR,Regar E and Serruys PW. First-in-man evaluation of intravascular optical frequency domain imaging (OFDI) of Terumo: a comparison with intravascular ultrasound and quantitative coronary angiography. EuroIntervention. 2011;6:1037-1045.

Chapter 11

Evaluation of vascular healing of polymer-free sirolimus-eluting stents in native coronary artery stenosis: a serial follow-up at three and six months with optical coherence tomography imaging

Pannipa Suwannasom, Yoshinobu Onuma, Edouard Benit, Olivier Gach, Clemens von Birgelen, Sjoerd H. Hofma, Yohei Sotomi, Xu Bo, Yao-Jun Zhang, Runlin Gao, Hector M. García-García, Joanna J. Wykrzykowska, Robbert J. de Winter, Patrick W. Serruys

Eurointervention 2016;12:e574-e583

ABSTRACT

Aim

Our aim was to assess vascular response after polymer-free sirolimus-eluting stent (SES) implantation by using an optical coherence tomography (OCT)-derived vascular Healing Score (HS), quantifying the deficiency of healing.

Methods and result

In a prospective, multicenter, single arm, open-label study, OCT examinations were performed at three months in 45 patients (47 lesions). Per protocol, 24 lesions that had not reached adequate vascular healing according to study criteria were scheduled for OCT examination at six months. The HS was calculated at two time points. Serial OCT imaging demonstrated that the proportion of covered stent struts increased from a median of 87.1% at three months to 98.6% at six months ($p<0.0001$). The neointimal thickness increased from a median of 82.8 μm to 112.2 μm ($p<0.0001$), whereas the median percentages of malapposed struts were 0.2% and 0.0% at the two respective time points. Neointimal volume obstruction increased from 6.3% to 12.8%, and the HS decreased from a median of 28.1 at three months to 2.4 at six months.

Conclusion

In patients who had inadequate vascular healing three months after polymer-free SES implantation, serial OCT showed almost complete vascular healing at six months.

(ClinicalTrials.gov Identifier: NCT01925027)

INTRODUCTION

Optical coherence tomography (OCT) has provided excellent imaging resolution of implanted devices and coronary arteries. At follow-up, OCT sheds light on the vascular healing process for the various coronary stent platforms.[1-3] Post-mortem data, demonstrating the relationship between uncovered stent strut and stent thrombosis has been reported.[4] The impact of permanent polymer drug-eluting stent (DES) on long-term complications (late and very late stent thrombosis) from delayed vascular healing has been well described in the literature.[5,6] Consequently, intensive clinical research has focused on the potential relationship between OCT findings (uncovered strut and stent malapposition) and clinical outcomes.

Complications created by the polymer have motivated researchers to design new coronary stent platforms without polymer coating. To evaluate the status of vascular healing systematically, the Healing Score (HS) has been introduced in clinical research.[7,8] The advantage of the HS is that it permits a relative assessment of the speed and degree of vascular "healing" in patients treated with different types of stents and at different points in time. The Nano Plus stent polymer-free stent (Lepu Medical, Beijing, China), is a polymer-free sirolimus eluting stent (SES) elutes sirolimus the drug from a reservoir made of abluminal nanomeric cavities, aiming at minimizing long-term complication that have been related to the polymer coating. Prior OCT examinations 3 months after Nano Plus implantation in 47 lesions showed that the strut coverage rate was 93.0%.[9]

The aim of our present study was to provide mechanistic insights into the vascular healing process after implantation of polymer-free SES, as assessed into the vascular healing process by serial assessment of lesions with OCT that were treated with polymer-free SES at 3 and 6 months.

METHODS

Patient population

The NANO Plus OCT study is a prospective, multicenter, single arm, open-label study, in coronary artery disease patients. The inclusion criteria and exclusion criteria have previously been described.[9] Briefly, inclusion criteria are; 1) stable angina or silent ischemia demonstrated by positive functional study with a *de novo* target lesion of >50% diameter stenosis (%DS); 2) planned intervention up to two *de novo* lesions in different epicardial vessels; 3) lesion length of less than 18 mm; 4) native coronary artery of 2.5-4.0 mm in diameter. All patients had OCT assessment scheduled at 3 months follow-up. Whenever the pre-specified criteria were not fulfilled on 3-month OCT imaging, the patients were scheduled for additional OCT assessment at 6 months. For the purpose of the study that

aimed at assessing vascular healing serially at 3 months and 6 months, the data was exclusively reported in lesions that had OCT assessment in both time points. The study protocol was approved by all institutional ethics committees and informed consent was obtained for every patient before any intervention was performed.

Device description

The Nano Plus stent is a drug-eluting stainless steel stent with a strut thickness of 91µm. A large number of pores with a diameter of 400 nm are present on the abluminal stent surface. The device releases sirolimus from the abluminal pores directly (i.e. without using any of a polymer coating) into the vessel wall; a total of 85% of the drug is released within 30 days.

OCT acquisition and analysis

The details of OCT acquisition have been previously described.[9] All OCT images were analyzed at an independent core laboratory (Cardialysis BV, Rotterdam, the Netherlands) with QIvus 2.2 software (Medis, Leiden University, Leiden, the Netherlands). The stent and lumen areas were semi-automatically traced at 1 mm intervals.

At 3-month follow-up, all lesions were evaluated by pre-specified OCT criteria, derived from the literature.[4,7,10,11] These criteria were: (i) percentage of covered struts >90%; (ii) no frame with a ratio of uncovered to total stent struts (RUTTS) of >30%; (iii) incomplete stent apposition area (ISA) ≤ 2 mm^2; (iv) intraluminal defect area (ILD) < 300 μm^2. If they were not fulfilled, the patients were scheduled for additional OCT assessment at 6 months. A covered strut was defined as having neointimal thickness >0 µm.[8,12] A ratio of uncovered to total stent struts (RUTTS) was calculated in every cross-section from number of uncovered struts divided by total number of struts.[4] Incomplete strut apposition was defined as a separation between strut and vessel wall with a distance greater than the thickness of the strut (i.e. >91µm). Intraluminal defect was defined as an irregularly shaped structure, either free from the vessel wall or attached to the vessel wall or the stent.

To quantify the degree of vascular healing status, the Healing Score (HS) was calculated at every time-point. Details of the HS components have been described.[8] The score consisted of 5 parameters as follows: (a) percentage of intraluminal defect (%ILD); (b) percentage of malapposed and uncovered struts (%MU); (c) percentage of uncovered struts alone (%U); (d) percentage of malapposition alone (%M); (e) presence of neointimal volume obstruction more than 30% (%NVO). The parameters were weighted according to the following formula: HS = [% ILDx4] + [% MUx3]+ [% Ux2]+ [% M] + [% NVO -30%] whenever %NVO is less than 30, the last component was set as 0.

Treatment allocation and follow-up procedure

All patients in this trial underwent stent implantation according to standard procedures. All patients received aspirin 75-100 mg per day indefinitely and a daily dose of clopidogrel 75 mg or prasugrel 10 mg or ticagrelor 90 mg bid for at least 4 months after the index-procedure.

Following the OCT examination at 3 months, all OCT pull-backs were assessed off-line by an independent Core Lab. When all pre-specified OCT criteria were met, patients were allowed to stop DAPT at 4 months but was advised to continue aspirin indefinitely according to standard guidelines.[13] By contrast, if any of the OCT criteria were not met, the patients were scheduled for repeat angiography and OCT examination at 6 months according to the protocol. If the 6-month OCT findings met all criteria, the patients were allowed to stop DAPT at 7 months, otherwise, the patients were requested to continue DAPT at least 12 months after the index procedure.

Patients who stopped DAPT either at 4 or 7 months according to the OCT finding were followed up at hospital or by a telephone call one month after their discontinuation of DAPT (5 or 8 months) in order to assess their vital status and to confirm the absence of major serious adverse events after the discontinuation of DAPT.

Quantitative coronary analysis

Two-dimensional quantitative coronary analysis (QCA) was performed at an independent core lab (Cardialysis BV, Rotterdam, The Netherlands) with the CAAS system (CAAS 5.9; Pie Medical BV, Maastricht, The Netherlands), using validated quantitative methods.[14]

Study endpoints

The primary endpoint was the change of Healing Scores (HS) from 3 to 6 months. The secondary angiographic endpoints were binary restenosis, late lumen loss (LLL), minimal lumen diameter (MLD) and %DS at 6 months. The secondary OCT endpoints were neointimal area and volume, mean stent lumen diameter, area and volume; minimal stent lumen diameter, area, and volume; mean neointimal thickness of the struts coverage; percentage of covered struts; and percentage of incomplete strut apposition area at 6 months.

Statistical analysis

The statistical analysis was performed by SAS version 9.2 (SAS Institute Inc., Cary, NC, USA). Categorical variables were summarized with frequencies and percentages. The continuous variables were reported as mean ± standard deviation (SD) or median and interquartile ranges (IQR 1^{st}-3^{rd}) as appropriate. Wilcoxon Signed Ranks test was used to compare continuous variables between serial OCT and QCA data. The categorical variables were compared by Fisher's exact test. A two sided p-value <0.05 was considered statistically significant.

RESULTS

Baseline clinical and angiographic characteristics.

The study population is described in **Fig. 1.** A total of 45 patients with 47 lesions received Nano Plus stents and all patients underwent repeat coronary angiography and OCT examination at 3 months. Twenty-seven patients (28 lesions) did not meet all OCT criteria at 3 months and were scheduled for OCT examination at 6 months. Out of 27 patients, 3 patients refused to undergo 6-month invasive angiography while 1 patient underwent clinically indicated target lesion revascularization without OCT assessment at 185 days. Finally, 23 patients with 24 lesions had serial coronary angiography and OCT assessment at 3 and 6 months. Baseline clinical and angiographic characteristics are presented in **Table 1**.

Serial angiographic and OCT examinations at 3 months and 6 months

The QCA assessment at 3 and 6 months is shown in **Table 2.** The in-stent MLD was 2.46±0.38 mm at 3 months and 2.25±0.45 mm at 6 months. The in-stent LLL was 0.14±0.06 mm at 3 months and 0.35±0.08 mm at 6 months.

The OCT analyses are shown in **Table 3**. At 3 months, 95.8% (23 lesions) had at least 1 frame with RUTTS >30% and decreased to 12.5% (3 lesions) at 6 months. Of note, fourteen lesions (58.3%) had a percentage of covered strut < 90% at 3 months while at 6 months only 2 lesions (8.3%) had such an incomplete coverage. The median number of frame with RUTTS > 30% decreased from 3.5 frames (range 1.3-7.0) at 3 months to 0.0 frame at 6 months, respectively. There was no case with intraluminal defect >300 μm^2 in both time points.

The proportion of covered stent struts increased from a median of 87.1% (75.4%-92.9%) at 3 months to 98.6% (95.6%-100.0%) at 6 months **(Fig 2).** The median of neointimal thickness increased from 82.8 μm (69.3-98.7) to 112.2 μm (97.9-146.6) between 3 and 6 months. Only 1 case still had persistent malapposition at 6 months and there was no newly detected stent malapposition. The median percentage of malapposed struts at 3 and 6 months was 0.2% (IQR 0.0%-1.9%) and 0.0% (IQR 0.0%-0.0%), respectively. The %NVO increased between 3 and 6 months from 6.3% (IQR 4.1%-9.6%) to 12.8% (IQR 8.5%-18.0%). The percentage of residual area stenosis increased from 14.6% (IQR 7.0%- 23.6%) to 21.0% (IQR 7.5%-32.8%), p=0.002. The HS significantly decreased from a median of 28.1 (IQR 12.3-49.9) at 3 months to 2.4 (0.0-9.6) at 6 months **(Fig 3 and 4).**

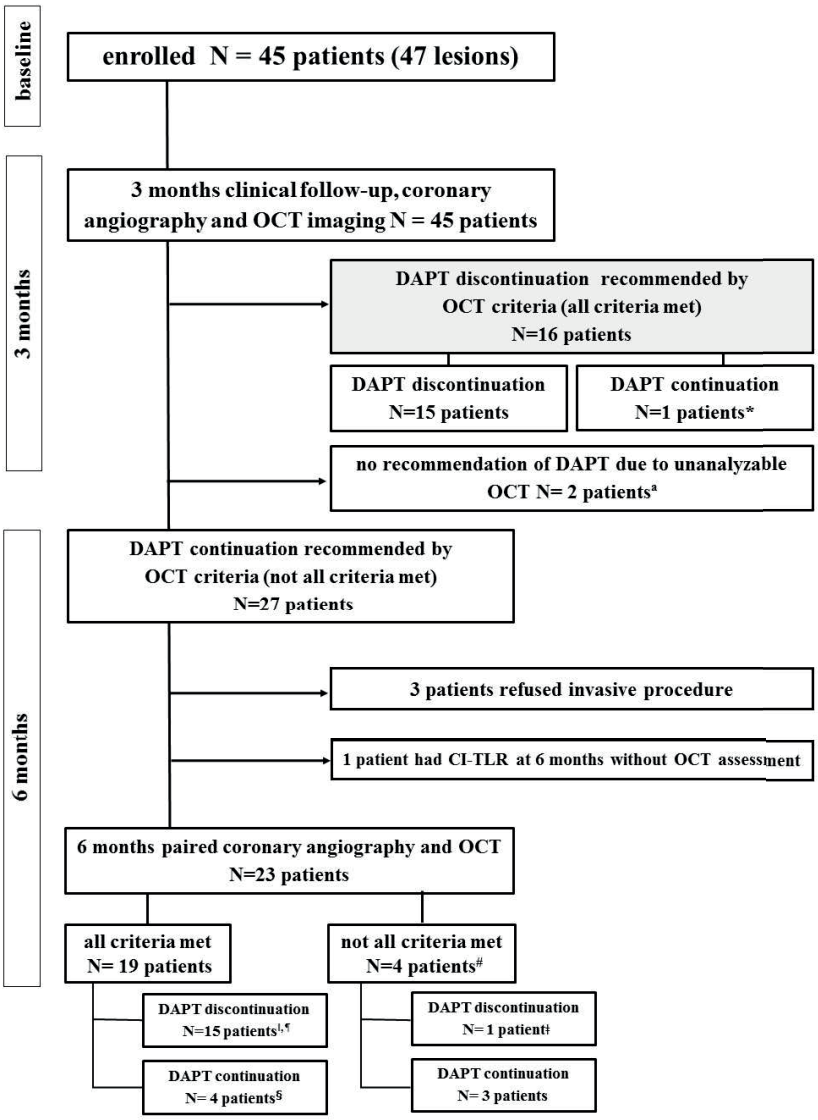

Figure 1. Study flow chart and follow-up.

*One patient was advised to continue DAPT according to his physician's opinion. [a]Two patients stopped clopidogrel after six-month OCT assessment due to fulfilment of OCT criteria. [#]No definite, probable, possible stent thrombosis reported at eight-month clinical follow-up. [‡]Clopidogrel was stopped due to dental procedure. aTwo patients had indication to use anticoagulant after stent implantation. One patient discontinued aspirin at one month and the other discontinued aspirin at three months after the index procedure. Both patients took the combination of anticoagulant and clopidogrel until six-month follow-up. After clopidogrel was discontinued at six months, the patients took only anticoagulant therapy. [¶]One patient underwent CABG due to progression of distal left main disease. [§]One patient had non-clinically indicated TLR at 184 days. CI-TLR: clinically indicated target lesion revascularisation; DAPT: dual antiplatelet therapy; OCT: optical coherence tomography

Table 1 Baseline clinical and angiographic characteristics

	Overall	Serial population
	n= 45 patients/47 lesions	n=23 patients/24 lesions
Age (years), mean±SD	64.0 ±9.8	68.6±9.5
Men, n(%)	33(73.3)	18(78.3)
Current smokers, n(%)	6(13.3)	1(4.3)
Diabetes, n(%)	5(11.1)	4(17.4)
Hypertension, n(%)	24(53.3)	12(52.2)
Hyperlipidemia, n(%)	37(82.2)	19(82.6)
Family history of CAD, n(%)	19(45.2)	8(34.8)
Previous CABG, n(%)	1(2.2)	1(4.3)
Previous PCI, n(%)	10(22.2)	5(21.7)
Previous myocardial infarction, n(%)	10(22.2)	5(21.7)
Stable angina, n(%)	30(66.7)	16(69.6)
Silent ischemia, n(%)	6(13.3)	3(13.0)
Target vessel		
Left anterior descending, n(%)	27(57.4)	12(50.0)
Left circumflex artery, n(%)	6(12.8)	4(16.7)
Right coronary artery, n(%)	14(29.8)	8(33.3)
AHA/ACC lesion classification		
B1, n(%)	20(42.6)	8(33.3)
B2, n(%)	25(53.2)	15(62.5)
C, n(%)	2(4.3)	1(4.2)
Moderate to heavy calcification, n(%)	8(17.0)	6(25.0)
Obstruction length (mm)	12.7±4.4	12.9±4.1
Diameter stenosis (%)	60.9±10.8	61.3±10.4
Reference vessel diameter (mm)	2.83 ± 0.46	2.81±0.47
Minimal lumen diameter (mm)	1.10 ± 0.35	1.09±0.37
Mean lumen diameter (mm)	2.51 ±0.39	2.49±0.38
Total nominal length of implanted stents per lesion (mm)	20.0±9.2	21.7±11.5
Number of device implanted per lesion (mm)	1.1±0.4	1.2±0.5
Mean nominal device diameter (mm)	3.6±1.5	3.19±0.41
Overlapping stents, n(%)	4(8.5)	2(8.7)

Data base on patients who had both OCT and coronary angiography at 3 and 6 months. Data are mean ± standard deviation or number (%). Abbreviation: AHA/ACC: American heart association/ American college of cardiology.

Antiplatelet therapy

Amongst 23 patients who received 6-month repeat OCT imaging, 21 patients had taken the following DAPT at 6 months; aspirin and clopidogrel 18(85.7%) patients, aspirin and ticagrelor 2(9.5%) patients and; aspirin and prasugrel in 1(4.8%) patient.

Table 2 Quantitative Coronary Angiography at 3 months and 6 months

	3 months	6 months	
	n=24 lesions	n=24 lesions	p-value†
Reference vessel diameter (mm)			
In-stent	2.84±0.43	2.77±0.44	0.03
In-segment	2.77±0.46	2.71±0.46	0.08
Minimal lumen diameter (mm)			
In-stent	2.46±0.38	2.25±0.45	0.001
In-segment	2.25±0.39	2.09±0.46	0.03
Mean lumen diameter (mm)			
In-stent	2.95±0.36	2.79±0.36	<0.001
In-segment	2.89±0.37	2.75±0.39	<0.001
Diameter stenosis (%)			
In-stent	12.7±9.1	17.6±12.3	0.02
In-segment	18.8±7.9	22.7±10.8	0.04
Late loss (mm)			
In-stent	0.14±0.06	0.35±0.08	<0.001
In-segment	0.06±0.04	0.22±0.07	0.005
Binary restenosis			
In-stent	0(0.0%)	0(0.0%)	1.0
In-segment	0(0.0%)	0(0.0%)	1.0

Data are mean ± standard deviation or number (%). p-values were calculated by Wilcoxon Signed Ranks Test.

Clinical outcomes

Throughout the 8-month period, no definite, probable or possible stent thrombosis was reported among 27 patients. There were three patients who underwent revascularization after 6-month angiographic follow-up. Two patients received target lesion revascularization and one patient underwent coronary bypass due to stable angina and progression of distal left main disease.

DISCUSSION

The present study was to provide a mechanistic interpretations of the vascular healing process in polymer-free SES in which the relative lack of neointimal growth was documented at 3 months. The main findings are; 1) an improvement in vascular healing as assessed by the HS was documented by a decrease of HS from 28.1 at 3 months to 2.4 at 6 months; 2) The angiographic late lumen loss and %NVO on OCT at 6 months were 0.35 mm and 12.8%, respectively; and 3) The absence of any definite or probable stent thrombosis up to 8 months.

Table 3 Optical coherence tomography analysis at 3 months and 6 months

	3 months	6 months	p-value
	n=24 lesions	n=24 lesions	
Strut level analysis			
Total analyzed struts, n	3833	3812	
Number of struts per cross-section, n	7.9±1.2	7.7±1.1	0.32
Percentage of covered struts	87.1(75.4-92.9)	98.6(95.6-100.0)	<0.001
Mean neointimal thickness, μm	82.8(69.3-98.7)	112.2(97.9-146.6)	<0.001
Number of malapposed struts, n	41	10	
Percentage of malapposed struts, %	0.2(0.0-1.9)	0(0.0-0.0)	0.008
Percentage of struts presence of both malapposed and uncovered, %	0.0(0.0-0.7)	0(0.0-0.0)	0.09
Cross-section level analysis			
Number of cross-sections per lesion, n	18(16-21)	18(17-21)	0.25
Mean reference lumen area, mm^2	7.08(5.27-8.51)	6.69(5.49-7.36)	0.003
Minimal lumen area, mm^2	5.85(4.49-6.98)	5.25(3.87-6.01)	<0.001
Mean lumen area, mm^2	7.75(6.39-8.51)	6.69(5.87-7.89)	<0.001
Minimal stent area, mm^2	6.68(5.98-7.42)	6.53(5.77-7.41)	0.10
Mean stent area, mm^2	8.25(6.72-9.27)	7.63(6.76-9.23)	0.03
Neointimal area, mm^2	0.47(0.35-0.73)	0.81(0.67-1.21)	<0.001
Mean ISA area, mm^2	0.01(0.00-0.07)	0.00(0.00-0.00)	0.01
Number of frame with RUTTS > 30% per lesion	3.5(1.3-7.0)	0.0(0.0-0.0)	<0.001
Lesion level analysis			
Healing Score	28.1(12.3-49.9)	2.4 (0.0-9.6)	<0.001
Mean area of ISA > 2 mm^2, n(%)	0(0.0%)	0(0.0%)	0.56
Intraluminal defect area > 300 μm^2, n(%)	0(0.0%)	0(0.0%)	1.00
Neointima volume, mm^3	7.5(5.9-14.2)	13.7(11.6-24.8)	<0.001
Percentage of neointimal volume obstruction	6.3(4.1-9.6)	12.8(8.5-18.0)	<0.001
Stent volume, mm^3	140.1(101.2-172.2)	139.6(102.5-158.0)	0.86
Lumen volume, mm^3	134.0(99.6-159.7)	120.1(93.4-145.7)	0.57
Mean lumen eccentricity index	0.87(0.82-0.89)	0.87(0.83-0.89)	0.33
Mean stent eccentricity index	0.89(0.85-0.92)	0.90(0.87-0.92)	0.12
Residual area stenosis	14.6(7.0-23.6)	21.0(7.5-32.8)	0.002

Data are median (Interquatile 1^{st} – 3^{rd}) or mean ± standard deviation. p-values were calculated by Wilcoxon Signed Ranks Test.

Initially, there was heterogeneity in the healing process at 3 months; 3 lesions had percentage of covered struts < 50%. The extremely low coverage might be related to: i) the presence of ISA, as malapposed struts generate high shear flow disturbance that is known to be a factor of retardation of neointimal growth[15]; ii) unfavorable characteristics of circulating endothelial progenitor cell in individual patients[16]; and iii) a heterogeneity in drug effect, potentially due to a defective manufacturing of certain stent batch.

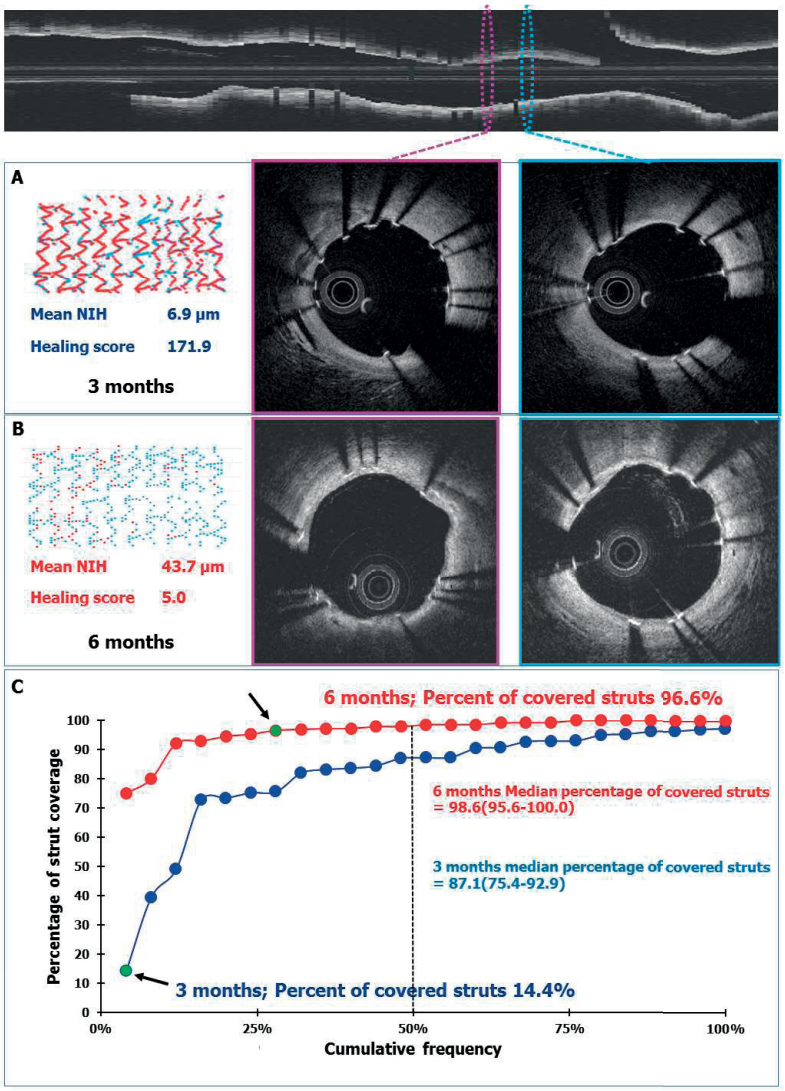

Figure 2. Example of optical coherence tomography and cumulative frequency curve of percentage of covered struts at three months and six months in 24 paired lesions.

Top panel shows the longitudinal view with corresponding cross-section samplings from two different in-stent segments (pink and blue ellipse). The follow-up OCT cross-sections at three months (middle and right-hand panel A) and six months (middle and right-hand panel B) are shown in coloured frames corresponding to the coloured cross-sections in the longitudinal view. The coverage of struts improved from three to six months. Panel A (left) shows a colour-coded spread-out sheet depicting a high proportion of uncovered struts (red dots) to covered struts (blue dots). At six-month follow-up (panel B, left), the spread-out sheet shows an improvement of strut coverage (fewer red dots). The HS dramatically decreased from 171.9 at three months to 5.0 at six months. The cumulative frequency curves of the percentage of covered struts at three months (blue) and six months (red) are shown in panel C. The green dots indicated by black arrows illustrate a shift from low to high percentage of strut coverage from three months to six months.

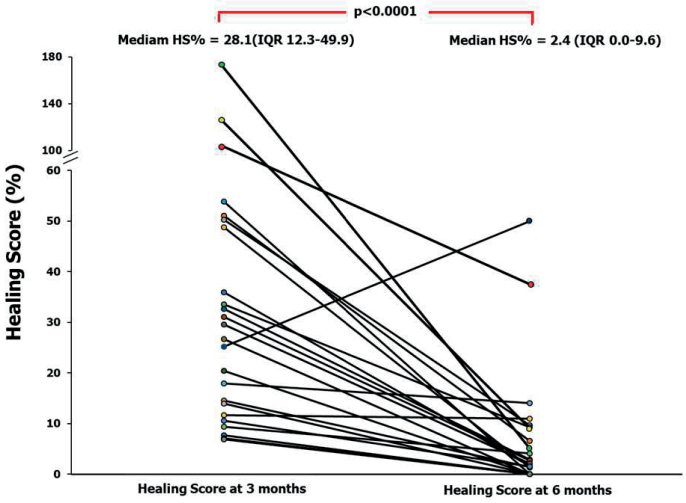

Figure 3. Temporal change of healing index at three-month and six-month follow-up in 24 paired lesions.

Can pathological criteria be applied as indicator of optimal vascular healing?

The OCT quantitative criteria used in the present study were derived from post-mortem histopathological study that showed a strong correlation of late stent thrombosis with RUTTS and number of uncovered struts.[4] Our OCT analysis at 3 months showed that 95.8% of lesions had RUTTS >30% while the percentage of strut coverage < 90% was observed in 58.3%. These findings reflect the weak relationship between OCT surrogate markers and their clinical prognostic value. The anatomo pathological criteria seem to overestimate the deficiencies of vascular healing status and they appear to be too stringent. The issues of applying the pathological criteria to the clinical research are, 1) the criteria were derived from post-mortem study of patients with late stent thrombosis and may thus reflect a certain selection bias since the denominator (patients alive having uncovered and malapposed struts) is unknown while the numerator (autopsied patients with stent thrombosis) is known. To prove the prognostic value of uncovered and malapposed struts in clinical practice, a huge sample size to show statistical significance will be needed. Since the incidence of stent thrombosis with combination of uncovered or malapposed struts is very low, the correlation may never be established, 2) the criteria were derived in the era of first-generation DES which had thicker struts that promoted recirculation zones with low endothelial shear stress behind the struts – a biological trigger for stent thrombosis[17], 3) the conventional DAPT used in these anatomo-pathological cases (ticlopidine or clopidogrel) was not as potent as contemporary antiplatelet agents such as ticagrelor or prasugrel.

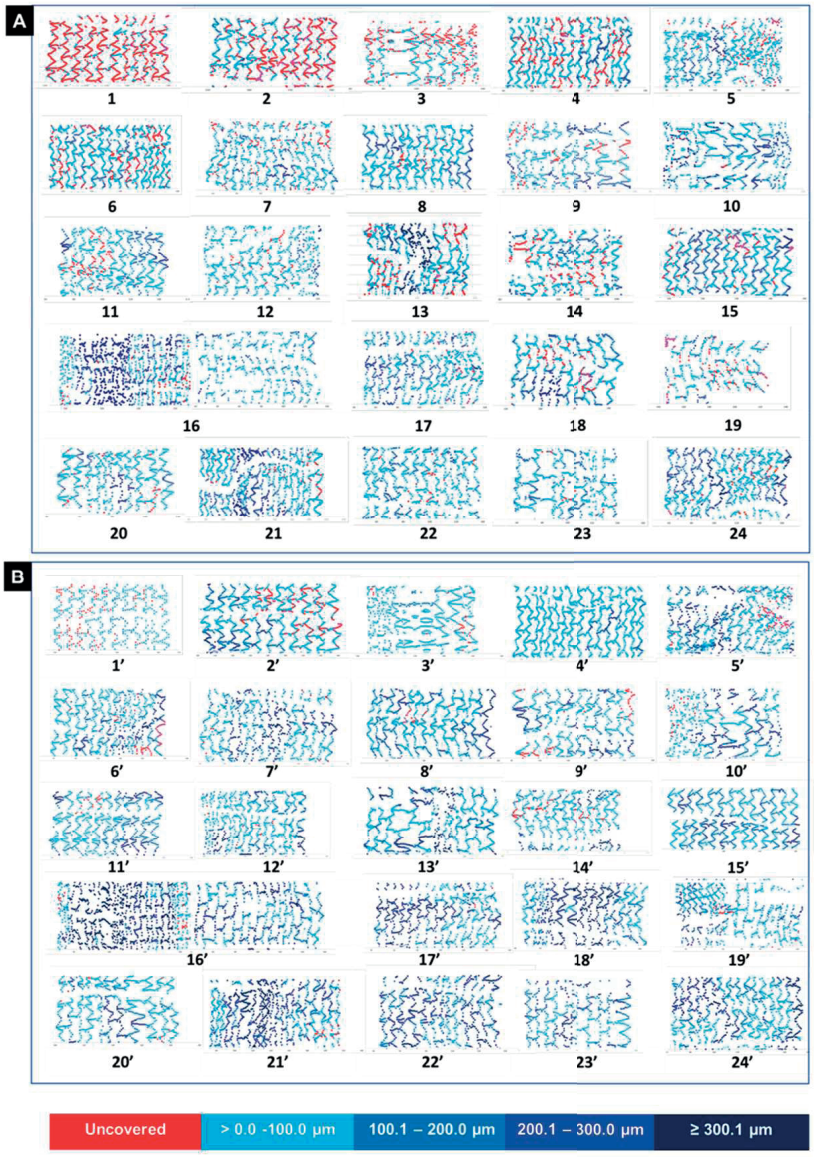

Figure 4. Spread-out sheets demonstrating the coverage status of the individual stents/patients at two time points (three and six months). Upper panel (A) demonstrates the coverage status of the individual stents at three months, while the lower panel (B) demonstrates the coverage status of the same stents at six months. Struts are colour coded according to their coverage status. Uncovered struts are depicted as red while covered struts are depicted as blue, with deepening colour of blue indicative of a thicker neointima (light blue colour indicates a neointimal thickness more than 0 µm to 100.0 µm, sustained blue indicates a neointimal thickness 100.1-200.0 µm, navy blue indicates a neointimal thickness 200.1-300.0 µm, dark blue indicates a neointimal thickness more than 300.1 µm).

Can OCT criteria be applied as a guidance for dual antiplatelet duration?

The current analysis showed that only onethird of lesions had adequate vascular healing at 3 months whereas vascular healing was almost complete at 6 months, without stent thrombosis. The present study did not pretend to detect lesions that were going to develop stent thrombosis; the study protocol recommended continuation of DAPT in order to potentially prevent patient from developing stent thrombosis. Previously, there has been sufficient evidence showing that abbreviated DAPT duration of 3 months[18] or 6 months[19-22] after polymer-coated DES implantation for low to moderate risk patients is safe. It has been recently demonstrated that DAPT duration can be even abbreviated to only 1 month after polymer-free DES implantation as reported in LEADERS FREE trial[23]. In the LEADERS FREE trial, polymer-free umirolimus-coated stent was compared with bare-metal stent (BMS) in a high risk of bleeding patients who underwent PCI. The results showed that a polymer-free umirolimus-coated stent was superior to a BMS with respect to the composite of cardiac death, myocardial infarction, or stent thrombosis when used with a 1-month course of DAPT. The rate of stent thrombosis did not differ significantly between the two groups, and more than half of the stent thromboses in both groups occurred during the first 30 days, when patients were prescribed DAPT. Consequently, invasive imaging is not a pragmatic requirement to determine whether DAPT has to be continued longer than 3 or 6 months in the polymer-free DES as reported in the present study. However, the consideration of abbreviated DAPT duration should be applied in specific stent platforms and in relation to similar lesions characteristics to those assessed in clinical trials.

Angiographic late lumen loss and OCT findings in polymer-free DES

The LLL of the NANO Plus stent at 3 and 6 months were 0.17 mm and 0.35 mm, respectively. These results are comparable to previous data of a polymer-free rapamycin-eluting stent that had LLL of 0.16 mm[24] and 0.47 mm[25] at 3 months and 6-8 months, respectively. Although NANO Plus had a higher angiographic in-stent LLL as compared to the first- and second-generation of DES (both permanent or biodegradable polymer-coated)[26-28], the risk of target lesion revascularization may still be low (<5% to 10%), according to the findings of a previous study with early generation DES[29]. A higher LLL may not necessarily translate into a higher target lesion revascularization rate among different DES platform.[30]

A recent study that compared FFR and MLA by OCT has clearly demonstrated that, with the exception of left main disease, an MLA greater >1.96 mm^2 is not generally associated with an FFR <0.80.[31] In our present study, the MLA was in general much higher than this meta-analysis-derived threshold that was recently proposed by D'Ascenzo et al [31].

Limitations

The limitations of this prospective study are (1) a relatively small sample size that was not powered to demonstrate the relationship between OCT findings and clinical outcomes, as stated in the protocol; (2) lesions that were treated in the present study were simple lesions, therefore, favorable vascular healing might be expected in these relatively short and less complex lesions; (3) a serial OCT follow-up was solely performed in inadequate vascular healing lesions at 3 months which is a potential cause of selection bias; (4) the lack of a direct comparison between the study devices and contemporary DES that are used in routine clinical practice and (5) the criteria of covered stent was defined as having a neointimal thickness more than 0 μm that may not be practical in clinical use.

CONCLUSION

In patients treated with polymer-free SES, serial OCT showed almost complete vascular healing at 6 months even when coverage was insufficient at 3 months. This suggests an adequate safety and efficacy profile of the device at that point in time. The implication of these findings should be evaluated in a large clinical trial.

Impact on daily practice.

The Nano Plus is a polymer-free DES that elutes sirolimus from a reservoir made of abluminal nanomeric cavities without the presence of a polymer. The Healing Score (HS), derived from OCT assessment showed that the polymer-free SES develops an almost complete vascular healing within this time interval.

REFERENCE

1. Kang SH, Park KW, Kang DY, et al. Biodegradable-polymer drug-eluting stents vs. bare metal stents vs. durable-polymer drug-eluting stents: a systematic review and Bayesian approach network meta-analysis. *European heart journal.* 2014;35(17):1147-1158.
2. Raber L, Zanchin T, Baumgartner S, et al. Differential healing response attributed to culprit lesions of patients with acute coronary syndromes and stable coronary artery after implantation of drug-eluting stents: an optical coherence tomography study. *International journal of cardiology.* 2014;173(2):259-267.
3. Kim BK, Ha J, Mintz GS, et al. Randomised comparison of strut coverage between Nobori biolimus-eluting and sirolimus-eluting stents: an optical coherence tomography analysis. *EuroIntervention.* 2014;9(12):1389-1397.
4. Finn AV, Joner M, Nakazawa G, et al. Pathological correlates of late drug-eluting stent thrombosis: strut coverage as a marker of endothelialization. *Circulation.* 2007;115(18):2435-2441.
5. Daemen J, Wenaweser P, Tsuchida K, et al. Early and late coronary stent thrombosis of sirolimus-eluting and paclitaxel-eluting stents in routine clinical practice: data from a large two-institutional cohort study. *Lancet.* 2007;369(9562):667-678.
6. Wenaweser P, Daemen J, Zwahlen M, et al. Incidence and correlates of drug-eluting stent thrombosis in routine clinical practice. 4-year results from a large 2-institutional cohort study. *Journal of the American College of Cardiology.* 2008;52(14):1134-1140.
7. Garcia-Garcia HM, Muramatsu T, Nakatani S, et al. Serial optical frequency domain imaging in STEMI patients: the follow-up report of TROFI study. *European heart journal cardiovascular Imaging.* 2014;15(9):987-995.
8. Raber L, Onuma Y, Brugaletta S, et al. Arterial healing following primary PCI using the Absorb everolimus-eluting bioresorbable vascular scaffold (Absorb BVS) versus the durable polymer everolimus-eluting metallic stent (XIENCE) in patients with acute ST-elevation myocardial infarction: rationale and design of the randomised TROFI II study. *EuroIntervention : journal of EuroPCR in collaboration with the Working Group on Interventional Cardiology of the European Society of Cardiology.* 2015;11(4).
9. Suwannasom P, Benit E, Gach O, et al. Short-term effects of Nano+™ polymer-free sirolimus-eluting stents on native coronary vessels: an optical coherence tomography imaging study. *EuroIntervention : journal of EuroPCR in collaboration with the Working Group on Interventional Cardiology of the European Society of Cardiology.* 2015;Asiaintervention 1(Issue 1):57-70.
10. Prati F, Di Vito L, Biondi-Zoccai G, et al. Angiography alone versus angiography plus optical coherence tomography to guide decision-making during percutaneous coronary intervention: the Centro per la Lotta contro l'Infarto-Optimisation of Percutaneous Coronary Intervention (CLI-OPCI) study. *EuroIntervention : journal of EuroPCR in collaboration with the Working Group on Interventional Cardiology of the European Society of Cardiology.* 2012;8(7):823-829.
11. Onuma Y, Thuesen L, van Geuns RJ, et al. Randomized study to assess the effect of thrombus aspiration on flow area in patients with ST-elevation myocardial infarction: an optical frequency domain imaging study--TROFI trial. *European heart journal.* 2013;34(14):1050-1060.
12. Takano M, Inami S, Jang IK, et al. Evaluation by optical coherence tomography of neointimal coverage of sirolimus-eluting stent three months after implantation. *The American journal of cardiology.* 2007;99(8):1033-1038.
13. Windecker S, Kolh P, Alfonso F, et al. 2014 ESC/EACTS Guidelines on myocardial revascularization: The Task Force on Myocardial Revascularization of the European Society of Cardiology (ESC)

and the European Association for Cardio-Thoracic Surgery (EACTS)Developed with the special contribution of the European Association of Percutaneous Cardiovascular Interventions (EAPCI). *European heart journal.* 2014;35(37):2541-2619.

14. van der Zwet PM, Reiber JH. A new approach for the quantification of complex lesion morphology: the gradient field transform; basic principles and validation results. *Journal of the American College of Cardiology.* 1994;24(1):216-224.
15. Foin N, Gutierrez-Chico JL, Nakatani S, et al. Incomplete stent apposition causes high shear flow disturbances and delay in neointimal coverage as a function of strut to wall detachment distance: implications for the management of incomplete stent apposition. *Circulation Cardiovascular interventions.* 2014;7(2):180-189.
16. De Winter RJ, Klomp M. Understanding the Role of Endothelial Progenitor Cells in Cardiovascular Disease, Coronary Artery Lesion Progression, and In-Stent Restenosis . *JACC: Cardiovascular Interventions.* 2010;3(1):87-89.
17. Koskinas KC, Chatzizisis YS, Antoniadis AP, Giannoglou GD. Role of endothelial shear stress in stent restenosis and thrombosis: pathophysiologic mechanisms and implications for clinical translation. *Journal of the American College of Cardiology.* 2012;59(15):1337-1349.
18. Kim BK, Hong MK, Shin DH, et al. A new strategy for discontinuation of dual antiplatelet therapy: the RESET Trial (REal Safety and Efficacy of 3-month dual antiplatelet Therapy following Endeavor zotarolimus-eluting stent implantation). *Journal of the American College of Cardiology.* 2012;60(15):1340-1348.
19. Valgimigli M, Campo G, Monti M, et al. Short- versus long-term duration of dual-antiplatelet therapy after coronary stenting: a randomized multicenter trial. *Circulation.* 2012;125(16):2015-2026.
20. Gwon HC, Hahn JY, Park KW, et al. Six-month versus 12-month dual antiplatelet therapy after implantation of drug-eluting stents: the Efficacy of Xience/Promus Versus Cypher to Reduce Late Loss After Stenting (EXCELLENT) randomized, multicenter study. *Circulation.* 2012;125(3):505-513.
21. Schulz-Schupke S, Byrne RA, Ten Berg JM, et al. ISAR-SAFE: a randomized, double-blind, placebo-controlled trial of 6 vs. 12 months of clopidogrel therapy after drug-eluting stenting. *European heart journal.* 2015;36(20):1252-1263.
22. Gilard M, Barragan P, Noryani AA, et al. 6- versus 24-month dual antiplatelet therapy after implantation of drug-eluting stents in patients nonresistant to aspirin: the randomized, multicenter ITALIC trial. *Journal of the American College of Cardiology.* 2015;65(8):777-786.
23. Urban P, Meredith IT, Abizaid A, et al. Polymer-free Drug-Coated Coronary Stents in Patients at High Bleeding Risk. *New England Journal of Medicine.* 2015;373(21):2038-2047.
24. Moore P, Barlis P, Spiro J, et al. A Randomized Optical Coherence Tomography Study of Coronary Stent Strut Coverage and Luminal Protrusion With Rapamycin-Eluting Stents. *JACC: Cardiovascular Interventions.* 2009;2(5):437-444.
25. Mehilli J, Byrne RA, Wieczorek A, et al. *Randomized trial of three rapamycin-eluting stents with different coating strategies for the reduction of coronary restenosis.* Vol 292008.
26. Morice MC, Serruys PW, Sousa JE, et al. A randomized comparison of a sirolimus-eluting stent with a standard stent for coronary revascularization. *The New England journal of medicine.* 2002;346(23):1773-1780.
27. Regar E, Serruys PW, Bode C, et al. Angiographic findings of the multicenter Randomized Study With the Sirolimus-Eluting Bx Velocity Balloon-Expandable Stent (RAVEL): sirolimus-eluting stents inhibit restenosis irrespective of the vessel size. *Circulation.* 2002;106(15):1949-1956.

28. Serruys PW, Ong AT, Piek JJ, et al. A randomized comparison of a durable polymer Everolimus-eluting stent with a bare metal coronary stent: The SPIRIT first trial. *EuroIntervention.* 2005;1(1):58-65.
29. Ellis SG, Popma JJ, Lasala JM, et al. Relationship between angiographic late loss and target lesion revascularization after coronary stent implantation: analysis from the TAXUS-IV trial. *Journal of the American College of Cardiology.* 2005;45(8):1193-1200.
30. Pocock SJ, Lansky AJ, Mehran R, et al. Angiographic surrogate end points in drug-eluting stent trials: a systematic evaluation based on individual patient data from 11 randomized, controlled trials. *Journal of the American College of Cardiology.* 2008;51(1):23-32.
31. D'Ascenzo F, Barbero U, Cerrato E, et al. Accuracy of intravascular ultrasound and optical coherence tomography in identifying functionally significant coronary stenosis according to vessel diameter: A meta-analysis of 2,581 patients and 2,807 lesions. *American heart journal.* 2015;169(5):663-673.

Chapter 12

Fate of Bioresorbable Vascular Scaffold Metallic Radio-Opaque Markers at the Site of Implantation After Bioresorption

Pannipa Suwannasom, Yoshinobu Onuma, Carlos M. Campos, Shimpei Nakatani, Yuki Ishibashi, Hiroki Tateishi, Maik J. Grundeken, Bojan Stanetic, Koen Nieman, Hans Jonker, Hector M. Garcia-Garcia, Patrick W. Serruys

JACC Cardiovasc Interv. 2015 Jul;8(8):1130-2.

The use of bioresorbable vascular scaffolds (BRS) is increasing in patients with coronary artery disease undergoing percutaneous coronary interventions. Because the devices are radiolucent on fluoroscopy, 2 adjacent cylindrical platinum markers are incorporated in the proximal and distal edges of the polymeric devices for precise scaffold deployment and post-dilation during the procedure. In addition, the metallic radio-opaque markers (MRMs) also provide anatomic landmarks for long-term follow-up when all the polymeric struts have been bioresorbed. There has been concern about the potential risk of MRM beads becoming dislodged from the device and embolized into the coronary bed after complete bioresorption of the polymeric struts. Beyond the biological hazard of MRMs embolization, the additional inconvenience is that the embolization may result in the incapacity to locate the coronary segment where the fully bioresorbed scaffold was implanted. Invasive assessment of BRS such as quantitative coronary angiography (QCA), intravascular ultrasound (IVUS), or optical coherence tomography (OCT) may be unable to detect the precise location of the MRMs either because of the resolution of the imaging technique (QCA) or as a result of wire artifact (IVUS, OCT) or mimicry by heavy calcium (IVUS). Multislice computed tomography coronary angiography (MSCT) has provided reliable assessment of the angiographic results up to 3 to 5 years (1,2) after scaffold implantation with accurate detection of the position of MRMs and their blooming effect without being dependent on the rate of image acquisition and wire artifact. In order to dispel the question of embolization of MRMs, we evaluated the persistent presence and location at 18 months of the MRMs following implantation of these fully bioresorbable scaffolds.

We retrospectively pooled data from the ABSORB trials (ABSORB Cohort A, ABSORB Cohort B, and ABSORB EXTEND) in which 943 patients with de novo native coronary artery lesions were treated with the fully resorbable everolimus-eluting Absorb scaffold (Abbott Vascular, Santa Clara, California); the details and primary outcome of each trial have been published (2–4). Of these 943 patients, 165 patients with 168 lesions underwent MSCT at 18 months. A list of the MSCT scanners, the acquisition protocol, and the MSCT analysis are described in the Online Appendix.

To establish the persistent presence of the MRMs in MSCT, both qualitative and quantitative evidence were required. The qualitative evidence was the ability to identify both proximal and distal MRMs position. Because calcified nodules (CN) could mimic MRMs, 4 criteria were used to identify the position of the radio-opaque markers: 1) typical location and orientation of the MRMs; 2) marker-to-marker length; 3) topographical relationship of the radio-opaque markers with anatomic landmarks visualized on MSCT and conventional coronary angiography; and 4) blooming artifact and its peak attenuation. The description of criteria and examples of MSCT images by using these 4 criteria are provided in Online Figure 1. The quantitative evidence is the MSCT scaffold length compared with its nominal length.

The statistical analysis is detailed in the Online Appendix.

A total of 168 lesions (12 lesions in ABSORB Cohort A, 61 lesions in ABSORB Cohort B, and 95 lesions in the ABSORB EXTEND study) were analyzed, and the study profile is shown in Online Figure 2. A total of 348 MRMs were evaluated by both quantitative and qualitative analyses; all MRMs were detected at the implantation site; and there was no evidence of marker embolization to distal vascular beds. The median MSCT scaffold length was 18.0 mm (ranging from 12 mm to 36 mm; interquartile range [IQR]: 17 to 19 mm) as well as the median nominal scaffold length was 18.0 mm (ranging from 12 mm to 28 mm) (Figure 1). The median difference in length between MSCT scaffold length and nominal scaffold length was 0.0 mm (IQR: −1.0 to 1.0 mm). There was a moderate correlation between MSCT mean lumen area (Mean LA) and QCA Mean LA ($r = 0.54$, $p < 0.0001$). A good correlation was observed between MSCT Mean LA and IVUS Mean LA, and between MSCT Mean LA and OCT Mean LA ($r = 0.74$ and $r = 0.73$, respectively; $p < 0.0001$) (Online Figure 3). The Mean LA measured by MSCT was comparable to QCA, but statistically lower than IVUS and OCT (Online Table 1). The reproducibility of the 4 criteria to identify MRMs from CN was good, $r = 0.97$; $p < 0.0001$ (Online Figure 4).

The attenuation of MRMs was approximately 30% higher than dense CN attenuation, but there was nevertheless a modest overlap of the attenuation values; MRM attenuation was sometimes lower than 1,000 HU as a result of the partial volume effect. The median peak density of MRMs was 1,368 HU (IQR: 1,158 to 1,715 HU) in contrast to the median peak density of CN that was 946 HU (IQR: 844 to 1,133 HU).

The main findings of this study are the following: 1) according to the criteria, all MRMs were identified and located at the site of the initial implantation; 2) the MSCT Mean LA was comparable to the Mean LA measured by QCA but lower than OCT and IVUS; and 3) the reproducibility in detecting of MRMs by using 4 criteria was high.

However, the distinction between calcified spots and metallic markers with computed tomography is also not easy to determine compared with OCT. The possible advantages of OCT are the ability to: 1) distinguish the MRMs from underlying calcium more clearly than MSCT; 2) measure the embedment of the struts; and 3) evaluate the thickness of neointima because of a higher axial resolution of around 10 to 15 μm as compared with MSCT.

The limitation in this study is that the study result was able to confirm the persistent presence of MRMs only at medium-term follow-up, and the long-term results still require investigation.

In conclusion, MRM recognition by MSCT is critical for precise noninvasive assessment of the coronary location of all MRMs. On the basis of our study criteria, there was no evidence of MRMs dislodgement and embolization 18 months after scaffold implantation.

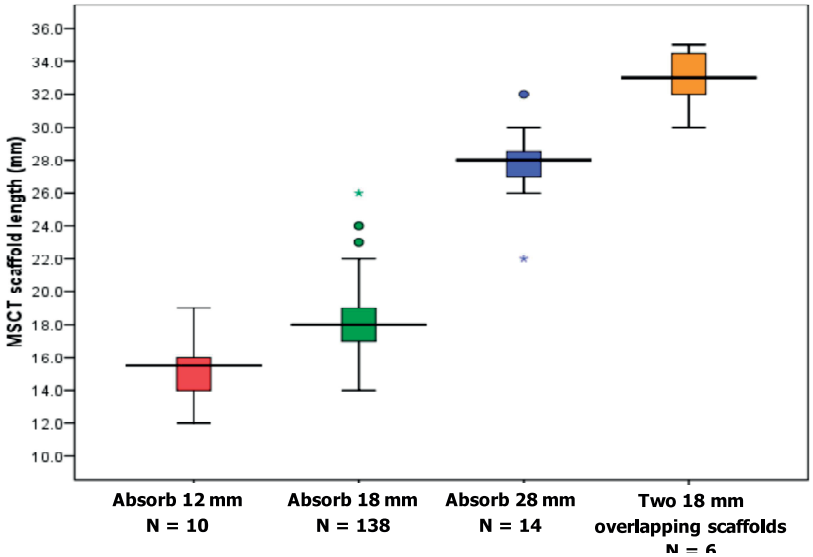

Figure 1. MSCT Scaffold Length Compared With Nominal Scaffold Length

The median and the 1st and 3rd quartiles of each multislice computed tomography (MSCT) scaffold length corresponding to its nominal length are shown in boxes, and the minimum and maximum values as whiskers. The asterisks and the dots above/below indicate the outlier cases.

REFERENCE

1. Onuma Y., Dudek D., Thuesen L., et al. (2013) Five-year clinical and functional multislice computed tomography angiographic results after coronary implantation of the fully resorbable polymeric everolimus-eluting scaffold in patients with de novo coronary artery disease: the ABSORB cohort A trial. J Am Coll Cardiol Intv 6:999–1009.
2. Serruys P.W., Onuma Y., Garcia-Garcia H.M., et al. (2014) Dynamics of vessel wall changes following the implantation of the absorb everolimus-eluting bioresorbable vascular scaffold: a multi-imaging modality study at 6, 12, 24 and 36 months. EuroIntervention 9:1271–1284.
3. Ormiston J.A., Serruys P.W., Regar E., et al. (2008) A bioabsorbable everolimus-eluting coronary stent system for patients with single de-novo coronary artery lesions (ABSORB): a prospective open-label trial. Lancet 371:899–907.
4. Abizaid A., Ribamar Costa J. Jr.., Bartorelli A.L., et al. (2014) The ABSORB EXTEND study: preliminary report of the twelve-month clinical outcomes in the first 512 patients enrolled. EuroIntervention 10:1396–1401.

APPENDIX - MSCT ACQUISITION PROTOCOL

CT scanners from all major manufacturers were used, including 64-slice CT (brilliance 64, Philips, Best, the Netherlands; CVi, GE Healthcare, Milwaukee, Wisconsin), 256-slice CT (iCT, Philips), 320-slice CT (Aquilion One, Toshiba, Nasu, Japan), 64-slice dual-source CT (Definition, Siemens AG Forchheim, Germany), and 128-slice dual-source CT (Definition Flash, Siemens). Standard acquisition techniques were analyzed, which included beta-blockers in patients with a fast heart rate, tube settings depending on patient size (80 to 140 kV), and axial scan protocols for patients with lower heart rates to reduce radiation doses, all at the discretion of the individual sites. Images were reconstructed using thin slices (0.5 to 0.67 mm) and medium smooth reconstruction filters, including 1 or several phases depending on the scan protocol. All data were stored on a DVD for core laboratory evaluation.

MSCT analysis

The MSCT images were analyzed on a dedicated workstation (Multi-Modality Workstation, Siemens AG) using a validated cardiovascular analysis package (syngo Circulation, Siemens AG, Forchheim, Germany). The analysts had to identify the position of proximal and distal MRMs in curved MPR, in addition, cross-sectional MPR also had to be evaluated to mark the center of MRMs. In order to differentiate MRMs from CN, the MRMs attenuation was evaluated by the peak Hounsfield Unit (HU) of points labeled as scaffold markers. Attenuation of calcified nodule suspected to be present in the scaffold area was measured within the scaffold, 5 mm proximal and distal to MRMs. MSCT scaffold length was obtained after marking the position of proximal and distal MRMs that provided automated segmentation length. The difference in length was calculated as nominal scaffold length minus MSCT scaffold length. Whenever the difference in length was more than 10 mm, the MSCT scaffold length was evaluated by a panel of two observers (PS and CC) in order to adjudicate the precise location of MRMs. The mean lumen area was performed by automatic segmentation of the vessel lumen and a center lumen line was created through the treated coronary branch. The cross-sectional views of the vessel were reconstructed at ~1-mm longitudinal steps from proximal to distal MRMs, the mean lumen areas within the treated lesion were determined and manual correction performed for each slice.

Statistical Analysis

Statistical analyses were performed with SPSS version 17.0 (SPSS Inc, Chicago, IL,USA). Continuous variables were presented as mean ± standard deviation or median and interquartile ranges (IQR 25-75). Pearson's correlation coefficient (*r*) was used to measure the correlation of MSCT with other invasive imaging technique (this analysis was

performed in only ABSORB Cohort B because of the timing of invasive coronary imaging were not different more than 6 months). Paired comparisons between the different imaging modalities were done by a paired t- test for continuous variables. Mean difference are based on paired data. Two observers blinded to the nominal scaffold length analyzed the persistent presence of the two markers. Inter-observer reproducibility was randomly performed in 50 patients. The agreement between the two observers on the MSCT scaffold length was estimated by Bland-Altman plots. A two-sided P value of less than 0.05 indicated statistical significance.

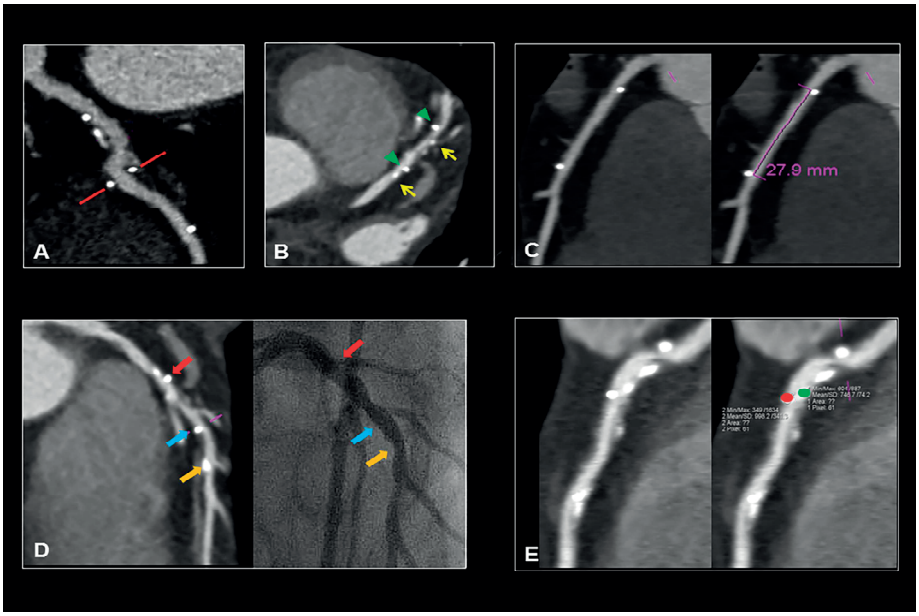

online appendix figure 1. Example of four criteria used in MSCT analysis for detecting the presence of metallic radiopaque markers

(A) Example of multislice computed tomography coronary angiography showing overlapping radiopaque markers (red) in Curved MPR; markers normally appeared as a round shape. Examples of four criteria applied to discriminate metallic radiopaque markers from nodular calcium; (B) 1) typical location and orientation of the MRMs. Markers (green arrowheads) are located on the opposite side at the proximal and distal edges of the scaffold while calcific nodules (yellow arrow) may be on the same side. (C) marker to marker length. In a single, non-overlap lesion, the 27.9 mm scaffold length was retrievable in Curved MPR view; (D) corresponding anatomical position of MRM on MSCT and conventional angiography at index procedure. The Absorb was deployed in the mid LAD, the proximal marker was easily identified (red block arrow) but distal radiopaque markers were difficult to discriminate from distal nodular calcium in Curved MPR view (left panel). The septal branch and 1st Diagonal branch from baseline conventional coronary angiography (right panel) were good anatomical landmarks to localize and identify the distal radiopaque marker (blue block arrow) from nodular calcium (orange block arrow); (E) blooming artefact and its peak intensity. Left panel show stretched Curved MPR view with two possible marker positions, their peak density values, 887 HU (green circle) and 1,634 HU (red circle) assisted the analyst in choosing the appropriate position of the markers.

MSCT: Multislice Computed Tomography, MPR: Multiplanar reconstruction, Absorb: Bioresorbable vascular scaffold, LAD: Left anterior descending artery, HU: Hounsfield units

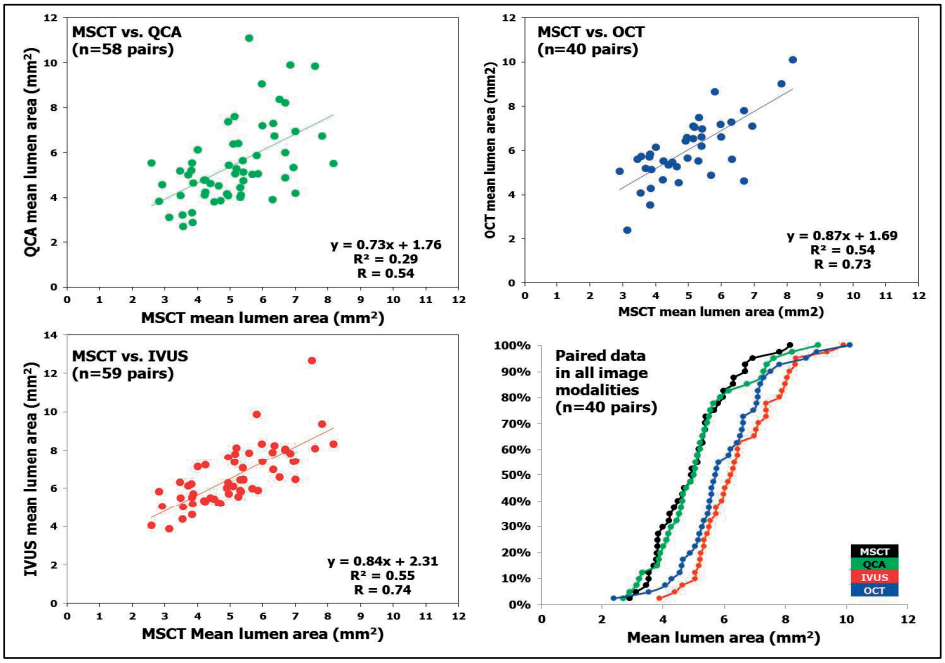

online appendix figure 2. The correlation of mean lumen area measured by MSCT and invasive coronary imaging.

Linear regression of minimal lumen area (MLA) measured by multislice computed tomography (X axis) and the different imaging modalities (y axis). The right lower panel depicts the cumulative curve of mean lumen area measured by different imaging techniques.

IVUS intravascular ultrasound; MSCT multislice computed tomography; OCT optical coherence tomography; QCA quantitative coronary angiography.

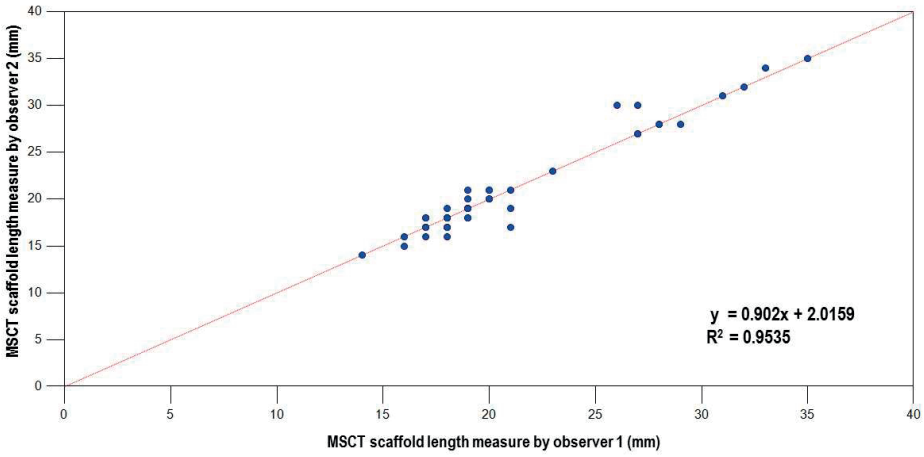

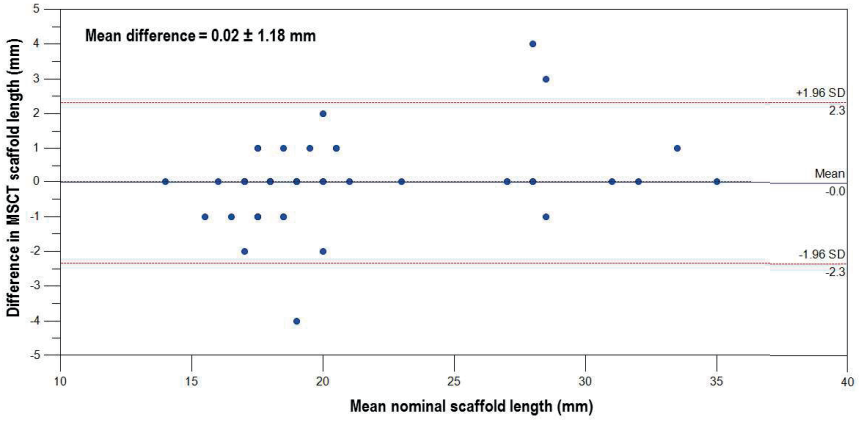

online appendix figure 3. Inter-observer variability and agreement of MSCT scaffold length for identifying radio-opaque markers.

Linear regression analysis plot depicting the inter-observer variability for the evaluation of the MSCT scaffold length, the correlation of MSCT scaffold length measured by two observers (panel A) was r = 0.97, p-value < 0.001. Bland-Altman plot (panel B) shows that the limit of agreement for identifying the position of MRMs was -2.3 to 2.3 mm. The inter-observer relative differences in length were 0.02 ±1.18 mm.

MSCT: Multislice Computed Tomography; MRMs: Metallic radiopaque markers

Supplementary Table 1 Mean stent length and mean lumen area measured by different imaging modalities*

A		B					
				MSCT	QCA	IVUS	OCT	nominal length
				n=61	n=58	n=59	n=40	18 mm
	Stent length (mm)							
		Mean±SD		19.6±2.8	14.8±1.7	20.0±2.9	17.8±1.1	18.0
	MSCT	Mean diff (A-B)			4.8	-0.4	1.7	1.6
		p-value			<0.0001	0.48	0.001	<0.0001
	QCA	Mean diff (A-B)				-5.3	-2.9	-3.2
		p-value				<0.0001	<0.0001	<0.0001
	IVUS	Mean diff (A-B)					2.3	2.0
		p-value					<0.0001	<0.0001
	OCT	Mean diff (A-B)						-0.2
		p-value						0.24
	Mean lumen area (mm2)			n=61	n=58	n=59	n=40	
		Mean±SD		5.11±1.32	5.48±1.79	6.63±1.52	6.02±1.48	
	MSCT	Mean diff (A-B)			-0.36	-1.47	-1.03	
		p-value			0.08	<0.0001	<0.0001	
	QCA	Mean diff (A-B)				-1.05	-0.89	
		p-value				<0.0001	<0.0001	
	IVUS	Mean diff (A-B)					0.45	
		p-value					0.001	

*Mean difference were calculated from paired data

IVUS intravascular ultrasound; OCT optical coherence tomography; MSCT multislice computed tomography; QCA quantitative coronary angiography; SD standard deviation

Chapter 13

Accuracy of coronary computed tomography angiography for bioresorbable scaffold luminal investigation: a comparison with optical coherence tomography

Carlos Collet, Yohei Sotomi, Rafael Cavalcante, Taku Asano, Yosuke Miyazaki, Erhan Tenekecioglu, Pieter Kistlaar, Yaping Zeng, Pannipa Suwannasom, Robbert J. de Winter, Koen Nieman, Patrick W. Serruys, Yoshinobu Onuma

Int J Cardiovasc Imaging. 2016 Nov 28. [Epub ahead of print].

ABSTRACT

To establish the accuracy of coronary computed tomography angiography (CTA) for in-scaffold quantitative evaluation with optical coherence tomography (OCT) as a reference. The translucent backbone of the bioresorbable scaffold allow us to evaluate non-invasively the coronary lumen with coronary CTA. In the ABSORB first-in-man studies, coronary CTA was shown to be feasible for quantitative luminal assessment. Nevertheless, a comparison with an intravascular modality with higher resolution has never been performed. In the ABSORB Cohort B trial, 101 patient with non-complex lesions were treated with the fully biodegradable vascular scaffold. For this analysis, all patients who underwent coronary CTA at 18 months and OCT within ±180 days were included. Coronary CTA and OCT data were analysed at an independent core laboratory for quantitative cross-sectional luminal dimensions. The primary objective was the accuracy and precision of coronary CTA for in-scaffold minimal lumen area assessment, with OCT as a reference. Among the 101 patients of the ABSORB Cohort B trial, 35 underwent both OCT and coronary CTA. The feasibility of quantitative evaluation was 74%. In the scaffolded segment, coronary CTA underestimated minimal lumen area by 9.8% (accuracy 0.39 mm^2, precision 1.0 mm^2, 95% limits of agreement −1.71 to 2.50 mm^2). A similar level of agreement was observed in the non-scaffolded segment. Compared to OCT, coronary CTA appears to be accurate for the estimation of in-scaffold luminal areas, with no difference compared to the non-scaffolded region.

INTRODUCTION

The field of interventional cardiology has been revolutionized by the introduction of the Absorb bioresorbable vascular scaffolds (Absorb BVS, Abbott Vascular, Santa Clara, CA). The restoration of the vascular integrity of the vessel might supersede the long-term limitations seen with permanent metallic stents [1]. At mid-term follow-up, randomised trials have shown comparable clinical results between bioresorbable vascular scaffolds (BVS) and cobalt-chromium everolimus-eluting stent for the treatment of non-complex coronary lesions [2, 3]. Also, the translucent backbone of the BVS allows for the non-invasive investigation of the coronary lumen with coronary CTA, thereby overcoming the limitations observed in patients previously revascularized with metallic stents [4].

In the ABSORB *first-in-man* trials (Cohort A and B), serial coronary CTA was performed. In these studies, high feasibility for quantitative in-scaffold luminal assessment was reported. In addition, the functional component of the treated region was assessed using computational fluid dynamics. Fractional flow reserve derived from coronary CTA (i.e., FFR_{CT}) was serially assessed. The persistence of FFR_{CT} normalization at long-term follow-up was observed [4]. The accuracy and precision of luminal geometry segmentation are of paramount importance for both quantitative luminal analysis and FFRCT computation.

Over the past two decades, major advances have been introduced in the field of computed tomography (i.e., the advent of 256 and 320-detectors scanners, dual-source CT, iterative algorithm for reconstructions, etc). With the best-in-class CT scanners available, the spatial resolution has been reported in the range of 250 microns. In contrast, invasive optical coherence tomography (OCT) has a resolution of 10–20 microns and is widely recognized as a gold standard for coronary luminal measurements [5]. Nevertheless, a comparison of in-scaffold luminal areas between coronary CTA and an intravascular modality with higher resolution have never been performed.

Therefore, the aim of this study was: (1) To assess the accuracy of coronary CTA for in-scaffold quantitative luminal analysis at mid-term follow-up with OCT as a reference and; (2) To validate the coronary CTA-derived luminal area measurement at the level of the radiopaque marker.

METHODS

Study design

In the ABSORB B (ABSORB Clinical Investigation Cohort B, Everolimus Eluting Coronary Stent System Clinical Investigation) trial, one hundred and one patients with non-complex de novo coronary lesion were enrolled at 12 centres between March and November

2009. Informed consent was obtained from all individual participants included in the study. The details of the trial have been previously described elsewhere [6]. Seventy-one patients underwent coronary CTA at 18 months with the use of at least a 64-detector (or higher) CT scanner [7]. In addition, patients were divided into two groups (B1 and B2) for serial invasive imaging (e.g., angiography, intravascular ultrasound and OCT) at different time points [6]. OCT was performed at 12 or 24-month follow-up in 28 and 31 patients in cohort B1 and B2, respectively [8]. All patients with coronary CTA and OCT evaluations were included in the present analysis (Fig. 1)

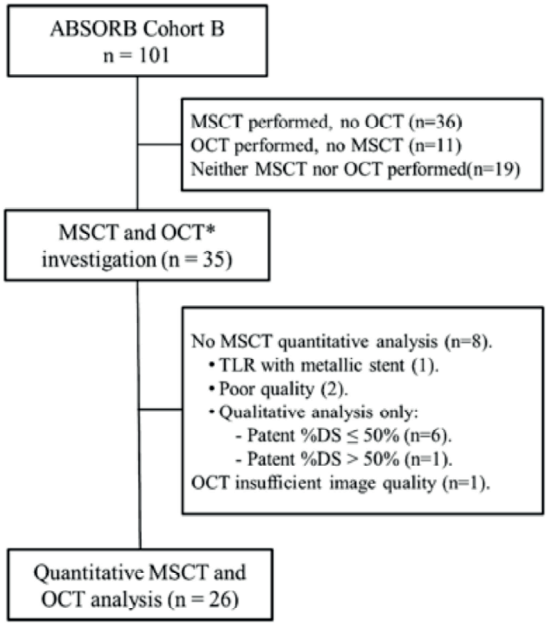

Figure 1. Flowchart of patients included in this analysis. From the overall ABSORB Cohort B cohort (n = 101), 35 patients underwent both coronary CTA and OCT analysis. Eight cases were non-analyzable. For this analysis 26 patients with both image modalities were included. *CTA* computed tomography angiography, *TLR* Target vessel revascularization, *OCT* Optical coherence tomography

Study device and procedure

The BVS balloon-expandable device consists of a polymer backbone of poly-l-lactide (PLLA) coated with a thin layer of a 1:1 mixture of poly(l-lactide-co-d, l-lactide) (PDLLA) polymer and the antiproliferative drug everolimus containing 100 μg everolimus/ cm^2 scaffold. All patients included in this study received a bioresorbable scaffold of 3 mm in diameter and 18 mm in length. The implant is radiolucent but has two platinum markers of 244 μm at each end that allows for easy visualisation on CTA [9]. Both PLLA and PDLLA are fully resorbable [10].

Coronary CTA Acquisition

Coronary CTA angiography was performed with different CT scanners: GE Lightspeed VCT 64-detector [10], Phillips Brilliance 64-detector [4], Siemens Flash 256-detector [15], Phillip Brilliance ICT 256-detector [6]. Standard acquisition techniques were used, which included beta-blockers in patients with heart rate >65 bpm, tube settings depending on patient body mass index (80–140 kV), and axial scan protocols for patients with lower heart rates to reduce radiation doses, all at the discretion of the individual sites [11]. Images were reconstructed using thin slices (0.5–0.67 mm) and medium smooth reconstruction filters in different phases. All data were stored on a DVD for core laboratory evaluation.

Coronary CTA analysis

Data from coronary CTA was analysed off-line by an independent Corelab (Cardialysis BV, Rotterdam, The Netherlands) using a validated cardiovascular analysis package (QAngioCT Research Edition version 3.0.14, Medis, Leiden, The Netherland). Vessel cross-sections were reconstructed at approximately 0.5 mm longitudinal increments, using the platinum scaffold markers as landmarks. Automatic lumen segmentation of the vessel lumen was performed; manual corrections using an attraction points tool was allowed. A window display setting of level 750 Hounsfield units and width 250 Hounsfield units were used for the analysis, and was adjusted if necessary. In addition, gradient images were used to assist the detection of the luminal contour. The minimal lumen area (MLA) was determined for each scaffold. The non-scaffolded lumen area was assessed 5 mm proximal and distal to each marker. To evaluate the concordance in the axial distribution of the MLA, each scaffold of 18 mm length was divided into three segments. The position of the scaffold MLA was measured from the distal radiopaque marker and compared from the distance obtained from OCT. Concordance was defined as localization of the MLA in the same scaffold segments (i.e., proximal, mid and distal). Additionally, to investigate the lumen contour tracing method at the level of the marker cross-section, three strategies were compared based on the agreement with the OCT-derived lumen area. The marker was divided in three parts by 2 parallel lines. Afterward, the extrapolation of the luminal contour through the marker artefact was manually drawn tangential to the first line i.e., closest to the lumen (first strategy), to the centre of the marker (second strategy) and to the second line (third strategy). The gradient image visualization tool was used to identify the centre of the marker.

Optical coherence tomography analysis

OCT acquisitions were performed using three different commercially available systems: the M2 and M3 Time- Domain Systems and the C7XR Fourier-Domain System (LightLab Imaging, Westford, Massachusetts). OCT images were acquired at frame rates of 15.6,

20, and 100 frames/s with pullback speeds of 2, 3, and 20 mm/s in the M2Time-Domain System,M3 Time- Domain System, and C7XR Fourier-Domain System (LightLab Imaging), respectively. All recordings were performed according to the recommended procedure for each OCT system [12]. The OCT measurements were performed with the QCU-CMS software version 4.69 (Leiden University Medical Center, Leiden, The Netherlands) by the core laboratory (Cardialysis BV, Rotterdam, the Netherlands). The following parameters were evaluated: MLA, lumen area at the proximal and distal marker cross-section, and the distance from the distal marker to the MLA. For the proximal and distal reference segments, the luminal area at the non-scaffolded region was measured at 5 mm from the proximal and distal radiopaque markers. Bifurcation segments in which the side branch occupied more than 45° of the cross-section were excluded in order to avoid tracing interpolation when quantifying the lumen [13]. In case the metallic marker of the scaffold could not be identified due to the wire shadow artefact or insufficient flush of blood, the cross-section and the associated proximal or distal edge cross-sections were not included in the analysis.

The primary objective was to assess the accuracy of coronary CTA for the measurement of in-scaffold minimal lumen area with OCT as a reference. The secondary objective was to validate the strategy of coronary CTA luminal contour tracing at the level of the radiopaque markers with matched OCT area as a reference.

Statistical analysis

Binary variables are presented as percentages and continuous variables as mean and standard deviation or median and interquartile range, as appropriate. Continuous variables with normal distributions were compared using *t* test. The level of agreement between methods at the cross-section level was determined using the Bland–Altman method and the Passing-Bablok regression analysis [14]. For the Bland–Altman method, data are given as plots showing the absolute difference between corresponding measurements of both methods (y-axis) against the average of both methods (x-axis). Accuracy was defined as the mean difference between OCT and coronary CTA and precision as the standard deviation of the difference. The 95% limits of agreement were calculated as mean bias $\pm$ 1.96 $\times$ standard deviation. For the Passing-Bablok regression analysis, the α and β coefficient assess for the systematic and proportional differences. If 0 is in the confident interval (CI) of α, and 1 is in the CI of β, the two methods are comparable. If 0 is not in the CI of α there is a systematic difference and if 1 is not in the CI of β then there is a proportional difference between the two methods. Intra and inter-observer variability were assessed using intra-class correlation coefficients. All statistical analyses were performed with SPSS software version 23.0 (IBM, Armonk, New York). This study was funded by Abbott Vascular.

RESULTS

Overall, 35 patients with both OCT and coronary CTA evaluations were included in this analysis. Baseline clinical and lesions characteristics are shown in Table 1. The mean age was 63.2 ± 9.0 years and 77% were male. The Left Anterior Descending artery was the most frequent treated vessel in 46% of the cases. Lesions were classified according to AHA/ACC as B1 and B2 in 90% of the cases. Images were acquired with a mean difference of 182 ± 19 days. CTA images were acquired with a mean heart rate of 53.8 ± 6.82 bpm. Coronary CTA quantitative analysis in the scaffold region was possible in 26 cases (76%) (Fig. 1). There were no systematic or proportional differences in minimum luminal area assessment between OCT and coronary CTA (4.48 ± 1.57 mm^2 OCT versus 4.04 ± 1.35 mm^2 coronary CTA, α coefficient −1.12 95% CI −4.78 to 0.66, β coefficient 1.12 95% CI 0.70 to 1.9) respectively. Coronary CTA underestimated luminal area by 9.8% in both scaffolded and non-scaffolded segments. In the scaffolded region, the accuracy and precision of coronary CTA at the MLA was 0.39 ± 1.0 mm^2 (95% limits of agreements −1.71 to 2.50 mm^2). In addition, the analysis of 31 matched cross-sections in the non-scaffolded segments at the proximal and distal edge showed similar level of agreement compared

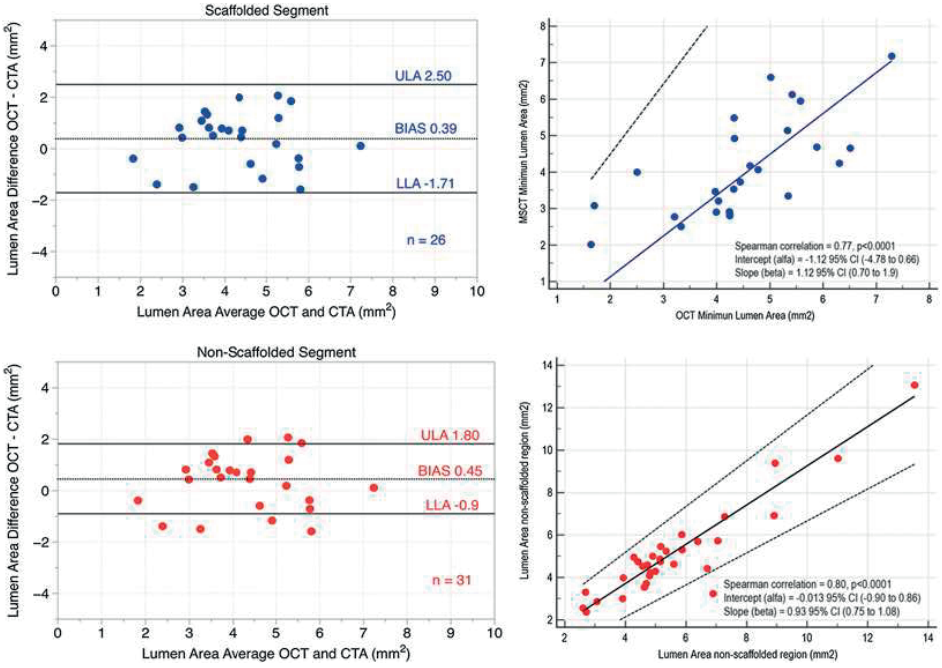

Figure 2. (Left side) Bland–Altman plots of the mean diferences in luminal areas between optical coherence tomography CTA in scaffolded (top) and non-scafolded segments (bottom). In the right side of the scatterplots with passing-Bablok analysis between modalities in both scafolded (top) and non-scafolded segments (bottom)

to the scaffolded region (accuracy 0.45 ± 0.70 mm^2, limits of agreement −0.92 to 1.82 mm^2, α coefficient −0.013 95% CI −0.9 to 0.86, β coefficient 0.93 95% CI 0.75–1.08) (Fig. 2). Concordance of axial in-scaffold MLA localization was observed in 77% of the cases (Case example Fig. 3). The intra-class correlation coefficient of in-scaffold MLA measurements for inter-observer agreement was 0.98 (95% CI 0.93–0.99; $p < 0.001$) and 0.98 (95% CI 0.94–0.99) for intra-observer agreement

Luminal assessment at the level of the radiopaque marker

Forty cross sections at the level of the radiopaque marker were evaluated (16 were excluded due to impossibility to identify the marker using OCT (n = 13) and overlap with a metallic stent (n = 3)). When the luminal contour was traced across the centre

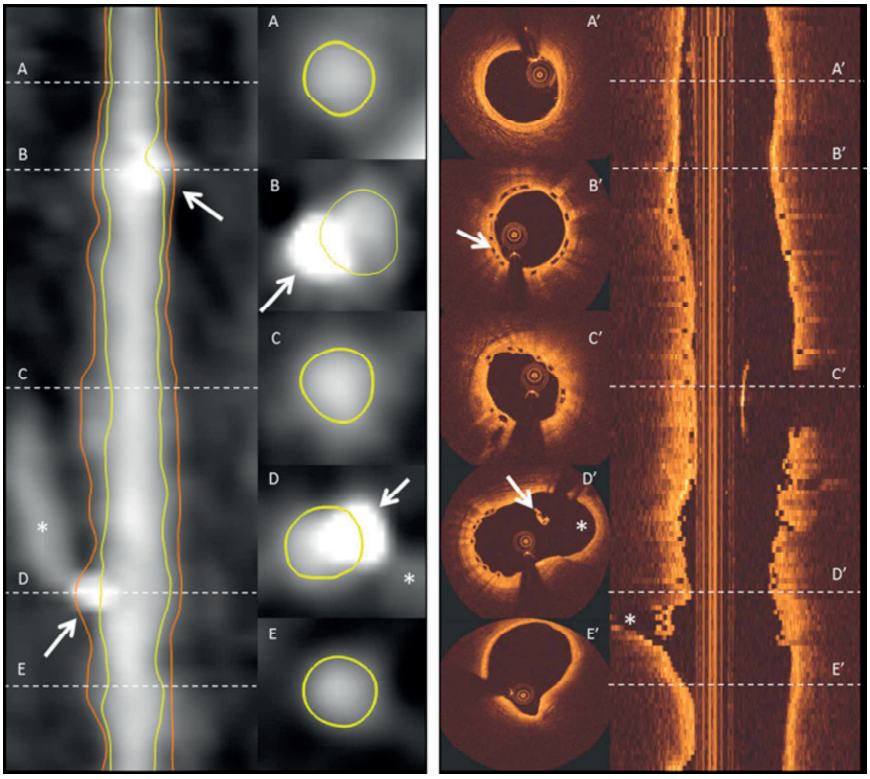

Figure 3. Case example of an coronary CTA straight multiplanar reconstruction image and optical coherence tomography correlating matched luminal areas at the scafold and non-scafolded segments. Panels a, a'and e, e' show the vessel lumen at the non-scafolded segments. Panels b, b' and d, d'show the cross-section at the level of the radiopaque markers, and panel c and c'correspond to the MLA. The MLA with coronary CTA (c) was 3.4 mm^2 and with 4.0 mm^2 with OCT (c'). The markers are shown with white arrows and a white stars identify the sidebranch. *CTA* computed tomography angiography, *MLA* Minimal lumen area

Table 1 Baseline characteristics

	Overall (n = 35)
Age (mean ± SD), years	63.2 ± 9.0
Male sex, n (%)	27 (77)
Diabetes mellitus, n (%)	2 (3)
Current smoker n (%)	9 (25)
Hyperlipidemia requiring medication, n (%)	27 (77)
Hypertension, n (%)	21 (60)
Prior PCTA, n (%)	7 (20)
Prior myocardial infarction, n (%)	10 (29)
Treated vessel	
Left anterior descending, n (%)	16 (46)
Left circumflex, n (%)	8 (23)
Right coronary artery, n (%)	11 (31)
AHA/ACC lesion classification	
A, n (%)	1 (3)
B1, n (%)	17 (48)
B2, n (%)	15 (42)
C, n (%)	2 (6)
Mean reference vessel diameter, (mm)	2.53 ± 0.57
Minimum luminal diameter, (mm)	1.05 ± 0.29
Diameter stenosis, (%)	56 ± 13.7

of the radiopaque marker (i.e., second strategy) the coronary CTA-derived lumen area showed a mean difference of the 0.48 mm^2 (limits of agreements −1.55 to 2.51 mm^2) with OCT-derived matched area as a reference. The inclusion in the luminal segmentation of one-third (first strategy) and two-thirds (third strategy) showed a mean difference of 1.21 mm^2 (limits of agreements −0.68 to 3.11 mm^2), and −0.58 mm^2 (limits of agreements −2.95 to 1.74 mm^2), respectively (Fig. 4). Figure 5 shows the overall agreement in MLA and marker cross-section luminal areas between OCT and coronary CTA.

DISCUSSION

The main findings of this analysis are (1) At 18 months, coronary CTA-derived in-scaffold minimal lumen area showed good agreement with OCT-derived minimal lumen area; (2) At the level of the marker with the blooming artefact, luminal segmentation through the centre of the marker showed the best agreement with the matched OCT-derived area; and (3) There was similar agreement between luminal measurement at the scaffolded and non-scaffolded segments.

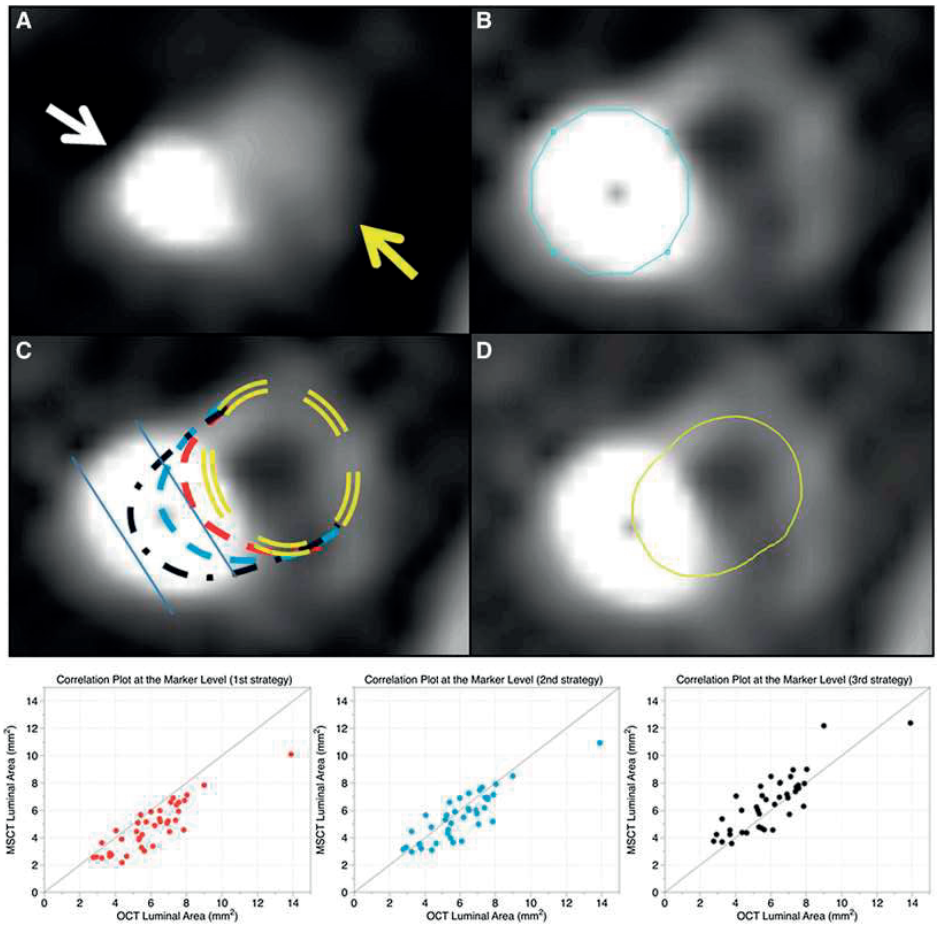

Figure 4. a) Cross-section at the level of the radiopaque marker with the blooming artefact (white arrows) and the coronary artery lumen (yellow arrow). b) CT-gradient image at the same cross-section, the radiopaque marker (blue line, area of 2.5 mm^2) is readily identified. c) Three strategies evaluated to measure the agreement between coronary CTA and OCT derived luminal areas (yellow double dash lines represents the position of the lumen with respect to the marker artefact); the first strategy in red dash line included in the luminal area 1.1 mm^2 of the blooming artefact without crossing the center of the marker; the second strategy in blue dash line included 2.3 mm^2 of the blooming artefact and crossed the center of the marker and the third strategy in black dash line included 3.2 mm^2 of the blooming artefact and the center of the marker. d) Contour tracing methods with the best agreement (second strategy, blue line) with the OCT-derived matched lumen area. In the bottom, the three tracing strategies are plotted against the OCT-derived lumen area. CTA computed tomography angiography, OCT optical coherence tomography

Non-invasive coronary CTA have demonstrated high accuracy for the evaluation of native coronary vessels compared to invasive coronary angiography. In the landmark multicentre CORE-64 study, coronary CTA showed high diagnostic accuracy for the detection of coronary lesions with diameter stenosis ≥50% [15]. Moreover, a meta-

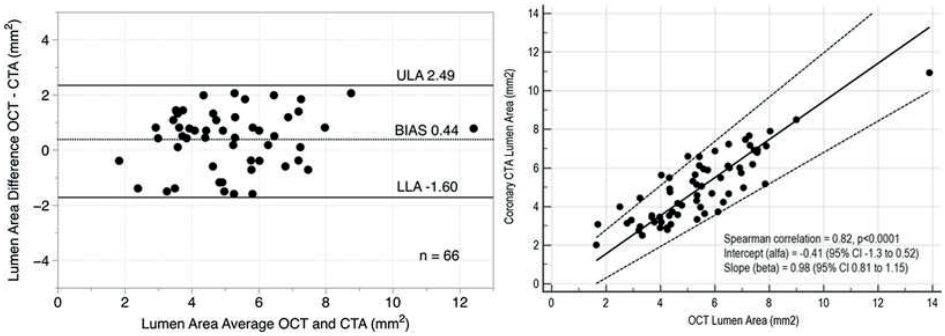

Figure 5. Bland–Altman scatter plot and Passing-Bablok analysis depicting the global agreement (MLA and radiopaque marker crosssection) between OCT and coronary CTA for quantitative luminal area assessment. *CTA* computed tomography angiography, *MLA* minimal lumen area, *OCT* optical coherence tomography

analysis assessing the accuracy of coronary CTA to measure coronary luminal area at the cross-section level found an excellent agreement (mean difference of 0.23 mm^2, CI 95% −0.07 to 0.48) compared to IVUS [16]. In this study, coronary CTA underestimated in-scaffold MLA by 0.39 mm^2 compared to OCT (4.48 ± 1.57 mm^2 OCT versus 4.04 ± 1.35 mm^2 CTA). Similar agreement was observed in the non-scaffolded region (mean difference 0.45 mm^2, limits of agreement −0.92 to 1.82 mm^2). These findings are comparable with previous reports comparing luminal areas derived from IVUS and coronary CTA in native coronary vessels [16].

Coronary CTA evaluation in segments treated with metallic stents is hampered by the presence of the metal; whereas the polymeric struts of the biodegradable scaffold do not interfere with non-invasive luminal evaluation [17]. Moreover, high concordance in axial MLA localization (77%) was observed. In three of the six cases with discordant MLA localization between modalities, the MLA derived from the OCT was at the level of the radiopaque marker. At this level, the blooming artefact from the radiopaque marker might have interfered with an appropriate luminal evaluation by coronary CTA; therefore, contributing to the relocation of the MLA.

The focal partial volume averaging and bean hardening artefacts at the scaffold marker cross-section makes coronary luminal segmentation challenging. Two 244 micron platinum markers at each site of scaffold create a blooming artefact leading to an artificial increase in the size of the structure that precludes appropriate visualization of the lumen boundary. At the marker cross-section, we reported the agreement between three coronary CTA luminal segmentation tracing strategies. The inclusion of the centre of the marker in the luminal area was associated with the higher accuracy (0.48 mm^2, 95% limits of agreements −1.55 to 2.51 mm^2). This is technically relevant, since automated luminal contour detection algorithms might recognized the blooming artefact

of the marker with high Hounsfield units (mean 1435 ± 412 HU) as dense calcium and exclude it from the lumen creating a systematic underestimation of the luminal area at the marker cross-section. Therefore, manual correction of the luminal contour in needed at this level. The accuracy of in-scaffold quantitative luminal analysis observed in this study supports the use of coronary CTA as the modality of choice for the follow-up of patients treated with bioresorbable vascular scaffolds. Also, the validation of the tracing methods through the center of the radiopaque marker provides further guidance for the quantitative segmentation of the lumen vessel.

To our knowledge this is the first study comparing coronary CTA in-scaffold luminal area dimensions with OCT. The small bias in the assessment of a clinically relevant non-ambiguous parameter, such as MLA, supports the use of coronary CTA angiography as an alternative method to quantify non-invasively in-scaffold luminal area and to further processing using computational fluid dynamics [18]. Indeed, non-invasive coronary CTA angiography have proven to the an accurate tool to assess endothelial shear stress and non-invasive fractional flow reserve [19, 20]. In the NXT Trial (Analysis of Coronary Blood Flow Using CT Angiography: Next Steps), coronary CTA-derived fractional flow reserve demonstrated high per-patient sensitivity 86% (95% CI 77–92%) and specificity 79% (95% CI 72–84%) to identify myocardial ischemia compared to invasive FFR [20]. In addition, Bourantas et al. have shown that coronary CTA-derived low shear stress correlates with coronary plaque progression in 3 years of follow up [21].

Limitations

The main limitation of this study in the inclusion of non-complex, non-calcified lesion in which coronary CTA has proven to have higher accuracy; therefore, this finding should be confirmed in a more complex population [22]. Also, the low incidence of in-scaffold restenosis limits the conclusion of this analysis to patent scaffolds. Moreover, the 3 mm scaffold diameter included in this study might have facilitated the quantitative assessment The accuracy of coronary CTA to investigate the commercially available 2.5 mm diameter scaffold is still unknown. Image acquisition was not performed at the same time; therefore, introducing a confounding factor. Nevertheless, the serial invasive angiography analysis in this population reported stable luminal dimensions in the timeframe evaluated in this study (i.e., after 12 months) [1]. And finally, due to the limitation in spatial resolution of coronary CTA coronary cross-section matched by OCT and coronary CTA may not be exactly identical.

CONCLUSION

Compared with OCT, coronary CTA appears to be accurate for the estimation of in-scaffold minimal lumen area 18-month post-implantation, with no difference compared to the non-scaffolded region.

REFERENCES

1. Serruys PW, Ormiston J, van Geuns RJ, de Bruyne B, Dudek D, Christiansen E et al (2016) A Polylactide bioresorbable scaffold eluting everolimus for treatment of coronary stenosis: 5-year follow-up. J Am Coll Cardiol 67(7):766–776
2. Stone GW, Gao R, Kimura T, Kereiakes DJ, Ellis SG, Onuma Y et al (2016) 1-year outcomes with the Absorb bioresorbable scaffold in patients with coronary artery disease: a patient-level, pooled meta-analysis. The Lancet 387(10025):1277–1289
3. Serruys PW, Chevalier B, Dudek D, Cequier A, Carrie D, Iniguez A et al (2015) A bioresorbable everolimus-eluting scaffold versus a metallic everolimus-eluting stent for ischaemic heart disease caused by de-novo native coronary artery lesions (ABSORB II): an interim 1-year analysis of clinical and procedural secondary outcomes from a randomised controlled trial. Lancet 385(9962):43–54
4. Onuma Y, Dudek D, Thuesen L, Webster M, Nieman K, Garcia-Garcia HM et al (2013) Five-year clinical and functional multislice computed tomography angiographic results after coronary implantation of the fully resorbable polymeric everolimus-eluting scaffold in patients with de novo coronary artery disease: the ABSORB cohort A trial. JACC Cardiovasc Interv 6(10):999–1009
5. Gutierrez-Chico JL, Serruys PW, Girasis C, Garg S, Onuma Y, Brugaletta S et al (2012) Quantitative multi-modality imaging analysis of a fully bioresorbable stent: a head-to-head comparison between QCA, IVUS and OCT. Int J Cardiovasc Imaging 28(3):467–478
6. Serruys PW, Onuma Y, Dudek D, Smits PC, Koolen J, Chevalier B et al (2011) Evaluation of the second generation of a bioresorbable everolimus-eluting vascular scaffold for the treatment of de novo coronary artery stenosis: 12-month clinical and imaging outcomes. J Am Coll Cardiol 58(15):1578–1588
7. Nieman K, Serruys PW, Onuma Y, van Geuns RJ, Garcia-Garcia HM, de Bruyne B et al (2013) Multislice computed tomography angiography for noninvasive assessment of the 18-month performance of a novel radiolucent bioresorbable vascular scaffolding device: the ABSORB trial (a clinical evaluation of the bioabsorbable everolimus eluting coronary stent system in the treatment of patients with de novo native coronary artery lesions). J Am Coll Cardiol 62(19):1813–1814
8. Zhang YJ, Iqbal J, Nakatani S, Bourantas CV, Campos CM, Ishibashi Y et al (2014) Scaffold and edge vascular response following implantation of everolimus-eluting bioresorbable vascular scaffold: a 3-year serial optical coherence tomography study. JACC Cardiovasc Interv 7(12):1361–1369
9. Suwannasom P, Onuma Y, Campos CM, Nakatani S, Ishibashi Y, Tateishi H et al (2015) Fate of bioresorbable vascular scaffold metallic radio-opaque markers at the site of implantation after bioresorption. JACC Cardiovasc Interv 8(8):1130–1132
10. Onuma Y, Serruys PW (2011) Bioresorbable scaffold: the advent of a new era in percutaneous coronary and peripheral revascularization? Circulation 123(7):779–797
11. Leipsic J, Abbara S, Achenbach S, Cury R, Earls JP, Mancini GJ et al (2014) SCCT guidelines for the interpretation and reporting of coronary CT angiography: a report of the Society of Cardiovascular Computed Tomography Guidelines Committee. J Cardiovasc Comput Tomogr 8(5):342–358
12. Tearney GJ, Regar E, Akasaka T, Adriaenssens T, Barlis P, Bezerra HG et al (2012) Consensus standards for acquisition, measurement, and reporting of intravascular optical coherence tomography studies: a report from the International Working Group for intravascular optical coherence tomography standardization and validation. J Am Coll Cardiol 59(12):1058–1072
13. Bezerra HG, Attizzani GF, Sirbu V, Musumeci G, Lortkipanidze N, Fujino Y et al (2013) Optical coherence tomography versus intravascular ultrasound to evaluate coronary artery disease and percutaneous coronary intervention. JACC Cardiovasc Interv 6(3):228–236

14. Altman DG, Bland JM (1986) Comparison of methods of measuring blood pressure. J Epidemiol Community Health 40(3):274–277
15. Arbab-Zadeh A, Miller JM, Rochitte CE, Dewey M, Niinuma H, Gottlieb I et al (2012) Diagnostic accuracy of computed tomography coronary angiography according to pre-test probability of coronary artery disease and severity of coronary arterial calcification. The CORE-64 (coronary artery evaluation using 64-row multidetector computed tomography angiography) International Multicenter Study. J Am Coll Cardiol 59(4):379–387
16. Fischer C, Hulten E, Belur P, Smith R, Voros S, Villines TC (2013) Coronary CT angiography versus intravascular ultrasound for estimation of coronary stenosis and atherosclerotic plaque burden: a meta-analysis. J Cardiovasc Comput Tomogr 7(4):256–266
17. Rief M, Zimmermann E, Stenzel F, Martus P, Stangl K, Greupner J et al (2013) Computed tomography angiography and myocardial computed tomography perfusion in patients with coronary stents: prospective intraindividual comparison with conventional coronary angiography. J Am Coll Cardiol 62(16):1476–1485
18. Sankaran S, Kim HJ, Choi G, Taylor CA (2016) Uncertainty quantification in coronary blood flow simulations: impact of geometry, boundary conditions and blood viscosity. J Biomech 49(12):2540–2547
19. Hetterich H, Jaber A, Gehring M, Curta A, Bamberg F, Filipovic N et al (2015) Coronary computed tomography angiography based assessment of endothelial shear stress and its association with atherosclerotic plaque distribution in-vivo. PLoS One 10(1):e0115408
20. Norgaard BL, Leipsic J, Gaur S, Seneviratne S, Ko BS, Ito H, et al (2014) Diagnostic performance of noninvasive fractional flow reserve derived from coronary computed tomography angiography in suspected coronary artery disease: the NXT trial (analysis of coronary blood flow using CT angiography: next steps). J Am Coll Cardiol 63(12):1145–1155
21. Bourantas CV, Papadopoulou SL, Serruys PW, Sakellarios A, Kitslaar PH, Bizopoulos P et al (2015) Noninvasive prediction of atherosclerotic progression: the PROSPECT-MSCT Study. JACC Cardiovasc Imaging 9(8):1009–1011
22. Toepker M, Schlett CL, Irlbeck T, Mahabadi AA, Bamberg F, Leidecker C et al (2010) Accuracy of dual-source computed tomography in quantitative assessment of low density coronary stenosis: a motion phantom study. Eur Radiol 20(3):542–548

Chapter 14

Imaging Outcomes of Bioresorbable Scaffold Overlap: An Optical Coherence Tomography Analysis from the ABSORB EXTEND Trial

Yohei Sotomi, Pannipa Suwannasom, Chiung-Jen Wu, Hiroki Tateishi, Wai-Fung Cheong, Wei-Ying Zhao, Susan Veldhof, Joanna J. Wykrzykowska, Robbert J. de Winter, Vasim Farooq, Alexandre Abizaid, Patrick W. Serruys, Yoshinobu Onuma

AsiaIntervention 2017;3:1-9

ABSTRACT

Aim

The purpose of this study is to assess the vascular response and vessel healing of overlapped Absorb scaffolds (Abbott Vascular, Santa Clara, California) compared to non-overlapped devices in human coronary arteries assessed by optical coherence tomography (OCT) in the same treated segment.

Methods and results

The ABSORB EXTEND [NCT01023789] trial is a prospective, single-arm, open-label clinical study which enrolled 800 patients. The planned overlap OCT subgroup in the ABSORB EXTEND was analyzed and two-year OCT follow-up was performed in 7 patients. In cross-section level analysis at baseline, lumen and abluminal scaffold areas were larger in overlap segments than in non-overlap segments, whereas endoluminal scaffold area was similar. At 2-year follow-up, lumen area and endoluminal scaffold areas were similar in both segments despite the neointimal area being larger in the overlap segments. The neointimal coverage was essentially fully complete in both non-overlap (99.4±0.8%) and overlap segments (99.8±0.4%) at 2-year follow-up.

Conclusions

The imaging results of this small OCT subgroup analysis in ABSORB EXTEND demonstrated substantial vessel healing and vascular response in the overlap segment of Absorb at 2-year follow-up comparable to the non-overlap segment.

INTRODUCTION

Overlap of Absorb scaffolds (Absorb BVS, Abbott Vascular, Santa Clara, California) is generally associated with a couple of issues: 1) Technically, thick struts (157 μm) could hinder implantation of the second Absorb device, which could result in difficult scaffold delivery or disruption of struts. 2) Overlap might be associated with increased risk of peri-procedural myocardial infarction. In the ABSORB II trial (n=501), treatment with overlap devices was the only independent determinant of peri-procedural myocardial infarction (Odds ratio: 5.07, 95% CI: 1.78-14.41, p=0.002).[1] 3) Animal study suggested delayed coverage of overlapping struts. In a juvenile porcine model, the overlapping Absorb scaffolds showed more delayed in tissue coverage than in non-overlap scaffolds [2].

The segments with overlapped scaffolds are possibly associated with delayed healing and greater neointimal growth compared to the segments with no overlapped scaffolds (non-overlap segments), which could result in smaller luminal dimension at follow-up. [2] However, the vessel healing and vascular response at segments with overlapped Absorb BVS in human coronary arteries have, thusfar, not yet been precisely evaluated by optical coherence tomography (OCT).

The purpose of the current study was to assess by OCT the vascular response and vessel healing in the Absorb scaffold overlap segments compared to the non-overlap segments in human coronary arteries.

METHODS

Study design

The ABSORB EXTEND Trial is a prospective, single-arm, open-label clinical study that has enrolled 812 patients at up to 100 global sites [NCT01023789]. Details on the study and the study device (Absorb BVS;Abbott Vascular) have been described previously. [3] Initially, a subset of up to 50 patients who receive planned overlapping Absorb BVS at selected sites with OCT capability was planned to be included in the OCT subgroup. In this OCT subgroup, OCT imaging after the BVS implantation and at 2-year follow-up were mandated in all patients. Despite the initial plan to include 50 patients with planned overlap, the actual OCT subgroup included only 14 patients. The main reasons were: i) small number of sites due to limited availability of OCT at the time of the study initiation in 2009; ii) prematured termination of the study; iii) low patient consent rate due to invasive imaging follow-up. The need for planned overlapping of BVS was determined by the investigator at the time of the index procedure.

The research ethics committee of each participating institution approved the protocol and all enrolled patients provided written informed consent before inclusion.

OCT Methodology

The image acquisition was performed with C7XR™ imaging console and the Dragonfly™ intravascular imaging catheter (both St. Jude Medical, St. Paul, MN, USA). Analysis of the OCT images was performed with the QCU-CMS software (Medis, Leiden, The Netherlands), using the methodology for BVS analysis described in the previous publication. [4] All analyses were performed at 1 mm longitudinal intervals within the non-overlap segment, and at 0.2 mm intervals within the overlap segment. In addition, the analysis for scaffold coverage was performed at 0.2 mm intervals in the whole scaffold segment.

Details of OCT analysis are illustrated in Figure 1. Definitions of OCT parameters were described in a previous publication.[4] Specifically in overlap segments, at baseline, the struts of the first (outer) and second (inner) scaffolds could appear stacked or overhanging. The strut of the inner scaffold could look malapposed in a cross-section, but it does not necessarily stand for absence of contact with other structures, since such struts are touching the other scaffold (Figure 1). [5] As a surrogate of vessel stretch, the abluminal side of the outer scaffold area ratio was calculated as the ratio of mean abluminal scaffold area of the outer scaffold in the overlap segment to the mean abluminal area of the single scaffold implanted in the adjacent non-overlap segments (5 mm of both sides). The endoluminal scaffold area ratio was also computed in the same way. At 2 years, the scaffold has already lost its mechanical integrity and could present late discontinuities as expected from the bioresorption process.[6] Therefore, it is not always possible to differentiate in an overlap segment the two layers of struts. In the current study, the analysis delineated the inner and outer contour of the struts without the distinction of two scaffolds. Wherever two struts were overhanging or stacked, the abluminal (endoluminal) border of outer (inner) struts were used to define the abluminal (endoluminal) scaffold contour (Figure 1).

With respect to coverage analysis, when the coverage thickness (the shortest distance from lumen contour to the endoluminal border of the strut black core) was ≥ 30μm in polymeric struts, the strut was defined as a covered strut. To allow full visualization of the spatial distribution of neointimal thickness and coverage status in the overlap devices, "spread-out-vessel graphs" – a visual representation of the vessel as if it had been cut along the reference angle (0°) and spread out on a flat surface – were created based upon previously described methodologies. [7]

Clinical follow-up

Definitions of all clinical endpoints were described elsewhere.[3] All study endpoint events were adjudicated by an independent clinical events committee (CEC) according to either protocol definitions and/or the Academic Research Consortium (ARC) definitions. All adverse events were reported to an independent data and safety monitoring board (DSMB), which reviewed the data to identify any safety issues related to the conduct of the study.

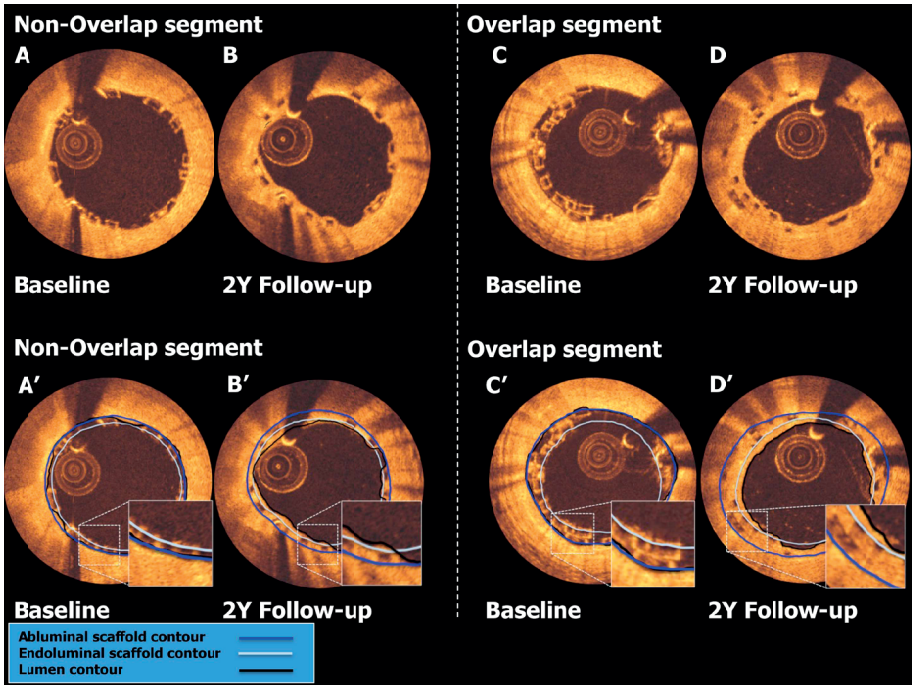

Figure 1. OCT methodology.
A) – D) Baseline and follow-up OCT images in the non-overlap and overlap segments, respectively. In the nonoverlap segment, the previously published methodology was applied (A′, B′)[4]. In the overlap segment, the endoluminal scaffold contour was drawn using the midpoint of the endoluminal black core border of "inner struts" at baseline (C′) and follow-up (D′). The abluminal scaffold contour was drawn using the midpoint of the abluminal black core border of "outer struts" at baseline (C′) and follow-up (D′).

Table 1. Diameter of target vessel(s), length of target lesion(s) and Absorb BVS size used.

Target Vessel Diameter Distal Dmax and Proximal Dmax	Length of target lesion(s)	BVS Size To Be Used
≥ 2.0 mm and ≤ 3.0 mm	≤ 14 mm	Single 2.5 x 18 mm
	> 14 mm and ≤ 22 mm	Single 2.5 x 28 mm
	> 22 mm and ≤ 28 mm	Two overlap 2.5 x 18 mm
≥ 2.5 mm and ≤ 3.3 mm	≤ 14 mm	Single 3.0 x 18 mm
	> 14 mm and ≤ 22 mm	Single 3.0 x 28 mm
	> 22 mm and ≤ 28 mm	Two overlap 3.0 x 18 mm
≥ 2.0 mm and ≤ 2.5 mm (Distal Dmax) ≥ 3.0 mm and ≤ 3.3 mm (Proximal Dmax)	> 22 mm and ≤ 28 mm	Overlap 2.5 x 18 with 3.0 x 18 mm

Table 2. Patient characteristics

Variables	N = 14
Baseline characteristics	
Age (years)	62±9
BMI (kg/m^2)	27.3±4.3
Male Sex, n (%)	12 (85.7)
Current Smoker, n (%)	2 (14.3)
Any Diabetes, n (%)	1 (7.1)
Diabetes Treated with Insulin, n (%)	0 (0)
Hypertension Requiring Medication, n (%)	7 (50.0)
Hypercholesterolemia Requiring Medication, n (%)	7 (50.0)
Prior MI, n (%)	2 (14.3)
Stable Angina, n (%)	13 (92.9)
Unstable Angina, n (%)	1 (7.1)
Lesion data	
Lesion location LAD/LCX/RCA	5/5/4
Lesion Class (ACC/AHA) A/B1/B2/C	0/6/7/1
Angulation (≥ 45°), n (%)	1 (7.1)
Calcification (Moderate or Severe), n (%)	2 (14.3)
Bifurcation, n (%)	3 (21.4)
Eccentric, n (%)	14 (100)
Pre-Procedure Thrombus, n (%)	0 (0)
Procedural data	
Pre dilatation, n (%)	14 (100)
Balloon diameter (mm)	2.61±0.28
Balloon pressure (atm)	13.7±3.2
Post dilatation, n (%)	9 (64.3)
Compliant balloon, n (%)	4 (29)
Non-compliant balloon, n (%)	5 (36)
Balloon diameter (mm)	3.14±0.17
Balloon pressure (atm)	17.3±4.0
Device, n (%)	
2.5x18; 2.5x18mm	1 (7.1)
3x18; 3x18mm	12 (85.7)
3.5x18; 3.5x18mm	1 (7.1)
Bailout with Xience PRIME (3.5x18mm), n (%)	2 (14.3)
Side branch occlusion, n (%)	1 (7.1)
Overlap length (mm) by post-procedural OCT	4.0 [2.0, 7.4]
Acute success, n (%)	14 (100)
QCA data	
Pre-procedural lesion length (mm)	15.1 [8.2, 21.0]
Pre-procedural RVD (mm)	2.5 [2.26, 2.55]

Table 2. Patient characteristics (continued)

Variables	N = 14
Pre-procedural DS% (%)	56.9±14.8
Post-procedural in-device DS% (%)	18.0±6.3
In-device acute gain (mm)	0.99±0.39

Data are expressed as mean ± standard deviation, number (frequency), and median [interquartile range]. BMI: body mass index; DS%: percent diameter stenosis; LAD: left anterior descending artery; LCX: left circumflex artery; MI: myocardial infarction; OCT: optical coherence tomography; QCA: quantitative coronary angiography; RCA: right coronary artery; RVD: reference vessel diameter

Statistical analysis

The normality of distribution of continuous data was examined with the Shapiro-Wilk test. Continuous variables with normal distribution are expressed as means ± standard deviations and those with unequal variance are expressed as medians and interquartile ranges [25th and 75th percentiles]. Categorical variables are expressed as numbers and frequencies. Group means for continuous variables with normal and non-normal distributions were compared using Student's *t*-test and Mann–Whitney *U*-test, respectively. Categorical variables were compared using the χ^2 test or Fischer's exact test, where appropriate. A mixed linear model with an assumed Gaussian distribution was used for the comparisons of continuous variables to take into an account the clustered nature of >1 struts and cross-sections analyzed from the same lesion, which might result in unknown correlations among measurements within the clusters. Statistical significance was assumed at a probability (*P*) value of <0.05. All statistical analyses were performed with SPSS (version 22.0.0, IBM, New York).

RESULTS

In the whole ABSORB EXTEND trial (N = 812), a total of 14 patients were enrolled in the planned overlap population (OCT subgroup). In these 14 patients, 1 patient died due to non-cardiac cause, and 13 patients underwent 2 years clinical followed-up. The median duration of follow-up was 748 [729-755] days. The baseline OCT data of 1 patient was not analyzable due to the poor image quality. Two-year invasive OCT follow-up was performed only in 7 patients.

Patient demographic data and procedural data

The baseline characteristics of the patients and procedural data are summarized in Table 2. A sensitivity analysis comparing baseline characteristics of patients with and without OCT surveillance at follow-up demonstrated that there was no significant difference between these cohorts.

Table 3. Baseline OCT data (13 cases)

	Non-Overlap Segment (N = 13*)	Overlap Segment (N = 13*)	P value
Baseline			
Total number of Struts, n	2571	4382	
Number of Struts per lesion, n	198±52	337±267	0.077
Lesion level analysis	N = 13	N = 13	
Lumen Area(mm^2)	7.00±0.92	7.96±1.37	0.046
Abluminal Scaffold Area(mm^2)	7.30±0.96	8.04±1.19	0.095
Endoluminal Scaffold Area(mm^2)	6.31±0.86	6.35±1.07	0.926
Strut Core Area(mm^2)	0.20±0.03	0.43±0.06	<0.001
Flow Area(mm^2)	6.80±0.90	7.53±1.36	0.118
Cross-section level analysis	N = 339	N = 324	
Lumen Area(mm^2)	6.98±1.26	7.94±1.24	<0.001
Abluminal Scaffold Area(mm^2)	7.29±1.30	8.01±1.10	<0.001
Endoluminal Scaffold Area(mm^2)	6.31±1.18	6.29±0.97	0.568
Strut Core Area(mm^2)	0.20±0.08	0.44±0.16	<0.001
Flow Area(mm^2)	6.78±1.24	7.50±1.22	<0.001

Data are expressed as mean ± standard deviation and number.
*The OCT baseline data (Case 14) was not analyzable due to poor quality of image.

Quantitative OCT findings at baseline and 2-year follow-up.

Table 3 shows the quantitative OCT findings at baseline in 13 patients at lesion level and cross-section level analyses. At cross section level analysis, no significant difference in endoluminal scaffold area was observed (6.31±1.18 mm^2 vs. 6.29±0.97 mm^2, p=0.568) between overlap and non-overlap segments.

Table 4 tabulates the quantitative OCT findings at baseline and 2-year follow-up in 7 patients with both baseline and follow-up OCT data. The time interval to OCT follow-up was 742 [724-754] days. At 2-year follow-up, both non-overlap and overlap segments presented with similar lumen area, abluminal scaffold area, endoluminal scaffold area, flow area, and neointimal area in lesion level analysis.

Serial changes of abluminal/endoluminal scaffold areas and flow area between the overlap segment and its margin (10 mm) are illustrated in the graph of Figure 2 (Representative Case 6 in Figure 3). Serial changes of all the cases (margin: 5mm) are shown in Figure 3. Post-dilatation was performed in 5 out of the 7 patients. Abluminal and endoluminal scaffold area ratios were 1.12±0.07 and 1.03±0.06, respectively. Outward vessel enlargement was still maintained at 2-year follow-up despite being after the disappearance of scaffold radial strength (12 months).

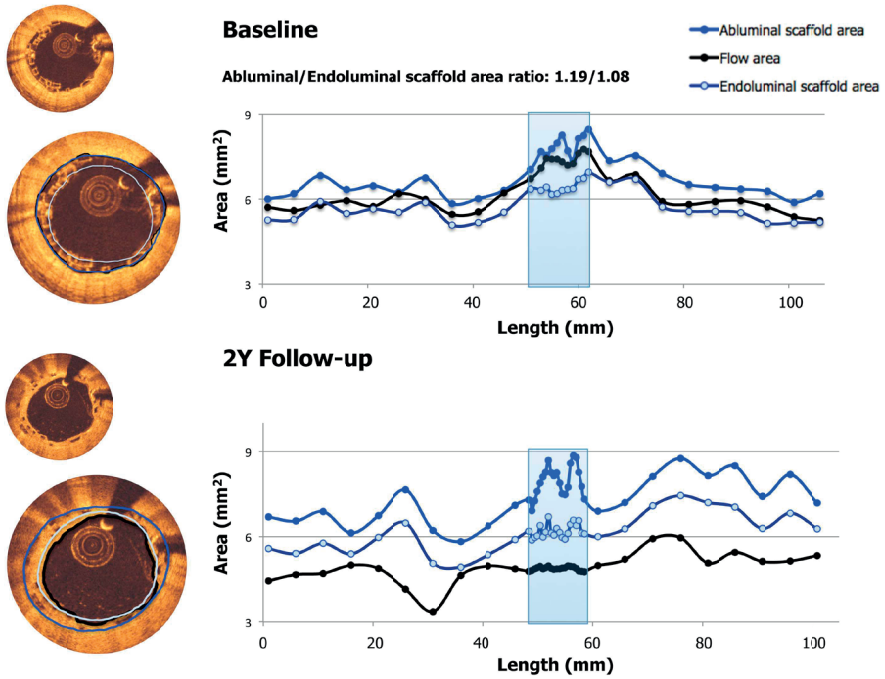

Figure 2. Vessel-scaffold interaction in overlap and non-overlap segments. Vessel-scaffold interaction in overlap and non-overlap segments of a representative case (case 6 in Figure 3) is indicated with OCT analysis images. The horizontal axis indicates the length of the lesion from distal to proximal. The vertical axis indicates the area of each cross-section (black: flow area; dark blue: abluminal scaffold area; light blue: endoluminal scaffold area). The overlap segment (blue shadow) and both 10 mm margins are illustrated.

Regarding the strut coverage analysis, 7828 struts in non-overlap segments and 1801 struts in overlap segments were analyzed. The neointimal coverage was almost completed in both segments at 2-year follow-up (Coverage rate in non-overlap segment vs. overlap segment, 99.4±0.8% vs. 99.8±0.4%, p=0.360). Spread-out-vessel graphs represent the spatial distribution of the neointimal thickness and coverage status along each overlap segment and non-overlap segments at 2-year follow-up (Figure 4).

Adverse event

The rate of ischaemia-driven(ID)major adverse cardiac event (all cardiac death, all myocardial infarction, or ischaemia-driven target lesion revascularization) at 2 years was 0% in the OCT subgroup. Preprocedural and post-procedural blood sample tests for cardiac enzymes (creatine kinase, creatine kinase-myocardial band, and troponin) were performed in 12 (85%) patients, and the periprocedural myocardial infarction rate (per protocol criteria) was 0 %. Of the 14 patients, 13 patients were on dual antiplatelet therapy at 1 year (1 patient discontinued the treatment before 1 year), and 3 patients

Table 4. Serial OCT data post-procedure and 2-year follow-up

	Baseline	2Y Follow-up	*P* value
Strut analysis			
Number of Struts per lesion, n			
Non-Overlap Segment	175±59	1118±197	-
Overlap Segment	283±265	257±74	-
P value†	0.351	<0.001	
Number of Uncovered Struts per lesion, n			
Non-Overlap Segment	-	7.0±9.4	-
Overlap Segment	-	0.9±1.7	-
P value†	-	0.163	
Coverage rate (%)			
Non-Overlap Segment	-	99.4±0.8	-
Overlap Segment	-	99.8±0.4	-
P value†	-	0.360	
Lesion level analysis			
Non-Overlap Segment	N = 7	N = 7	
Overlap Segment	N = 7	N = 7	
Lumen Area (mm^2)			
Non-Overlap Segment	6.98±1.18	5.58±2.01	0.138
Overlap Segment	8.25±1.73	6.09±2.30	0.071
P value†	0.133	0.663	
Abluminal Scaffold Area (mm^2)			
Non-Overlap Segment	7.33±1.23	8.02±2.52	0.529
Overlap Segment	8.26±1.50	9.23±3.16	0.476
P value†	0.233	0.445	
Endoluminal Scaffold Area (mm^2)			
Non-Overlap Segment	6.34±1.09	6.81±2.20	0.619
Overlap Segment	6.56±1.35	7.48±2.84	0.453
P value†	0.744	0.632	
Strut Core Area (mm^2)			
Non-Overlap Segment	0.20±0.04	0.21±0.05	0.804
Overlap Segment	0.41±0.07	0.36±0.10	0.284
P value†	<0.001	0.004	
Flow Area (mm^2)			
Non-Overlap Segment	6.78±1.15	5.58±2.01	0.195
Overlap Segment	7.84±1.71	6.09±2.30	0.133
P value†	0.197	0.663	
Neointimal Area (mm^2)			
Non-Overlap Segment		2.24±0.63	

Table 4. Serial OCT data post-procedure and 2-year follow-up (continued)

	Baseline	2Y Follow-up	*P* value
Overlap Segment		2.78±0.85	
P value†		0.206	
Cross-section level analysis			
Non-Overlap Segment	N = 174	N = 211	
Overlap Segment	N = 143	N = 142	
Lumen Area (mm^2)			
Non-Overlap Segment	6.89±1.50	5.56±2.20	<0.001
Overlap Segment	8.12±1.55	5.69±1.96	<0.001
P value†	<0.001	0.735	
Abluminal Scaffold Area (mm^2)			
Non-Overlap Segment	7.24±1.56	8.02±2.76	<0.001
Overlap Segment	8.18±1.33	8.69±2.68	0.001
P value†	<0.001	0.001	
Endoluminal Scaffold Area (mm^2)			
Non-Overlap Segment	6.27±1.40	6.81±2.42	<0.001
Overlap Segment	6.52±1.21	7.01±2.43	<0.001
P value†	0.030	0.834	
Strut Core Area (mm^2)			
Non-Overlap Segment	0.20±0.08	0.21±0.09	0.788
Overlap Segment	0.40±0.13	0.35±0.15	0.015
P value†	<0.001	<0.001	
Flow Area (mm^2)			
Non-Overlap Segment	6.69±1.47	5.56±2.20	<0.001
Overlap Segment	7.72±1.54	5.69±1.96	<0.001
P value†	<0.001	0.735	
Neointimal Area (mm^2)			
Non-Overlap Segment	-	2.25±0.95	-
Overlap Segment	-	2.65±0.81	-
P value†	-	<0.001	-
Abluminal scaffold area ratio (overlap vs. non-overlap)	1.12±0.07	-	-

Data are expressed as mean ± standard deviation and number.
† Non-overlap segment vs. Overlap segment

were still on dual antiplatelet therapy at 2 years. One patient died due to a non-cardiac cause 345 days after the index procedure. Two patients underwent the ID non-target vessel revascularization by PCI 188 days and 409 days after the index procedure, respectively. One patient underwent Non-ID-target lesion revascularization by PCI 707 days after the index procedure due to in-scaffold restenosis.

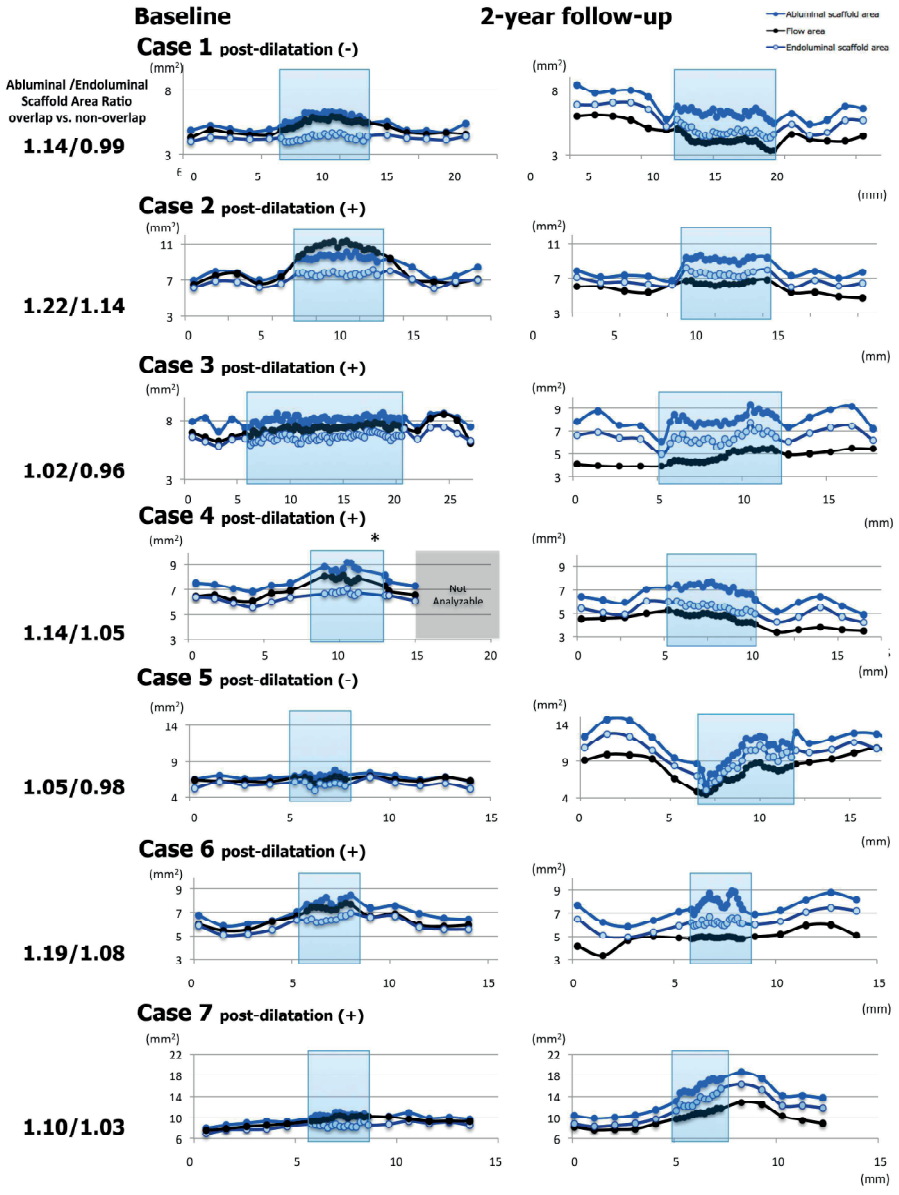

Figure 3. Vessel-scaffold interaction in all cases. Vessel-scaffold interactions in overlap (blue shadow) and non-overlap segments of all the cases are shown. The horizontal axis indicates the length of the lesion from the distal to proximal. The vertical axis indicates the area of each cross-section (black: flow area; dark blue: abluminal scaffold area; light blue: endoluminal scaffold area). The overlap segments and both 5 mm margins are illustrated. * In case 4, some cross-sections in the overlap segments and proximal site of the scaffolded lesion were not analysable due to insufficient image quality.

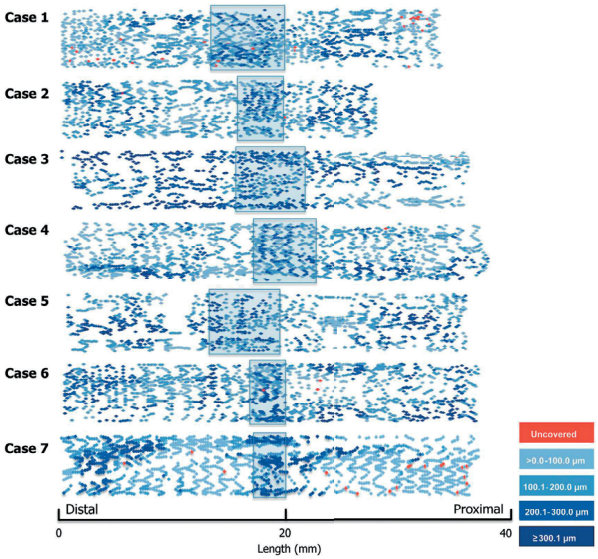

Figure 4. The spatial distribution of the neointimal thickness and coverage status along each overlap segment and non-overlap segment at two-year follow-up. The horizontal axis indicates the distance from the distal edge of the implanted devices to the struts in the overlap and non-overlap segments. The vertical axis indicates the angle where the strut is located in the circular cross-section with respect to the centre of gravity of the vessel (0° to 360°). The neointimal thickness of each strut is colour-coded as indicated in the figure. Overlap segments (light blue square) show a mixture of light blue and dark blue, indicating the thinner neointima of "inner struts" and thicker neointima of "outer struts".

DISCUSSION

The major findings of the present study are: 1) post-procedure, both overlap and non-overlap segments presented similar endoluminal scaffold area; 2) at 2-year follow-up, the neointimal coverage of the BVS struts was almost completed in both overlap segments and non-overlap segments; 3) the flow area in the overlap segments at 2-year follow-up was not different from the flow area in the non-overlap segments despite the neointimal response being greater in the overlap segments. Consequently, the treated segments showed a homogeneous lumen area through the scaffold segment.

Luminal dimension at overlap segment

The lumen area at baseline was larger in the overlap segment than in the no-overlap segment. This could compensate for the greater neointimal growth at overlap segment than at non-overlap segment, resulting in the equivalent luminal dimensions at follow-up. As shown in Figure 3, post-dilatation aligned the scaffold endoluminal surface at overlap segments, resulting in the greater outward enlargement of vessel due to double layers of struts compared to non-overlap segments. To maintain equivalent luminal

dimension after neointimal coverage at overlap segment as compared to non-overlap segments, appropriate post-dilatation might be necessary. However, safety of this technique needs to be evaluated in further trials, since this technique could be a cause of coronary perforation. [8]

Technical issues with overlap Absorb scaffolds

According to a European perspective for BVS use,[9] keeping the overlap to a minimum to avoid delays in healing is mandated due to the relatively thick struts of the Absorb scaffolds.[2] The thick struts of the Absorb scaffold could also hinder implantation of the second Absorb scaffold, which could result in difficulty of scaffold delivery or disruption of struts.

For an optimal overlap of Absorb scaffolds, the "marker-to-marker" (~1 mm of overlap) and "scaffold-to-scaffold" (no overlap) techniques are recommended by the European perspective.[9] In the marker-to-marker configuration, which appears to be the best to avoid gap restenosis, the second scaffold is advanced until the distal balloon markers line up with the proximal marker beads of the implanted scaffold. As such, the markers of the second scaffold will be adjacent to the markers of the deployed scaffold. Enhanced stent visualization-guided implantation would also be helpful.[10] Attention should be paid to scaffold size selection and placement order (i.e., starting with the distal scaffold is preferred) to avoid damage at the overlap site.

In the ABSORB EXTEND trial, planned overlapping of scaffolds was permitted in lesions with an overlap of 1 mm to 4 mm. As a result, the overlap length obtained by post-procedural OCT was 4.0 [2.0, 7.4mm] in this study population. In spite of the overlap length being relatively longer than the expert recommendation, procedure success was achieved in all patients and no strut disruption was observed.

It is noteworthy that the endoluminal scaffold area in the overlap segments was similar to that in the non-overlap segments post-procedure [representative case (Case 6) shown in Figure 2]. Post-dilatation made the transition between overlap and non-overlap smooth, which consequently resulted in outward enlargement of the outer scaffold and vessel wall.

Delayed coverage and greater neointimal response in overlap Absorb scaffolds

In a juvenile porcine model, the overlap Absorb scaffolds showed more delay in tissue coverage than in non-overlap scaffolds [2]. It is likely that the larger strut thickness of the stacked-like Absorb scaffolds (approximately 300 μm) in overlap segments lead to a greater neointimal response compared with that in the non-overlap segment. Thicker, rectangular (non-streamlined) struts, characteristic of the Absorb, may theoretically increase the device area exposed to low endothelial oscillatory shear stress areas, leading to the local accumulation of growth factors, mitogenic cytokines, and platelets, which

promote neointimal formation until a smooth lumen surface is achieved. [13] Delayed coverage of overlapped struts presumably results from that greater neointimal response which has a longer duration. Despite these concerns raised from the preclinical studies, overall coverage rate of the overlap segments at 2-year follow-up was achieved in 99.8% of struts, a figure similar to the non-overlap segments. Lumen area was similar between overlap and non-overlap segments in spite of the greater neointimal response in the overlap segments. Despite a large abluminal scaffold area ratio (overlap segment versus non-overlap segment), exuberant neointima in response to barotrauma was not observed.

Study limitation

The first limitation is the small number of patients included in our study, low imaging follow-up rate (50%) and consequent selection bias, despite the data representing one of the largest early registries. The small sample size did not permit drawing any conclusions on clinical relevance. The second limitation is the follow-up timing. The OCT follow-up in this study was performed 2 years after the index procedure. The results confirmed the completed strut coverage at least at that time point. However, the serial changes of neointimal coverage of overlap BVS struts in humans still remain to be elucidated. Lastly, the challenges of OCT assessment for overlap segment should be acknowledged. Artifacts of OCT such as elongation and repetition could also interfere with the results. [14] Therefore, OCT results should be interpreted with caution.

CONCLUSIONS

Despite the expectation that overlapping scaffold struts would occupy more of the luminal area than non-overlapping struts, both overlap and non-overlap segments showed similar endoluminal areas post-implantation and excellent vessel healing and vascular response at 2 years follow-up. The results from this small OCT substudy therefore support the feasibility of overlapping scaffolds when needed for longer lesions if acute lumen expansion is achieved similar to non-overlapped segments using good implant techniques.

Impact on daily practice

Results from the present OCT study might support the feasibility of overlapping scaffolds when needed for longer lesions if acute lumen expansion is achieved similar to non-overlapped segments using good implant techniques. Since the patient number of our analysis was very limited, the results should be interpreted with caution, and further investigation in a prospective fashion might be necessary to elucidate the impact of overlap Absorb scaffolds on clinical outcomes.

REFERENCES

1. Ishibashi Y, Muramatsu T, Nakatani S, Sotomi Y, Suwannasom P, Grundeken MJ, Cho YK, Garcia-Garcia HM, van Boven AJ, Piek JJ, Sabate M, Helqvist S, Baumbach A, McClean D, de Sousa Almeida M, Wasungu L, Miquel-Hebert K, Dudek D, Chevalier B, Onuma Y, Serruys PW. Incidence and Potential Mechanism(s) of Post-Procedural Rise of Cardiac Biomarker in Patients With Coronary Artery Narrowing After Implantation of an Everolimus-Eluting Bioresorbable Vascular Scaffold or Everolimus-Eluting Metallic Stent. JACC Cardiovasc Interv 2015;8(8):1053-63.
2. Farooq V, Serruys PW, Heo JH, Gogas BD, Onuma Y, Perkins LE, Diletti R, Radu MD, Raber L, Bourantas CV, Zhang Y, van Remortel E, Pawar R, Rapoza RJ, Powers JC, van Beusekom HM, Garcia-Garcia HM, Virmani R. Intracoronary optical coherence tomography and histology of overlapping everolimus-eluting bioresorbable vascular scaffolds in a porcine coronary artery model: the potential implications for clinical practice. JACC Cardiovasc Interv 2013;6(5):523-32.
3. Abizaid A, Ribamar Costa J, Jr., Bartorelli AL, Whitbourn R, van Geuns RJ, Chevalier B, Patel T, Seth A, Stuteville M, Dorange C, Cheong WF, Sudhir K, Serruys PW. The ABSORB EXTEND study: preliminary report of the twelve-month clinical outcomes in the first 512 patients enrolled. EuroIntervention 2015;10(12):1396-401.
4. Nakatani S, Sotomi Y, Ishibashi Y, Grundeken MJ, Tateishi H, Tenekecioglu E, Zeng Y, Suwannasom P, Regar E, Radu MD, Raber L, Bezerra H, Costa MA, Fitzgerald P, Prati F, Costa RA, Dijkstra J, Kimura T, Kozuma K, Tanabe K, Akasaka T, Di Mario C, Serruys PW, Onuma Y. Comparative analysis method of permanent metallic stents (XIENCE) and bioresorbable poly-L-lactic (PLLA) scaffolds (Absorb) on optical coherence tomography at baseline and follow-up. EuroIntervention 2015;11(6).
5. Farooq V, Onuma Y, Radu M, Okamura T, Gomez-Lara J, Brugaletta S, Gogas BD, van Geuns RJ, Regar E, Schultz C, Windecker S, Lefevre T, Brueren BR, Powers J, Perkins LL, Rapoza RJ, Virmani R, Garcia-Garcia HM, Serruys PW. Optical coherence tomography (OCT) of overlapping bioresorbable scaffolds: from benchwork to clinical application. EuroIntervention 2011;7(3):386-99.
6. Onuma Y, Serruys PW, Muramatsu T, Nakatani S, van Geuns RJ, de Bruyne B, Dudek D, Christiansen E, Smits PC, Chevalier B, McClean D, Koolen J, Windecker S, Whitbourn R, Meredith I, Garcia-Garcia HM, Veldhof S, Rapoza R, Ormiston JA. Incidence and imaging outcomes of acute scaffold disruption and late structural discontinuity after implantation of the absorb Everolimus-Eluting fully bioresorbable vascular scaffold: optical coherence tomography assessment in the ABSORB cohort B Trial (A Clinical Evaluation of the Bioabsorbable Everolimus Eluting Coronary Stent System in the Treatment of Patients With De Novo Native Coronary Artery Lesions). JACC Cardiovasc Interv 2014;7(12):1400-11.
7. Raber L, Zaugg S, Windecker S, Juni P. Intricacies in the analysis and interpretation of optical coherence tomography findings. EuroIntervention 2014;9(12):1374-7.
8. Pichette M, Chevalier F, Genereux P. Coronary artery perforation at the level of two-overlapping bioresorbable vascular scaffolds: The importance of vessel sizing and scaffold thickness. Catheter Cardiovasc Interv 2015;86(4):686-91.
9. Tamburino C, Latib A, van Geuns RJ, Sabate M, Mehilli J, Gori T, Achenbach S, Alvarez MP, Nef H, Lesiak M, Di Mario C, Colombo A, Naber CK, Caramanno G, Capranzano P, Brugaletta S, Geraci S, Araszkiewicz A, Mattesini A, Pyxaras SA, Rzeszutko L, Depukat R, Diletti R, Boone E, Capodanno D, Dudek D. Contemporary practice and technical aspects in coronary intervention with bioresorbable scaffolds: a European perspective. EuroIntervention 2015;11(1):45-52.
10. Biscaglia S, Campo G, Tebaldi M, Tumscitz C, Pavasini R, Fileti L, Secco GG, Di Mario C, Ferrari R. Bioresorbable vascular scaffold overlap evaluation with optical coherence tomography after

implantation with or without enhanced stent visualization system (WOLFIE study): a two-centre prospective comparison. Int J Cardiovasc Imaging 2016;32(2):211-23.

11. Serruys PW, Chevalier B, Dudek D, Cequier A, Carrié D, Iniguez A, Dominici M, van der Schaaf RJ, Haude M, Wasungu L, Veldhof S, Peng L, Staehr P, Grundeken MJ, Ishibashi Y, Garcia-Garcia HM, Onuma Y. A bioresorbable everolimus-eluting scaffold versus a metallic everolimus-eluting stent for ischaemic heart disease caused by de-novo native coronary artery lesions (ABSORB II): an interim 1-year analysis of clinical and procedural secondary outcomes from a randomised controlled trial. The Lancet 2015;385(9962):43-54.
12. Kawamoto T, Okura H, Koyama Y, Toda I, Taguchi H, Tamita K, Yamamuro A, Yoshimura Y, Neishi Y, Toyota E, Yoshida K. The relationship between coronary plaque characteristics and small embolic particles during coronary stent implantation. J Am Coll Cardiol 2007;50(17):1635-40.
13. Koskinas KC, Chatzizisis YS, Antoniadis AP, Giannoglou GD. Role of endothelial shear stress in stent restenosis and thrombosis: pathophysiologic mechanisms and implications for clinical translation. J Am Coll Cardiol 2012;59(15):1337-49.
14. Farooq V, Gogas BD, Okamura T, Heo JH, Magro M, Gomez-Lara J, Onuma Y, Radu MD, Brugaletta S, van Bochove G, van Geuns RJ, Garcia-Garcia HM, Serruys PW. Three-dimensional optical frequency domain imaging in conventional percutaneous coronary intervention: the potential for clinical application. Eur Heart J 2013;34(12):875-85.

Chapter 15

Development and receding of a coronary artery aneurysm after implantation of a fully bioresorbable scaffold

Shimpei Nakatani, Yuki Ishibashi, Pannipa Suwannasom, Maik J. Grundeken, Evald Høj Christiansen, Yoshinobu Onuma, Patrick W. Serruys

Circulation 2015;24;131(8):764-7.

ABSTRACT

A 83-year-old man included in the ABSORB cohort B trial underwent successful percutaneous coronary intervention of the middle left anterior descending artery with a 3.0×18-mm bioresorbable scaffold (Absorb, Abbott Vascular, CA) that was postdilated with a 3.0-mm noncompliant balloon at 24 atm (Figure 1A and 1B). The 2-dimensional and 3-dimensional (3D) optical coherence tomography (OCT) confirmed the absence of structural discontinuity after the procedure (Figure 2B and Figure 3A'). At 6 months, the planned angiography showed the absence of restenosis but an ectasia in the scaffolded segment (Figure 1C). Intravascular ultrasound revealed a focal vessel and lumen enlargement (17.93 mm^2 [Δ+20.5%] and 6.99 mm^2 [Δ+9.6%], respectively, in the matched cross-section analysis; Figure 2C), whereas 3D OCT suggested a deformation of the scaffold in the 2-mm segment of the ectasia (Figure 3B'). At 18 months, the planned multislice computed tomography showed lumen dilatation in the scaffolded segment (Figure 1D). At 2 years, on angiography, the ectatic lesion in the scaffold became aneurysmal (50% increase compared with the adjacent reference vessel; Figure 1E). Intravascular imaging revealed the increase in the vessel area and lumen area (20.90 mm2 [Δ+40.5%] on intravascular ultrasound and 10.91 mm2 [Δ+35.7%] on OCT, respectively, from baseline; Figure 1E and 1F), whereas 3D OCT showed a focal cleavage of the scaffold rings and a bulge of the vessel in the segment free from the scaffold struts (Figure 3C and C'). Five years after implantation, angiography revealed that the aneurysm was still present but had become smaller compared with the previous time points (Figure 1F). Intravascular ultrasound and OCT demonstrated the diminished vessel and lumen area (17.11 mm^2 [Δ−18.1%] and 8.78 mm^2 [Δ−19.5%], respectively, from 2 years; Figure 2G and 2H), making the scaffold indiscernible on OCT.

In general, aneurysm after drug-eluting device implantation is attributed to residual dissection and deep arterial wall injury and to inflammatory and allergic reactions to the drug, polymer, or device such as metal. In rare cases, a fully bioresorbable poly(L-lactide) acid prosthesis can cause inflammation[1]. Further insight can be obtained from the 3D reconstructions of the OCT signal (Figure 3A', 3B', and 3C'), in which the pattern of the struts can qualitatively outline the time history of the aneurysmal expansion. From implantation to 6 months, the wall distended and displaced the strut pattern without an apparent change in intracrown angulations, indicating a wall distention that occurred while the strut material was still continuous and minimally degraded. Further expansion from 6 to 24 months occurred in part after substantial polymer degradation had already occurred, as evidenced by the widening of intracrown angulations or complete separation of strut segments, indicating that strut migration follows wall migration entirely and continuity of struts has diminished to subpattern levels. Cross-sectional and longitudinal reconstructions of these segments appear to show that, although diameter

is substantially distended, the arterial wall thickness over and under the struts is uniform in nature, an appearance inconsistent with severe inflammatory reactions to polymer.

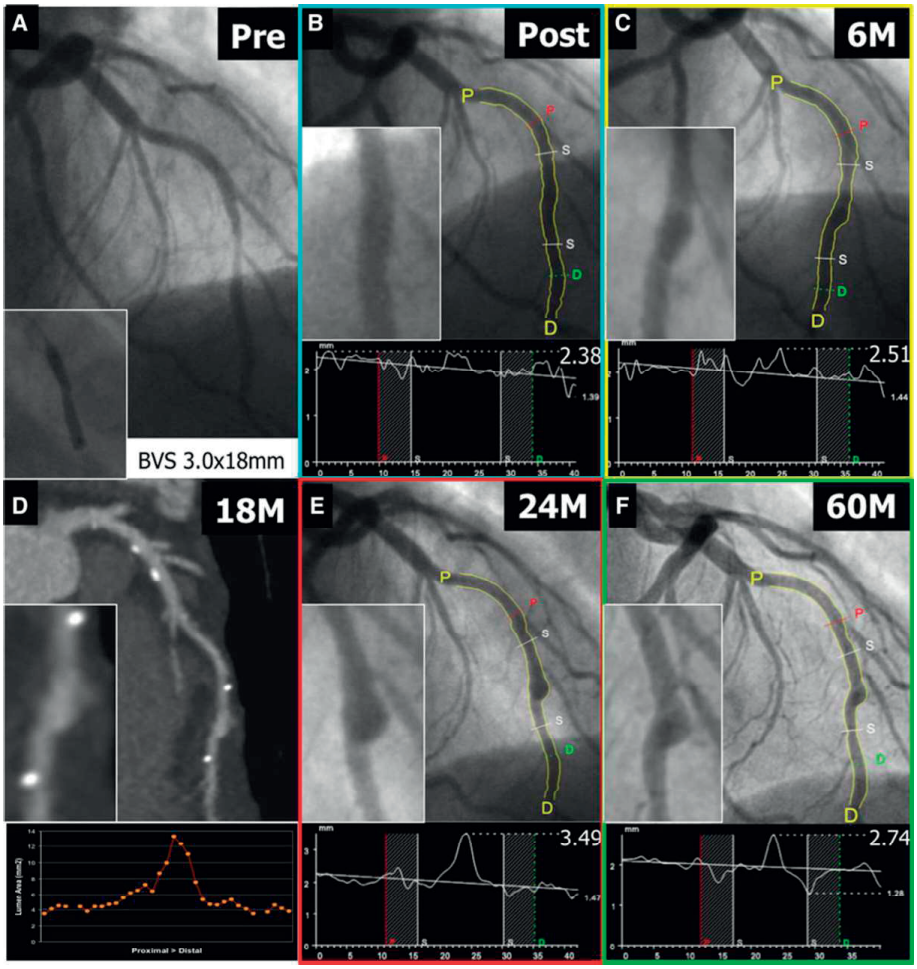

Figure 1. Coronary angiography of the left anterior descending artery before (A) and after (B) intervention at baseline. At 6 months, the planned angiography showed an ectasia in the scaffolded segment (C). The planned multislice computed tomography showed lumen dilatation in the scaffolded segment at 18 months (D). Repeat angiography demonstrated that the ectatic lesion in the scaffold became aneurysmal at 2 years (E) and diminished at 5 years (F).

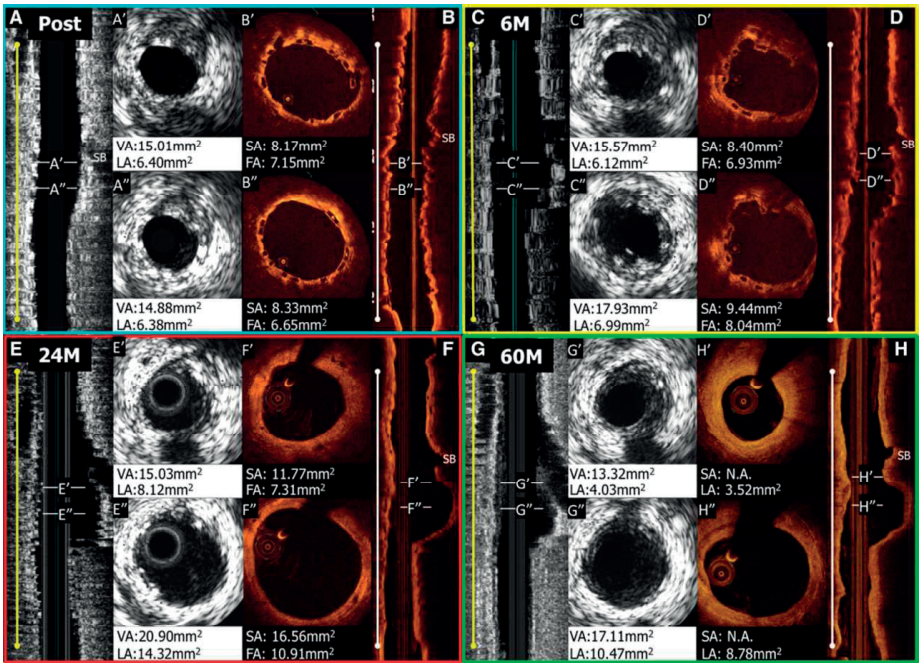

Figure 2. Intravascular ultrasound (IVUS) and optical coherence tomography (OCT) images from matched sites (aneurysm site and near proximal site) after the procedure (A and B), at 6 months (C and D), at 2 years (E and F), and at 5 years (G and H) after scaffold implantation. The white lines in the longitudinal view indicate the sites corresponding to the cross sections of A′ to H″. Postprocedural OCT showed some malapposed struts but confirmed the absence of structural discontinuity. At 6 months, IVUS revealed a focal vessel and lumen enlargement (C″). IVUS and OCT revealed the increase in the vessel and the lumen area at 2 years (E″ and F″) and the subsequent decrease in the aneurysm, with the scaffold becoming indiscernible on OCT at 5 years (G″ and H″). FA indicates flow area; LA, lumen area; SA, scaffold area; and VA, vessel area.

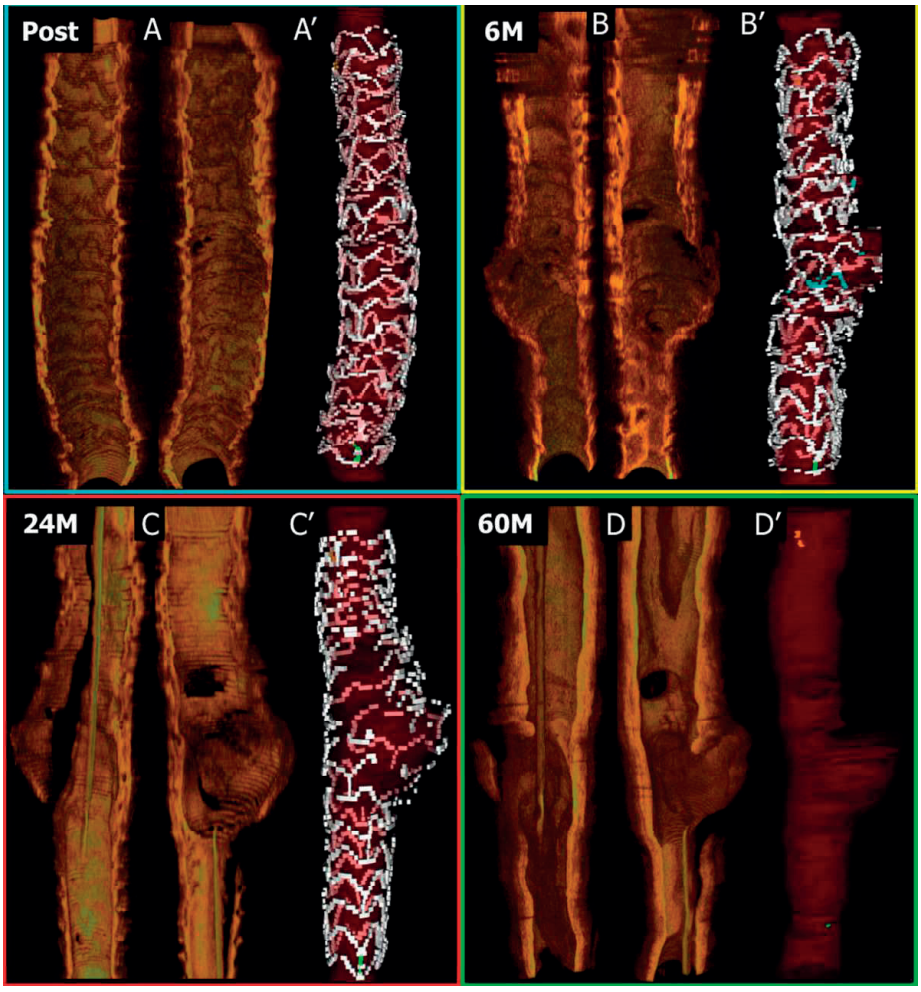

Figure 3. Three-dimensional (3D) reconstruction of cross-sectional images corresponding to the scaffold segment. A′ through D′ are reconstructed for emphasizing the scaffold structure. 3D optical coherence tomography (OCT) confirmed the absence of structural discontinuity after the procedure. At 6 months, 3D OCT suggested a deformation of the scaffold in the 2-mm segment corresponding to the ectasia (B and B′). At 2 years, 3D OCT showed a focal cleavage of the scaffold rings and a bulge of the vessel in the segment free from the scaffold struts (C and C′). At 5 years, the aneurysm started to reduce, with the scaffold becoming indiscernible on OCT (D and D′). In A′ to D′, the yellow and green dots indicate the proximal and distal radiopaque makers. The blue struts indicate malapposed struts.

REFERENCES

1. Katsuragi YT, Gomi A, Sunaga A, Miyazaki K, Kamochi H, Arai F, Fukushima N, Sugawara Y. Intracerebral foreign body granuloma caused by a resorbable plate with passive intraosseous translocation after cranioplasty. J Neurosurg Pediatr. 2013;12:622–625.

Chapter 16

Change in lumen eccentricity and asymmetry after treatment with Absorb bioresorbable vascular scaffolds in the ABSORB Cohort B trial: a five-year serial optical coherence tomography imaging study

Pannipa Suwannasom, Yohei Sotomi, Taku Asano, Jaryl Ng Chen Koon, Hiroki Tateishi, Yaping Zheng, Erhan Tenekecioglu, Joanna J. Wykrzykowska, Nicolas Foin, Robbert J. de Winter, John A. Ormiston, Patrick W. Serruys, Yoshinobu Onuma

EuroIntervention 2017;12(18):e2244-e2252

ABSTRACT

Aims

The aim of the study was to investigate long-term changes in lumen eccentricity and asymmetry at 5 years after implantation of the Absorb bioresorbable vascular scaffold (BVS)

Methods and results

Out of 101 patients from Absorb cohort B trial, 28 patients(29 lesions) with serial Optical Coherence Tomography(OCT) examination at 4 different time points(Cohort B1: post-procedure,6 months, 2, and 5 years[n=13]; Cohort B2:post-procedure,1, 3, and 5 years[n=16]) were evaluated. The longitudinal variance in lumen diameter was assessed by asymmetry index(AI). Asymmetric lesion was defined as AI > 0.3. The circularity of the lumen or scaffold was evaluated by the eccentricity index calculated as minimal divided by maximal luminal or scaffold diameter per cross-section. The lowest lumen eccentricity index within a scaffold segment (EI_L)< 0.7 was defined as eccentric lesion. Post-procedure, eccentric lesion was observed in 72.4% and became concentric in 93.1% at 5 years (post EI_L 0.67±0.05 vs. 5-year EI_L 0.80±0.10, p=0.03) with a modest reduction of the lumen area from baseline to 5 years by 0.75±0.32 mm^2. Asymmetric lumen morphology was observed in 93.1%(n=27) post implantation and persisted until 5-year follow-up. On serial OCT analyses, there was a substantial increase in the scaffold EI during the first two years (post 0.70±0.06, 6-month 0.76±0.08, 2-year 0.85±0.07), then remained stable whereas the lumen circularity further improved. There were no significant differences in major adverse cardiac events regarding the lumen morphology over the 5-year follow-up.

Conclusion

In patients treated with Absorb BVS, the cross-sectional circularity improved over 5-year while the variance in longitudinal diameters remained. Regaining of lumen circularity is mainly caused by reshaping of the scaffold during the first 2 years.

INTRODUCTION

Bioresorbable vascular scaffold (BVS) technology has been developed to eliminate the deleterious caging effect of the permanent metallic stent. The mechanical behavior of the BVS is different from the metallic drug-eluting stents(DES). BVS exhibits more lumen eccentricity and asymmetry than metallic everolimus-eluting stent (EES) as assessed by intravascular ultrasound (IVUS) post-implantation. Eccentricity and asymmetry of the device may cause an inhomogenous strut distribution, which theoretically may decrease local drug concentration[1] and alter shear stress, therefore promoting scaffold failure.

As demonstrated previously, the BVS struts gradually disappear over time, the initial eccentricity and asymmetry of the lumen may also change according to the full resorption of the struts and the remodeling of the vessel wall. Without the permanent metallic caging, the vessels may remodel and return to their physiologic and morphologic original state. Karanasos et al. reported that after full resorption of the first-generation BVS (ABSORB Cohort A, n=4), the lumen asymmetry index decreased over time.[2] However, the long-term lumen adaptation after the second-generation BVS implantation has never been explored.

The aim of this study was to investigate using optical coherence tomography (OCT) the eccentricity and asymmetry of the lumen at 5 years after implantation of Absorb BVS (Abbott Vascular, Santa Clara, CA, USA) and their impacts to the long-term clinical outcomes.

METHODS

Study design and study device

The ABSORB Cohort B trial was a multicenter, prospective, open-label trial that included 101 patients (102 lesions) treated with the second-generation Absorb scaffold. The first 45 patients (Cohort B1) underwent invasive coronary imaging follow up at 6-months, 2-, and 5-year follow up, while the other 56 patients (B2) underwent the same at 1-, 3-, and 5-year follow up. The long-term clinical outcomes were reported in all patients who had baseline OCT assessment. The clinical endpoints definitions have been published elsewhere[3]. The long-term changes of lumen morphology were exclusively reported only in lesions that had serial OCT assessment at all time points. The study protocol was approved by all institutional ethics committees and informed consent was obtained for every patient before any intervention was performed.

The Absorb BVS (Abbott Vascular, Santa Clara, California) is comprised of a Poly-L lactide (PLLA) backbone coated with an amorphous drug-eluting coating matrix composed of Poly-D, L-lactide (PDLLA) polymer containing everolimus 100 μg/cm^2. A pair of

radiopaque platinum markers are located at the proximal and distal ends of the scaffold. The details of the study and treatment procedure have been previously described [4].

Imaging acquisition and analysis

OCT acquisition

Over the last five years OCT techniques have evolved. OCT acquisition in this study was performed using 4 different commercially available systems: the M2 and M3 Time-Domain Systems and the C7 and C8 Fourier-Domain Systems (LightLab Imaging, Westford, Massachusetts, USA). The details of the image acquisition have been previously described[5].

OCT data analysis

The OCT images acquired post-procedure and at follow-up were analyzed off-line, using proprietary LightLab software (St. Jude Medical Inc., Massachusetts, USA) and Q-IVUS 3.0 (Medis Medical Imaging systems, Leiden, The Netherlands). The scaffold segments and the 5-mm segments adjacent to both edges were analyzed at 1 mm intervals by an independent core laboratory (Cardialysis, Rotterdam, The Netherlands).

OCT lumen eccentricity and lumen asymmetry

Lumen diameters in each cross-section were measured through each gravitational center for each sectorial degree[6]. The variance in lumen diameter throughout the scaffold was assessed by an asymmetry index. The asymmetry index was calculated per scaffold segment as (1 – [minimal lumen diameter/ maximal lumen diameter])[7]. A lesion was characterized as an asymmetric lesion when the value of AI was over 0.3[1,8,9]. Conversely, a lesion with AI ≤ 0.3 was defined as a symmetric lesion.

The eccentricity index was calculated as a parameter for the circularity of cross-section using the formula of minimal luminal diameter divided by maximal luminal diameter from the same cross-section[10]. This parameter was calculated in all analyzed frames and the most eccentric lumen shape in the scaffold segment was identified as the lowest value of eccentricity index (EI_L). A lesion with $EI_L \geq 0.7$ was defined as concentric while $EI_L < 0.7$ was defined as an eccentric lesion. The distinction between the method of calculation of eccentricity index and asymmetry index is illustrated and detailed in Figure 1.

Reference lumen area (RLA) was estimated as the mean lumen area between the 5 mm proximal and distal segments to the edges of the BVS[8]. Area stenosis(%) was calculated from (1- [lumen area at the cross-section of interest/RLA]) x100.

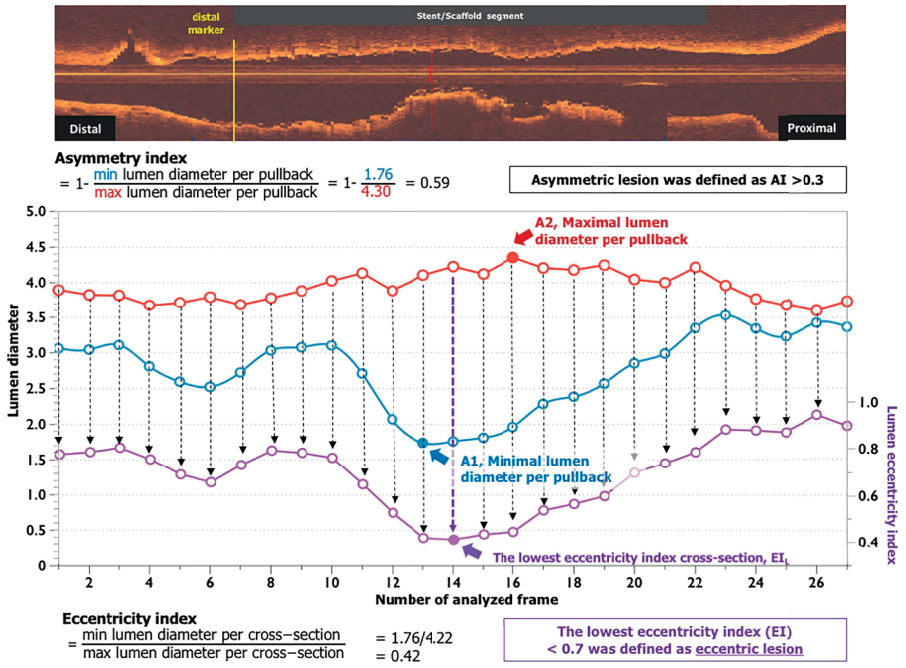

Figure 1. Figure 1 The differences between the methods to calculate eccentricity index and asymmetry index.

Asymmetry index was calculated per scaffold segment as (1 – minimal lumen diameter/ maximal lumen diameter). Minimal lumen diameter was the minimal value of minimal lumen diameter throughout scaffold segment (A1 in figure), maximal lumen diameter was the maximal value of maximal lumen diameter throughout scaffold segment (A2 in figure). Therefore, the minimum lumen diameter and maximum lumen diameter could derive from different cross-section in the scaffold segment.

On one hand, the eccentricity index used the formula of minimal lumen diameter divided by maximal lumen diameter in the same cross-section. This parameter was calculated in all analyzed frames as shown in individual purple dot. The most eccentric lumen shape in scaffold segment was identified as the lowest value of eccentricity index.

Abbreviation: AI: asymmetry index; EI: eccentricity index

Co-localization of post-procedural and follow-up OCT

Two post-procedural cross sections were used as references to compare the changes of lumen area and the lumen eccentricity index at follow-up. The first cross-section was the site of post-procedural lowest eccentricity index(EI_L), the second cross-section was the site of post procedural highest eccentricity index (EI_H). The distance from the first cross-section comprising of the distal marker to the EI_L or EI_H cross-section were measured in the longitudinal view respectively. Co-localization of the corresponding cross-sections at all time points was performed by using the distance from the distal markers and topographical landmarks such as: side branch (SB); vein; pericardium; position and configuration of calcifications to assure a precise co-localization procedure. The serial

changes of lumen area, lumen EI and neointimal thickness (reported as mean value of minimal, maximal and mean) in matched cross sections were evaluated.

Statistical Analysis

All statistical analyses were performed using IBM SPSS Statistics, version 23.0 (IBM Corp, Armonk, NY). OCT analysis was performed per lesion. All continuous variables were presented as mean±standard deviation (SD) or median and interquartile range (IQR; 1st to 3rd quartile) as appropriate. Pairwise comparisons were performed by a Wilcoxon signed-rank test. All reported p-values were 2-sided, and values of $p < 0.05$ were considered statistically significant.

RESULTS

Baseline clinical, angiographic characteristics and procedural details

Out of 101 patients in the entire cohort, 28 patients (29 lesions) had serial OCT at all time points. Thirteen lesions from Cohort B1 and 16 lesions from Cohort B2 were included in the analysis as shown in flow chart (Figure 2). The patient, lesion and procedural characteristics are shown in table 1. Post-dilation was performed in 19 lesions (65.5%) with a maximal post balloon dilation pressure of 17.79±5.32 atm.

Lumen morphology at baseline

The baseline OCT results are detailed in table 2. The post-procedural residual area stenosis was 1.0% (IQR -14.1%;13.2%) and the asymmetry index was 0.39±0.06. Out of 29 lesions, asymmetric morphology (AI > 0.3) was observed in 93.1% of lesions (n=27). The lumen EI_L was 0.67±0.05. Twenty-one lesions (72.4%) were classified as eccentric lesions. The highest eccentricity index (EI_H) was 0.92±0.03.

Lumen morphology at 5 years

Overall and individual changes in lumen morphology are presented in figure 3. On average, both the asymmetry index and eccentricity index increased from post-procedure to 5 years (asymmetry index: post 0.36±0.05 vs. 5-year 0.44±0.11, p<0.001; eccentricity index: post 0.67±0.05 vs. 5-year 0.72±0.09, p=0.01), indicating that the lumen became more concentric but longitudinally more asymmetric. The percentage of eccentric lesions decreased to 27.6% whereas the proportion of asymmetric lesions remained unchanged(93.1%).

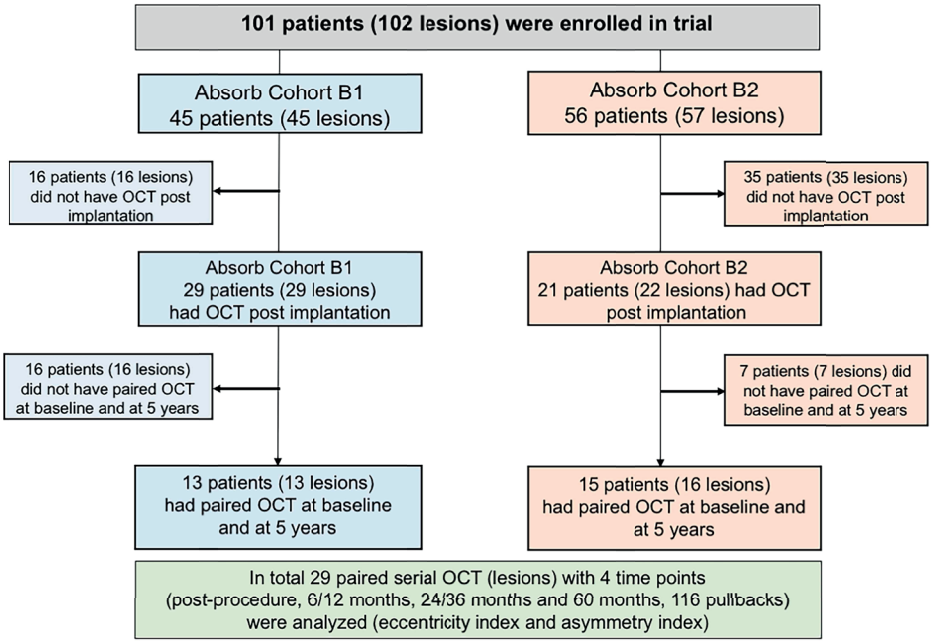

Figure 2. Study flow chart
Abbreviation: OCT: optical coherence tomography, other abbreviations see Figure 1

Baseline lumen morphology and the long-term clinical outcomes

At baseline, there were 50 patients who had OCT assessment post-procedure. The asymmetry index was 0.36±0.07 and asymmetric morphology (AI > 0.3) was observed in 80% of lesions. The graphical presentation in figure 4 shows that the major adverse cardiac event (composite of cardiac death, all myocardial infarction and ischemic driven target lesion revascularization) occurred 10% in the asymmetric lesions and 10% in the symmetric lesions, p=1.00. Similarly, there were no significant differences in the eccentric lesions and concentric lesions (11.1% vs. 7.1%, p=0.68) over 5-year follow-up.

Serial changes of lumen morphology up to 5 years

The changes in the eccentricity index at the site of the EI_L were assessed in matched cross-section at all time points (Figure 5). The lumen EI_L substantially increased from baseline to 2-year follow-up in parallel with the scaffold eccentricity index (Fig 5A). In the first 2 years after implantation, the improvement of lumen circularity was basically driven by reshaping of the scaffold. From 1 year to 3 years, the scaffold eccentricity index did not change whereas the lumen circularity further improved (Fig 5B). In this period, the continuous growth of neointima contributed to the regaining of lumen circularity,

Table 1 Baseline patient, lesion characteristics and procedural details

	Overall
	$N_P = 28$, $N_L=29$
Baseline patient characteristics	
Age, mean ± SD	61.4±9.4
Male sex	20(71.4)
Hypertension	17(60.7)
Hyperlipidemia	24(85.7)
Diabetes	1(3.6)
Current smokers	10(35.7)
Previous myocardial infarction	9(33.3)
Previous PCI	7(25.0)
Stable angina	23(82.1)
Baseline lesion characteristics	
Target vessel	
Left anterior descending	15(51.7)
Left circumflex	6(20.7)
Right coronary artery	8(27.6)
AHA/ACC lesion classification*	
Type B1 lesion	20(69.0)
Type B2 lesion	8(27.6)
Moderate/severe calcification	4(13.3)
Procedural characteristics	
Pre-dilation performed	29(100)
Semi-compliant balloon used for pre-dilation	27(93.1)
Maximal pre-dilatation balloon diameter, mm	2.63±0.22
Length of pre-dilatation balloon, mm	12.62±1.61
Maximal pre-dilatation pressure, atm	12.00±3.14
Diameter of scaffold implanted, mm	3.0
Scaffold length, mm	18.0
Maximal device balloon inflation pressure, atm	13.17±2.90
Post-dilation balloon performed	19(65.5)
Maximal post-dilatation balloon diameter, mm	3.18±0.19
Maximal post-dilatation pressure, atm	17.79±5.32
Length of post-dilatation balloon, mm	11.70±3.13

Data are shown in mean±SD or median (IQR 1st-3rd) or n(%).* One missing data in Cohort B2.
Abbreviation: PCI:percutaneous coronary intervention; ACC- American College of Cardiology, AHA- American Heart Association

Table 2 OCT findings post-procedure and 5-year follow-up

	post-procedure	5 years	p-value*
	N=29	N=29	
Reference lumen area, mm^2	6.22±1.68	5.83±1.51	0.19
Minimal lumen area, mm^2	5.96±0.93	3.84±1.35	<0.001
Mean lumen area, mm^2	7.40±1.05	5.98±1.30	<0.001
Minimal lumen diameter, mm	2.40±0.26	1.95±0.39	<0.001
Maximal lumen diameter, mm	3.72±0.26	3.53±0.45	<0.001
Minimal scaffold area, mm^2	6.19±0.93	n/a	
Mean scaffold area, mm^2	7.56±0.98	n/a	
Residual area stenosis (%)	1.0 (-14.1;13.2)	34.1 (18.5;45.3)	<0.001
Scaffold Asymmetry index	0.36±0.05	0.44±0.11	<0.001
In-scaffold lowest lumen eccentricity index (EI_L)	0.67±0.05	0.72±0.09	0.01
In-scaffold highest lumen eccentricity index (EI_H)	0.92±0.03	0.94±0.02	0.002
Matched cross-section data at the site of the lowest eccentricity index post-procedure			
Lumen area at the site of EI_L, mm^2	6.83±1.37	6.09±1.69	0.049
Lumen eccentricity index	0.67±0.05	0.80±0.10	<0.001
Area stenosis at the site of EI_L(%)	-13.1 (-38.4;6.4)	-1.3 (-22.3;11.9)	0.11
Matched cross-section data at the site of the highest eccentricity index post-procedure			
Lumen area at the site of EI_H, mm^2	7.65±1.37	6.19±2.09	<0.001
Lumen eccentricity index	0.92±0.03	0.87±0.06	0.008
Area stenosis at the site of EI_H(%)	-26.7 (-48.4;-11.5)	-1.1 (-28.5;13.5)	0.004

Data are shown in mean±SD or median (IQR 1st-3rd) or n(%).The comparison was performed by Wilcoxon Signed Rank test.; *Comparison between baseline and 5 years

Abbreviation: EI_L : post-procedural lowest eccentricity index per pull back; EI_H : post-procedural highest eccentricity index per pull back

which eventually resulted in similar eccentricity of the lumen and scaffold at 3 years (Fig 5B). Serial changes of neointimal thickness at EI_L and EI_H cross-sections were tabulated in table 3. The neointimal thickness of EI_H cross-section was comparable to that of EI_L cross-section.

At 5-year follow-up, there was a substantial increase in the eccentricity index from baseline (0.67±0.05 to 0.80±0.10, p<0.001). The cross-section became more concentric in 82.8% with a modest reduction of the lumen area from baseline to 5 years by 0.75±0.32 mm^2. However, the reduction of lumen did not create a significant area stenosis at the site of EI_L (post-procedure -13.1%[IQR -38.4%; 6.4%] vs. 5-year -1.3%[IQR -22.3%;11.9%], p=0.14).

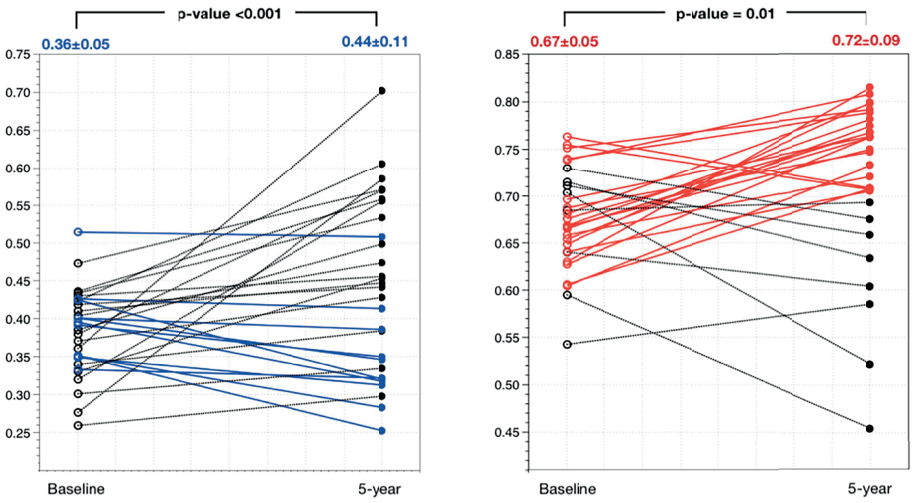

Figure 3. Individual asymmetry index (3A) and eccentricity index (3B) changes of the lumen between baseline and 5 years.
Figure 3A shows individual changes in the asymmetry index where blue lines connect individual case that asymmetry index improves (lower than baseline), the dotted black lines connect the individual case that asymmetry index becomes worse (higher than baseline).
Figure 3B shows individual changes in the eccentricity index where red lines connect individual case that eccentricity index becomes concentric (EI ≥ 0.7) whereas the dotted black lines connect the individual case that becomes eccentric (EI < 0.7).
Abbreviation: see Figure 1

DISCUSSION

The main findings of the current analysis are the following: 1) the polymeric device has a high incidence of asymmetry (93.1%) and eccentricity (72.4%) of the lumen post-implantation; 2) at 5-year follow-up, the lumen shape of the scaffold segment became more circular; 3) nevertheless, the lumen asymmetry did not improve in the long-term follow-up, suggesting that longitudinal heterogeneity of the lumen diameters persisted.

Recently, the prospective randomized controlled ABSORB II trial comparing the Absorb BVS and Xience stent reported that high AI (> 0.3) was associated with an increase in device-oriented composite endpoint (DoCE) mainly driven from myocardial infarction[11], suggesting that the heterogeneity in lumen diameters and lumen areas throughout the scaffold could have pathophysiologic implications in early- and medium-term follow-up. However, the current analysis showed that the asymmetric lesions as well as eccentric lesions were not associated with MACE at 5-year follow-up. The discrepancy of the results might be explained by small sample size and low event rates in the trial.

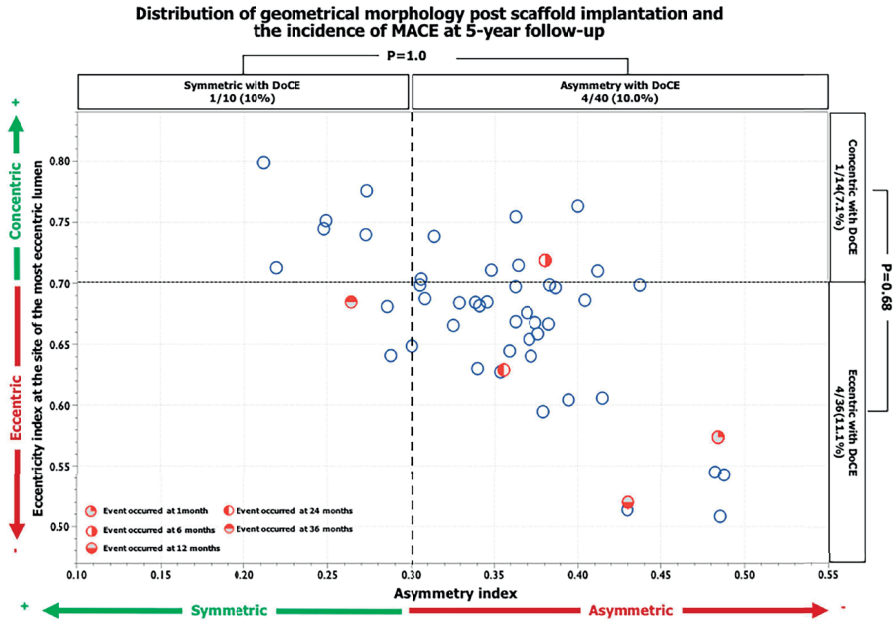

Figure 4. Distribution of geometrical morphology after scaffold implantation and the incidence of DoCE over 5-year follow-up

The scatter plot represents the asymmetry index (AI) on the x axis and the eccentricity index (EI) at the site of the most eccentric lumen on the y axis. Red dots represented cases with major adverse cardiac events.

In the previous studies where IVUS and OCT were used, both modalities showed that the eccentricity did not affect the neointimal growth[12,13]. The current analysis also showed similar findings; the neointimal thickness between the EI_L- and EI_H- cross-section was comparable.

Practical implication

Recent IVUS studies demonstrated that post-procedural asymmetry of stent or scaffold is the independent determinant of device-oriented clinical events (DoCE) irrespective of the expansion index[11]. However, the attempt to correct eccentricity and asymmetry of the lumen may be troublesome. Both pre- and post- aggressive dilation may correct the lumen eccentricity (calculated in one cross-section), on the other hand, it may not be able to change the gap between minimal and maximal lumen diameters due to the fact that the balloon also increases the lumen diameters in both cross-sections (see Fig 1). Aggressive lesion preparation with systematic non-compliant balloon in combination with routine high pressure post-dilation (with non-compliance balloon) previously reported by Mattasini et al[14] would be the strategy of choice to avoid the eccentric and asymmetric lumen morphology.

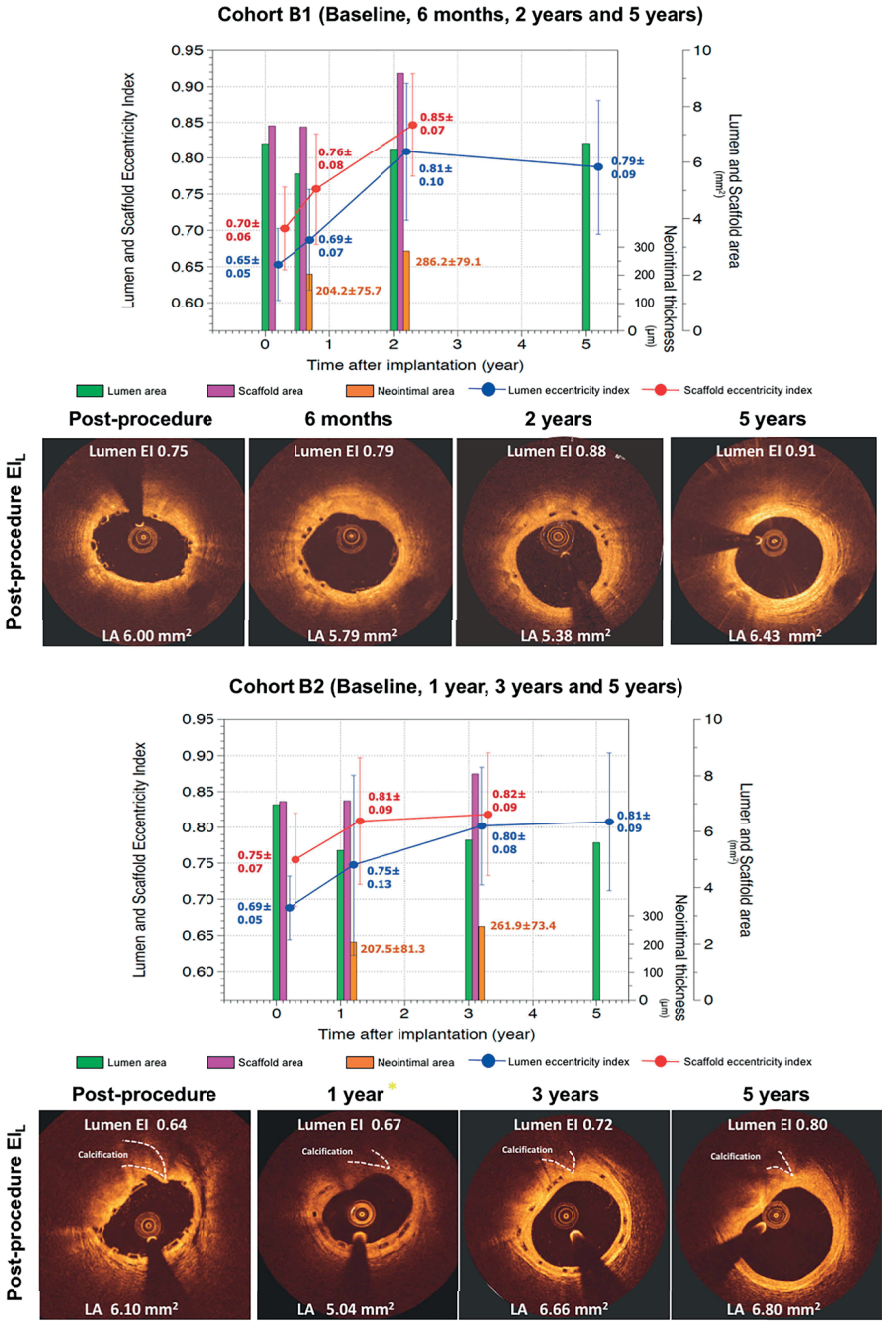

Figure 5.Serial changes of lumen and scaffold area and lumen and scaffold eccentricity index of matched cross-sections at the site of the lowest value of the post procedural eccentricity index in cohort B1 (5A) and cohort B2 (5B)

The bar graphs in green and magenta colors represent lumen area and scaffold area, respectively. The bar graphs in orange represent the neointimal thickness in micrometer. The blue circle and vertical lines represent the mean and standard error of the mean of EI_L post-procedure whereas the red circle and vertical lines represent the mean and standard error of the mean of the scaffold eccentricity index at the same cross-section. The EI_L substantially increased from baseline to 2-year follow-up (blue line panel A), in parallel with the scaffold eccentricity index (red line panel A). In the first 2 years after implantation, the improvement of lumen circularity is basically driven by the reshaping of the scaffold area. From 1 year to 3 years, the eccentricity of the scaffold did not change whereas the lumen circularity further improved (blue line panel B). The continuous growth of neointimal tissue also contributed to the regaining of lumen circularity and eventually resulted in similar eccentricity of the lumen and scaffold area at 3 years (bar graph in orange color).

So far, the evidence of the eccentric and asymmetric lumen morphology post-implantation and clinical outcomes is sparse. The online OCT guidance during procedure to correct asymmetric and eccentric lumen morphology with shear stress analysis would be of interest in further clinical trials.

Limitation

There are several limitations in the present study that need to be addressed. First, the analysis was solely based on the cases that had serial OCT at all time-points, therefore, it was inevitable to have a small sample size with potential selection bias. The findings should be interpreted with caution as the ABSORB cohort B included relatively simple lesion characteristics. The results of the present study may not be applicable in complex lesions. In addition, the data was derived from subgroup analysis, therefore, it is hypothesis generating in nature. Second, pre-procedure OCT images were not available, pre-existing asymmetric or eccentric lesions certainly affect the scaffold morphology after deployment. Third, the software and catheters were different because of technology advancement throughout the study period. However, both eccentricity and asymmetry indices were calculated by using ratio of lumen diameters, thus, the values would not be influenced by the different types of OCT systems. Forth, because of the limited penetration of OCT, the present analysis was unable to assess whether there was a relationship between the lumen morphological changes and plaque burden, plaque progression or regression, alteration of plaque type and vessel remodeling. To address questions raised above, co-localization of OCT and IVUS images is a prerequisite. Further analyses of plaque composition, vascular remodeling and wall shear stress profiling as assessed by IVUS may provide more mechanistic details of luminal change over time.

CONCLUSION

In patients treated with bioresorbable scaffolds, the cross-sectional circularity improved over 5 years while the variance in longitudinal diameters remained without creating a

Table 3 Comparison of neointimal thickness between the lowest eccentricity index cross-section and the highest eccentricity index cross-section

Matched cross-section data	6 months	1 year	2 years	3 years
	(N=13, L13)	(N=15,L=16)	(N=13, L13)	(N=15, L=16)
At the site of the lowest eccentricity index post-procedure (EI_L)				
Minimal neointimal thickness at the site of EI_L*, μm	15.8±18.3	72.5±69.9	113.8±66.2	105.0±61.5
Maximal neointimal thickness at the site of EI_L*, μm	460.8±340.8	400.6±140.3	466.2±150.6	412.5±97.6
Mean neointimal thickness at the site of EI_L, μm	204.2±75.7	207.5±81.3	286.2±79.1	261.9±73.4
At the site of the highest eccentricity index post-procedure(EI_H)				
Minimal neointimal thickness at the site of EI_H*, μm	95.4±75.9	71.9±64.0	129.2±74.9	127.5±67.1
Maximal neointimal thickness at the site of EI_H*, μm	340.8±130.4	363.1±216.6	403.9±140.2	370.6±139.5
Mean neointimal thickness at the site of EI_H, μm	216.9±89.5	196.3±75.5	253.9±78.5	240.0±74.1
Comparison of neointimal thickness				
p-value for minimal neointimal thickness#	0.007	0.08	0.58	0.30
p-value for maximal neointimal thickness**	0.18	0.55	0.19	0.33
p-value for mean neointimal thickness†	0.79	0.56	0.21	0.27

Data are shown in mean±SD or median (IQR 1st-3rd) or n(%). *represent as mean value; #comparison between minimal neointimal thickness of EI_L and EI_H ;** comparison between maximal neointimal thickness of EI_L and EI_H; †comparison between mean neointimal thickness of EI_L and EI_H

Abbreviation: EI_L : post procedural lowest eccentricity index value in scaffold segment; EI^H : post procedural highest eccentricity index value in scaffold segment

significant stenosis. Regaining of lumen circularity is mainly caused by reshaping of the scaffold during the first 2 years.

Impact on daily practice

The polymeric device has a high incidence of asymmetry and eccentricity of the lumen post-implantation. The previous IVUS data showed that post-procedural asymmetric lesion is associated with 1-year clinical events mainly driven from MI. The present study demonstrated that at 5-year follow-up, the lumen could regain its circularity but the asymmetry of the lumen still persisted. The asymmetric lesions were not associated with MACE at 5-year follow-up, albeit in a limited sample size. The strategies to avoid eccentricity and asymmetry of the lumen post-implantation remain challenging and need further investigation

REFERENCES

1. Brugaletta S, Gomez-Lara J, Diletti R, et al. Comparison of in vivo eccentricity and symmetry indices between metallic stents and bioresorbable vascular scaffolds: insights from the ABSORB and SPIRIT trials. *Catheterization and cardiovascular interventions.* 2012;79(2):219-228.
2. Hwang C-W, Wu D, Edelman ER. Physiological Transport Forces Govern Drug Distribution for Stent-Based Delivery. *Circulation.* 2001;104(5):600-605.
3. Karanasos A, Simsek C, Gnanadesigan M, et al. OCT assessment of the long-term vascular healing response 5 years after everolimus-eluting bioresorbable vascular scaffold. *Journal of the American College of Cardiology.* 2014;64(22):2343-2356.
4. Serruys PW, Ormiston J, van Geuns RJ, et al. A Polylactide Bioresorbable Scaffold Eluting Everolimus for Treatment of Coronary Stenosis: 5-Year Follow-Up. *Journal of the American College of Cardiology.* 2016;67(7):766-776.
5. Tateishi H, Suwannasom P, Sotomi Y, et al. Edge Vascular Response After Resorption of the Everolimus-Eluting Bioresorbable Vascular Scaffold- A 5-Year Serial Optical Coherence Tomography Study. *Circulation journal : official journal of the Japanese Circulation Society.* 2016;80(5):1131-1141.
6. Gogas BD, Serruys PW, Diletti R, et al. Vascular response of the segments adjacent to the proximal and distal edges of the ABSORB everolimus-eluting bioresorbable vascular scaffold: 6-month and 1-year follow-up assessment: a virtual histology intravascular ultrasound study from the first-in-man ABSORB cohort B trial. *JACC Cardiovascular interventions.* 2012;5(6):656-665.
7. Tsuchida K, Garcia-Garcia HM, Ong AT, et al. Revisiting late loss and neointimal volumetric measurements in a drug-eluting stent trial: analysis from the SPIRIT FIRST trial. *Catheterization and cardiovascular* 2006;67(2):188-197.
8. de Jaegere P, Mudra H, Figulla H, et al. Intravascular ultrasound-guided optimized stent deployment. Immediate and 6 months clinical and angiographic results from the Multicenter Ultrasound Stenting in Coronaries Study (MUSIC Study). *Eur Heart J.* 1998;19(8):1214-1223.
9. Mintz GS, Nissen SE, Anderson WD, et al. American College of Cardiology Clinical Expert Consensus Document on Standards for Acquisition, Measurement and Reporting of Intravascular Ultrasound Studies (IVUS). A report of the American College of Cardiology Task Force on Clinical Expert Consensus Documents. *Journal of the American College of Cardiology.* 2001;37(5):1478-1492.
10. von Birgelen C, Gil R, Ruygrok P, et al. Optimized expansion of the Wallstent compared with the Palmaz-Schatz stent: on-line observations with two- and three-dimensional intracoronary ultrasound after angiographic guidance. *American heart journal.* 1996;131(6):1067-1075.
11. Suwannasom P, Sotomi Y, Ishibashi Y, et al. The Impact of Post-Procedural Asymmetry, Expansion, and Eccentricity of Bioresorbable Everolimus-Eluting Scaffold and Metallic Everolimus-Eluting Stent on Clinical Outcomes in the ABSORB II Trial. *JACC Cardiovascular interventions.* 2016;9(12):1231-1242.
12. Kim BK, Ko YG, Oh S, et al. Comparisons of the effects of stent eccentricity on the neointimal hyperplasia between sirolimus-eluting stent versus paclitaxel-eluting stent. *Yonsei medical journal.* 2010;51(6):823-831.
13. Kaneda H, Ako J, Honda Y, et al. Impact of asymmetric stent expansion on neointimal hyperplasia following sirolimus-eluting stent implantation. *The American journal of cardiology.* 2005;96(10):1404-1407.
14. Mattesini A, Secco GG, Dall'Ara G, et al. ABSORB biodegradable stents versus second-generation metal stents: a comparison study of 100 complex lesions treated under OCT guidance. *JACC Cardiovascular interventions.* 2014;7(7):741-750.

Chapter 17

Edge Vascular Response After Resorption of the Everolimus-Eluting Bioresorbable Vascular Scaffold: A 5-Year Serial Optical Coherence Tomography Study

Hiroki Tateishi, Pannipa Suwannasom, Yohei Sotomi, Shimpei Nakatani, Yuki Ishibashi, Erhan Tenekecioglu, Mohammad Abdelghani, Rafael Cavalcante, Yaping Zeng, Maik J. Grundeken, Felipe N. Albuquerque, Susan Veldhof, Yoshinobu Onuma, Patrick W. Serruys

Circ J. 2016 Apr 25;80(5):1131-41

ABSTRACT

Background

The edge vascular response (EVR) has been linked to important prognostic implications in patients treated with permanent metallic stents. We aimed to investigate the relationship of EVR with the geometric changes in the everolimus-eluting bioresorbable scaffold using serial optical coherence tomography (OCT) analysis.

Methods and Results

In the first-in-man ABSORB trial, 28 patients (29 lesions) underwent serial OCT at 4 different time points (Cohort B1: post-procedure, 6, 24, and 60 months [n=13]; Cohort B2: post-procedure, 12, 36, and 60 months [n=15]) following implantation of the scaffold. In Cohort B1, there was no significant luminal change at the distal or proximal edge segment throughout the entire follow-up. In contrast, there was a significant reduction of the lumen flow area (LFA) of the scaffold between post-procedure and 6 months (-1.03 ± 0.49 mm^2 [$P<0.001$]), whereas between 6 and 60 months the LFA remained stable ($+0.31\pm1.00$ mm^2 [$P=0.293$]). In Cohort B2, there was a significant luminal reduction of the proximal edge between post-procedure and 12 months (-0.57 ± 0.74 mm^2 [$P=0.017$]), whereas the lumen area remained stable (-0.26 ± 1.22 mm^2 [$P=0.462$]) between 12 and 60 months. The scaffold LFA showed a change similar to that observed in Cohort B1.

Conclusions

Our study demonstrated a reduction in the scaffold luminal area in the absence of major EVR, suggesting that the physiological continuity of the lumen contour is restored long term.

The advent of the metallic stent has been a major breakthrough in the treatment of patients with ischemic coronary artery disease. In the era of the bare-metal stent (BMS), the edge vascular response (EVR) was defined as a reduction in the lumen area mainly from an increase in plaque/media and lumen area within the first 1–2 mm of the device.[1,2] In the era of radioactive stents, EVR became a more prominent effect.[3] In the drug-eluting stent (DES) era, although several studies have demonstrated effective inhibition of neointimal hyperplasia, the EVR was mostly focal and located at the proximal stent edge.[4–7] The rigidity of the metal encaging the vessel can potentially lead to a life-long loss of pulsatility and distensibility of the coronary arterial wall in the stented segment and a compliance mismatch between the stented and adjacent segments of the vessel. In the bioresorbable scaffold (BRS) era, a variety of polymers with different chemical compositions, mechanical properties, and bioresorption duration became available. The polymer most frequently used is poly-L-lactide (PLLA).[8] After completion of the bioresorption process, the struts become integrated into the surrounding vessel wall,[9,10] and the strut voids are no longer visible on optical coherence tomography (OCT) at 5 years after implantation.[11] Our group has previously demonstrated no major changes in lumen area at both the distal and proximal edges of the scaffold at 6 months using intravascular ultrasound (IVUS) analysis. However, at long-term follow-up (1 and 2 years), especially at the proximal edge, there was a slight but statistically significant lumen loss (LL) without any significant change in the lumen area of the distal edge.[12,13]

The aim of the present study was to describe the EVR and its relationship with the scaffold throughout the entire follow-up period of 60 months using serial OCT analysis.

METHODS

Study Design and Study Device

The ABSORB Cohort B trial (clinicaltrials.gov NCT00856856, Study Sponsor Abbott Vascular) is a non-randomized, multicenter, single-arm prospective, open-label trial that included 101 patients (102 lesions) treated with the 2nd-generation Absorb scaffold. The first 45 patients (Cohort B1) underwent intravascular imaging follow-up with OCT at 6, 24, and 60 months, whereas the other 56 patients (B2) underwent the same at 12, 36, and 60 months follow-up.

The Absorb scaffold (Abbott Vascular, Santa Clara, CA, USA) consists of a PLLA scaffold, a coating layer of poly-D,L-lactide (PDLLA) and the antiproliferative drug everolimus, a pair of radiopaque platinum markers at the proximal and distal ends of the scaffold, and a balloon catheter delivery system.[14] The details of the study and treatment procedure have been previously described.[15–18]

OCT Image Acquisition

Over the past 5 years OCT techniques have evolved. OCT acquisition in this study was performed using 4 different commercially available systems: the M2 and M3 Time-Domain Systems and the C7 and C8 Fourier-Domain Systems (LightLab Imaging, Westford, MA, USA). OCT images were acquired at a frame rate of 15.6, 20, 100, 180 frames/s with a pullback speed of 2, 3, 20, 18 mm/s in the M2 (n=11), M3 (n=11), C7 (n=174), and C8 (n=39), respectively. All image acquisition was performed according to the recommended procedure for each OCT system.[19] None of the OCT images was acquired with the occlusion technique.[16–18] If the 5-mm edge segment had a side branch with an ostium diameter ≥1.5 mm, the analysis included only those frames between the scaffold margin and the ostium of the side branch. If the ostium diameter of the side branch was less than 1.5 mm, the frames at the ostium of the side branch were excluded. In addition, we excluded subjects who required a bailout stent, subjects with a scaffold implantation adjacent to a previously deployed stent, subjects in whom the edge segment was not fully documented, and frames with insufficient assessment of the entire lumen circumference because of inadequate blood clearance, air bubbles or contrast filling the extremity of the OCT catheter.[20]

OCT Data Analysis

The OCT images acquired post-procedure and at follow-up were analyzed off-line, using proprietary LightLab software (St. Jude Medical Inc, MA, USA) and Q-IVUS 3.0 (Medis Medical Imaging systems, Leiden, The Netherlands). Truly serial OCT data were used in patients who underwent OCT examinations at all 4 time points. Lumen flow area (LFA) of the scaffold segment and the 5-mm segments adjacent to both edges were analyzed at 1-mm intervals by an independent core laboratory (Cardialysis, Rotterdam, The Netherlands). Adjusting for the pullback speed, the analysis of continuous cross-sections was performed at each 1-mm longitudinal interval.[16–18]

As a specific additional approach, frame-by-frame analyses were performed for the 5-mm edge segment and the transitional region between the edge and scaffold segment. The transitional region was defined as a 4-mm region including both the 2 mm of the lumen vessel adjacent to the scaffold edge and the 2-mm margins of the scaffold. The LFA (ie, the effective lumen filled by circulating blood) was defined as the lumen area minus the strut area.[16,21] At follow-up, LFA was equal to the lumen area if no malapposed struts were found. Details of the LFA measurements have been previously described.[21]

Definition of the Scaffolded Segment

At 3 years, most of the scaffold struts remained visible as a black core, so the scaffold edges were defined as the first and last cross-sections with circumferentially visible struts.[13] At 5 years, the struts are no longer visible, so only the platinum marker was visu-

alized as evidence and location of the bioresorbed scaffold. However, in a few patients visualization of the marker was masked by the guidewire shadow. Furthermore, poor image acquisition because of inadequate blood clearance, contrast filling the OCT catheter, artifact from tangential signal drop out, or other reflective structures (eg, mineralization) was a limiting factor. Accordingly, in the present study localization of the edges of the scaffold was performed as follows: (1) when both the proximal and distal markers could be identified, the scaffold segment was defined as the segment between the first cross-section of the distal marker and the last cross-section of the proximal marker; (2) when the marker could not be clearly identified, we used anatomical landmarks on previous OCT images and another imaging modality, such as coronary angiography or IVUS, to localize the edge of the bioresorbed body of the scaffold; (3) when the marker could be identified only on one side, the scaffold length (18 mm) was used to assume the localization of the other edge of the scaffold.

IVUS Greyscale Analysis

Treated vessels post-procedure were examined with phased array IVUS catheters (EagleEye™; Volcano Corporation, Rancho Cordova, CA, USA) using a pullback speed of 0.5 mm/s.[16–18,22] The region of interest, beginning 5 mm distal to and extending 5 mm proximal to the treated segment, was examined. Lumen area, vessel area, plaque burden at the edge segment, and significant residual reference segment stenosis,[23] defined as a reference minimum lumen (CSA <4 mm^2) plus plaque burden <70%, are shown in Table 1.

Assessment of Procedural Performance and Postprocedural Findings on OCT

According to the IVUS-MUSIC criteria,[24] we calculated the expansion index (=minimum scaffold area/reference lumen area), the percentage of residual area stenosis (%RAS: =[reference lumen area-minimum scaffold area]/reference lumen area×100), and the scaffold-artery ratio (the ratio of nominal scaffold diameter to the mean reference diameter, the ratio of the post-dilatation balloon nominal diameter to the mean reference diameter, and the ratio of expected scaffold diameter from pressure to mean reference diameter). The procedural details are summarized in Table 1 and the adequacy of expansion was evaluated based on the MUSIC criteria.

The frequency of non-flow-limiting edge dissection, which was identified on postprocedural OCT, is shown in Table 1, as well as intra-scaffold dissection, tissue protrusion, and thrombus, which were identified in the 2-mm margin of the scaffold segment in accordance with previous reports.[25,26]

Table 1. Lesion Characteristics and Procedural Parameters at the Lesion Level in Patients With Serial OCT Analysis

Variable	B1+B2 (n=29)	B1 (n=13)	B2 (n=16)	P value (B1 vs. B2)
Target-lesion vessel (LAD/LCx/RCA)	15/6/8	6/4/3	9/2/5	0.87
AHA classification (A/B1/B2/C)	0/20/8/0	0/10/3/0	0/10/5/0	0.56
Stent implantation				
Scaffold size diameter, mm	3.0	3.0	3.0	–
Scaffold inflation pressure, atm	13.17±2.90	14.15±2.51	12.37±3.03	0.51
Expected scaffold diameter, mm	3.30±0.11	3.32±0.90	3.26±0.13	0.40
Expected scaffold area, mm^2	8.58±0.55	8.67±0.47	8.38±0.65	0.41
Post-dilatation				
Balloon dilatation after device implantation, n (%)	19/29 (65.5)	9/13 (69.2)	10/16 (62.5)	0.71
Maximal diameter of post-dilatation balloon (nominal pressure), mm	3.18±0.19	3.22±0.23	3.15±0.17	0.49
Post-dilatation balloon area (nominal pressure), mm^2	7.98±0.82	8.31±0.90	7.61±0.64	0.09
Length of post-dilatation balloon inflation, mm	11.70±3.13	11.22±3.11	12.09±3.23	0.55
Maximal post-dilatation balloon inflation, atm	17.79±5.32	18.00±6.00	17.60±4.95	0.86
No. of inflations performed	2.26±2.00	2.22±1.99	2.44±2.19	0.94
Ratio of post-dilatation balloon nominal diameter to nominal stent diameter	1.06±0.05	1.08±0.06	1.04±0.04	0.09
Scaffold-artery ratio on postprocedural OCT				
Ratio of nominal scaffold diameter to mean reference diameter	1.10±0.14	1.11±0.17	1.10±0.11	0.77
Ratio of post-dilatation balloon nominal diameter to mean reference diameter	1.16±0.13	1.20±0.16	1.14±0.09	0.27
Ratio of expected scaffold diameter according to dilatation pressure to mean reference diameter	1.21±0.15	1.22±0.15	1.20±0.10	0.56
Postprocedural OCT findings				
Mean reference lumen area, mm^2	6.20±1.65	6.14±2.06	6.31±1.51	0.71
Mean reference diameter, mm	2.76±0.34	2.77±0.43	2.75±0.27	0.94
Mean scaffold area, mm^2	7.56±0.98	7.59±1.38	7.66±0.91	0.79

Table 1. Lesion Characteristics and Procedural Parameters at the Lesion Level in Patients With Serial OCT Analysis (continued)

Variable	B1+B2 (n=29)	B1 (n=13)	B2 (n=16)	P value (B1 vs. B2)
Minimal scaffold area, mm^2	6.19±0.93	6.23±1.28	6.33±0.76	0.72
Expansion index	1.04±0.21	1.05±0.16	1.04±0.20	0.74
Percentage of residual area stenosis (%RAS)	−4.16±21.20	−5.35±16.06	−3.80±19.95	0.73
Edge segment after procedure				
Proximal non-flow-limiting edge dissection, number (%)	7/26 (26.9)	2/10 (20.0)	5/16 (31.3)	0.53
Distal non-flow-limiting edge dissection, number (%)	6/27 (22.2)	3/13 (23.1)	3/14 (21.4)	0.92
2-mm scaffold margin after procedure				
Proximal intra-scaffold dissection, n (%)	8/29 (27.6)	3/13 (23.1)	5/16 (31.3)	0.62
Distal intra-scaffold dissection, n (%)	3/28 (10.7)	0/13	3/15 (20.0)	0.09
Proximal intra-scaffold thrombus, n (%)	3/29 (10.3)	1/13 (7.7)	2/16 (12.5)	0.67
Distal intra-scaffold thrombus, n (%)	2/28 (7.1)	1/13 (7.7)	1/15 (6.7)	0.92
Tissue prolapse at proximal 2-mm margin of scaffold, n (%)	22/29 (75.9)	11/13 (84.6)	11/16 (75.9)	0.32
Tissue prolapse at distal 2-mm margin of scaffold, n (%)	23/28 (82.1)	12/15 (80.0)	11/13 (84.6)	0.75
Greyscale IVUS findings at the reference segment				
Proximal mean reference lumen area, mm^2	7.55±2.10	7.62±2.64	7.50±1.66	0.89
Distal mean reference lumen area, mm^2	6.37±1.36	5.98±0.98	6.64±1.56	0.28
Proximal mean vessel area, mm^2	14.15±3.48	14.03±4.64	14.24±2.41	0.89
Distal mean vessel area, mm^2	11.10±3.51	10.26±3.78	11.69±3.33	0.36
Residual plaque burden at proximal edge segment, %	46.05±10.26	44.65±11.93	47.16±9.06	0.56
Residual plaque burden at distal edge segment, %	38.83±17.40	36.66±18.46	40.34±17.22	0.64
Significant residual stenosis at the proximal edge segment, n (%)	1/23 (4.3)	1/11 (9.1)	0	–
Significant residual stenosis at the distal edge segment, n (%)	1/22 (4.5)	0	1/13 (7.7)	–

IVUS, intravascular ultrasound; LAD, left anterior descending; LCx, left circumflex artery; OCT, optical coherence tomography; RCA, right coronary artery.

Statistical Analysis

Continuous variables are presented as mean±standard deviation (SD) or median and interquartile range. Normality of the data was determined with the Shapiro-Wilk test and verified by histogram. For the overall assessment, Wilcoxon signed-rank test adjusted by the Bonferroni correction was used to compare EVR within groups at different time points, while for the truly serial follow-up assessment, paired t-test or Wilcoxon signed-rank test was used to compare EVR within groups at different time points without adjustment. A P-value <0.05 was considered statistically significant. All statistical analyses were performed with IBM SPSS Statistics 22 (IBM Co, NY, USA) and MedCalc (ver. 14.12.0, MedCalc Software, Ostend, Belgium).

RESULTS

Study Population and OCT Image Acquisition

A total of 235 OCT pullbacks were analyzed in 90 patients (Cohort B1: 40 patients, 40 lesions; Cohort B2: 50 patients, 51 lesions). At 5-year follow-up, OCT was performed in 52 patients (53 lesions) [Cohort B1: 22 patients (22 lesions); Cohort B2: 30 patients (31 lesions)] (Figures S1A,B). According to the criteria described in the Methods section, we excluded a total of 14 distal edges and 15 proximal edges for the following reasons: 4 edges were not documented on the pullback; 2 edges had overlap with a previously deployed DES; 4 edges had been treated with bailout DES deployment; 1 edge because of DES overlapping the scaffold segment for target lesion revascularization (TLR), and the remaining 18 edges because of a large side branch (≥1.5 mm), insufficient assessment of the entire lumen, or inadequate contrast clearance.

During the 5-year follow-up, of the entire cohort of 101 patients, 11 patients underwent TLR, and 1 of them underwent TLR twice during the entire follow-up. Of these 11 patients (12 TLR), only 3 patients had preprocedural OCT images and were noted to have TLR for edge restenosis (2 proximal, 1 distal). These 3 cases were excluded and thus the study reports exclusively the evolution of the edges in patients who had an uneventful follow-up.

Over the entire follow-up period, 13 patients (13 lesions) of Cohort B1 and 15 patients (16 lesions) of Cohort B2 had serial OCT follow-up images (Figures S2A,B).

Assessment of Procedural Performance on Postprocedural OCT

The scaffold-artery ratio, which indicates the adequate and appropriate ratio for optimal scaffold expansion, was 1.10±0.14 for the ratio of nominal scaffold diameter to the mean reference diameter, and 1.16±0.13 for the ratio of the post-dilatation balloon nominal diameter to the mean reference diameter (Table 1).

Table 1 shows the procedural details and OCT performance parameters that were used to evaluate the stent expansion and scaffold-artery ratio. The expansion index was 1.04±0.21 and the %RAS was −4.16±21.20, suggesting that optimal scaffold expansion was achieved in this population.

Edge dissections were identified at the proximal edge segment (26.9%), and at the distal edge segment (22.2%) immediately post-procedure. Tissue prolapse was identified in most of the lesions; however, there was no more than 500 μm of tissue prolapse (data not shown). Greyscale IVUS analysis showed no large plaque burden of the edge segment (proximal: 46.05±10.26%, distal: 38.83±17.40%). Only 1 significant residual stenosis at the proximal edge segment and 1 significant residual stenosis at the distal edge segment were identified.

Change in the LFA of the Scaffold Segment

Figure 1A shows the LFA of the entire scaffold segment as well as the proximal and distal 5-mm edges. The 4 time points are illustrated by the different lines: the black line illustrates the postprocedural contour of the edge and scaffold, which is over-expanded with respect to the edge with a "step-up" and a "step down" at the site of the scaffold implantation. The major change in the first 12 months was a reduction in flow area without any further change in the luminal dimensions after 12 months, so the LFA curves of 12, 36, and 60 months are more or less superimposed in Figure 1A. Figure 1B shows similar profile for the patients who had serial OCT at 6, 24, and 60 months.

EVR and the Change in Lumen Area of the Scaffold Subsegment

The mean LFA, minimal LFA, as well as the changes in the mean LFA over time for both edges and scaffolds at all the time points in the 2 cohorts are shown in the Table S1. The lumen area of the distal edges did not change significantly throughout the entire follow-up period, but there was a trend toward a decrease in the lumen area of the proximal edges over the same period (7.17±2.45 mm^2 post-procedure vs. 6.05±1.80 mm^2 at 60 months [P=0.214] for Cohort B1; 7.95±3.50 mm^2 post-procedure vs. 6.12±1.71 mm^2 at 60 months [P=0.022] for Cohort B2). After the initial and significant decreases in the mean and minimal LFA of the scaffold documented at either 6 months or 12 months, no further significant changes in these parameters were observed.

To further assess the changes in the lumen area of the edge segment, truly serial assessment was performed at 6, 24 and 60 months (Cohort B1) and at 12, 36 and 60 months (Cohort B2) (Tables 2A,B; Figures 2A,B).

At 12, 36 and 60 months (B2), there was a significant reduction of the LFA at the distal margin between post-procedure and 12 months (at the 1-mm margin: 6.92±1.15 mm^2 vs. 5.60±1.75 mm^2, and 2-mm margin: 7.36±1.04 mm^2 vs. 5.64±1.30 mm^2, both P-values=0.001) (Table 2A; Figure 2A). However, there were no significant changes of

the LFA at either the 1-mm or 2-mm distal margins of the scaffold between 12 months and 60 months (at the 1-mm margin: 5.60±1.75 mm^2 vs. 4.99±2.19 mm^2 [P=0.116]; at the 2-mm margin: 5.64±1.30 mm^2 vs. 5.18±1.96 mm^2 [P=0.211]) (Figure 2A).

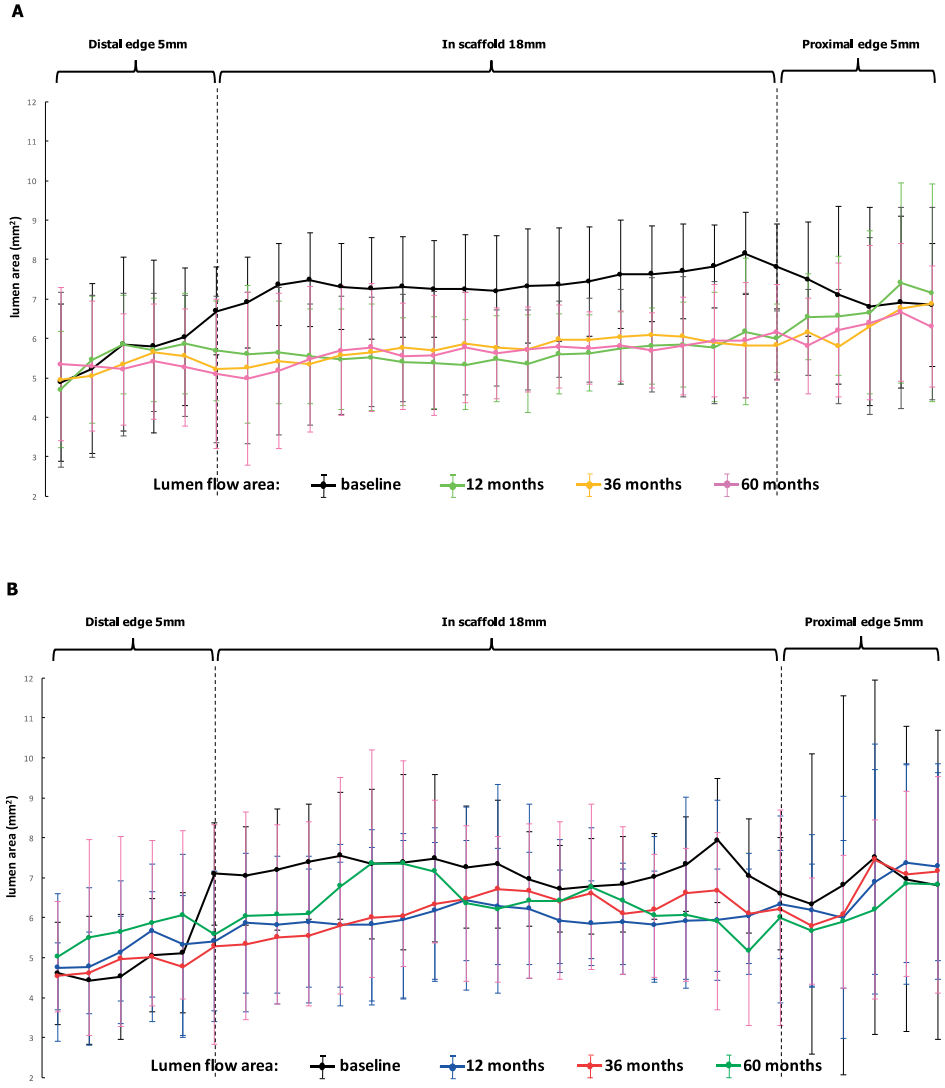

Figure 1. Mean values of the lumen area of the target segment with every 1-mm analysis. Lumen area of the entire scaffold segment as well as the proximal and distal 5-mm edges. The 4 time points are illustrated by lines of different colors. (A) Cohort B2 at 12, 36 and 60 months; (B) Cohort B1 at 6, 24 and 60 months. The respective absolute values and the delta changes as well as the statistical significance are tabulated in Tables 2A,B.

Table 2. Changes in Lumen Area at Both the Distal and Proximal Edges on Serial OCT Analysis (A) Cohort B2 at 12, 36 and 60 Months, (B) Cohort B1 at 6, 24 and 60 Months

(A)	BL (n)	1Y (n)	3Y (n)	5Y (n)	1Y-BL Difference P value	3Y-1Y Difference P value	5Y-3Y Difference P value	5Y-1Y Difference P value	3Y-BL Difference P value	5Y-BL Difference P value
Distal edge 5 mm (mm^2)	5.71±1.82 (n=13)	5.70±1.21 (n=14)	5.41±1.59 (n=14)	5.41±1.41 (n=13)	+0.07±1.09 0.821	−0.29±0.79 0.191	0.00±0.78 0.985	−0.29±0.82 0.209	−0.15±0.92 0.591	−0.22±1.34 0.584
Distal scaffold (mm^2)	7.35±1.02 (n=16)	5.75±1.26 (n=16)	5.73±1.77 (n=16)	5.45±1.75 (n=16)	−1.60±1.21 <0.001	−0.02±0.89 0.926	−0.28±1.04 0.301	−0.30±1.13 0.307	−1.62±1.77 0.002	−1.90±1.72 <0.001
Mid-scaffold (mm^2)	7.13±1.31 (n=16)	5.48±0.83 (n=16)	5.84±1.12 (n=16)	5.69±1.14 (n=16)	−1.66±1.21 <0.001	+0.37±0.78 0.079	−0.15±0.70 0.394	+0.21±0.84 0.331	−1.29±1.47 0.003	−1.45±1.53 0.002
Proximal scaffold (mm^2)	7.51±1.17 (n=16)	5.80±0.67 (n=16)	5.93±1.07 (n=16)	5.88±1.01 (n=16)	−1.70±1.16 <0.001	+0.13±0.90 0.584	−0.05±0.66 0.782	+0.08±0.90 0.727	−1.58±1.46 0.001	−1.62±1.38 <0.001
Whole scaffold (mm^2)	7.32±0.89 (n=16)	5.68±0.74 (n=16)	5.75±1.06 (n=16)	5.66±1.10 (n=16)	−1.63±1.00 <0.001	+0.07±0.76 0.724	−0.09±0.43 0.418	−0.02±0.81 0.917	−1.57±1.07 <0.001	−1.65±1.10 <0.001
Proximal edge 5 mm (mm^2)	7.20±1.75 (n=13)	6.70±1.53 (n=13)	6.36±1.61 (n=12)	6.22±1.83 (n=13)	−0.57±0.74 0.017	−0.12±0.73 0.564	−0.14±0.94 0.596	−0.26±1.22 0.462	−0.84±1.27 0.027	−0.98±1.66 0.047
(B)	BL (n)	6M (n)	2Y (n)	5Y (n)	6M-BL Difference P value	2Y-6M Difference P value	5Y-2Y Difference P value	5Y-6M Difference P value	2Y-BL Difference P value	5Y-BL Difference P value
Distal edge 5 mm (mm^2)	4.94±1.23 (n=12)	5.39±1.83 (n=12)	4.95±1.26 (n=10)	5.61±2.08 (n=11)	+0.59±0.89 0.0520	−0.21±1.09 0.542	+0.21±0.78 0.391	+0.22±1.03 0.479	+0.22±0.86 0.433	+0.74±1.31 0.088
Distal scaffold (mm^2)	7.27±1.40 (n=13)	5.78±1.61 (n=13)	5.58±1.73 (n=13)	6.30±2.14 (n=13)	−1.50±0.69 <0.001	−0.20±0.98 0.477	+0.72±0.73 0.004	+0.52±1.57 0.253	−1.70±0.95 <0.001	−0.97±1.51 0.039
Mid-scaffold (mm^2)	7.19±1.48 (n=13)	6.16±1.29 (n=13)	6.44±1.80 (n=13)	6.67±1.72 (n=13)	−1.03±0.74 <0.001	+0.28±1.80 0.589	+0.23±1.34 0.544	−0.52±1.56 0.222	0.51±1.43 0.201	−0.75±2.01 0.251
Proximal scaffold (mm^2)	7.42±1.11 (n=13)	6.12±0.95 (n=13)	6.52±1.67 (n=13)	6.12±1.47 (n=13)	−1.31±0.83 <0.001	+0.40±1.64 0.396	−0.40±1.51 0.361	+0.00±1.05 0.996	−0.91±1.46 0.045	−1.31±0.73 <0.001
Whole scaffold (mm^2)	7.06±1.23 (n=13)	6.04±1.19 (n=13)	6.17±1.44 (n=13)	6.34±1.51 (n=13)	−1.03±0.49 <0.001	+0.13±1.28 0.716	+0.17±0.63 0.338	+0.31±1.00 0.293	−0.90±1.16 0.016	−0.72±0.96 0.019
Proximal edge 5 mm (mm^2)	6.37±3.18 (n=11)	6.63±2.68 (n=11)	6.73±2.70 (n=11)	6.69±2.61 (n=10)	+0.32±1.33 0.488	+0.09±0.66 0.612	−0.04±0.72 0.855	−0.06±0.80 0.801	−0.43±0.91 0.191	−0.22±1.31 0.625

Values are presented as mean±standard deviation. The edge segments were evaluated by Wilcoxon signed-rank test, while the subsegments of scaffold were evaluated by paired t-test. A significant level for each paired comparison is 0.05. BL, baseline; OCT, optical coherence tomography; 6M, 6 months; 1Y, 1 year; 2Y, 2 years; 3Y, 3 years; 5Y, 5 years.

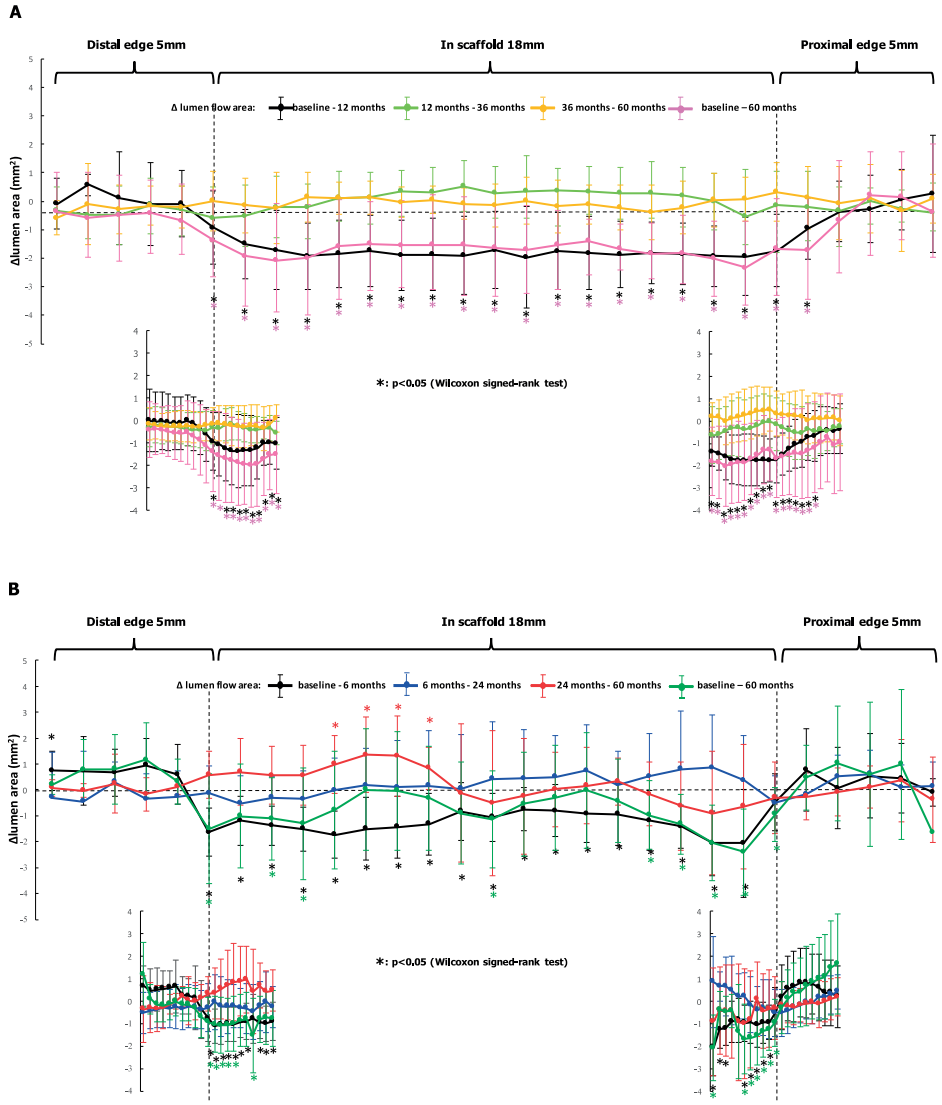

Figure 2. Change in lumen area of both edges and in-scaffold through the entire follow-up. (A) Cohort B2 at 12, 36 and 60 months: mean lumen area of the 18-mm in-scaffold segment decreased from baseline to 12-month (black line), extending into the first 1-mm proximal edge. There is a continuous pattern of luminal reduction extending from the in-scaffold margin to the first 1-mm of both the distal and proximal edges from baseline to 12 months; however, significant luminal reduction in-scaffold extends into only the first 1-mm proximal edge. (B) Cohort B1 at 6, 24 and 60 months: mean lumen area of the 18-mm in-scaffold segment decreased from baseline to 6-month (black line); however, there is no further significant change in the following 54 months. There is a trend toward an increase at the 5-mm distal edge in the first 6 months following device implantation without a following significant change from 6 to 60 months. In contrast, there is no significant change in lumen area at the proximal edge segment throughout the entire follow-up in this cohort. The 200-µm analysis at the transitional region reveals that although there is a continuous pattern of luminal reduction extending from the in-scaffold margin to the first 1-mm of both the distal and proximal edges in the first 6 months, significant lumen reduction is observed only at the in-scaffold margin.

At 6, 24 and 60 months (B1), there was a trend toward an increase in the lumen area of the distal edge (4.94±1.23 mm^2 post-procedure vs. 5.39±1.83 mm^2 at 6 months [P=0.052]; 5.61±2.08 mm^2 at 60 months [P=0.088, vs. post-procedure]) (Table 2B; Figure 2B). There was also a significant reduction of the LFA at both the 1-mm and 2-mm distal margins of the scaffold between post-procedure and 6 months (at the 1-mm margin: 7.05±1.23 mm^2 vs. 5.86±1.76 mm^2 [P=0.005], and at the 2-mm margin: 7.20±1.52 mm^2 vs. 5.82±1.71 mm^2 [P=0.001]) (Figure 2B).

At 12, 36 and 60 months (B2), the proximal edge lumen area of the first 1-mm edge decreased significantly between post-procedure and 12 months (7.49±1.45 mm^2 vs. 6.55±1.08 mm^2 [P=0.019]). In contrast there was no significant change of the lumen area at the first 1-mm edge between 12 months and 60 months (6.55±1.08 mm^2 vs. 5.81±1.22 mm^2 [P=0.508]) (Figure 2A).

At 6, 24 and 60 months (B1), no significant change was observed in the lumen of the proximal edge segment (6.37±3.18 mm^2 post-procedure, 6.63±2.68 mm^2 at 6 months, 6.73±2.70 mm^2 at 24 months, 6.69±2.61 mm^2 at 60 months, P=0.889) (Table 2B; Figure 2B).

In this cohort (B1), the 2-mm proximal margin of the scaffold segment also showed a significant reduction of LFA at the 2-mm proximal margin of the scaffold between post-procedure and 6 months (at the 1-mm margin: 7.05±1.43 mm^2 vs. 6.04±1.19 mm^2 [P=0.003]; at the 2-mm margin: 7.94±1.54 mm^2 vs. 5.94±1.28 mm^2 [P=0.002]) (Figure 2B). A similar change was observed at 12, 36 and 60 months (B2) between post-procedure and 12 months (at the 1-mm margin: 8.15±1.04 mm^2 vs. 6.17±1.85 mm^2 [P=0.002]; at the 2-mm margin: 7.83±1.06 mm^2 vs. 5.78±1.38 mm^2 [P=0.001]) (Figure 2A). However, there was no change in the LFA in the 2-mm proximal margin of the scaffold between 12 months and 60 months (at the 1-mm margin: 6.17±1.85 mm^2 vs. 5.95±1.47 mm^2 [P=0.638]; at the 2-mm margin: 5.78±1.38 mm^2 vs. 5.94±1.42 mm^2 [P=0.532]) (Figure 2A).

DISCUSSION

The main findings of the present study are: (1) in the first 12 months following device implantation, there was a significant reduction of the lumen of the scaffold, while in the following 48 months no significant change was demonstrated; (2) the change in lumen area at the edge segment within the first year can be more precisely localized in the so-called transitional region and the lumen reduction at the edges seems to be geometric prolongation of the scaffold reduction; (3) the scaffold segment and the lumen area in the transitional region no longer change after the first year of follow-up and the lumen contour of the edges aligned with the contour of the scaffold after 1 year; (4) no cases of TLR for either proximal or distal edge restenosis occurred after 3 years.

Because of the long-term follow-up and serial follow-up, this study was limited to a small number of observations. In view of the limited number of patients documented so far worldwide, we believed that Cohorts B1 and B2 should be pooled because both have follow-up at 5 years. Although some cases of aneurysmal changes were responsible for some heterogeneity of the lumen contours in Cohort B1 and there are some differences in the temporal changes of lumen area measurements between the 2 cohorts, the lumen contours of both cohorts presented a similar profile through the entire period (Figures 1A,B).

In order to fully document and evaluate the temporal changes in luminal contours, we deliberately selected cases of patients with truly serial OCT analyses. Furthermore, from a nosologic point of view, EVR and edge restenosis have to be differentiated. EVR is a general observation made at the scaffold edges, whereas edge restenosis is a truly pathologic phenomenon resulting from focal exuberance of neointima eventually combined with constrictive remodeling and progression of the atherosclerotic process.[2] For this reason and to fully understand EVR we excluded the 3 cases of edge restenosis that could be related to other pathologic mechanisms such as the presence of active plaque at the edge of the scaffold, defect in the manufacturing process and coating of the scaffold edge or intense barotrauma during post-dilatation outside the scaffold. All these specific phenomena could induce true restenosis of the edge.[27]

The present study describes a frame interval of 200 μm, the transition between the native vessel wall and the neointima that has fully integrated the polymeric material.

Previously, a late vascular response to DES was primarily attributed to a delay in strut healing because of subsequent drug toxicity and polymer-induced inflammation followed by hypersensitivity reactions.[27,28] A preclinical study in non-atherosclerotic pigs treated with the Absorb scaffold showed the disappearance of inflammatory response associated with the scaffold after 2, 3, or 4 years, as evidenced by the absence of the polylactide at 3 years and its replacement by malleable proteoglycan, which was demonstrated by gel permeation chromatography.[9] However, those findings were derived from a non-diseased vessel, and could be at variance with the inflammatory response observed in a diseased vessel.

In clinical studies, we have demonstrated the return of vasomotion of the scaffold segment at 12 months, which indicates that the device has lost its mechanical integrity at around 12 months.[17] Other clinical studies have shown that the malleable matrix of proteoglycan, which fills the strut void of the scaffold, can be pushed outward and expanded; the expansion of the scaffold matrix compensates for the continuing growth of neointimal hyperplasia between and on the top of the struts.[22]

In the present study, the postprocedural luminal dimensions of the scaffold and edge were characterized by a "step-up and step-down" in luminal area measurements (Figure 3) that implies excellent deployment and expansion of the device without systematic OCT or IVUS guidance, as performed by Mattesini et al[29] or according to the

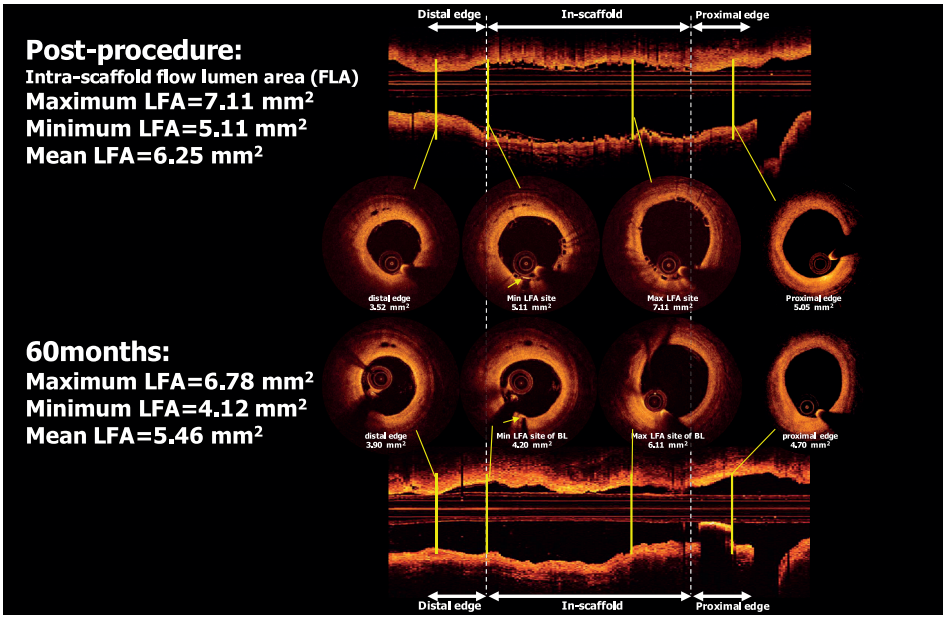

Figure 3. Representative longitudinal images at both edges and in-scaffold at post-procedure and 60 months. The longitudinal image shows both the edges and the postprocedural scaffold, with a "step-up and step-down" at the site of the scaffold implantation. In the following 48 months, the target vessel evolves to resemble a "straight tube" because of the filling of the gap between the initial expansion of the scaffold and the final lumen at 60 months. BL, baseline; LFA, lumen flow area.

MUSIC Study criteria.[24] Although non-flow-limiting edge dissection occurred frequently, these 2 cohorts have good long-term OCT results that were presumably related to the small residual plaque burden at the edge segment immediately post-procedure.

We show that the growth of neointimal tissue between baseline and 12 months fills almost perfectly the gap between the initial expansion of the strut and the final lumen at 60 months, because the dimension of the lumen did not change between 12, 36, and 60 months (Figure 3).

Previously, using the first iteration of the device with a faster bioresorption we demonstrated that scaffold implantation transiently reduced vascular compliance, which disappeared after 24 months.[15,30] After completion of bioresorption, unlike a metal cage, the disappearance of the "step up-step down" in vascular compliance and the cyclic strain at the scaffold edges might theoretically correct the early disturbances in shear stress at the edges and finally lead to laminar flow in the scaffold segment, including the transitional region, and the distal and proximal edge segments (Figure 4).[30,31] Moreover, exposing the endothelial cells to a homogeneous shear stress can potentially prevent neointimal growth and neoatherosclerosis in the late phase in all regions (scaffold, transitional region, and edge segment).[32–35]

According to the results from the late phase (between 2–3 and 5 years), the favorable lumen evolution of the scaffold itself apparently abrogated the EVR phenomenon. At the present time there is no comparable late observation of metallic DES.

Clinical Implications

Although metallic stented segments showed positive vessel remodeling up to 2 years,[36,37] and no late analysis is available, in contrast the latest report of the ABSORB Cohort B trial at 5 years demonstrated a decrease in plaque media together with adaptive, constrictive remodeling of the vessel area on IVUS analysis at 5 years.[38] Our study demonstrated a reduction of the scaffold luminal area in the absence of major EVR, suggesting that the physiological continuity of the lumen contour is restored long term. Loss of the mechanical property of the scaffold allows restoration of the endothelial shear stress, which is the frictional force on the vessel lining as blood flows through it, and cyclic strain, which is the force generated by the stretching of the vessel wall during systole and is affected by vessel distensibility. Furthermore, the interaction of shear stress and cyclic strain controls cell signaling. Cyclic strain stimulates eNOS gene regulation and steady-state levels of prostacyclin are increased when the shear stress force is applied in a pulsatile fashion.[39] The present study showed no late LL, so we could expect fewer cases of late TLR.

Study Limitations

This was an observational study and the OCT assessment was limited to a small number of observations, which were, however, serial and performed long term. We used 2 different OCT systems (TD- and FD-OCT) because OCT techniques evolved over the study period. Validity of the OCT measurements between 2 different systems has been established.[40] Regarding size discrepancy between the 2 modalities, we minimized it because none of the OCT images was acquired using the occlusion technique.[16–18,22]

An inherent limitation of a first-in-man trial is that the lesion subset may be relatively simple and likely not reflective of "real-world lesions". The postprocedural luminal dimensions of the scaffold and edge were characterized by a "step-up and step-down" in luminal area measurements (Figure 3), which implied excellent deployment and expansion of the device that in itself may constitute a favorable selection bias bound to the "first in man" nature of the study; Mattesini et al have reported a similar luminal area increase when a metallic DES or BRS was implanted under OCT guidance.[29] In the BMS era the IVUS-MUSIC criteria for optimal BMS implantation resulted in the lowest binary restenosis rate (9.7%) ever observed.[24]

In order to fully document and evaluate the temporal changes in luminal contour, we deliberately selected cases of patients with truly serial OCT analyses. To fully understand EVR, we excluded the 3 cases of edge restenosis (see Discussion).

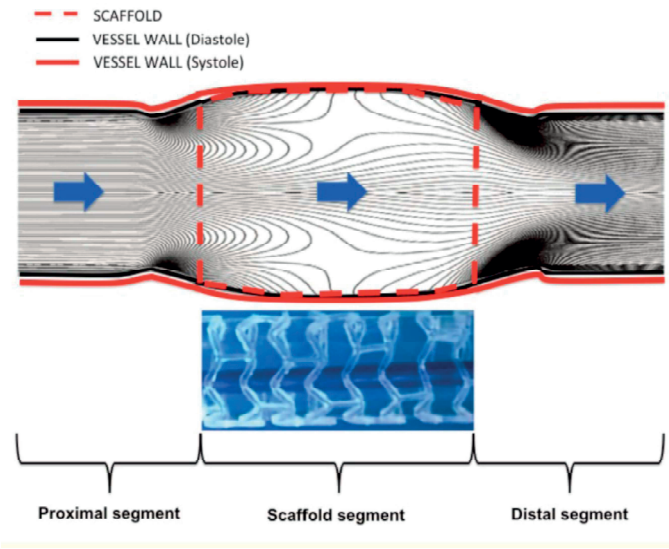

Figure 4. Compliance mismatch after scaffold implantation with alteration in flow. In this diagram the mismatch in compliance created by the scaffold (red dotted line) is indicated as a "bump" in the vessel wall compared with the proximal and distal segments. Instantaneous vortices fields calculated by a mathematical model are also shown, indicating the presence of turbulence at the proximal and distal edges. Instantaneous vorticity fields reconstructed according to Tortoriello A, et al.[31] (Reproduced with permission from Brugaletta S, et al.[30])

There were some differences in the sequential and temporal changes of OCT area measurements between Cohorts B1 and B2 which may raise a concern about the potential patient heterogeneity. The small sample size precludes a formal univariate or multivariable analysis of the differences between cohorts.

CONCLUSIONS

The key observation was global reduction of the scaffolded lumen in the absence of major EVR, suggesting that the physiological continuity of the lumen boundaries after bioresorption of the scaffold are restored long term.

REFERENCES

1. Weissman NJ, Wilensky RL, Tanguay JF, Bartorelli AL, Moses J, Williams DO, et al. Extent and distribution of in-stent intimal hyperplasia and edge effect in a non-radiation stent population. Am J Cardiol 2001; 88: 248–252.
2. Serruys PW, Degertekin M, Tanabe K, Russell ME, Guagliumi G, Webb J, et al. Vascular responses at proximal and distal edges of paclitaxel-eluting stents: Serial intravascular ultrasound analysis from the TAXUS II trial. Circulation 2004; 109: 627–633.
3. Serruys PW, Kay IP. I like the candy, i hate the wrapper: The (32)P radioactive stent. Circulation 2000; 101: 3–7.
4. Popma JJ, Leon MB, Moses JW, Holmes DR Jr, Cox N, Fitzpatrick M, et al. Quantitative assessment of angiographic restenosis after sirolimus-eluting stent implantation in native coronary arteries. Circulation 2004; 110: 3773–3780.
5. Windecker S, Serruys PW, Wandel S, Buszman P, Trznadel S, Linke A, et al. Biolimus-eluting stent with biodegradable polymer versus sirolimus-eluting stent with durable polymer for coronary revascularisation (LEADERS): A randomised non-inferiority trial. The Lancet 2008; 372: 1163–1173.
6. García-García HM, Gonzalo N, Tanimoto S, Meliga E, de Jaegere P, Serruys PW. Characterization of edge effects with paclitaxel-eluting stents using serial intravascular ultrasound radiofrequency data analysis: The BETAX (BEside TAXus) study. Rev Esp Cardiol (English Version) 2008; 61: 1013–1019.
7. Serruys PW, Silber S, Garg S, van Geuns RJ, Richardt G, Buszman PE, et al. Comparison of zotarolimus-eluting and everolimus-eluting coronary stents. N Engl J Med 2010; 363: 136–146.
8. Onuma Y, Serruys PW. Bioresorbable scaffold: The advent of a new era in percutaneous coronary and peripheral revascularization? Circulation 2011; 123: 779–797.
9. Onuma Y, Serruys PW, Perkins LE, Okamura T, Gonzalo N, Garcia-Garcia HM, et al. Intracoronary optical coherence tomography and histology at 1 month and 2, 3, and 4 years after implantation of everolimus-eluting bioresorbable vascular scaffolds in a porcine coronary artery model: An attempt to decipher the human optical coherence tomography images in the ABSORB trial. Circulation 2010; 122: 2288–2300.
10. Nakatani S, Onuma Y, Ishibashi Y, Eggermont J, Zhang YJ, Campos CM, et al. Temporal evolution of strut light intensity after implantation of bioresorbable polymeric intracoronary scaffolds in the ABSORB Cohort B trial: An application of a new quantitative method based on optical coherence tomography. Circ J 2014; 78: 1873–1881.
11. Karanasos A, Simsek C, Serruys P, Ligthart J, Witberg K, van Geuns RJ, et al. Five-year optical coherence tomography follow-up of an everolimus-eluting bioresorbable vascular scaffold: Changing the paradigm of coronary stenting? Circulation 2012; 126: e89–e91.
12. Gogas BD, Bourantas CV, Garcia-Garcia HM, Onuma Y, Muramatsu T, Farooq V, et al. The edge vascular response following implantation of the Absorb everolimus-eluting bioresorbable vascular scaffold and the XIENCE V metallic everolimus-eluting stent: First serial follow-up assessment at six months and two years: Insights from the first-in-man ABSORB Cohort B and SPIRIT II trials. EuroIntervention 2013; 9: 709–720.
13. Gogas BD, Serruys PW, Diletti R, Farooq V, Brugaletta S, Radu MD, et al. Vascular response of the segments adjacent to the proximal and distal edges of the ABSORB everolimus-eluting bioresorbable vascular scaffold: 6-month and 1-year follow-up assessment: A virtual histology intravascular ultrasound study from the first-in-man ABSORB cohort B trial. JACC Cardiovasc Interv 2012; 5: 656–665.

14. Oberhauser J, Hossainy S, Rapoza R. Design principles and performance of bioresorbable polymeric vascular scaffolds. EuroIntervention 2009; 5: F15–F22.
15. Serruys PW, Ormiston JA, Onuma Y, Regar E, Gonzalo N, Garcia-Garcia HM, et al. A bioabsorbable everolimus-eluting coronary stent system (ABSORB): 2-year outcomes and results from multiple imaging methods. Lancet 2009; 373: 897–910.
16. Serruys PW, Onuma Y, Ormiston JA, de Bruyne B, Regar E, Dudek D, et al. Evaluation of the second generation of a bioresorbable everolimus drug-eluting vascular scaffold for treatment of de novo coronary artery stenosis: Six-month clinical and imaging outcomes. Circulation 2010; 122: 2301–2312.
17. Serruys PW, Onuma Y, Dudek D, Smits PC, Koolen J, Chevalier B, et al. Evaluation of the second generation of a bioresorbable everolimus-eluting vascular scaffold for the treatment of de novo coronary artery stenosis: 12-month clinical and imaging outcomes. J Am Coll Cardiol 2011; 58: 1578–1588.
18. Ormiston JA, Serruys PW, Onuma Y, van Geuns RJ, de Bruyne B, Dudek D, et al. First serial assessment at 6 months and 2 years of the second generation of absorb everolimus-eluting bioresorbable vascular scaffold: A multi-imaging modality study. Circ Cardiovasc Interv 2012; 5: 620–632.
19. Tearney GJ, Regar E, Akasaka T, Adriaenssens T, Barlis P, Bezerra HG, et al. Consensus standards for acquisition, measurement, and reporting of intravascular optical coherence tomography studies: A report from the International Working Group for Intravascular Optical Coherence Tomography Standardization and Validation. J Am Coll Cardiol 2012; 59: 1058–1072.
20. Zhang YJ, Iqbal J, Nakatani S, Bourantas CV, Campos CM, Ishibashi Y, et al. Scaffold and edge vascular response following implantation of everolimus-eluting bioresorbable vascular scaffold: A 3-year serial optical coherence tomography study. JACC Cardiovasc Interv 2014; 7: 1361–1369.
21. Nakatani S, Sotomi Y, Ishibashi Y, Grundeken MJ, Tateishi H, Tenekecioglu E, et al. Comparative analysis method of permanent metallic stents (XIENCE) and bioresorbable poly-L-lactic (PLLA) scaffolds (Absorb) on optical coherence tomography at baseline and follow-up. EuroIntervention 2015 Octber 9, doi:10.4244/EIJY15M10_03.
22. Serruys PW, Onuma Y, Garcia-Garcia HM, Muramatsu T, van Geuns RJ, de Bruyne B, et al. Dynamics of vessel wall changes following the implantation of the absorb everolimus-eluting bioresorbable vascular scaffold: A multi-imaging modality study at 6, 12, 24 and 36 months. EuroIntervention 2014; 9: 1271–1284.
23. Fujii K, Carlier SG, Mintz GS, Yang YM, Moussa I, Weisz G, et al. Stent underexpansion and residual reference segment stenosis are related to stent thrombosis after sirolimus-eluting stent implantation: An intravascular ultrasound study. J Am Coll Cardiol 2005; 45: 995–998.
24. de Jaegere P, Mudra H, Figulla H, Almagor Y, Doucet S, Penn I, et al. Intravascular ultrasound-guided optimized stent deployment: Immediate and 6 months clinical and angiographic results from the Multicenter Ultrasound Stenting in Coronaries Study (MUSIC Study). Eur Heart J 1998; 19: 1214–1223.
25. Gonzalo N, Serruys PW, Okamura T, Shen ZJ, Onuma Y, Garcia-Garcia HM, et al. Optical coherence tomography assessment of the acute effects of stent implantation on the vessel wall: A systematic quantitative approach. Heart 2009; 95: 1913–1919.
26. Radu MD, Räber L, Heo JH, Gogas BD, Jørgensen E, Kelbæk H, et al. Natural history of optical coherence tomography-detected non-flow-limiting edge dissections following drug-eluting stent implantation. EuroIntervention 2014; 9: 1085–1094.
27. Gogas BD, Samady H. Shedding light on scaffold vascular response. JACC Cardiovasc Interv 2014; 7: 1370–1373.

28. Hiranuma N, Shinke T, Nakazawa G, Otake H, Matsumoto D, Ijichi T, et al. Optical coherence tomography and histopathology assessment after implantation of first- and second-generation drug-eluting stents in a porcine coronary model. Circ J 2014; 78: 2665–2673.
29. Mattesini A, Secco GG, Dall'Ara G, Ghione M, Rama-Merchan JC, Lupi A, et al. ABSORB biodegradable stents versus second-generation metal stents: A comparison study of 100 complex lesions treated under OCT guidance. JACC Cardiovasc Interv 2014; 7: 741–750.
30. Brugaletta S, Gogas BD, Garcia-Garcia HM, Farooq V, Girasis C, Heo JH, et al. Vascular compliance changes of the coronary vessel wall after bioresorbable vascular scaffold implantation in the treated and adjacent segments. Circ J 2012; 76: 1616–1623.
31. Tortoriello A, Pedrizzetti G. Flow-tissue interaction with compliance mismatch in a model stented artery. J Biomech 2004; 37: 1–11.
32. Wentzel JJ, Whelan DM, van der Giessen WJ, van Beusekom HM, Andhyiswara I, Serruys PW, et al. Coronary stent implantation changes 3-D vessel geometry and 3-D shear stress distribution. J Biomech 2000; 33: 1287–1295.
33. Schwarzacher SP, Tsao PS, Ward M, Hayase M, Niebauer J, Cooke JP, et al. Effects of stenting on adjacent vascular distensibility and neointima formation: Role of nitric oxide. Vasc Med 2001; 6: 139–144.
34. Benard N, Coisne D, Donal E, Perrault R. Experimental study of laminar blood flow through an artery treated by a stent implantation: Characterisation of intra-stent wall shear stress. J Biomech 2003; 36: 991–998.
35. Nakazawa G, Otsuka F, Nakano M, Vorpahl M, Yazdani SK, Ladich E, et al. The pathology of neoatherosclerosis in human coronary implants bare-metal and drug-eluting stents. J Am Coll Cardiol 2011; 57: 1314–1322.
36. Wilson GJ, Nakazawa G, Schwartz RS, Huibregtse B, Poff B, Herbst TJ, et al. Comparison of inflammatory response after implantation of sirolimus- and paclitaxel-eluting stents in porcine coronary arteries. Circulation 2009; 120: 141–149, 141–142.
37. Garcia-Garcia HM, Serruys PW, Campos CM, Onuma Y. Differential impact of five coronary devices on plaque size: Insights from the ABSORB and SPIRIT trials. Int J Cardiol 2014; 175: 441–445.
38. Serruys PW, Ormiston J, van Geuns RJ, de Bruyne B, Dudek D, Christiansen E, et al. A polylactide bioresorbable scaffold eluting everolimus for treatment of coronary stenosis: 5-year follow-up. J Am Coll Cardiol 2016; 67: 766–776.
39. Serruys PW, Garcia-Garcia HM, Onuma Y. From metallic cages to transient bioresorbable scaffolds: Change in paradigm of coronary revascularization in the upcoming decade? Eur Heart J 2012; 33: 16–25.
40. Takarada S, Imanishi T, Liu Y, Ikejima H, Tsujioka H, Kuroi A, et al. Advantage of next-generation frequency-domain optical coherence tomography compared with conventional time-domain system in the assessment of coronary lesion. Catheter Cardiovasc Interv 2010; 75: 202–206.

A

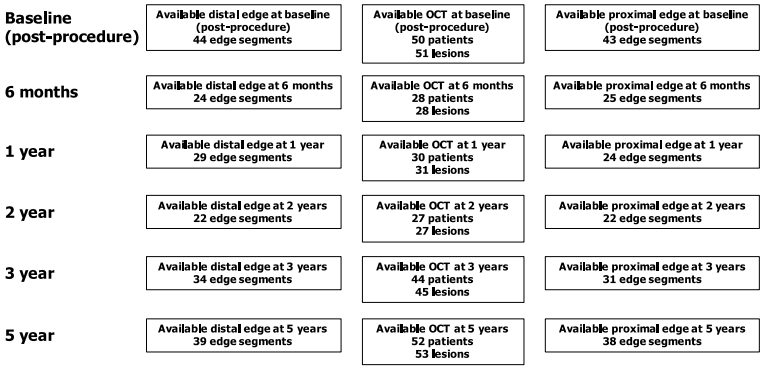

B

Distal edge segment at the post procedure		Proximal edge segment at the post procedure	
DES (previously implanted or implanted by bail-out procedure)	5	Edge was not documented within the pull-back	3
Edge was not documented within the pull-back	1	SB>1.5mm	5
SB>1.5mm	1		
Distal edge segment at 6 months		**Proximal edge segment at 6 months**	
DES (previously implanted or implanted by bail-out procedure)	3	Edge was not documented within the pull-back	1
Inadequate contrast flush	1	SB>1.5mm	2
Distal edge segment at 1 year		**Proximal edge segment at 1 year**	
DES (previously implanted or implanted by bail-out procedure)	1	Inadequate contrast flush	1
SB>1.5mm	1	SB>1.5mm	6
Distal edge segment at 2 years		**Proximal edge segment at 2 years**	
DES (previously implanted or implanted by bail-out procedure)	3	Edge was not documented within the pull-back	2
Edge was not documented within the pull-back	1	SB>1.5mm	3
Insufficient assessment of lumen	1		
Distal edge segment at 3 years		**Proximal edge segment at 3 years**	
DES (previously implanted or implanted by bail-out procedure)	2	DES (previously implanted or implanted by bail-out procedure)	2
Edge was not documented within the pull-back	1	Inadequate contrast flush	6
Insufficient assessment of lumen	1	Edge was not documented within the pull-back	1
Inadequate contrast flush	3	SB>1.5mm	5
SB>1.5mm	4		
Distal edge segment at 5 years		**Proximal edge segment at 5 years**	
DES (previously implanted or implanted by bail-out procedure)	5	DES (previously implanted or implanted by bail-out procedure)	2
Edge was not documented within the pull-back	2	Edge was not documented within the pull-back	2
SB>1.5mm	7	Insufficient assessment of lumen	2
		SB>1.5mm	9

online appendix figure 1. (A) Study profile through the entire follow-up. (B) Number of exclusions at each time point. DES, drug-eluting stent; OCT, optical coherence tomography.

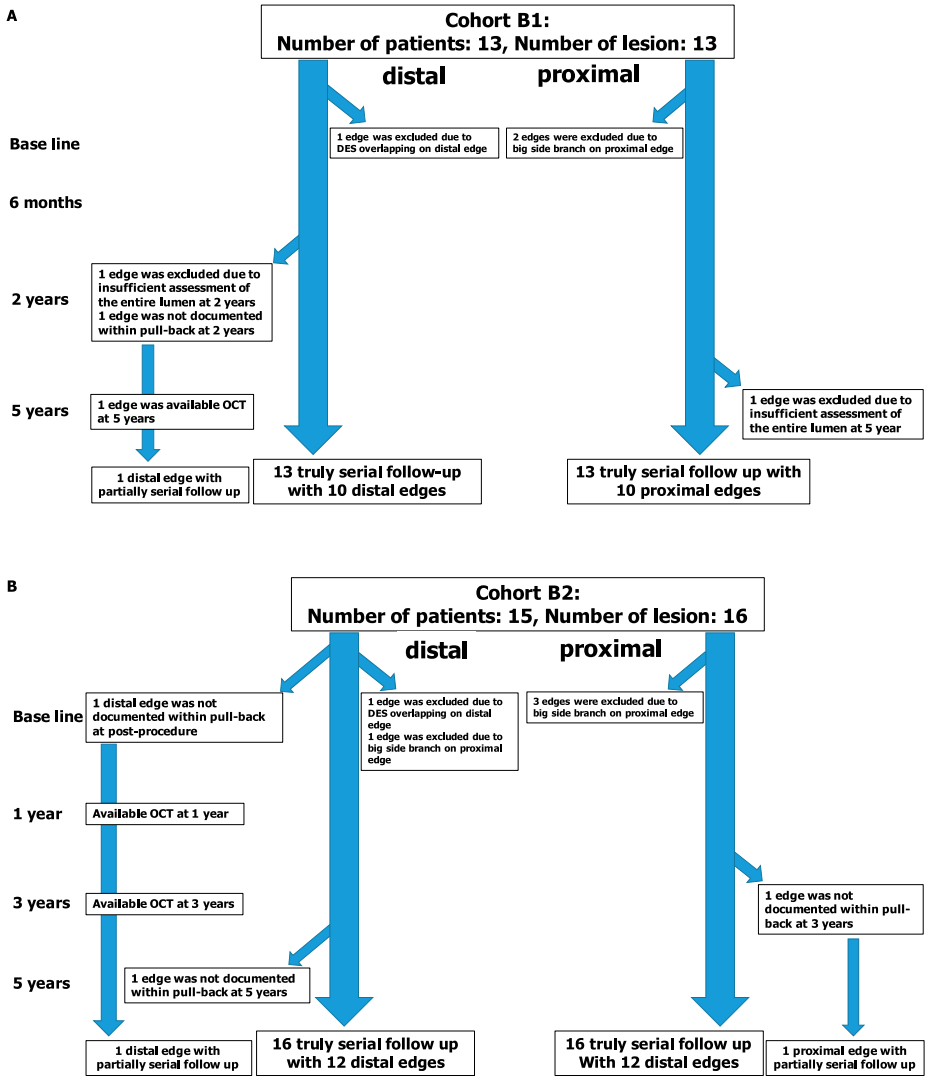

online appendix figure 2. Study profile of the serial OCT analysis. (A) Cohort B2 at 12, 36 and 60 months; (B) for Cohort B1 at 6, 24 and 60 months. DES, drug-eluting stent; OCT, optical coherence tomography.

Table S1. Mean Lumen Area and Changes Over Time at Both Edges and In-Scaffold (A) Cohort B2 at 12, 36 and 60 Months, (B) Cohort B1 at 6, 24 and 60 Months

(A)	BL (B2) No. of lesion	1Y (B2) No. of lesion	3Y (B2) No. of lesion	5Y (B2) No. of lesion	1Y-BL(B2) Difference p-values	1Y-3Y(B2) Difference p-values	5Y-3Y(B2) Difference p-values	3Y-BL(B2) Difference p-values	5Y-BL(B2) Difference p-values	5Y-1Y(B2) Difference p-values
Distal edge (mm^2)	5.86±1.56 (n=21)	5.65±1.80 (n=29)	5.90±1.58 (n=34)	5.40±1.28 (n=21)	-0.21±0.48 0.917	+0.25±0.42 0.619	-0.50±0.41 0.239	+0.04±0.44 0.979	-0.18±0.44 0.352	-0.25±0.46 0833
Mean lumen area in scaffold (mm^2)	7.51±1.31 (n=22)	5.92±1.69 (n=31)	6.01±1.54 (n=45)	5.68±1.86 (n=31)	-1.60±0.43 <0.001	+0.10±0.38 0.946	-0.34±0.35 0.871	-1.49±0.38 <0.001	-1.83±0.37 <0.001	-0.24±0.39 0.782
Minimum lumen area in scaffold (mm^2)	5.95±0.96 (n=22)	4.31±1.40 (n=31)	4.49±1.45 (n=45)	4.00±1.41 (n=31)	-1.64±0.35 <0.001	+0.18±0.34 0.737	-0.49±0.34 0.118	-1.46±0.30 <0.001	-1.95±0.35 <0.001	-0.30±0.36 0.263
Proximal edge (mm^2)	7.95±3.50 (n=20)	7.20±3.20 (n=24)	6.58±1.96 (n=31)	6.12±1.71 (n=21)	-0.75±0.95 0.146	-0.62±0.69 0.708	-0.47±0.53 0.330	-1.37±0.84 0.0342	-1.83±0.85 0.022	-1.09±0.70 0.316
(B)	BL (B1) No. of lesion	6M (B1) No. of lesion	2Y (B1) No. of lesion	5Y (B1) No. of lesion	6M-BL(B1) Difference p-values	2Y-6M(B1) Difference p-values	5Y-2Y(B1) Difference p-values	2Y-BL(B1) Difference p-values	5Y-BL(B1) Difference p-values	5Y-6M(B1) Difference p-values
Distal edge (mm^2)	5.73±1.78 (n=23)	6.03±2.34 (n=24)	5.59±2.19 (n=22)	6.00±2.03 (n=18)	+0.31±0.60 0.909	-0.44±0.67 0.442	+0.41±0.67 0.277	-0.13±0.59 0.590	+0.27±0.59 0.576	-0.03±0.69 0.809
Mean lumen area in scaffold (mm^2)	7.15±1.19 (n=29)	6.34±1.50 (n=28)	5.93±1.75 (n=27)	6.68±2.03 (n=22)	-0.80±0.36 <0.001	-0.42±0.44 0.241	+0.75±0.54 0.107	-1.22±0.40 <0.001	-0.47±0.49 0.345	+0.34±0.50 0.241
Minimum lumen area in scaffold (mm^2)	5.83±1.23 (n=29)	4.89±1.43 (n=28)	4.22±1.45 (n=27)	4.19±1.91 (n=22)	-0.94±0.35 <0.001	-0.67±0.39 0.035	-0.02±0.48 0.421	-1.61±0.36 <0.001	-1.64±0.47 <0.001	-0.69±0.47 0.058
Proximal edge (mm^2)	7.17±2.45 (n=23)	7.08±2.50 (n=25)	6.54±1.97 (n=22)	6.05±1.80 (n=17)	-0.09±0.69 0.805	-0.53±0.65 0.560	-0.49±0.61 0.413	-0.62±0.66 0.413	-1.11±0.70 0.214	-1.02±0.70 0.224

Values are presented as mean±standard error. A significant level for each paired comparison is 0.013 after adjustment for multiplicity using the Bonferroni correction. BL, baseline; 6M, 6 months; 1Y, 1 year; 2Y, 2 years; 3Y, 3 years; 5Y, 5 years.

Chapter 18

Serial Assessment of Tissue Precursors and Progression of Coronary Artery Calcification Analyzed by Fusion of Intravascular Ultrasound and Optimal Coherent Tomography: A Five Years Follow-up of Scaffolded and Non-scaffolded Arteries.

Yaping Zeng, Hiroki Tateishi, Rafael Cavalcante, Erhan Tenekecioglu, Pannipa Suwannasom, Yohei Sotomi, Carlos Collet, Shaoping Nie, Hans Jonker, Jouke Dijkstra, Maria D. Radu, Lorenz Räber, Dougal R. McClean, Robert-Jan van Geuns, Evald Høj Christiansen, Therese Fahrni, Jacques J. Koolen, Yoshinobu Onuma, Nico Bruining, Patrick W. Serruys

JACC Cardiovasc Imaging (accepted for publication)

ABSTRACT

Objectives

To assess calcium growth with fused greyscale-IVUS, virtual histology-IVUS (VHIVUS) and OCT from baseline to 5-year follow-up in patients treated with Bioresorbable Vascular Scaffolds (BVS).

Background

Intravascular ultrasound (IVUS) and optical coherence tomography (OCT) have individual strengths in assessing plaque composition and volume. Fusion of images of these methods could potentially help coronary plaque assessment.

Methods

Anatomic landmarks and endoluminal radiopaque markers were used to fuse OCT and IVUS images and match baseline and follow-up.

Results

Seventy-two VH-IVUS and OCT paired matched cross-section in- and out-scaffold segments were fused at baseline and follow-up. In total, 46 calcified plaques at follow-up weredetected by the fusion method (33 in-, 13 out-scaffold), showing either calcium progression (52.2%) or de novo calcifications(47.8%). On OCT, calcification volume increased from baselineto follow-up by 2.3±2.4 mm^3 (p=0.001). The baseline VH tissue precursors of dense calcium(DC) at follow-up were necrotic core (NC) in 73.9% and Fibrous/Fibrofatty (F/FF) in 10.9%. In 15.2%, calcium was already present at baseline. Precursors on OCT were lipid pool in 71.2%, fibrous in 4.3%, and fibrocalcific plaque in 23.9%.

Conclusions

The use of OCT/IVUS fusion imaging shows similar calcium growth in-and outscaffold segments. NC is the most frequent precursor of calcification. The scaffold resorption process creates a tissue layer that recaps the calcified plaques.

INTRODUCTION

Coronary atherosclerotic plaque characterization with intravascular imaging is important for assessing atherosclerosis, planning percutaneous coronary interventions and predicting outcomes (1). Intravascular ultrasound (IVUS) and optical coherence tomography(OCT) are the two mostwidely used intracoronary imaging techniques.

The main advantage of IVUS lies on its deep penetration ability that offers a cross-section of the entire vessel wall and allows the detection of deep calcification. Its main disadvantages are a limited resolution and the strong reflection of the ultrasound waves by endoluminal calcium that creates a shadow behind the calcium that precludes assessment of the extent and depth of calcification(2).

Virtual-histology IVUS (VH-IVUS) increases the usefulness of IVUS by characterizing tissue components and allowing for better risk stratification(1). However, stent/scaffold struts are incorrectly recognized as dense calcium (DC) surrounded by necrotic core (NC) on VH. Moreover, VH algorithm also incorrectly inputs fibrofatty signal in the shadow behind DC(3,4).

OCT allows for a detailed assessment of near-lumen plaque characteristics due to its high resolution (10-20μm), including features related to plaque vulnerability like thin fibrous caps. OCT can also assess calcifications more accurately due to the fact that the light can cross calcified area without being excessively reflected, and without substantial attenuation allowing for the visualization of the real extension of calcification plaque along its longitudinal-and axial distribution, at least in the relatively superficial layer of the vessel wall(5). However, the high resolution comes at the cost of limited depth of penetration(6). Therefore, OCT is unable to detect deep calcium.

The feasibility and advantages of combining the individual strengths of both technologies in vivo have been described (7). The feasibility of off-line fusion images of co-registered IVUS/OCT has been previously described(8).

The objective of the present study is to comprehensively assess the serial progression of calcification at 5-year follow-up after Bioresorbable Vascular Scaffold(BVS) implantation using matched fusion images of IVUS/OCT. We sought to evaluate calcium progression and describe the baseline(BL) tissue precursors of calcification at long-term follow-up.

METHODS

Study design

In the cohort B1,B2 (n=101)28 patients with 29 lesions underwent IVUS and OCT assessment BL and 5-year(9)(supplement Figure1). OCT, greyscale-IVUS(GS-IVUS) and VHIVUS images were displayed simultaneously and screened concomitantly frame by frame to match using the radiopaque markers and/or anatomical marks at each time

point (supplement Figure2). Then the matched cross-section selected were co-localized between 2 time points. Each cross section was subdivided in four quadrants and the presence of each type of atherosclerotic plaque was assessed in each quadrant(7).

GS-IVUS acquisition

Post-implantation and 5-year images were obtained with 20MHz, phased-array IVUS catheters (Eagle Eye,Volcano Corp.,Rancho Cordova, California,USA) using an automated pullback of 0.5mm/second. Semi-automatic detection of both lumen and external elastic membrane were performed with the QCU-CMS-Research software v4.69 (Medis, Leiden, the Netherlands). Calcification on GS-IVUS was defined as bright echoes with acoustic shadowing(2).

IVUS radiofrequency analysis

On VH-IVUS analysis, "pseudo" DC/NC related to the scaffold strut was defined as confluent, non-interrupted white color surrounded by red color, located near the lumen contour. DC located behind the struts and separated from the struts was considered as real DC at baseline(10). The "white color" was then defined as calcification if the confluent white color area exceeded 0.0625mm^2(0.25mm*0.25mm), considering the resolution of 20MHz IVUS catheters used in the study(2). To determine the major baseline tissue precursor of calcifications at 5-year, fusion images weighting VH information in topographically matched calcified areas at follow-up were used (Figure4). The baseline VH tissue precursor was determined as the major tissue component comprising approximately 50% of the total tissue.

OCT image acquisition and analysis

OCT acquisition was performed using C7/C8 frequency domain systems (Light Lab Imaging, Westford, Massachusetts, USA)(11). The OCT images acquired baseline and follow-up were analyzed off-line at 100μm or 200μm longitudinal intervals within the region of interest (ROI) using QCU-CMS .

Three tissue components were identified based on the consensus of 5 analysts as: Fibrous; Fibrocalcific; Lipid pool (lipid/necrotic core)(11)(supplement). The baseline OCT tissue precursor of calcifications at follow-up was defined as the tissue component comprising approximately 50% in topographically matched calcified area.

Matching cross-section and ROI definition

The matching of multimodalities at one time point and at follow-up is performed according to the following criteria: the presence of platinum marker (BVS) and common anatomical landmarks such as side branch(SB), vein, pericardium, position and configuration of calcified plaque, characteristic lumen shape and circumferential profile of plaque thickness, and/or positional or directional relationship among all the landmarks above

(Figure1). The following cross-section will not be included in the analysis(supplement). ROI was defined as scaffold segment and 5-mm proximal and distal.

Fusion cross-section of IVUS/OCT

The principles of fusion image have been previously described(8). In summary, the matched GS-IVUS, VH-IVUS and OCT images were adjusted and fused in Adobe Photo Shop elements 12 software (Adobe Systems Incorporated, San Jose, CA, USA) (Figure 1). Detailed processes are as the following:

1. The size of OCT and IVUS images were adjusted by matching the calibration line of 1 mm. The original square shape of both IVUS and OCT images were well defined, so that the matching of 1 mm calibration line between OCT and IVUS images was maintained, thus allowing for the matching of square image areas.
2. The 2-dimensional cross-section images were rotated using cross-sectional landmarks according to the following hierarchy: a) side branch; b) calcification; c) lumen shape; d) circumferential plaques.
3. To optimize the overlay of IVUS on top of OCT images, the transparency function of Adobe Photoshop was used to allow the simultaneous visibility of the structures in the underlying OCT images. As a suitable default setting for overlaying IVUS on top of OCT images, a transparency of 60-70% for the grayscale IVUS images, and 70-80% for VH-IVUS images were applied.

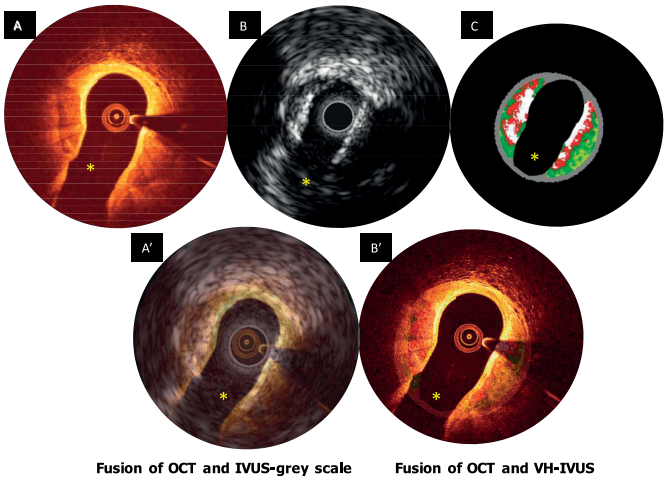

Figure 1. Matching and fusion method in ABSORB Cohort B.
The yellow asterisk indicates the side branch. Two calcifications are shown at the ostium of the side branch. Image A, B and C show the matched OCT, GS-IVUS and VH-IVUS images using the side branches and 2 calcifications as anatomical landmarks. The "green color" (fibrofatty) in panel C is an artefact of the VH measurement: the ultrasound waves are completely reflected by the calcium and there is basically no backscattering signal stemming from the shadow area located behind the main ultrasound reflection. Image A' and B' show the fusion images of OCT/GS-IVUS, and OCT/VH- IVUS, respectively.

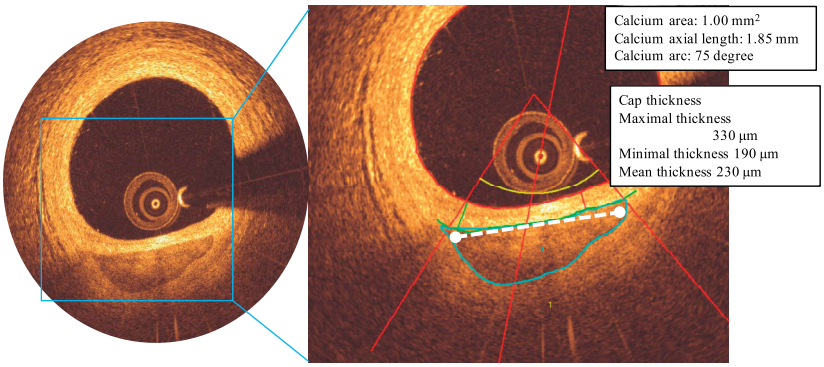

Figure 2. Assessment of calcification: calcium area was characterized by the appearance of signal-poor heterogeneous images with sharp borders. Calcium arc (yellow) was measured from the gravitational center of the lumen to the two lateral extremities of the calcium. Calcium axial length (white dash line) in each cross-section was measured as the maximal geometric length. The maximal(green), minimal(red), and mean cap thickness overlying calcification are measured.

Calcium assessment by fusion IVUS/OCT

To assess the diagnostic accuracy of calcium detection of each individual modality as compared to the fusion images, the cross-section of each modality were evaluated by 3 teams of 2 cardiologists who were blind to the images of the other modalities baseline and 5-year using the criteria described above.

After having assessed individually the presence or absence of calcification in each imaging modality, a group of five cardiologists assessed by consensus the diagnosis of calcification in matched cross-section. Calcification was diagnosed by fusion when qualitative and quantitative criteria were met by at least 2 imaging modalities. Sensitivity and specificity of each modality were determined using the fusion image as comparator.

OCT/IVUS calcification measurements

The following OCT parameters were assessed (Figure2): calcium area, volume, arc, axial and longitudinal length and intima thickness overlying calcifications(12) ; calcium volume was calculated based on the disk summation method(supplement).

Automatic quantitative echogenicity analysis

Echogenicity classify the plaque components into 5 categories based on their grey-level intensity on IVUS: calcified, upperechogenic, hyperechogenic, hypoechogenic, and unknown(13).

Statistical analysis

Continuous variables are presented as mean±standard deviation (SD) or median and inter quartile ranges (IQR) as appropriate and compared with paired T-test or Wilcoxon

signed-rank test for baseline vs follow-up comparisons and independent T-test and Mann-Whitney test for in- vs out-scaffold. Binary variables are summarized as counts and percentages and compared with Chisquare or Fisher's exact test. For each imaging modality alone, sensitivity and specificity for calcium detection were determined using the fusion method as the comparator. The agreement for calcium detection between each modality and the fusion method was assessed with Cohen's Kappa(κ)statistic. As the data in the study have multi-level structure, a mixed effects model was used. Patients were implemented as random effect, in- or out- scaffold segment was input as fixed effect into the model. A two-sided p-value<0.05 indicated statistical significance. All analyses were performed with SPSS version 22(IBM Corp, Armonk, NY).

RESULTS

Study population and case selection

Out of 28 patients with complete 5-year in the ABSORB Cohort B trial, 15 cases (16 lesions), with all three imaging modalities (GS-IVUS, VH-IVUS and OCT) available, were included in the present analysis. Baseline clinical characteristics of the study population are summarized (Table 1), IVUS measurements at baseline and 5-year are shown in Table 2. Cases imaged with time domain-OCT were excluded from the analysis (supplement Figure1). In the 16 coronary lesions, at baseline, 72 cross-sections (4.6±1.4 cross-sections/lesion) of each of the three imaging modalities (GS-IVUS, VH-IVUS and OCT) were matched and fused using the criteria stated above. These fused cross-sections were further matched with the corresponding 72 fused cross-sections of the 5-years follow-up assessment. These comprise the study database of 72 pairs of matched, fused (GS-IVUS, VH-IVUS and OCT) cross-sections.

No calcification was observed in 33 (41.8%) of these 72 pairs of cross-sections (i.e. at neither time point). In the other 39 pairs (58.2%) of fused cross-sections, 46 calcified area pools were detected at 5-years follow-up. These 46 calcified area pools represented either calcium progression from baseline (n=24) or de novo calcification (n=22) (Figure 3). Of note, calcium was detected by VH only at baseline in 22 cross-section. To definitely determine the true significance of this isolated VH signal, follow-up fusion images were assessed and calcification was confirmed in 13/22 cross-section. In the remaining 9 cross-section, the VH signal of calcification, either disappeared or persisted only as an isolated VH signal not confirmed by the fusion method.

Diagnostic accuracy of calcification with fusion or individual modality

Table 3 shows sensitivity and specificity of each individual modality in detecting calcium at 2 time points using the fusion modality as the comparator.

Analysis of tissue precursor of calcification on OCT and VH-IVUS

On VH-IVUS the tissue precursors of DC at baseline were NC (n=34, 73.9%) and F/FF (n=5,10.9%). In the remaining 7(15.2%) calcifications, calcium was already present at baseline. On OCT, precursors were lipid pool (n=33, 71.2%), fibrous(n=2, 4.3%) and fibrocalcific tissue (n=11, 23.9%).

OCT calcium measurements

An overall increase in calcium area was observed both in-scaffold Δ: 0.37(0.25, 0.74) mm2 and out-scaffold Δ: 0.39(0.21, 1.2) mm2 (p=0.098,in-vs out-scaffold). Mixed effects model showed a similar trend (p=0.117).

Table 1 Baseline patient characteristics (15 patients, 16 lesions).

	15 cases, 16 lesions
Age, years (mean±SD)	59.14±7.16
Male, n (%)	9 (60%)
Hypertension requiring medication	8 (53.3%)
Hypercholesterolemia requiring medication	9 (60.0 %)
Diabetes mellitus requiring medication	0
Myocardial infarction history	4 (26.7 %)
Cardiac Intervention history	2 (13.3%)
Current smokers	4 (26.7%)
Family history of CHD	10 (66.7%)
Clinical presentation	
Stable	12 (80%)
Non-ST-ACS	1 (6.7%)
Silent ischemia	0
Target vessel	
Left anterior descending	9 (56.2%)
Left circumflex	3 (18.8%)
Right coronary artery	4 (25%)
AHA/ACC lesion classification	
A	0
B1	11 (68.8%)
Type B2/C lesion	5 (31.3%)
Statin using at 5 years	14 (93.3%)
Rosuvastatin (%)	3 (21.4%)
Atorvastatin (%)	7 (50%)
Simvastatin (%)	5 (35.7%)
Lipid profile at 5 years (mmol/L)	
Total Cholesterol	3.7±0.7
LDL	1.6±0.5
HDL	1.0±0.3
Triglyceride	2.3±0.4

Table 2 IVUS measurements at baseline and 5-year follow-up

	Baseline	5-year	Differ 5y-BL	P
Scaffold segment (16 paired measurements)				
Vessel area, mm^2	14.4(13.0,16.8)	14.2(11.5,15.5)	-0.6(-1.3,0.36)	0.121
Lumen area, mm^2	6.4(5.8,7)	6.3(5.9,7.2)	0.15(-0.24,0.88)	0.352
Plaque area, mm^2	8.4(6.6,10.0)	7.4(6.2,8.5)	-0.82(-1.5,- 0.24)	0.044
Plaque burden, %	55.8±5.8	52.8±6.1	-3.0±6.7	0.094
Proximal edge (7 paired measurements)				
Vessel area, mm^2	13.5(12.4,14.9)	13.1(12.1,14.8)	-0.28(-1.0,0.06)	0.128
Lumen area, mm^2	8.4(6.2,8.8)	6.2(5.8,8.0)	-0.76(-1.1,0)	0.091
Plaque area, mm^2	6.1(5.8,6.2)	6.8(6.3,7.7)	0.54(0.05,0.74)	0.176
Plaque burden,%	43.7±10.3	51.4±6.0	7.8±14.9	0.219
Distal edge (9 paired measurements)				
Vessel area, mm^2	11.1(9.2,15.9)	11.4(9.9,15.0)	-0.31(-0.68,0.64)	0.767
Lumen area, mm^2	6.3(5.1,7.1)	5.7(5.0,6.8)	-0.07(-1.1,0.43)	0.515
Plaque area, mm^2	5.1(4.2,8.4)	5.2(4.8,7.8)	-0.01(-1.2,1.6)	0.953
Plaque burden,%	46.5±14.9	51.2±4.8	4.6±13.5	0.334

Data are shown in mean±SD or median (interquartile range 1st-3rd quartile).

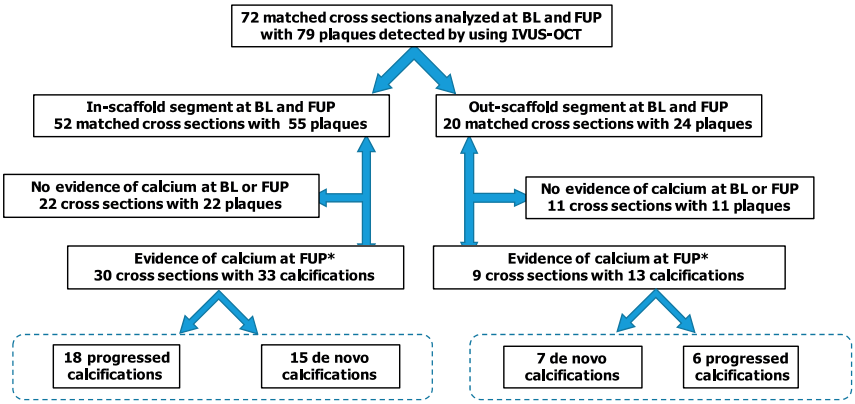

Figure 3. Flow chart of the cross-section selection.
Seventy-two cross-section (79 pools) matched for GS-IVUS, VH-IVUS and OCT images baseline and follow-up were analyzed. *no calcification was observed at BL that was present at FUP. BL=baseline; FUP=follow-up.

The assessment of serial changes in intima thickness overlying the calcified plaque as well as the axial calcium length and arc was analyzable in 14 plaques (9 in-and 5 out-scaffold) at both time points. Minimal intima thickness overlying calcium increased significantly more in-scaffold (Δ:180μm±152μm) than out-scaffold segments (Δ:16μm±116μm) (p=0.034, in-vs out-scaffold), although it was statistically non-significant (p=0.079) after mixed effects analysis. Overall, the mean intima thickness, maximal

intima thickness, axial calcium length and arc significantly increased at follow-up with no differences between in- and out-scaffold segments before and after using the mixed effects model(Table 4).

Longitudinal calcium length (BL:1.8mm±0.71mm vs 5-years:3.6mm±2.0mm, p=0.003) and volume (0.83±0.64mm^3 vs 3.1±2.5mm^3,p=0.001) significantly increased at follow-up.

Table 3. Diagnostic accuracy of individual OCT, GS-IVUS, and VH-IVUS for the calcification detection of coronary atherosclerotic plaque at baseline and 5-year follow up- comparison with fusion method.

Pooled BL and 5Y						
OCT	OCT(-)	OCT(+)	Sensitivity	Specificity	Kappa	P value
Fusion(-)	88	0	70%	100%	0.722	<0.001
Fusion(+)	21	49				
GS-IVUS	GS-IVUS(-)	GS-IVUS(+)				
Fusion(-)	88	0	95.70%	100%	0.961	<0.001
Fusion(+)	3	67				
VH-IVUS	VH-IVUS(-)	VH-IVUS(+)				
Fusion(-)	62	26	100%	70.50%	0.679	<0.001
Fusion(+)	0	70				
Baseline						
OCT	OCT(-)	OCT(+)				
Fusion(-)	55	0	58.30%	100%	0.661	<0.001
Fusion(+)	10	14				
GS-IVUS	GS-IVUS(-)	GS-IVUS(+)				
Fusion(-)	55	0	87.50%	100%	0.907	<0.001
Fusion(+)	3	21				
VH-IVUS	VH-IVUS(-)	VH-IVUS(+)				
Fusion(-)	33	22	100%	60%	0.477	<0.001
Fusion(+)	0	24				
5-year						
OCT	OCT(-)	OCT(+)				
Fusion(-)	33	0	76.10%	100%	0.727	<0.001
Fusion(+)	11	35				
GS-IVUS	GS-IVUS(-)	GS-IVUS(+)				
Fusion(-)	33	0	100%	100%	1	<0.001
Fusion(+)	0	46				
VH-IVUS	VH-IVUS(-)	VH-IVUS(+)				
Fusion(-)	29	4	100%	87.90%	0.894	<0.001
Fusion(+)	0	46				

Data are shown in n(%).GS-IVUS=Greyscale-IVUS; VH-IVUS=virtual histology-IVUS

Table 4. Evolution from baseline to 5-year follow-up of 46 calcifications detected by fusion at follow-up in 39 cross-section; 14 progressed calcifications detectable on OCT and 21 detectable on GS-IVUS at both time points.

Calcium area (n=46) measured on OCT in de novo or progressed calcifications	Baseline	5-year	Differ 5y-BL	P value 5y-BL
Calcium area, mm2				
In-scaffold (n=33)	0.22±0.32	0.70±0.41	0.48±0.32	<0.001
Out-scaffold (n=13)	0.19±0.30	1.04±1.14	0.85±1.0	0.003
P value in-and out-scaffold	0.774	0.199	0.098	
N=14 progressed calcifications detectable on OCT				
Minimal intima thickness overlying calcium, µm				
In-scaffold (n=9)	92±53	272±149	180±152	0.002
Out-scaffold (n=5)	223±156	239±119	16±116	0.345
P value in- and out-scaffold	0.031	0.629	0.034	
Maximal intima thickness overlying calcium, µm				
In-scaffold(n=9)	303(181,480)	355(254,519)	95(40,283)	0.209
Out-scaffold(n=5)	248(141,333)	278(204,447)	55(24,87)	0 345
P value in- and out-scaffold	0.482	0.274	0.16	
Mean intima thickness overlying calcium, µm				
In-scaffold(n=9)	217±117	361±183	144±141	0.005
Out-scaffold(n=5)	238±111	265±109	27±38	0.147
P value in- and out-scaffold	0.721	0.31	0.066	
Arc on OCT, degree				
In-scaffold(n=9)	30±13	46±17	16±14	0.003
Out-scaffold(n=5)	34±24	70±19	36±30	0.03
P value in- and out-scaffold	0.694	0.139	0.057	
Axial length, mm				
In-scaffold(n=9)	0.89(0.51,1.08)	1.1(0.64,1.4)	0.42(0.17,0.77)	0.002
Out-scaffold(n=5)	0.53(0.38,0.79)	0.95(0.70,1.2)	0.45(0.1,1.2)	0.028
P value in- and out-scaffold	0.261	0.936	0.851	
Calcium volume and longitudinal length assessed in 13 progressed calcifications detectable on OCT*				
Longitudinal length, mm (n=13)	1.8±0.71	3.6±2.0	1.7±2.0	0.003
Volume,mm3(n=13)	0.83±0.64	3.1±2.5	2.3±2.4	0.001
N =21 progressed calcifications detectable on IVUS	Baseline	5-year	Differ 5y-BL	P value 5y-BL
Arc on IVUS, degree				
In-scaffold (n=16)	43±21	59±23	16±13	0.002
Out-scaffold (n=5)	34±24	69±31	35±28	0.018
P value in- and out-scaffold	0.35	0.442	0.134	

Data are shown in n, mean±SD or median (interquartile range 1st-3rd quartile). *13 separate calcified volumes were quantified by OCT, 2 continuous calcified cross-section belong to one continuous calcified volume.

IVUS calcification arc measurements

GS-IVUS detected calcium at both time points in 21 plaques. An overall increase in calcium arc was observed with no difference between in-scaffold (Δ:16degree±13degree) and out-scaffold (Δ:35degree±28 degree) (p=0.134, in- vs out-scaffold), and the similar trend was observed after mixed effect analysis (p=0.075) (Table 4).

Calcium assessment with IVUS echogenicity

IVUS echogenicity was evaluated in 39 cross sections containing 46 calcified area pools. An increase in calcium area was observed with no difference between in- Δ:0.21mm^2(0.1, 0.28) and out-scaffold segments Δ:0.22mm^2(0.03, 0.37) (p=0.881, in-vs out-scaffold), after applying mixed effects model, p=0.887 (supplement Table 1).

DISCUSSION

The findings of the present study can be summarized as follows: 1) Fusion OCT/IVUS images provide a comprehensive assessment of coronary artery calcification; 2) Calcification progresses to a similar extent in- and out-scaffold segments, suggesting that calcification is a global phenomenon not influenced by the presence of the scaffold; 3) The intima thickness overlying calcium in-scaffold is thicker than out-scaffold segments and may constitute a new endoluminal lining isolating the calcified plaque from the lumen; 4) VH-IVUS has a high sensitivity for detection of calcification; 5) Lipid pool and NC are the most frequent precursors of calcifications at follow-up.

Calcification detection with fusion of OCT and IVUS

Coronary artery calcium affects the pathophysiologic development of atherosclerosis and triggers cardiac events. In addition, its severity and endoluminal topography affects interventional strategy and clinical events(14). In the present study, calcification was evaluated by fusion of OCT, GS-IVUS and VH-IVUS, which improved the diagnostic accuracy of calcification combining the individual strengths of each modality. As for the diagnostic accuracy of individual modalities in detecting calcification, GS-IVUS at BL showed lower sensitivity than VH, which could be explained by the fact that the complex classification tree and algorithm for tissue analysis of VH-IVUS relies on backscattering of the radiofrequency signal whereas GS-IVUS only detects the envelope of the ultrasonic signal.

In the analysis, the specificity of OCT was high but the sensitivity was limited. Among possible reasons of the low sensitivity are the limited penetration of OCT which precludes the detection of deep calcium deposits, guide-wire artifact and tangential signal drop-out. VH-IVUS, on the other hand, showed 100% sensitivity and low specificity for calcium

detection. Some isolated, localized VH-IVUS DC signals at baseline were considered as artifacts when not confirmed by greyscale and/or OCT calcium detection. Interestingly, some of these isolated VH signals (13/22) became fully calcified plaques at follow-up in the same topographic area detected by the fusion method(Figure4). This unexpected finding might reopen the debate on the diagnostic value of VH-IVUS for detection of calcium(15,16). The validation study with VH-IVUS obtained from 45MHz rotation IVUS has demonstrated the capacity of VH algorithm to detect microcalcification in ROI as small as 0.25mm*0.25mm (3).

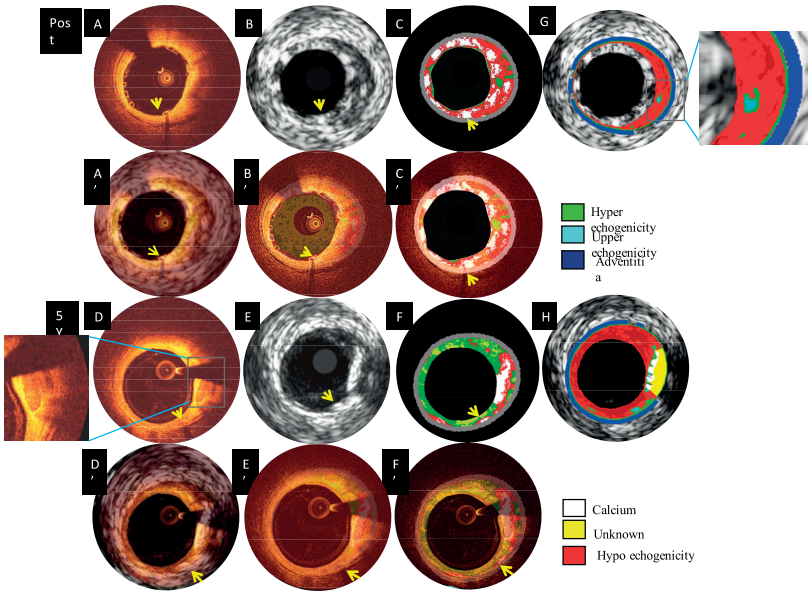

Figure 4. Serial analyses of a calcification by fusion of OCT and IVUS images baseline and follow-up.
The yellow arrow indicates the platinum marker at 6 o'clock. Image A-C show the matched cross-section of OCT, GS-IVUS and VH-IVUS baseline whereas image D-F show matched cross-section at follow-up. Image A, at 1 to 5 o'clock shows a lipid pool plaque with low light intensity, high light attenuation and unclear border. Image C shows mixed plaque composition of necrotic core, fibrous tissue and dense calcium; struts on VH-IVUS are identified as pseudo dense calcium. Image A', B' show the fusion of OCT/GS-IVUS, OCT/VH-IVUS respectively. Image C' emphasizes the VH information of image B' by selecting lower threshold of transparency. The calcium spot with sharp borders (image D) corresponds to the lipid rich plaque on image A. Image D' and E' show the fusion of OCT/GS-IVUS and OCT/VH-IVUS respectively. Image F' emphasizes the VH information of image E' by selecting lower threshold of transparency. Image G shows the echogenicity analysis behind the strut at baseline, upper echogenicity with light blue color progressed to calcium at follow-up (image H; white). The color legend of each echogenicity classification is provided.

Calcified plaque development and precursors

In the present study, calcifications (calcium area, arc, axial length, calcified echogenicity) were shown to increase to a similar extent both in- and out-scaffold segments. This implies a global calcification phenomenon unrelated to the implantation of the scaffold. Calcium progression has been shown in patients on secondary prevention and statin treatment(17). This natural history is thought to reflect a plaque stabilizing phenomenon associated with lipid lowering therapy(18).

Previous data have shown indirectly that, at follow-up, atherosclerosis regresses by decreasing its necrotic core content and increasing its dense calcium content in average(17-19). Our study is the first report to date to clearly and directly demonstrate that phenomenon at the plaque and cross-section level. Only by this meticulous paired, matched analysis of in vivo data with long-term follow-up, we were able to demonstrate the transformation of NC into calcium since the vast majority of tissue precursors were NC or lipid pool. The molecular mechanisms for this transformation remain largely unclear, but "mineral deposit", "osteoprotegerin" and efferocytosis of macrophage are the possible mechanisms(20,21). Co-registration of MSCT and fluoride-18 positron emission tomography (PET) have clearly demonstrated dynamic and inflammatory changes in calcified lesions. Fluoride is uptaken by macrophages, liposomes and microcalcification. In addition, NC on VH-IVUS has been co-localized with calcification visualized by MSCT and 18F PET(22).

Regulatory bodies in Europe and the United States have raised concerns over bioresorption of fully bioresobable scaffold in polylactide: local acidification and transient detection (Von Kossa staining) of calcification around the degraded scaffold strut has been reported in pre-clinical model as earlier as 28 days, but disappeared at long-term follow-up(23). Despite these reassuring pre-clinical data, clinicians remain concerned by the long term outcome of the polylactide bioresorbable scaffold. For instance, in pre-clinical studies it has been demonstrated that metallic bioresorbable scaffold in magnesium evolves in soft amorphous hydroxyapatite of calcium(24).

Progression and development of new calcified plaque should not been confused with neoatherosclerosis of which the OCT features are very specific(25). It has to be emphasized that the lumen area in the present series was 6.4mm2 at baseline and 6.3mm2 at 5-year with no sign of restenosis or luminal encroachment (Table 2).

Re-capping of the calcified plaque

Despite the appearance and progression of calcifications, the new lesions could be considered stable for the following reasons: at 5-year follow-up, a moderately thick layer of neointima(272±149µm) is located on top of each calcified plaque in-scaffold segment (Figure4:D,F'). The minimal intima thickness overlying the calcification increased significantly more in-scaffold segments at 5-year follow-up when compared to out-

scaffold segments. The term "re-capping of the plaque" has been coined to describe this phenomenon(12).

This "cap" overlying the calcification is likely due to the integration of the polymeric struts into the vessel wall, which isolates the lumen from the underlying calcium and the surrounding lipid/necrotic core. The "cap" may transform the unstable phenotype of plaque to stable one by covering the calcific spots and TCFA with neointima(12); Furthermore, calcium with a homogenous thick cap will have less effect on the shear stress than spotty superficial calcium(26).

Strengths and Limitations

This study represents the longest natural history of evolution of plaques analyzed serially by fusion IVUS/OCT. There are nevertheless some methodological limitations. First, precise and careful matching of images acquired with a sampling rate as different as 1 frame/sec from VH to 100/180 frames/sec for OCT considerably reduces the number of analyzable cross-sections per lesion. The goal of the paper was not to unravel clinical implications, but to generate hypotheses. Therefore caution should be exercised when extrapolating the study results given the limited number of cross-section.

Secondly, the lack of intracoronary images pre-procedure renders the analysis of true tissue composition more complex, since strut artifact are detected as "pseudo" DC and NC on VH-IVUS images. To account for that, we excluded struts from the IVUS images according to a previously validated method(10).

Third, we have not used any automated imaging software specifically validated to create fused images. Therefore, the display of the presented images is purely exploratory, but may serve as a preamble for further development of dedicated software application on imaging based on photoacoustic systems(27), as well as hybrid technique(28).

Forth, the data of lipid profile and medications in this study were collected as general clinical information. It was clearly stipulated in the protocol that the investigators had to follow the guidelines of the ESC (at the time of the trial design, target LDL<2mmol/L). In the present study at 5 years, 14/15 patients were treated with HMCoA reductase inhibitor (i.e.,3 Rosuvastatin,7 Atorvastatin, 5 Simvastatin). The Low-density lipoprotein (LDL) was well controlled and decreased from baseline (2.6±0.5 mmol/L) to 5-year (1.6±0.5mmol/L). All the patients presented with at least 1 calcification in the selected 72 fused cross sections. The limited number of observation does not allow any physiopathological or pharmacological interpretation.

Fifth, our findings are limited to segments treated with BVS and cannot be extrapolated to segments treated with metallic stents or untreated ones. Of note, due to the fact that the struts get resorbed at around 2 years of follow-up, we can speculate that at 5 years, the behavior of the vascular wall should be close to that of an untreated segment.

Finally, since no validation against histology was performed to the present time, our results should be cautiously interpreted as hypothesis generating regarding the potential benefits of hybrid imaging techniques.

CONCLUSIONS

With the use of OCT/IVUS fusion imaging we demonstrate in-vivo similar calcium growth in- and non-scaffold segments in patients treated with BVS. Necrotic core is the most frequent precursor of calcification. The scaffold resorption process creates a tissue layer that recaps calcified plaques.

PERSPECTIVES

Competency in medical knowledge

Both OCT and IVUS alone have limitations in evaluating calcification. In this study, by fusing OCT/IVUS, we have shown that similar calcium growth in- and out-scaffold segments in patients treated with BVS. NC is the most frequent precursor of calcification.

Translational outlook

In the future, co-registration of OCT/IVUS techniques, e.g., an acquisition with hybrid catheter will likely be in clinical practice. Future research is needed to define whether calcification is a sign of plaque progression or stabilization of coronary atherosclerosis. What's the molecular mechanism, and how to use pharmacological intervention targeting calcification to stabilize the plaque?

REFERENCES

1. Shan P, Mintz GS, McPherson JA et al. Usefulness of Coronary Atheroma Burden to Predict Cardiovascular Events in Patients Presenting With Acute Coronary Syndromes (from the PROSPECT Study). Am J Cardiol 2015;116:1672-7.
2. Mintz GS, Nissen SE, Anderson WD et al. American College of Cardiology Clinical Expert Consensus Document on Standards for Acquisition, Measurement and Reporting of Intravascular Ultrasound Studies (IVUS). A report of the American College of Cardiology Task Force on Clinical Expert Consensus Documents. J Am Coll Cardiol 2001;37:1478-92.
3. Campos CM, Fedewa RJ, Garcia-Garcia HM et al. Ex vivo validation of 45 MHz intravascular ultrasound backscatter tissue characterization. Eur Heart J Cardiovasc Imaging 2015;16:1112-9.
4. Tolle M, Reshetnik A, Schuchardt M, Hohne M, van der Giet M. Arteriosclerosis and vascular calcification: causes, clinical assessment and therapy. European journal of clinical investigation 2015;45:976-85.
5. Kume T, Okura H, Kawamoto T et al. Assessment of the coronary calcification by optical coherence tomography. EuroIntervention 2011;6:768-72.
6. Kubo T, Imanishi T, Takarada S et al. Assessment of culprit lesion morphology in acute myocardial infarction: ability of optical coherence tomography compared with intravascular ultrasound and coronary angioscopy. Journal of the American College of Cardiology 2007;50:933-9.
7. Gonzalo N, Garcia-Garcia HM, Regar E et al. In vivo assessment of high-risk coronary plaques at bifurcations with combined intravascular ultrasound and optical coherence tomography. JACC Cardiovascular imaging 2009;2:473-82.
8. Raber L, Heo JH, Radu MD et al. Offline fusion of co-registered intravascular ultrasound and frequency domain optical coherence tomography images for the analysis of human atherosclerotic plaques. EuroIntervention 2012;8:98-108.
9. Serruys PW, Ormiston J, van Geuns RJ et al. A Polylactide Bioresorbable Scaffold Eluting Everolimus for Treatment of Coronary Stenosis: 5-Year Follow-Up. Journal of the American College of Cardiology 2016;67:766-76.
10. Brugaletta S, Garcia-Garcia HM, Garg S et al. Temporal changes of coronary artery plaque located behind the struts of the everolimus eluting bioresorbable vascular scaffold. The international journal of cardiovascular imaging 2011;27:859-66.
11. Tearney GJ, Regar E, Akasaka T et al. Consensus standards for acquisition, measurement, and reporting of intravascular optical coherence tomography studies: a report from the International Working Group for Intravascular Optical Coherence Tomography Standardization and Validation. J Am Coll Cardiol 2012;59:1058-72.
12. Bourantas CV, Serruys PW, Nakatani S et al. Bioresorbable vascular scaffold treatment induces the formation of neointimal cap that seals the underlying plaque without compromising the luminal dimensions: a concept based on serial optical coherence tomography data. EuroIntervention 2014;11:746-56.
13. Campos CM, Ishibashi Y, Eggermont J et al. Echogenicity as a surrogate for bioresorbable everolimus-eluting scaffold degradation: analysis at 1-, 3-, 6-, 12- 18, 24-, 30-, 36- and 42-month follow-up in a porcine model. Int J Cardiovasc Imaging 2015;31:471-82.
14. Mintz GS. Intravascular imaging of coronary calcification and its clinical implications. JACC Cardiovascular imaging 2015;8:461-71.

15. Stone GW, Mintz GS. Letter by Stone and Mintz regarding article, "unreliable assessment of necrotic core by virtual histology intravascular ultrasound in porcine coronary artery disease". Circ Cardiovasc Imaging 2010;3:e4; author reply e5.
16. Thim T, Hagensen MK, Wallace-Bradley D et al. Unreliable assessment of necrotic core by virtual histology intravascular ultrasound in porcine coronary artery disease. Circ Cardiovasc Imaging 2010;3:384-91.
17. Nasu K, Tsuchikane E, Katoh O et al. Effect of fluvastatin on progression of coronary atherosclerotic plaque evaluated by virtual histology intravascular ultrasound. JACC Cardiovascular interventions 2009;2:689-96.
18. Raber L, Taniwaki M, Zaugg S et al. Effect of high-intensity statin therapy on atherosclerosis in non-infarct-related coronary arteries (IBIS-4): a serial intravascular ultrasonography study. Eur Heart J 2015;36:490-500.
19. Banach M, Serban C, Sahebkar A et al. Impact of statin therapy on coronary plaque composition: a systematic review and meta-analysis of virtual histology intravascular ultrasound studies. BMC medicine 2015;13:229.
20. Otsuka F, Sakakura K, Yahagi K, Joner M, Virmani R. Has our understanding of calcification in human coronary atherosclerosis progressed? Arteriosclerosis, thrombosis, and vascular biology 2014;34:724-36.
21. Van Campenhout A, Golledge J. Osteoprotegerin, vascular calcification and atherosclerosis. Atherosclerosis 2009;204:321-9.
22. Doris MK, Newby DE. Identification of early vascular calcification with F-sodium fluoride: potential clinical application. Expert Rev Cardiovasc Ther 2016:1-11.
23. Onuma Y, Serruys PW, Perkins LE et al. Intracoronary optical coherence tomography and histology at 1 month and 2, 3, and 4 years after implantation of everolimus-eluting bioresorbable vascular scaffolds in a porcine coronary artery model: an attempt to decipher the human optical coherence tomography images in the ABSORB trial. Circulation 2010;122:2288-300.
24. Campos CM, Muramatsu T, Iqbal J et al. Bioresorbable drug-eluting magnesium-alloy scaffold for treatment of coronary artery disease. Int J Mol Sci 2013;14:24492-500.
25. Taniwaki M, Windecker S, Zaugg S et al. The association between in-stent neoatherosclerosis and native coronary artery disease progression: a long-term angiographic and optical coherence tomography cohort study. European heart journal 2015;36:2167-76.
26. Vengrenyuk Y, Carlier S, Xanthos S et al. A hypothesis for vulnerable plaque rupture due to stress-induced debonding around cellular microcalcifications in thin fibrous caps. Proceedings of the National Academy of Sciences of the United States of America 2006;103:14678-83.
27. Kim J, Lee D, Jung U, Kim C. Photoacoustic imaging platforms for multimodal imaging. Ultrasonography 2015;34:88-97.
28. Bourantas CV, Jaffer FA, Gijsen FJ, van Soest G, Madden SP,Courtney BK, Fard AM, Tenekecioglu E, Zeng Y, van der Steen AF, Emelianov S, Muller J, Stone PH, Marcu L, Tearney GJ, Serruys PW. Hybrid intravascular imaging: recent advances, technical considerations, and current applications in the study of plaque pathophysiology.. European heart journal 2016; [Epub ahead of print]

APPENDIX

Method

OCT image acquisition and analysis

1)Fibrous plaque = high backscattering and a relatively homogeneous OCT signal; 2) Fibrocalcific plaque = contains OCT evidence of fibrous tissue along with calcium that appears as a signal-poor or heterogeneous region with a sharply delineated border on leading, trailing, and/or lateral edges; 3)Lipid pool (lipid/necrotic core) = signal-poor regions with poorly defined or diffuse borders

Matching cross sections and ROI definition

1. No anatomical landmarks in the cross section; 2. Poor OCT image quality due to inadequate contrast flush and/or any artifact; 3. Either lumen or vessel in both OCT and IVUS images unable to be delineated in more than 180 degrees of the vessel or lumen circumference.

OCT/IVUS calcification measurements

Analyst identified the superficial calcific tissue and marked their location. In particular, two markers were placed at the two lateral extremities of the calcified tissue. Then, their circumferential position was determined with respect to the gravitational center of the lumen area, and expressed as an arc taking the position at 3 o'clock as the 0 degree(1) . Calcium axial length in a single cross section was measured as the maximal geometric length of calcification. Minimal, maximal and mean intima thickness on top of calcium were detected by the QCU-CMS software automatically. Calcium longitudinal length was measured from every single frame (C7: 200 μm/frame, C8: 100 or 200 μm/frame) of the entire calcification.

Calcium volume was calculated based on the disk summation method(2). In addition, the unique aspect of the co-registration is to use the presence of an endoluminal radiopaque marker, to select with extreme precision and the matched image on OCT and guarantee the co-registration of OCT, IVUS, and VH-IVUS. Around that single selected OCT frame, we could analyze proximally and distally the adjacent cross sections including calcification in order to measure the length, the volume and the arc of the calcification. The selected, co-registered image is the starting point for the OCT analysis of the plaque volume, and the length of the calcification.

The arc of calcification on IVUS was determined based on a validated method(3).

Automatic quantitative echogenicity analysis

The histograms of the reference adventitial areas of the individual frames are combined into a global adventitia grey-level intensity histogram and the median value is computed as a threshold. Cross-section pixels with an intensity lower than the median value are classified as hypoechogenic, pixels with an intensity higher than the median value threshold are classified as hyperechogenic. An in-house developed acoustic shadow detection algorithm was used to determine calcified plaque which is typically identified in IVUS images as a highly echogenic area creating an acoustic shadow. Highly echogenic areas with a grey-level intensity higher than the high-intensity threshold but without acoustic shadow behind them are classified as upperechogenic, while highly echogenic areas with acoustic shadow are classified as calcified and the shadow itself is classified as unknown(4, 5). To diminish the effect of struts, echogenicity was analyzed behind the struts(6).

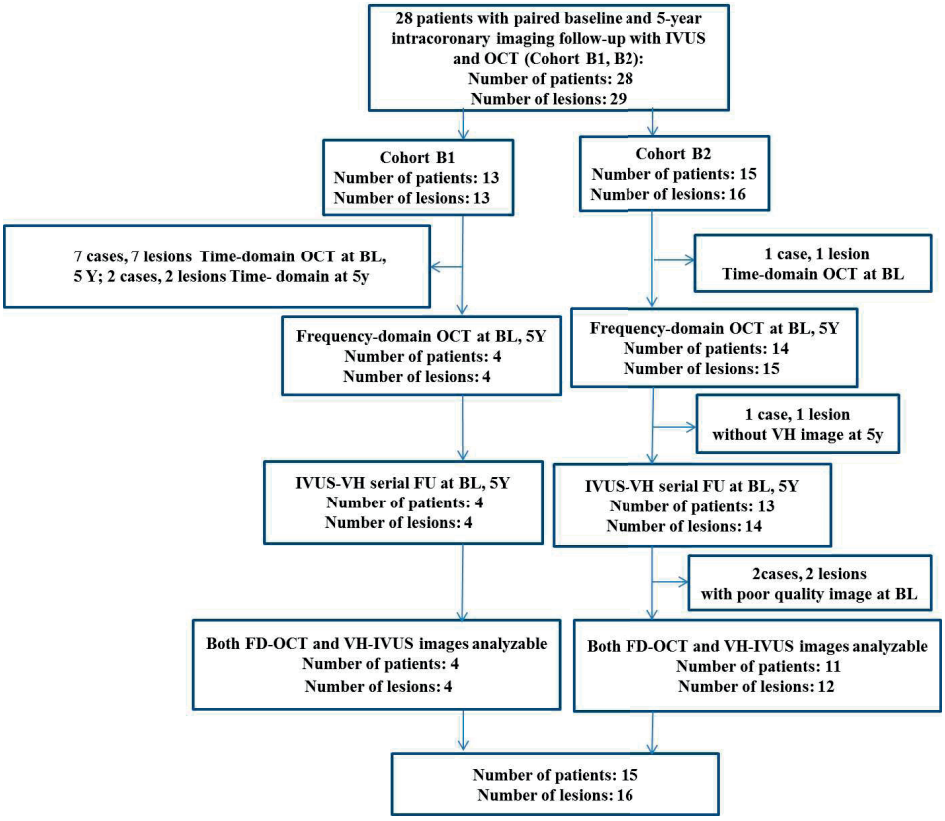

online appendix figure 1. Flow chart of the patient selection in ABSORB Cohort B1 and B2, baseline and at 5-year follow-up (28 cases, 29 lesions).

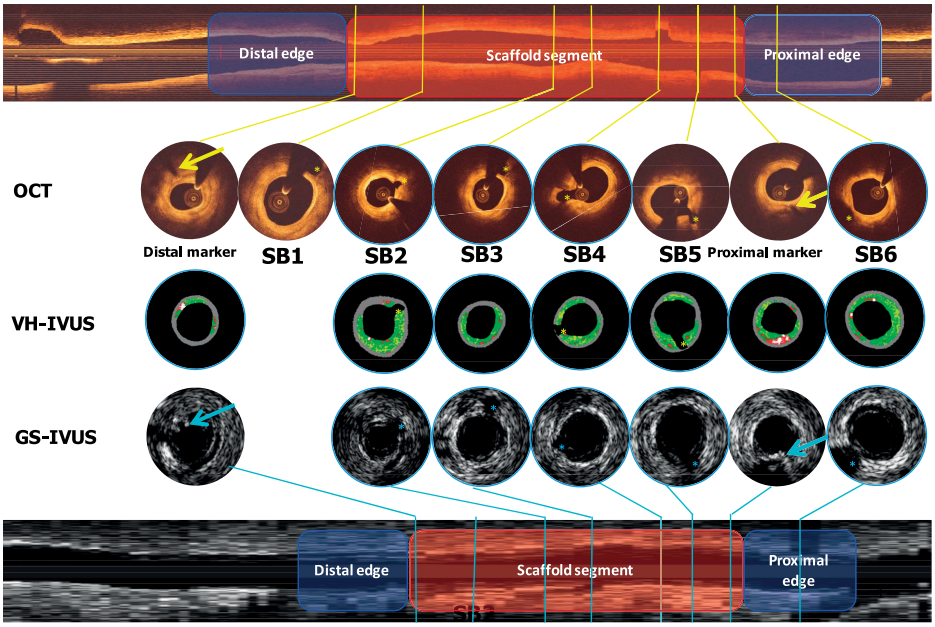

online appendix figure 2. Matching OCT, greyscale-IVUS and VH-IVUS images using radiopaque markers and side branches

*Arrows indicate the metallic radiopaque markers; asterisks indicate the side branches; SB1 on VH-IVUS and GS-IVUS could not be matched with OCT images.

SB=side branch; GS=greyscale-IVUS.

Supplementary Table 1 Evolution from baseline to 5-year follow-up of 39 fused cross sections 4 containing 46 calcifications detected by echogenicity.

	Baseline	5-year	Differ 5y-BL	P value 5y-BL
Calcium, mm^2				
In-scaffold (n=30)	0(0, 0.0425)	0.23(0.12, 0.37)	0.21(0.1, 0.28)	<0.001
Out-scaffold (n=9)	0(0, 0.07)	0.22(0.03, 0.47)	0.22(0.03, 0.37)	0.012
P value in- and out-scaffold	0.967	0.713	0.881	
Upper echogenicity				
In-scaffold (n=30)	0.1(0.03,0.33)	0.07(0.03, 0.14)	0(-0.26, 0.06)	0.160
Out-scaffold (n=9)	0.06(0.02, 0.18)	0.11(0.04, 0.20)	0.05(-0.05, 0.1)	0.441
P value in- and out-scaffold	0.308	0.431	0.199	
Hyper echogenicity				
In-scaffold (n=30)	0.17(0.07, 0.30)	0.11(0.06,0.22)	-0.05(-0.15, 0.1)	0.270
Out-scaffold (n=9)	0.08(0.03, 0.23)	0.13(0.06, 0.23)	0.05(-0.1, 0.13)	0.441
P value in- and out-scaffold	0.229	0.593	0.309	

Data are shown in median (interquartile range 1st-3rd quartile).

SAMENVATTING VAN HET PROEFSCHRIFT

DEEL A: EEN OVERZICHT VAN DE BIOLOGISCH-OPLOSBARE STENT (SCAFFOLD) IN DE BEHANDELING VAN CORONAIRE HARTZIEKTE

Het is 30 jaar geleden sinds de Percutane Transluminale Coronaire Angioplastiek (PTCA) in de klinische praktijk werd geïntroduceerd[1]. Sindsdien heeft de behandeling van coronaire hartziekte een enorme vooruitgang geboekt die de overlevingskansen van patiënten aanzienlijk heeft verbeterd, in het bijzonder in de setting van acuut vaatlijden[2]. Percutane coronaire interventie-technologie heeft zich ontwikkeld van ballon angioplastiek via de metalen stent[3,4] uiteindelijk naar de medicijn-afgevende stent (DES)[5,6]. Na introductie is de werkzaamheid van de DES aangetoond via het verlagen van in-stent restenose, maar met de eerste DES generatie openbaarde zich ook het risico op late en zeer late stent thrombosis[7,8] als gevolg van de aanwezigheid van een permanente polymer[9,10] en dikke metalen stent struts. Om bovenstaande beperkingen te overwinnen is de biologisch-oplosbare technologie inclusief een antiproliferatief geneesmiddel ontwikkeld welke vervolgens geen vreemd materiaal achterlaat dat zou kunnen leiden tot stent thrombosis[11]. In **hoofdstuk 2** beschrijven we het landschap van materialen en technologieën op het gebied van de biologisch-oplosbare scaffold (BRS). Verschillende materialen hebben een verschillende chemische samenstelling, mechanische eigenschappen en biologische absorptie tijden. De huidige soorten BRS bestaan uit ofwel een polymeer of een bio-oplosbase metaallegering. Tot op heden hebben 2 polymere en 1 metaallegering oplosbare stent CE-markering gekregen. De biologisch-oplosbare vasculaire scaffold (ABSORB BVS, Abbott Vascular, Santa Clara, California, USA) is de meest uitgebreid bestudeerd BRS. Naast de behandeling van coronaire hartziekte kan BRS ook gebruikt worden in perifere vasculaire ziekten en aangeboren hartafwijkingen.

DEEL B: MULTIMODALE BEELDVORMING VOOR PROCEDURELE PLANNING

Bij patiënten met meervatscoronairlijden, is de angiografische SYNTAX score gebruikt om de anatomische complexiteit van kransslagaders[12,13] te kwantificeren. Het blijkt echter dat de klinische co-morbiditeit ook van invloed is op de resultaten van revascularization[14,15]. Als gevolg hiervan werd de SYNTAX Score II ontwikkeld een combinatie van de anatomische SYNTAX score en klinische variabelen met prognostische impact[16]. De SYNTAX Score II is gevalideerd in een grote externe populatie op basis van de angiografische gegevens[16]. Maar, de SYNTAX Score II is nooit toegepast in de niet-invasieve coronaire computed tomografie angiografie (CCTA). In **hoofdstuk 3**, tonen we aan dat de CCTA SYNTAX Score II een uitstekende overeenkomst laat zien met de invasieve coronaire angiografie (ICA) SYNTAX Score II, terwijl het afgeleide Heart Team behandelingsadvies op basis van CCTA en ICA een matige overeenkomst toont. CCTA lijkt veelbelovend in

het begeleiden van de beslissing van het Heart Team met betrekking tot de keuze van revascularisatie strategie bij patiënten met meervatscoronairlijden.

Er is gerapporteerd dat IVUS-begeleide DES implantatie betere resultaten heeft dan angiografie-begeleide implantatie[17]. Hoewel, de resultaten van een meta-analyse[18] zijn misschien niet toepasbaar voor de BVS implantatie, immers de studies werden uitgevoerd in metalen stents. Door de limitatie van scaffold expansie, is bepaling van de dimensie van het bloedvat één van de essentiële stappen tijdens BVS implantatie, echter het belang van kwantitatieve angiografische begeleiding op de klinische resultaten is niet bekend. In **hoofdstuk 4** hebben we onderzoek gedaan naar de relatie tussen klinische resultaten en maximale diameter (Dmax) door middel van kwantitatieve coronaire analyse (QCA), de implantatie van een te grote BVS scaffold in een relatief klein bloedvat lijkt te worden geassocieerd met een hoger 1-jaar major Adverse Cardiac Events (MACE) percentage gedreven door meer peri-procedure myocard infarcten (MI). Met de bevindingen uit het vorige hoofdstuk, is de hypothese dat een té grote BVS wordt geassocieerd met een relatieve té lage unfolding van de scaffold. Echter, deze hypothese is nooit gevalideerd versus de feitelijke bevindingen van intracoronaire beelden. Bovendien is het effect van over dimensionering op de finale BVS expansie versus everolimus-afgevende metalen stent (EES) nooit onderzocht. In **hoofdstuk 5** onderzochten we de daadwerkelijke status na implantatie van een te grote stent door middel van intracoronaire ultrasound imaging (IVUS). We vonden dat implantatie van een te grote scaffold of stent geassocieerd is met de onder-deployment van stents wat niet kon worden gecorrigeerd door additionele agressieve post-dilatatie. De belangrijkste mechanismen waardoor een té grote stent bijdraagt aan peri-procedurele MI was de relatieve toename in de strut 'voetafdruk' van de onder-deployment van de scaffold. De bevinding benadrukt het belang van een juiste bloedvat en stent dimensie tijdens BVS implantatie.

DEEL C: MULTIMODALE BEELDVORMING VOOR DE BEPALING VAN DE ACUTE PRESTATIES VAN DE STENT

We onderzochten ook de verschillen in acute prestatie tussen de polymere BRS en de metalen DES platforms. Voorheen was er geen in-vivo kwantitatieve beoordeling van de mate van vaatletsel en was de mate van vaatletsel nooit vergeleken in-vivo tussen metalen stents en polymere scaffolds. In **hoofdstuk 6** beschrijven we een nieuwe specifieke optical coherence tomography (OCT)-afgeleide methode voor de kwantitatieve en nauwkeurige evaluatie van bloedvat schade door analyse van inbedding van de stent struts als een surrogaat marker. We vonden een hoge reproduceerbaarheid voor in-vivo kwantitatieve beoordeling van scaffold / stent inbedding met OCT. Door middel van dit

nieuwe OCT algoritme, konden wij het verschil in lumen dimensiemetingen tussen OCT en QCA in de polymere scaffold en de metalen stent beoordelen. In **hoofdstuk 7** hebben we de invloed van radio-opaciteit op de QCA analyse besproken. Theoretisch zou de radio-opaciteit van metalen stents invloed kunnen hebben op de densitometrische en edge software analyse van QCA, terwijl, de radiolucente eigenschappen van polymere BRS geen invloed hebben op de QCA analyse[17]. Echter, de toegenomen strut uitsteeksels van polymere BRS in het lumen kunnen de intracoronaire laminaire stroming verstoren, wat weer kan leiden tot een onderschatting van de lumen afmeting vanwege een verandering in het contact van het contrastmiddel met de bloedvat wand[18]. We vonden dat verschil in radio-opaciteit tussen polymeer en metaal de edge detectiemethode van QCA analyse verschillend kan beïnvloeden voor de beoordeling van polymere BRS en metalen stents. Vergeleken met OCT, resulteert QCA van de ABSORB polymere scaffold tot een ernstige onderschatting van de luminale dimensie (nauwkeurigheid -0,30 mm) in vergelijking met de XIENCE metalen stents (nauwkeurigheid -0,14 mm). De afstand van de strut uitsteeksels was lager in de ABSORB dan in de XIENCE arm (135 ± 27 µm versus 18 ± 26 µm, p <0,001), en kan hebben bijgedragen aan de waargenomen verschillen.

De discrepantie tussen QCA en OCT gegevens tussen de polymere BRS en metalen stent heeft geleid tot bezorgdheid betreffende acute expansie en lumen toename (gain) bij het gebruik van een polymere stent. In **hoofdstuk 8,** onderzochten wij met IVUS de acute gain ter plaatse van de pre-procedure minimale lumen area tussen de polymere BRS en metalen stent. We vonden dat de polymere BRS een lagere acute gain heeft dan de metalen stent. Bovendien, werd plaque morfologie op de plaats van de MLA dwarsdoorsnede niet onafhankelijk geassocieerd met acute gain. Verder hebben we de prognostische waarde van de post-procedure IVUS bevindingen tussen de twee platforms onderzocht. In **hoofdstuk 9** hebben we aangetoond dat BVS implantatie vaker wordt geassocieerd met post-procedurele asymmetrische en excentrische morfologie in vergelijking met de metalen EES. Slechts 8,0% van de BVS arm en 20,0% van de metalen EES arm bereikt optimale scaffold / stent expansie (p <0,001). Op 1 jaar was er geen statistisch significant verschil in de Device georiënteerde Compositie Eindpunten (DoCE) tussen beide stents (BVS 5,2% vs. EES 3,1%; p = 0,29). Post-procedurele stent asymmetrie en excentriciteit waren gerelateerd aan hogere aantallen eindpunten terwijl er geen relevantie was voor de expansie-status. Post-procedurele stent asymmetrie werd onafhankelijk geassocieerd met DoCE voornamelijk als gevolg van peri-procedurele MI na een percutane coronaire interventie. Toch moet deze aanpak worden gezien als een hypothese genererende aanpak vanwege het geringe aantal eindpunten.

DEEL D: MULTIMODALE BEELDVORMING VOOR DE EVALUATIE VAN DE VEILIGHEID EN DE WERKZAAMHEID VAN STENT VAN KORTE TOT MIDDELLANGE TERMIJN FOLLOW-UP

Ondanks de therapeutische successen van DES in vermindering van restenose en revascularisatie in vergelijking met BMS zijn er nog steeds pogingen een nieuwe BMS generatie te ontwikkelen met vergelijkbare prestaties als DES, maar ook zorgt voor een kortere periode van dubbele antibloedplaatjes therapie (DAPT). De oppervlakte-modificatie technologie is een van de nieuwe methoden die een effectieve remming van de neointima groei en een snelle genezing in preklinische studies[19,20] heeft aangetoond. In **hoofdstuk 10**, presenteerden we de gegevens van de eerste-patiënten studie die was opgezet om de veiligheid en de haalbaarheid van de oppervlakte-modificatie technologie (BMS_{mod}) te testen voor de behandeling van nieuwe coronaire vernauwingen. De BMS_{mod} is een CoCr stent met een oppervlaktebehandeling door het wijzigen van de samenstelling van de native oxide laag. In vitro studies toonden aan dat het behandelde oppervlak verminderde bloedplaatjes adhesie en een verhoogde neutrofiel-vrijgelaten eiwit "cathelicidin" heeft, wat op zijn beurt vorming van neointimal verminderde. De verwachting was dat BMS_{mod} minder in-stent restenose zou hebben. Ondanks de conceptuele voordelen van oppervlaktemodificatie en effectieve remming van de groei van neointima in diermodellen, toonde deze FIM studie aan dat de biocompatibiliteit-gerichte oppervlakte-modificatie niet voldoende is om de neointimale groei te beperken. We gebruikten OCT inbedding analyse (zoals eerder beschreven in **hoofdstuk 6**) om de mate van schade te kwantificeren en te correleren met de neointima reactie. We vonden dat de correlatie van de neointima reactie en de inplantingsdiepte in deze studie niet zo sterk was als in de histologische beoordeling. Een deel van het verschil kan verklaard worden door de verschillende eigenschappen van zieke humane kransslagader weefsel in vergelijking met gezonde varkens modellen, als ook beperkingen van de OCT resolutie om media verstoring te detecteren.

Naast de ontwikkeling van biologisch-oplosbare polymeer-beklede DES en oppervlakte-modificatie BMS, werden polymeervrije DES voorgesteld als een van de oplossingen om de complicatie veroorzaakt door de permanente polymeer te overwinnen. In **hoofdstuk 11** hebben we uitvoerig de vasculaire genezing na implantatie van polymeer-vrije SES met de OCT genezing score op drie en zes maanden geëvalueerd. De seriële OCT toonde een bijna volledige vasculaire genezing aan op zes maanden, zelfs wanneer op drie maanden deze dekking nog onvoldoende was. Deze surrogaat beeldvorming bevinding, en het ontbreken van elke definitieve of mogelijke stent trombose tot acht maanden suggereert een toereikende veiligheid en werkzaamheid van de stent. Onlangs heeft de Leaders-Free trial[21] gemeld dat de DAPT periode kan worden ingekort tot één maand na implantatie van de polymeer-free-biolimus eluerende stent. Verdere

studies met klinische eindpunten zullen nodig zijn om te testen of een verkorte DAPT periode toegepast kan worden bij andere stents (anders dan de polymeervrije-biolimus eluerende stent) en in relatie tot soortgelijke laesie karakteristieken.

DEEL E: MULTIMODALE BEELDVORMING VOOR DE EVALUATIE VAN DE VEILIGHEID EN DE WERKZAAMHEID VAN STENT IN LANGE-TERMIJN FOLLOW-UP

De veiligheid en werkzaamheid van de nieuwe coronaire stent kan aantrekkelijk zijn voor de korte en middellange termijn follow-up. Het is echter de ervaring van de interventionele cardiologen dat onvoorziene complicaties van de nieuwe coronaire stent zich vaak voordoen op de langere termijn follow-up. Bijvoorbeeld, late en zeer late stent trombose in de eerste generatie DES kwam pas 5 jaar na de eerste-in-man studie naar voren. Daarom is het verplicht om de veiligheid en werkzaamheid van het nieuwe platform op lange termijn follow-up te volgen. Naast de klinische follow-up, geeft de coronaire beeldvorming zowel invasief als niet-invasief, mechanistische inzichten in de respons van het bloedvat die kan helpen om vervolgens de nieuwe coronaire stent platform te verbeteren.

Door de radiolucente eigenschap van de polymere BRS, is coronaire computed tomography angiography (CCTA) de alternatieve keuze voor de lange termijn follow-up. In **hoofdstuk 12** hebben we de haalbaarheid van CCTA aangetoond om de aanhoudende aanwezigheid en de locatie van de metalen radio-opake markers (MrMs) 18 maanden na implantatie van de Absorb BVS te evalueren. Wij hebben 4 criteria vastgesteld om de positie van MrMs versus de verkalkte nodules (CN) te bepalen: 1) typische locatie en oriëntatie van de MrMs; 2) marker-tot-marker lengte; 3) topografische relatie van de MrMs met de anatomische oriëntatiepunten gevisualiseerd met behulp van CCTA en conventionele coronaire angiografie; en 4) blooming artefact en de peak demping. De reproduceerbaarheid van de 4 criteria om MrMs van CN te identificeren was goed, $r = 0,97$; $p < 0,0001$. Wanneer we de CCTA gemiddelde lumen area (LA) met andere beeldvormende modaliteiten vergelijken, was de gemiddelde CCTA vergelijkbaar met de Mean LA gemeten door QCA, maar lager dan OCT en IVUS. In **hoofdstuk 13** hebben we de nauwkeurigheid van CCTA om minimale LA te evalueren verder onderzocht in vergelijking met OCT. We vonden dat CCTA, de minimale LA onderschat met 9,8% (nauwkeurigheid 0,39 mm^2, precisie 1,0 mm^2, 95% grenzen van de agreement -1,71 tot 2,50 mm^2). Op het niveau van de marker met de blooming artefact, toonde luminale segmentatie door het centrum van de marker de beste overeenkomst met het OCT-afgeleide gebied; en er was soortgelijke overeenkomst tussen luminale meting bij de scaffold en non-scaffold segmenten.

In **hoofdstuk 14** hebben we gebruik gemaakt van OCT om de vasculaire respons en vasculaire genezing na 2 jaar in 7 patiënten met overlappende geïmplanteerde scaffolds te evalueren. In preklinische studies, toonden de overlappende segmenten een vertraagde dekking in vergelijking met niet-overlappende scaffolds segmenten. In tegenstelling tot de preklinische data, vonden we in patiënten op twee jaar follow-up dat de neointima bekleding nagenoeg volledig was in zowel niet-overlappende (99,4 ± 0,8%) als overlappende segmenten (99,8 ± 0,4%). We vonden ook dat de endoluminale area's tussen overlap en niet-overlappende segmenten vergelijkbaar waren. Aangezien het aantal patiënten in onze analyse zeer beperkt was, moeten de resultaten voorzichtig geïnterpreteerd worden.

In **hoofdstuk 15,** hebben we het gebruik van multimodale beeldvorming gebruikt wordt om het mechanisme van coronaire aneurysma bij het scaffold segment aan te tonen. Zoals beschreven in **hoofdstuk 9,** heeft BVS vaker asymmetrische en excentrieke morfologie tentoongesteld dan metalen EES onmiddellijk post-implantatie. In **hoofdstuk 16**, hebben we de veranderingen in lumen excentriciteit en asymmetrie op 5 jaar na de implantatie van Absorb BVS met behulp van OCT verder onderzocht. We vonden dat de vorm van het lumen van het scaffold segment ronder werd voornamelijk veroorzaakt door vervorming van de scaffold tijdens de eerste 2 jaar. Echter, het asymmetrische lumen vertoonde geen verbetering op lange termijn follow-up. We onderzochten ook de lange-termijn edge vasculaire reactie, in **hoofdstuk 17**, en vonden een vermindering van het luminale scaffold gebied in de afwezigheid van grote edge vasculaire respons dat suggereert dat de fysiologische continuïteit van de lumen contour hersteld op de lange termijn. In **hoofdstuk 18** hebben we gebruik gemaakt van multimodale beeldvorming om de progressie / regressie van verkalkte plaque door middel van de fusie van greyscale-IVUS, virtuele histologie-IVUS (VH-IVUS) en OCT van baseline tot 5 jaar follow-up na Absorb BVS implantatie volledig te kunnen beoordelen. De OCT / IVUS fusie imaging heeft aangetoond dat de progressie van verkalkte plaque vergelijkbaar was tussen de scaffold segments en de segmenten zonder scaffolds. De necrotische kern was de meest voorkomende voorbode van verkalking. Het scaffold resorptie proces creëerde een tissue laag die de verkalkte plaques opnieuw insloten.

SUMMARY

PART A: AN OVERVIEW OF BIORESORBABLE VASCULAR SCAFFOLD IN THE TREATMENT OF CORONARY ARTERY DISEASE

It has been 30 years since the percutaneous transluminal coronary angioplasty (PTCA) was introduced into the clinical practice[1]. Since then, the treatment of coronary artery disease has made tremendous progress in improving patient's survival, especially in the setting of acute coronary syndrome[2]. Percutaneous coronary intervention technology has evolved from the balloon angioplasty to the BMS[3,4] and finally to the DES[5,6]. After its introduction, DES has proven its efficacy in terms of reducing in-stent restenosis rate, however, the first-generation DES also came with the risk of late and very late stent thrombosis[7,8] due to the presence of permanent polymer[9,10] and thick metallic strut. In order to overcome the above limitations, bioresorbable technology has been developed to offer transient scaffolding and eluting an antiproliferative drug, subsequently, leaving no foreign material behind which could potentially trigger the stent thrombosis[11]. In **chapter 2**, we describe the landscape of materials and technologies in the field of BRS. Different materials have different chemical compositions, mechanical properties, and bioabsorption times. The current BRSs are composed of either a polymer or bioresorbable metal alloy. To date, there are 2 polymeric BRSs and 1 metal alloy BRS that acquired CE mark. Polymeric Absorb Bioresorbable Vascular Scaffold (ABSORB BVS, Abbott Vascular, Santa Clara, California, USA) is the most extensively studied BRS. In addition to the treatment of coronary artery disease, BRS could also expand its use to peripheral vascular disease and congenital heart abnormalities.

PART B: MULTIMODALITY IMAGING FOR PROCEDURAL PLANNING

In patients with multi-vessel CAD, the angiographic SYNTAX score has been used to quantify the anatomical complexity of coronary[12,13]. However, it appears that the clinical comorbidities also play a major role in the outcomes after revascularization[14,15]. Consequently, the SYNTAX score II was formulated by the combination of angiographic SYNTAX and the clinical variables with prognostic impact[16]. The SYNTAX score II has been validated in large external population based on the angiographic data[16]. However, the SYNTAX score II has never been applied in the non-invasive coronary computed tomographic angiography (CCTA). In **chapter 3**, we demonstrate that CCTA SYNTAX score II shows excellent agreement with invasive angiography SYNTAX score II, whereas the SYNTAX score II derived Heart Team treatment recommendations based on CCTA and ICA show moderate agreement. Coronary CTA appears to be promising in guiding the Heart Team decision regarding the choice of revascularization strategy in patients with multi-vessel coronary disease.

It has been reported that IVUS-guided DES implantation has better outcomes than angiography-guided implantation[17]. However, the results of meta-analyses[18]might not be applicable to the BVS implantation because the studies were performed in metallic stents. Due to the limitation of scaffold expansion, the vessel sizing is one of the essential steps during the BVS implantation, however, the impact of quantitative angiographic guidance on clinical outcomes is unknown. In **chapter 4**, we investigated the relationship between clinical outcomes and maximal diameter (Dmax) by QCA, we found that implantation of an oversized Absorb scaffold in a relatively small vessel appears to be associated with a higher 1-year MACE rate driven by more frequent periprocedural MI. From the findings of the previous chapter, it has been hypothesized that BVS oversizing is associated with a relative under-deployment of device. However, this hypothesis has never been validated against the actual findings from intracoronary imaging. Furthermore, the impact of device oversizing on the final expansion in the BVS versus metallic everolimus-eluting stent(EES) has never been investigated. In **chapter 5**, we investigated the actual deployment status after implantation of oversized device confirmed by IVUS. We found that implantation of oversized scaffold or stent are associated with the under-deployment of devices and it could not be corrected with subsequent aggressive post-dilation. The major mechanism, by which device oversizing contributed to the periprocedural MIs was the relatively increase in strut footprint from the underdeployment of the scaffold. The finding emphasizes the importance of vessel and device sizing in BVS implantation.

PART C: MULTIMODALITY IMAGING FOR ASSESSMENT OF ACUTE DEVICE PERFORMANCE

We also explored the differential acute device performance between the polymeric BRS and metallis DES platforms. Previously, there was no in vivo quantitative assessment of the degree of vessel injury and the degree of vessel injury has never been compared in vivo between metallic stents and polymeric scaffolds. In **chapter 6**, we described a new specific OCT-derived method for the quantitative and accurate evaluation of vessel injury by using embedment of struts as a surrogate marker. We found a high reproducibility for in vivo quantitative assessment of scaffold/stent embedment by OCT. Based on the above chapter, the new OCT algorithm enabled us to assess the difference in lumen dimension measurements between optical OCT and QCA in the polymeric bioresorbable scaffold and metallic stent. In **chapter 7**, we discussed the influence of material radio-opacity on the QCA analysis. Theoretically, the radiopacity of metallic stents could impact the densitometric and edge software analysis of QCA, in contrast the radiolucent property of polymeric BRS should not impact the QCA analysis[17]. However, the increased

strut protrusion of polymeric BRS into the lumen could hinder the intracoronary laminar flow, which in turn might result in underestimation of the lumen dimension due to altered contact of the contrast medium with the vessel wall[18]. We found that the difference in radioopacity of polymer and metal does differentially influence the edge detection method of QCA for the assessment of polymeric BRS and metallic stents. When compared to OCT, QCA of the Absorb polymeric scaffolds led to a more severe underestimation of the luminal dimension (accuracy –0.30 mm) than with the XIENCE metallic stents (accuracy –0.14 mm). The protrusion distance of struts was larger in the Absorb arm than in the XIENCE arm (135±27 μm vs. 18±26 μm, p<0.001), and may have contributed to the observed differences.

The discrepancy between QCA and OCT data between the polymeric BRS and metallic stent has raised concern about the acute expansion and lumen gain with the use of a polymeric device. In **chapter 8**, we investigated, by IVUS, the acute gain at the site of pre-procedural minimal lumen area between polymeric BRS and metallic stent. We found that polymeric BRS has lower acute gain than the metallic stent. In addition, plaque morphology at the MLA cross-section was not independently associated with acute gain. We further explored the prognostic value of post-procedural IVUS findings between the two platforms. In **chapter 9**, we demonstrated that BVS implantation is more frequently associated with post-procedural asymmetric and eccentric morphology compared to metallic EES. Only 8.0% of the BVS arm and 20.0% of the metallic EES arm achieved optimal scaffold/stent expansion ($p < 0.001$). At 1 year, there was no statistically significant difference in the DoCE between both devices (BVS 5.2% vs. EES 3.1%; $p = 0.29$). Post-procedural devices asymmetry and eccentricity were related to higher event rates while there was no relevance to the expansion status. Post-procedural device asymmetry was independently associated with DoCE, mainly driven by peri-procedural MI, following percutaneous coronary intervention. However, this approach should be viewed as hypothesis generating due to low event rates.

PART D: MULTIMODALITY IMAGING FOR EVALUATING SAFETY AND EFFICACY OF STENT FROM SHORT- TO MEDIUM TERM FOLLOW-UP

Despite the therapeutic successes achieved by DES in reduction of restenosis and target vessel revascularization compared with BMS, there is still a considerable effort to develop a new BMS generation that has a comparable performance to DES but also allows for a shorter duration of dual antiplatelet therapy. The surface-modification technology is one of the novel methods that has demonstrated an effective inhibition of neointimal growth and rapid healing in pre-clinical studies[19,20]. In **chapter 10**, we presented the data from the first-in-man study that was designed to test the safety and feasibility of

the surface-modification technology (BMS_{mod}) for treating de novo coronary lesions. The BMS_{mod} is a CoCr stent that underwent surface treatment by modifying native oxide layer composition. In vitro studies showed that treated surface reduced platelet adhesion and increased neutrophil-released protein "cathelicidin", which in turn reduced neointimal formation. Therefore, BMS_{mod} was expected to have less in-stent restenosis. Despite the conceptual advantages of surface modification and effective inhibition of neointimal growth in animal models, this FIM study showed that the biocompatibility-focused surface modification is not sufficient to reduce the neointimal growth. We used OCT embedment analysis (as described previously in **chapter 6**) to quantify the degree of injury and correlated it with the neointimal response. We found that the correlation of the neointimal response and the embedment depth in the present study was not as strong as in the histological assessment. Part of the discrepancy might be explained by the different properties of diseased human coronary artery tissue as compared to healthy porcine models, as well as limitations of OCT resolution to detect media disruption.

Besides the development of biodegradable polymer-coated DES and surface-modification BMS, polymer-free DES has been proposed as one of the solutions to overcome the complication created by the permanent polymer. In **Chapter 11**, we comprehensively evaluated the vascular healing after implantation of polymer-free SES with OCT healing score at three and six months. The serial OCT showed almost complete vascular healing at six months, even when coverage was insufficient at three months. This imaging surrogate finding, together with the absence of any definite or probable stent thrombosis up to eight months, suggests an adequate safety and efficacy profile of the device. Recently, the LEADERS FREE trial[21] reported that DAPT duration can be abbreviated to only one month after polymer-free biolimus-eluting stents implantation. Further trials with clinical end-points will be needed to test whether abbreviated DAPT duration could be applied in stent platforms other than polymer-free biolimus-eluting stent and in relation to similar lesion characteristics to those assessed in clinical trials.

PART E: MULTIMODALITY IMAGING FOR EVALUATING SAFETY AND EFFICACY OF STENT IN LONG-TERM FOLLOW-UP

The safety and efficacy of the new coronary stent may appear attractive in the short and medium-term follow-up. However, it has been the experience of the interventional cardiologists that often the unforeseen complication of the new coronary stent platform occurred at longer term follow-up. For example, late and very late stent thrombosis in first-generation DES that emerged 5 years after the first-in-man study. Therefore, it is mandatory to monitor the safety and efficacy of the new platform in long-term follow-up. The coronary imaging, either invasive or non-invasive, provides mechanistic insights

into the vessel response that may help to subsequently improve the new coronary stent platform.

Due to the radiolucent property of the polymeric BRS, CCTA is the alternative choices for long-term follow-up. In **chapter 12**, we demonstrated the feasibility of CCTA to evaluate the persistent presence and location at 18 months of the metallic radio-opaque markers (MRMs) following implantation of the Absorb BVS. We established 4 criteria to identify the position of MRMs from the calcified nodules (CN): 1) typical location and orientation of the MRMs; 2) marker-to-marker length; 3) topographical relationship of the MRMs with anatomic landmarks visualized on CCTA and conventional coronary angiography; and 4) blooming artifact and its peak attenuation. The reproducibility of the 4 criteria to identify MRMs from CN was good, r=0.97; $p < 0.0001$. When compared the CCTA mean lumen area (LA) with other imaging modalities, the CCTA Mean LA was comparable to the Mean LA measured by QCA but lower than OCT and IVUS. In **chapter 13**, we then further assessed the accuracy of CCTA to evaluate minimal LA compared with OCT. We found that CCTA underestimated minimal LA by 9.8% (accuracy 0.39 mm^2, precision 1.0 mm^2, 95% limits of agreement −1.71 to 2.50 mm^2). At the level of the marker with the blooming artefact, luminal segmentation through the center of the marker showed the best agreement with the matched OCT-derived area and there was similar agreement between luminal measurement at the scaffold and non-scaffold segments.

In **chapter 14**, we used OCT to evaluate the vascular response and vascular healing at 2 years in 7 patients with overlapped implanted scaffolds. In pre-clinical studies, the overlapped segment showed delayed delayed coverage than in non-overlapped scaffolds segment. In contrast to the pre-clinical data, we found that neointimal coverage was essentially complete in both non-overlap (99.4±0.8%) and overlap segments (99.8±0.4%) at two-year follow-up. We also noted that the endoluminal areas were comparable between overlap and non-overlap segments. Since the number of patients in our analysis was very limited, the results should be interpreted with caution.

In **chapter 15**, we demonstrated the multimodality imaging used to explore the mechanism of the coronary artery aneurysm at the scaffold segment. As presented in chapter 9 that BVS exhibited asymmetric and eccentric morphology more frequently than metallic EES immediately, post-implantation, in **chapter 16**, we further explored the changes of lumen eccentricity and asymmetry at 5 years after implantation of Absorb BVS by using OCT. We found that the lumen shape of the scaffold segment became more circular mainly caused by reshaping of the scaffold during the first 2 years. However, the lumen asymmetry did not improve in the long-term follow-up. We also investigated the long-term edge vascular response, in **chapter 17**, we found a reduction in the scaffold luminal area in the absence of major edge vascular response, suggesting that the physiological continuity of the lumen contour is restored in the long term. In **chapter 18**, we used multimodality imaging to comprehensively assess the progression/regression of

calcified plaque with fused greyscale-IVUS, virtual histology-IVUS (VH-IVUS) and OCT from baseline to 5-year follow-up after Absorb BVS implantation. The OCT/IVUS fusion imaging demonstrated that the progression of calcified plaque was similar between scaffolded segment and non-scaffolded segments. Necrotic core was the most frequent precursor of calcification. The scaffold resorption process created a tissue layer that recapped and sealed calcified plaques.

REFERENCE

1. Gruntzig A. Transluminal dilatation of coronary-artery stenosis. *Lancet (London, England).* 1978;1(8058):263.
2. Van de Werf F, Bax J, Betriu A, et al. Management of acute myocardial infarction in patients presenting with persistent ST-segment elevation: the Task Force on the Management of ST-Segment Elevation Acute Myocardial Infarction of the European Society of Cardiology. *European heart journal.* 2008;29(23):2909-2945.
3. Serruys PW, de Jaegere P, Kiemeneij F, et al. A comparison of balloon-expandable-stent implantation with balloon angioplasty in patients with coronary artery disease. Benestent Study Group. *The New England journal of medicine.* 1994;331(8):489-495.
4. Sigwart U, Puel J, Mirkovitch V, Joffre F, Kappenberger L. Intravascular stents to prevent occlusion and restenosis after transluminal angioplasty. *The New England journal of medicine.* 1987;316(12):701-706.
5. Morice MC, Serruys PW, Sousa JE, et al. A randomized comparison of a sirolimus-eluting stent with a standard stent for coronary revascularization. *The New England journal of medicine.* 2002;346(23):1773-1780.
6. Sousa JE, Costa MA, Abizaid A, et al. Lack of neointimal proliferation after implantation of sirolimus-coated stents in human coronary arteries: a quantitative coronary angiography and three-dimensional intravascular ultrasound study. *Circulation.* 2001;103(2):192-195.
7. Daemen J, Wenaweser P, Tsuchida K, et al. Early and late coronary stent thrombosis of sirolimus-eluting and paclitaxel-eluting stents in routine clinical practice: data from a large two-institutional cohort study. *Lancet (London, England).* 2007;369(9562):667-678.
8. Wenaweser P, Daemen J, Zwahlen M, et al. Incidence and correlates of drug-eluting stent thrombosis in routine clinical practice. 4-year results from a large 2-institutional cohort study. *Journal of the American College of Cardiology.* 2008;52(14):1134-1140.
9. Finn AV, Joner M, Nakazawa G, et al. Pathological correlates of late drug-eluting stent thrombosis: strut coverage as a marker of endothelialization. *Circulation.* 2007;115(18):2435-2441.
10. John MC, Wessely R, Kastrati A, et al. Differential Healing Responses in Polymer- and Nonpolymer-Based Sirolimus-Eluting Stents. *JACC: Cardiovascular Interventions.* 2008;1(5):535-544.
11. Onuma Y, Serruys PW. Bioresorbable scaffold: the advent of a new era in percutaneous coronary and peripheral revascularization? *Circulation.* 2011;123(7):779-797.
12. Serruys PW, Morice MC, Kappetein AP, et al. Percutaneous coronary intervention versus coronary-artery bypass grafting for severe coronary artery disease. *The New England journal of medicine.* 2009;360(10):961-972.
13. Windecker S, Kolh P, Alfonso F, et al. 2014 ESC/EACTS Guidelines on myocardial revascularization: The Task Force on Myocardial Revascularization of the European Society of Cardiology (ESC) and the European Association for Cardio-Thoracic Surgery (EACTS)Developed with the special contribution of the European Association of Percutaneous Cardiovascular Interventions (EAPCI). *European heart journal.* 2014;35(37):2541-2619.
14. Iqbal J, Vergouwe Y, Bourantas CV, et al. Predicting 3-Year Mortality After Percutaneous Coronary Intervention. *JACC: Cardiovascular Interventions.* 2014;7(5):464.
15. Farooq V, Vergouwe Y, Räber L, et al. Combined anatomical and clinical factors for the long-term risk stratification of patients undergoing percutaneous coronary intervention: the Logistic Clinical SYNTAX score. *European heart journal.* 2012;33(24):3098.

16. Farooq V, van Klaveren D, Steyerberg EW, et al. Anatomical and clinical characteristics to guide decision making between coronary artery bypass surgery and percutaneous coronary intervention for individual patients: development and validation of SYNTAX score II. *Lancet (London, England)*. 2013;381(9867):639-650.
17. Witzenbichler B, Maehara A, Weisz G, et al. Relationship between intravascular ultrasound guidance and clinical outcomes after drug-eluting stents: the assessment of dual antiplatelet therapy with drug-eluting stents (ADAPT-DES) study. *Circulation*. 2014;129(4):463-470.
18. Elgendy IY, Mahmoud AN, Elgendy AY, Bavry AA. Outcomes With Intravascular Ultrasound-Guided Stent Implantation: A Meta-Analysis of Randomized Trials in the Era of Drug-Eluting Stents. *Circulation Cardiovascular interventions*. 2016;9(4):e003700.
19. Kolandaivelu K, Bailey L, Buzzi S, et al. Ultra-Hydrophilic Stent Platforms Promote Early Vascular Healing and Minimize Late Tissue Response - A Potential Alternative to Second-Generation Drug Eluting Stents. *EuroIntervention*. 2016.
20. Milleret V, Ziogas A, Buzzi S, Heuberger R, Zucker A, Ehrbar M. Effect of oxide layer modification of CoCr stent alloys on blood activation and endothelial behavior. *Journal of biomedical materials research Part B, Applied biomaterials*. 2015;103(3):629-640.
21. Urban P, Meredith IT, Abizaid A, et al. Polymer-free Drug-Coated Coronary Stents in Patients at High Bleeding Risk. *New England Journal of Medicine*. 2015;373(21):2038-2047.

Future perspectives

INTEGRATION OF CCTA IN CLINICAL PRACTICE: FROM TREATMENT PLANNING TO LONG-TERM CLINICAL FOLLOW-UP

In 2017, percutaneous coronary intervention (PCI) celebrates the 40th anniversary of the first procedure which was performed back in 1977[1]. The continuous improvement of PCI technique resulted in excellent outcomes and made PCI equals to CABG for revascularization in selected patients[2]. In parallel with the advent of stents and surgical techniques, coronary imaging both invasive and non-invasive have also evolved to support the field. In this thesis, we showed the feasibility of using CCTA to assess SYNTAX score II compared with invasive angiographic SYNTAX score II. The future studies should focus on 1) improvement of image resolution that offers image qualities close to the invasive coronary angiography. This would enable the Heart Team to select revascularization strategies solely with non-invasive imaging. The concept is currently studied in the ongoing SYNTAX III Revolution trial[3]. The SYNTAX III Revolution trial is a prospective, multicenter, all-comers randomized trial that will randomize two Heart Teams to select between CABG or PCI according to either ICA or CCTA. The trial will prove the concept of a pure non-invasive coronary anatomy assessment to accurately select the most appropriate revascularization strategy for patients with multi-vessel CAD; 2) incorporating CT-derived FFR in clinical decision. To date, the indications for revascularization in patients with stable angina or silent ischaemia required the diameter stenosis > 50% with documented ischemia or fractional flow reserved (FFR) ≤ 0.80[2]. The CT-derived FFR estimates virtual hyperemia by the calculation, therefore, the technique does not require additional image acquisition and pharmacological agent to induce hyperemic stage during scanning. CT-derived FFR also provided high and superior diagnostic performance despite the presence of calcification[4], hence, it would compensate the reduced performance according to the calcium artifacts that interfered the quantification of the lumen[5]. Currently, there are two methods for deriving FFR from CCTA. The three-dimensional (3D) modeling is provided by Heartflow, Inc (Redwood City, California, USA), the 3D method requires offline analysis. Another method is a simplified one-dimensional (1D) analysis (cFFR) from Siemens Healthcare (Forchheim, Germany) that can be performed at on-site workstations[6]. If the on-site cFFR is commercially available, the future practices may include CT-derived FFR for consideration of revascularization strategies; 3) development on-site algorithm that can automatically calculate SYNTAX score from CCTA and CCTA-derived FFR. The automatic CCTA-SYNTAX score and CCTA functional SYNTAX score will reduce the inter-observer variability and shorten time for image interpretation, consequently, it will support Heart Team decision.

Besides the benefit of CCTA for preprocedural planning, CCTA has been considered as a non-invasive tool to detect in-stent restenosis. The latest generation scanner, with a nominal spatial resolution of 230 μm and new postprocessing algorithm allowed reli-

able detection and quantification of in-stent restenosis with low radiation exposure[7]. However, the research in this field still needs improvement of 1) postprocessing algorithm that provides QCA information in the intervene and non-intervene vessels with short analysis time; 2) valid offline algorithm for the analysis of plaque morphology to assess the progression and regression of plaque burden attributed to the long-term prognosis of the patients[8]. The above features will support the penetration of CCTA in clinical practice.

IMPROVEMENT OF PCI TECHNIQUE: THE ROLE OF INTRA-CORONARY IMAGING DURING THE PROCEDURE

Recently, ILUMIEN III trial[9] has reported that 59%, 63% and 79% of stents that were deployed under OCT-, IVUS- and angiographic guidance could not fully dilate despite following the sizing and post-dilation protocol. In this thesis, we showed that post-dilation might have little effect to improve scaffold expansion if the initial sizing was inappropriate. The above findings reflected that the interventional cardiologists should change their attitude toward the role of intracoronary imaging during PCI. Previously, such technologies were limited to evaluate the expansion of stent and acute complication after stenting. The accumulating evidence showed that intracoronary imaging should be a systematic approach for both pre- and post-procedure[10,11]. An adequate lesion preparation is the most important step during the procedure and need guidance from intracoronary imaging. It has recently been demonstrated that the balloon-artery ratio was associated with the expansion of devices[12]. In the heavy calcified lesions, adequate lesion preparation with debulking devices either balloon or atherectomy plays a key role to achieve optimal stent expansion[13]. It is crucial to establish the standard and simple algorithms to guide lesion preparation and assess whether the lesions are adequately prepared or not. All of these research questions can be elucidated with systematic approach of intracoronary imaging to explore the mechanistic effect of each strategy employed during the procedure.

Further research should assess the role of intravascular imaging guidance in more complex lesions than in ILUMIEN III[9] trial, for instance, diffuse and calcified lesion, bifurcation lesion and ACS setting to clarify its impact on clinical outcomes. In addition, the assessment of underlying plaque morphology is also essential as the findings may change the initial strategies of the procedure[10] and result in the more favourable outcomes[11]. If the current technologies allow, an automatic plaque morphology profile should be developed and integrated into the on-line work stations. This supporting feature will decrease the inter- and intra- observer variability in image interpretation and ease of procedural planning. For example, in the long calcified lesion, the plaque

morphology profile would facilitate the operator's decision whether they would call for debulking devices immediately instead of spending their efforts with many kind of balloons to dilate non-dilatable lesions.

There has been concern about the amount of contrast media and the scanning length when the OCT was used during the procedure. The new method, ECG-triggered Heartbeat OCT pullback has facilitated coronary artery imaging at a rate of 500 frames per second and a pullback speed of 100 mm per second[14,15]. This feature took 0.5 seconds for image acquisition, therefore, it can reduce motion artifacts from ventricular contraction and also enable imaging of a long coronary artery segment in one cardiac cycle. The short imaging time also decreased the amount of contrast dye required for blood clearing, which would reduce the risk of contrast-induced nephropathy[16].

Besides the direct assessment of the stent expansion, intracoronary imaging also allows intracoronary vascular profiling of coronary arteries that made possible to study microenvironment within the coronary arteries. The advancement of computed fluid dynamic (CFD) extend our current understanding of low endothelial shear stress (ESS) as a factor that contributes to in-stent restenosis and stent thrombosis[17] along with established risk factors. The CFD model showed that the thick and rectangular stent design (non-streamlined stent strut) may precipitate stent thrombosis by amplifying platelet activation on top of the strut and attenuating the endothelial production of anticoagulants in low-ESS regions downstream of struts[17]. The new DES systems should therefore change from non-streamlined stent strut (thick and rectangular) to streamlined stent strut (thin and oval) that would promote more physiologic ESS environment to prevent stent thrombosis[18] and ESS may require to be tested in the new stent platform before conducting the first-in-man trial.

It is well established that low local endothelial shear stress is one of predictors of plaque progression and lumen narrowing[19], however, the data is available for the lesions treated with BMS and permanent metallic DES but less is known in lesions treated with BRS. Serial intracoronary vascular profiling in the lesions treated with BRS from post-implantation until the scaffold complete bioresorbtion will provide the mechanistic insight into the role of ESS in the remodeling of vessels after BRS implantation.

INTRACORONARY IMAGING IN TAILORING THE TREATMENT IN ACS PATIENT

The high resolution of OCT brought new knowledge in the treatment of acute coronary syndrome patients. Recently, Jia et al reported that one-fourh of patients with ACS caused by plaque erosion could be treated with conservative treatment without stenting[20]. The intracoronary imaging will play more role in tailoring the treatment in ACS

patient as it can be treated differently depend on the individual risk of bleeding and underlying mechanism of ACS.

ASSESSMENT STENT PERFORMANCE BETWEEN NEW BRS PLATFORM AND METALLIC STENT

In this thesis, we discussed that the material radio-opacity has a significant impact on the QCA assessment. The trialists should be aware of this limitation when the stent performance between new polymeric BRS platforms and permanent metallic DES will be compared in the future studies. In order to accurately evaluate the acute lumen gain, intracoronary imaging especially OCT should be employed to provide the actual luminal gain unless the strut thickness between the two platforms is comparable.

INTRACORONARY IMAGING IN TRANSLATING PRE-CLINICAL STUDIES RESULTS TO THE FIRST-IN-MAN TRIAL

In this thesis, we found that the surface-modified coronary system appeared to be safe in clinical use. However, we also found that the neointimal hyperplasia in the surface-modified coronary system was not substantially reduced as previously reported in the pre-clinical studies. The discrepancy between the results of animal models and FIM study raised the concern about the translation from pre-clinical studies to the first-in-man coronary stent trial. The pre-clinical studies mainly focused on the compatibility of the device with the biological environment without testing per se the anti-restenotic property of the device[21,22]. In the future pre-clinical studies, a certain level of injury should be induced and quantified by imaging to establish the relationship observed between vessel injury and neointimal hyperplasia[23] before conducting the first-in-man trial. In addition, the quantification of the degree of vessel injury by using level of strut embedment as described in the thesis was limited by the OCT penetration to detect media disruption and underlying plaque. This limitation should be solved by high-definition 60-MHz IVUS catheter[24] or miniature integrated IVUS-OCT imaging catheter[25]. These kind of catheters would provide high resolution and deep penetration for a better assessment of coronary structures.

REFERENCE

1. Gruntzig A. Transluminal dilatation of coronary-artery stenosis. *Lancet (London, England).* 1978;1(8058):263.
2. Windecker S, Kolh P, Alfonso F, et al. 2014 ESC/EACTS Guidelines on myocardial revascularization: The Task Force on Myocardial Revascularization of the European Society of Cardiology (ESC) and the European Association for Cardio-Thoracic Surgery (EACTS)Developed with the special contribution of the European Association of Percutaneous Cardiovascular Interventions (EAPCI). *European heart journal.* 2014;35(37):2541-2619.
3. Cavalcante R, Onuma Y, Sotomi Y, et al. Non-invasive Heart Team Assessment of Multivessel Coronary Disease with Coronary Computed Tomography Angiography Based on SYNTAX Score II Treatment Recommendations: Design and Rationale of the Randomized SYNTAX III Revolution trial. *EuroIntervention.* 2016.
4. Norgaard BL, Gaur S, Leipsic J, et al. Influence of Coronary Calcification on the Diagnostic Performance of CT Angiography Derived FFR in Coronary Artery Disease: A Substudy of the NXT Trial. *JACC Cardiovascular imaging.* 2015;8(9):1045-1055.
5. Budoff MJ, Min JK. FFR Derived From Coronary CT Angiography. *JACC: Cardiovascular Imaging.* 2015;8(9):1056.
6. Min JK, Hasegawa JT, Machacz SF, O'Day K. Costs and clinical outcomes for non-invasive versus invasive diagnostic approaches to patients with suspected in-stent restenosis. *The international journal of cardiovascular imaging.* 2016;32(2):309-315.
7. Andreini D, Pontone G, Mushtaq S, et al. Coronary in-stent restenosis: assessment with CT coronary angiography. *Radiology.* 2012;265(2):410-417.
8. Voros S, Rinehart S, Qian Z, et al. Coronary Atherosclerosis Imaging by Coronary CT Angiography. *JACC: Cardiovascular Imaging.* 2011;4(5):537.
9. Ali ZA, Maehara A, Généreux P, et al. Optical coherence tomography compared with intravascular ultrasound and with angiography to guide coronary stent implantation (ILUMIEN III: OPTIMIZE PCI): a randomised controlled trial. *The Lancet.*388(10060):2618-2628.
10. Wijns W, Shite J, Jones MR, et al. Optical coherence tomography imaging during percutaneous coronary intervention impacts physician decision-making: ILUMIEN I study. *European heart journal.* 2015.
11. Witzenbichler B, Maehara A, Weisz G, et al. Relationship Between Intravascular Ultrasound Guidance and Clinical Outcomes After Drug-Eluting Stents: The ADAPT-DES Study. *Circulation.* 2013.
12. Brown AJ, McCormick LM, Braganza DM, Bennett MR, Hoole SP, West NEJ. Expansion and malapposition characteristics after bioresorbable vascular scaffold implantation. *Catheterization and Cardiovascular Interventions.* 2014;84(1):37-45.
13. Kubo T, Shimamura K, Ino Y, et al. Superficial Calcium Fracture After PCI as Assessed by OCT. *JACC: Cardiovascular Imaging.* 2015;8(10):1228.
14. Jang S-J, Park H-S, Song JW, et al. ECG-Triggered, Single Cardiac Cycle, High-Speed, 3D, Intracoronary OCT. *JACC: Cardiovascular Imaging.* 2016;9(5):623.
15. Wang T, Pfeiffer T, Regar E, et al. Heartbeat OCT and Motion-Free 3D In Vivo Coronary Artery Microscopy. *JACC: Cardiovascular Imaging.* 2016;9(5):622-623.
16. Kim TS, Park H-S, Jang S-J, et al. Single cardiac cycle three-dimensional intracoronary optical coherence tomography. *Biomedical Optics Express.* 2016;7(12):4847-4858.
17. Koskinas KC, Chatzizisis YS, Antoniadis AP, Giannoglou GD. Role of Endothelial Shear Stress in Stent Restenosis and Thrombosis. *Journal of the American College of Cardiology.* 2012;59(15):1337.

18. Koskinas KC, Chatzizisis YS, Antoniadis AP, Giannoglou GD. Role of endothelial shear stress in stent restenosis and thrombosis: pathophysiologic mechanisms and implications for clinical translation. *Journal of the American College of Cardiology.* 2012;59(15):1337-1349.
19. Stone PH, Saito S, Takahashi S, et al. Prediction of progression of coronary artery disease and clinical outcomes using vascular profiling of endothelial shear stress and arterial plaque characteristics: the PREDICTION Study. *Circulation.* 2012;126(2):172-181.
20. Jia H, Dai J, Hou J, et al. Effective anti-thrombotic therapy without stenting: intravascular optical coherence tomography-based management in plaque erosion (the EROSION study). *European heart journal.* 2016.
21. van Beusekom H, Sorop O, Weymaere M, Duncker D, van der Giessen W. The neointimal response to stents eluting tacrolimus from a degradable coating depends on the balance between polymer degradation and drug release. *EuroIntervention : journal of EuroPCR in collaboration with the Working Group on Interventional Cardiology of the European Society of Cardiology.* 2008;4(1):139-147.
22. Onuma Y, Serruys P, den Heijer P, et al. MAHOROBA, first-in-man study: 6-month results of a biodegradable polymer sustained release tacrolimus-eluting stent in de novo coronary stenoses. *European heart journal.* 2009;30(12):1477-1485.
23. Schwartz RS, Huber KC, Murphy JG, et al. Restenosis and the proportional neointimal response to coronary artery injury: results in a porcine model. *Journal of the American College of Cardiology.* 1992;19(2):267-274.
24. Chin CY, Maehara A, Fall K, Mintz GS, Ali ZA. Imaging Comparisons of Coregistered Native and Stented Coronary Segments by High-Definition 60-MHz Intravascular Ultrasound and Optical Coherence Tomography. *JACC: Cardiovascular Interventions.* 2016;9(12):1305.
25. Li X, Li J, Jing J, et al. Integrated IVUS-OCT Imaging for Atherosclerotic Plaque Characterization. *IEEE J Sel Top Quantum Electron.* 2014;20(2):7100108.

Appendices

Authors and affiliations
Curriculum vitae
Portfolio
List of publications
Acknowledgement

AUTHORS AND AFFILIATIONS

Mohammad Abdelghani, MD
Academic Medical Center, University of Amsterdam, Amsterdam, The Netherlands

Alexandre Abizaid, MD
Instituto de Cardiologia Dante Pazzanese, Sao Paulo, Brazil

Felipe N. Albuquerque, MD
Montefiore Medical Center, Albert Einstein College of Medicine, New York, New York

Taku Asano, MD
Academic Medical Center, University of Amsterdam, Amsterdam, The Netherlands

Adrian Banning, MD
Oxford Heart Centre, Oxford University Hospitals, Oxford, United Kingdom

Paul Barragan, MD
Polyclinique les Fleurs, Ollioules, France

Antonio L. Bartorelli, MD
Centro Cardiologico Monzino, IRCCS, University of Milan, Milan, Italy

Edouard Benit, MD
Hasselt Heart Centre, Jessa Ziekenhuis, Hasselt, Belgium

Xu Bo, MBBS
Fu Wai Hospital, National Center for Cardiovascular Diseases, Chinese Academy of Medical Sciences, Beijing, China"

Nico Bruining, PhD
ThoraxCenter, Erasmus Medical Center, Rotterdam, The Netherlands

Stefano Buzzi, PhD
Qvanteq AG, Zurich, Switzerland

Gianluca Campo, MD
Cardiology Unit, Azienda Ospedaliera-Universitaria di Ferrara, Cona, Italy

Carlos M. Campos, MD PhD

ThoraxCenter, Erasmus Medical Center, Rotterdam, The Netherlands
Jaryl Ng Chen Koon, B.Eng
National Heart Centre Singapore; Duke-NUS Medical School,Singapore

Wai-Fung Cheong, PhD

Abbott Vascular, Santa Clara, CA, USA

Bernard Chevalier, MD

Institut Cardiovasculaire Paris Sud, Massy, France

Yun-Kyeong Cho, MD

ThoraxCenter, Erasmus Medical Center, Rotterdam, The Netherlands

Evald Høj Christiansen, MD

Department of Cardiology, Aarhus University Hospital, Skejby Hospital, Aarhus, Denmark.

Carlos Collet, MD

Academic Medical Center, University of Amsterdam, Amsterdam, The Netherlands

Roberto Corti, MD

HerzKlinik Hirslanden, Zurich, Switzerland

Joost Daemen, MD PhD

Thoraxcenter, Erasmus Medical Center, Rotterdam, The Netherlands

Gianluigi de Maria MD

John Radcliffe Hospital, Oxford, United Kingdom

Robbert J. de Winter, MD PhD

Academic Medical Center, University of Amsterdam, Amsterdam, The Netherlands

Jouke Dijkstra, PhD

Division of Image Processing, Department of Radiology, Leiden University Medical Center, Leiden, Netherlands

Jeroen Eggermont, PhD

Division of Image Processing, Department of Radiology, Leiden University Medical Center, Leiden, Netherlands

Mohaned Egred, MD

Freeman Hospital, Newcastle upon Tyne, England

Javier Escaned, MD PhD

Hospital Clinico San Carlos / Faculty of Medicine Complutense University and Centro Nacional de Investigaciones Cardiovasculares Carlos III (CNIC), Madrid, Spain

Therese Fahrni, RN

Department of Cardiology, Swiss Cardiovascular Center, University Hospital, Bern, Switzerland

Jean Fajadet, MD

Department of Cardiology, Pasteur Hospital, Toulouse, France

Vasim Farooq, MD PhD

Manchester Heart Centre, Manchester Royal Infirmary, Central Manchester, University Hospitals NHS Trust, Manchester, United Kingdom"

Nicolas Foin, PhD

National Heart Centre Singapore; Duke-NUS Medical School,Singapore

Olivier Gach, MD PhD

CHU de Liege, Liege, Belgium

Runlin Gao, MD

Fu Wai Hospital, National Center for Cardiovascular Diseases, Chinese Academy of Medical Sciences, Beijing, China

Hector M. García-García, MD PhD

Thoraxcenter, Erasmus Medical Center, Rotterdam, The Netherlands

Anthony H. Gershlick, MD

Glenfield Hospital, Leicester, United Kingdom

Alexander Ghanem, MD

Department of Medicine/Cardiology, University of Bonn, Bonn, Germany

Maik J. Grundeken, MD PhD

Academic Medical Center, University of Amsterdam, Amsterdam, The Netherlands

Steven Haine, MD

Antwerp University Hospital, Antwerp, Belgium

Jonathan Hill, MD

King's College Hospital, London, England

Sjoerd H. Hofma, MD PhD

Medisch Centrum Leeuwarden, Leeuwarden, The Netherlands

Yuki Ishibashi, MD PhD

Thoraxcenter, Erasmus Medical Center, Rotterdam, The Netherlands

Hans Jonker, BsC

Cardialysis BV, Rotterdam, the Netherland

Takeshi Kimura, MD PhD

Department of Cardiovascular Medicine, Kyoto University Hospital, Kyoto, Japan

Pieter Kistlaar , PhD

Division of Image Processing, Department of Radiology, Leiden University Medical Center, Leiden, Netherlands

Jacques J. Koolen, MD PhD

Cardiology, Catharina Ziekenhuis, Eindhoven, the Netherlands

Ron Kornowski, MD

Rabin Medical Center, Petah Tikva, Israel

Ken Kozuma, MD PhD

Teikyo University Hospital,Tokyo, Japan

Robin P. Kraak, MD

Academic Medical Center, University of Amsterdam, Amsterdam, The Netherlands

David J. Kurz, MD

Cardiology, Triemli Hospital, Zurich, Switzerland

Irene M. Lang, MD

Division of Cardiology, Department of Internal Medicine II, Medical University of Vienna, Vienna, Austria

Maciej Lesiak, MD

1st Department of Cardiology, Medical University of Poznan, Poland;

Shengnan Liu, MD

Division of Image Processing, Department of Radiology, Leiden University Medical Center, Leiden, Netherlands

Carlos Macaya, MD

Hospital Universitario Clínico San Carlos, Madrid, Spain

Dougal R. McClean, MD

Department of Cardiology, Christchurch Hospital, Christchurch, New Zealand

Yosuke Miyazaki, MD PhD

Thoraxcenter, Erasmus Medical Center, Rotterdam, The Netherlands

Marie-Angele Morel , BsC

Cardialysis BV, Rotterdam, The Netherlands

Shimpei Nakatani, MD PhD

Thoraxcenter, Erasmus Medical Center, Rotterdam, The Netherlands

Shaoping Nie, MD

The Emergency & Critical Care Center of Beijing Anzhen Hospital, Capital Medical University, Beijing, the People's Republic of China.

Koen Nieman, MD PhD

Thoraxcenter, Erasmus Medical Center, Rotterdam, The Netherlands

Yoshinobu Onuma, MD PhD

Thoraxcenter, Erasmus Medical Center, Rotterdam, The Netherlands

John A. Ormiston, MBChB

Auckland City Hospital, Auckland, New Zealand

Jeffrey J. Popma, MD

Beth Israel Deaconess Medical Center, Boston, MA, USA

Lorenz Räber, MD PhD

Department of Cardiology, Bern University Hospital, Bern, Switzerland.

Maria D. Radu, MD PhD

Department of Cardiology, Rigshospitalet, Copenhagen, Denmark

Richard J. Rapoza, PhD

Abbott Vascular, Santa Clara, California

Marco Roffi, MD PhD

Division of Cardiology, University Hospital, Geneva, Switzerland

Nicola Ryan, MD

Hospital Clinico San Carlos / Faculty of Medicine Complutense University and Centro Nacional de Investigaciones Cardiovasculares Carlos III (CNIC), Madrid, Spain

Patrick W.J.C Serruys, MD PhD

International Centre for Circulatory Health, NHLI, Imperial College London, London, UK

Pieter C. Smits, MD PhD

Maasstad Ziekenhuis, Rotterdam, the Netherlands

Yohei Sotomi, MD

Academic Medical Center, University of Amsterdam, Amsterdam, The Netherlands

Rod Stables , MD

Liverpool Heart and Chest Hospital NHS Foundation Trust, Liverpool, United Kingdom

Bojan Stanetic, MD

Department of Cardiology, University Clinical Centre of the Republic of Srpska, Banja Luka, Bosnia and Herzegovina.

Gregg W. Stone, MD

Columbia University Medical Center, New York-Presbyterian Hospital, and the Cardiovascular Research Foundation, New York, NY, USA

Pannipa Suwannasom, MD

Academic Medical Center, University of Amsterdam, Amsterdam, The Netherlands
Northern Region Heart Center, Faculty of Medicine, Chiang Mai University, Chiang Mai, Thailand

Kengo Tanabe, MD PhD

Division of Cardiology, Cardiac Intensive Care Unit, Mitsui Memorial Hospital, Tokyo, Japan

Hiroki Tateishi, MD PhD

Thoraxcenter, Erasmus Medical Center, Rotterdam, The Netherlands

Erhan Tenekecioglu, MD

Thoraxcenter, Erasmus Medical Center, Rotterdam, The Netherlands

Jan G. Tijssen, PhD

Academic Medical Center, University of Amsterdam, Amsterdam, The Netherlands

Gerrit-Anne van Es, PhD

Cardialysis BV, Rotterdam, The Netherlands

Robert-Jan van Geuns, MD PhD

Thoraxcenter, Erasmus Medical Center, Rotterdam, The Netherlands

Susan Veldhof, RN

Abbott Vascular, Diegem, Belgium

Clemens von Birgelen, MD PhD

Department of Cardiology, Thoraxcentrum Twente, Medisch Spectrum Twente, Enschede, the Netherlands

Robert Whitbourn, MD

St. Vincent's Hospital, Fitzroy, Victoria, Australia

Stephan Windecker, MD

Bern University Hospital, Bern, Switzerland

Chiung-Jen Wu, MD

Division of Cardiology, Department of Internal Medicine, Kaohsiung Chang Gung Memorial Hospital and Chang Gung University College of Medicine, Kaohsiung, Taiwan

Joanna J. Wykrzykowska, MD PhD

Academic Medical Center, University of Amsterdam, Amsterdam, The Netherlands

Yaping Zeng, MD PhD

Thoraxcenter, Erasmus Medical Center, Rotterdam, The Netherlands

Yao-Jun Zhang, MD PhD

Nanjing First Hospital, Nanjing Medical University, Nanjing, China

Wei-Ying Zhao, PhD

Abbott Vascular, Santa Clara, CA, USA

Arik Zucker, MSc

Qvanteq AG, Zurich, Switzerland

CURRICULUM VITAE

Name	Pannipa Suwannasom
Date of Birth	November 21, 1982
Place of Birth	Uttaradit, Thailand
Nationality	Thai
Professional Address	Division of Cardiology, Department of Internal Medicine, Maharaj Nakorn Chiang Mai Hospital, Faculty of Medicine, Chiang Mai University Room 0805, 8th floor, Sripat Building, 110 Intavaroros Road, Sripoom, Muang, Chiang Mai, 50200, Thailand
E-mail	pannipa.s@cmu.ac.th
Education:	
2000-2006	MD (First class honour): Faculty of Medicine, Chiang Mai University, Chiang Mai, Thailand
2006-2010	Board of Internal Medicine: Faculty of Medicine, Chiang Mai University, Chiang Mai, Thailand
2010-2012	Board of Cardiology: Faculty of Medicine, Chiang Mai University, Chiang Mai, Thailand
2012-2013	Certificate in Interventional Cardiology: Faculty of Medicine, Chiang Mai University, Chiang Mai, Thailand
Training and working experiences:	
2006 - 2010	Resident of Internal Medicine, Faculty of Medicine, Chiang Mai University, Chiang Mai, Thailand
2010 - 2012	Fellow in Cardiology, Faculty of Medicine, Chiang Mai University, Chiang Mai, Thailand
2012 - 2013	Interventional Cardiology Fellow, Faculty of Medicine, Chiang Mai University, Chiang Mai, Thailand
2013- 2014	Interventional cardiologist at Northern Region Heart Center, Faculty of Medicine, Chiang Mai University, Chiang Mai, Thailand
2014- 2016	Research fellowship in Interventional Cardiology, Academic medical center, University of Amsterdam, Amsterdam, The Netherlands
2017-present	Lecturer, Division of Cardiology, Department of Internal Medicine, Faculty of Medicine, Chiang Mai University, Chiang Mai, Thailand
License and Certification	
2006	Thai Full Medical license (#34216)
2010	Board Certified Member of the Royal College of Physician of Thailand in Internal Medicine (#21482/2553)
2012	Board Certified Member of the Royal College of Physician of Thailand in Cardiology (#24777/2555)
2013	Board Certified Member of the Royal College of Physician of Thailand in Interventional Cardiology (#155/2556)
2017	Fellow of the European Society of Cardiology (FESC)

PHD PORTFOLIO

Name PhD student: Pannipa Suwannasom
PhD period: May 2015 - June 2016
Co-supervisors: dr. J.J. Wykrzykowska and dr. Y. Onuma
Supervisors: prof. dr. R.J. de Winter and prof. dr. P.W.J.C. Serruys

PhD training	**Year**	**ECTS**
Specific courses		
- NIHES Summer Program Courses on Epidemiology	2013	4.0
Presentations and conferences		
- EuroPCR, Paris (attendant)	2014	1.0
- AsiaPCR, Singapore (oral presentation)	2015	1.0
- American College of Cardiology (ACC) scientific sessions, San Diego (poster)	2015	1.0
- European Society of Cardiology (ESC) scientific sessions, London (poster)	2015	1.0
- Transcatheter Cardiovascular Therapeutics (TCT), San Francisco (poster)	2015	1.0
- EuroPCR, Paris (1 invited speaker, 2 oral presentation)	2016	2.0
- SOLACI/SBHCI 2016 Congress, Rio De Janeiro (e-poster)	2016	0.8
- European Society of Cardiology (ESC) scientific sessions, Rome (attendant)	2016	1.0
Other academic activities		
- Local associated editor and regular reviewer for EuroIntervention and AsiaIntervention	2014-present	4.0
Awards and Prizes		
First place in the category e-poster in SOLACI/SBHCI 2016 Congress	2016	

LIST OF PUBLICATION

INCLUDED IN THESIS

Part A

1. **Suwannasom P**, Sotomi Y, Tateishi H, Erhan Tenekecioglu E, Zeng Y, Kraak RP, Wykrzykowska JJ, de Winter RJ, Serruys PW, Onuma Y. *Bioresorbable drug-eluting scaffolds for treatment of vascular disease: reviewed.* Expert Opin Drug Deliv. 2016;13(5):725-39.

Part B

2. Cavalcante R*, **Suwannasom P ***, Sotomi Y, Onuma Y, Collet C, Ryan N, de Maria G, Morel MA, van Es GA, Farooq V, Banning A, Escaned J, Serruys PW. On behalf of the SYNTAX II Study Group. *Noninvasive Coronary Computed Tomography Angiography Based Heart Team Assessment Using The SYNTAX Score II For The Selection Of The Revascularization Strategy In Patients With Multivessel Coronary Artery Disease: An Analysis Of The SYNTAX II Trial*. (Submitted)
3. Ishibashi Y, Nakatani S, Sotomi Y, **Suwannasom P**, Grundeken MJ, Garcia-Garcia HM, Bartorelli AL, Whitbourn R, Chevalier B, Abizaid A, Ormiston JA, Rapoza RJ, Veldhof S, Onuma Y, Serruys PW. *Relation Between Bioresorbable Scaffold Sizing Using QCA-Dmax and Clinical Outcomes at 1 Year in 1,232 Patients From 3 Study Cohorts (ABSORB Cohort B, ABSORB EXTEND, and ABSORB II).* JACC Cardiovasc Interv. 2015 Nov;8(13):1715-26.
4. **Suwannasom P**, Sotomi Y, Tenekecioglu E, Wykrzykowska JJ,Haine S, Stables R, Adrian Banning AP, Ghanem A, Reith S, Campo G, de Winter RJ, Chevalier B, Onuma Y, Serruys PW. *Impact of devices oversizing on final device expansion and clinical outcomes after everolimus-eluting bioresorbable vascular scaffold and everolimus-eluting metallic stent implantation in the ABSORB II trial.* (Submitted)

Part C

5. Sotomi Y, Tateishi H, **Suwannasom P**, Dijkstra J, Eggermont J, Liu S, Tenekecioglu E, Zheng Y, Abdelghani M, Cavalcante R, de Winter RJ, Wykrzykowska JJ, Onuma Y, Serruys PW, Kimura T. *Quantitative assessment of the stent/scaffold strut embedment analysis by optical coherence tomography.* Int J Cardiovasc Imaging. 2016 Jun;32(6):871-83.
6. Sotomi Y, Onuma Y, **Suwannasom P**, Tateishi H, Tenekecioglu E, Zheng Y, Cavalcante R, Jonker H, Stone GW, Popma JJ, Kozuma K, Tanabe K, de Winter RJ, Wykrzykowska JJ, Serruys PW, Kimura T. *Is quantitative coronary angiography reliable in assessing the lumen gain after treatment with the everolimus eluting bioresorbable polylactide scaffold:*

a quantitative coronary angiography and optical coherence tomography comparison in the Absorb Japan randomized trial? EuroIntervention. 2016 Oct 10;12(8):e998-e1008

7. Sotomi Y*, Ishibashi Y*, **Suwannasom P**, Nakatani S , Cho YK , Grundeken M, Zeng Y, Tateishi H , Smits PC, Barragan P, Kornowski R , Gershlick AH, Windecker S, van Geuns RJ , Bartorelli AL, de Winter RJ, Tijssen JP, Onuma Y, Serruys PW. *Acute Gain in Minimal Lumen Area Following Implantation of Everolimus-Eluting ABSORB Biodegradable Vascular Scaffolds or Xience Metallic Stents: Intravascular Ultrasound Assessment from the ABSORB II Trial.* JACC Cardiovasc Interv. 2016 Jun 27;9(12):1216-27
8. **Suwannasom P**, Sotomi Y, Ishibashi Y , Cavalcante R , Albuquerque FN , Macaya C, Ormiston J , Hill J, Lang I , Egred M, Fajadet J, Lesiak M , Tijssen J, Wykrzykowska JJ, de Winter RJ, Chevalier B, Onuma Y, Serruys PW. *The impact of post-procedural asymmetry, expansion and eccentricity of bioresorbable everolimus-eluting scaffold and metallic everolimus-eluting stent on clinical outcomes in the ABSORB II trial.* JACC Cardiovasc Interv. 2016 Jun 27;9(12):1231-42.

Part D

9. **Suwannasom P**, Sotomi Y, Corti R, Kurz D, Roffi M, von Birgelen C, Buzzi S, Zucker A, Dijkstra J, Wykrzykowska JJ, de Winter RJ, Windecker S, Onuma Y, Serruys PW, Daemen J, Räber L. *First-in-Man 6-month results of Surface-modified Coronary Stent System in native coronary stenosis.* EuroIntervention. 2017; 12(17):2118-2127
10. **Suwannasom P**, Onuma Y, Benit E, Gach O, von Birgelen C, Hofma SH, Sotomi Y,Bo X, Zhang YJ, Gao R, García-García HM, Wykrzykowska JJ, de Winter RJ, Serruys PW. *Evaluation of vascular healing of polymer-free sirolimus-eluting stents in native coronary artery stenosis: a serial follow-up at 3 and 6 months with optical coherence tomography imaging.* Eurointervention 2016;12:e574-e583

Part E

11. **Suwannasom P**, Onuma Y, Campos CM, Nakatani S, Ishibashi Y, Tateishi H, Grundeken MJ, Stanetic BM, Nieman K, Jonker H, Garcia-Garcia HM, Serruys PW: On behalf of the investigators of ABSORB Cohort A, B and EXTEND trials. *Fate of Bioresorbable Vascular Scaffold Metallic Radio-Opaque Markers at the Site of Implantation After Bioresorption.* JACC Cardiovasc Interv. 2015 Jul;8(8):1130-2.
12. Collet C, Sotomi Y, Cavalcante R, Asano T, Miyazaki Y,Tenekecioglu E, Kistlaar P, Zeng Y, **Suwannasom P**, de Winter RJ, Nieman K, Serruys PW, Onuma Y. *Accuracy of coronary computed tomography angiography for bioresorbable scaffold luminal investigation: a comparison with optical coherence tomography.* Int J Cardiovasc Imaging. 2016 Nov 28. [Epub ahead of print].
13. Sotomi Y, **Suwannasom P**, Tateishi H, Farooq V, Wu CJ, Cheong WF, Zhao W, Veldhof S, de Winter RJ, Wykrzykowska JJ, Abizaid A, Serruys PW, Onuma Y, on behalf of the

ABSORB EXTEND investigators. *Imaging Outcomes of Bioresorbable Scaffold Overlap: An Optical Coherence Tomography Analysis from the ABSORB EXTEND Trial.* AsiaIntervention 2017;3:1-9. (non-Pubmed listed).

14. Nakatani S, Ishibashi Y, **Suwannasom P**, J Grundeken M, Høj Christiansen E, Onuma Y, Serruys PW; *ABSORB Cohort B Investigators. Development and receding of a coronary artery aneurysm after implantation of a fully bioresorbable scaffold.* Circulation 2015;24;131(8):764-7.
15. **Suwannasom P,** Sotomi Y, Asano T, Koon JN, Tateishi H, Zeng Y, Tenekecioglu E, Wykrzykowska JJ, Foin N, de Winter RJ, Ormiston JA, Serruys PW, Onuma Y. *Change in lumen eccentricity and asymmetry after treatment with Absorb bioresorbable vascular scaffolds in the ABSORB Cohort B trial: a five-year serial optical coherence tomography imaging study*. EuroIntervention. 2017;12(18):e2244-e2252
16. Hiroki T, **Suwannasom P**, Sotomi Y, Nakatani S, Ishibashi Y, Tenekecioglu E, Abdelgani M, Cavalcante R, Zeng Y, Grundeken M, Albuquerque FA, Veldhof S, Onuma Y, Serruys PW. *Edge Vascular Response After Resorption of the Everolimus-Eluting Bioresorbable Vascular Scaffold: A 5-Year Serial Optical Coherence Tomography Study.* Circ J. 2016 Apr 25;80(5):1131-41
17. Zeng Y*, Tateishi H*, Cavalcante R, Tenekecioglu E, **Suwannasom P**, Sotomi Y, Collet C, Nie S, Jonker H, Dijkstra J, Radu M, Räber L, Onuma Y, Serruys PW. *Serial Assessment of Tissue Precursors and Progression of Coronary Artery Calcification Analyzed by Fusion of Intravascular Ultrasound and Optimal Coherent Tomography:A Five Years Follow-up of Scaffolded and Nonscaffolded Arteries.* JACC Cardiovasc Imaging (accepted for publication).

PUBLISHED ARTICLES, NOT INCLUDED IN THESIS (FIRST AUTHOR)

18. **Suwannasom P**, Benit E, Gach O, von Birgelen C, Hofma S, Bo X, Zhang Y-J, Nakatani S, Ishibashi Y, Onuma Y, García-García HM, Gao R, Serruys PW. *Short-term effects of Nano+™ polymer-free sirolimus-eluting stents on native coronary vessels: an optical coherence tomography imaging study.* AsiaIntervention 2015;1:57-70. (non-Pubmed listed).
19. **Suwannasom P**, Sotomi Y, Onuma Y, Serruys PW. *Reply: Predictors of Bioresorbable Everolimus-Eluting Scaffold Failure at Intravascular Ultrasound Examination: Asymmetry Versus Expansion.* JACC Cardiovasc Interv. 2016 Sep 26;9(18):1971-2
20. **Suwannasom P**, Serruys PW. *DAPT: a historical accident in the pharmacological treatment of post-percutaneous coronary intervention*. EuroIntervention. 2016 Apr 20;11(13):1449-50.

PUBLISHED ARTICLES, NOT INCLUDED IN THESIS (CO-AUTHORSHIPS)

21. Ishibashi Y, Muramatsu T, Nakatani S, Sotomi Y, **Suwannasom P**, Grundeken MJ, Cho YK, Garcia-Garcia HM, van Boven AJ, Piek JJ, Sabaté M, Helqvist S, Baumbach A, McClean D, de Sousa Almeida M, Wasungu L, Miquel K, Dudek D, Chevalier B, Onuma Y, Patrick W. Serruys PW. *Incidence and Potential Mechanism(s) of Post-procedural Rise of Cardiac Biomarker in Patients with Coronary Artery Narrowing after Implantation of an Everolimus Eluting Bioresorbable Vascular Scaffold or Everolimus Eluting Metallic Stent*. JACC Cardiovasc Interv. 2015 Jul;8(8):1053-63.
22. Nakatani S, Sotomi Y, Ishibashi Y, Grundeken MJ, Tateishi H, Tenekecioglu E, Zeng Y, **Suwannasom P**, Regar E, Radu MD, Räber L, Bezerra H, Costa MA, Fitzgerald P, Prati F, Costa RA, Dijkstra J, Kimura T, Kozuma K, Tanabe K, Akasaka T, Di Mario C, Serruys PW, Onuma Y. *Comparative analysis method of permanent metallic stents (XIENCE) and bioresorbable poly-L-lactic (PLLA) scaffolds (Absorb) on optical coherence tomography at baseline and follow-up*. EuroIntervention. 2015 Oct 9;11(6). [Epub ahead of print]
23. Grundeken MJ, White RM, Hernandez JB, Dudek D, Cequier A, Haude M, van Boven AJ, Piek JJ, Helqvist S, Sabate M, Baumbach A, **Suwannasom P**, Ishibashi Y, Staehr P, Veldhof S, Cheong WF, de Winter RJ, Garcia-Garcia HM, Wykrzykowska JJ, Onuma Y, Serruys PW, Chevalier B. *The incidence and relevance of site-reported versus patient reported angina: insights from the ABSORB II randomized trial comparing Absorb everolimus eluting bioresorbable scaffold with XIENCE everolimus eluting metallic stent*. Eur Heart J Qual Care Clin Outcomes(2015) published online: 13 October 2015 (non-Pubmed listed).
24. Campos CM, Costa F, Garcia-Garcia HM, Bourantas C, **Suwannasom P**, Valgimigli M, Morel MA, Windecker S, Serruys PW. *Anatomic Characteristics and Clinical Implications of Angiographic Coronary Thrombus: Insights From a Patient-Level Pooled Analysis of SYNTAX, RESOLUTE, and LEADERS Trials.* Circ Cardiovasc Interv. 2015;8:e002279.
25. Escaned J, Banning A, Farooq V, Echavarria-Pinto M, Garcia-Garcia HM, Ryan N, Cavalcante e Silva R, Campos CM, Stanetic BM, Ishibashi Y, **Suwannasom P**, Kappetein AP, Taggart D, Morel Van Es GA, Serruys PW, on behalf of the SYNTAX II Study Group. *Rationale and design of the SYNTAX II trial evaluating the short to long-term outcomes of state-of-the-art percutaneous coronary revascularisation in patients with de novo three vessels disease*. EuroIntervention. 2016 Jun 12;12(2):e224-34
26. Cavalcante R, Sotomi Y, Lee CW, Ahn JM, Farooq V, Tateishi H,Tenekecioglu E, Zeng Y, **Suwannasom P**, Collet C, Albuquerque FN, Onuma Y, Park SJ, Serruys PW. *Outcomes After Percutaneous Coronary Intervention or Bypass Surgery in Patients With Unprotected Left Main Disease*. J Am Coll Cardiol. 2016 Sep 6;68(10):999-1009.
27. Cavalcante R, Sotomi Y, Zeng Y, Lee CW, Ahn JM, Collet C, Tenekecioglu E, **Suwannasom P**, Onuma Y, Park SJ, Serruys PW. *Coronary bypass surgery versus stenting in*

multivessel disease involving the proximal left anterior descending coronary artery. Heart. 2016 Sep 20. [Epub ahead of print]

28. Sotomi Y, Cavalcante R, Shlofmitz RA, **Suwannasom P**, Tateishi H, Tenekecioglu E, Zheng Y, Abdelghani M, de Winter RJ, Wykrzykowska JJ, Onuma Y, Serruys PW. *Quantification by optical coherence tomography imaging of the ablation volume obtained with the Orbital Atherectomy System in calcified coronary lesions.* EuroIntervention. 2016 Oct 20;12(9):1126-1134.
29. Collet C, Cavalcante R, **Suwannasom P**, Bittencourt MS, Serruys PW. *Letter to Editor: Coronary plaque quantification and fractional flow reserve by coronary computed tomography angiography identify ischemia-causing lesions.* European Heart Journal: Published online 29 February 2016
30. Serruys PW, **Suwannasom P**, Nakatani S, Onuma Y. *Snowshoe Versus Ice Skate for Scaffolding of Disrupted Vessel Wall.* JACC Cardiovasc Interv. 2015:8(7):910-913.
31. Collet C, Sotomi Y, Cavalcante R, **Suwannasom P**, Tenekecioglu E, Onuma Y, Serruys PW. *Coronary stent thrombosis: what have we learned?* J Thorac Dis 2016;8(7):1398-1405.
32. Cummins P, **Suwannasom P**, Zhang YJ, Hayashida K, Yeo KH, Byrne RA, Naber CK, Tan HC. *Proceedings from an AsiaIntervention think tank meeting, May 2016*. AsiaIntervention 2016;2:80-81
33. Campos CM, **Suwannasom P**, Koenig W, Serruys PW, Garcia-Garcia HM. *Darapladib for the treatment of cardiovascular disease*. Expert Rev Cardiovasc Ther. 2015;13(1):33-48.
34. Campos CM, **Suwannasom P**, Nakatani S, Onuma Y, Serruys PW, Garcia-Garcia HM. *Short- and Long-term Evaluation of Bioresorbable Scaffolds by Optical Coherence Tomography.* Interventional Cardiology Clinics. 2015:4(3):333–349.
35. Sotomi Y, **Suwannasom P**, Tenekecioglu E, Tateishi H, Abdelghani M, Serruys PW, Onuma Y. *Differential aspects between cobalt-chromium everolimus drug-eluting stent and Absorb everolimus bioresorbable vascular scaffold: from bench to clinical use.* Expert Rev Cardiovasc Ther. 2015 Oct;13(10):1127-1145.
36. de Araújo Gonçalves P, Rodríguez-Granillo GA, Spitzer E, **Suwannasom P**, Loewe C, Nieman K, Garcia-Garcia HM. *Functional Evaluation of Coronary Disease by CT Angiography*. JACC Cardiovasc Imaging. 2015 Nov;8(11):1322-35.
37. Zeng Y, Tateishi H, **Suwannasom P**, Tenekecioglu E, Silva RC, Sotomi Y, Onuma Y, Serruys PW. *Progression of calcification after implantation of a fully bioresorbable scaffold: A serial and combined IVUS-OCT follow-up of 5 years.* Int J Cardiol. 2016 Apr 15;209:176-8.
38. Tenekecioglu E, Bourantas CV, Abdelghani M, Tateishi H, Sotomi Y, **Suwannasom P**, Onuma Y, Yılmaz M, Serruy PW. *Optimisation of percutaneous coronary intervention*

: Indispensable for Bioresorbable scaffolds. Expert Rev Cardiovasc Ther. 2016 Jul 4. [Epub ahead of print]

39. Sotomi Y, Collet C, Cavalcante R, Morel MA, **Suwannasom P**, Farooq V, van Gameren M, Onuma Y, Serruys PW. *Tools and Techniques - Clinical: SYNTAX score II calculator.* EuroIntervention. 2016 May 17;12(1):120-3.
40. Sotomi Y, Shammas NW, **Suwannasom P**, Campos CM, Wykrzykowska JJ, de Winter RJ, Dijkstra J, Serruys PW, Onuma Y. *Impact of the Orbital Atherectomy System on a Peripheral Calcified Lesion: Quantitative Analysis by Intravascular Echogenicity.* JACC Cardiovasc Interv. 2015 Sep 9 [Epub ahead of print]
41. Sotomi Y, **Suwannasom P**, Serruys PW, Onuma Y. *Possible Mechanical Causes of Scaffold Thrombosis: Insights from Case Reports with Intracoronary Imaging.* EuroIntervention. 2016 Oct 25 [Epub ahead of print]
42. Lee CW, Ahn JM , Cavalcante R, Sotomi Y, Onuma Y, **Suwannasom P**, Tenekecioglu E, Yun SC, Park DW, Kang SJ, Lee SW, Kim YH, Park SW, Serruys PW, Park SJ. *Coronary Artery Bypass Surgery Versus Drug-Eluting Stent Implantation for Left Main or Multivessel Coronary Artery Disease: A Meta-Analysis of Individual Patient Data.* JACC: Cardiovascular Interventions Dec 2016, 9 (24) 2481-2489.
43. Tenekecioglu E, Albuquerque F, Sotomi Y, Zeng Y, **Suwannasom P**, Tateishi H, Cavalcante R, Ishibashi Y, Nakatani S, Abdelghani M, Dijkstra J, Bourantas C, Collet C, Karanosos A, Radu M, Wang A, Takashi Muramatsu T, Landmesser U, Okamura T, Regar E, Raber L, Guagliumi G, Pyo R, Onuma Y, Serruys PW. *Intracoronary Optical Coherence Tomography: Clinical and Research Applications and Intravascular Imaging Software Overview.* Catheter Cardiovasc Interv. 2017 Jan 21. [Epub ahead of print]
44. Zeng Y*, Cavalcante R*, Tenekecioglu E, **Suwannasom P**, Sotomi Y, Collet C, Abdelghani M, Jonker H, Digne F, Horstkotte D, Zehender M, Indolfi C, Saia F, Fiorilli R, Chevalier B, Bolognese L, Goicolea J, Nie S, Onuma Y, Serruys PW; investigators of Absorb II study. *Comparative assessment of "plaque/media" change on three modalities of IVUS immediately after implantation of either everolimus-eluting bioresorbable vascular scaffold or everolimus-eluting metallic stent in Absorb II study.* Int J Cardiovasc Imaging. 2016 Dec 23. [Epub ahead of print] *Authors contributed equally
45. Sotomi Y, Miyazaki Y,Collet C, Asano T, **Suwannasom P**, Tijssen J, de Winter RJ, Waksman R, Lipinski MJ, Onuma Y, Serruys PW. *Does acute coronary syndrome impact on the incidence of thrombosis after the implantation of Absorb bioresorbable vascular scaffold?* EuroIntervention 2017;12:1-3
46. Collet C, **Suwannasom P**, Almeida M, Onuma Y, Serruys PW. *Coronary bioresorbable vascular scaffold radiopaque marker embolization.* Eur Heart J. 2017 Feb 8. [Epub ahead of print]
47. Miyazaki Y*, **Suwannasom P***, Sotomi Y, Abdelghani M, Tummala K, Katagiri Y, Asano T, Tenekecioglu E, Zeng Y, Cavalcante R, Collet C, Onuma Y, Serruys PW. *Single or*

dual antiplatelet therapy after PCI. Nat Rev Cardiol. 2017 Feb 9. [Epub ahead of print]
*Authors contributed equally

ACKNOWLEDGEMENTS

This thesis would not have been accomplished without huge support of people around me. I would like to express my sincere gratitude to my promotors, co-promotors, colleagues, friends and family for their continued support and encouraging me to go forward in research field. I wish in particular to thank:

Prof. Patrick Serruys: Meeting Prof. Serruys in 2013 was the start of the journey. At that time, I was about to complete my training in interventional cardiology and was replaced my boss to participate AsiaPCR-SingLive in Singapore. I popped in the bioresorbable scaffold session, the new platform that just launched in Southeast Asia at that time. Many slides were projected during the presentationbut the most sexy-catchy one was the slide with OCT cross-section after complete bioresorption of the scaffold from the ABSORB cohort A trial. At that moment, I was eager to learn more about intracoronary imaging and started to figure out who was the speaker, then, I realized that the speaker was the father of SYNTAX trial "Prof. Patrick W. Serruys".

In the afternoon, I joined small lunch meeting that dedicated for BVS and Prof. Serruys was there to answer all questions. After stay hesitating since appetizer, main course and dessert, I decided to ask him whether I would have any chance to join research team in Rotterdam. Prof. answered by handing his iPhone to me and said "put your contact there, send your CV to my email, do you have my email address?" At that time, I was so excited and assumed that it meant "yes", I said that I did not have but I would certainly find it in NEJM at the address of correspondence. Later, I managed to visit Rotterdam for an interview in August 2013 and finally joined the team in April 2014.

Dearest my promotor Professor Serruys, I'm eternally grateful for everything you have taught me both academic and non-academic issues. It is my great honour and privilege to work with one of the pioneers of Interventional Cardiology. It was always a pleasure to work with you in your office (so called "fish tank" for the fellows) during the weekend to discuss on the methodology of our manuscripts, review the manuscripts before submission, review OCT, IVUS, MSCT for the upcoming meetings and review topics of your lectures. Your incredible memory of all previous publications (already 2,000+) always made us amazing. It appeared to me that there was no area in interventional cardiology that you have never explored. You have in depth knowledge in every topics. You are the most energetic person I have ever seen, your positive stimulus has navigated all fellows to become the real scientists. Your endless enthusiasm put all projects in their shape. Thanks for granting me to work in many projects, it enabled me to learn the "Serruys methodology of work" which I have no doubt why you have a great achievement in your career. It begins with excellent planning, helicopter view, consistency, transparency, never give up to any problems but solution will always deliver, I will keep refining myself for these.

Despite a very tight schedule during the day, Prof. is very kind to read fellow's manuscripts carefully every pages, numbers and space. Your patience in reading and teaching fellows to write and think in scientific way was remarkable. From five types of mentor, you are all of them: Educator, Challenger, Moderator, Career planner, Connector. I don't know how can you work like this for more than four decades to guide all naive fellows and later, majority of them become famous independent researchers in the field. Thanks for being our pillar, our resource of inspiration, I really proud of myself for having been your fellow.

Dr.Yoshinobu Onuma: my dearest co-promotor. Yoshi sensei, thank you so much for always being mentor, friend and brother. Whenever I stepped to your office, there was always a solution and practical advice. You always give a helping hand to all fellows despite your schedule is also tight, your presence has saved many fellows who were about to be decapitated in the "fish tank". Despite the outstanding expertise of yours, you are always stay humble as you keep saying that "at least I know something", which indeed I would like to change to "I know everything". I sincerely admire your intelligence, hard work, perfection, generosity and broad minded, sometimes you helped other until you had no time for yourself. Thank you for teaching me a lot in imaging analysis; CEC adjudication; statistical analysis; writing the manuscripts, your comments are always sharp and even sharper after two glasses of Chardonnay!

Besides our serious work in Cardialysis, it was a great fun outside the office. The remarkable one is drinking! Thank you for all the happy moments we shared together. I will never forget the first day in Gaucho and new year drink with you and Pieter in LaBru. Thanks for everything you have helped me. I hope to keep our friendships closely and continue our collaboration in the future.

prof. Robbert J. de Winter and Dr.Joanna Wykrzykowska : Dear Prof. de Winter, Dear Joanna, thanks for including me in your team and your continuous support. I deeply appreciated your excellent advices and hope to continue our collaborations in various topics.

Rotterdam research fellows

Yohei: Dearest Sotomi sensei, my best friend. Thanks for being such a great colleague, friend and brother. Working with you was an enjoyable task, although some projects we did together were so gut-wrenching. I'm so sorry that my paragraph in the manuscript was always "illegal" to your opinion. Anyway thank for all of your kind suggestions. I loved our fruitful conversation during lunch time from research methodology to the non-academic issues such as family, music, TV series (Big Bang). You are the intelligent, hard-worker, positive thinking and reliable guy I have met. I trust that you will prosper in this field and I look very much forward to continuing our research collaborations throughout the rest of our career path. I would also thanks to your family (your mother and Aya) to let me join your family occasions, I hope to meet them again if I have chance to join CCT and hope to be able to welcome you to Thailand as well.

Hiroki: Dear Tate-chan, thanks for being such a great friend and great "drink" company after 10 PM. You are the one who never say "no" to my requests, thanks for your kind assistance in many projects. You are a good listener and always support me whenever I faced difficult situations. It was a great fun to learn Japanese from you, oniisan!.

Yuki and Shimpei: Dear Yuki, master of QCA and Shimpei, master of OCT, thanks for always being my consultants, I truly appreciate our warm friendship.

Carlos Campos: Dear Carlos, you are the only one who kept trying to speak Thai with self learning technique by closing nostrils, however, I must admit that you did it well. It was my great pleasure and lots of fun to work with you in SYNTAX and echogenicity projects, still nobody can beat your "7 minutes" IVUS analysis. I hope that we can continue our collaboration in the future.

Maik: Dear Maik, the only native dutch fellow in the office. Thanks for helping us in all about Dutch issues. I hope that you will become a great Interventional Cardiologist soon.

Rafael: Dear Rafa, master of rotablator, statistic, wine and cooking. Your Brazillian BBQ was heaven! Thank you for your kind friendship, look forward to seeing you in euroPCR every year.

I would also thank all my colleagues: Erhan Tenekecioglu, Mohammed Abdelghani, Yaping Zeng, Carlos Collet, Yosuke Miyazaki, Taku Asano, Bojan Stanetic, Ernest Spitzer, Amsterdam research fellow: Robin P. Kraak, Martina Nassif, for their kind friendship.

Hanny: Dear Hanny, I would never have this thesis without your help. Our 15 minutes conversation in the early morning became the most important task of the day for me. It was not only to be the first one who claimed for time slot to work with Prof. but also the time to have good personal advices. Now, it was the memorable moment. I always admired the way you dealt with Prof. super busy schedule, you could manage to meet all requests (even sometimes fellows were not allowed to enter your room with big A4 paper quoted "Do not enter, unless you are PWS" in front of the door. My dear paranymph, my heartful thanks for all of your support. Please consider Chiang Mai next time for your vacation, I am more than happy to welcome you.

Cardialysis: It was a great experience to be involved in scientific work and got support by professional teams in Cardialysis: Gerrit-Anne van Es, Rob Schneijdenberg, Maurice Vorage, Timo van Laun, Bianca Backx, Jeannette Fong-Pien-Joe, Stefanie Leeflang, Ana Guimaraes, Ravindra Pawar, Jamal Khachabi, Marije Hoogen, Andre Boogaards, ex-cardialysis: Hector Garcia-Garcia and Linda Korthout. Special thanks to Monique Schuijer, I'm grateful for your endless support in all projects I have been involved. Everything went well only when your hands touched those projects. Eric van Remortel and Ton de Vries, many thanks for your statistical support. Ton, we still have one trip to go to see Maeslantkering. Hans Jonker, thanks for your technical support, no matter chaotic output they were, you could manage to change from "god" language to "human" language. It

was amazing that you can control everything and make all fellows happy just only one click, Haartlijk Bedunkt! Osama Soliman, your cocktail was so fantastic and I'm looking forward to visiting your kitchen again.

Marie-Angele: my angel. The mother of "SYNTAX score". Besides the serious academic work, you have a magic that can gather everyone together: nieuwe haring when Schmidt-Zeevis still close to our office, the sinterklass who visited fellow office with honour artificial black petes (Yoshi and Linda), the barbecue party that make the policemen kept checking us until party finished, the farewell party for ex-fellows. You are big sister for all fellows in Cardialysis and also the rescuer for us. I owed a special thank for kindly translating my thesis into Dutch though you were busy. I appreciated your invitation for new year party and afternoon tea when my family came to Rotterdam, I will never forget the precious moment with you.

EuroIntervention office: It is my great privilege to be part of EuroIntervention editorial team. Dear Paul, the best managing editor ever. You are hard-worker but also have a ton of humour at the same time. I always enjoyed your afternoon entertainment, funny VDO clip in YouTube or old songs (sorry, I was born too late). Thanks for St.Patrick's day hat, you carried it all the way from Beijing to R'Dam just only I could not get one from Paddy Murphy and O'chea. Sylvie, assistant managing editor, Merci Beaucoup! thank you so much for all of your support, you always encouraged me to have positive thinking when I had doubt of my capability. I hope that I will have chance to see your live dance performance very soon.

Dien de Boer: Dearest Dien, thanks for your support during my stay. It was always positive energy when I visited Naarden. I loved our conversation during the evening walk to greet "happy sheep", I hope to do it with you every year.

Division of Cardiology, Chiang Mai University: I wish to thank to all my colleagues for ongoing support since I was a fellow in training until I became a young staff. I feel greatly indebted to Dr.Srun Kuanprasert, the first mentor who inspired me to choose cardiology and interventional cardiology for my career. Without you, I would not be here today. It is always a great pleasure to work with you and I always feel secured when we stand together even the procedure is the complex one. Thanks for your endless supports and encouragement that push me forward. Also, I extend my sincerest thanks to for all nurses and employees in cathlab, cardiac care units, med-noninvasive unit and cardiology back office. We are and will always be a great team.

Family: I am indebted to my parents **Payon** and **Suree**, grandmother **Kamolwan** and my sisters **Thitirat** and **Supattana** for their infinite love and support. Thanks for teaching me how importance of education; for believing in me and allowing me to follow my dream. There is no word to express how much I love you, this thesis represents as my dedication to you all.